

لجنة الميكانيك
تقدم لكم..

[المكتبة التخصصية]



<http://www.Mech.MuslimEngineer.Net>



[FB.com/Groups/Mid.Group](https://www.facebook.com/Groups/Mid.Group)



0789434018



MechFet

Principles of Measurement Systems



We work with leading authors to develop the strongest educational materials in engineering, bringing cutting-edge thinking and best learning practice to a global market.

Under a range of well-known imprints, including Prentice Hall, we craft high quality print and electronic publications which help readers to understand and apply their content, whether studying or at work.

To find out more about the complete range of our publishing, please visit us on the World Wide Web at:
www.pearsoned.co.uk

Principles of Measurement Systems

Fourth Edition

John P. Bentley

*Emeritus Professor of Measurement Systems
University of Teesside*



Harlow, England • London • New York • Boston • San Francisco • Toronto • Sydney • Singapore • Hong Kong
Tokyo • Seoul • Taipei • New Delhi • Cape Town • Madrid • Mexico City • Amsterdam • Munich • Paris • Milan

Pearson Education Limited

Edinburgh Gate
Harlow
Essex CM20 2JE
England

and Associated Companies throughout the world

Visit us on the World Wide Web at:
www.pearsoned.co.uk

First published 1983
Second Edition 1988
Third Edition 1995

Fourth Edition published 2005

© Pearson Education Limited 1983, 2005

The right of John P. Bentley to be identified as author of this work has been asserted by him in accordance with the Copyright, Designs and Patents Act 1988.

All rights reserved. No part of this publication may be reproduced, stored in a retrieval system, or transmitted in any form or by any means, electronic, mechanical, photocopying, recording or otherwise, without either the prior written permission of the publisher or a licence permitting restricted copying in the United Kingdom issued by the Copyright Licensing Agency Ltd, 90 Tottenham Court Road, London W1T 4LP.

ISBN 0 130 43028 5

British Library Cataloguing-in-Publication Data

A catalogue record for this book is available from the British Library

Library of Congress Cataloging-in-Publication Data

Bentley, John P., 1943–

Principles of measurement systems / John P. Bentley. – 4th ed.
p. cm.

Includes bibliographical references and index.

ISBN 0-13-043028-5

1. Physical instruments. 2. Physical measurements. 3. Engineering instruments.
4. Automatic control. I. Title.

QC53.B44 2005

530.8–dc22

2004044467

10 9 8 7 6 5 4 3 2 1
10 09 08 07 06 05

Typeset in 10/12pt Times by 35
Printed in Malaysia

The publisher's policy is to use paper manufactured from sustainable forests.

To Pauline, Sarah and Victoria

Contents

Preface to the fourth edition
Acknowledgements

xi
xiii

Part A General Principles

1

1	The General Measurement System	3
1.1	Purpose and performance of measurement systems	3
1.2	Structure of measurement systems	4
1.3	Examples of measurement systems	5
1.4	Block diagram symbols	7
2	Static Characteristics of Measurement System Elements	9
2.1	Systematic characteristics	9
2.2	Generalised model of a system element	15
2.3	Statistical characteristics	17
2.4	Identification of static characteristics – calibration	21
3	The Accuracy of Measurement Systems in the Steady State	35
3.1	Measurement error of a system of ideal elements	35
3.2	The error probability density function of a system of non-ideal elements	36
3.3	Error reduction techniques	41
4	Dynamic Characteristics of Measurement Systems	51
4.1	Transfer function $G(s)$ for typical system elements	51
4.2	Identification of the dynamics of an element	58
4.3	Dynamic errors in measurement systems	65
4.4	Techniques for dynamic compensation	70
5	Loading Effects and Two-port Networks	77
5.1	Electrical loading	77
5.2	Two-port networks	84
6	Signals and Noise in Measurement Systems	97
6.1	Introduction	97
6.2	Statistical representation of random signals	98
6.3	Effects of noise and interference on measurement circuits	107
6.4	Noise sources and coupling mechanisms	110
6.5	Methods of reducing effects of noise and interference	113

7	Reliability, Choice and Economics of Measurement Systems	125
7.1	Reliability of measurement systems	125
7.2	Choice of measurement systems	140
7.3	Total lifetime operating cost	141

Part B	Typical Measurement System Elements	147
---------------	--	------------

8	Sensing Elements	149
8.1	Resistive sensing elements	149
8.2	Capacitive sensing elements	160
8.3	Inductive sensing elements	165
8.4	Electromagnetic sensing elements	170
8.5	Thermoelectric sensing elements	172
8.6	Elastic sensing elements	177
8.7	Piezoelectric sensing elements	182
8.8	Piezoresistive sensing elements	188
8.9	Electrochemical sensing elements	190
8.10	Hall effect sensors	196
9	Signal Conditioning Elements	205
9.1	Deflection bridges	205
9.2	Amplifiers	214
9.3	A.C. carrier systems	224
9.4	Current transmitters	228
9.5	Oscillators and resonators	235
10	Signal Processing Elements and Software	247
10.1	Analogue-to-digital (A/D) conversion	247
10.2	Computer and microcontroller systems	260
10.3	Microcontroller and computer software	264
10.4	Signal processing calculations	270
11	Data Presentation Elements	285
11.1	Review and choice of data presentation elements	285
11.2	Pointer-scale indicators	287
11.3	Digital display principles	289
11.4	Light-emitting diode (LED) displays	292
11.5	Cathode ray tube (CRT) displays	295
11.6	Liquid crystal displays (LCDs)	299
11.7	Electroluminescence (EL) displays	302
11.8	Chart recorders	304
11.9	Paperless recorders	306
11.10	Laser printers	307

Part C Specialised Measurement Systems**311**

12	Flow Measurement Systems	313
12.1	Essential principles of fluid mechanics	313
12.2	Measurement of velocity at a point in a fluid	319
12.3	Measurement of volume flow rate	321
12.4	Measurement of mass flow rate	339
12.5	Measurement of flow rate in difficult situations	342
13	Intrinsically Safe Measurement Systems	351
13.1	Pneumatic measurement systems	353
13.2	Intrinsically safe electronic systems	362
14	Heat Transfer Effects in Measurement Systems	367
14.1	Introduction	367
14.2	Dynamic characteristics of thermal sensors	369
14.3	Constant-temperature anemometer system for fluid velocity measurements	374
14.4	Katharometer systems for gas thermal conductivity and composition measurement	378
15	Optical Measurement Systems	385
15.1	Introduction: types of system	385
15.2	Sources	387
15.3	Transmission medium	393
15.4	Geometry of coupling of detector to source	398
15.5	Detectors and signal conditioning elements	403
15.6	Measurement systems	409
16	Ultrasonic Measurement Systems	427
16.1	Basic ultrasonic transmission link	427
16.2	Piezoelectric ultrasonic transmitters and receivers	428
16.3	Principles of ultrasonic transmission	436
16.4	Examples of ultrasonic measurement systems	447
17	Gas Chromatography	461
17.1	Principles and basic theory	461
17.2	Typical gas chromatograph	465
17.3	Signal processing and operations sequencing	468
18	Data Acquisition and Communication Systems	475
18.1	Time division multiplexing	476
18.2	Typical data acquisition system	477
18.3	Parallel digital signals	478
18.4	Serial digital signals	479
18.5	Error detection and correction	487
18.6	Frequency shift keying	490
18.7	Communication systems for measurement	493

19	The Intelligent Multivariable Measurement System	503
19.1	The structure of an intelligent multivariable system	503
19.2	Modelling methods for multivariable systems	507

<i>Answers to Numerical Problems</i>	515
<i>Index</i>	521



Preface to the fourth edition

Measurement is an essential activity in every branch of technology and science. We need to know the speed of a car, the temperature of our working environment, the flow rate of liquid in a pipe, the amount of oxygen dissolved in river water. It is important, therefore, that the study of measurement forms part of engineering and science courses in further and higher education. The aim of this book is to provide the fundamental principles of measurement which underlie these studies.

The book treats measurement as a coherent and integrated subject by presenting it as the study of measurement systems. A measurement system is an information system which presents an observer with a numerical value corresponding to the variable being measured. A given system may contain four types of element: sensing, signal conditioning, signal processing and data presentation elements.

The book is divided into three parts. *Part A (Chapters 1 to 7)* examines general systems principles. This part begins by discussing the static and dynamic characteristics that individual elements may possess and how they are used to calculate the overall system measurement error, under both steady and unsteady conditions. In later chapters, the principles of loading and two-port networks, the effects of interference and noise on system performance, reliability, maintainability and choice using economic criteria are explained. *Part B (Chapters 8 to 11)* examines the principles, characteristics and applications of typical sensing, signal conditioning, signal processing and data presentation elements in wide current use. *Part C (Chapters 12 to 19)* examines a number of specialised measurement systems which have important industrial applications. These are flow measurement systems, intrinsically safe systems, heat transfer, optical, ultrasonic, gas chromatography, data acquisition, communication and intelligent multivariable systems.

The fourth edition has been substantially extended and updated to reflect new developments in, and applications of, technology since the third edition was published in 1995. Chapter 1 has been extended to include a wider range of examples of basic measurement systems. New material on **solid state sensors** has been included in Chapter 8; this includes **resistive gas**, **electrochemical** and **Hall effect** sensors. In Chapter 9 there is now a full analysis of **operational amplifier circuits** which are used in measurement systems. The section on **frequency to digital conversion** in Chapter 10 has been expanded; there is also new material on **microcontroller** structure, software and applications. Chapter 11 has been extensively updated with new material on **digital displays**, **chart and paperless recorders** and **laser printers**. The section on **vortex flowmeters** in Chapter 12 has been extended and updated. Chapter 19 is a new chapter on **intelligent multivariable measurement systems** which concentrates on structure and modelling methods. There are around 35 additional problems in this new edition; many of these are at a basic, introductory level.

Each chapter in the book is clearly divided into sections. The topics to be covered are introduced at the beginning and reviewed in a conclusion at the end. Basic and important equations are highlighted, and a number of references are given at the end of each chapter; these should provide useful supplementary reading. The book contains about 300 line diagrams and tables and about 140 problems. At the end of the book there are answers to all the numerical problems and a comprehensive index.

This book is primarily aimed at students taking modules in measurement and instrumentation as part of degree courses in instrumentation/control, mechanical, manufacturing, electrical, electronic, chemical engineering and applied physics. Much of the material will also be helpful to lecturers and students involved in HNC/HND and foundation degree courses in technology. The book should also be useful to professional engineers and technicians engaged in solving practical measurement problems.

I would like to thank academic colleagues, industrial contacts and countless students for their helpful comments and criticism over many years. Thanks are again especially due to my wife Pauline for her constant support and help with the preparation of the manuscript.

John P. Bentley
Guisborough, December 2003

Acknowledgements

We are grateful to the following for permission to reproduce copyright material:

Figure 2.1(b) from *Repeatability and Accuracy*, Council of the Institution of Mechanical Engineers (Hayward, A.T.J., 1977); Figure 2.17(a) from Measurement of length in *Journal Institute Measurement & Control*, Vol. 12, July (Scarr, A., 1979), Table 5.1 from Systems analysis of instruments in *Journal Institute Measurement & Control*, Vol. 4, September (Finkelstein, L. and Watts, R.D., 1971), Table 7.3 from The application of reliability engineering to high integrity plant control systems in *Measurement and Control*, Vol. 18, June (Hellyer, F.G., 1985), and Figures 8.4(a) and (b) from Institute of Measurement and Control; Tables 2.3 and 2.4 from *Units of Measurement poster*, 8th edition, 1996, and Figures 15.22(a) and (b) from Wavelength encoded optical fibre sensors in *N.P.L. News*, No. 363 (Hutley, M.C., 1985), National Physical Laboratory; Figure 7.1 from The Institution of Chemical Engineers; Table 7.1 from Instrument reliability in *Instrument Science and Technology: Volume 1* (Wright, R.I., 1984), and Figure 16.14 from Medical and industrial applications of high resolution ultrasound in *Journal of Physics E: Scientific Instruments*, Vol. 18 (Payne, P.A., 1985), Institute of Physics Publishing Ltd.; Table 7.2 from The reliability of instrumentation in *Chemistry and Industry*, 6 March 1976, Professor F. Lees, Loughborough University; Table 8.2 from BS 4937: 1974 *International Thermocouple Reference Tables*, and Table 12.1 and Figure 12.7 from BS 1042: 1981 *Methods of measurement of fluid flow in closed conduits*, British Standards Institution; Figure 8.2(a) from *Instrument Transducers: An Introduction to their Performance and Design*, 2nd edition, Oxford University Press (Neubert, H.K.P., 1975); Figure 8.3(a) from *Technical Information on Two-point NTC Thermistors*, 1974, Mullard Ltd.; Table 8.4 from *Technical Data on Ion Selective Electrodes*, 1984, E.D.T. Research; Figures 8.4(b) and (c) from Thick film polymer sensors for physical variables in *Measurement and Control*, Vol. 33, No. 4, May, Institute of Measurement and Control and Professor N. White, University of Southampton (Papakostas, T.V. and White, N., 2000); Figures 8.8(a), (b) and (c) from Thick film chemical sensor array allows flexibility in specificity in *MTEC 1999, Sensor and Transducer Conference*, NEC Birmingham, Trident Exhibitions and Dr. A Cranny, University of Southampton (Jeffrey, P.D. *et al.*, 1999); Figure 8.10 from Ceramics put pressure on conventional transducers in *Process Industry Journal*, June, Endress and Hauser Ltd. (Stokes, D., 1991); Figure 8.23(b) from Piezoelectric devices: a step nearer problem-free vibration measurement in *Transducer Technology*, Vol. 4, No. 1 (Purdy, D., 1981), and Figure 8.24 from IC sensors boost potential of measurement systems in *Transducer Technology*, Vol. 8, No. 4 (Noble, M., 1985), Transducer Technology; Figure 8.25(b) from *Analysis with Ion Selective Electrodes*, John Wiley

and Sons Ltd. (Bailey, P.L., 1976); Figure 8.25(c) from pH facts – the glass electrode in *Kent Technical Review*, Kent Industrial Measurements Ltd., E.I.L Analytical Instruments (Thompson, W.); Figure 8.26(a) from *Electrical Engineering: Principles and Applications*, 2nd edition, reprinted by permission of Pearson Education Inc., Upper Saddle River, NJ, USA (Hambley, A.R.); Table 10.5 from Appendix A, *MCS BASIC-52 User's Manual*, Intel Corporation; Figure 11.10(c) from Instrumentation T 292 Block 6, part 2 Displays, 1986, The Open University Press; Figures 11.12(a) and (b) from Trident Displays technical literature on EL displays, Trident Microsystems Ltd. and M.S. Caddy and D. Weber; Figure 12.11(a) from Kent Process Control Ltd., Flow Products; Figure 15.10 from *Optical Fibre Communications* (Keiser, G., 1983), and Figure 15.12(b) from *Measurement Systems: Application and Design* (Doebelin, E.O., 1976), McGraw-Hill Book Co. (USA); Table 16.1 from Piezoelectric transducers in *Methods of Experimental Physics*, Vol. 19, Academic Press (O'Donnell, M., Busse, L.J. and Miller, J.G., 1981); Table 16.2 from *Ultrasonics: Methods and Applications*, Butterworth and Co. (Blitz, J., 1971); Figure 16.15 from ultrasonic image of Benjamin Stefan Morton, Nottingham City Hospital NHS Trust and Sarah Morton; Figure 17.5 from Process gas chromatography in *Talanta 1967*, Vol. 14, Pergamon Press Ltd. (Pine, C.S.F., 1967); Error Detection System in Section 18.5.2 from *Technical Information on Kent P4000 Telemetry Systems*, 1985, Kent Automation Systems Ltd.

In some instances we have been unable to trace the owners of copyright material, and we would appreciate any information that would enable us to do so.

Part A

General Principles

1

The General Measurement System

1.1

Purpose and performance of measurement systems

We begin by defining a **process** as a system which generates **information**. Examples are a chemical reactor, a jet fighter, a gas platform, a submarine, a car, a human heart, and a weather system.

Table 1.1 lists **information variables** which are commonly generated by processes: thus a car generates displacement, velocity and acceleration variables, and a chemical reactor generates temperature, pressure and composition variables.

Table 1.1 Common information/measured variables.

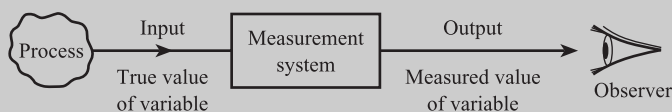
Acceleration	Density
Velocity	Viscosity
Displacement	Composition
Force–Weight	pH
Pressure	Humidity
Torque	Temperature
Volume	Heat/Light flux
Mass	Current
Flow rate	Voltage
Level	Power

We then define the **observer** as a person who needs this information from the process. This could be the car driver, the plant operator or the nurse.

The purpose of the **measurement system** is to link the observer to the process, as shown in Figure 1.1. Here the observer is presented with a number which is the current value of the information variable.

We can now refer to the information variable as a **measured variable**. The input to the measurement system is the **true value** of the variable; the system output is the **measured value** of the variable. In an ideal measurement system, the measured

Figure 1.1 Purpose of measurement system.



value would be equal to the true value. The **accuracy** of the system can be defined as the closeness of the measured value to the true value. A perfectly accurate system is a theoretical ideal and the accuracy of a real system is quantified using **measurement system error** E , where

$$E = \text{measured value} - \text{true value}$$

$$E = \text{system output} - \text{system input}$$

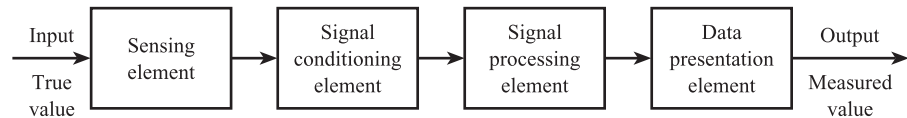
Thus if the measured value of the flow rate of gas in a pipe is $11.0 \text{ m}^3/\text{h}$ and the true value is $11.2 \text{ m}^3/\text{h}$, then the error $E = -0.2 \text{ m}^3/\text{h}$. If the measured value of the rotational speed of an engine is 3140 rpm and the true value is 3133 rpm , then $E = +7 \text{ rpm}$. Error is the main performance indicator for a measurement system. The procedures and equipment used to establish the true value of the measured variable will be explained in Chapter 2.

1.2

Structure of measurement systems

The measurement system consists of several elements or blocks. It is possible to identify four types of element, although in a given system one type of element may be missing or may occur more than once. The four types are shown in Figure 1.2 and can be defined as follows.

Figure 1.2 General structure of measurement system.



Sensing element

This is in contact with the process and gives an output which depends in some way on the variable to be measured. Examples are:

- Thermocouple where millivolt e.m.f. depends on temperature
- Strain gauge where resistance depends on mechanical strain
- Orifice plate where pressure drop depends on flow rate.

If there is more than one sensing element in a system, the element in contact with the process is termed the primary sensing element, the others secondary sensing elements.

Signal conditioning element

This takes the output of the sensing element and converts it into a form more suitable for further processing, usually a d.c. voltage, d.c. current or frequency signal. Examples are:

- Deflection bridge which converts an impedance change into a voltage change
- Amplifier which amplifies millivolts to volts
- Oscillator which converts an impedance change into a variable frequency voltage.

Signal processing element

This takes the output of the conditioning element and converts it into a form more suitable for presentation. Examples are:

- Analogue-to-digital converter (ADC) which converts a voltage into a digital form for input to a computer
- Computer which calculates the measured value of the variable from the incoming digital data.

Typical calculations are:

- Computation of total mass of product gas from flow rate and density data
- Integration of chromatograph peaks to give the composition of a gas stream
- Correction for sensing element non-linearity.

Data presentation element

This presents the measured value in a form which can be easily recognised by the observer. Examples are:

- Simple pointer-scale indicator
- Chart recorder
- Alphanumeric display
- Visual display unit (VDU).

1.3

Examples of measurement systems

Figure 1.3 shows some typical examples of measurement systems.

Figure 1.3(a) shows a temperature system with a thermocouple sensing element; this gives a millivolt output. Signal conditioning consists of a circuit to compensate for changes in reference junction temperature, and an amplifier. The voltage signal is converted into digital form using an analogue-to-digital converter, the computer corrects for sensor non-linearity, and the measured value is displayed on a VDU.

In Figure 1.3(b) the speed of rotation of an engine is sensed by an electromagnetic tachogenerator which gives an a.c. output signal with frequency proportional to speed. The Schmitt trigger converts the sine wave into sharp-edged pulses which are then counted over a fixed time interval. The digital count is transferred to a computer which calculates frequency and speed, and the speed is presented on a digital display.

The flow system of Figure 1.3(c) has an orifice plate sensing element; this gives a differential pressure output. The differential pressure transmitter converts this into a current signal and therefore combines both sensing and signal conditioning stages. The ADC converts the current into digital form and the computer calculates the flow rate, which is obtained as a permanent record on a chart recorder.

The weight system of Figure 1.3(d) has two sensing elements: the primary element is a cantilever which converts weight into strain; the strain gauge converts this into a change in electrical resistance and acts as a secondary sensor. There are two signal conditioning elements: the deflection bridge converts the resistance change into

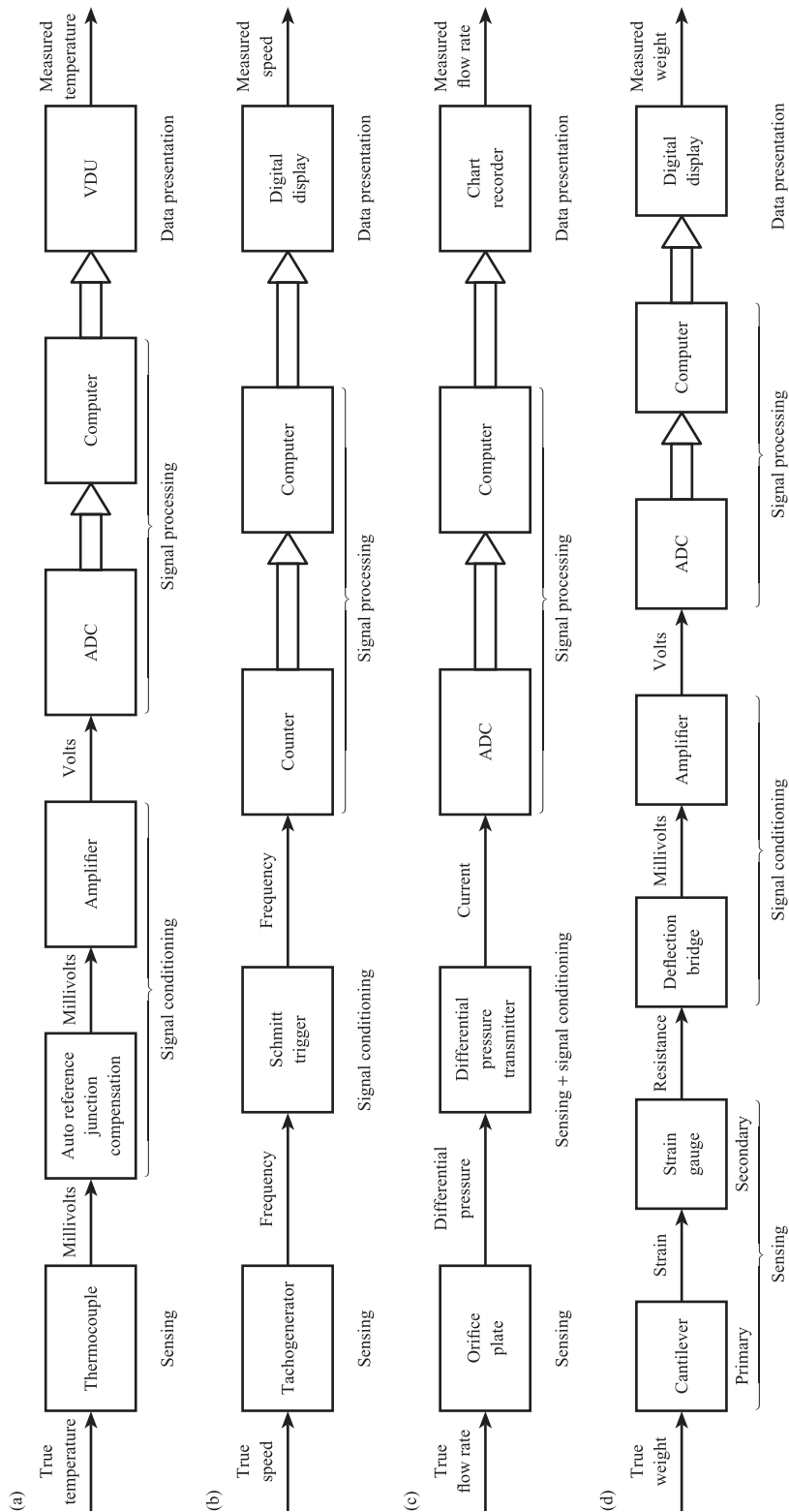


Figure 1.3 Examples of measurement systems.

millivolts and the amplifier converts millivolts into volts. The computer corrects for non-linearity in the cantilever and the weight is presented on a digital display.

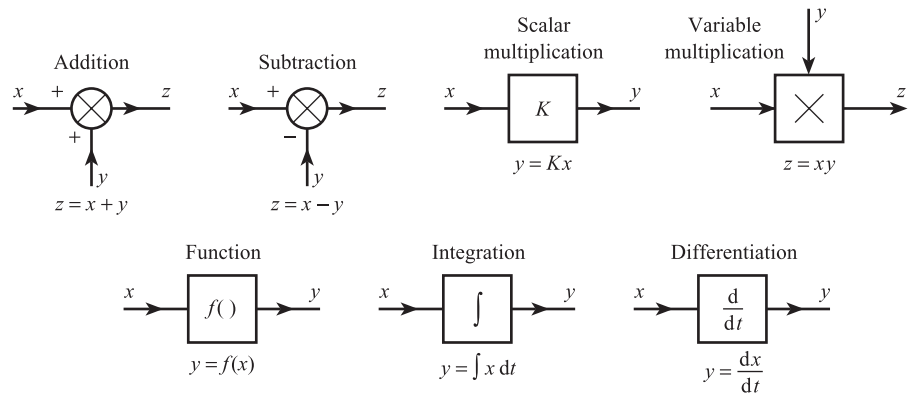
The word '**transducer**' is commonly used in connection with measurement and instrumentation. This is a manufactured package which gives an output voltage (usually) corresponding to an input variable such as pressure or acceleration. We see therefore that such a transducer may incorporate both sensing and signal conditioning elements; for example a weight transducer would incorporate the first four elements shown in Figure 1.3(d).

It is also important to note that each element in the measurement system may itself be a system made up of simpler components. Chapters 8 to 11 discuss typical examples of each type of element in common use.

1.4 Block diagram symbols

A block diagram approach is very useful in discussing the properties of elements and systems. Figure 1.4 shows the main block diagram symbols used in this book.

Figure 1.4 Block diagram symbols.



Conclusion

This chapter has defined the purpose of a measurement system and explained the importance of **system error**. It has shown that, in general, a system consists of four types of element: **sensing**, **signal conditioning**, **signal processing** and **data presentation** elements. Typical examples have been given.

2

Static Characteristics of Measurement System Elements



Figure 2.1 Meaning of element characteristics.

In the previous chapter we saw that a measurement system consists of different types of element. The following chapters discuss the characteristics that typical elements may possess and their effect on the overall performance of the system. This chapter is concerned with static or steady-state characteristics; these are the relationships which may occur between the output O and input I of an element when I is either at a constant value or changing slowly (Figure 2.1).

2.1

Systematic characteristics

Systematic characteristics are those that can be exactly quantified by mathematical or graphical means. These are distinct from statistical characteristics which cannot be exactly quantified and are discussed in Section 2.3.

Range

The input range of an element is specified by the minimum and maximum values of I , i.e. I_{MIN} to I_{MAX} . The output range is specified by the minimum and maximum values of O , i.e. O_{MIN} to O_{MAX} . Thus a pressure transducer may have an input range of 0 to 10^4 Pa and an output range of 4 to 20 mA; a thermocouple may have an input range of 100 to 250 °C and an output range of 4 to 10 mV.

Span

Span is the maximum variation in input or output, i.e. input span is $I_{\text{MAX}} - I_{\text{MIN}}$, and output span is $O_{\text{MAX}} - O_{\text{MIN}}$. Thus in the above examples the pressure transducer has an input span of 10^4 Pa and an output span of 16 mA; the thermocouple has an input span of 150 °C and an output span of 6 mV.

Ideal straight line

An element is said to be linear if corresponding values of I and O lie on a straight line. The **ideal straight line** connects the minimum point A(I_{MIN} , O_{MIN}) to maximum point B(I_{MAX} , O_{MAX}) (Figure 2.2) and therefore has the equation:

$$O - O_{\text{MIN}} = \left[\frac{O_{\text{MAX}} - O_{\text{MIN}}}{I_{\text{MAX}} - I_{\text{MIN}}} \right] (I - I_{\text{MIN}}) \quad [2.1]$$

Ideal straight line equation

$$O_{\text{IDEAL}} = KI + a \quad [2.2]$$

where:

$$K = \text{ideal straight-line slope} = \frac{O_{\text{MAX}} - O_{\text{MIN}}}{I_{\text{MAX}} - I_{\text{MIN}}}$$

and

$$a = \text{ideal straight-line intercept} = O_{\text{MIN}} - KI_{\text{MIN}}$$

Thus the ideal straight line for the above pressure transducer is:

$$O = 1.6 \times 10^{-3}I + 4.0$$

The ideal straight line defines the ideal characteristics of an element. Non-ideal characteristics can then be quantified in terms of deviations from the ideal straight line.

Non-linearity

In many cases the straight-line relationship defined by eqn [2.2] is not obeyed and the element is said to be **non-linear**. Non-linearity can be defined (Figure 2.2) in terms of a function $N(I)$ which is the difference between actual and ideal straight-line behaviour, i.e.

$$N(I) = O(I) - (KI + a) \quad [2.3]$$

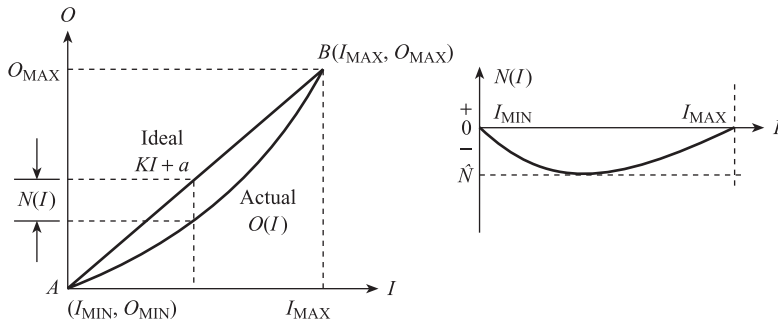
or

$$O(I) = KI + a + N(I) \quad [2.4]$$

Non-linearity is often quantified in terms of the maximum non-linearity \hat{N} expressed as a percentage of full-scale deflection (f.s.d.), i.e. as a percentage of span. Thus:

$$\text{Max. non-linearity as a percentage of f.s.d.} = \frac{\hat{N}}{O_{\text{MAX}} - O_{\text{MIN}}} \times 100\% \quad [2.5]$$

Figure 2.2 Definition of non-linearity.



As an example, consider a pressure sensor where the maximum difference between actual and ideal straight-line output values is 2 mV. If the output span is 100 mV, then the maximum percentage non-linearity is 2% of f.s.d.

In many cases $O(I)$ and therefore $N(I)$ can be expressed as a polynomial in I :

$$O(I) = a_0 + a_1 I + a_2 I^2 + \dots + a_q I^q + \dots + a_m I^m = \sum_{q=0}^m a_q I^q \quad [2.6]$$

An example is the temperature variation of the thermoelectric e.m.f. at the junction of two dissimilar metals. For a copper–constantan (Type T) thermocouple junction, the first four terms in the polynomial relating e.m.f. $E(T)$, expressed in μV , and junction temperature $T^\circ\text{C}$ are:

$$E(T) = 38.74T + 3.319 \times 10^{-2}T^2 + 2.071 \times 10^{-4}T^3 - 2.195 \times 10^{-6}T^4 + \text{higher-order terms up to } T^8 \quad [2.7a]$$

for the range 0 to 400°C .^[1] Since $E = 0 \mu\text{V}$ at $T = 0^\circ\text{C}$ and $E = 20\,869 \mu\text{V}$ at $T = 400^\circ\text{C}$, the equation to the ideal straight line is:

$$E_{\text{IDEAL}} = 52.17T \quad [2.7b]$$

and the non-linear correction function is:

$$\begin{aligned} N(T) &= E(T) - E_{\text{IDEAL}} \\ &= -13.43T + 3.319 \times 10^{-2}T^2 + 2.071 \times 10^{-4}T^3 \\ &\quad - 2.195 \times 10^{-6}T^4 + \text{higher-order terms} \end{aligned} \quad [2.7c]$$

In some cases expressions other than polynomials are more appropriate: for example the resistance $R(T)$ ohms of a thermistor at $T^\circ\text{C}$ is given by:

$$R(T) = 0.04 \exp\left(\frac{3300}{T + 273}\right) \quad [2.8]$$

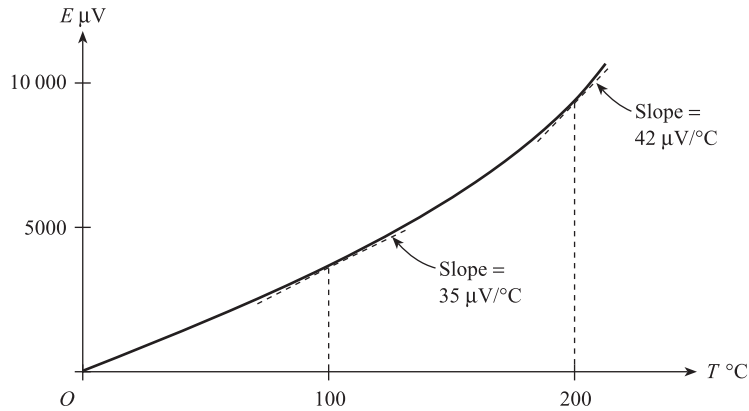
Sensitivity

This is the change ΔO in output O for unit change ΔI in input I , i.e. it is the ratio $\Delta O/\Delta I$. In the limit that ΔI tends to zero, the ratio $\Delta O/\Delta I$ tends to the **derivative** dO/dI , which is the rate of change of O with respect to I . For a linear element dO/dI is equal to the slope or gradient K of the straight line; for the above pressure transducer the sensitivity is $1.6 \times 10^{-3} \text{ mA/Pa}$. For a non-linear element $dO/dI = K + dN/dI$, i.e. sensitivity is the **slope** or **gradient** of the output versus input characteristics $O(I)$. Figure 2.3 shows the e.m.f. versus temperature characteristics $E(T)$ for a Type T thermocouple (eqn [2.7a]). We see that the gradient and therefore the sensitivity vary with temperature: at 100°C it is approximately $35 \mu\text{V}/^\circ\text{C}$ and at 200°C approximately $42 \mu\text{V}/^\circ\text{C}$.

Environmental effects

In general, the output O depends not only on the signal input I but on environmental inputs such as ambient temperature, atmospheric pressure, relative humidity, supply voltage, etc. Thus if eqn [2.4] adequately represents the behaviour of the element under ‘standard’ environmental conditions, e.g. 20°C ambient temperature,

Figure 2.3
Thermocouple sensitivity.



1000 millibars atmospheric pressure, 50% RH and 10 V supply voltage, then the equation must be modified to take account of deviations in environmental conditions from 'standard'. There are two main types of environmental input.

A **modifying** input I_M causes the linear sensitivity of an element to change. K is the sensitivity at standard conditions when $I_M = 0$. If the input is changed from the standard value, then I_M is the **deviation** from standard conditions, i.e. (new value – standard value). The sensitivity changes from K to $K + K_M I_M$, where K_M is the change in sensitivity for unit change in I_M . Figure 2.4(a) shows the modifying effect of ambient temperature on a linear element.

An **interfering** input I_I causes the straight line intercept or zero bias to change. a is the zero bias at standard conditions when $I_I = 0$. If the input is changed from the standard value, then I_I is the **deviation** from standard conditions, i.e. (new value – standard value). The zero bias changes from a to $a + K_I I_I$, where K_I is the change in zero bias for unit change in I_I . Figure 2.4(b) shows the interfering effect of ambient temperature on a linear element.

K_M and K_I are referred to as environmental coupling constants or sensitivities. Thus we must now correct eqn [2.4], replacing KI with $(K + K_M I_M)I$ and replacing a with $a + K_I I_I$ to give:

$$O = KI + a + N(I) + K_M I_M I + K_I I_I \quad [2.9]$$

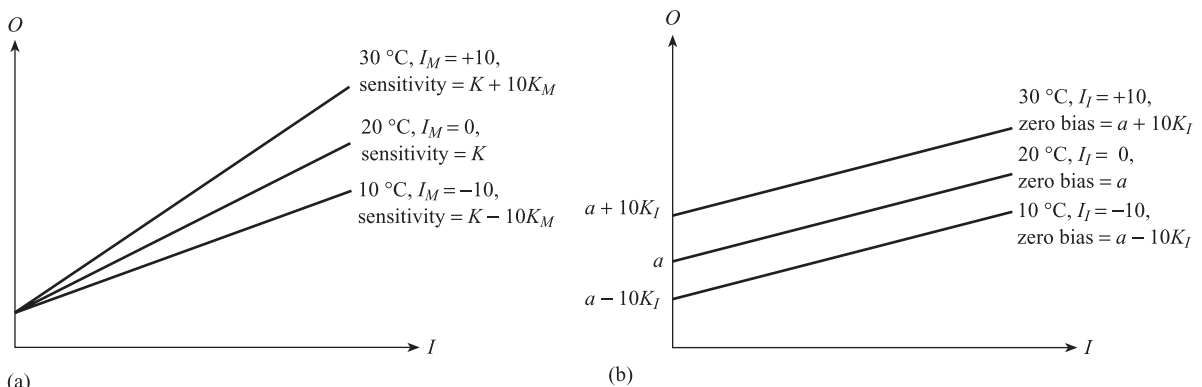
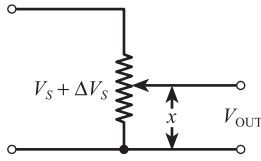


Figure 2.4 Modifying and interfering inputs.



If x is the fractional displacement, then
 $V_{OUT} = (V_s + \Delta V_s)x$
 $= V_s x + \Delta V_s x$

Figure 2.5

An example of a modifying input is the variation ΔV_s in the supply voltage V_s of the potentiometric displacement sensor shown in Figure 2.5. An example of an interfering input is provided by variations in the reference junction temperature T_2 of the thermocouple (see following section and Section 8.5).

Hysteresis

For a given value of I , the output O may be different depending on whether I is increasing or decreasing. Hysteresis is the difference between these two values of O (Figure 2.6), i.e.

$$\text{Hysteresis } H(I) = O(I)_{I\downarrow} - O(I)_{I\uparrow} \quad [2.10]$$

Again hysteresis is usually quantified in terms of the maximum hysteresis \hat{H} expressed as a percentage of f.s.d., i.e. span. Thus:

$$\text{Maximum hysteresis as a percentage of f.s.d.} = \frac{\hat{H}}{O_{MAX} - O_{MIN}} \times 100\% \quad [2.11]$$

A simple gear system (Figure 2.7) for converting linear movement into angular rotation provides a good example of hysteresis. Due to the 'backlash' or 'play' in the gears the angular rotation θ , for a given value of x , is different depending on the direction of the linear movement.

Resolution

Some elements are characterised by the output increasing in a series of discrete steps or jumps in response to a continuous increase in input (Figure 2.8). Resolution is defined as the largest change in I that can occur without any corresponding change in O .

Figure 2.6 Hysteresis.

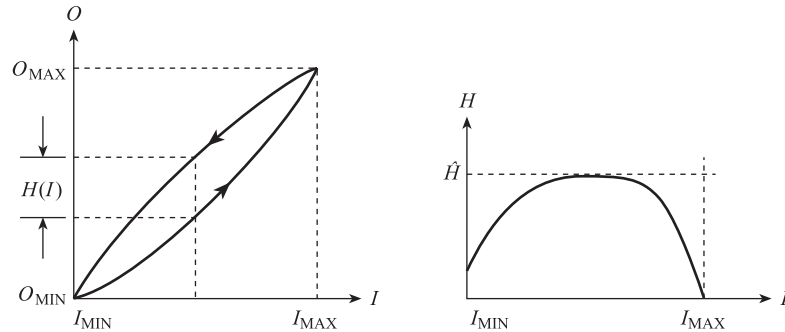


Figure 2.7 Backlash in gears.

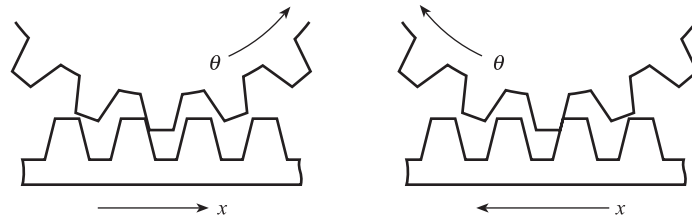
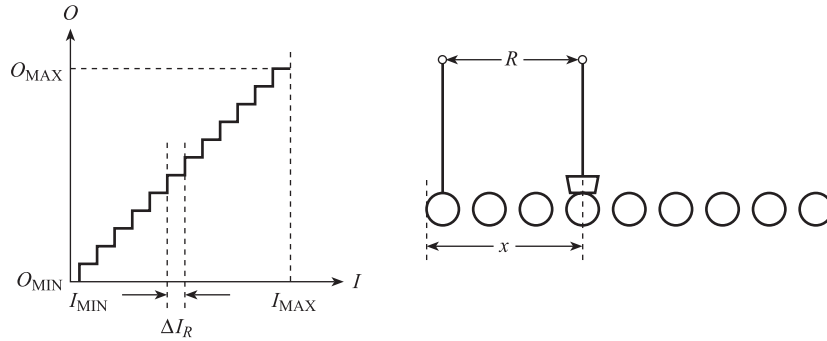


Figure 2.8 Resolution and potentiometer example.



Thus in Figure 2.8 resolution is defined in terms of the width ΔI_R of the widest step; resolution expressed as a percentage of f.s.d. is thus:

$$\frac{\Delta I_R}{I_{\text{MAX}} - I_{\text{MIN}}} \times 100\%$$

A common example is a wire-wound potentiometer (Figure 2.8); in response to a continuous increase in x the resistance R increases in a series of steps, the size of each step being equal to the resistance of a single turn. Thus the resolution of a 100 turn potentiometer is 1%. Another example is an analogue-to-digital converter (Chapter 10); here the output digital signal responds in discrete steps to a continuous increase in input voltage; the resolution is the change in voltage required to cause the output code to change by the least significant bit.

Wear and ageing

These effects can cause the characteristics of an element, e.g. K and a , to change slowly but systematically throughout its life. One example is the stiffness of a spring $k(t)$ decreasing slowly with time due to wear, i.e.

$$k(t) = k_0 - bt \quad [2.12]$$

where k_0 is the initial stiffness and b is a constant. Another example is the constants a_1 , a_2 , etc. of a thermocouple, measuring the temperature of gas leaving a cracking furnace, changing systematically with time due to chemical changes in the thermocouple metals.

Error bands

Non-linearity, hysteresis and resolution effects in many modern sensors and transducers are so small that it is difficult and not worthwhile to exactly quantify each individual effect. In these cases the manufacturer defines the performance of the element in terms of error bands (Figure 2.9). Here the manufacturer states that for any value of I , the output O will be within $\pm h$ of the ideal straight-line value O_{IDEAL} . Here an exact or systematic statement of performance is replaced by a statistical statement in terms of a probability density function $p(O)$. In general a probability density function $p(x)$ is defined so that the integral $\int_{x_1}^{x_2} p(x) dx$ (equal to the area under the curve in Figure 2.10 between x_1 and x_2) is the probability P_{x_1, x_2} of x lying between x_1 and x_2 (Section 6.2). In this case the probability density function is rectangular (Figure 2.9), i.e.

Figure 2.9 Error bands and rectangular probability density function.

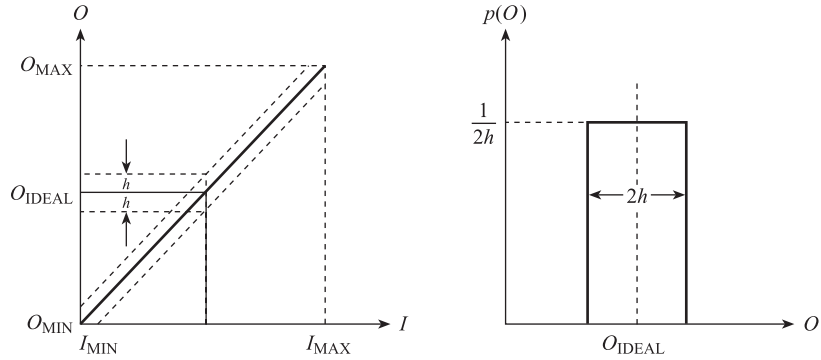
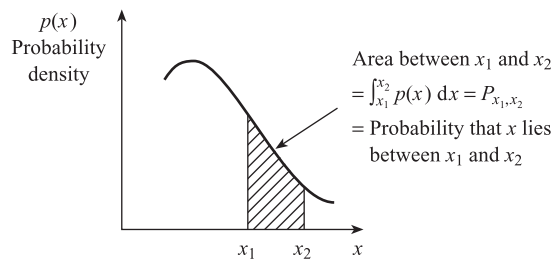


Figure 2.10 Probability density function.



$$p(O) \begin{cases} = \frac{1}{2h} & O_{\text{IDEAL}} - h \leq O \leq O_{\text{IDEAL}} + h \\ = 0 & O > O_{\text{IDEAL}} + h \\ = 0 & O_{\text{IDEAL}} - h > O \end{cases} \quad [2.13]$$

We note that the area of the rectangle is equal to unity: this is the probability of O lying between $O_{\text{IDEAL}} - h$ and $O_{\text{IDEAL}} + h$.

2.2

Generalised model of a system element

If hysteresis and resolution effects are not present in an element but environmental and non-linear effects are, then the steady-state output O of the element is in general given by eqn [2.9], i.e.:

$$O = KI + a + N(I) + K_M I_M I + K_I I_I \quad [2.9]$$

Figure 2.11 shows this equation in block diagram form to represent the **static** characteristics of an element. For completeness the diagram also shows the transfer function $G(s)$, which represents the **dynamic** characteristics of the element. The meaning of transfer function will be explained in Chapter 4 where the form of $G(s)$ for different elements will be derived.

Examples of this general model are shown in Figure 2.12(a), (b) and (c), which summarise the static and dynamic characteristics of a strain gauge, thermocouple and accelerometer respectively.

Figure 2.11 General model of element.

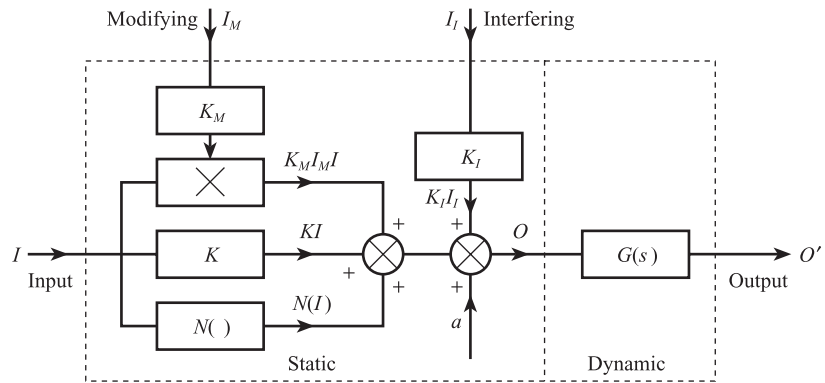
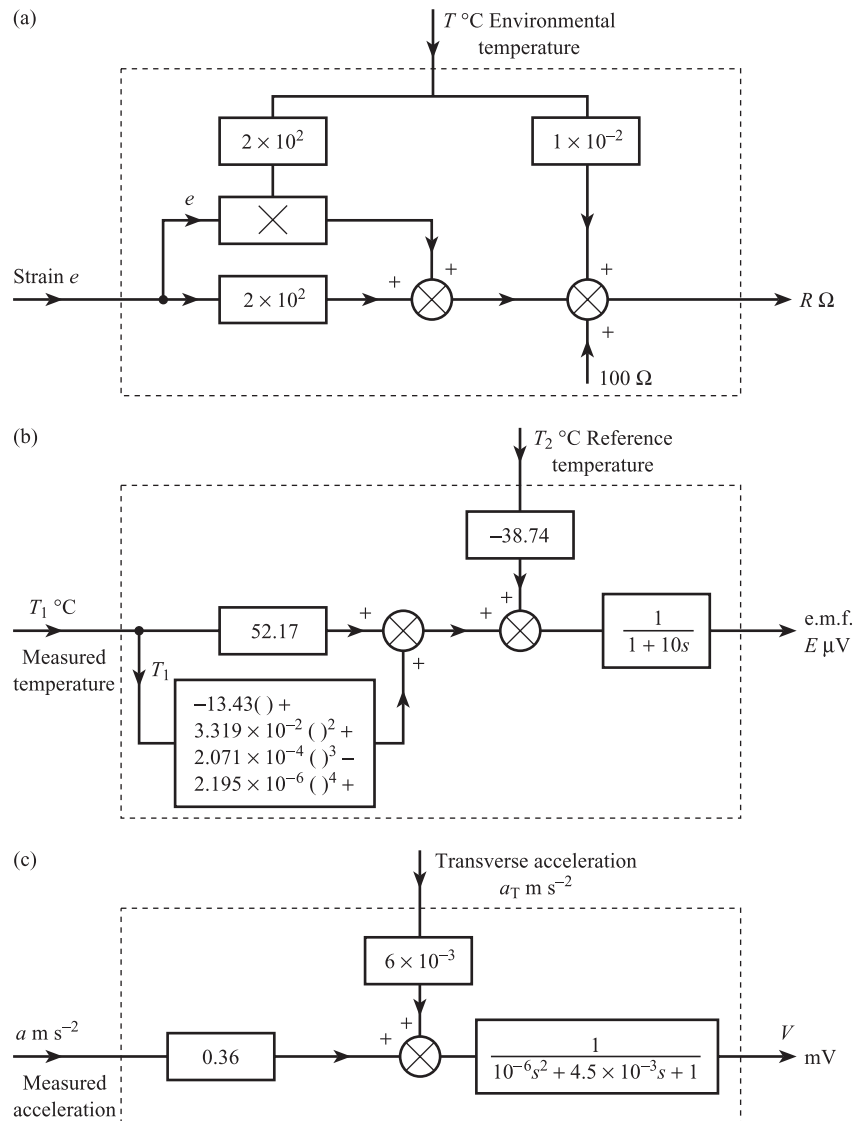


Figure 2.12 Examples of element characteristics:
(a) Strain gauge
(b) Copper–constantan thermocouple
(c) Accelerometer.



The strain gauge has an unstrained resistance of $100\ \Omega$ and gauge factor (Section 8.1) of 2.0. Non-linearity and dynamic effects can be neglected, but the resistance of the gauge is affected by ambient temperature as well as strain. Here temperature acts as both a modifying and an interfering input, i.e. it affects both gauge sensitivity and resistance at zero strain.

Figure 2.12(b) represents a copper–constantan thermocouple between 0 and $400\ ^\circ\text{C}$. The figure is drawn using eqns [2.7b] and [2.7c] for ideal straight-line and non-linear correction functions; these apply to a single junction. A thermocouple installation consists of two junctions (Section 8.5) – a measurement junction at $T_1\ ^\circ\text{C}$ and a reference junction at $T_2\ ^\circ\text{C}$. The resultant e.m.f. is the difference of the two junction potentials and thus depends on both T_1 and T_2 , i.e. $E(T_1, T_2) = E(T_1) - E(T_2)$; T_2 is thus an interfering input. The model applies to the situation where T_2 is small compared with T_1 , so that $E(T_2)$ can be approximated by $38.74\ T_2$, the largest term in eqn [2.7a]. The dynamics are represented by a first-order transfer function of time constant 10 seconds (Chapters 4 and 14).

Figure 2.12(c) represents an accelerometer with a linear sensitivity of $0.35\ \text{mV m}^{-1}\ \text{s}^2$ and negligible non-linearity. Any transverse acceleration a_T , i.e. any acceleration perpendicular to that being measured, acts as an interfering input. The dynamics are represented by a second-order transfer function with a natural frequency of 250 Hz and damping coefficient of 0.7 (Chapters 4 and 8).

2.3

Statistical characteristics

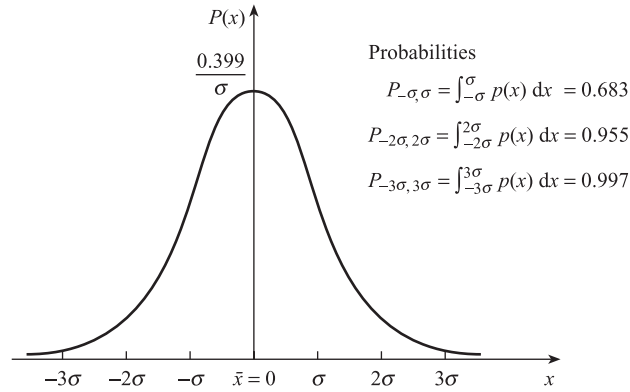
2.3.1 Statistical variations in the output of a single element with time – repeatability

Suppose that the input I of a single element, e.g. a pressure transducer, is held constant, say at 0.5 bar, for several days. If a large number of readings of the output O are taken, then the expected value of 1.0 volt is not obtained on every occasion; a range of values such as 0.99, 1.01, 1.00, 1.02, 0.98, etc., scattered about the expected value, is obtained. This effect is termed a lack of **repeatability** in the element. Repeatability is the ability of an element to give the same output for the same input, when repeatedly applied to it. Lack of repeatability is due to random effects in the element and its environment. An example is the vortex flowmeter (Section 12.2.4): for a fixed flow rate $Q = 1.4 \times 10^{-2}\ \text{m}^3\ \text{s}^{-1}$, we would expect a constant frequency output $f = 209\ \text{Hz}$. Because the output signal is not a perfect sine wave, but is subject to random fluctuations, the measured frequency varies between 207 and 211 Hz.

The most common cause of lack of repeatability in the output O is random fluctuations with time in the environmental inputs I_M, I_I : if the coupling constants K_M, K_I are non-zero, then there will be corresponding time variations in O . Thus random fluctuations in ambient temperature cause corresponding time variations in the resistance of a strain gauge or the output voltage of an amplifier; random fluctuations in the supply voltage of a deflection bridge affect the bridge output voltage.

By making reasonable assumptions for the probability density functions of the inputs I, I_M and I_I (in a measurement system random variations in the input I to

Figure 2.13 Normal probability density function with $\bar{x} = 0$.



a given element can be caused by random effects in the previous element), the probability density function of the element output O can be found. The most likely probability density function for I , I_M and I_I is the normal or Gaussian distribution function (Figure 2.13):

Normal probability density function

$$p(x) = \frac{1}{\sigma\sqrt{2\pi}} \exp\left[-\frac{(x - \bar{x})^2}{2\sigma^2}\right] \quad [2.14]$$

where: \bar{x} = mean or expected value (specifies centre of distribution)
 σ = standard deviation (specifies spread of distribution).

Equation [2.9] expresses the independent variable O in terms of the independent variables I , I_M and I_I . Thus if ΔO is a small deviation in O from the mean value \bar{O} , caused by deviations ΔI , ΔI_M and ΔI_I from respective mean values \bar{I} , \bar{I}_M and \bar{I}_I , then:

$$\Delta O = \left(\frac{\partial O}{\partial I}\right)\Delta I + \left(\frac{\partial O}{\partial I_M}\right)\Delta I_M + \left(\frac{\partial O}{\partial I_I}\right)\Delta I_I \quad [2.15]$$

Thus ΔO is a linear combination of the variables ΔI , ΔI_M and ΔI_I ; the partial derivatives can be evaluated using eqn [2.9]. It can be shown^[2] that if a dependent variable y is a linear combination of independent variables x_1 , x_2 and x_3 , i.e.

$$y = a_1x_1 + a_2x_2 + a_3x_3 \quad [2.16]$$

and if x_1 , x_2 and x_3 have normal distributions with standard deviations σ_1 , σ_2 and σ_3 respectively, then the probability distribution of y is also normal with standard deviation σ given by:

$$\sigma = \sqrt{a_1^2\sigma_1^2 + a_2^2\sigma_2^2 + a_3^2\sigma_3^2} \quad [2.17]$$

From eqns [2.15] and [2.17] we see that the standard deviation of ΔO , i.e. of O about mean O , is given by:

Standard deviation
of output for a
single element

$$\sigma_0 = \sqrt{\left(\frac{\partial O}{\partial I}\right)^2 \sigma_I^2 + \left(\frac{\partial O}{\partial I_M}\right)^2 \sigma_{I_M}^2 + \left(\frac{\partial O}{\partial I_I}\right)^2 \sigma_{I_I}^2} \quad [2.18]$$

where σ_I , σ_{I_M} and σ_{I_I} are the standard deviations of the inputs. Thus σ_0 can be calculated using eqn [2.18] if σ_I , σ_{I_M} and σ_{I_I} are known; alternatively if a calibration test (see following section) is being performed on the element then σ_0 can be estimated directly from the experimental results. The corresponding mean or expected value \bar{O} of the element output is given by:

Mean value of output
for a single element

$$\bar{O} = K\bar{I} + a + N(\bar{I}) + K_M\bar{I}_M + K_I\bar{I}_I \quad [2.19]$$

and the corresponding probability density function is:

$$p(O) = \frac{1}{\sigma_0 \sqrt{2\pi}} \exp\left[-\frac{(O - \bar{O})^2}{2\sigma_0^2}\right] \quad [2.20]$$

2.3.2 Statistical variations amongst a batch of similar elements – tolerance

Suppose that a user buys a batch of similar elements, e.g. a batch of 100 resistance temperature sensors, from a manufacturer. If he then measures the resistance R_0 of each sensor at 0 °C he finds that the resistance values are not all equal to the manufacturer's quoted value of 100.0 Ω . A range of values such as 99.8, 100.1, 99.9, 100.0 and 100.2 Ω , distributed statistically about the quoted value, is obtained. This effect is due to small random variations in manufacture and is often well represented by the normal probability density function given earlier. In this case we have:

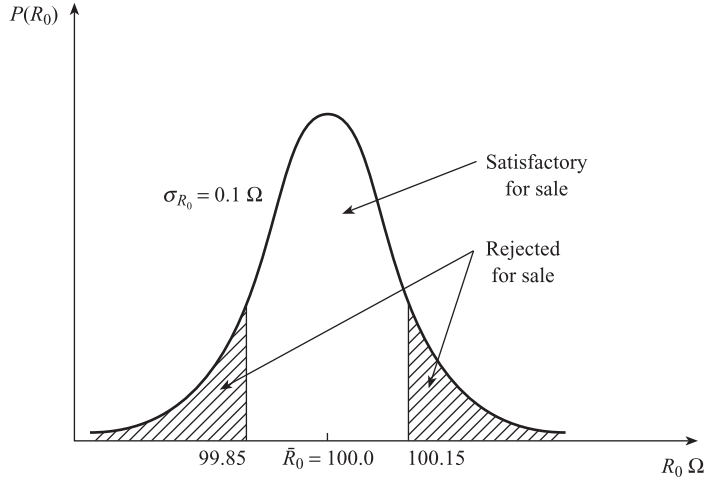
$$p(R_0) = \frac{1}{\sigma_{R_0} \sqrt{2\pi}} \exp\left[-\frac{(R_0 - \bar{R}_0)^2}{2\sigma_{R_0}^2}\right] \quad [2.21]$$

where \bar{R}_0 = mean value of distribution = 100 Ω and σ_{R_0} = standard deviation, typically 0.1 Ω . However, a manufacturer may state in his specification that R_0 lies within ± 0.15 Ω of 100 Ω for all sensors, i.e. he is quoting **tolerance** limits of ± 0.15 Ω . Thus in order to satisfy these limits he must reject for sale all sensors with $R_0 < 99.85$ Ω and $R_0 > 100.15$ Ω , so that the probability density function of the sensors bought by the user now has the form shown in Figure 2.14.

The user has two choices:

- He can design his measurement system using the manufacturer's value of $R_0 = 100.0$ Ω and accept that any individual system, with $R_0 = 100.1$ Ω say, will have a small measurement error. This is the usual practice.
- He can perform a calibration test to measure R_0 as accurately as possible for each element in the batch. This theoretically removes the error due to uncertainty in R_0 but is time-consuming and expensive. There is also a small remaining uncertainty in the value of R_0 due to the limited accuracy of the calibration equipment.

Figure 2.14
Tolerance limits.



This effect is found in any batch of ‘identical’ elements; significant variations are found in batches of thermocouples and thermistors, for example. In the general case we can say that the values of parameters, such as linear sensitivity K and zero bias a , for a batch of elements are distributed statistically about mean values \bar{K} and \bar{a} .

2.3.3 Summary

In the general case of a batch of several ‘identical’ elements, where each element is subject to random variations in environmental conditions with time, both inputs I , I_M and I_I and parameters K , a , etc., are subject to statistical variations. If we assume that each statistical variation can be represented by a normal probability density function, then the probability density function of the element output O is also normal, i.e.:

$$p(O) = \frac{1}{\sigma_0 \sqrt{2\pi}} \exp \left[\frac{-(O - \bar{O})^2}{2\sigma_0^2} \right] \quad [2.20]$$

where the mean value \bar{O} is given by:

*Mean value of output
for a batch of elements*

$$\bar{O} = \bar{K}\bar{I} + \bar{N}(\bar{I}) + \bar{a} + \bar{K}_M\bar{I}_M + \bar{K}_I\bar{I}_I \quad [2.22]$$

and the standard deviation σ_0 is given by:

*Standard deviation
of output for a batch
of elements*

$$\sigma_0 = \sqrt{\left(\frac{\partial O}{\partial I} \right)^2 \sigma_I^2 + \left(\frac{\partial O}{\partial I_M} \right)^2 \sigma_{I_M}^2 + \left(\frac{\partial O}{\partial I_I} \right)^2 \sigma_{I_I}^2 + \left(\frac{\partial O}{\partial K} \right)^2 \sigma_K^2 + \left(\frac{\partial O}{\partial a} \right)^2 \sigma_a^2 + \dots} \quad [2.23]$$

Tables 2.1 and 2.2 summarise the static characteristics of a chromel–alumel thermocouple and a millivolt to current temperature transmitter. The thermocouple is

Table 2.1 Model for chromel–alumel thermocouple.

Model equation	$E_{T,T_a} = a_0 + a_1(T - T_a) + a_2(T^2 - T_a^2) \quad (50 \text{ to } 150 \text{ }^\circ\text{C})$
Mean values	$\bar{a}_0 = 0.00, \bar{a}_1 = 4.017 \times 10^{-2}, \bar{a}_2 = 4.66 \times 10^{-6}, \bar{T}_a = 10$
Standard deviations	$\sigma_{a_0} = 6.93 \times 10^{-2}, \sigma_{a_1} = 0.0, \sigma_{a_2} = 0.0, \sigma_{T_a} = 6.7$
Partial derivatives	$\frac{\partial E}{\partial a_0} = 1.0, \quad \frac{\partial E}{\partial T_a} = -4.026 \times 10^{-2}$
Mean value of output	$\bar{E}_{T,T_a} = \bar{a}_0 + \bar{a}_1(\bar{T} - \bar{T}_a) + \bar{a}_2(\bar{T}^2 - \bar{T}_a^2)$
Standard deviation of output	$\sigma_E^2 = \left(\frac{\partial E}{\partial a_0}\right)^2 \sigma_{a_0}^2 + \left(\frac{\partial E}{\partial T_a}\right)^2 \sigma_{T_a}^2$

Table 2.2 Model for millivolt to current temperature transmitter.

Model equation	$i = KE + K_M E \Delta T_a + K_I \Delta T_a + a$ 4 to 20 mA output for 2.02 to 6.13 mV input ΔT_a = deviation in ambient temperature from 20 °C
Mean values	$\bar{K} = 3.893, \bar{a} = 3.864, \Delta \bar{T}_a = -10$ $\bar{K}_M = 1.95 \times 10^{-4}, \bar{K}_I = 2.00 \times 10^{-3}$
Standard deviations	$\sigma_a = 0.14, \sigma_{\Delta T_a} = 6.7$ $\sigma_K = 0.0, \sigma_{K_M} = 0.0, \sigma_{K_I} = 0.0$
Partial derivatives	$\frac{\partial i}{\partial E} = 3.891, \quad \frac{\partial i}{\partial \Delta T_a} = 2.936 \times 10^{-3}, \quad \frac{\partial i}{\partial a} = 1.0$
Mean value of output	$\bar{i} = \bar{K}\bar{E} + \bar{K}_M \bar{E} \Delta \bar{T}_a + \bar{K}_I \Delta \bar{T}_a + \bar{a}$
Standard deviation of output	$\sigma_i^2 = \left(\frac{\partial i}{\partial E}\right)^2 \sigma_E^2 + \left(\frac{\partial i}{\partial \Delta T_a}\right)^2 \sigma_{\Delta T_a}^2 + \left(\frac{\partial i}{\partial a}\right)^2 \sigma_a^2$

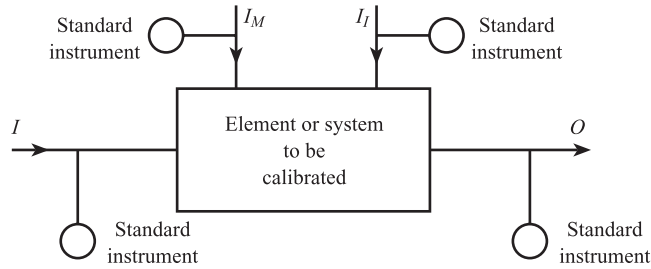
characterised by non-linearity, changes in reference junction (ambient temperature) T_a acting as an interfering input, and a spread of zero bias values a_0 . The transmitter is linear but is affected by ambient temperature acting as both a modifying and an interfering input. The zero and sensitivity of this element are adjustable; we cannot be certain that the transmitter is set up exactly as required, and this is reflected in a non-zero value of the standard deviation of the zero bias a .

2.4

Identification of static characteristics – calibration

2.4.1 Standards

The static characteristics of an element can be found experimentally by measuring corresponding values of the input I , the output O and the environmental inputs I_M and I_I , when I is either at a constant value or changing slowly. This type of experiment is referred to as **calibration**, and the measurement of the variables I , O , I_M and I_I must be accurate if meaningful results are to be obtained. The instruments and techniques used to quantify these variables are referred to as **standards** (Figure 2.15).

Figure 2.15 Calibration of an element.

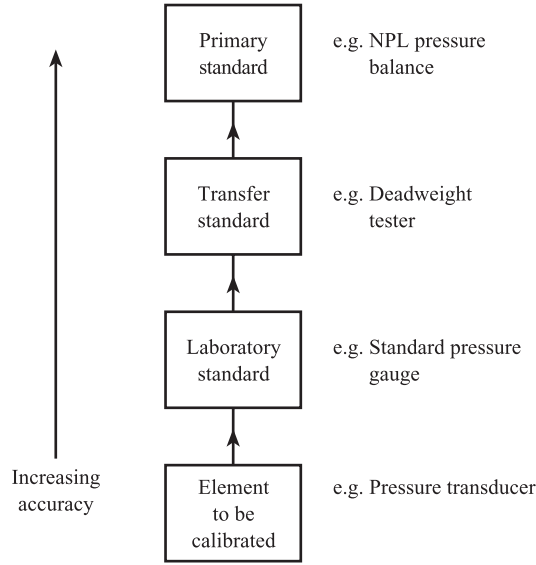
The **accuracy** of a measurement of a variable is the closeness of the measurement to the true value of the variable. It is quantified in terms of measurement error, i.e. the difference between the measured value and the true value (Chapter 3). Thus the accuracy of a laboratory standard pressure gauge is the closeness of the reading to the true value of pressure. This brings us back to the problem, mentioned in the previous chapter, of how to establish the true value of a variable. We define the true value of a variable as the measured value obtained with a standard of ultimate accuracy. Thus the accuracy of the above pressure gauge is quantified by the difference between the gauge reading, for a given pressure, and the reading given by the ultimate pressure standard. However, the manufacturer of the pressure gauge may not have access to the ultimate standard to measure the accuracy of his products.

In the United Kingdom the manufacturer is supported by the National Measurement System. **Ultimate** or **primary** measurement standards for key physical variables such as time, length, mass, current and temperature are maintained at the National Physical Laboratory (NPL). Primary measurement standards for other important industrial variables such as the density and flow rate of gases and liquids are maintained at the National Engineering Laboratory (NEL). In addition there is a network of laboratories and centres throughout the country which maintain **transfer** or **intermediate** standards. These centres are accredited by UKAS (United Kingdom Accreditation Service). Transfer standards held at accredited centres are calibrated against national primary and secondary standards, and a manufacturer can calibrate his products against the transfer standard at a local centre. Thus the manufacturer of pressure gauges can calibrate his products against a transfer standard, for example a deadweight tester. The transfer standard is in turn calibrated against a primary or secondary standard, for example a pressure balance at NPL. This introduces the concept of a **traceability ladder**, which is shown in simplified form in Figure 2.16.

The element is calibrated using the laboratory standard, which should itself be calibrated using the transfer standard, and this in turn should be calibrated using the primary standard. Each element in the ladder should be significantly more accurate than the one below it.

NPL are currently developing an **Internet calibration** service.^[3] This will allow an element at a remote location (for example at a user's factory) to be calibrated directly against a national primary or secondary standard without having to be transported to NPL. The traceability ladder is thereby collapsed to a single link between element and national standard. The same input must be applied to element and standard. The measured value given by the standard instrument is then the true value of the input to the element, and this is communicated to the user via the Internet. If the user measures the output of the element for a number of true values of input, then the characteristics of the element can be determined to a known, high accuracy.

Figure 2.16 Simplified traceability ladder.



2.4.2 SI units

Having introduced the concepts of standards and traceability we can now discuss different types of standards in more detail. The International System of Units (SI) comprises seven base units, which are listed and defined in Table 2.3. The units of all physical quantities can be derived from these base units. Table 2.4 lists common physical quantities and shows the derivation of their units from the base units. In the United Kingdom the National Physical Laboratory (NPL) is responsible for the

Table 2.3 SI base units (after National Physical Laboratory ‘Units of Measurement’ poster, 1996^[4]).

Time: second (s)	The second is the duration of 9 192 631 770 periods of the radiation corresponding to the transition between the two hyperfine levels of the ground state of the caesium-133 atom.
Length: metre (m)	The metre is the length of the path travelled by light in vacuum during a time interval of 1/299 792 458 of a second.
Mass: kilogram (kg)	The kilogram is the unit of mass; it is equal to the mass of the international prototype of the kilogram.
Electric current: ampere (A)	The ampere is that constant current which, if maintained in two straight parallel conductors of infinite length, of negligible circular cross-section, and placed 1 metre apart in vacuum, would produce between these conductors a force equal to 2×10^{-7} newton per metre of length.
Thermodynamic temperature: kelvin (K)	The kelvin, unit of thermodynamic temperature, is the fraction 1/273.16 of the thermodynamic temperature of the triple point of water.
Amount of substance: mole (mol)	The mole is the amount of substance of a system which contains as many elementary entities as there are atoms in 0.012 kilogram of carbon-12.
Luminous intensity: candela (cd)	The candela is the luminous intensity, in a given direction, of a source that emits monochromatic radiation of frequency 540×10^{12} hertz and that has a radiant intensity in that direction of (1/683) watt per steradian.

Table 2.4 SI derived units (after National Physical Laboratory Units of Measurement poster, 1996^[4]).

Examples of SI derived units expressed in terms of base units

Quantity	SI unit	
	Name	Symbol
area	square metre	m ²
volume	cubic metre	m ³
speed, velocity	metre per second	m/s
acceleration	metre per second squared	m/s ²
wave number	1 per metre	m ⁻¹
density, mass density	kilogram per cubic metre	kg/m ³
specific volume	cubic metre per kilogram	m ³ /kg
current density	ampere per square metre	A/m ²
magnetic field strength	ampere per metre	A/m
concentration (of amount of substance)	mole per cubic metre	mol/m ³
luminance	candela per square metre	cd/m ²

SI derived units with special names

Quantity	SI unit			
	Name	Symbol	Expression in terms of other units	Expression ^a in terms of SI base units
plane angle ^b	radian	rad		m · m ⁻¹ = 1
solid angle ^b	steradian	sr		m ² · m ⁻² = 1
frequency	hertz	Hz		s ⁻¹
force	newton	N		m kg s ⁻²
pressure, stress	pascal	Pa	N/m ²	m ⁻¹ kg s ⁻²
energy, work quantity of heat	joule	J	N m	m ² kg s ⁻²
power, radiant flux	watt	W	J/s	m ² kg s ⁻³
electric charge, quantity of electricity	coulomb	C		s A
electric potential, potential difference, electromotive force	volt	V	W/A	m ² kg s ⁻³ A ⁻¹
capacitance	farad	F	C/V	m ⁻² kg ⁻¹ s ⁴ A ²
electric resistance	ohm	Ω	V/A	m ² kg s ⁻³ A ⁻²
electric conductance	siemens	S	A/V	m ⁻² kg ⁻¹ s ³ A ²
magnetic flux	weber	Wb	V s	m ² kg s ⁻² A ⁻¹
magnetic flux density	tesla	T	Wb/m ²	kg s ⁻² A ⁻¹
inductance	henry	H	Wb/A	m ² kg s ⁻² A ⁻²
Celsius temperature	degree Celsius	°C		K
luminous flux	lumen	lm	cd sr	cd · m ² · m ⁻² = cd
illuminance	lux	lx	lm/m ²	cd · m ² · m ⁻⁴ = cd · m ⁻²
activity (of a radionuclide)	becquerel	Bq		s ⁻¹
absorbed dose, specific energy imparted, kerma	gray	Gy	J/kg	m ² s ⁻²
dose equivalent	sievert	Sv	J/kg	m ² s ⁻²

Table 2.4 (*cont'd*)

Examples of SI derived units expressed by means of special names

Quantity	SI unit		
	Name	Symbol	Expression in terms of SI base units
dynamic viscosity	pascal second	Pa s	$\text{m}^{-1} \text{kg s}^{-1}$
moment of force	newton metre	N m	$\text{m}^2 \text{kg s}^{-2}$
surface tension	newton per metre	N/m	kg s^{-2}
heat flux density, irradiance	watt per square metre	W/m^2	kg s^{-3}
heat capacity, entropy	joule per kelvin	J/K	$\text{m}^2 \text{kg s}^{-2} \text{K}^{-1}$
specific heat capacity, specific entropy	joule per kilogram kelvin	$\text{J}/(\text{kg K})$	$\text{m}^2 \text{s}^{-2} \text{K}^{-1}$
specific energy	joule per kilogram	J/kg	$\text{m}^2 \text{s}^{-2}$
thermal conductivity	watt per metre kelvin	$\text{W}/(\text{m K})$	$\text{m kg s}^{-3} \text{K}^{-1}$
energy density	joule per cubic metre	J/m^3	$\text{m}^{-1} \text{kg s}^{-2}$
electric field strength	volt per metre	V/m	$\text{m kg s}^{-3} \text{A}^{-1}$
electric charge density	coulomb per cubic metre	C/m^3	$\text{m}^{-3} \text{s A}$
electric flux density	coulomb per square metre	C/m^2	$\text{m}^{-2} \text{s A}$
permittivity	farad per metre	F/m	$\text{m}^{-3} \text{kg}^{-1} \text{s}^4 \text{A}^2$
permeability	henry per metre	H/m	$\text{m kg s}^{-2} \text{A}^{-2}$
molar energy	joule per mole	J/mol	$\text{m}^2 \text{kg s}^{-2} \text{mol}^{-1}$
molar entropy, molar heat capacity	joule per mole kelvin	$\text{J}/(\text{mol K})$	$\text{m}^2 \text{kg s}^{-2} \text{K}^{-1} \text{mol}^{-1}$
exposure (X and γ rays)	coulomb per kilogram	C/kg	$\text{kg}^{-1} \text{s A}$
absorbed dose rate	gray per second	Gy/s	$\text{m}^2 \text{s}^{-3}$

Examples of SI derived units formed by using the radian and steradian

Quantity	SI unit	
	Name	Symbol
angular velocity	radian per second	rad/s
angular acceleration	radian per second squared	rad/s^2
radiant intensity	watt per steradian	W/sr
radiance	watt per square metre steradian	$\text{W m}^{-2} \text{sr}^{-1}$

^a Acceptable forms are, for example, $\text{m} \cdot \text{kg} \cdot \text{s}^{-2}$, m kg s^{-2} ; m/s , $\frac{\text{m}}{\text{s}}$ or $\text{m} \cdot \text{s}^{-1}$.

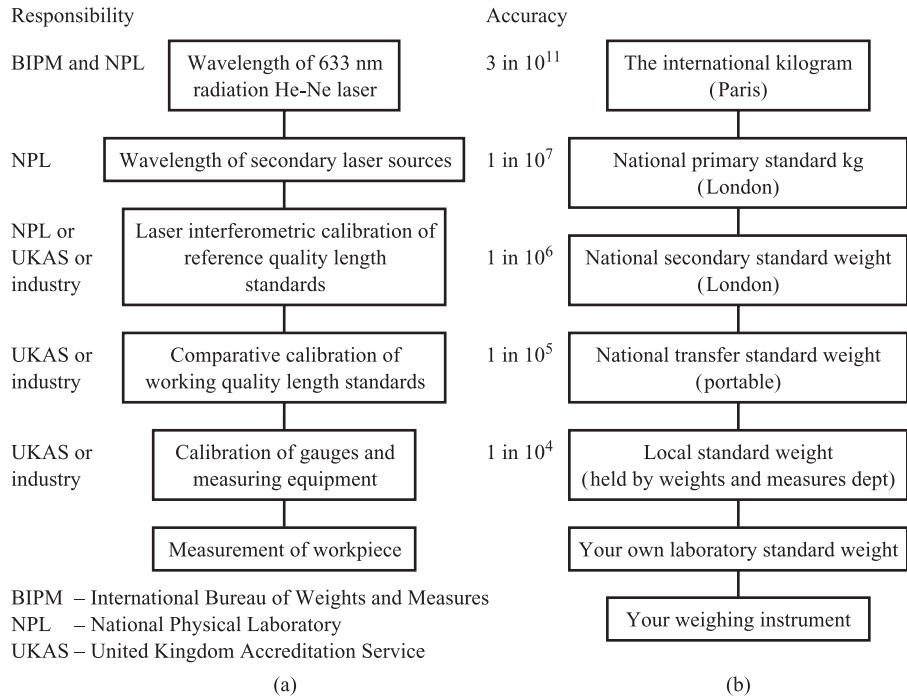
^b The CIPM (1995) decided that the radian and steradian should henceforth be designated as dimensionless derived units.

physical realisation of all of the base units and many of the derived units mentioned above. The NPL is therefore the custodian of ultimate or primary standards in the UK. There are secondary standards held at United Kingdom Accreditation Service (UKAS) centres. These have been calibrated against NPL standards and are available to calibrate transfer standards.

At NPL, the **metre** is realised using the wavelength of the 633 nm radiation from an iodine-stabilised helium–neon laser. The reproducibility of this primary standard

Figure 2.17

Traceability ladders:
 (a) length (adapted from Scarr^[5])
 (b) mass (reprinted by permission of the Council of the Institution of Mechanical Engineers from Hayward^[6]).



is about 3 parts in 10^{11} , and the wavelength of the radiation has been accurately related to the definition of the metre in terms of the velocity of light. The primary standard is used to calibrate secondary laser interferometers which are in turn used to calibrate precision length bars, gauges and tapes. A simplified traceability ladder for length^[5] is shown in Figure 2.17(a).

The international prototype of the **kilogram** is made of platinum–iridium and is kept at the International Bureau of Weights and Measures (BIPM) in Paris. The British national copy is kept at NPL and is used in conjunction with a precision balance to calibrate secondary and transfer kilogram standards. Figure 2.17(b) shows a simplified traceability ladder for mass and weight.^[6] The weight of a mass m is the force mg it experiences under the acceleration of gravity g ; thus if the local value of g is known accurately, then a force standard can be derived from mass standards. At NPL deadweight machines covering a range of forces from 450 N to 30 MN are used to calibrate strain-gauge load cells and other weight transducers.

The **second** is realised by caesium beam standards to about 1 part in 10^{13} ; this is equivalent to one second in 300 000 years! A uniform timescale, synchronised to 0.1 microsecond, is available worldwide by radio transmissions; this includes satellite broadcasts.

The **ampere** has traditionally been the electrical base unit and has been realised at NPL using the Ayrton-Jones current balance; here the force between two current-carrying coils is balanced by a known weight. The accuracy of this method is limited by the large deadweight of the coils and formers and the many length measurements necessary. For this reason the two electrical base units are now chosen to be the **farad** and the **volt** (or watt); the other units such as the ampere, ohm, henry and joule are derived from these two base units with time or frequency units, using

Ohm's law where necessary. The farad is realised using a calculable capacitor based on the Thompson–Lampard theorem. Using a.c. bridges, capacitance and frequency standards can then be used to calibrate standard resistors. The primary standard for the volt is based on the Josephson effect in superconductivity; this is used to calibrate secondary voltage standards, usually saturated Weston cadmium cells. The ampere can then be realised using a modified current balance. As before, the force due to a current I is balanced by a known weight mg , but also a separate measurement is made of the voltage e induced in the coil when moving with velocity u . Equating electrical and mechanical powers gives the simple equation:

$$eI = mgu$$

Accurate measurements of m , u and e can be made using secondary standards traceable back to the primary standards of the kilogram, metre, second and volt.

Ideally **temperature** should be defined using the thermodynamic scale, i.e. the relationship $PV = R\theta$ between the pressure P and temperature θ of a fixed volume V of an ideal gas. Because of the limited reproducibility of real gas thermometers the International Practical Temperature Scale (IPTS) was devised. This consists of:

- (a) several highly reproducible fixed points corresponding to the freezing, boiling or triple points of pure substances under specified conditions;
- (b) standard instruments with a known output versus temperature relationship obtained by calibration at fixed points.

The instruments interpolate between the fixed points.

The numbers assigned to the fixed points are such that there is exactly 100 K between the freezing point (273.15 K) and boiling point (373.15 K) of water. This means that a change of 1 K is equal to a change of 1 °C on the older Celsius scale. The exact relationship between the two scales is:

$$\theta \text{ K} = T \text{ °C} + 273.15$$

Table 2.5 shows the primary fixed points, and the temperatures assigned to them, for the 1990 version of the International Temperature Scale – ITS90.^[7] In addition there are primary standard instruments which **interpolate** between these fixed points. Platinum resistance detectors (PRTD – Section 8.1) are used up to the freezing point of silver (961.78 °C) and radiation pyrometers (Section 15.6) are used at higher temperatures. The resistance $R_T \Omega$ of a PRTD at temperature $T \text{ °C}$ (above 0 °C) can be specified by the quadratic equation

$$R_T = R_0(1 + \alpha T + \beta T^2)$$

where R_0 is the resistance at 0 °C and α , β are constants. By measuring the resistance at three adjacent fixed points (e.g. water, gallium and indium), R_0 , α and β can be calculated. An interpolating equation can then be found for the standard, which relates R_T to T and is valid between the water and indium fixed points. This primary standard PRTD, together with its equation, can then be used to calibrate secondary and transfer standards, usually PRTDs or thermocouples depending on temperature range.

The standards available for the base quantities, i.e. length, mass, time, current and temperature, enable standards for derived quantities to be realised. This is illustrated in the methods for calibrating liquid flowmeters.^[8] The actual flow rate through the meter is found by weighing the amount of water collected in a given time, so that the accuracy of the flow rate standard depends on the accuracies of weight and time standards.

Table 2.5 The primary fixed points defining the International Temperature Scale 1990 – ITS90.

Equilibrium state	θ K	T °C
Triple point of hydrogen	13.8033	–259.3467
Boiling point of hydrogen at a pressure of 33 321.3 Pa	17.035	–256.115
Boiling point of hydrogen at a pressure of 101 292 Pa	20.27	–252.88
Triple point of neon	24.5561	–248.5939
Triple point of oxygen	54.3584	–218.7916
Triple point of argon	83.8058	–189.3442
Triple point of mercury	234.3156	–38.8344
Triple point of water	273.16	0.01
Melting point of gallium	302.9146	29.7646
Freezing point of indium	429.7485	156.5985
Freezing point of tin	505.078	231.928
Freezing point of zinc	692.677	419.527
Freezing point of aluminium	933.473	660.323
Freezing point of silver	1234.93	961.78
Freezing point of gold	1337.33	1064.18
Freezing point of copper	1357.77	1084.62

National primary and secondary standards for **pressure** above 110 kPa use pressure balances.^[3] Here the force pA due to pressure p acting over an area A is balanced by the gravitational force mg acting on a mass m , i.e.

$$pA = mg$$

or

$$p = mg/A$$

Thus standards for pressure can be derived from those for mass and length, though the local value of gravitational acceleration g must also be accurately known.

2.4.3 Experimental measurements and evaluation of results

The calibration experiment is divided into three main parts.

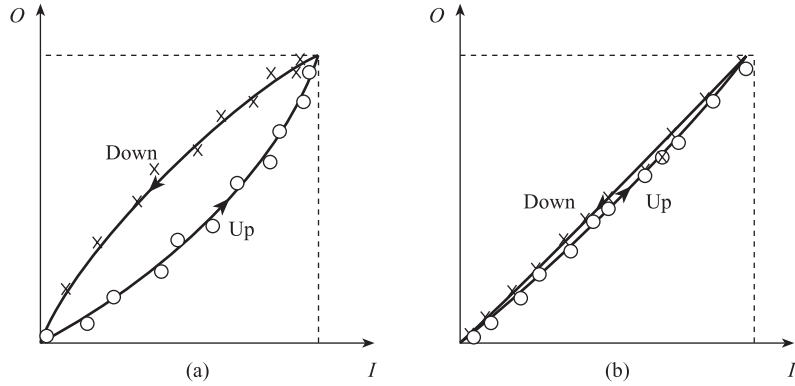
O versus I with $I_M = I_I = 0$

Ideally this test should be held under ‘standard’ environmental conditions so that $I_M = I_I = 0$; if this is not possible all environmental inputs should be measured. I should be increased slowly from I_{MIN} to I_{MAX} and corresponding values of I and O recorded at intervals of 10% span (i.e. 11 readings), allowing sufficient time for the output to settle out before taking each reading. A further 11 pairs of readings should be taken with I decreasing slowly from I_{MAX} to I_{MIN} . The whole process should be repeated for two further ‘**ups**’ and ‘**downs**’ to yield two sets of data: an ‘**up**’ set $(I_i, O_i)_{i\uparrow}$ and a ‘**down**’ set $(I_j, O_j)_{j\downarrow}$, $i, j = 1, 2, \dots, n$ ($n = 33$).

Computer software regression packages are readily available which fit a polynomial, i.e. $O(I) = \sum_{q=0}^{q=m} a_q I^q$, to a set of n data points. These packages use a ‘least squares’ criterion. If d_i is the deviation of the polynomial value $O(I_i)$ from the data value O_i , then $d_i = O(I_i) - O_i$. The program finds a set of coefficients a_0, a_1, a_2 , etc.,

Figure 2.18

(a) Significant hysteresis
(b) Insignificant hysteresis.



such that the sum of the squares of the deviations, i.e. $\sum_{i=1}^{i=n} d_i^2$, is a minimum. This involves solving a set of linear equations.^[9]

In order to detect any hysteresis, separate regressions should be performed on the two sets of data $(I_i, O_i)_{I\uparrow}$, $(I_j, O_j)_{I\downarrow}$, to yield two polynomials:

$$O(I)_{I\uparrow} = \sum_{q=0}^q a_q^{\uparrow} I^q \quad \text{and} \quad O(I)_{I\downarrow} = \sum_{q=0}^q a_q^{\downarrow} I^q$$

If the hysteresis is significant, then the separation of the two curves will be greater than the scatter of data points about each individual curve (Figure 2.18(a)). Hysteresis $H(I)$ is then given by eqn [2.10], i.e. $H(I) = O(I)_{I\downarrow} - O(I)_{I\uparrow}$. If, however, the scatter of points about each curve is greater than the separation of the curves (Figure 2.18(b)), then H is not significant and the two sets of data can then be combined to give a single polynomial $O(I)$. The slope K and zero bias a of the ideal straight line joining the minimum and maximum points $(I_{\text{MIN}}, O_{\text{MIN}})$ and $(I_{\text{MAX}}, O_{\text{MAX}})$ can be found from eqn [2.3]. The non-linear function $N(I)$ can then be found using eqn [2.4]:

$$N(I) = O(I) - (KI + a) \quad [2.24]$$

Temperature sensors are often calibrated using appropriate fixed points rather than a standard instrument. For example, a thermocouple may be calibrated between 0 and 500 °C by measuring e.m.f.'s at ice, steam and zinc points. If the e.m.f.–temperature relationship is represented by the cubic $E = a_1 T + a_2 T^2 + a_3 T^3$, then the coefficients a_1, a_2, a_3 can be found by solving three simultaneous equations (see Problem 2.1).

O versus I_M, I_I at constant I

We first need to find which environmental inputs are interfering, i.e. which affect the zero bias a . The input I is held constant at $I = I_{\text{MIN}}$, and one environmental input is changed by a known amount, the rest being kept at standard values. If there is a resulting change ΔO in O , then the input I_i is interfering and the value of the corresponding coefficient K_i is given by $K_i = \Delta O / \Delta I_i$. If there is no change in O , then the input is not interfering; the process is repeated until all interfering inputs are identified and the corresponding K_i values found.

We now need to identify modifying inputs, i.e. those which affect the sensitivity of the element. The input I is held constant at the mid-range value $\frac{1}{2}(I_{\text{MIN}} + I_{\text{MAX}})$ and each environmental input is varied in turn by a known amount. If a change in input

produces a change ΔO in O and is not an interfering input, then it must be a modifying input I_M and the value of the corresponding coefficient K_M is given by

$$K_M = \frac{1}{I} \frac{\Delta O}{\Delta I_M} = \frac{2}{I_{\text{MIN}} + I_{\text{MAX}}} \frac{\Delta O}{\Delta I_M} \quad [2.25]$$

Suppose a change in input produces a change ΔO in O and it has already been identified as an interfering input with a known value of K_I . Then we must calculate a non-zero value of K_M before we can be sure that the input is also modifying. Since

$$\Delta O = K_I \Delta I_{I,M} + K_M \Delta I_{I,M} \frac{I_{\text{MIN}} + I_{\text{MAX}}}{2}$$

then

$$K_M = \frac{2}{I_{\text{MIN}} + I_{\text{MAX}}} \left[\frac{\Delta O}{\Delta I_{I,M}} - K_I \right] \quad [2.26]$$

Repeatability test

This test should be carried out in the normal working environment of the element, e.g. out on the plant, or in a control room, where the environmental inputs I_M and I_I are subject to the random variations usually experienced. The signal input I should be held constant at mid-range value and the output O measured over an extended period, ideally many days, yielding a set of values O_k , $k = 1, 2, \dots, N$. The mean value of the set can be found using

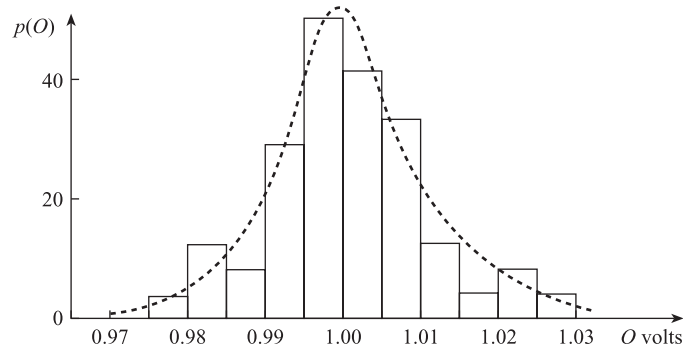
$$\bar{O} = \frac{1}{N} \sum_{k=1}^N O_k \quad [2.27]$$

and the standard deviation (root mean square of deviations from the mean) is found using

$$\sigma_0 = \sqrt{\frac{1}{N} \sum_{k=1}^N (O_k - \bar{O})^2} \quad [2.28]$$

A histogram of the values O_k should then be plotted in order to estimate the probability density function $p(O)$ and to compare it with the normal form (eqn [2.20]). A repeatability test on a pressure transducer can be used as an example of the construction of a histogram. Suppose that $N = 50$ and readings between 0.975 and 1.030 V are obtained corresponding to an expected value of 1.000 V. The readings are grouped into equal intervals of width 0.005 V and the number in each interval is found, e.g. 12, 10, 8, etc. This number is divided by the total number of readings, i.e. 50, to give the probabilities 0.24, 0.20, 0.16, etc. of a reading occurring in a given interval. The probabilities are in turn divided by the interval width 0.005 V to give the probability densities 48, 40 and 32 V^{-1} plotted in the histogram (Figure 2.19). We note that the area of each rectangle represents the probability that a reading lies within the interval, and that the total area of the histogram is equal to unity. The mean and standard deviation are found from eqns [2.27] and [2.28] to be $\bar{O} = 0.999$ V and $\sigma_0 = 0.010$ V respectively. Figure 2.19 also shows a normal probability density function with these values.

Figure 2.19 Comparison of histogram with normal probability density function.



Conclusion

The chapter began by discussing the **static** or **steady-state** characteristics of measurement system elements. **Systematic characteristics** such as non-linearity and environmental effects were first explained. This led to the **generalised model** of an element. **Statistical** characteristics, i.e. repeatability and tolerance, were then discussed. The last section explained how these characteristics can be measured experimentally, i.e. **calibration** and the use and types of **standards**.

References

- [1] IEC 584.1:1995 *International Thermocouple Reference Tables*, International Electrotechnical Committee.
- [2] KENNEDY J B and NEVILLE A 1986 *Basic Statistical Methods for Engineers and Scientists*, 3rd edn, pp. 345–60. Harper and Row, New York.
- [3] STUART P R 1987 ‘Standards for the measurement of pressure’, *Measurement and Control*, vol. 20, no. 8, pp. 7–11.
- [4] National Physical Laboratory 1996 *Units of Measurement*, poster, 8th edn.
- [5] SCARR A 1979 ‘Measurement of length’, *Journal of the Institute of Measurement and Control*, vol. 12, July, pp. 265–9.
- [6] HAYWARD A T J 1977 *Repeatability and Accuracy*, p. 34. Mechanical Engineering Publications, London.
- [7] TC Ltd 2001 *Guide to Thermocouple and Resistance Thermometry*, issue 6.0.
- [8] HAYWARD A T J 1977 ‘Methods of calibrating flowmeters with liquids – a comparative survey’, *Transactions of the Institute of Measurement and Control*, vol. 10, pp. 106–16.
- [9] FREUND J E 1984 *Modern Elementary Statistics*, 6th edn, pp. 401–34. Prentice Hall International, Englewood Cliffs, NJ.

Problems

- 2.1 The e.m.f. at a thermocouple junction is $645 \mu\text{V}$ at the steam point, $3375 \mu\text{V}$ at the zinc point and $9149 \mu\text{V}$ at the silver point. Given that the e.m.f.–temperature relationship is of the form $E(T) = a_1T + a_2T^2 + a_3T^3$ (T in $^\circ\text{C}$), find a_1 , a_2 and a_3 .
- 2.2 The resistance $R(\theta)$ of a thermistor at temperature θ K is given by $R(\theta) = \alpha \exp(\beta/\theta)$. Given that the resistance at the ice point ($\theta = 273.15$ K) is $9.00 \text{ k}\Omega$ and the resistance at the steam point is $0.50 \text{ k}\Omega$, find the resistance at 25°C .
- 2.3 A displacement sensor has an input range of 0.0 to 3.0 cm and a standard supply voltage $V_s = 0.5$ volts. Using the calibration results given in the table, estimate:
- The maximum non-linearity as a percentage of f.s.d.
 - The constants K_f , K_M associated with supply voltage variations.
 - The slope K of the ideal straight line.

Displacement x cm	0.0	0.5	1.0	1.5	2.0	2.5	3.0
Output voltage millivolts ($V_s = 0.5$)	0.0	16.5	32.0	44.0	51.5	55.5	58.0
Output voltage millivolts ($V_s = 0.6$)	0.0	21.0	41.5	56.0	65.0	70.5	74.0

- 2.4 A liquid level sensor has an input range of 0 to 15 cm . Use the calibration results given in the table to estimate the maximum hysteresis as a percentage of f.s.d.

Level h cm	0.0	1.5	3.0	4.5	6.0	7.5	9.0	10.5	12.0	13.5	15.0
Output volts h increasing	0.00	0.35	1.42	2.40	3.43	4.35	5.61	6.50	7.77	8.85	10.2
Output volts h decreasing	0.14	1.25	2.32	3.55	4.43	5.70	6.78	7.80	8.87	9.65	10.2

- 2.5 A repeatability test on a vortex flowmeter yielded the following 35 values of frequency corresponding to a constant flow rate of $1.4 \times 10^{-2} \text{ m}^3 \text{ s}^{-1}$: 208.6; 208.3; 208.7; 208.5; 208.8; 207.6; 208.9; 209.1; 208.2; 208.4; 208.1; 209.2; 209.6; 208.6; 208.5; 207.4; 210.2; 209.2; 208.7; 208.4; 207.7; 208.9; 208.7; 208.0; 209.0; 208.1; 209.3; 208.2; 208.6; 209.4; 207.6; 208.1; 208.8; 209.2; 209.7 Hz.
- Using equal intervals of width 0.5 Hz , plot a histogram of probability density values.
 - Calculate the mean and standard deviation of the data.
 - Sketch a normal probability density function with the mean and standard deviation calculated in (b) on the histogram drawn in (a).

- 2.6 A platinum resistance sensor is used to interpolate between the triple point of water (0°C), the boiling point of water (100°C) and the freezing point of zinc (419.6°C). The corresponding resistance values are 100.0Ω , 138.5Ω and 253.7Ω . The algebraic form of the interpolation equation is:

$$R_T = R_0(1 + \alpha T + \beta T^2)$$

where $R_T \Omega$ = resistance at $T^\circ\text{C}$
 $R_0 \Omega$ = resistance at 0°C
 α, β = constants.

Find the numerical form of the interpolation equation.

- 2.7 The following results were obtained when a pressure transducer was tested in a laboratory under the following conditions:

- I Ambient temperature 20 °C, supply voltage 10 V (standard)
 II Ambient temperature 20 °C, supply voltage 12 V
 III Ambient temperature 25 °C, supply voltage 10 V

Input (barg)	0	2	4	6	8	10
Output (mA)						
I	4	7.2	10.4	13.6	16.8	20
II	4	8.4	12.8	17.2	21.6	28
III	6	9.2	12.4	15.6	18.8	22

- (a) Determine the values of K_M , K_I , a and K associated with the generalised model equation $O = (K + K_M I_M)I + a + K_I I_I$.
 (b) Predict an output value when the input is 5 barg, $V_S = 12$ V and ambient temperature is 25 °C.

Basic problems

- 2.8 A force sensor has an output range of 1 to 5 V corresponding to an input range of 0 to 2×10^5 N. Find the equation of the ideal straight line.
 2.9 A differential pressure transmitter has an input range of 0 to 2×10^4 Pa and an output range of 4 to 20 mA. Find the equation to the ideal straight line.
 2.10 A non-linear pressure sensor has an input range of 0 to 10 bar and an output range of 0 to 5 V. The output voltage at 4 bar is 2.20 V. Calculate the non-linearity in volts and as a percentage of span.
 2.11 A non-linear temperature sensor has an input range of 0 to 400 °C and an output range of 0 to 20 mV. The output signal at 100 °C is 4.5 mV. Find the non-linearity at 100 °C in millivolts and as a percentage of span.
 2.12 A thermocouple used between 0 and 500 °C has the following input–output characteristics:

Input T °C	0	100	200	300	500
Output E μ V	0	5268	10 777	16 325	27 388

- (a) Find the equation of the ideal straight line.
 (b) Find the non-linearity at 100 °C and 300 °C in μ V and as a percentage of f.s.d.
 2.13 A force sensor has an input range of 0 to 10 kN and an output range of 0 to 5 V at a standard temperature of 20 °C. At 30 °C the output range is 0 to 5.5 V. Quantify this environmental effect.
 2.14 A pressure transducer has an output range of 1.0 to 5.0 V at a standard temperature of 20 °C, and an output range of 1.2 to 5.2 V at 30 °C. Quantify this environmental effect.
 2.15 A pressure transducer has an input range of 0 to 10^4 Pa and an output range of 4 to 20 mA at a standard ambient temperature of 20 °C. If the ambient temperature is increased to 30 °C, the range changes to 4.2 to 20.8 mA. Find the values of the environmental sensitivities K_I and K_M .

- 2.16 An analogue-to-digital converter has an input range of 0 to 5 V. Calculate the resolution error both as a voltage and as a percentage of f.s.d. if the output digital signal is:
- (a) 8-bit binary
 - (b) 16-bit binary.
- 2.17 A level transducer has an output range of 0 to 10 V. For a 3 metre level, the output voltage for a falling level is 3.05 V and for a rising level 2.95 V. Find the hysteresis as a percentage of span.

3 The Accuracy of Measurement Systems in the Steady State

In Chapter 1 we saw that the input to a measurement system is the true value of the variable being measured. Also, if the measurement system is complete, the system output is the measured value of the variable. In Chapter 2 we defined accuracy in terms of measurement error, i.e. the difference between the measured and true values of a variable. It follows therefore that accuracy is a property of a complete measurement system rather than a single element. Accuracy is quantified using measurement error E where:

$$\begin{aligned} E &= \text{measured value} - \text{true value} \\ &= \text{system output} - \text{system input} \end{aligned} \quad [3.1]$$

In this chapter we use the static model of a single element, developed previously, to calculate the output and thus the measurement error for a complete system of several elements. The chapter concludes by examining methods of reducing system error.

3.1 Measurement error of a system of ideal elements

Consider the system shown in Figure 3.1 consisting of n elements in series. Suppose each element is ideal, i.e. perfectly linear and not subject to environmental inputs. If we also assume the intercept or bias is zero, i.e. $a = 0$, then:

Input/output equation for ideal element with zero intercept

$$O_i = K_i I_i \quad [3.2]$$

for $i = 1, \dots, n$, where K_i is the linear sensitivity or slope (eqn [2.3]). It follows that $O_2 = K_2 I_2 = K_2 K_1 I$, $O_3 = K_3 I_3 = K_3 K_2 K_1 I$, and for the whole system:

$$O = O_n = K_1 K_2 K_3 \dots K_i \dots K_n I \quad [3.3]$$

Figure 3.1.

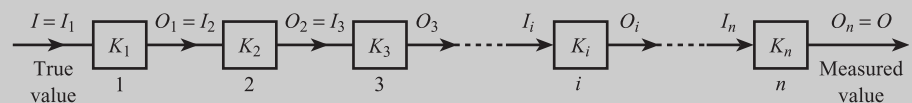
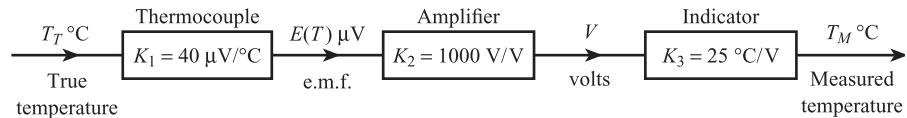


Figure 3.2 Simple temperature measurement system.



If the measurement system is complete, then $E = O - I$, giving:

$$E = (K_1 K_2 K_3 \dots K_n - 1)I \quad [3.4]$$

Thus if

$$K_1 K_2 K_3 \dots K_n = 1 \quad [3.5]$$

we have $E = 0$ and the system is perfectly accurate. The temperature measurement system shown in Figure 3.2 appears to satisfy the above condition. The indicator is simply a moving coil voltmeter (see Chapter 11) with a scale marked in degrees Celsius so that an input change of 1 V causes a change in deflection of 25 °C. This system has $K_1 K_2 K_3 = 40 \times 10^{-6} \times 10^3 \times 25 = 1$ and thus appears to be perfectly accurate. The system is not accurate, however, because none of the three elements present is ideal. The thermocouple is non-linear (Chapter 2), so that as the input temperature changes the sensitivity is no longer 40 $\mu\text{V } ^\circ\text{C}^{-1}$. Also changes in reference junction temperature (Figure 2.12(b)) cause the thermocouple e.m.f. to change. The output voltage of the amplifier is also affected by changes in ambient temperature (Chapter 9). The sensitivity K_3 of the indicator depends on the stiffness of the restoring spring in the moving coil assembly. This is affected by changes in environmental temperature and wear, causing K_3 to deviate from 25 $^\circ\text{C V}^{-1}$. Thus the condition $K_1 K_2 K_3 = 1$ cannot be always satisfied and the system is in error.

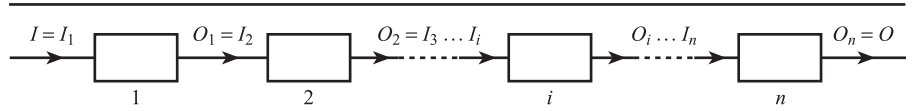
In general the error of any measurement system depends on the non-ideal characteristics – e.g. non-linearity, environmental and statistical effects – of every element in the system. Thus in order to quantify this error as precisely as possible we need to use the general model for a single element developed in Sections 2.2 and 2.3.

3.2 The error probability density function of a system of non-ideal elements

In Chapter 2 we saw that the probability density function of the output $p(O)$ of a single element can be represented by a normal distribution (eqn [2.20]). The mean value \bar{O} of the distribution is given by eqn [2.22], which allows for non-linear and environmental effects. The standard deviation σ_0 is given by [2.23], which allows for statistical variations in inputs I , I_M and I_I with time, and statistical variations in parameters K , a , etc., amongst a batch of similar elements. These equations apply to each element in a measurement system of n elements and can be used to calculate the system error probability density function $p(E)$ as shown in Table 3.1.

Equations [3.6] (based on [2.22]) show how to calculate the mean value of the output of each element in turn, starting with \bar{O}_1 for the first and finishing with $\bar{O}_n = \bar{O}$ for the n th. The mean value \bar{E} of the system error is simply the difference between the mean value of system output and mean value of system input (eqn [3.7]). Since the probability densities of the outputs of the individual elements are normal, then, using the result outlined in Section 2.3, the probability density function of the

Table 3.1 General calculation of system $p(E)$.



Mean values of element outputs

$$\begin{aligned}
 \bar{I}_1 &= \bar{I} \\
 \bar{I}_2 &= \bar{O}_1 = \bar{K}_1 \bar{I}_1 + \bar{N}_1(\bar{I}_1) + \bar{a}_1 + \bar{K}_{M_1} \bar{I}_{M_1} \bar{I}_1 + \bar{K}_{I_1} \bar{I}_{I_1} \\
 \bar{I}_3 &= \bar{O}_2 = \bar{K}_2 \bar{I}_2 + \bar{N}_2(\bar{I}_2) + \bar{a}_2 + \bar{K}_{M_2} \bar{I}_{M_2} \bar{I}_2 + \bar{K}_{I_2} \bar{I}_{I_2} \\
 &\vdots \\
 \bar{I}_{i+1} &= \bar{O}_i = \bar{K}_i \bar{I}_i + \bar{N}_i(\bar{I}_i) + \bar{a}_i + \bar{K}_{M_i} \bar{I}_{M_i} \bar{I}_i + \bar{K}_{I_i} \bar{I}_{I_i} \\
 &\vdots \\
 \bar{O} &= \bar{O}_n = \bar{K}_n \bar{I}_n + \bar{N}_n(\bar{I}_n) + \bar{a}_n + \bar{K}_{M_n} \bar{I}_{M_n} \bar{I}_n + \bar{K}_{I_n} \bar{I}_{I_n}
 \end{aligned} \tag{3.6}$$

Mean value of system error

$$\bar{E} = \bar{O} - \bar{I} \tag{3.7}$$

Standard deviations of element outputs

$$\begin{aligned}
 \sigma_{I_1}^2 &= 0 \\
 \sigma_{I_2}^2 &= \sigma_{O_1}^2 = \left(\frac{\partial O_1}{\partial I_1} \right)^2 \sigma_{I_1}^2 + \left(\frac{\partial O_1}{\partial I_{M_1}} \right)^2 \sigma_{I_{M_1}}^2 + \left(\frac{\partial O_1}{\partial I_{I_1}} \right)^2 \sigma_{I_{I_1}}^2 + \left(\frac{\partial O_1}{\partial K_1} \right)^2 \sigma_{K_1}^2 + \dots \\
 \sigma_{I_3}^2 &= \sigma_{O_2}^2 = \left(\frac{\partial O_2}{\partial I_2} \right)^2 \sigma_{I_2}^2 + \left(\frac{\partial O_2}{\partial I_{M_2}} \right)^2 \sigma_{I_{M_2}}^2 + \left(\frac{\partial O_2}{\partial I_{I_2}} \right)^2 \sigma_{I_{I_2}}^2 + \left(\frac{\partial O_2}{\partial K_2} \right)^2 \sigma_{K_2}^2 + \dots \\
 &\vdots \\
 \sigma_{I_{i+1}}^2 &= \sigma_{O_i}^2 = \left(\frac{\partial O_i}{\partial I_i} \right)^2 \sigma_{I_i}^2 + \left(\frac{\partial O_i}{\partial I_{M_i}} \right)^2 \sigma_{I_{M_i}}^2 + \left(\frac{\partial O_i}{\partial I_{I_i}} \right)^2 \sigma_{I_{I_i}}^2 + \left(\frac{\partial O_i}{\partial K_i} \right)^2 \sigma_{K_i}^2 + \dots \\
 \sigma_O^2 &= \sigma_{O_n}^2 = \left(\frac{\partial O_n}{\partial I_n} \right)^2 \sigma_{I_n}^2 + \left(\frac{\partial O_n}{\partial I_{M_n}} \right)^2 \sigma_{I_{M_n}}^2 + \left(\frac{\partial O_n}{\partial I_{I_n}} \right)^2 \sigma_{I_{I_n}}^2 + \left(\frac{\partial O_n}{\partial K_n} \right)^2 \sigma_{K_n}^2 + \dots
 \end{aligned} \tag{3.8}$$

Standard deviation of system error

$$\sigma_E = \sigma_O \tag{3.9}$$

Error probability density function

$$p(E) = \frac{1}{\sigma_E \sqrt{2\pi}} \exp \left[-\frac{1}{2\sigma_E^2} (E - \bar{E})^2 \right] \tag{3.10}$$

system output O and system error E is also normal (eqn [3.10]). Equations [3.8] (based on [2.23]) show how to calculate the standard deviation of the output of each element in turn, starting with σ_{O_1} for the first, and finishing with σ_{O_n} for the n th. We note that the standard deviation of the system input is zero and that the standard deviation of the error is equal to that of the system output (eqn [3.9]).

We now use the temperature measurement system shown in Figure 3.3 as an example of the calculation of \bar{E} and σ_E . This consists of a platinum resistance temperature detector, current transmitter and recorder.

Table 3.2 gives the models for each of the elements in the temperature measurement system. In (a), the platinum resistance temperature detector is characterised by

Figure 3.3 Temperature measurement system.

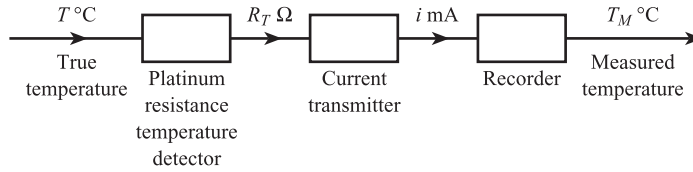


Table 3.2 Models for temperature measurement system elements.

(a) Platinum resistance temperature detector

Model equation	$R_T = R_0(1 + \alpha T + \beta T^2)$
Individual mean values	$\bar{R}_0 = 100.0 \Omega$, $\bar{\alpha} = 3.909 \times 10^{-3}$, $\bar{\beta} = -5.897 \times 10^{-7}$ (between 100 and 130 °C)
Individual standard deviations	$\sigma_{R_0} = 4.33 \times 10^{-2}$, $\sigma_{\alpha} = 0.0$, $\sigma_{\beta} = 0.0$
Partial derivatives	$\frac{\partial R_T}{\partial R_0} = 1.449$ at $T = 117 \text{ °C}$
Overall mean value	$\bar{R}_T = \bar{R}_0(1 + \bar{\alpha}\bar{T} + \bar{\beta}\bar{T}^2)$
Overall standard deviation	$\sigma_{R_T}^2 = \left(\frac{\partial R_T}{\partial R_0}\right)^2 \sigma_{R_0}^2$

(b) Current transmitter

Model equation	4 to 20 mA output for 138.5 to 149.8 Ω input (100 to 130 °C) ΔT_a = deviation of ambient temperature from 20 °C $i = KR_T + K_M R_T \Delta T_a + K_I \Delta T_a + a$
Individual mean values	$\bar{K} = 1.4134$, $\bar{K}_M = 1.4134 \times 10^{-4}$, $\bar{K}_I = -1.637 \times 10^{-2}$ $\bar{a} = -191.76$, $\bar{\Delta T}_a = -10$
Individual standard deviations	$\sigma_K = 0.0$, $\sigma_{K_M} = 0.0$, $\sigma_{K_I} = 0.0$ $\sigma_a = 0.24$, $\sigma_{\Delta T_a} = 6.7$
Partial derivatives	$\frac{\partial i}{\partial R_T} = 1.413$, $\frac{\partial i}{\partial \Delta T_a} = 4.11 \times 10^{-3}$, $\frac{\partial i}{\partial a} = 1.00$
Overall mean value	$\bar{i} = \bar{K}\bar{R}_T + \bar{K}_M \bar{R}_T \bar{\Delta T}_a + \bar{K}_I \bar{\Delta T}_a + \bar{a}$
Overall standard deviation	$\sigma_i^2 = \left(\frac{\partial i}{\partial R_T}\right)^2 \sigma_{R_T}^2 + \left(\frac{\partial i}{\partial \Delta T_a}\right)^2 \sigma_{\Delta T_a}^2 + \left(\frac{\partial i}{\partial a}\right)^2 \sigma_a^2$

(c) Recorder

Model equation	$T_M = Ki + a$
Individual mean values	$\bar{K} = 1.875$, $\bar{a} = 92.50$ (100 to 130 °C record for 4 to 20 mA input)
Individual standard deviations	$\sigma_K = 0.0$, $\sigma_a = 0.10$
Partial derivatives	$\frac{\partial T_M}{\partial i} = 1.875$, $\frac{\partial T_M}{\partial a} = 1.00$
Overall mean value	$\bar{T}_M = \bar{K}\bar{i} + \bar{a}$
Overall standard deviation	$\sigma_{T_M}^2 = \left(\frac{\partial T_M}{\partial i}\right)^2 \sigma_i^2 + \left(\frac{\partial T_M}{\partial a}\right)^2 \sigma_a^2$

Table 3.3 Summary of calculation of \bar{E} and σ_E for temperature system.Mean \bar{E}

$$\begin{aligned}\bar{T} &= 117 \text{ }^\circ\text{C} & \bar{R}_T &= 144.93 \text{ } \Omega \\ \bar{i} &= 13.04 \text{ mA} & \bar{T}_M &= 116.95 \text{ }^\circ\text{C} \\ \bar{E} &= \bar{T}_M - \bar{T} = -0.005 \text{ }^\circ\text{C}\end{aligned}$$

Standard deviation σ_E

$$\begin{aligned}\sigma_T^2 &= 0 \\ \sigma_{R_T}^2 &= \left(\frac{\partial R_T}{\partial R_0} \right)^2 \sigma_{R_0}^2 = 39.4 \times 10^{-4} \\ \sigma_i^2 &= \left(\frac{\partial i}{\partial R_T} \right)^2 \sigma_{R_T}^2 + \left(\frac{\partial i}{\partial \Delta T_a} \right)^2 \sigma_{\Delta T_a}^2 + \left(\frac{\partial i}{\partial a} \right)^2 \sigma_a^2 \\ &= 78.7 \times 10^{-4} + 8.18 \times 10^{-4} + 5.76 \times 10^{-2} \\ &= 6.62 \times 10^{-2} \\ \sigma_{T_M}^2 &= \left(\frac{\partial T_M}{\partial i} \right)^2 \sigma_i^2 + \left(\frac{\partial T_M}{\partial a} \right)^2 \sigma_a^2 = 24.3 \times 10^{-2} \\ \sigma_E &= \sigma_{T_M} = 0.49 \text{ }^\circ\text{C}\end{aligned}$$

a small amount of non-linearity and a spread of values of R_0 (resistance at 0 °C). The current transmitter (b) is linear but temperature acts as both a modifying and an interfering input. The zero bias and sensitivity are adjustable: we cannot be certain that the transmitter will be set up exactly as stated in the table, and this is reflected in the non-zero value of σ_a . In (c) the recorder is linear but again calibration uncertainties are modelled by a non-zero value of σ_a .

Table 3.3 summarises the calculation of \bar{E} and σ_E for the system when the mean value \bar{T} of the true temperature is 117 °C. The corresponding mean values for the system are resistance $\bar{R}_T = 144.93 \text{ } \Omega$ (Table 3.2(a)), current $\bar{i} = 13.04 \text{ mA}$ (Table 3.2(b)) and measured temperature $\bar{T}_M = 116.95 \text{ }^\circ\text{C}$ (Table 3.2(c)). The mean error is therefore $\bar{E} = -0.05 \text{ }^\circ\text{C}$. The standard deviations σ_{R_T} , σ_i and σ_{T_M} are calculated using Table 3.2 to give $\sigma_E = 0.49 \text{ }^\circ\text{C}$.

Modelling using error bands

In Section 2.1 we saw that in situations where element non-linearity, hysteresis and environmental effects are small, their overall effect is quantified using error bands. Here a systematic statement of the exact element input/output relationship (e.g. eqn [2.9]) is replaced by a statistical statement. The element output is described by a rectangular probability density function, of width $2h$, centred on the ideal straight line value $O_{\text{IDEAL}} = KI + a$. If every element in the system is described in this way, then the mean output value \bar{O} will have the ideal value $\bar{O}_i = K_i \bar{I}_i + a_i$ for each element in the system. In the special case $a_i = 0$ for all i , $\bar{O}_i = K_i \bar{I}_i$, the mean value of system output is given by

$$\bar{O} = K_1 K_2 \dots K_i \dots K_n \bar{I}$$

and the mean value of error $\bar{E} = \bar{O} - \bar{I}$. In the special case $K_1 K_2 \dots K_i \dots K_n = 1$, $\bar{E} = 0$ (Table 3.4). The error probability density function $p(E)$ is the result of

Table 3.4 \bar{E} and σ_E
for system of elements
described by error bands.

$I = I_1$	$\boxed{K_1, h_1}$	$O_1 = I_2$	$\boxed{K_2, h_2}$	\dots	$\boxed{K_i, h_i}$	\dots	$\boxed{K_n, h_n}$	$O_n = O$
	1		2		i		n	
	$\bar{O}_i = K_i \bar{I}_i$							
	$\bar{O} = K_1 K_2 \dots K_i \dots K_n \bar{I}$							
	$\bar{E} = \bar{O} - \bar{I} [= 0, \text{ if } K_1 K_2 \dots K_n = 1]$							
	$\sigma_{I_1}^2 = 0$							
	$\sigma_{O_1}^2 = \sigma_{I_1}^2 = \frac{h_1^2}{3}$							
	$\sigma_{O_2}^2 = \sigma_{O_1}^2 = K_2^2 \sigma_{I_1}^2 + \frac{h_2^2}{3}$							
	\vdots							
	$\sigma_{O_i}^2 = \sigma_{O_{i-1}}^2 = K_i^2 \sigma_{I_{i-1}}^2 + \frac{h_i^2}{3}$							
	\vdots							
	$\sigma_{O_n}^2 = \sigma_{O_{n-1}}^2 = K_n^2 \sigma_{I_{n-1}}^2 + \frac{h_n^2}{3}$							
	$\sigma_E = \sigma_0$							

combining n rectangular distributions, each of width $2h_i$, $i = 1, 2, \dots, n$. If $n > 3$, then the resultant distribution $p(E)$ approximates to a normal distribution; the larger the value of n the closer the distribution is to normal.

In order to calculate the standard deviation σ_E of $p(E)$ we return to eqns [2.16] and [2.17]. If a dependent variable y is a linear combination of independent random variables x_1, x_2, x_3 , i.e.

$$y = a_1 x_1 + a_2 x_2 + a_3 x_3 \quad [2.16]$$

then the standard deviation σ of the probability distribution of y is given by

$$\sigma^2 = a_1^2 \sigma_1^2 + a_2^2 \sigma_2^2 + a_3^2 \sigma_3^2 \quad [2.17]$$

Equation [2.17] applies whatever the probability distributions of the individual x_1, x_2, x_3 are, provided that the individual standard deviations $\sigma_1, \sigma_2, \sigma_3$ are small.^[1] Consider the i th element in Table 3.4 with sensitivity K_i and error band width $2h_i$. The standard deviation σ_{O_i} of the output O_i is equal to

$$\sigma_{O_i}^2 = \sigma^2 \text{ due to input} + \sigma^2 \text{ due to element}$$

If σ_{I_i} is the standard deviation of the input I_i , then this contributes $K_i \sigma_{I_i}$ to the output standard deviation. The standard deviation of the rectangular distribution of width $2h_i$, due to the element, is $h_i/\sqrt{3}$. We therefore have:

$$\sigma_{O_i}^2 = K_i^2 \sigma_{I_i}^2 + h_i^2/3$$

Table 3.4 gives the calculation procedure for a complete system of n elements described by error bands.

3.3 Error reduction techniques

In the two previous sections we saw that the error of a measurement system depends on the non-ideal characteristics of every element in the system. Using the calibration techniques of Section 2.4, we can identify which elements in the system have the most dominant non-ideal behaviour. We can then devise compensation strategies for these elements which should produce significant reductions in the overall system error. This section outlines compensation methods for non-linear and environmental effects.

One of the most common methods of correcting a non-linear element is to introduce a **compensating non-linear element** into the system. This method is illustrated in Figure 3.4. Given a non-linear element, described by $U(I)$, we need a compensating element $C(U)$, such that the overall characteristics $C[U(I)]$ of the elements together are as close to the ideal straight line as possible. The method is illustrated in Figure 3.4 by the use of a deflection bridge to compensate for the non-linear characteristics of a thermistor. A detailed procedure for the design of the bridge is given in Section 9.1.

The most obvious method of reducing the effects of environmental inputs is that of **isolation**, i.e. to isolate the transducer from environmental changes so that effectively $I_M = I_I = 0$. Examples of this are the placing of the reference junction of a thermocouple in a temperature-controlled enclosure, and the use of spring mountings to isolate a transducer from the vibrations of the structure to which it is attached. Another obvious method is that of **zero environmental sensitivity**, where the element is completely insensitive to environmental inputs, i.e. $K_M = K_I = 0$. An example of this is the use of a metal alloy with zero temperature coefficients of expansion and resistance as a strain gauge element. Such an ideal material is difficult to find, and in practice the resistance of a metal strain gauge is affected slightly by changes in ambient temperature.

A more successful method of coping with environmental inputs is that of **opposing environmental inputs**. Suppose that an element is affected by an environmental

Figure 3.4 Compensating non-linear element.

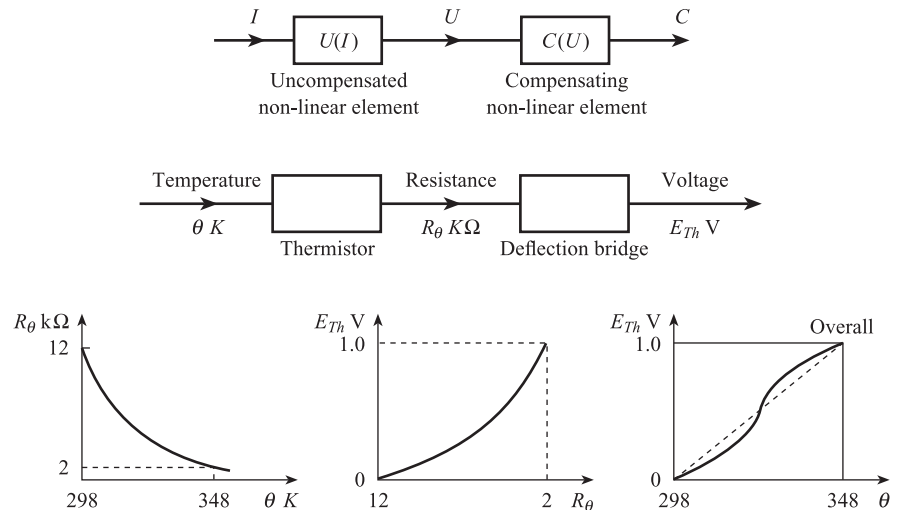
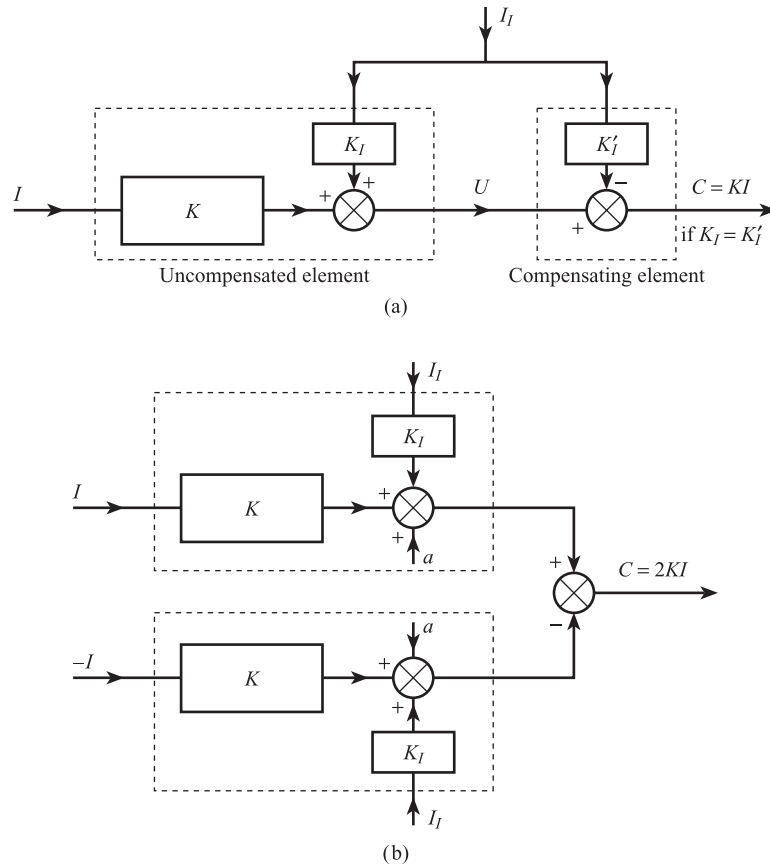


Figure 3.5 Compensation for interfering inputs:
 (a) Using opposing environmental inputs
 (b) Using a differential system.



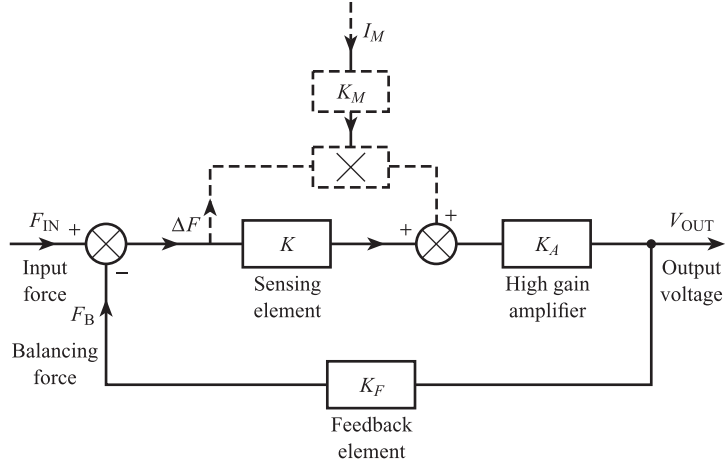
input; then a second element, subject to the same environmental input, is deliberately introduced into the system so that the two effects tend to cancel out. This method is illustrated for interfering inputs in Figure 3.5 and can be easily extended to modifying inputs.

An example is compensation for variations in the temperature T_2 of the reference junction of a thermocouple. For a copper–constantan thermocouple (Figure 2.12(b)), we have $K_I I_I$ equal to $-38.74 T_2 \mu\text{V}$ so that a compensating element giving an output equal to $+38.74 T_2 \mu\text{V}$ is required. The design of the reference junction compensation element is discussed in Sections 8.5 and 9.1 and Problem 9.2.

An example of a **differential system** (Figure 3.5(b)) is the use of two matched strain gauges in adjacent arms of a bridge to provide compensation for ambient temperature changes. One gauge is measuring a tensile strain $+e$ and the other an equal compressive strain $-e$. The bridge effectively subtracts the two resistances so that the strain effect is doubled and the environmental effects cancel out.

The use of **high-gain negative feedback** is an important method of compensating for modifying inputs and non-linearity. Figure 3.6 illustrates the technique for a force transducer. The voltage output of a force-sensing element, subject to a modifying input, is amplified by a high-gain amplifier. The amplifier output is fed back to an element (e.g. a coil and permanent magnet) which provides a balancing force to oppose the input force.

Figure 3.6 Closed loop force transducer.



Ignoring the effects of the modifying input for the moment we have:

$$\Delta F = F_{IN} - F_B \quad [3.11]$$

$$V_{OUT} = KK_A \Delta F \quad [3.12]$$

$$F_B = K_F V_{OUT} \quad [3.13]$$

i.e.

$$\frac{V_{OUT}}{KK_A} = F_{IN} - K_F V_{OUT}$$

giving

Equation for force transducer with negative feedback

$$V_{OUT} = \frac{KK_A}{1 + KK_A K_F} F_{IN} \quad [3.14]$$

If the amplifier gain K_A is made large such that the condition

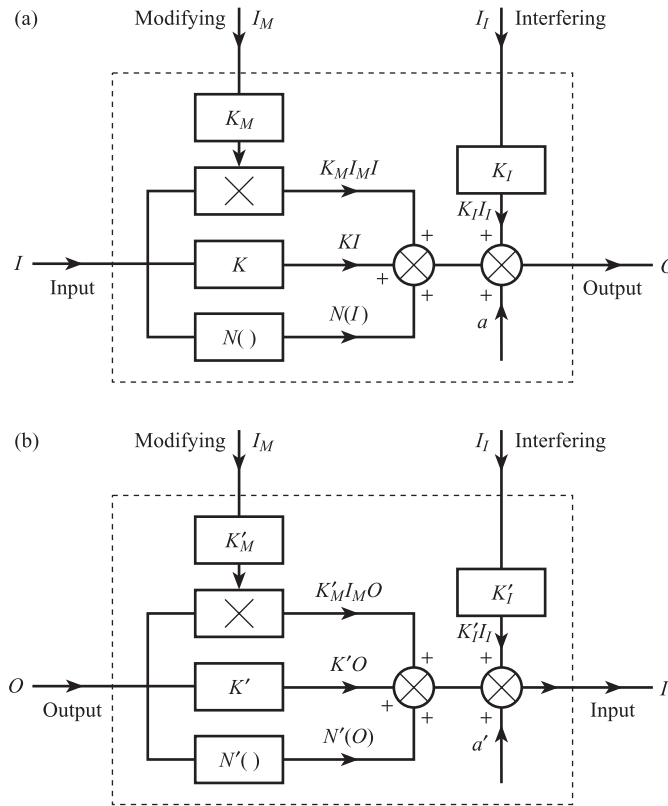
$$KK_A K_F \gg 1 \quad [3.15]$$

is satisfied, then $V_{OUT} \approx \frac{1}{K_F} F_{IN}$. This means that the system output depends only on the gain K_F of the feedback element and is independent of the gains K and K_A in the forward path. This means that, provided the above condition is obeyed, changes in K and K_A due to modifying inputs and/or non-linear effects have negligible effect on V_{OUT} . This can be confirmed by repeating the above analysis with K replaced by $K + K_M I_M$, giving

$$V_{OUT} = \frac{(K + K_M I_M) K_A}{1 + (K + K_M I_M) K_A K_F} F_{IN} \quad [3.16]$$

which again reduces to $V_{OUT} \approx \frac{F_{IN}}{K_F}$ if $(K + K_M I_M) K_A K_F \gg 1$. We now, of course, have to ensure that the gain K_F of the feedback element does not change due to non-linear or environmental effects. Since the amplifier provides most of the required power, the feedback element can be designed for low power-handling capacity,

Figure 3.7 Models for system element:
(a) Direct
(b) Inverse.



giving greater linearity and less susceptibility to environmental inputs. A commonly used device which employs this principle is discussed in Section 9.4.

The rapid fall in the cost of digital integrated circuits in recent years has meant that microcontrollers are now widely used as signal-processing elements in measurement systems (Chapter 10). This means that the powerful techniques of **computer estimation of measured value** can now be used. For this method, a good model of the elements in the system is required. In Sections 2.1 and 2.2 we saw that the steady-state output O of an element is in general given by an equation of the form:

Direct equation

$$O = KI + a + N(I) + K_M I_M I + K_I I_I \quad [2.9]$$

This is the **direct equation** (Figure 3.7(a)); here O is the dependent variable, which is expressed in terms of the independent variables I , I_M and I_I . In Section 2.4.2 we saw how the direct equation could be derived from sets of data obtained in a calibration experiment. In Section 3.2 eqn [2.9] was used to derive the error probability density function for a complete measurement system.

The steady-state characteristics of an element can also be represented by an alternative equation. This is the **inverse equation** (Figure 3.7(b)); here the signal input I is the dependent variable and the output O and environmental inputs I_I and I_M are the independent variables. The general form of this equation is:

Inverse equation

$$I = K'O + N'(O) + a' + K'_M I_M O + K'_I I_I \quad [3.17]$$

where the values of K' , $N'()$, a' , etc., are quite different from those for the direct equation. For example, the direct and inverse equations for a copper–constantan (type T) thermocouple with reference junction at 0 °C are:

DIRECT

$$E = 3.845 \times 10^{-2}T + 4.682 \times 10^{-5}T^2 - 3.789 \times 10^{-8}T^3 + 1.652 \times 10^{-11}T^4 \text{ mV}$$

INVERSE

$$T = 25.55E - 0.5973E^2 + 2.064 \times 10^{-2}E^3 - 3.205 \times 10^{-4}E^4 \text{ °C} \quad [3.18]$$

where E is the thermocouple e.m.f. and T the measured junction temperature between 0 and 400 °C. Both equations were derived using a least squares polynomial fit to IEC 584.1 data; for the direct equation E is the dependent variable and T the independent variable; for the inverse equation T is the dependent variable and E the independent variable. While the direct equation is more useful for **error estimation**, the inverse equation is more useful for **error reduction**.

The use of the inverse equation in computer estimation of measured value is best implemented in a number of stages; with reference to Figure 3.8(a), these are:

1. Treat the uncompensated system as a single element. Using the calibration procedure of Section 2.4.2 (or any other method of generating data) the parameters K' , a' , etc. in the inverse model equation:

$$I = K'U + N'(U) + a' + K'_M I_M U + K'_I I_I \quad [3.19]$$

representing the overall behaviour of the uncompensated system can be found. This procedure will enable major environmental inputs I_M and I_I to be identified (there may be more than one of each type).

2. The uncompensated system should be connected to the estimator. This consists firstly of a computer which stores the model parameters K' , a' , $N'()$, etc. If errors due to environmental inputs are considered significant, then environmental sensors to provide the computer with estimates I'_M , I'_I , of these inputs are also necessary. The output U of the uncompensated system is also fed to the computer.
3. The computer then calculates an initial estimate I' of I using the inverse equation:

$$I' = K'U + N'(U) + a' + K'_M I'_M U + K'_I I'_I \quad [3.20]$$

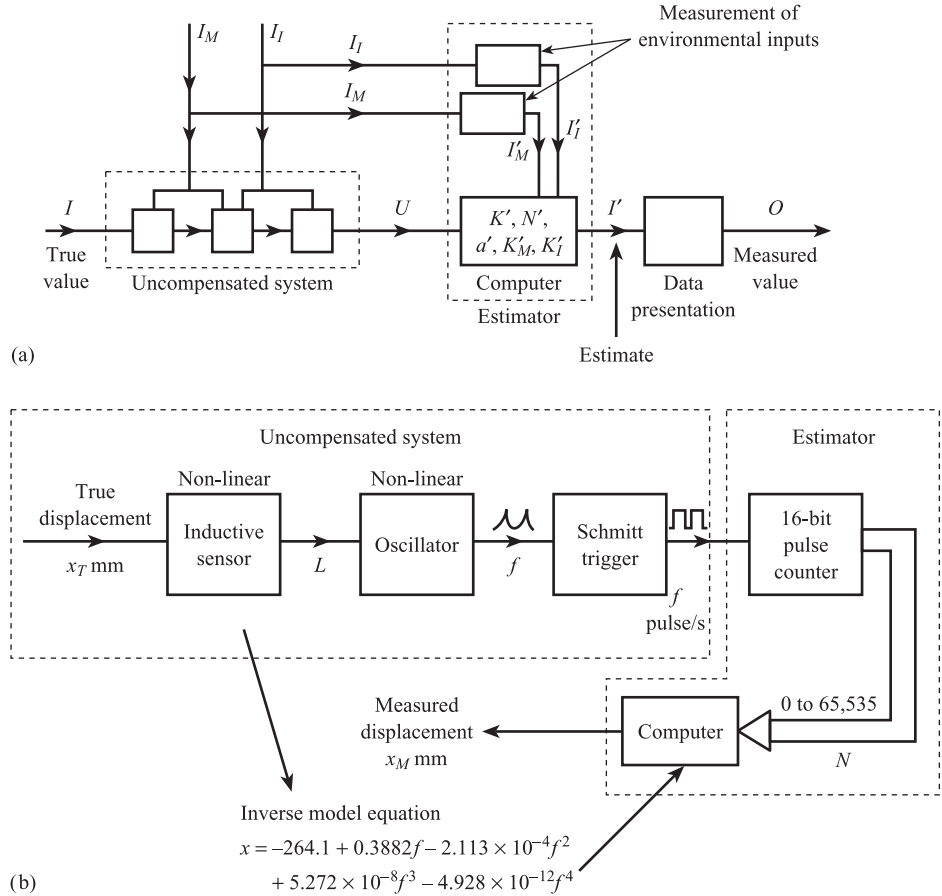
4. The data presentation element then displays the measured value O , which should be close to I' . In applications not requiring the highest accuracy the procedure can be terminated at this stage.
5. If high accuracy is required, then it may be possible to further improve the estimator by calibrating the complete system. Values of system output O are measured for a range of known standard inputs I and the corresponding values of system error $E = O - I$ are calculated. These error values will be mainly due to random effects but may also contain a small systematic component which can be corrected for.
6. An attempt should now be made to fit the data set (O_i, E_i) , $i = 1, 2, \dots, n$, by a least squares straight line of the form:

$$E = kO + b \quad [3.21]$$

where b is any residual zero error and k specifies any residual scale error. There is little point in attempting a polynomial fit at this stage.

Figure 3.8 Computer estimation of measured value using inverse model equation:

(a) Principles
(b) Example of displacement measurement system.



7. The correlation coefficient:

$$r = \frac{\sum_{i=1}^{i=n} O_i E_i}{\sqrt{\sum_{i=1}^{i=n} O_i^2 \times \sum_{i=1}^{i=n} E_i^2}} \quad [3.22]$$

between E and O data should now be evaluated. If the magnitude of r is greater than 0.5, then there is reasonable correlation between the E and O data; this means the systematic error of eqn [3.7] is present and we can proceed to stage 8 to correct for it. If the magnitude of r is less than 0.5, then there is no correlation between the E and O data; this means that the errors E are purely random and no correction can be made.

8. If appropriate, eqn [3.21] can be used to calculate an improved measured value:

$$O' = O - E = O - (kO + b) \quad [3.23]$$

The displacement measurement system of Figure 3.8(b) shows this method. The uncompensated system consists of an inductive displacement sensor, an oscillator (Section 9.5) and a Schmitt trigger (Section 10.1.4). The sensor has a non-linear

relation between inductance L and displacement x , the oscillator a non-linear relation between frequency f and inductance L . This means that the inverse model equation, relating displacement x and frequency f of the Schmitt trigger output signal, has the non-linear form shown. The estimator consists of a 16-bit pulse counter and a computer. The computer reads the state of the counter at the beginning and end of a fixed time interval and thus measures the frequency f of the pulse signal. The computer then calculates x from the inverse model equation using model coefficients stored in memory.

Conclusion

This chapter has shown how to find the **error** of a complete measurement system under **steady-state** conditions. **Measurement error** was first defined and then the **error probability density function** was derived, firstly for a general system of non-ideal elements and then for the typical example of a temperature measurement system. The last section discussed a range of methods for **error reduction**.

Reference

- [1] KENNEDY J B and NEVILLE A 1986 *Basic Statistical Methods for Engineers and Scientists*, 3rd edn, pp. 345–60. Harper and Row, New York.

Problems

- 3.1 A measurement system consists of a chromel–alumel thermocouple (with cold junction compensation), a millivolt-to-current converter and a recorder. Table Prob. 1 gives the model equations, and parameters for each element. Assuming that all probability distributions are normal, calculate the mean and standard deviation of the error probability distribution, when the input temperature is 117 °C.

Table Prob. 1.

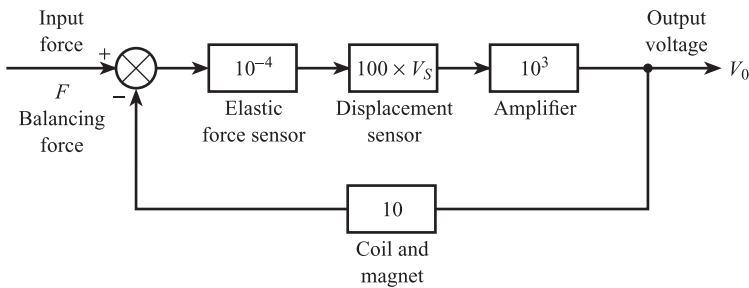
	Chromel–alumel thermocouple	e.m.f.-to-current converter	Recorder
Model equation	$E = C_0 + C_1T + C_2T^2$	$i = K_1E + K_ME\Delta T_a + K_I\Delta T_a + a_1$	$T_M = K_2i + a_2$
Mean values	$\bar{C}_0 = 0.00$ $\bar{C}_1 = 4.017 \times 10^{-2}$ $\bar{C}_2 = 4.66 \times 10^{-6}$	$\bar{K}_1 = 3.893$ $\Delta T_a = -10$ $\bar{a}_1 = -3.864$ $\bar{K}_M = 1.95 \times 10^{-4}$ $\bar{K}_I = 2.00 \times 10^{-3}$	$\bar{K}_2 = 6.25$ $\bar{a}_2 = 25.0$
Standard deviations	$\sigma_{C_0} = 6.93 \times 10^{-2}$ $\sigma_{C_1} = \sigma_{C_2} = 0$	$\sigma_{a_1} = 0.14, \sigma_{\Delta T_a} = 10$ $\sigma_{K_1} = \sigma_{K_M} = \sigma_{K_I} = 0$	$\sigma_{a_2} = 0.30$ $\sigma_{K_2} = 0.0$

Table Prob. 2.

Element	Linear sensitivity K	Error bandwidth $\pm h$
Pressure sensor	$10^{-4} \Omega \text{ Pa}^{-1}$	$\pm 0.005 \Omega$
Deflection bridge	$4 \times 10^{-2} \text{ mV } \Omega^{-1}$	$\pm 5 \times 10^{-4} \text{ mV}$
Amplifier	10^3 mV mV^{-1}	$\pm 0.5 \text{ mV}$
Recorder	250 Pa mV^{-1}	$\pm 100 \text{ Pa}$

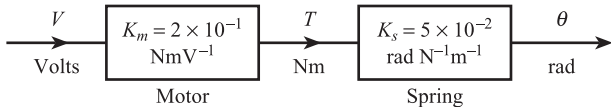
- 3.2
- A pressure measurement system consists of a pressure sensor, deflection bridge, amplifier and recorder. Table Prob. 2 gives the linear sensitivities and error bandwidths for each element in the system.
- (a)
- Calculate the standard deviation σ_E of the error distribution function.
- (b)
- Given that the recorder is incorrectly adjusted so that its sensitivity is 225 Pa mV^{-1} , calculate the mean error \bar{E} for an input pressure of $5 \times 10^3 \text{ Pa}$.
- 3.3
- Figure Prob. 3 shows a block diagram of a force transducer using negative feedback. The elastic sensor gives a displacement output for a force input; the displacement sensor gives a voltage output for a displacement input. V_s is the supply voltage for the displacement sensor.
- (a)
- Calculate the output voltage V_0 when
- (i)
- $V_s = 1.0 \text{ V}, F = 50 \text{ N}$
- (ii)
- $V_s = 1.5 \text{ V}, F = 50 \text{ N}$.
- (b)
- Comment on the practical significance of the variation of the supply voltage V_s .

Figure Prob. 3.



- 3.4
- Figure Prob. 4 is a block diagram of a voltmeter. The motor produces a torque T proportional to voltage V , and the output angular displacement θ of the spring is proportional to T . The stiffness K_s of the spring can vary by $\pm 10\%$ about the nominal value of $5 \times 10^{-2} \text{ rad N}^{-1}\text{m}^{-1}$. Given that the following are available:
- (i)
- a d.c. voltage amplifier of gain 1000
- (ii)
- a voltage subtraction unit
- (iii)
- a stable angular displacement transducer of sensitivity 100 V rad^{-1} ,
- (a)
- draw a block diagram of a modified system using these components, which reduces the effect of changes in K_s ;
- (b)
- calculate the effect of a 10% increase in K_s on the sensitivity of the **modified** system.

Figure Prob. 4.



3.5 A temperature measurement system consists of a thermocouple, an amplifier, an 8-bit analogue-to-digital converter and a microcontroller with display facilities. Table Prob. 5 gives the model equations and parameters for each element in the system. The temperature of the thermocouple measurement junction is T_1 °C and the temperature of the reference junction is T_2 °C. The microcontroller corrects for T_2 having a non-zero mean value.

- Estimate the mean and standard deviation of the error probability density function when the input temperature T_1 is 100 °C. Treat rectangular distribution as normal with $\sigma = h/\sqrt{3}$.
- Explain briefly what modifications should be made to the system to reduce the quantities calculated in (a).

Table Prob. 5.

	Thermocouple	Amplifier	Analogue-to-digital converter	Microcontroller with display
Model equations	$E_{T_1, T_2} = a_0 + a_1(T_1 - T_2) + a_2(T_1^2 - T_2^2)$	$V = K_1 E_{T_1, T_2} + b_1$	$n = K_2 V + b_2$	$T_m = K_3 n + b_3$
Mean values	$\bar{a}_0 = 0$ $\bar{a}_1 = 4.3796 \times 10^{-2}$ $\bar{a}_2 = -1.7963 \times 10^{-5}$ $\bar{T}_2 = 20$	$\bar{K}_1 = 255$ $\bar{b}_1 = 0.0$	$\bar{K}_2 = 0.1$ $\bar{b}_2 = 0.0$ n rounded to nearest integer	$\bar{K}_3 = 1.0$ $\bar{b}_3 = 20$
Statistical distributions	Normal with $\sigma_{a_0} = 0.05$ $\sigma_{T_2} = 2.0$ $\sigma_{a_1} = \sigma_{a_2} = 0.0$	Normal with $\sigma_{b_1} = 5.0$ $\sigma_{K_1} = 0.0$	b_2 has a rectangular distribution of width ± 0.5 $\sigma_{K_2} = 0.0$	$\sigma_{K_3} = 0.0$ $\sigma_{b_3} = 0.0$

3.6 A fluid velocity measurement system consists of a pitot tube, a differential pressure transmitter, an 8-bit analogue-to-digital converter and a microcontroller with display facilities. Table Prob. 6 gives the model equations and parameters for each element in the system. The microcontroller calculates the measured value of velocity assuming a constant density.

- Estimate the mean and standard deviation of the error probability density function assuming the true value of velocity v_T is 14.0 m s⁻¹. Use the procedure of Table 3.1, treating the rectangular distributions as normal with $\sigma = h/\sqrt{3}$.
- Explain briefly what modifications could be made to the system to reduce the quantities calculated in (a).

Table Prob. 6.

	Pitot tube	Differential pressure transmitter	Analogue-to-digital converter	Microcontroller with display
Model equations	$\Delta P = \frac{1}{2} \rho v_T^2$	$i = K_1 \Delta P + a_1$	$n = K_2 i + a_2$	$v_M = K_3 \sqrt{n - 51}$
Mean values	$\bar{\rho} = 1.2$	$\bar{K}_1 = 0.064$ $\bar{a}_1 = 4.0$	$\bar{K}_2 = 12.80$ $\bar{a}_2 = 0.0$ n rounded off to nearest integer	$\bar{K}_3 = 1.430$
Half-widths of rectangular distribution	$h_\rho = 0.1$	$h_{a_1} = 0.04$	$h_{a_2} = 0.5$	$h_{K_3} = 0.0$

- 3.7 A temperature measurement system consists of a thermistor, bridge and recorder. Table Prob. 7 gives the model equations, mean values and standard deviations for each element in the system. Assuming all probability distributions are normal, calculate the mean and standard deviation of the error probability density function for a true input temperature of 320 K.

Table Prob. 7.

	Thermistor	Bridge	Recorder
Model equations	$R_\theta = K_1 \exp\left(\frac{\beta}{\theta}\right)$	$V_0 = V_s \left\{ \frac{1}{1 + \frac{3.3}{R_\theta}} - a_1 \right\}$	$\theta_M = K_2 V_0 + a_2$
Mean values	$\bar{K}_1 = 5 \times 10^{-4} \text{ k}\Omega$ $\bar{\beta} = 3 \times 10^3 \text{ K}$	$\bar{V}_s = -3.00 \text{ V}$ $\bar{a}_1 = 0.77$	$\bar{K}_2 = 50.0 \text{ K/V}$ $\bar{a}_2 = 300 \text{ K}$
Standard deviations	$\sigma_{K_1} = 0.5 \times 10^{-4}$ $\sigma_\beta = 0$	$\sigma_{V_s} = 0.03$ $\sigma_{a_1} = 0.01$	$\sigma_{K_2} = 0.0$ $\sigma_{a_2} = 3.0$

Basic problems

- 3.8 A force measurement system consists of four elements with sensitivities 10^{-2} , 5×10^{-2} , 10^3 and 1.9. Find the system error for a true value input of 10 kN.
- 3.9 A level measurement system consists of three linear elements with sensitivities of 0.050, 21.5 and 0.99. Find the system error for a true value input of 5.0 metres.

4 Dynamic Characteristics of Measurement Systems

If the input signal I to an element is changed suddenly, from one value to another, then the output signal O will not instantaneously change to its new value. For example, if the temperature input to a thermocouple is suddenly changed from 25 °C to 100 °C, some time will elapse before the e.m.f. output completes the change from 1 mV to 4 mV. The ways in which an element responds to sudden input changes are termed its **dynamic characteristics**, and these are most conveniently summarised using a **transfer function** $G(s)$. The first section of this chapter examines the dynamics of typical elements and derives the corresponding transfer function. The next section examines how standard test signals can be used to identify $G(s)$ for an element. If the input signal to a multi-element measurement system is changing rapidly, then the waveform of the system output signal is in general different from that of the input signal. Section 4.3 explains how this **dynamic error** can be found, and the final section outlines **dynamic compensation** methods that can be used to minimise errors.

4.1 Transfer function $G(s)$ for typical system elements

4.1.1 First-order elements

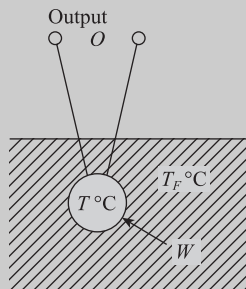


Figure 4.1 Temperature sensor in fluid.

A good example of a first-order element is provided by a temperature sensor with an electrical output signal, e.g. a thermocouple or thermistor. The bare element (not enclosed in a sheath) is placed inside a fluid (Figure 4.1). Initially at time $t = 0^-$ (just before $t = 0$), the sensor temperature is equal to the fluid temperature, i.e. $T(0^-) = T_F(0^-)$. If the fluid temperature is suddenly raised at $t = 0$, the sensor is no longer in a steady state, and its dynamic behaviour is described by the **heat balance equation**:

$$\text{rate of heat inflow} - \text{rate of heat outflow} = \frac{\text{rate of change of sensor heat content}}{[4.1]}$$

Assuming that $T_F > T$, then the rate of heat outflow will be zero, and the rate of heat inflow W will be proportional to the temperature difference ($T_F - T$). From Chapter 14 we have

$$W = UA(T_F - T) \text{ watts} \quad [4.2]$$

where $U \text{ W m}^{-2} \text{ }^\circ\text{C}^{-1}$ is the overall heat transfer coefficient between fluid and sensor and $A \text{ m}^2$ is the effective heat transfer area. The increase of heat content of the sensor is $MC[T - T(0-)]$ joules, where $M \text{ kg}$ is the sensor mass and $C \text{ J kg}^{-1} \text{ }^\circ\text{C}^{-1}$ is the specific heat of the sensor material. Thus, assuming M and C are constants:

$$\text{rate of increase of sensor heat content} = MC \frac{d}{dt} [T - T(0-)] \quad [4.3]$$

Defining $\Delta T = T - T(0-)$ and $\Delta T_F = T_F - T_F(0-)$ to be the deviations in temperatures from initial steady-state conditions, the differential equation describing the sensor temperature changes is

$$UA(\Delta T_F - \Delta T) = MC \frac{d\Delta T}{dt}$$

i.e.

$$\frac{MC}{UA} \frac{d\Delta T}{dt} + \Delta T = \Delta T_F \quad [4.4]$$

This is a **linear differential equation** in which $d\Delta T/dt$ and ΔT are multiplied by constant coefficients; the equation is **first order** because $d\Delta T/dt$ is the highest derivative present. The quantity MC/UA has the dimensions of time:

$$\frac{\text{kg} \times \text{J} \times \text{kg}^{-1} \times \text{ }^\circ\text{C}^{-1}}{\text{W} \times \text{m}^{-2} \times \text{ }^\circ\text{C}^{-1} \times \text{m}^2} = \frac{\text{J}}{\text{W}} = \text{seconds}$$

and is referred to as the **time constant** τ for the system. The differential equation is now:

*Linear first-order
differential equation*

$$\tau \frac{d\Delta T}{dt} + \Delta T = \Delta T_F \quad [4.5]$$

While the above differential equation is a perfectly adequate description of the dynamics of the sensor, it is not the most useful representation. The transfer function based on the Laplace transform of the differential equation provides a convenient framework for studying the dynamics of multi-element systems. The Laplace transform $\tilde{f}(s)$ of a time-varying function is defined by:

*Definition of Laplace
transform*

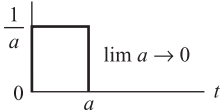
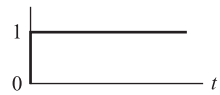
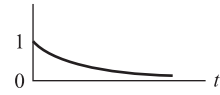
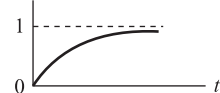


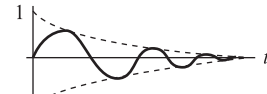

$$\tilde{f}(s) = \int_0^\infty e^{-st} f(t) dt \quad [4.6]$$

where s is a complex variable of the form $\sigma + j\omega$ where $j = \sqrt{-1}$.

Table 4.1 gives Laplace transforms for some common standard functions $f(t)$. In order to find the transfer function for the sensor we must find the Laplace transform of eqn [4.5]. Using Table 4.1 we have:

$$\tau[s\tilde{\Delta T}(s) - \Delta T(0-)] + \tilde{\Delta T}(s) = \Delta \tilde{T}_F(s) \quad [4.7]$$

Table 4.1 Laplace transforms of common time functions $f(t)$.^a

$\mathcal{L}[f(t)] = \tilde{f}(s) = \int_0^{\infty} e^{-st} f(t) dt$			
Function	Symbol	Graph	Transform
1st derivative	$\frac{d}{dt}f(t)$		$s\tilde{f}(s) - f(0-)$
2nd derivative	$\frac{d^2}{dt^2}f(t)$		$s^2\tilde{f}(s) - sf(0-) - \dot{f}(0-)$
Unit impulse	$\delta(t)$		1
Unit step	$\mu(t)$		$\frac{1}{s}$
Exponential decay	$\exp(-\alpha t)$		$\frac{1}{s + \alpha}$
Exponential growth	$1 - \exp(-\alpha t)$		$\frac{\alpha}{s(s + \alpha)}$
Sine wave	$\sin \omega t$		$\frac{\omega}{s^2 + \omega^2}$
Phase-shifted sine wave	$\sin(\omega t + \phi)$		$\frac{\omega \cos \phi + s \sin \phi}{s^2 + \omega^2}$
Exponentially damped sine wave	$\exp(-\alpha t) \sin \omega t$		$\frac{\omega}{(s + \alpha)^2 + \omega^2}$
Ramp with exponential decay	$t \exp(-\alpha t)$		$\frac{1}{(s + \alpha)^2}$

^a Initial conditions are at $t = 0-$, just prior to $t = 0$.

where $\Delta T(0-)$ is the temperature deviation at initial conditions prior to $t = 0$. By definition, $\Delta T(0-) = 0$, giving:

$$\tau s \Delta \tilde{T}(s) + \Delta \tilde{T}(s) = \Delta \tilde{T}_F(s)$$

i.e.

$$(\tau s + 1) \Delta \tilde{T}(s) = \Delta \tilde{T}_F(s) \quad [4.8]$$

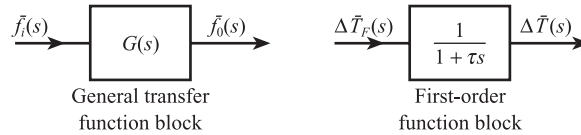
The transfer function $G(s)$ of an element is defined as the ratio of the Laplace transform of the output to the Laplace transform of the input, provided the initial conditions are zero. Thus:

Definition of element
transfer function

$$G(s) = \frac{\bar{f}_0(s)}{\bar{f}_i(s)} \quad [4.9]$$

and $\bar{f}_0(s) = G(s)\bar{f}_i(s)$; this means the transfer function of the output signal is simply the product of the element transfer function and the transfer function of the input signal. Because of this simple relationship the transfer function technique lends itself to the study of the dynamics of multi-element systems and block diagram representation (Figure 4.2).

Figure 4.2 Transfer function representation.



From eqns [4.8] and [4.9] the transfer function for a first-order element is:

Transfer function for
a first-order element

$$G(s) = \frac{\Delta \bar{T}(s)}{\Delta \bar{T}_F(s)} = \frac{1}{1 + \tau s} \quad [4.10]$$

The above transfer function only relates changes in sensor temperature to changes in fluid temperature. The overall relationship between changes in sensor output signal O and fluid temperature is:

$$\frac{\Delta \bar{O}(s)}{\Delta \bar{T}_F(s)} = \frac{\Delta O}{\Delta T} \frac{\Delta \bar{T}(s)}{\Delta \bar{T}_F(s)} \quad [4.11]$$

where $\Delta O/\Delta T$ is the **steady-state sensitivity** of the temperature sensor. For an ideal element $\Delta O/\Delta T$ will be equal to the slope K of the **ideal straight line**. For non-linear elements, subject to small temperature fluctuations, we can take $\Delta O/\Delta T = dO/dT$, the derivative being evaluated at the steady-state temperature $T(0-)$ around which the fluctuations are taking place. Thus for a copper–constantan thermocouple measuring small fluctuations in temperature around 100 °C, $\Delta E/\Delta T$ is found by evaluating dE/dT at 100 °C (see Section 2.1) to give $\Delta E/\Delta T = 35 \mu\text{V } ^\circ\text{C}^{-1}$. Thus if the time constant of the thermocouple is 10 s the overall dynamic relationship between changes in e.m.f. and fluid temperature is:

$$\frac{\Delta \bar{E}(s)}{\Delta \bar{T}_F(s)} = 35 \times \frac{1}{1 + 10s} \quad [4.12]$$

In the general case of an element with static characteristics given by eqn [2.9] and dynamic characteristics defined by $G(s)$, the effect of small, rapid changes in ΔI is evaluated using Figure 4.3, in which steady-state sensitivity $(\partial O/\partial I)_{I_0} = K + K_M I_M + (dN/dI)_{I_0}$, and I_0 is the steady-state value of I around which the fluctuations are

Figure 4.3 Element model for dynamic calculations.

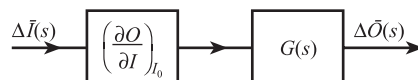
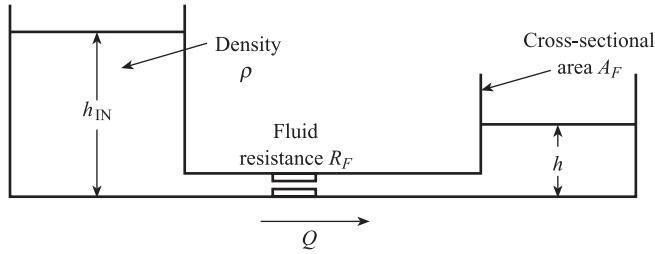


Table 4.2 Analogous first-order elements.

Fluidic



$$\text{Volume flow rate } Q = \frac{1}{R_F} (P_{IN} - P)$$

$$\text{Pressures } P_{IN} = h_{IN} \rho g, P = h \rho g$$

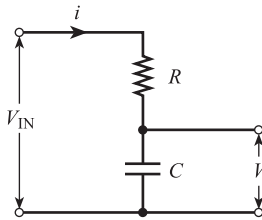
$$A_F \frac{dh}{dt} = Q = \frac{\rho g}{R_F} (h_{IN} - h)$$

$$\frac{A_F R_F}{\rho g} \frac{dh}{dt} + h = h_{IN}$$

i.e.

$$\tau_F \frac{dh}{dt} + h = h_{IN}, \tau_F = \frac{A_F R_F}{\rho g}$$

Electrical



$$V_{IN} - V = iR$$

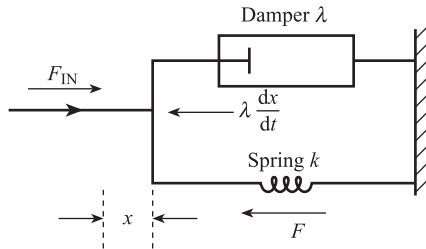
$$\text{Charge } q = CV, \text{ current } i = \frac{dq}{dt} = \frac{C dV}{dt}$$

$$RC \frac{dV}{dt} + V = V_{IN}$$

i.e.

$$\tau_E \frac{dV}{dt} + V = V_{IN}, \tau_E = RC$$

Mechanical



$$F_{IN} - F = \lambda \frac{dx}{dt}, \lambda \text{ N s m}^{-1} = \text{damping constant}$$

$$\text{Displacement } x = \frac{F}{k}, k \text{ N m}^{-1} = \text{spring stiffness}$$

$$\frac{\lambda}{k} \frac{dF}{dt} + F = F_{IN}$$

$$\tau_M \frac{dF}{dt} + F = F_{IN}, \tau_M = \frac{\lambda}{k}$$

$$\text{Thermal } \tau_{Th} = \frac{MC}{UA} = R_{Th} C_{Th}; R_{Th} = \frac{1}{UA}, C_{Th} = MC$$

$$\text{Fluidic } \tau_F = \frac{A_F R_F}{\rho g} = R_F C_F; R_F = R_F, C_F = \frac{A_F}{\rho g}$$

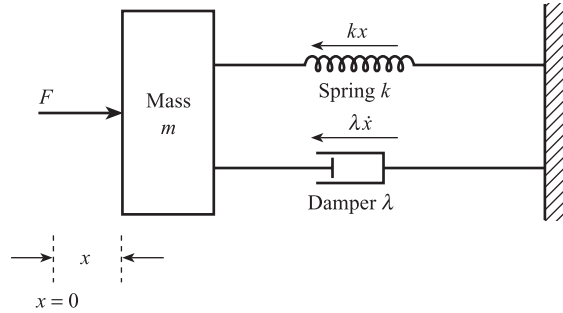
$$\text{Electrical } \tau_E = RC = R_E C_E; R_E = R, C_E = C$$

$$\text{Mechanical } \tau_M = \frac{\lambda}{k} = R_M C_M; R_M = \lambda, C_M = \frac{1}{k}$$

taking place. Table 4.2 shows analogous fluidic, electrical and mechanical elements, which are also described by a first-order transfer function $G(s) = 1/(1 + \tau s)$. All four elements are characterised by ‘resistance’ and ‘capacitance’ as illustrated in the table. Temperature, pressure, voltage and force are analogous ‘driving’ or effort variables; heat flow rate, volume flow rate, current and velocity are analogous ‘driven’ or flow variables. These analogies are discussed further in Section 5.2.

Figure 4.4

Mass–spring–damper model of elastic force sensor.



4.1.2 Second-order elements

The elastic sensor shown in Figure 4.4, which converts a force input F into a displacement output x , is a good example of a second-order element. The diagram is a conceptual model of the element, which incorporates a mass m kg, a spring of stiffness k N m⁻¹, and a damper of constant λ N s m⁻¹. The system is initially at rest at time $t = 0^-$ so that the initial velocity $\dot{x}(0^-) = 0$ and the initial acceleration $\ddot{x}(0^-) = 0$. The initial input force $F(0^-)$ is balanced by the spring force at the initial displacement $x(0^-)$, i.e.

$$F(0^-) = kx(0^-) \quad [4.13]$$

If the input force is suddenly increased at $t = 0$, then the element is no longer in a steady state and its dynamic behaviour is described by Newton's second law, i.e.

resultant force = mass × acceleration

i.e.

$$F - kx - \lambda\dot{x} = m\ddot{x} \quad [4.14]$$

and

$$m\ddot{x} + \lambda\dot{x} + kx = F$$

Defining ΔF and Δx to be the deviations in F and x from initial steady-state conditions:

$$\begin{aligned} \Delta F &= F - F(0^-), & \Delta x &= x - x(0^-) \\ \Delta \dot{x} &= \dot{x}, & \Delta \ddot{x} &= \ddot{x} \end{aligned} \quad [4.15]$$

the differential equation now becomes:

$$m\Delta\ddot{x} + \lambda\Delta\dot{x} + kx(0^-) + k\Delta x = F(0^-) + \Delta F$$

which, using [4.13], reduces to:

$$m\Delta\ddot{x} + \lambda\Delta\dot{x} + k\Delta x = \Delta F$$

i.e.

$$\frac{m}{k} \frac{d^2\Delta x}{dt^2} + \frac{\lambda}{k} \frac{d\Delta x}{dt} + \Delta x = \frac{1}{k} \Delta F \quad [4.16]$$

This is a **second-order linear differential equation** in which Δx and its derivatives are multiplied by constant coefficients and the highest derivative present is $d^2\Delta x/dt^2$. If we define

$$\text{undamped natural frequency } \omega_n = \sqrt{\frac{k}{m}} \text{ rad/s}$$

and

$$\text{damping ratio } \xi = \frac{\lambda}{2\sqrt{km}} \quad [4.17]$$

then $m/k = 1/\omega_n^2$, $\lambda/k = 2\xi/\omega_n$, and [4.16] can be expressed in the standard form:

Linear second-order differential equation

$$\frac{1}{\omega_n^2} \frac{d^2 \Delta x}{dt^2} + \frac{2\xi}{\omega_n} \frac{d\Delta x}{dt} + \Delta x = \frac{1}{k} \Delta F \quad [4.18]$$

In order to find the transfer function for the element we require the Laplace transform of eqn [4.18]. Using Table 4.1 we have:

$$\begin{aligned} & \frac{1}{\omega_n^2} [s^2 \Delta \bar{x}(s) - s\Delta x(0-) - \Delta \dot{x}(0-)] + \frac{2\xi}{\omega_n} [s\Delta \bar{x}(s) - \Delta x(0-)] + \Delta \bar{x}(s) \\ &= \frac{1}{k} \Delta \bar{F}(s) \end{aligned} \quad [4.19]$$

Since $\Delta \dot{x}(0-) = \dot{x}(0-) = 0$ and $\Delta x(0-) = 0$ by definition, [4.19] reduces to:

$$\left[\frac{1}{\omega_n^2} s^2 + \frac{2\xi}{\omega_n} s + 1 \right] \Delta \bar{x}(s) = \frac{1}{k} \Delta \bar{F}(s) \quad [4.20]$$

Thus

$$\frac{\Delta \bar{x}(s)}{\Delta \bar{F}(s)} = \frac{1}{k} G(s)$$

where $1/k$ = steady-state sensitivity K , and

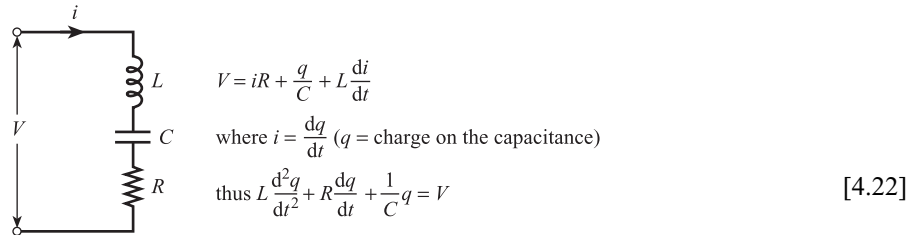
Transfer function for a second-order element

$$G(s) = \frac{1}{\frac{1}{\omega_n^2} s^2 + \frac{2\xi}{\omega_n} s + 1} \quad [4.21]$$

Figure 4.5 shows an analogous electrical element, a series L - C - R circuit.

Comparing eqns [4.14] and [4.22] we see that q is analogous to x , V is analogous to F , and L , R and $1/C$ are analogous to m , λ and k respectively (see Table 5.1). The electrical circuit is also described by the above second-order transfer function with $\omega_n = 1/\sqrt{LC}$ and $\xi = (R/2)\sqrt{C/L}$.

Figure 4.5
Series L - C - R circuit.



4.2 Identification of the dynamics of an element

In order to identify the transfer function $G(s)$ of an element, standard input signals should be used. The two most commonly used standard signals are step and sine wave. This section examines the response of first- and second-order elements to step and sine wave inputs.

4.2.1 Step response of first- and second-order elements

From Table 4.1 we see that the Laplace transform of a step of unit height $u(t)$ is $\bar{f}(s) = 1/s$. Thus if a first-order element with $G(s) = 1/(1 + \tau s)$ is subject to a unit step input signal, the Laplace transform of the element output signal is:

$$\bar{f}_o(s) = G(s)\bar{f}_i(s) = \frac{1}{(1 + \tau s)s} \quad [4.23]$$

Expressing [4.23] in partial fractions, we have:

$$\bar{f}_o(s) = \frac{1}{(1 + \tau s)s} = \frac{A}{(1 + \tau s)} + \frac{B}{s}$$

Equating coefficients of constants gives $B = 1$, and equating coefficients of s gives $0 = A + B\tau$, i.e. $A = -\tau$. Thus:

$$\bar{f}_o(s) = \frac{1}{s} - \frac{\tau}{(1 + \tau s)} = \frac{1}{s} - \frac{1}{(s + 1/\tau)} \quad [4.24]$$

Using Table 4.1 in reverse, i.e. finding a time signal $f(t)$ corresponding to a transform $\bar{f}(s)$, we have:

$$f_o(t) = u(t) - \exp\left(\frac{-t}{\tau}\right)$$

and since $u(t) = 1$ for $t > 0$:

Response of first-order element to unit step

$$f_o(t) = 1 - \exp\left(\frac{-t}{\tau}\right) \quad [4.25]$$

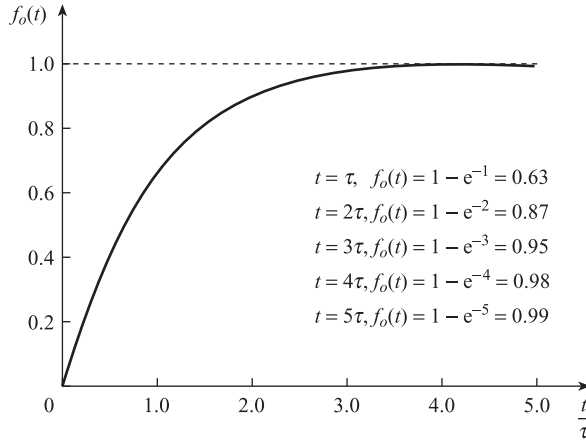
The form of the response is shown in Figure 4.6.

As an example of the use of eqn [4.25], consider the temperature sensor of Section 4.1.1. Initially the temperature of the sensor is equal to that of the fluid, i.e. $T(0-) = T_F(0-) = 25^\circ\text{C}$, say. If T_F is suddenly raised to 100°C , then this represents a step change ΔT_F of height 75°C . The corresponding *change* in sensor temperature is given by $\Delta T = 75(1 - e^{-t/\tau})$ and the actual temperature T of the sensor at time t is given by:

$$T(t) = 25 + 75(1 - e^{-t/\tau}) \quad [4.26]$$

Thus at time $t = \tau$, $T = 25 + (75 \times 0.63) = 72.3^\circ\text{C}$. By measuring the time taken for T to rise to 72.3°C we can find the time constant τ of the element.

Figure 4.6 Response of a first-order element to a unit step.



If the second-order element with transfer function

$$G(s) = \frac{1}{\frac{1}{\omega_n^2} s^2 + \frac{2\xi}{\omega_n} s + 1}$$

is subject to a unit step input signal, then the Laplace transform of the element output signal is:

$$\bar{f}_o(s) = \frac{1}{\left(\frac{1}{\omega_n^2} s^2 + \frac{2\xi}{\omega_n} s + 1 \right) s} \quad [4.27]$$

Expressing [4.27] in partial fractions we have:

$$\bar{f}_o(s) = \frac{As + B}{\left(\frac{1}{\omega_n^2} s^2 + \frac{2\xi}{\omega_n} s + 1 \right)} + \frac{C}{s} \quad [4.27]$$

where $A = -1/\omega_n^2$, $B = -2\xi/\omega_n$, $C = 1$. This gives:

$$\begin{aligned} \bar{f}_o(s) &= \frac{1}{s} - \frac{(s + 2\xi\omega_n)}{s^2 + 2\xi\omega_n s + \omega_n^2} \\ &= \frac{1}{s} - \frac{(s + 2\xi\omega_n)}{(s + \xi\omega_n)^2 + \omega_n^2(1 - \xi^2)} \\ &= \frac{1}{s} - \frac{(s + \xi\omega_n)}{(s + \xi\omega_n)^2 + \omega_n^2(1 - \xi^2)} - \frac{\xi\omega_n}{(s + \xi\omega_n)^2 + \omega_n^2(1 - \xi^2)} \end{aligned} \quad [4.28]$$

There are three cases to consider, depending on whether ξ is greater than 1, equal to 1, or less than 1. For example, if $\xi = 1$ (**critical damping**) then:

$$\bar{f}_o(s) = \frac{1}{s} - \frac{1}{s + \omega_n} - \frac{\omega_n}{(s + \omega_n)^2} \quad [4.29]$$

Using Table 4.1 we have:

Response of second-order element to a unit step, critical damping $\xi = 1$

$$f_o(t) = 1 - e^{-\omega_n t} (1 + \omega_n t) \quad [4.30]$$

Using standard tables it can be shown that if $\xi < 1$ (**underdamping**) then:

Second-order step response, underdamping $\xi < 1$

$$f_o(t) = 1 - e^{-\xi \omega_n t} \left[\cos \omega_n \sqrt{1 - \xi^2} t + \frac{\xi}{\sqrt{1 - \xi^2}} \sin \omega_n \sqrt{1 - \xi^2} t \right] \quad [4.31]$$

and if $\xi > 1$ (**overdamping**) then:

Second-order step response, overdamping $\xi > 1$

$$f_o(t) = 1 - e^{-\xi \omega_n t} \left[\cosh \omega_n \sqrt{\xi^2 - 1} t + \frac{\xi}{\sqrt{\xi^2 - 1}} \sinh \omega_n \sqrt{\xi^2 - 1} t \right] \quad [4.32]$$

We consider the case of the underdamped response with $\xi < 1$, given by eqn [4.31]. Here the **damped angular frequency** of the oscillations is given by:

$$\omega_d = \omega_n \sqrt{1 - \xi^2}$$

where ω_n is the natural or undamped angular frequency. The corresponding period T_d of the damped oscillations is given by:

$$T_d = \frac{2\pi}{\omega_d} = \frac{2\pi}{\omega_n \sqrt{1 - \xi^2}}$$

The time T_p at which the first oscillation peak occurs is correspondingly given by:

$$T_p = T_d/2 = \frac{\pi}{\omega_n \sqrt{1 - \xi^2}}$$

The **settling time** T_s taken for the response to settle out at the steady-state value is governed by the exponential decay term $e^{-\xi \omega_n t}$. When $t = 5/\xi \omega_n$, i.e. $\xi \omega_n t = 5$, then $e^{-5} = 0.0067$. The time for the response to settle out approximately within 1% is therefore:

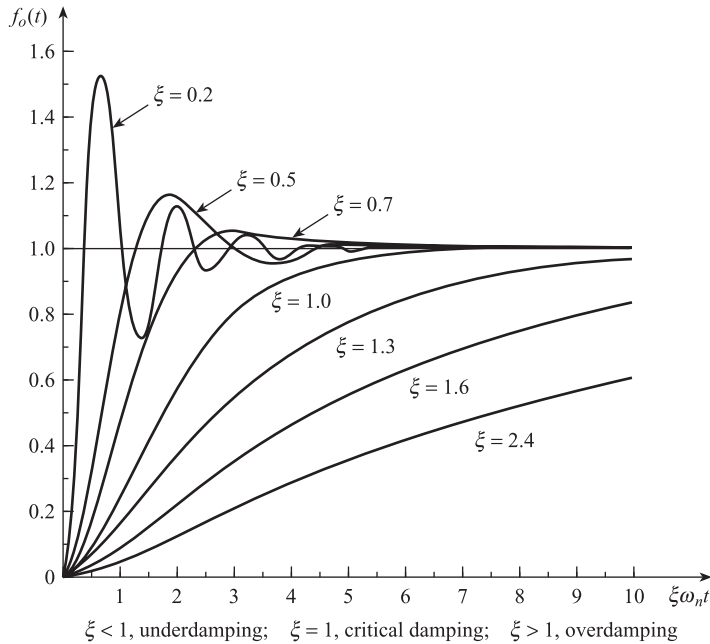
$$T_s = 5/\xi \omega_n$$

From Figure 4.7, we see that T_s is minimum when $\xi = 0.7$. The response $f_o(t)$ has a maximum value f_o^p at the peak of the first oscillation. The difference $(f_o^p - 1)$ between maximum and steady-state values of $f_o(t)$, for $\xi < 1$, is termed the **maximum overshoot** and is given by:

$$\exp \left[\frac{-\pi \xi}{\sqrt{1 - \xi^2}} \right]$$

and depends only on ξ . Thus for $\xi < 1$, an estimate of ξ can be found from measurement of maximum overshoot and then, knowing ξ , ω_n can be estimated from measurements of T_d , T_p and/or T_s .

Figure 4.7 Response of a second-order element to a unit step.



The form of the responses is shown in Figure 4.7. As an example consider the step response of a force sensor with stiffness $k = 10^3 \text{ N m}^{-1}$, mass $m = 10^{-1} \text{ kg}$ and damping constant $\lambda = 10 \text{ N s m}^{-1}$. The steady-state sensitivity $K = 1/k = 10^{-3} \text{ m N}^{-1}$, natural frequency $\omega_n = \sqrt{k/m} = 10^2 \text{ rad s}^{-1}$ and damping coefficient $\xi = \lambda/2\sqrt{km} = 0.5$. Initially at time $t = 0^-$, a steady force $F(0^-) = 10 \text{ N}$ causes a steady displacement of $(1/10^3) \times 10 \text{ metre}$, i.e. 10 mm . Suppose that at $t = 0$ the force is suddenly increased from 10 to 12 N, i.e. there is a step change ΔF of 2 N. The resulting change $\Delta x(t)$ in displacement is found using

$$\Delta x(t) = \text{steady-state sensitivity} \times \text{step height} \times \text{unit step response } f_o(t) \quad [4.33]$$

i.e.

$$\begin{aligned} \Delta x(t) &= \frac{1}{10^3} \times 2 \times [1 - e^{-50t} (\cos 86.6t + 0.58 \sin 86.6t)] \text{ metre} \\ &= 2[1 - e^{-50t} (\cos 86.6t + 0.58 \sin 86.6t)] \text{ mm} \end{aligned} \quad [4.34]$$

Here the damped angular frequency $\omega_d = 86.6 \text{ rad/s}$ and the period of the damped oscillations $T_d = 72.6 \text{ ms}$. The maximum overshoot is 0.16, giving $f_o^p = 1.16$ so that the maximum value of Δx is 2.32 mm. This occurs at time $T_p = 36.3 \text{ ms}$. Eventually as t becomes large Δx tends to 2 mm, i.e. x settles out at a new steady-state value of 12 mm with a settling time T_s of 100 ms.

4.2.2 Sinusoidal response of first- and second-order elements

From Table 4.1 we see that the Laplace transform of sine wave $f(t) = \sin \omega t$, with unit amplitude and angular frequency ω , is $\bar{f}(s) = \omega/(s^2 + \omega^2)$. Thus if a sine wave of amplitude \hat{f} is input to a first-order element, then the Laplace transform of the output signal is

$$\bar{f}_o(s) = \frac{1}{(1 + \tau s)} \frac{\hat{I} \cdot \omega}{(s^2 + \omega^2)} \quad [4.35]$$

Expressing [4.35] in partial fractions we have

$$\bar{f}_o(s) = \frac{A}{(1 + \tau s)} + \frac{Bs + C}{s^2 + \omega^2} \quad [4.36]$$

where:

$$A = \frac{\omega \tau^2 \hat{I}}{(1 + \tau^2 \omega^2)}, \quad B = \frac{-\omega \tau \hat{I}}{(1 + \tau^2 \omega^2)}, \quad C = \frac{\omega \hat{I}}{(1 + \tau^2 \omega^2)}$$

so that:

$$\begin{aligned} \bar{f}_o(s) &= \frac{\omega \tau^2 \hat{I}}{(1 + \tau^2 \omega^2)} \frac{1}{(1 + \tau s)} + \frac{\hat{I}}{(1 + \tau^2 \omega^2)} \left\{ \frac{-\omega \tau s + \omega}{s^2 + \omega^2} \right\} \\ &= \frac{\omega \tau^2 \hat{I}}{(1 + \tau^2 \omega^2)} \frac{1}{(1 + \tau s)} + \frac{\hat{I}}{\sqrt{1 + \tau^2 \omega^2}} \left\{ \frac{\omega \frac{1}{\sqrt{1 + \tau^2 \omega^2}} + s \frac{-\omega \tau}{\sqrt{1 + \tau^2 \omega^2}}}{s^2 + \omega^2} \right\} \\ &= \frac{\omega \tau^2 \hat{I}}{(1 + \tau^2 \omega^2)} \frac{1}{(1 + \tau s)} + \frac{\hat{I}}{\sqrt{1 + \tau^2 \omega^2}} \left\{ \frac{\omega \cos \phi + s \sin \phi}{s^2 + \omega^2} \right\} \end{aligned} \quad [4.37]$$

where

$$\cos \phi = \frac{1}{\sqrt{1 + \tau^2 \omega^2}}, \quad \sin \phi = \frac{-\omega \tau}{\sqrt{1 + \tau^2 \omega^2}}$$

Using Table 4.1 we have:

$$f_o(t) = \underbrace{\frac{\omega \tau \hat{I}}{1 + \tau^2 \omega^2}}_{\text{Transient term}} e^{-t/\tau} + \underbrace{\frac{\hat{I}}{\sqrt{1 + \tau^2 \omega^2}} \sin(\omega t + \phi)}_{\text{Sinusoidal term}} \quad [24.38]$$

In a sine wave test experiment, we wait until the transient term has decayed to zero and measure the sinusoidal signal:

$$f_o(t) = \frac{\hat{I}}{\sqrt{1 + \tau^2 \omega^2}} \sin(\omega t + \phi) \quad [4.39]$$

which remains. We see therefore that the output signal is also a sine wave of frequency ω but with amplitude $\hat{I}/\sqrt{1 + \tau^2 \omega^2}$, and shifted in phase by $\phi = -\tan^{-1}(\omega \tau)$ relative to the input sine wave. These amplitude and phase results can be found directly from the transfer function $G(s) = 1/(1 + \tau s)$ without having to use the table of transforms. If we replace s by $j\omega$ ($j = \sqrt{-1}$) in $G(s)$ we form the complex number $G(j\omega) = 1/(1 + j\tau\omega)$. The **magnitude** $|G(j\omega)| = 1/\sqrt{1 + \tau^2 \omega^2}$ of this complex number is equal to the ratio of output amplitude to input amplitude, and the **angle** or **argument** $\arg G(j\omega) = -\tan^{-1}(\omega \tau)$ is equal to the phase difference ϕ between output and input sine waves. Figure 4.8 shows amplitude ratio versus frequency and phase versus frequency graphs for a first-order element; these are known as the **frequency response** characteristics of the element. From the above equations we see that when $\omega \tau = 1$,

Figure 4.8 Frequency response characteristics of first-order element with

$$G(s) = \frac{1}{1 + \tau s}.$$

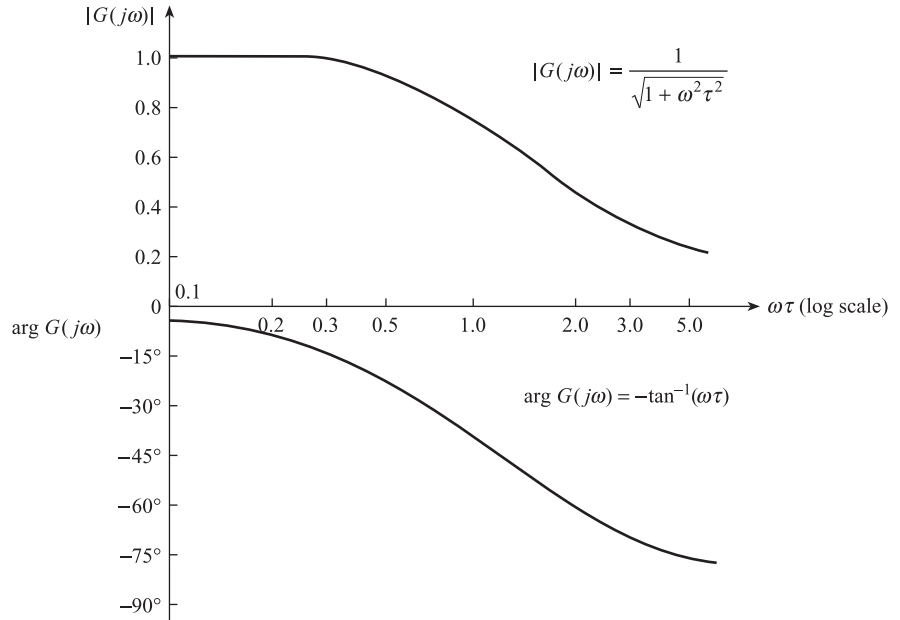


Figure 4.9 Frequency response of an element with linear dynamics.



i.e. $\omega = 1/\tau$, the amplitude ratio $= 1/\sqrt{2}$ and phase difference $\phi = -45^\circ$. These results enable the value of τ to be found from experimental frequency response data.

The above results can be generalised to an element with steady-state sensitivity K (or $\partial O/\partial I$) and transfer function $G(s)$, subject to a sinusoidal input signal $I = \hat{I} \sin \omega t$ as in Figure 4.9. In the steady state we can make four statements about the output signal:

- O is also a sine wave.
- The frequency of O is also ω .
- The amplitude of O is $\hat{O} = K|G(j\omega)|\hat{I}$.
- The phase difference between O and I is $\phi = \arg G(j\omega)$.

Using the above rules we can quickly find the amplitude ratio and phase relations for a second-order element with:

$$G(s) = \frac{1}{\frac{1}{\omega_n^2} s^2 + \frac{2\xi}{\omega_n} s + 1}$$

Here we have:

$$G(j\omega) = \frac{1}{\frac{1}{\omega_n^2} (j\omega)^2 + \frac{2\xi}{\omega_n} (j\omega) + 1}$$

so that

Frequency response characteristics of second-order element

$$\begin{aligned} \text{Amplitude ratio} &= |G(j\omega)| = \frac{1}{\sqrt{\left(1 - \frac{\omega^2}{\omega_n^2}\right)^2 + 4\xi^2 \frac{\omega^2}{\omega_n^2}}} \\ \text{Phase difference} &= \arg G(j\omega) = -\tan^{-1} \left[\frac{2\xi\omega/\omega_n}{1 - \omega^2/\omega_n^2} \right] \end{aligned} \quad [4.40]$$

These characteristics are shown graphically in Figure 4.10; both amplitude ratio and phase characteristics are critically dependent on the value of ξ .

We note that for $\xi < 0.7$, $|G(j\omega)|$ has a maximum value which is greater than unity. This maximum value is given by:

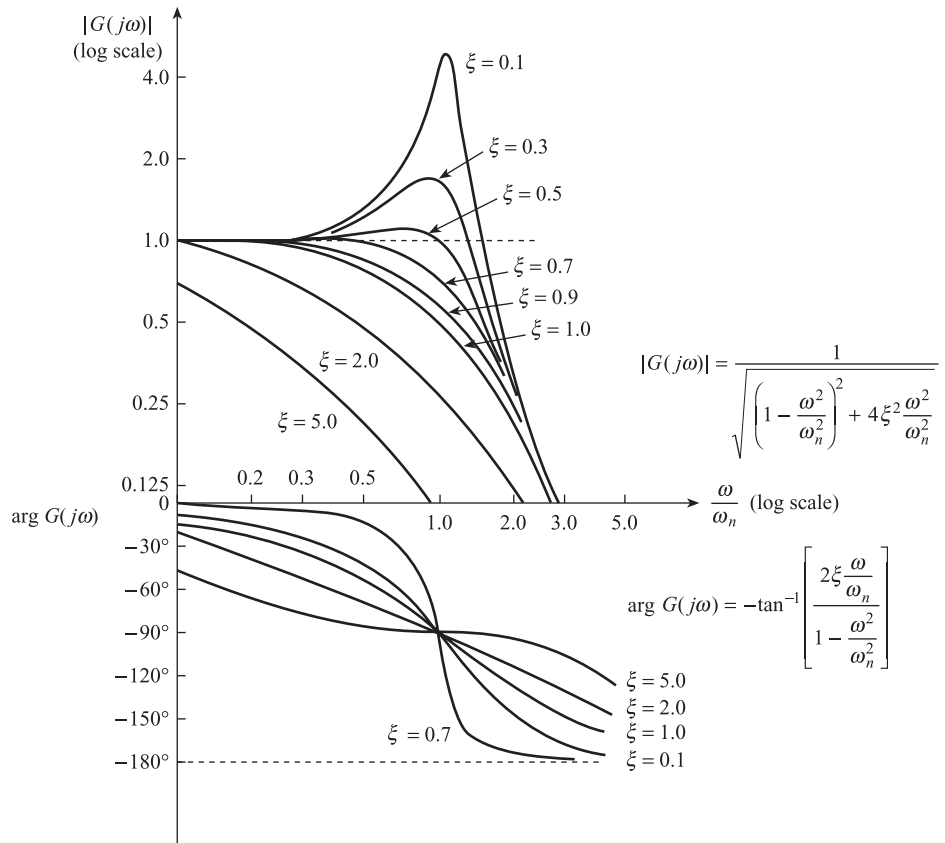
$$|G(j\omega)|_{\text{MAX}} = \frac{1}{2\xi\sqrt{1-\xi^2}}$$

and occurs at the **resonant frequency** ω_R where:

$$\omega_R = \omega_n \sqrt{1 - 2\xi^2}, \quad \xi < 1/\sqrt{2}$$

Figure 4.10 Frequency response characteristics of second-order element with

$$G(s) = \frac{1}{\frac{1}{\omega_n^2} s^2 + \frac{2\xi}{\omega_n} s + 1}$$

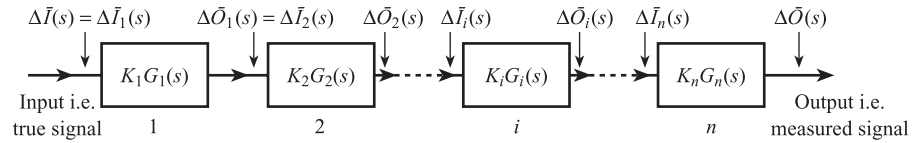


Thus by measuring $|G(j\omega)|_{\text{MAX}}$ and ω_R , ξ and ω_n can be found. An alternative to plotting $|G(j\omega)|$ versus ω is a graph of the number of decibels N dB versus ω , where $N = 20 \log_{10}|G(j\omega)|$. Thus if $|G(j\omega)| = 1$, $N = 0$ dB; if $|G(j\omega)| = 10$, $N = +20$ dB; and if $|G(j\omega)| = 0.1$, $N = -20$ dB.

4.3 Dynamic errors in measurement systems

Figure 4.11 shows a complete measurement system consisting of n elements. Each element i has ideal steady-state and linear dynamic characteristics and can therefore be represented by a constant steady-state sensitivity K_i and a transfer function $G_i(s)$.

Figure 4.11 Complete measurement system with dynamics.



We begin by assuming that the steady-state sensitivity $K_1 K_2 \dots K_i \dots K_n$ for the overall system is equal to 1, i.e. the system has no steady-state error (Section 3.1). The system transfer function $G(s)$ is the product of the individual element transfer functions, i.e.

Transfer function for complete measurement system

$$\frac{\Delta \bar{O}(s)}{\Delta \bar{I}(s)} = G(s) = G_1(s) G_2(s) \dots G_i(s) \dots G_n(s) \quad [4.41]$$

In principle we can use eqn [4.41] to find the system output signal $\Delta O(t)$ corresponding to a time-varying input signal $\Delta I(t)$. We first find the Laplace transform $\Delta \bar{I}(s)$ of $\Delta I(t)$, then using [4.9] the Laplace transform of the output signal is $\Delta \bar{O}(s) = G(s) \Delta \bar{I}(s)$. By expressing $\Delta \bar{O}(s)$ in partial fractions, and using standard tables of Laplace transforms, we can find the corresponding time signal $\Delta O(t)$. Expressing this mathematically:

$$\Delta O(t) = \mathcal{L}^{-1}[G(s) \Delta \bar{I}(s)] \quad [4.42]$$

where \mathcal{L}^{-1} denotes the inverse Laplace transform. The dynamic error $E(t)$ of the measurement system is the difference between the measured signal and the true signal, i.e. the difference between $\Delta O(t)$ and $\Delta I(t)$:

Dynamic error of a measurement system

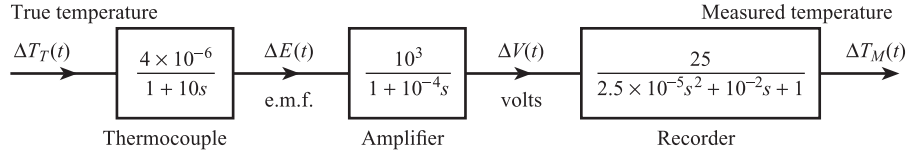
$$E(t) = \Delta O(t) - \Delta I(t) \quad [4.43]$$

Using [4.42] we have:

$$E(t) = \mathcal{L}^{-1}[G(s) \Delta \bar{I}(s)] - \Delta I(t) \quad [4.44]$$

The simple temperature measurement system (Figure 4.12), first introduced in Section 3.1, provides a good example of dynamic errors. The thermocouple has a time constant of 10 s, the amplifier has a time constant of 10^{-4} s (Chapter 9), and the recorder (Chapter 11) is a second-order element with $\omega_n = 200$ rad/s and $\xi = 1.0$. The overall steady-state sensitivity of the system is unity.

Figure 4.12 Simple temperature measurement system with dynamics.



We can now calculate the dynamic error of the system for a step input of +20 °C, i.e. $\Delta T_T(t) = 20u(t)$ and $\Delta \tilde{T}_T(s) = 20(1/s)$. Thus the Laplace transform of the output signal is:

$$\begin{aligned} \Delta \tilde{T}_M(s) &= 20 \frac{1}{s} \frac{1}{(1 + 10s)} \frac{1}{(1 + 10^{-4}s)} \frac{1}{(1 + 1/200s)^2} \\ &= 20 \left\{ \frac{1}{s} - \frac{A}{(s + 0.1)} - \frac{B}{(s + 10^4)} - \frac{Cs + D}{(s + 200)^2} \right\} \end{aligned} \quad [4.45]$$

Using Table 4.1 and eqn [4.30],

$$\Delta T_M(t) = 20 \{ u(t) - A e^{-0.1t} - B e^{-10^4 t} - E e^{-200t}(1 + 200t) \}$$

and the dynamic error:

$$\begin{aligned} E(t) &= \Delta T_M(t) - \Delta T_T(t) \\ &= -20 \{ A e^{-0.1t} + B e^{-10^4 t} - E e^{-200t}(1 + 200t) \} \end{aligned} \quad [4.46]$$

where the negative sign indicates too low a reading. The $B e^{-10^4 t}$ term decays to zero after about 5×10^{-4} s, and the $E e^{-200t}(1 + 200t)$ term decays to zero after about 25 ms. The $A e^{-0.1t}$ term, which corresponds to the 10 s time constant of the thermocouple, takes about 50 s to decay to zero and so has the greatest effect on the dynamic error.

We can use the rules developed in Section 4.2.2 to find the dynamic error of a system, with transfer function $G(s)$ subject to a sinusoidal input $\Delta I(t) = \hat{I} \sin \omega t$. From Figure 4.9 we have:

$$\Delta O(t) = |G(j\omega)| \hat{I} \sin(\omega t + \phi)$$

giving

$$E(t) = \hat{I} \{ |G(j\omega)| \sin(\omega t + \phi) - \sin \omega t \} \quad [4.47]$$

where $\phi = \arg G(j\omega)$.

Suppose that the above temperature measurement system is measuring a sinusoidal temperature variation of amplitude $\hat{T}_T = 20$ °C and period $T = 6$ s, i.e. angular frequency $\omega = 2\pi/T \approx 1.0$ rad s⁻¹. The frequency response function $G(j\omega)$ is:

$$G(j\omega) = \frac{1}{(1 + 10j\omega)(1 + 10^{-4}j\omega)[1 + 10^{-2}j\omega + 2.5 \times 10^{-5}(j\omega)^2]} \quad [4.48]$$

so that at $\omega = 1$

$$|G(j\omega)|_{\omega=1} = \frac{1}{\sqrt{(1 + 100)(1 + 10^{-8})[(1 - 2.5 \times 10^{-5})^2 + 10^{-4}]}} \approx 0.10$$

and

$$\arg G(j\omega)_{\omega=1} \approx 0 - \tan^{-1}(10) - \tan^{-1}(10^{-4}) - \tan^{-1}(10^{-2}) \approx -85^\circ \quad [4.49]$$

We note from the above equations that the values of $|G(j\omega)|$ and $\arg G(j\omega)$ at $\omega = 1$ are determined mainly by the 10 s time constant; the dynamic characteristics of the other elements will only begin to affect the system performance at much higher frequencies. Since $T_T(t) = 20 \sin t$ and $T_M(t) = 0.1 \times 20 \sin(t - 85^\circ)$, the error is:

$$E(t) = 20\{0.1 \sin(t - 85^\circ) - \sin t\} \quad [4.50]$$

We note that in the case of a sine wave input, the output recording is also a sine wave, i.e. the **waveform** of the signal is unaltered even though there is a reduction in amplitude and a phase shift.

In practice the input signal to a measurement system is more likely to be **periodic** rather than a simple sine wave. A periodic signal is one that repeats itself at equal intervals of time T , i.e. $f(t) = f(t + T) = f(t + 2T)$ etc. where T is the period. One example of a periodic measurement signal is the time variation of the temperature inside a diesel engine; another is the vibration of the casing of a centrifugal compressor. In order to calculate dynamic errors for periodic signals, we need to use **Fourier analysis**. Any periodic signal $f(t)$ with period T can be expressed as a series of sine and cosine waves; these have frequencies which are **harmonics** of the fundamental frequency $\omega_1 = 2\pi/T$ rad s⁻¹, i.e.

Fourier series for periodic signal

$$f(t) = a_0 + \sum_{n=1}^{\infty} a_n \cos n\omega_1 t + \sum_{n=1}^{\infty} b_n \sin n\omega_1 t \quad [4.51]$$

where

$$a_n = \frac{2}{T} \int_{-T/2}^{+T/2} f(t) \cos n\omega_1 t \, dt$$

$$b_n = \frac{2}{T} \int_{-T/2}^{+T/2} f(t) \sin n\omega_1 t \, dt \quad [4.52]$$

and

$$a_0 = \frac{1}{T} \int_{-T/2}^{+T/2} f(t) \, dt = \text{average value of } f(t) \text{ over } T$$

If $f(t) = \Delta I(t)$, where $\Delta I(t)$ is the deviation of measurement input signal $I(t)$ from steady-state or d.c. value I_0 , then $a_0 = 0$. If we also assume that $f(t)$ is odd, i.e. $f(t) = -f(-t)$, then $a_n = 0$ for all n , i.e. there are only sine terms present in the series. This simplifying assumption does not affect the general conclusions drawn in the following section. The system input signal is thus given by

$$\Delta I(t) = \sum_{n=1}^{\infty} \hat{I}_n \sin n\omega_1 t \quad [4.53]$$

where $\hat{I}_n = b_n$ is the amplitude of the n th harmonic at frequency $n\omega_1$. In order to find $\Delta O(t)$, let us first suppose that only the n th harmonic $\hat{I}_n \sin n\omega_1 t$ is input to the system. From Figure 4.9 the corresponding output signal is

$$\hat{I}_n |G(jn\omega_1)| \sin(n\omega_1 t + \phi_n)$$

where $\phi_n = \arg G(jn\omega_1)$.

We now require to use the principle of superposition, which is a basic property of linear systems (i.e. systems described by linear differential equations). This can be stated as follows:

If an input $I_1(t)$ causes an output $O_1(t)$ and an input $I_2(t)$ causes an output $O_2(t)$, then an input $I_1(t) + I_2(t)$ causes an output $O_1(t) + O_2(t)$, provided the system is linear.

This means that if the total input signal is the sum of many sine waves (equation [4.53]), then the total output signal is the sum of the responses to each sine wave, i.e.

$$\Delta O(t) = \sum_{n=1}^{\infty} \hat{I}_n |G(jn\omega_1)| \sin(n\omega_1 t + \phi_n) \quad [4.54]$$

The dynamic error is thus

Dynamic error of system with periodic input signal

$$\Delta E(t) = \sum_{n=1}^{\infty} \hat{I}_n \{ |G(jn\omega_1)| \sin(n\omega_1 t + \phi_n) - \sin n\omega_1 t \} \quad [4.55]$$

As an example, suppose that the input to the temperature measurement system is a square wave of amplitude 20°C and period $T = 6\text{ s}$ (i.e. $\omega_1 = 2\pi/T \approx 1\text{ rad s}^{-1}$). The Fourier series for the input signal is:

$$\Delta T_T(t) = \frac{80}{\pi} \left[\sin t + \frac{1}{3} \sin 3t + \frac{1}{5} \sin 5t + \frac{1}{7} \sin 7t + \dots \right] \quad [4.56]$$

Figure 4.13 shows the waveforms of the input square wave and the first four Fourier components with frequencies 1, 3, 5 and 7 rad s^{-1} .

Figure 4.14 shows the amplitude–frequency and phase–frequency relationships for the input temperature; these define the frequency spectrum of the signal. The spectrum consists of a number of lines at frequencies $\omega_1, 3\omega_1, 5\omega_1$, etc., of decreasing length to represent the smaller amplitudes of the higher harmonics. In practical cases we can terminate or truncate the series at a harmonic where the amplitude is negligible; in this case we choose $n = 7$. In order to find the output signal, i.e. the recorded waveform, we need to evaluate the magnitude and argument of $G(j\omega)$ at $\omega = 1, 3, 5$ and 7 rad s^{-1} . Thus

$$|G(j)| \approx 0.100, \quad |G(3j)| \approx 0.033, \quad |G(5j)| \approx 0.020, \quad |G(7j)| \approx 0.014$$

and

$$\begin{aligned} \arg G(j) &\approx -85^\circ, & \arg G(3j) &\approx -90^\circ, \\ \arg G(5j) &\approx -92^\circ, & \arg G(7j) &\approx -93^\circ \end{aligned} \quad [4.57]$$

Again the above values are determined mainly by the 10 s thermocouple time constant; the highest signal frequency $\omega = 7$ is still well below the natural frequency of the recorder $\omega_n = 200$. The system output signal is:

$$\begin{aligned} \Delta T_M(t) = \frac{80}{\pi} [&0.100 \sin(t - 85^\circ) + 0.011 \sin(3t - 90^\circ) \\ &+ 0.004 \sin(5t - 92^\circ) + 0.002 \sin(7t - 93^\circ)] \end{aligned} \quad [4.58]$$

Figure 4.13 Waveforms for input square wave and Fourier components.

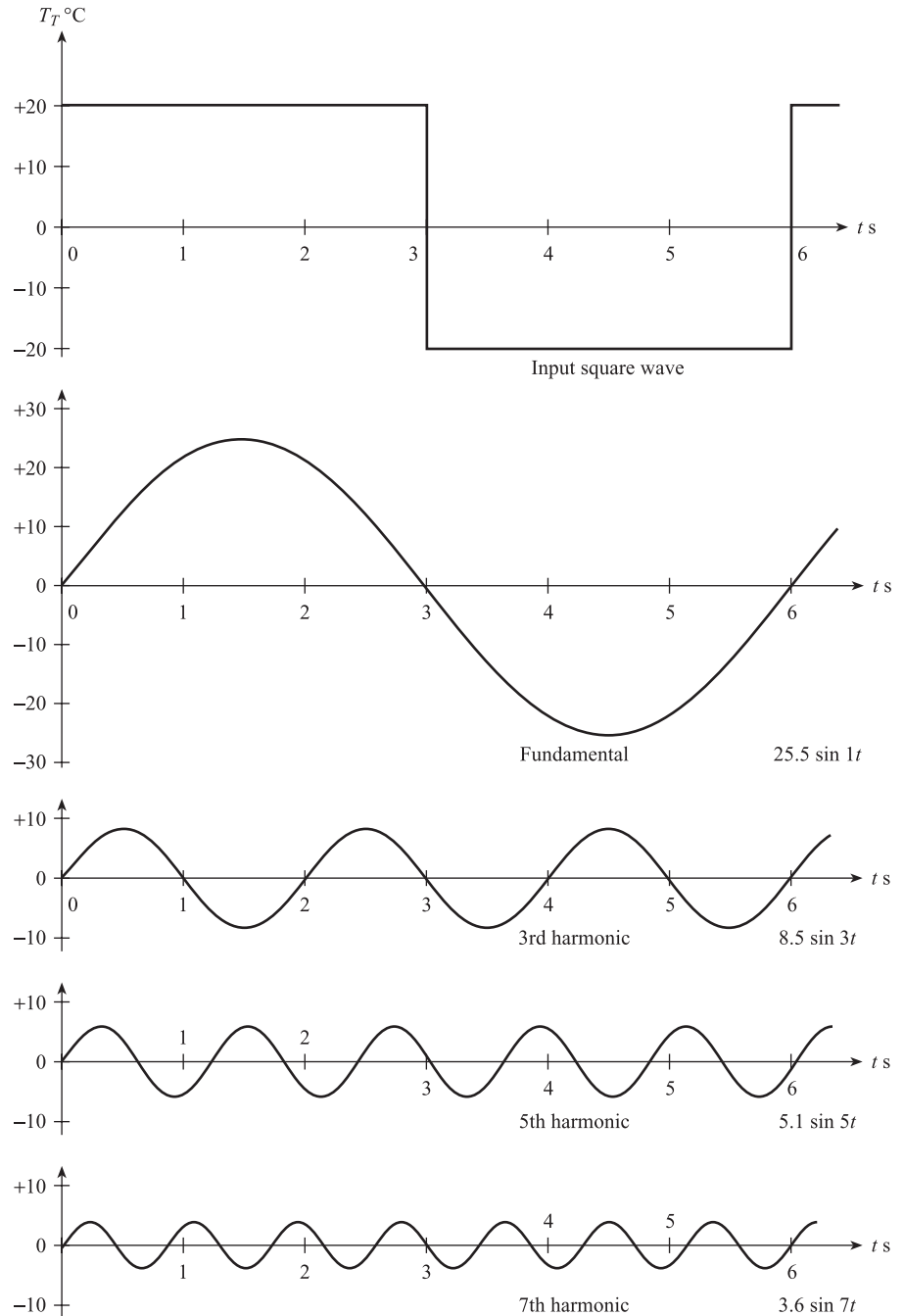


Figure 4.14 shows the system frequency response characteristics, the output signal frequency spectrum and the output waveform. We note that, in the output signal, the amplitudes of the 3rd, 5th and 7th harmonics have been reduced relative to the amplitude of the fundamental. The recorded waveform has therefore a different **shape** from the input signal as well as being reduced in amplitude and changed in phase.

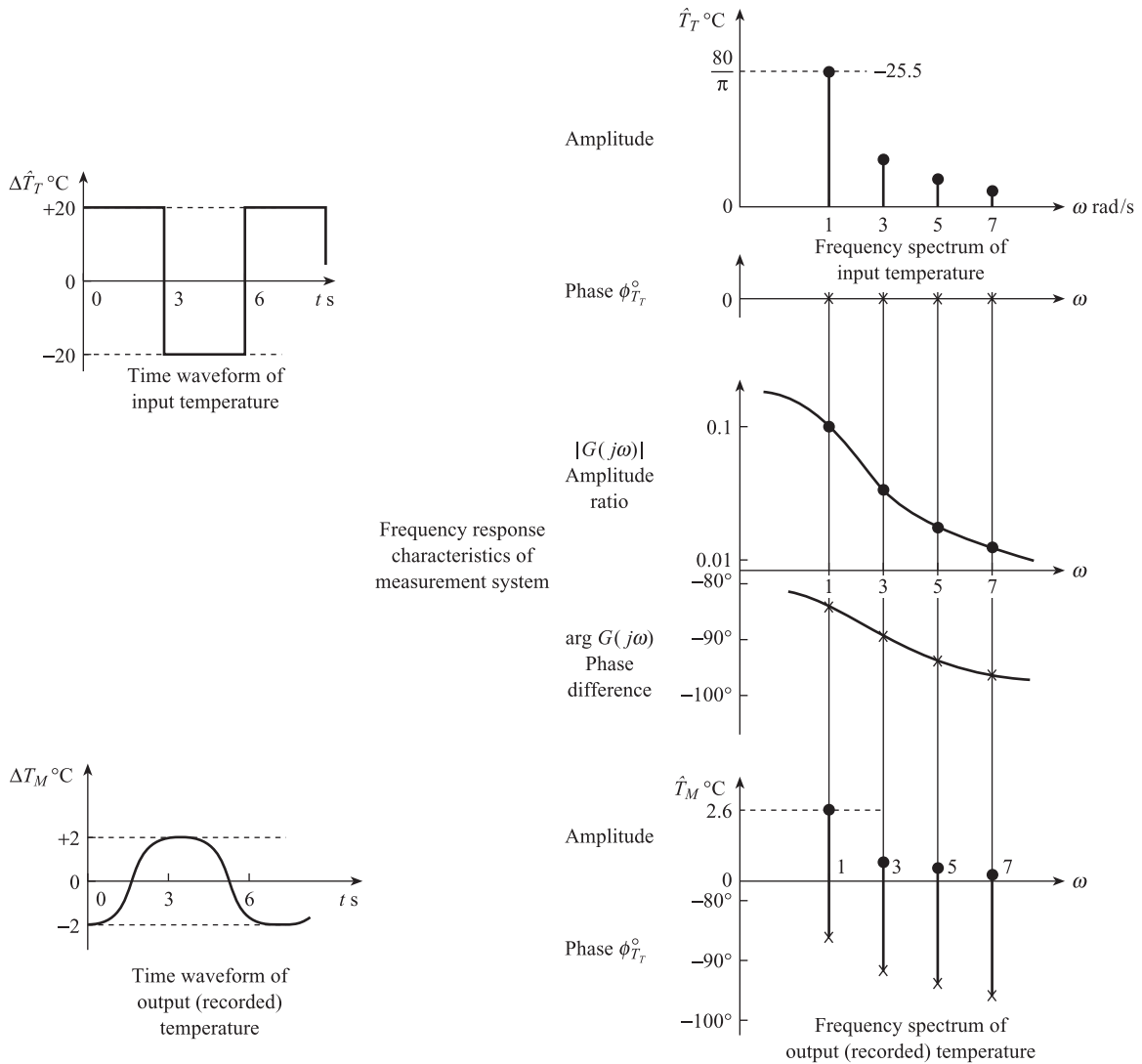


Figure 4.14 Calculation of dynamic errors with periodic input signal.

The above ideas can be extended to calculating the dynamic error for **random** input signals. Random signals can be represented by continuous frequency spectra (Chapter 6).

4.4

Techniques for dynamic compensation

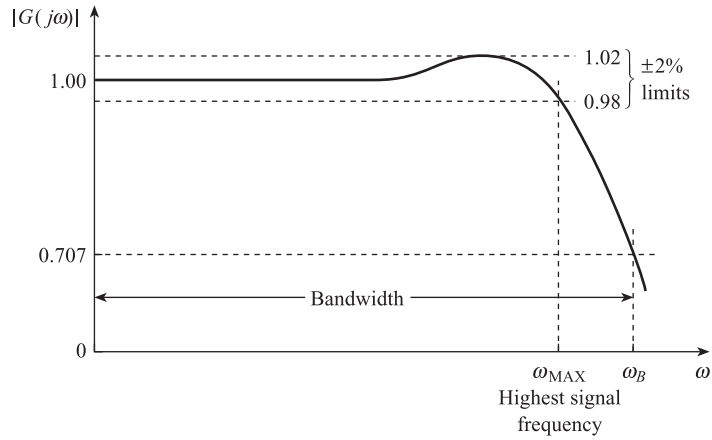
From eqn [4.55] we see that in order to have $E(t) = 0$ for a periodic signal, the following conditions must be obeyed:

$$|G(j\omega_1)| = |G(j2\omega_1)| = \dots = |G(jn\omega_1)| = \dots = |G(jm\omega_1)| = 1$$

$$\arg G(j\omega_1) = \arg G(j2\omega_1) = \dots = \arg G(jn\omega_1) = \dots = \arg G(jm\omega_1) = 0$$

[4.59]

Figure 4.15 Percentage limits and bandwidth.



where m is the order of the **highest significant harmonic**. For a random signal (Chapter 6) with a continuous frequency spectrum containing frequencies between 0 and ω_{MAX} , we require:

$$|G(j\omega)| = 1 \quad \text{and} \quad \arg G(j\omega) = 0 \quad \text{for} \quad 0 < \omega \leq \omega_{\text{MAX}} \quad [4.60]$$

The above conditions represent a theoretical ideal which will be difficult to realise in practice. A more practical criterion is one which limits the variation in $|G(j\omega)|$ to a few per cent for the frequencies present in the signal. For example the condition

$$0.98 < |G(j\omega)| < 1.02 \quad \text{for} \quad 0 < \omega \leq \omega_{\text{MAX}} \quad [4.61]$$

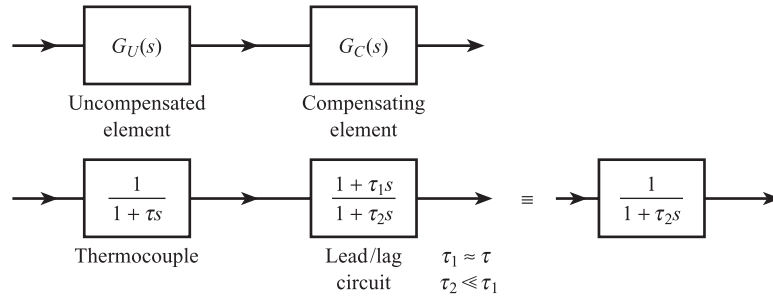
will ensure that the dynamic error is limited to $\approx \pm 2$ per cent for a signal containing frequencies up to $\omega_{\text{MAX}}/2\pi$ Hz (Figure 4.15).

Another commonly used criterion is that of **bandwidth**. The bandwidth of an element or a system is the range of frequencies for which $|G(j\omega)|$ is greater than $1/\sqrt{2}$. Thus the bandwidth of the system, with frequency response shown in Figure 4.15, is 0 to ω_B rad s⁻¹. The highest signal frequency ω_{MAX} must be considerably less than ω_B . Since, however, there is a 30% reduction in $|G(j\omega)|$ at ω_B , bandwidth is not a particularly useful criterion for complete measurement systems.

Bandwidth is commonly used in specifying the frequency response of amplifiers (Chapter 9); a reduction in $|G(j\omega)|$ from 1 to $1/\sqrt{2}$ is equivalent to a decibel change of $N = 20 \log(1/\sqrt{2}) = -3.0$ dB. A first-order element has a bandwidth between 0 and $1/\tau$ rad s⁻¹.

If a system fails to meet the specified limits on dynamic error $E(t)$, i.e. the system transfer function $G(s)$ does not satisfy a condition such as [4.61], then the first step is to identify which elements in the system dominate the dynamic behaviour. In the temperature measurement system of the previous section, the dynamic error is almost entirely due to the 10 s time constant of the thermocouple.

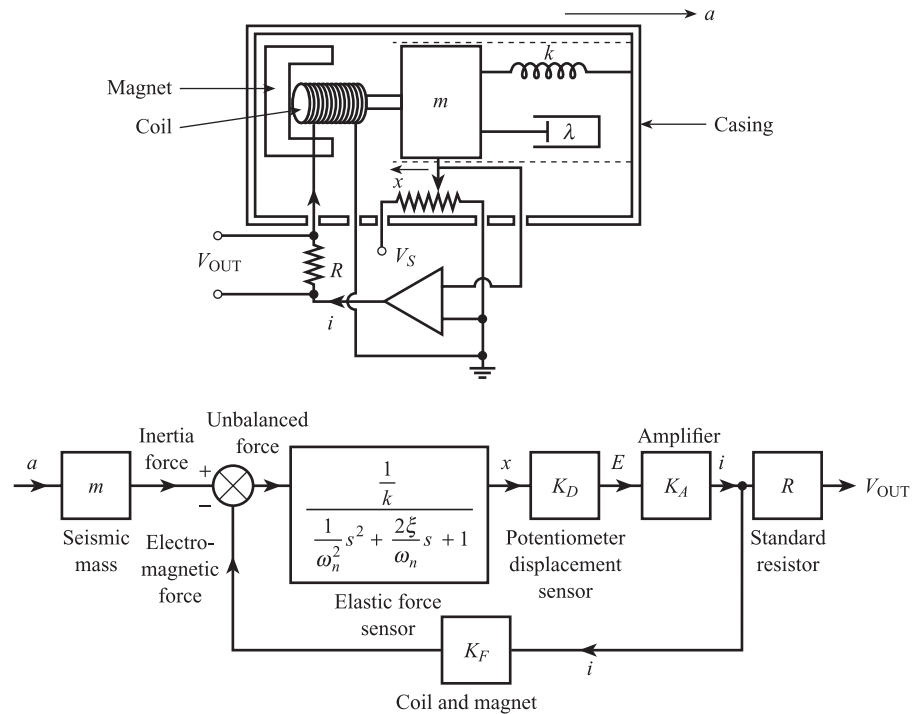
Having identified the dominant elements in the system, the most obvious method of improving dynamic response is that of **inherent design**. In the case of a first-order temperature sensor with $\tau = MC/UA$, τ can be minimised by minimising the mass/area ratio M/A – for example by using a thermistor in the form of a thin flake. In the case of a second-order force sensor with $\omega_n = \sqrt{k/m}$, ω_n can be maximised by maximising k/m , i.e. by using high stiffness k and low mass m . Increasing k , however, reduces the steady-state sensitivity $K = 1/k$.

Figure 4.16 Open-loop dynamic compensation.

From second-order step and frequency response graphs we see that the optimum value of damping ratio ξ is around 0.7. This value ensures minimum settling time for the step response and $|G(j\omega)|$ closest to unity for the frequency response.

Another possible method is that of **open-loop dynamic compensation** (Figure 4.16). Given an uncompensated element or system $G_U(s)$, a compensating element $G_C(s)$ is introduced into the system, such that the overall transfer function $G(s) = G_U(s)G_C(s)$ satisfies the required condition (for example eqn [4.61]). Thus if a lead/lag circuit (Figure 9.12) is used with a thermocouple (Figure 4.16), the overall time constant is reduced to τ_2 so that $|G(j\omega)|$ is close to unity over a wider range of frequencies. The main problem with this method is that τ can change with heat transfer coefficient U , thus reducing the effectiveness of the compensation (Chapter 14).

Another method is to incorporate the element to be compensated into a closed-loop system with **high-gain negative feedback**. An example of this is the constant temperature anemometer system for measuring fluid velocity fluctuations (Section 14.3). Another example is the closed-loop accelerometer shown in schematic and block diagram form in Figure 4.17.

Figure 4.17 Schematic and block diagram of closed-loop accelerometer.

The applied acceleration a produces an inertia force ma on the seismic mass m (Chapter 8). This is balanced by the force of the permanent magnet on the current feedback coil. Any imbalance of forces is detected by the elastic force element to produce a displacement which is detected by a potentiometric displacement sensor (Chapter 5). The potentiometer output voltage is amplified, giving a current output which is fed to the feedback coil through a standard resistor to give the output voltage.

Analysis of the block diagram shows that the overall system transfer function is:

$$\frac{\Delta \bar{V}(s)}{\Delta \bar{a}(s)} = \frac{mR}{K_F} \left\{ \frac{1}{\frac{k}{K_A K_D K_F} \frac{1}{\omega_n^2} s^2 + \frac{2\xi}{\omega_n} \frac{ks}{K_A K_D K_F} + \left(1 + \frac{1}{K_A K_D K_F}\right)} \right\} \quad [4.62]$$

If K_A is made large so that $K_A K_D K_F / k \gg 1$ (Chapter 3), then the system transfer function can be expressed in the form:

$$\frac{\Delta \bar{V}(s)}{\Delta \bar{a}(s)} = \frac{K_s}{\frac{1}{\omega_{ns}^2} s^2 + \frac{2\xi_s}{\omega_{ns}} s + 1}$$

where

$$\begin{aligned} \text{system steady-state sensitivity} \quad K_s &= \frac{mR}{K_F} \\ \text{system natural frequency} \quad \omega_{ns} &= \omega_n \sqrt{\frac{K_A K_D K_F}{k}} \\ \text{system damping ratio} \quad \xi_s &= \xi \sqrt{\frac{k}{K_A K_D K_F}} \end{aligned} \quad [4.63]$$

We see that the system natural frequency ω_{ns} is now much greater than that of the elastic force element itself. The system damping ratio ξ_s is much less than ξ , but by making ξ large a value of $\xi_s \approx 0.7$ can be obtained. Furthermore the system steady-state sensitivity depends only on m , K_F and R , which can be made constant to a high degree.

Conclusion

The **dynamic characteristics** of typical measurement system elements were initially discussed; in particular the **transfer functions** of **first-** and **second-order** elements were derived. The response of both first- and second-order elements to **step** and **sine wave inputs** was then studied. A general description of the **dynamic error** of a complete measurement system was then developed and applied to a temperature measurement system subject to step, sine wave and **periodic** input signals. Finally methods of **dynamic compensation**, which reduce dynamic error, were explained.

Problems

- 4.1 A temperature measurement system consists of linear elements and has an overall steady-state sensitivity of unity. The dynamics of the system are determined by the first-order transfer function of the sensing element. At time $t = 0$, the sensing element is suddenly transferred from air at 20°C to boiling water. One minute later the element is suddenly transferred back to air. Using the data given below, calculate the system dynamic error at the following times: $t = 10, 20, 50, 120$ and 300 s.

Sensor data

Mass = 5×10^{-2} kg

Surface area = 10^{-3} m²

Specific heat = $0.2 \text{ J kg}^{-1} ^\circ\text{C}^{-1}$

Heat transfer coefficient for air = $0.2 \text{ W m}^{-2} ^\circ\text{C}^{-1}$

Heat transfer coefficient for water = $1.0 \text{ W m}^{-2} ^\circ\text{C}^{-1}$

- 4.2 A force sensor has a mass of 0.5 kg, stiffness of $2 \times 10^2 \text{ N m}^{-1}$ and a damping constant of 6.0 N s m^{-1} .
- Calculate the steady-state sensitivity, natural frequency and damping ratio for the sensor.
 - Calculate the displacement of the sensor for a steady input force of 2 N .
 - If the input force is suddenly increased from 2 to 3 N , derive an expression for the resulting displacement of the sensor.
- 4.3 A force measurement system consists of linear elements and has an overall steady-state sensitivity of unity. The dynamics of the system are determined by the second-order transfer function of the sensing element, which has a natural frequency $\omega_n = 40 \text{ rad s}^{-1}$ and a damping ratio $\xi = 0.1$. Calculate the system dynamic error corresponding to the periodic input force signal:

$$F(t) = 50(\sin 10t + \frac{1}{3} \sin 30t + \frac{1}{5} \sin 50t)$$

- 4.4 An uncompensated thermocouple has a time constant of 10 s in a fast-moving liquid.
- Calculate the bandwidth of the thermocouple frequency response.
 - Find the range of frequencies for which the amplitude ratio of the uncompensated thermocouple is flat within $\pm 5\%$.
 - A lead/lag circuit with transfer function $G(s) = (1 + 10s)/(1 + s)$ is used to compensate for thermocouple dynamics. Calculate the range of frequencies for which the amplitude ratio of the compensated system is flat within $\pm 5\%$.
 - The velocity of the liquid is reduced, causing the thermocouple time constant to increase to 20 s. By sketching $|G(j\omega)|$ explain why the effectiveness of the above compensation is reduced.
- 4.5 An elastic force sensor has an effective seismic mass of 0.1 kg, a spring stiffness of 10 N m^{-1} and a damping constant of 14 N s m^{-1} .
- Calculate the following quantities:
 - sensor natural frequency
 - sensor damping ratio
 - transfer function relating displacement and force.
 - The above sensor is incorporated into a closed-loop, force balance accelerometer. The following components are also present:

Potentiometer displacement sensor: sensitivity 1.0 V m^{-1}
 Amplifier: voltage input, current output, sensitivity 40 A V^{-1}
 Coil and magnet: current input, force output, sensitivity 25 N A^{-1}
 Resistor: 250Ω .

- (i) Draw a block diagram of the accelerometer.
- (ii) Calculate the overall accelerometer transfer function.
- (iii) Explain why the dynamic performance of the accelerometer is superior to that of the elastic sensor.

4.6 A load cell consists of an elastic cantilever and a displacement transducer. The cantilever has a stiffness of 10^2 N m^{-1} , a mass of 0.5 kg and a damping constant of 2 N s m^{-1} . The displacement transducer has a steady-state sensitivity of 10 V m^{-1} .

- (a) A package of mass 0.5 kg is suddenly dropped onto the load cell. Use eqn [4.31] to derive a numerical equation describing the corresponding time variation of the output voltage ($g = 9.81 \text{ m s}^{-2}$).
- (b) The load cell is used to weigh packages moving along a conveyor belt at the rate of 60 per minute. Use the equation derived in (a) to explain why the load cell is unsuitable for this application. Explain what modifications to the load cell are necessary.

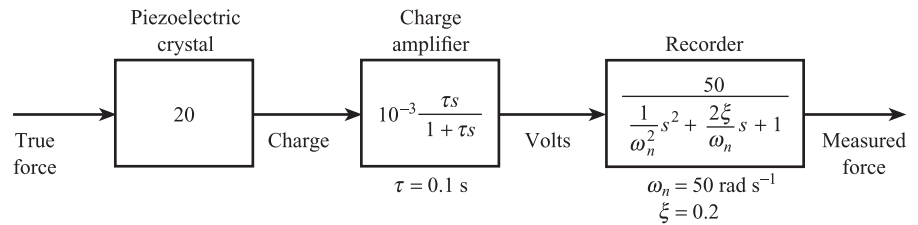
4.7 A force measurement system consisting of a piezoelectric crystal, charge amplifier and recorder is shown in Figure Prob. 7.

- (a) Calculate the system dynamic error corresponding to the force input signal:

$$F(t) = 50(\sin 10t + \frac{1}{3} \sin 30t + \frac{1}{5} \sin 50t)$$

- (b) Explain briefly the system modifications necessary to reduce the error in (a) (hint: see Figure 8.22).

Figure Prob. 7.



4.8 A thermocouple is used to measure the temperature inside a vessel, which is part of a high-speed batch process. At time $t = 0$, with the vessel at an initial temperature of 50°C , the vessel is instantaneously filled with gas at 150°C . One minute later, instantaneously the gas is removed and the vessel is filled with liquid at 50°C . The thermocouple can be regarded as having linear steady-state characteristics and first-order dynamics.

- (a) Use the data given below to sketch a graph of how the thermocouple e.m.f. changes with time. The axes of the graph should have suitable scales and the answer should include supporting numerical calculations.
- (b) Comment on whether the thermocouple is suitable for this application.
- (c) What modifications should be made?

Data

Thermocouple sensitivity	$= 40 \mu\text{V } ^\circ\text{C}^{-1}$
Thermocouple mass	$= 5 \times 10^{-2} \text{ kg}$
Thermocouple specific heat	$= 0.2 \text{ J kg}^{-1} ^\circ\text{C}^{-1}$
Thermocouple surface area	$= 10^{-3} \text{ m}^2$
Heat transfer coefficient for gas	$= 0.2 \text{ W m}^{-2} ^\circ\text{C}^{-1}$
Heat transfer coefficient for liquid	$= 1.0 \text{ W m}^{-2} ^\circ\text{C}^{-1}$

Response of first-order element, with unit sensitivity, to unit step:

$$F^0(t) = 1 - \exp\left(-\frac{t}{\tau}\right)$$

- 4.9 A temperature measurement system for a gas reactor consists of linear elements and has an overall steady-state sensitivity of unity. The temperature sensor has a time constant of 5.0 s; an *ideal* low-pass filter with a cut-off frequency of 0.05 Hz is also present. The input temperature signal is periodic with period 63 s and can be approximated by the Fourier series:

$$T(t) = 10(\sin \omega_0 t + \frac{1}{2} \sin 2\omega_0 t + \frac{1}{3} \sin 3\omega_0 t + \frac{1}{4} \sin 4\omega_0 t)$$

where ω_0 is the angular frequency of the fundamental component.

- (a) Calculate expressions for the time response of:
- (i) the system output signal
 - (ii) the system dynamic error.
- (b) Explain what modifications are necessary to the system to minimise the dynamic error in (a).

Note

An ideal low-pass filter has a gain of one and zero phase shift up to the cut-off frequency. The gain is zero above the cut-off frequency.

5

Loading Effects and Two-port Networks

In our discussion of measurement systems no consideration has yet been given to the effects of **loading**. One important effect is that of **inter-element loading** where a given element in the system may modify the characteristics of the previous element (for example by drawing current). In turn, the characteristics of this element may be modified by the following element in the system. Inter-element loading is normally an electrical loading effect which is described in the first section of this chapter using **Thévenin** and **Norton equivalent circuits**. The second section begins by discussing the analogies between electrical and non-electrical variables. This means that mechanical and thermal systems can be described by equivalent circuits and sensing elements by **two-port networks**. Two-port networks are then used to describe **process loading**; here the introduction of the sensing element into the process or system being measured causes the value of the measured variable to change. Finally two-port networks are used to describe **bilateral transducers** which use reversible physical effects.

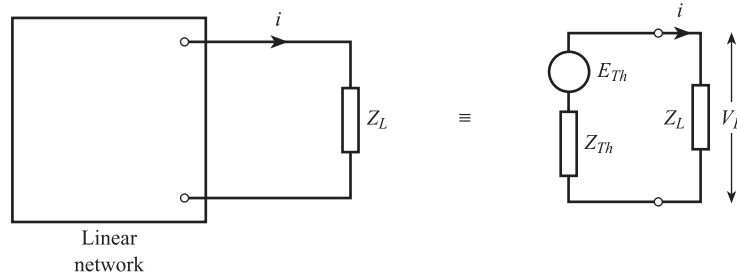
5.1

Electrical loading

We have so far represented measurement systems as blocks connected by single lines where the transfer of information and energy is in terms of one variable only. Thus in the temperature measurement system of Figure 3.2 the information transfer between elements is in terms of voltage only. No allowance can therefore be made for the amplifier drawing current from the thermocouple and the indicator drawing current from the amplifier. In order to describe both voltage and current behaviour at the connection of two elements, we need to represent each element by equivalent circuits characterised by two terminals. The connection is then shown by two lines.

5.1.1 Thévenin equivalent circuit

Thévenin's theorem states that any network consisting of linear impedances and voltage sources can be replaced by an equivalent circuit consisting of a voltage source E_{Th} and a series impedance Z_{Th} (Figure 5.1). The source E_{Th} is equal to the open circuit voltage of the network across the output terminals, and Z_{Th} is the impedance looking back into these terminals with all voltage sources reduced to zero and replaced by their internal impedances. Thus connecting a load Z_L across the output

Figure 5.1 Thévenin equivalent circuit.

terminals of the network is equivalent to connecting Z_L across the Thévenin circuit. The current i in Z_L is then simply given by:

$$i = \frac{E_{Th}}{Z_{Th} + Z_L} \quad [5.1]$$

and the voltage V_L across the load by:

Loading of Thévenin equivalent circuit

$$V_L = iZ_L = E_{Th} \frac{Z_L}{Z_{Th} + Z_L} \quad [5.2]$$

From eqn [5.2] we see that if $Z_L \gg Z_{Th}$, then $V_L \rightarrow E_{Th}$; i.e. in order to get **maximum voltage transfer** from the network to the load, the load impedance should be *far greater* than the Thévenin impedance for the network. In order to get **maximum power transfer** from network to load, the load impedance should be equal to the network impedance; i.e. $Z_L = Z_{Th}$.^[1] (An example of the calculation of E_{Th} and Z_{Th} for a potentiometer displacement transducer is given in the following section and for a deflection bridge in Section 9.1.)

We can now discuss the Thévenin equivalent circuit for the temperature measurement system of Figure 3.2. The thermocouple may be represented by $Z_{Th} = 20 \, \Omega$ (resistive) and $E_{Th} = 40T \, \mu\text{V}$, where T is the measurement junction temperature, if non-linear and reference junction temperature effects are ignored. The amplifier acts both as a load for the thermocouple and as a voltage source for the indicator. Figure 5.2 shows a general equivalent circuit for an amplifier with two pairs of terminals. Using typical amplifier data (Chapter 9), we have input impedance $Z_{IN} = R_{IN} = 2 \times 10^6 \, \Omega$, closed-loop voltage gain $A = 10^3$, and output impedance $Z_{OUT} = R_{OUT} = 75 \, \Omega$. The indicator is a resistive load of $10^4 \, \Omega$. The complete equivalent circuit for the system is shown in Figure 5.3, and using eqn [5.2] we have:

$$V_{IN} = 40 \times 10^{-6} T \left(\frac{2 \times 10^6}{2 \times 10^6 + 20} \right) \quad [5.3]$$

$$V_L = 1000 V_{IN} \left(\frac{10^4}{10^4 + 75} \right)$$

If the indicator scale is drawn so that a change of 1 V in V_L causes a change in deflection of $25 \, ^\circ\text{C}$, then the measured temperature $T_M = 25V_L$. This gives:

Figure 5.2 Equivalent circuit for amplifier.

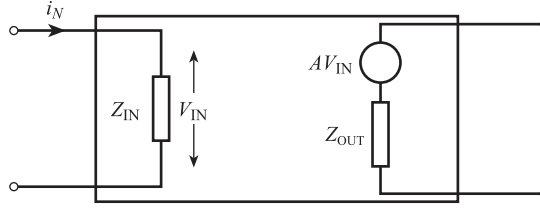
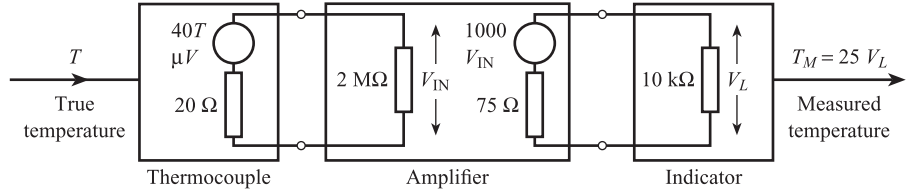


Figure 5.3 Thévenin equivalent to temperature measurement system.



$$T_M = \left(\frac{2 \times 10^6}{2 \times 10^6 + 20} \right) \left(\frac{10^4}{10^4 + 75} \right) T = 0.9925T \quad [5.4]$$

i.e. we have to introduce the factor $Z_L/(Z_{Th} + Z_L)$ at every interconnection of two elements to allow for loading. The loading error = $-0.0075T$; this is in addition to the steady-state error due to element imperfections calculated in Chapter 3.

The loading error in the above example is small, but if care is not taken it can be very large. Suppose a pH glass electrode (Chapter 8), with sensitivity 59 mV per pH, i.e. $E_{Th} = 59\text{pH mV}$ and $Z_{Th} = R_{Th} = 10^9 \Omega$, is directly connected to an indicator with $Z_L = R_L = 10^4 \Omega$ and a scale of sensitivity $\frac{1}{59}\text{pH/mV}$. The measured pH is:

$$\text{pH}_M = 59\text{pH} \left(\frac{10^4}{10^4 + 10^9} \right) \frac{1}{59} \approx 10^{-5}\text{pH} \quad [5.5]$$

i.e. there will be effectively a zero indication for any non-zero value.

This problem is solved by connecting the electrode to the indicator via a **buffer amplifier**. This is characterised by large Z_{IN} , small Z_{OUT} and unity gain $A = 1$. For example, an operational amplifier with a field effect transistor (FET) input stage connected as a voltage follower (Figure 9.9) would have $Z_{IN} = 10^{12} \Omega$, $Z_{OUT} = 10 \Omega$. The indicated pH value for the modified system (Figure 5.4) is:

$$\text{pH}_M = \frac{10^{12}}{10^{12} + 10^9} \times \frac{10^4}{10^4 + 10} \text{pH} \quad [5.6]$$

and the loading error is now -0.002pH , which is negligible.

Figure 5.4 Equivalent circuit for pH measurement system.

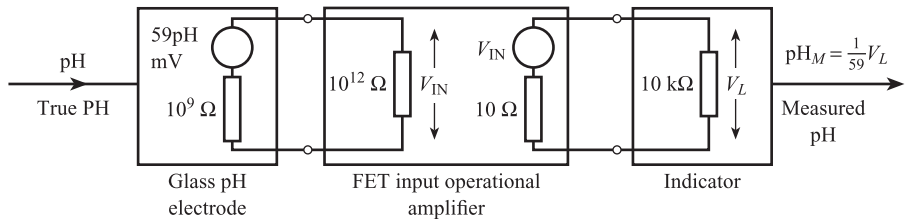
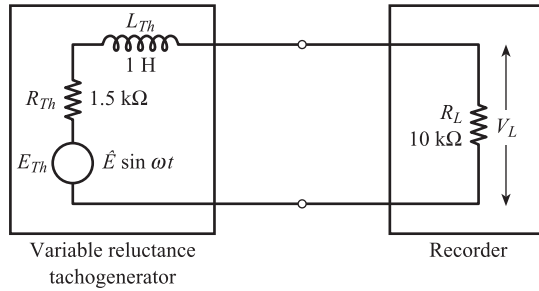


Figure 5.5 A.C. loading of tachogenerator.

An example of a.c. loading effects is given in Figure 5.5, which shows the equivalent circuit for a variable reluctance tachogenerator connected to a recorder. The Thévenin voltage E_{Th} for the tachogenerator is a.c. with an amplitude \hat{E} and angular frequency ω , both proportional to the mechanical angular velocity ω_r (Section 8.4). In this example, $\hat{E} = (5.0 \times 10^{-3}) \omega_r$ volts and $\omega = 6\omega_r$ rad s^{-1} . The Thévenin impedance Z_{Th} for the tachogenerator is an inductance and resistance in series (coil surrounding magnet), i.e. $Z_{Th} = R_{Th} + j\omega L_{Th}$. Thus if $\omega_r = 10^3$ rad s^{-1} :

$$\hat{E} = 5 \text{ V}, \quad \omega = 6 \times 10^3 \text{ rad s}^{-1}$$

and

$$Z_{Th} = 1.5 + 6.0j \text{ k}\Omega$$

so that the amplitude of the recorded voltage is

$$\hat{V}_L = \hat{E} \frac{R_L}{|Z_{Th} + R_L|} = 5 \frac{10}{\sqrt{(11.5)^2 + (6.0)^2}} = 3.85 \text{ V} \quad [5.7]$$

If the recorder scale sensitivity is set at $1/(5 \times 10^{-3})$ rad s^{-1} V^{-1} , then the recorded angular velocity is 770 rad s^{-1} . This error can be removed either by increasing the recorder impedance, or by changing the recorder sensitivity to allow for loading effects. A better alternative is to replace the recorder by a counter which measures the frequency rather than the amplitude of the tachogenerator signal (Section 10.3).

5.1.2 Example of Thévenin equivalent circuit calculation: potentiometric displacement sensor

Figure 5.6 shows a schematic diagram of a potentiometric sensor for measuring displacements d . The resistance of the potentiometer varies linearly with displacement.

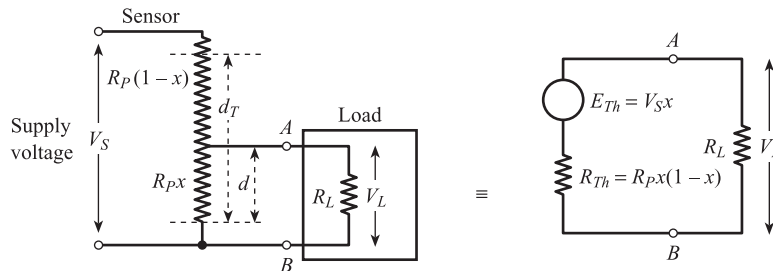
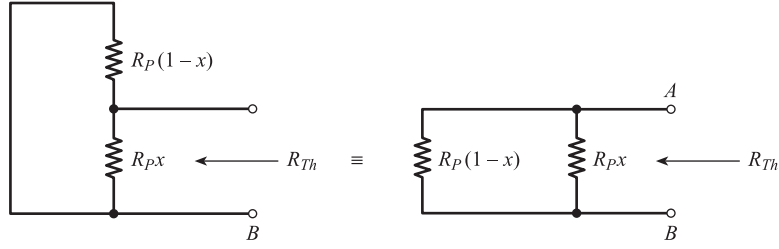
Figure 5.6 Potentiometer displacement sensor and Thévenin equivalent circuit.

Figure 5.7 Calculation of R_{Th} for potentiometer.



Thus if $x = d/d_T$ is the fractional displacement, the corresponding resistance is R_px , where $R_p \Omega$ is the total resistance of the potentiometer. The Thévenin voltage E_{Th} is the open circuit voltage across the output terminals AB . The ratio between E_{Th} and supply voltage V_S is equal to the ratio of fractional resistance R_px to total resistance R_p ; that is

$$\frac{E_{Th}}{V_S} = \frac{R_px}{R_p}, \quad \text{giving} \quad E_{Th} = V_S x \quad [5.8]$$

The Thévenin impedance Z_{Th} is found by setting supply voltage $V_S = 0$, replacing the supply by its internal impedance (assumed to be zero), and calculating the impedance looking back into the terminals AB as shown in Figure 5.7. Thus:

$$\frac{1}{R_{Th}} = \frac{1}{R_px} + \frac{1}{R_p(1-x)}$$

giving

$$R_{Th} = R_px(1-x) \quad [5.9]$$

Thus the effect of connecting a resistive load R_L (recorder or indicator) across the terminals AB is equivalent to connecting R_L across the Thévenin circuit. The load voltage is thus:

$$V_L = E_{Th} \frac{R_L}{R_{Th} + R_L} = V_S x \frac{R_L}{R_px(1-x) + R_L}$$

i.e.

*Voltage–displacement
relationship for a
loaded potentiometer*

$$V_L = V_S x \frac{1}{(R_p/R_L)x(1-x) + 1} \quad [5.10]$$

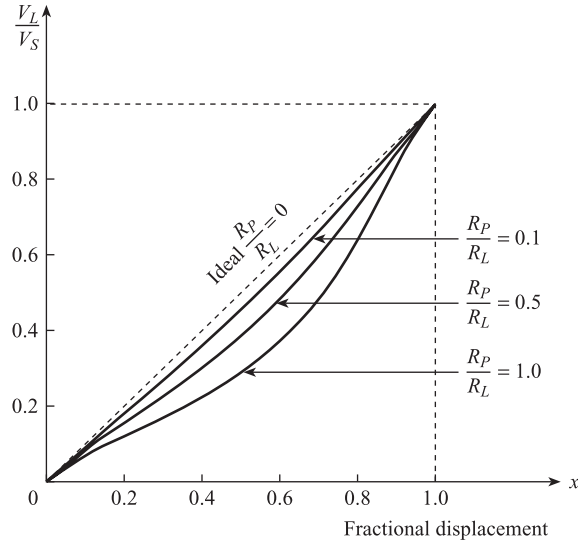
The relationship between V_L and x is non-linear, the amount of non-linearity depending on the ratio R_p/R_L (Figure 5.8). Thus the effect of loading a linear potentiometric sensor is to introduce a non-linear error into the system given by:

$$N(x) = E_{Th} - V_L = V_S x \left\{ 1 - \frac{1}{(R_p/R_L)x(1-x) + 1} \right\}$$

i.e.

$$N(x) = V_S \left\{ \frac{x^2(1-x)(R_p/R_L)}{1 + (R_p/R_L)x(1-x)} \right\} \quad [5.11]$$

Figure 5.8 Non-linear characteristics of loaded potentiometer.



which reduces to:

$$N(x) \approx V_S(R_P/R_L)(x^2 - x^3)$$

if $R_P/R_L \ll 1$ (the usual situation). $N(x)$ has a maximum value of $\hat{N} = \frac{4}{27}V_S(R_P/R_L)$ when $x = \frac{2}{3}$, corresponding to $dN/dx = 0$ and negative d^2N/dx^2 . Expressing \hat{N} as a percentage of full-scale deflection or span V_S volts gives:

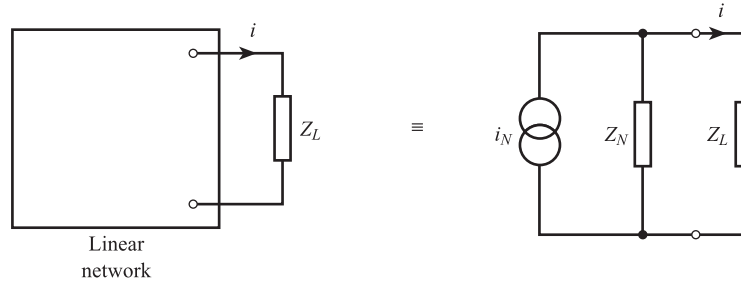
$$\hat{N} = \frac{400}{27} \frac{R_P}{R_L} \% \approx 15 \frac{R_P}{R_L} \% \quad [5.12]$$

Non-linearity, sensitivity and maximum power requirements are used to specify the values of R_P and V_S for a given application. Suppose that a 10 cm range potentiometer is to be connected to a 10 k Ω recorder. If the maximum non-linearity must not exceed 2%, then we require $15R_P/R_L \leq 2$, i.e. $R_P \leq \frac{20}{15} \times 10^3 \Omega$; thus a 1 k Ω potentiometer would be suitable.

Since sensitivity $dV_L/dx \approx V_S$, the greater V_S the higher the sensitivity, but we must satisfy the requirement that power dissipation V_S^2/R_P should not exceed maximum value \hat{W} watts. If $\hat{W} = 0.1$ W we require $V_S \leq \sqrt{0.1 \times 10^3}$, i.e. $V_S \leq 10$ V; if $V_S = 10$ V, then corresponding sensitivity = 1.0 V cm⁻¹.

5.1.3 Norton equivalent circuit

Norton's theorem states that any network consisting of linear impedances and voltage sources can be replaced by an equivalent circuit consisting of a current source i_N in parallel with an impedance Z_N (Figure 5.9). Z_N is the impedance looking back into the output terminals with all voltage sources reduced to zero and replaced by their internal impedances, and i_N is the current which flows when the terminals are short circuited. Connecting a load Z_L across the output terminals of the network is equivalent to connecting Z_L across the Norton circuit. The voltage V_L across the load is given by $V_L = i_N Z$, where $1/Z = 1/Z_N + 1/Z_L$, giving:

Figure 5.9 Norton equivalent circuit.*Loading of Norton equivalent circuit*

$$V_L = i_N \frac{Z_N \cdot Z_L}{Z_N + Z_L} \quad [5.13]$$

From eqn [5.13] we note that if $Z_L \ll Z_N$, then $V_L \rightarrow i_N Z_L$; i.e. in order to develop the maximum current through the load, the load impedance should be *far smaller* than the Norton impedance for the network.

A common example of a current source is an electronic differential pressure transmitter giving an output current signal, range 4 to 20 mA, proportional to an input differential pressure, typical range 0 to 2×10^4 Pa (Section 9.4). Figure 5.10 shows a typical equivalent circuit for the transmitter connected to a recorder via a cable. Using eqn [5.13], the voltage across the total load $R_C + R_R$ of recorder and cable is

$$V_L = i_N \frac{R_N(R_C + R_R)}{R_N + R_C + R_R} \quad [5.14]$$

and the ratio $V_R/V_L = R_R/(R_C + R_R)$, giving the recorder voltage:

$$V_R = i_N R_R \frac{R_N}{R_N + R_C + R_R} \quad [5.15]$$

Using the data given, we have $V_R = 0.9995 i_N R_R$, so that the recorded voltage deviates from the desired range of 1 to 5 V by only 0.05%.

A second example of a current generator is provided by a piezoelectric crystal acting as a force sensor. If a force F is applied to any crystal, then the atoms of the crystal undergo a small displacement x proportional to F . For a piezoelectric material the crystal acquires a charge q proportional to x , i.e. $q = Kx$. The crystal can therefore be regarded as a Norton current source of magnitude $i_N = dq/dt = K(dx/dt)$,

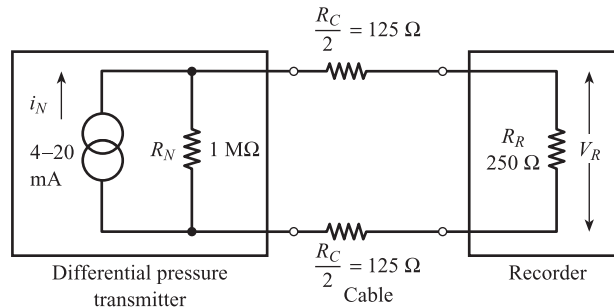
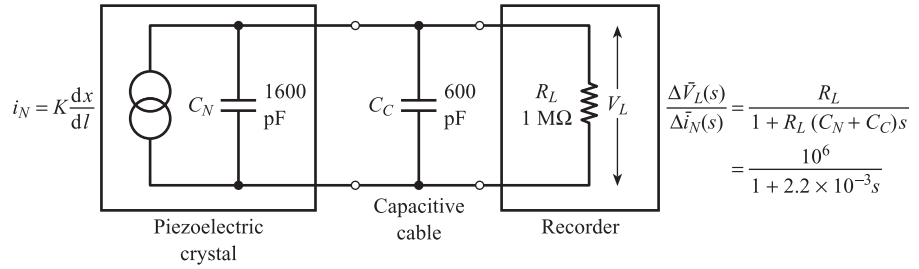
Figure 5.10 Typical current source and load.

Figure 5.11 Piezoelectric force measurement system.



where dx/dt is the velocity of the atomic deformations. This effect is discussed more fully in Section 8.7, where we see that the crystal acts as a capacitance C_N in parallel with the current source i_N . Figure 5.11 shows the equivalent circuit and typical component values for a crystal connected via a capacitive cable C_C to a recorder acting as a resistive load R_L . The voltage V_L across the load is given by $i_N Z$, where Z is the impedance of C_N , C_C and R_L in parallel. Since

$$\frac{1}{Z} = C_N s + C_C s + \frac{1}{R_L}$$

$$Z = \frac{R_L}{1 + R_L(C_N + C_C)s}$$

where s denotes the Laplace operator. The transfer function relating dynamic changes in source current and recorder voltage is thus:

$$\frac{\Delta \bar{V}_L(s)}{\Delta \bar{i}_N(s)} = \frac{R_L}{1 + R_L(C_N + C_C)s} \quad [5.16]$$

Thus the effect of electrical loading in this example is to introduce a first-order transfer function into the force measurement system; this will affect dynamic accuracy.

5.2 Two-port networks

5.2.1 Generalised effort and flow variables

We have seen in the previous section how electrical loading effects can be described using a pair of variables, voltage and current. Voltage is an example of an **across** or **effort variable** y ; current is an example of a **through** or **flow variable** \dot{x} . An effort variable drives a flow variable through an impedance. Other examples of effort/flow pairs are force/velocity, torque/angular velocity, pressure difference/volume flow rate and temperature difference/heat flow rate.^[2] Each y – \dot{x} pair has the following properties:

- The product $y\dot{x}$ represents power in watts.
- The ratio y/\dot{x} represents impedance.

The only exception is the thermal variables where the product has the dimensions of watts and temperature. Table 5.1 lists the effort/flow pairs for different forms of energy and for each pair defines the related quantities of impedance, stiffness, compliance

Table 5.1 Flow/effort variables and related quantities.

Variables	$\frac{d}{dt} \dot{x}$	$\int \dot{x} dt$	Flow \dot{x}	Effort y	Impedance $\frac{y}{\dot{x}}$	Stiffness $\frac{y}{\int \dot{x} dt}$	Compliance $\frac{\int \dot{x} dt}{y}$	Inertance $\frac{y}{d\dot{x}/dt}$
Mechanical-translation	acceleration	displacement	velocity	force	$\frac{\text{force}}{\text{velocity}} =$ damping constant	$\frac{\text{force}}{\text{displacement}} =$ mechanical stiffness	$\frac{\text{displacement}}{\text{force}} =$ 1 mech. stiffness	$\frac{\text{force}}{\text{acceleration}} =$ mass
Mechanical-rotation	angular acceleration	angular displacement	angular velocity	torque	$\frac{\text{torque}}{\text{ang. velocity}} =$ damping constant	$\frac{\text{torque}}{\text{angular disp.}} =$ mechanical stiffness	$\frac{\text{angular disp.}}{\text{torque}} =$ 1 mech. stiffness	$\frac{\text{torque}}{\text{angular accn}} =$ moment of inertia
Electrical	$\frac{d}{dt}$ (current)	charge	current	voltage	$\frac{\text{voltage}}{\text{current}} =$ electrical resistance	$\frac{\text{voltage}}{\text{charge}} =$ 1 elect. capacitance	$\frac{\text{charge}}{\text{voltage}} =$ electrical capacitance	$\frac{\text{voltage}}{d(\text{current})/dt} =$ inductance
Fluidic		volume	volume flow rate	pressure	$\frac{\text{pressure}}{\text{vol. flow rate}} =$ fluidic resistance	$\frac{\text{pressure}}{\text{volume}} =$ 1 fluid capacitance	$\frac{\text{volume}}{\text{pressure}} =$ fluidic capacitance	$\frac{\text{pressure}}{d(\text{flow rate})/dt} =$ fluidic inertance
Thermal		heat	heat flow rate	temperature	$\frac{\text{temperature}}{\text{heat flow rate}} =$ thermal resistance	$\frac{\text{temperature}}{\text{heat}} =$ 1 therm. capacitance	$\frac{\text{heat}}{\text{temperature}} =$ thermal capacitance	

Source: adapted from Finkelstein and Watts, 1971^[2].

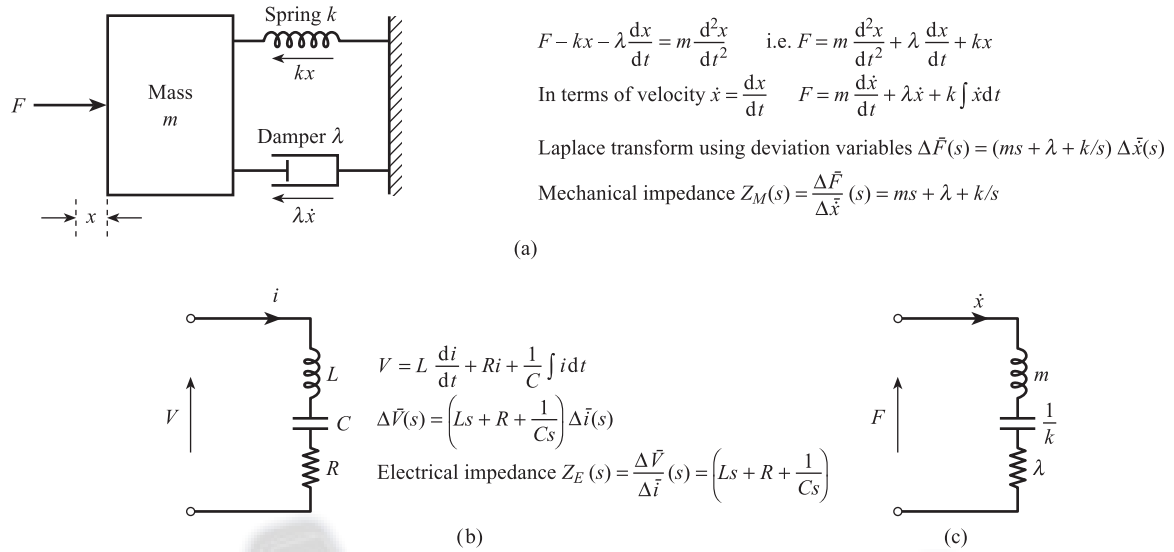


Figure 5.12 Equivalent circuit for a mechanical system:

- (a) Parallel mechanical system
 (b) Series electrical circuit
 (c) Equivalent mechanical circuit.

and inductance. Thus we see that the concept of impedance is applicable to mechanical, fluidic and thermal systems as well as electrical. For a mechanical system, mass is analogous to electrical inductance, damping constant is analogous to electrical resistance, and $1/\text{stiffness}$ is analogous to electrical capacitance. For a thermal system, thermal resistance is analogous to electrical resistance, and thermal capacitance is analogous to electrical capacitance. This means we can generalise the electrical equivalent circuits of Thévenin and Norton to non-electrical systems.

Figure 5.12(a) shows a parallel mechanical system consisting of a mass m , spring stiffness k and damper constant λ . Figure 5.12(b) shows a series electrical circuit consisting of an inductance L , a capacitance C and a resistance R . Since mechanical impedance is the ratio of force/velocity, the mechanical impedance transfer function is

$$Z_M(s) = \frac{\Delta \bar{F}}{\Delta \dot{\bar{x}}} = ms + \lambda + \frac{k}{s} \quad [5.17]$$

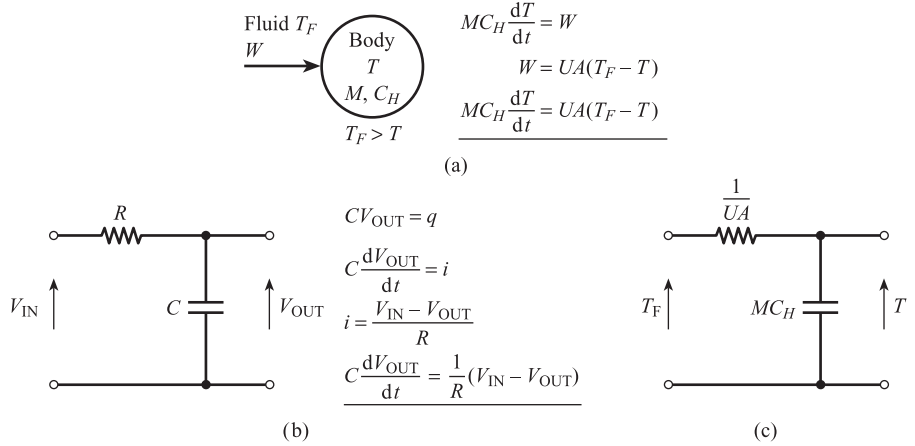
The impedance transfer function for the electrical circuit is

$$Z_E(s) = \frac{\Delta \bar{V}}{\Delta \bar{i}} = Ls + R + \frac{1}{Cs} \quad [5.18]$$

We see that these have a similar form, with m corresponding to L , λ corresponding to R , and k corresponding to $1/C$. Thus the parallel mechanical system can be represented by an equivalent circuit consisting of an inductive element m , a resistive element λ and a capacitive element $1/k$ in series (Figure 5.12(c)).

Figure 5.13(a) shows a thermal system consisting of a body at temperature T immersed in a fluid at temperature T_F . The body has a mass M , specific heat C_H and surface area A ; U is the heat transfer coefficient between the body and the fluid. Figure 5.13(b) shows a series electrical circuit with resistance R , capacitance C , input voltage V_{IN} and output voltage V_{OUT} . The differential equation for the thermal system is:

Figure 5.13 Equivalent circuit for a thermal system:
 (a) Thermal system
 (b) Electrical circuit
 (c) Equivalent thermal circuit.



$$MC_H \frac{dT}{dt} = UA(T_F - T) \quad [5.19]$$

and the differential equation for the electrical circuit is:

$$C \frac{dV_{OUT}}{dt} = \frac{1}{R}(V_{IN} - V_{OUT}) \quad [5.20]$$

We see that the equations have a similar form and the temperature effort variables T_F and T are analogous to the voltage effort variables V_{IN} and V_{OUT} . Heat flow W is analogous to current flow i , UA is analogous to $1/R$, i.e. the reciprocal of electrical resistance, and MC_H is analogous to electrical capacitance C . Thus the thermal system can be represented by an equivalent circuit consisting of a resistive element $1/UA$ in series with a capacitive element MC_H as in Figure 5.13(c).

5.2.2 Two-port networks

We saw in Section 5.1 that the electrical output of a sensing element such as a thermocouple or piezoelectric crystal can be represented by a Thévenin or Norton equivalent circuit. The sensor has therefore two output terminals which allow both voltage and current flow to be specified; this is referred to as an electrical output port. The sensing element will have a mechanical, thermal or fluidic input; we saw in the previous section that mechanical and thermal systems can be represented by equivalent circuits which show the relation between the corresponding effort and flow variables. Thus the input to a mechanical or thermal sensor can be represented by two input terminals which allow both the effort and flow variables to be specified; this is either a mechanical or a thermal input port. Thus a sensing element can be represented by a **two-port** or four-terminal network. Figure 5.14(a) shows a two-port representation of a mechanical sensor with input mechanical port and output electrical port; Figure 5.15(a) shows the two-port representation of a thermal sensor.

Figures 5.14(b) and (c) show the detailed two-port networks for a range of mechanical sensing elements. Figure 5.14(b) shows the equivalent circuit for sensing elements with a Thévenin equivalent circuit at the electrical output port. Z_M is the input mechanical impedance; E_{Th} and Z_{Th} are the Thévenin voltage and impedance. For a displacement sensor E_{Th} is proportional to displacement x , i.e.

Figure 5.14 Mechanical sensing elements as two-port networks:
(a) Overall two-port representation
(b) Equivalent circuit with Thévenin output
(c) Equivalent circuit with Norton output.

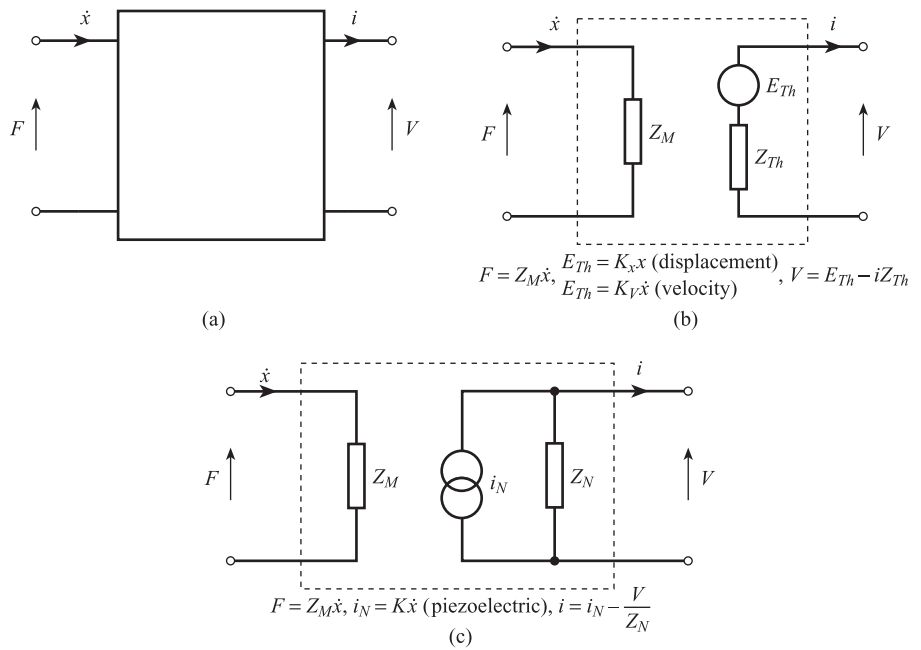
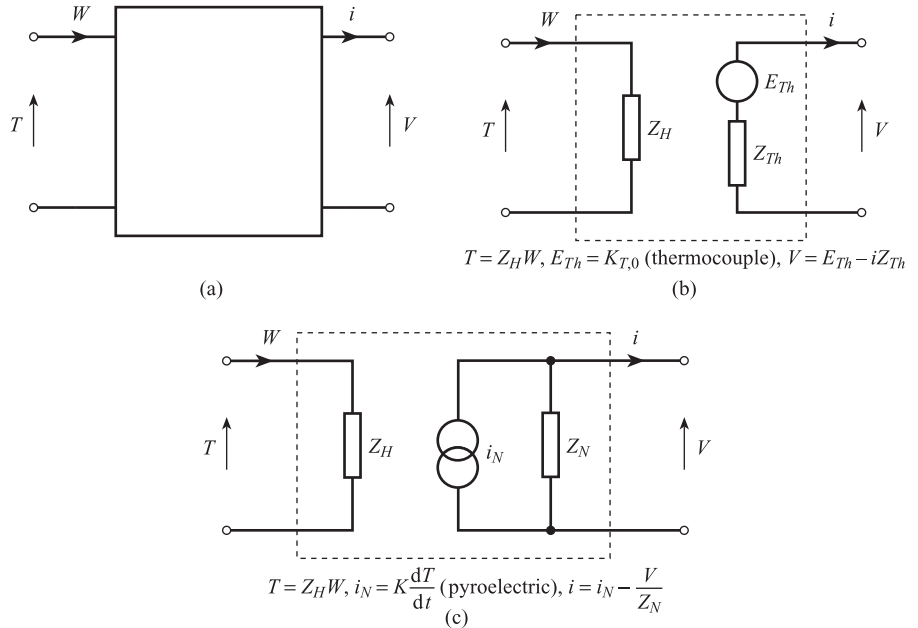


Figure 5.15 Thermal sensing elements as two-port networks:
(a) Overall two-port representation
(b) Equivalent circuit with Thévenin output
(c) Equivalent circuit with Norton output.



$$E_{Th} = K_x x \quad [5.21]$$

where K_x is the sensitivity and $x = \int \dot{x} dt$.

For a potentiometer displacement sensor (Section 5.1.2) $K_x = V_s$ (supply voltage), and for a linear variable differential transformer (LVDT, Section 8.3.2) K_x is the slope of the linear portion of the a.c. voltage versus displacement characteristics. For a velocity sensor, E_{Th} is proportional to velocity \dot{x} , i.e.

$$E_{Th} = K_V \dot{x} \quad [5.22]$$

For an electromagnetic linear velocity sensor (Section 12.5.1) $K_V = Bl$ where B is the applied magnetic field and l the length of the conductor. In the case of an electromagnetic angular velocity sensor or tachogenerator (Section 8.4) we have $E_{Th} = K_V \omega_r$, where ω_r is the angular velocity and $K_V = dN/d\theta$ the rate of change of flux N with angle θ . Figure 5.14(c) shows the equivalent circuit for sensing elements with a Norton equivalent circuit i_N , Z_N at the electrical output port. For a piezoelectric sensor i_N is proportional to velocity \dot{x} (Section 8.7), i.e.

$$i_N = K \dot{x} \quad [5.23]$$

where $K = dk$, d is the charge sensitivity to force and k is the stiffness of the crystal.

Figures 5.15(b) and (c) show the detailed two-port networks for two examples of thermal sensing elements. Figure 5.15(b) shows the equivalent circuit for a sensing element with a Thévenin equivalent circuit E_{Th} , Z_{Th} at the electrical output port; Z_H is the thermal input impedance. For a thermocouple temperature sensor (Section 8.5) with the reference junction at 0 °C we have $E_{Th} = E_{T,0}$ where $E_{T,0}$ is the e.m.f. at the measured junction at T °C and is given by the power series

$$E_{T,0} = a_1 T + a_2 T^2 + a_3 T^3 + \dots \quad [5.24]$$

Figure 5.15(c) shows the equivalent circuit for a sensing element with a Norton equivalent circuit i_N , Z_N at the electrical output port. For a pyroelectric detector (Section 15.5.1) i_N is proportional to rate of change of temperature dT/dt , i.e.

$$i_N = K \frac{dT}{dt} \quad [5.25]$$

where $K = A(dP/dT)$, A is the area of the electrodes and dP/dT is the slope of the polarisation temperature characteristics.

5.2.3 Process loading

Having introduced the concepts of equivalent circuits and two-port networks for mechanical and thermal systems, we can now use these concepts to study examples of how a primary sensing element can ‘load’ the process or element being measured.

Figure 5.16 shows a mechanical system or ‘process’ represented by a mass, spring and damper. The force F applied to the ‘process’ is being measured by a force sensor, consisting of an elastic element in conjunction with a potentiometric displacement sensor. The elastic force sensor can also be represented by a mass spring and damper (Section 4.1.2). Under steady-state conditions when both velocity $\dot{x} = 0$ and acceleration $\ddot{x} = 0$, we have the following force balance equations:

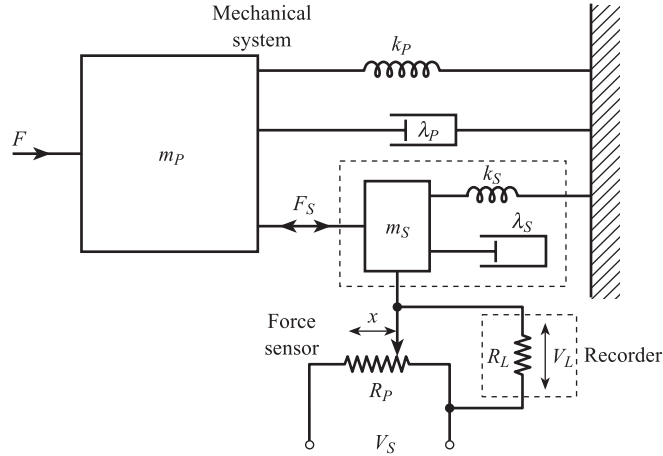
$$\begin{aligned} \text{process} \quad F &= k_p x + F_s \\ \text{sensor} \quad F_s &= k_s x \end{aligned} \quad [5.26]$$

showing that the relationship between the measured force F_s and the true force F is:

*Steady-state loading
of mechanical system*

$$F_s = \frac{k_s}{k_s + k_p} F = \frac{1}{1 + k_p/k_s} F \quad [5.27]$$

Figure 5.16 Loading of mechanical system by force sensor.



We see that in order to minimise the loading error in the steady state the sensor stiffness k_s should be very much greater than the process stiffness k_p .

Under unsteady conditions when \dot{x} and \ddot{x} are non-zero, Newton's second law gives the following differential equations:

$$\text{process} \quad F - k_p x - \lambda_p \dot{x} - F_s = m_p \ddot{x} \quad [5.28]$$

$$\text{sensor} \quad F_s - k_s x - \lambda_s \dot{x} = m_s \ddot{x}$$

i.e.

$$m_p \frac{d\dot{x}}{dt} + \lambda_p \dot{x} + k_p \int \dot{x} dt = F - F_s \quad [5.29]$$

$$m_s \frac{d\dot{x}}{dt} + \lambda_s \dot{x} + k_s \int \dot{x} dt = F_s$$

Using the analogues given earlier, the sensor can be represented by F_s driving \dot{x} through the mechanical L, C, R circuit $m_s, 1/k_s, \lambda_s$; and the process can be represented by $F - F_s$ driving \dot{x} through the mechanical L, C, R circuit $m_p, 1/k_p, \lambda_p$. If $\Delta x, \Delta F$ and ΔF_s are deviations from initial steady conditions, then the Laplace transforms of eqns [5.29] are:

$$\left(m_p s + \lambda_p + \frac{k_p}{s} \right) \overline{\Delta \dot{x}} = \Delta \bar{F} - \Delta \bar{F}_s \quad [5.30]$$

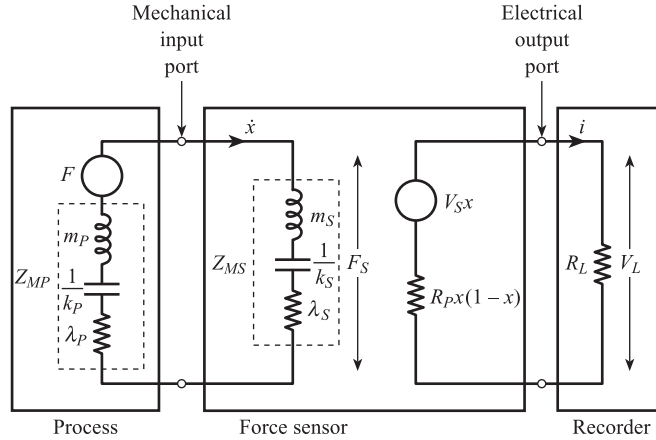
$$\left(m_s s + \lambda_s + \frac{k_s}{s} \right) \overline{\Delta \dot{x}} = \Delta \bar{F}_s$$

Using Table 5.1 we can define mechanical impedance transfer functions by $Z_M(s) = \Delta \bar{F}(s) / \overline{\Delta \dot{x}}(s)$, so that:

$$\text{process impedance} \quad Z_{MP}(s) = m_p s + \lambda_p + \frac{k_p}{s} \quad [5.31]$$

$$\text{sensor impedance} \quad Z_{MS}(s) = m_s s + \lambda_s + \frac{k_s}{s}$$

Figure 5.17 Equivalent circuit for complete system showing a force sensor as a two-port network.



From [5.30] and [5.31] the relationship between measured and actual dynamic changes in force is:

Dynamic loading of mechanical system

$$\Delta \bar{F}_S(s) = \frac{Z_{MS}}{Z_{MS} + Z_{MP}} \Delta \bar{F}(s) \quad [5.32]$$

Thus in order to minimise dynamic loading effects, sensor impedance Z_{MS} should be very much greater than process impedance Z_{MP} . Figure 5.17 shows the equivalent circuit for the system: process, force sensor and recorder.

Figure 5.18 shows a hot body, i.e. a thermal ‘process’ whose temperature T_P is being measured by a thermocouple sensor. Under unsteady conditions, heat flow rate considerations give the following differential equations (Section 4.1):

$$\begin{aligned} \text{process} \quad M_P C_P \frac{dT_P}{dt} &= W_P - W_S, & W_P &= U_P A_P (T_F - T_P) \\ \text{sensor} \quad M_S C_S \frac{dT_S}{dt} &= W_S, & W_S &= U_S A_S (T_P - T_S) \end{aligned} \quad [5.33]$$

Figure 5.18 Loading of thermal ‘process’ by thermocouple temperature sensor.

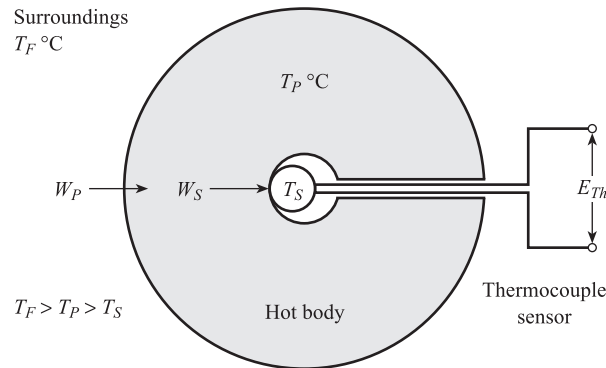
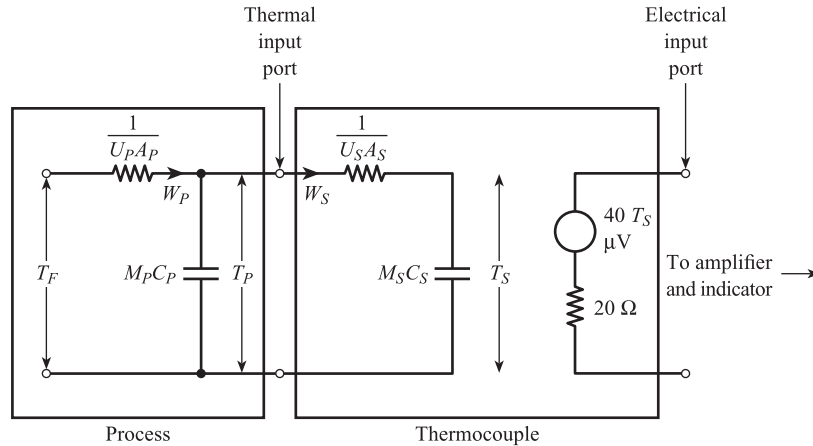


Figure 5.19 Equivalent circuit for thermal system showing thermocouple as a two-port network.



where M denotes masses

C denotes specific heats

U denotes heat transfer coefficients

A denotes heat transfer areas.

The quantities $M_P C_P$ and $M_S C_S$ have the dimensions of heat/temperature and are analogous to electrical capacitance. The quantities $U_P A_P$ and $U_S A_S$ have the dimensions of heat flow rate/temperature and are analogous to $1/(\text{electrical resistance})$. The equivalent circuit for the process and thermocouple is shown in Figure 5.19. We see that the relationship between T_F and T_P depends on the potential divider $1/U_P A_P, M_P C_P$, and the relationship between T_P and T_S depends on the potential divider $1/(U_S A_S), M_S C_S$. Again the thermocouple can be represented as a two-port network with a thermal input port and an electrical output port.

In conclusion we see that the representation of measurement system elements by two-port networks enables both **process** and **inter-element** loading effects to be quantified.

5.2.4 Bilateral transducers

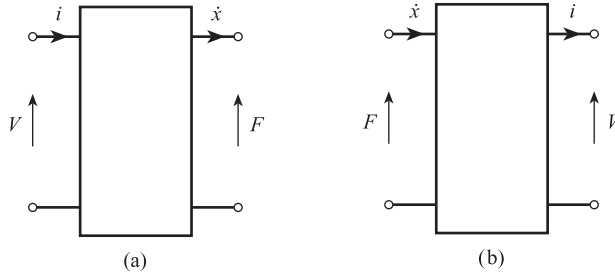
Bilateral transducers are associated with reversible physical effects. In a reversible effect the same device can, for example, convert mechanical energy into electrical energy and also convert electrical energy into mechanical energy. When the device converts electrical energy into mechanical energy it acts as a **transmitter** or **sender**.

This can be represented by a two-port network with an input electrical port and an output mechanical port as in Figure 5.20(a). When the device converts mechanical energy into electrical energy it acts as a **receiver** or **sensor**, and can be represented by an input mechanical port and an output electrical port as in Figure 5.20(b).

The piezoelectric effect is a common example of a reversible effect (Section 8.7). In the **direct effect** a force F applied to the crystal produces a charge q , proportional to F , according to:

$$q = dF \quad [5.34]$$

Figure 5.20 Bilateral transducers:
(a) Transmitter/sender
(b) Receiver/sensor.



i.e. this is a conversion of mechanical energy to electrical energy and the device acts as a receiver or sensor. In the **inverse effect** a voltage V applied to the crystal produces a mechanical deformation x , proportional to V , according to:

$$x = dV \quad [5.35]$$

This is a conversion of electrical energy to mechanical energy and the device acts as a transmitter or sender. The detailed equivalent circuits for a piezoelectric transmitter and receiver are given in Section 16.2.1.

Another reversible physical effect is the **electromagnetic effect**. In the direct effect, a conductor of length l moving with velocity \dot{x} perpendicular to a magnetic field B has a voltage

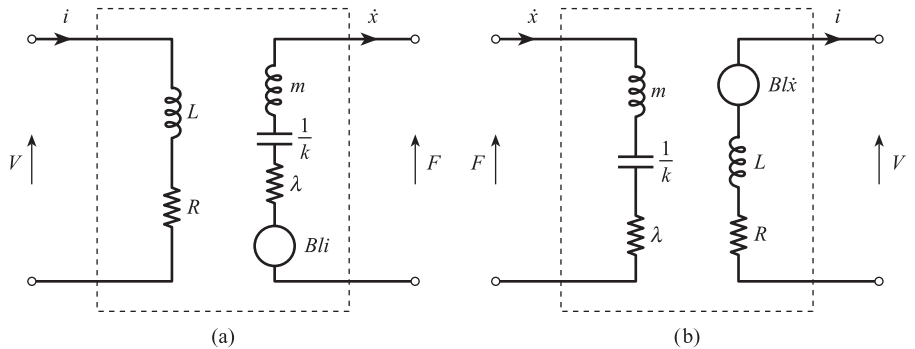
$$E = Bl\dot{x} \quad [5.36]$$

induced across the ends of the conductor. This is a conversion of mechanical to electrical energy and the device acts as a receiver or sensor. In the inverse effect a conductor of length l carrying a current i in a transverse magnetic field B experiences a force

$$F = Bli \quad [5.37]$$

This is a conversion of electrical to mechanical energy and the device acts as a transmitter or sender. Figure 5.21 gives the detailed equivalent circuits for an electromagnetic transmitter and receiver. At the electrical ports the applied voltage drives a current through the electrical impedance L, R ; at the mechanical ports the applied force drives a velocity through the mechanical impedance $m, 1/k, \lambda$. The transmitter can be used as a voltage indicator (Section 11.2) and the receiver as a velocity sensor (Sections 5.1.1 and 8.4).

Figure 5.21 Equivalent circuits for bilateral electromagnetic transducers:
(a) Transmitter/sender
(b) Receiver/sensor.



Conclusion

We have seen how the use of equivalent circuits and two-port networks has enabled both inter-element and process loading effects to be described.

References

- [1] BELL E C and WHITEHEAD R W 1979 *Basic Electrical Engineering and Instrumentation for Engineers*, Granada, London, pp. 46–7.
- [2] FINKELSTEIN L and WATTS R D 1971 ‘Systems analysis of instruments’, *Journal of the Institute of Measurement and Control*, vol. 4, Sept., pp. 236–7.

Problems

- 5.1 A glass pH electrode with a sensitivity of 59 mV pH^{-1} and a resistance of $10^9 \Omega$ is used to measure pH in the range 0 to 15. The electrode is to be connected to a recorder of input range 0 to 100 mV and resistance 100Ω using a buffer amplifier of unity gain and output resistance 100Ω .
 - (a) Calculate the input impedance of the amplifier, and the sensitivity of the recorder scale necessary to obtain an accurate recording of pH.
 - (b) The resistance of the electrode increases to $2 \times 10^9 \Omega$ due to chemical action. Calculate the resulting measurement error in the above system, as a percentage of full scale, for a true pH of 7.
- 5.2 The motion of a hydraulic ram is to be recorded using a potentiometer displacement sensor connected to a recorder. The potentiometer is 25 cm long and has linear resistance displacement characteristics. A set of potentiometers with maximum power rating of 5 W and resistance values ranging from 250 to 2500Ω in 250Ω steps is available. The recorder has a resistance of 5000Ω and the non-linear error of the system must not exceed 2% of full scale. Find:
 - (a) the maximum potentiometer sensitivity that can be obtained;
 - (b) the required potentiometer resistance and supply voltage in order to achieve maximum sensitivity.
- 5.3 An electronic differential transmitter gives a current output of 4 to 20 mA linearly related to a differential pressure input of 0 to 10^4 Pa . The Norton impedance of the transmitter is $10^5 \Omega$. The transmitter is connected to an indicator of impedance 250Ω via a cable of total resistance 500Ω . The indicator gives a reading between 0 and 10^4 Pa for an input voltage between 1 and 5 V. Calculate the system measurement error, due to loading, for an input pressure of $5 \times 10^3 \text{ Pa}$.
- 5.4 A sensor with mass 0.1 kg, stiffness 10^3 N m^{-1} and damping constant 10 N s m^{-1} is used to measure the force on a mechanical structure of mass 5 kg, stiffness 10^2 N m^{-1} and damping constant 20 N s m^{-1} . Find the transfer function relating measured and actual changes in force.

Basic problems

- 5.5 A linear thermocouple with a sensitivity of $0.04 \text{ mV}/^\circ\text{C}$ and resistance of 100Ω is connected to a load with a resistance of $1 \text{ k}\Omega$. Find the voltage across the load for a temperature of 250°C .
- 5.6 A potentiometer displacement sensor has a supply voltage of 15 V and a resistance of $50 \text{ k}\Omega$. The fractional displacement of the wiper is 0.3 . Find the Thévenin voltage and resistance for the circuit.
- 5.7 A potentiometer has a supply voltage of 10 V , a resistance of $10 \text{ k}\Omega$ and a length of 10 cm . A recorder of resistance $10 \text{ k}\Omega$ is connected across the potentiometer. Calculate the Thévenin equivalent circuit for the sensor and the recorder voltage for each of the following displacements:
- 2 cm
 - 5 cm
 - 8 cm .
- 5.8 A potentiometer has a total length of 10 cm and a resistance of 100Ω .
- Calculate the supply voltage so that power dissipation $= 1 \text{ W}$.
 - Draw the Thévenin equivalent circuit for 7 cm displacement.
 - The potentiometer is connected to a recorder with a resistance R_L . Find R_L such that the recorder voltage is 5% less than the open circuit voltage at 7 cm displacement.
- 5.9 A pressure transducer consists of a Bourdon tube elastic element connected to a potentiometer displacement sensor. The input range of the Bourdon tube is 0 to 10^4 Pa and the output range is 0 to 1 cm . The potentiometer has a length of 1 cm , a resistance of $10 \text{ k}\Omega$ and a supply voltage of 10 V . If the input pressure is $5 \times 10^3 \text{ Pa}$, calculate:
- the displacement of the potentiometer wiper (assume a linear Bourdon tube)
 - the open circuit transducer output voltage
 - the voltage indicated by a voltmeter of resistance $10 \text{ k}\Omega$ connected across the potentiometer.

6

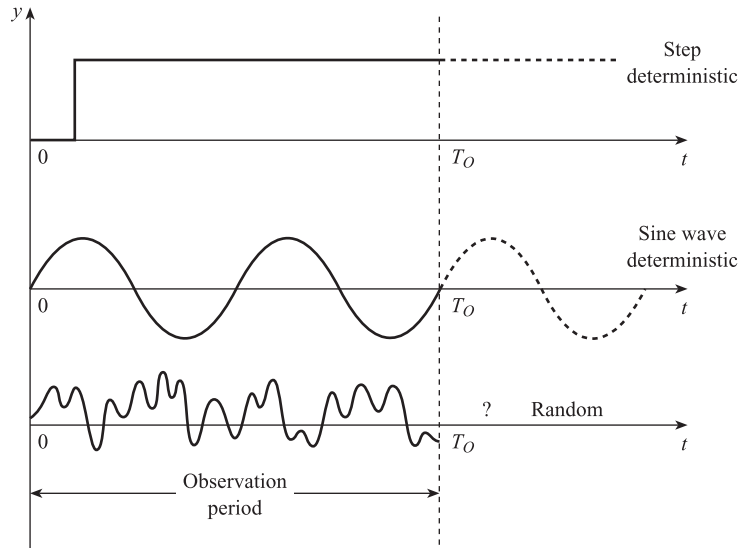
Signals and Noise in Measurement Systems

6.1

Introduction

In Chapter 4 we studied the dynamic response of measurement systems to step, sine wave and square wave input signals. These signals are examples of **deterministic signals**: a deterministic signal is one whose value at any future time can be exactly predicted. Thus if we record these signals for an observation period T_o (Figure 6.1), the future behaviour of the signal, once the observation period is over, is known exactly. The future behaviour of real processes, such as chemical reactors, blast furnaces and aircraft, will depend on unknown factors such as the type of feedstock, reliability of equipment, changes in throughput and atmospheric conditions, and cannot be known in advance. This means that the future value of measured variables, such as reactor temperature, flow in a pipe and aircraft speed, *cannot* be exactly predicted. Thus in real measurement applications the input signal to the measurement system is not deterministic but **random**. If a random signal is recorded for an observation period T_o (Figure 6.1) the behaviour of the signal, once the observation period is over, is *not* known exactly. However, five statistical quantities – mean, standard deviation, probability density function, power spectral density and autocorrelation function – are used to estimate the behaviour of random signals. These are defined and explained in Section 6.2.

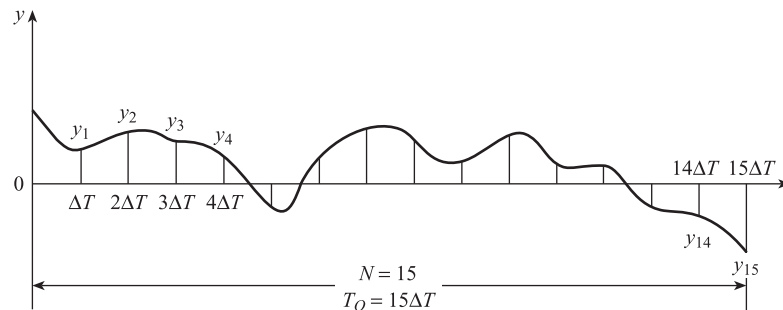
Random variations in the measured input variable produce corresponding random variations in the electrical output signals of elements in the system. More precisely the Thévenin voltage and Norton current signals defined in Chapter 5 vary randomly with time and will be referred to as the **measurement signal**. Examples are random fluctuations in the millivolt output of a thermocouple, random fluctuations in the current output of a differential pressure transmitter, and random fluctuations in the amplitude and frequency of the a.c. output voltage of a variable reluctance tachogenerator. However, unwanted electrical signals may also be present in the measurement circuit. These may be due to sources inside the measurement circuit or caused by coupling to sources outside the circuit. The magnitude of the unwanted signal may be comparable to or larger than that of the measurement signal itself, resulting in a measurement error for the overall system. This is an example of the **interfering inputs** discussed in Chapter 2. The unwanted signal then may be either random, e.g. signals caused by the random motion of electrons, or deterministic, e.g. sinusoidal signals at 50 Hz caused by power cables. Unwanted random signals are usually referred to as **noise signals** and unwanted deterministic signals as **interference signals**.

Figure 6.1 Deterministic and random signals.

Sections 6.3 and 6.4 discuss the sources of noise and interference signals and how they affect the measurement circuit. Section 6.5 examines ways of reducing the effects of noise and interference.

6.2 Statistical representation of random signals

Figure 6.2 shows a recording of a section of a random signal obtained during an observation period T_o . Since the signal is random we cannot write down a continuous algebraic equation $y(t)$ for the signal voltage y at time t . We can, however, write down the values y_1 to y_N of N samples taken at equal intervals ΔT during T_o . The first sample y_1 is taken at $t = \Delta T$, the second y_2 is taken at $t = 2\Delta T$, and the i th y_i is taken at $t = i\Delta T$, where $i = 1, \dots, N$. The sampling interval $\Delta T = T_o/N$ must satisfy the Nyquist sampling theorem, which is explained in Section 10.1. We can now use these samples to calculate statistical quantities for the observed section of the signal. These observed statistical quantities will provide a good estimate of the future behaviour of the signal, once the observation period is over, provided:

Figure 6.2 Sampling of a random signal.

- (a) T_O is sufficiently long, i.e. N is sufficiently large;
- (b) the signal is **stationary**, i.e. long-term statistical quantities do not change with time.

6.2.1 Mean \bar{y}

For a signal defined in terms of a continuous function $y(t)$ in the interval 0 to T_O , the mean is given by:

Mean for continuous signal

$$\bar{y} = \frac{1}{T_O} \int_0^{T_O} y(t) dt \quad [6.1]$$

If, however, the signal is represented by the set of sampled values y_i we have

Mean for sampled signal

$$\bar{y} = \frac{1}{N} \sum_{i=1}^{i=N} y_i \quad [6.2]$$

6.2.2 Standard deviation σ

This is a measure of the average spread or deviation of the signal from the mean value \bar{y} . In the continuous case:

Standard deviation for continuous signal

$$\sigma^2 = \frac{1}{T_O} \int_0^{T_O} [y(t) - \bar{y}]^2 dt \quad [6.3]$$

and in the sampled case:

Standard deviation for sampled signal

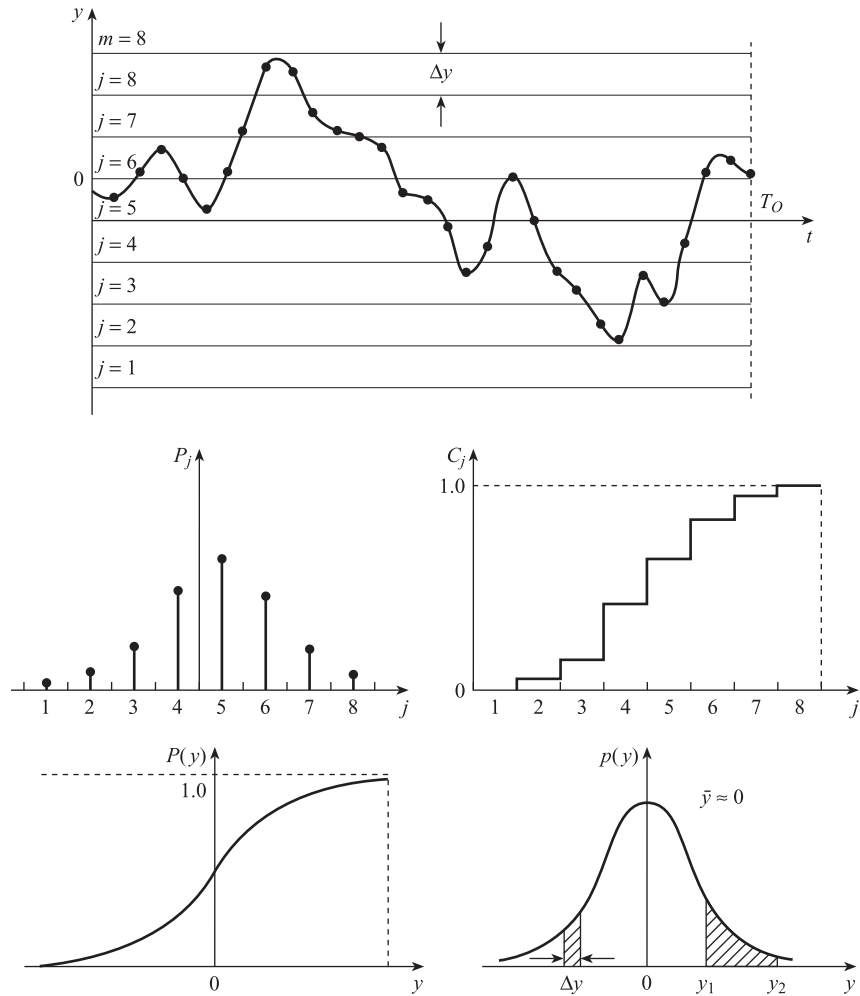
$$\sigma^2 = \frac{1}{N} \sum_{i=1}^{i=N} (y_i - \bar{y})^2 \quad [6.4]$$

In the special case that $\bar{y} = 0$, the standard deviation σ is equal to the **root mean square** (r.m.s.) value y_{rms} , where:

$$y_{\text{rms}} = \sqrt{\frac{1}{T_O} \int_0^{T_O} y^2 dt} \quad [6.5]$$

or

$$y_{\text{rms}} = \sqrt{\frac{1}{N} \sum_{i=1}^{i=N} y_i^2} \quad [6.6]$$

Figure 6.3 Probability and probability density.

6.2.3 Probability density function $p(y)$

This is a function of signal value y and is a measure of the probability that the signal will have a certain range of values. Figure 6.3 shows the set of sample values y_i and the y axis divided into m sections each of width Δy . We can then count the number of samples occurring within each section, i.e. n_1 in section 1, n_2 in section 2, n_j in section j , etc., where $j = 1, \dots, m$. The **probability** P_j of the signal occurring in the j th section is thus:

$$P_j = \frac{\text{number of times sample occurs in the } j\text{th section}}{\text{total number of samples}} \quad [6.7]$$

$$= \frac{n_j}{N}, \quad j = 1, \dots, m$$

The **cumulative probability** C_j is the total probability that the signal will occur in the first j sections and is given by:

Cumulative probability

$$\begin{aligned} C_j &= P_1 + P_2 + \dots + P_j \\ &= \frac{1}{N}(n_1 + n_2 + \dots + n_j) \end{aligned} \quad [6.8]$$

Figure 6.3 shows the corresponding forms of P_j and C_j . The final value of C_j when $j = m$ is:

$$\begin{aligned} C_m &= \frac{1}{N}(n_1 + n_2 + \dots + n_m) \\ &= \frac{1}{N} \times N = 1 \quad (\text{since } n_1 + n_2 + \dots + n_m = N) \end{aligned} \quad [6.9]$$

i.e. the total probability of finding the signal in all m sections is unity. In the limit as the interval Δy tends to zero the discrete cumulative probability C_j tends to a continuous function (Figure 6.3). This is the **cumulative probability distribution function** (c.d.f.) $P(y)$, which is defined by:

Cumulative probability
distribution function

$$P(y) = \lim_{\Delta y \rightarrow 0} C_j \quad [6.10]$$

The **probability density function** (p.d.f.) $p(y)$ is more commonly used and is the derivative of $P(y)$, i.e.

Probability density
function

$$p(y) = \frac{dP}{dy} \quad [6.11]$$

Thus the probability $P_{y,y+\Delta y}$ that the signal will lie between y and $y + \Delta y$ is given by:

$$P_{y,y+\Delta y} = \Delta P = p(y)\Delta y \quad [6.12]$$

i.e. by the area of a strip of height $p(y)$ and width Δy . Similarly the probability P_{y_1,y_2} that the signal will lie between y_1 and y_2 is given by:

$$P_{y_1,y_2} = \int_{y_1}^{y_2} p(y) dy \quad [6.13]$$

i.e. the area under the probability density curve between y_1 and y_2 . The total area under the probability density curve is equal to unity, corresponding to the total probability of the signal having any value of y . The normal probability density function (Section 2.3), i.e.

$$p(y) = \frac{1}{\sigma\sqrt{2\pi}} \exp\left[-\frac{(y - \bar{y})^2}{2\sigma^2}\right] \quad [6.14]$$

usually provides an adequate description of the amplitude distribution of random noise signals.

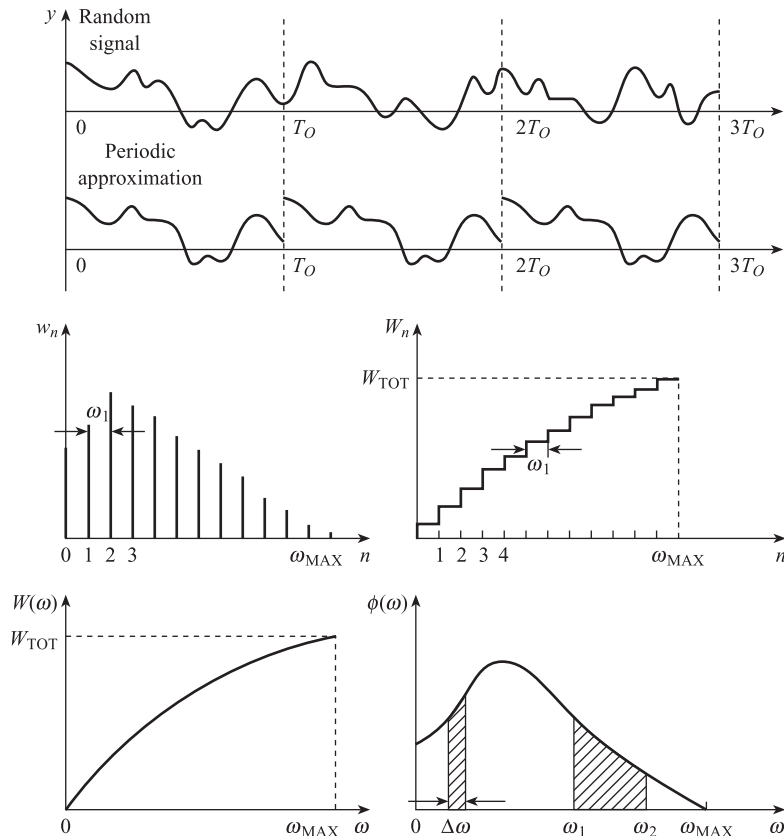
6.2.4 Power spectral density $\phi(\omega)$

If we record a random signal for several observation periods, each of length T_O (Figure 6.4), the waveform will be different for each period. However, the average signal power will be approximately the same for each observation period. This means that signal power is a **stationary** quantity which can be used to quantify random signals. In Section 4.3 we saw that a **periodic** signal can be expressed as a **Fourier series**, i.e. a sum of sine and cosine waves with frequencies which are harmonics of the fundamental frequency. The power in a periodic signal is therefore distributed amongst these harmonic frequencies. A random signal is not periodic and cannot be represented by Fourier series but does contain a large number of closely spaced frequencies. Power spectral density is a stationary quantity which is a measure of how the power in a random signal is distributed amongst these different frequencies.

In order to explain the meaning of $\phi(\omega)$ we approximate the random signal by a periodic signal (Figure 6.4) in which the waveform recorded during the first observation period T_O is exactly repeated during each subsequent observation period. This periodic approximation is valid:

- in the limit that the observation period, i.e. the signal period T_O , becomes large,
- provided we use it to calculate the power distribution in the signal.

Figure 6.4 Power spectrum and power spectral density.



The Fourier series for a voltage signal with period T_O is

$$y(t) = a_0 + \sum_{n=1}^{\infty} a_n \cos n\omega_1 t + \sum_{n=1}^{\infty} b_n \sin n\omega_1 t \quad [4.51a]$$

where the fundamental frequency $\omega_1 = 2\pi/T_O$, $a_0 = \text{mean } \bar{y}$, and

*Fourier series
coefficients for
sampled signal*

$$\begin{aligned} a_n &= \frac{2}{N} \sum_{i=1}^{i=N} y_i \cos(n\omega_1 i \Delta T) = \frac{2}{N} \sum_{i=1}^{i=N} y_i \cos\left(2\pi n \frac{i}{N}\right) \\ b_n &= \frac{2}{N} \sum_{i=1}^{i=N} y_i \sin(n\omega_1 i \Delta T) = \frac{2}{N} \sum_{i=1}^{i=N} y_i \sin\left(2\pi n \frac{i}{N}\right) \end{aligned} \quad [6.15]$$

Equations [6.15] use the set of sample values y_i and are equivalent to eqns [4.52] for the Fourier coefficients of a continuous signal. If the n th harmonic $a_n \cos n\omega_1 t$ is applied across a 1Ω resistor, the instantaneous power in the resistor at time t is $a_n^2 \cos^2 n\omega_1 t$ watts, and the average power over period T_O is:

$$a_n^2 \frac{1}{T_O} \int_0^{T_O} \cos^2 n\omega_1 t \, dt = \frac{a_n^2}{2} \quad [6.16]$$

Similarly the average power in a 1Ω resistor due to $b_n \sin n\omega_1 t$ is $b_n^2/2$, so that the power due to the n th harmonic at frequency $n\omega_1$ is:

*Power due to
nth harmonic*

$$w_n = \frac{1}{2}(a_n^2 + b_n^2) \quad [6.17]$$

Figure 6.4 shows that the relationship between w_n and ω is a series of lines at the harmonic frequencies $n\omega_1$. This is referred to as the **power spectrum** of the signal and is terminated at ω_{MAX} , the harmonic frequency beyond which w_n becomes negligible. The **cumulative power** W_n is the total power in a 1Ω resistor due to the first n harmonics and the d.c. component a_0 , i.e.

Cumulative power

$$W_n = w_0 + w_1 + w_2 + \dots + w_n \quad [6.18]$$

The diagram shows the relation between W_n and ω ; it is in the form of a staircase, each step having width ω_1 . At $\omega = \omega_{\text{MAX}}$, $W_n = W_{\text{TOT}}$, the total power in the signal. However, in the limit that signal period $T_O \rightarrow \infty$, $\omega_1 \rightarrow 0$ and W_n becomes a continuous function of ω . This is the **cumulative power function** (c.p.f.) $W(\omega)$, which is defined by:

*Cumulative power
function*

$$W(\omega) = \lim_{\omega_1 \rightarrow 0} W_n \quad [6.19]$$

The **power spectral density** (PSD) $\phi(\omega)$ is more commonly used and is the derivative of $W(\omega)$ (Figure 6.4), i.e.

Power spectral density

$$\phi(\omega) = \frac{dW}{d\omega} \quad [6.20]$$

The PSD ϕ has units watt s rad⁻¹ or W/Hz. Thus the power produced in a 1 Ω resistor due to frequencies between ω and $\omega + \Delta\omega$ is:

$$W_{\omega, \omega + \Delta\omega} = \Delta W = \phi(\omega) \Delta\omega \text{ watts} \quad [6.21]$$

i.e. the area of a strip of height $\phi(\omega)$ and width $\Delta\omega$. Similarly the power due to frequencies between ω_1 and ω_2 is:

$$W_{\omega_1, \omega_2} = \int_{\omega_1}^{\omega_2} \phi(\omega) d\omega \text{ watts} \quad [6.22]$$

i.e. the area under the power spectral density curve between ω_1 and ω_2 . The total area under the PSD curve is the total power in the signal, i.e.

$$W_{\text{TOT}} = \int_0^{\omega_{\text{MAX}}} \phi(\omega) d\omega \text{ watts} \quad [6.23]$$

Internal noise sources in electrical circuits can often be regarded as **white noise**, which has a uniform PSD over an infinite range of frequencies, i.e.

$$\phi(\omega) = A, \quad 0 \leq \omega \leq \infty \quad [6.24]$$

Another useful representation for both noise and measurement signals is a power spectral density which is constant up to a cut-off frequency ω_c and zero for higher frequencies (**band limited white noise**):

$$\phi(\omega) = \begin{cases} A, & 0 \leq \omega \leq \omega_c \\ 0, & \omega > \omega_c \end{cases} \quad [6.25]$$

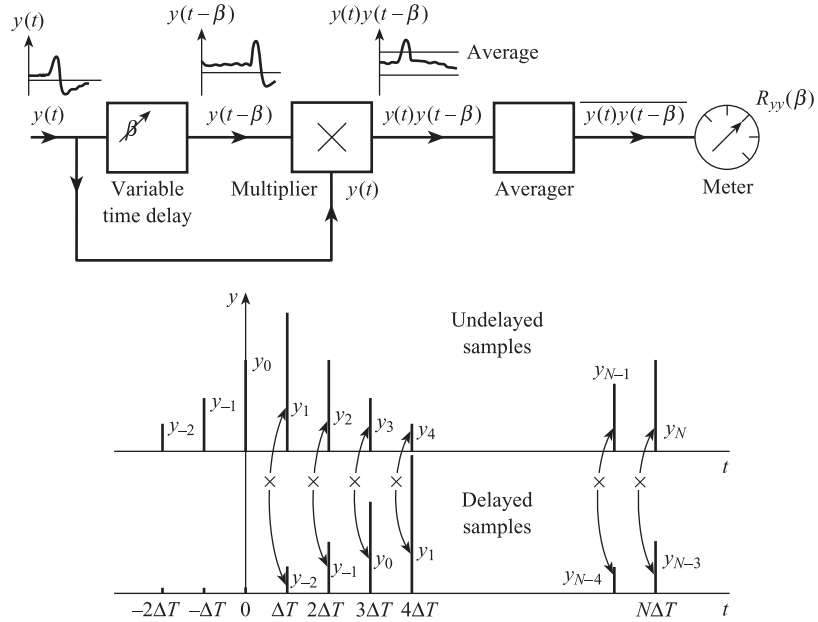
i.e. $W_{\text{TOT}} = A\omega_c$.

The maximum frequency ω_{MAX} for a measurement signal depends on the nature of the measured variable. Thus the vibration displacement of part of a machine may contain frequencies up to many kHz, whereas the temperature variations in a chemical reactor may only contain frequencies up to 0.01 Hz. In order to accurately measure random fluctuations in a measured variable, the transfer function $G(s)$ for the measurement system must satisfy the conditions of Section 4.4, i.e. $|G(j\omega)| = 1$ and $\arg G(j\omega) = 0$ for all ω up to ω_{MAX} .

6.2.5 Autocorrelation function

Figure 6.5 shows a block diagram of a simple correlator. The input signal $y(t)$ is passed through a variable time delay unit to give a delayed signal $y(t - \beta)$. The signals $y(t)$ and $y(t - \beta)$ are multiplied together to give the product waveform $y(t)y(t - \beta)$. This product waveform is passed through an averager and the average value $\overline{y(t)y(t - \beta)}$ is displayed on a meter: this is the **autocorrelation coefficient** R_{yy} . If the time delay β is altered, the shape of the product waveform changes, causing the meter reading R_{yy} to change. The relationship between R_{yy} and time delay β is the **autocorrelation function** $R_{yy}(\beta)$ of the signal. We note that $R_{yy}(\beta)$ has a maximum value

Figure 6.5
Autocorrelation
and evaluation of
autocorrelation coefficient
 $R_{yy}(3\Delta T)$.



$R_{yy}(0)$ when $\beta = 0$; this is because the corresponding product waveform is $y^2(t)$, which is always positive and has a maximum average value.

If the signal is defined by a continuous function $y(t)$ in the interval 0 to T_o , then $R_{yy}(\beta)$ can be evaluated using:

*Autocorrelation
function of a
continuous signal*

$$R_{yy}(\beta) = \lim_{T_o \rightarrow \infty} \frac{1}{T_o} \int_0^{T_o} y(t)y(t-\beta) dt \quad [6.26]$$

Thus, if $y(t) = b \sin(\omega_1 t + \phi)$,

$$\begin{aligned} R_{yy}(\beta) &= b^2 \lim_{T_o \rightarrow \infty} \frac{1}{T_o} \int_0^{T_o} \sin(\omega_1 t + \phi) \sin[\omega_1(t - \beta) + \phi] dt \\ &= b^2 \lim_{T_o \rightarrow \infty} \frac{1}{T_o} \int_0^{T_o} \frac{1}{2} \{ \cos \omega_1 \beta - \cos[\omega_1(2t - \beta) + 2\phi] \} dt \\ &= \frac{b^2}{2} \cos \omega_1 \beta \lim_{T_o \rightarrow \infty} \frac{1}{T_o} \int_0^{T_o} dt - \frac{b^2}{2} \lim_{T_o \rightarrow \infty} \frac{1}{T_o} \int_0^{T_o} \cos[\omega_1(2t - \beta) + 2\phi] dt \\ &= \frac{b^2}{2} \cos \omega_1 \beta \end{aligned} \quad [6.27]$$

since the average value of $\cos[\omega_1(2t - \beta) + 2\phi]$ is zero. Thus the autocorrelation function of a sinusoidal signal is a cosine function of the same frequency, but the phase information ϕ in the sine wave is lost. The autocorrelation function of any periodic signal has the same period as the signal itself (see Problem 6.2).

A random signal is usually characterised by a set of N sample values y_i . Since information is only available at discrete time intervals, the time delay β is normally an integer multiple of the sampling interval ΔT , i.e.

$$\beta = m\Delta T, \quad m = 0, 1, 2, \dots \quad [6.28]$$

In this case the autocorrelation function of the signal is found by evaluating the set of autocorrelation coefficients $R_{yy}(m\Delta T)$, which are given by:

*Autocorrelation
coefficient for
sampled signal*

$$R_{yy}(m\Delta T) = \lim_{N \rightarrow \infty} \frac{1}{N} \sum_{i=1}^{i=N} y_i y_{i-m} \quad [6.29]$$

where y_i is the sample value at time $i\Delta T$ and y_{i-m} the value at time $(i-m)\Delta T$ (m sampling intervals earlier). Figure 6.5 shows the evaluation of $R_{yy}(3\Delta T)$ for a sampled waveform; this involves calculating the products $y_1 y_{-2}$, $y_2 y_{-1}$, $y_3 y_0$, \dots , $y_N y_{N-3}$, summing, and dividing by N .

The autocorrelation function of a random signal can also be found from the power spectral density $\phi(\omega)$. To illustrate this we first consider a periodic signal which is the sum of three harmonics:

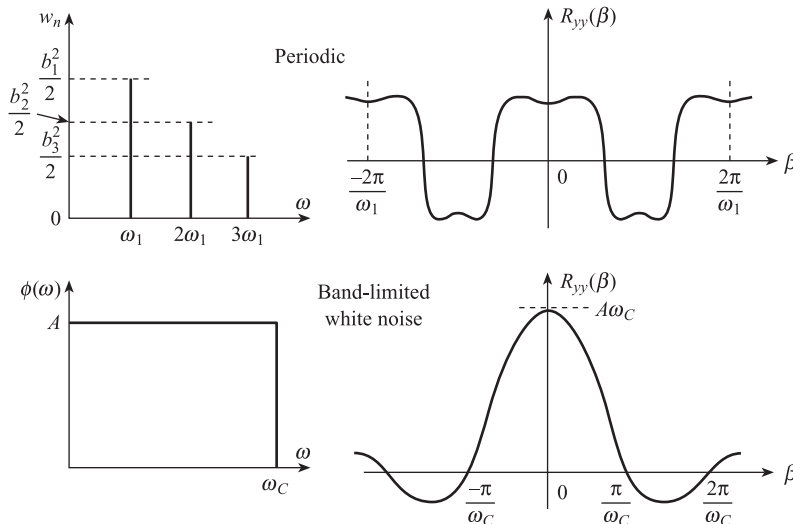
$$y(t) = b_1 \sin \omega_1 t + b_2 \sin 2\omega_1 t + b_3 \sin 3\omega_1 t$$

Using eqn [6.27] the autocorrelation function is:

$$R_{yy}(\beta) = \frac{b_1^2}{2} \cos \omega_1 \beta + \frac{b_2^2}{2} \cos 2\omega_1 \beta + \frac{b_3^2}{2} \cos 3\omega_1 \beta$$

which has period $2\pi/\omega_1$ (Figure 6.6). Using eqn [6.17], the power spectrum of the signal consists of three lines at frequencies ω_1 , $2\omega_1$ and $3\omega_1$ with heights $b_1^2/2$, $b_2^2/2$ and $b_3^2/2$ respectively. Thus the power spectrum can be obtained from the autocorrelation function by Fourier analysis. Similarly the autocorrelation function can be obtained from the power spectrum by adding the harmonics together as in Fourier synthesis. For random signals, $R_{yy}(\beta)$ and $\phi(\omega)$ are related by the Fourier transform or Wiener–Khinchin relations:

Figure 6.6 Relationships between power spectrum and autocorrelation function for periodic and random signals.



$$\begin{aligned}
 R_{yy}(\beta) &= \int_0^\infty \phi(\omega) \cos \omega\beta \, d\omega \\
 \phi(\omega) &= \frac{2}{\pi} \int_0^\infty R_{yy}(\beta) \cos \omega\beta \, d\beta
 \end{aligned}
 \tag{6.30}$$

Thus for a signal with $\phi(\omega)$ constant up to ω_c and zero for higher frequencies we have:

$$R_{yy}(\beta) = \int_0^{\omega_c} A \cos \omega\beta \, d\omega = A \left[\frac{\sin \omega\beta}{\beta} \right]_0^{\omega_c} = A \frac{\sin \omega_c \beta}{\beta}
 \tag{6.31}$$

The form of both functions is shown in Figure 6.6; we see that $R_{yy}(\beta)$ has its first zero crossings at $\beta = \pm\pi/\omega_c$, i.e. the width of the central ‘spike’ is $2\pi/\omega_c$. Thus a rapidly varying random signal has a high value of ω_c , i.e. a broad power spectrum but a narrow autocorrelation function, that falls off sharply as β is increased. A slowly varying random signal, however, has a low value of ω_c , i.e. a narrow power spectrum but a broad autocorrelation function that falls slowly as β is increased.

6.2.6 Summary

In order to specify a random signal we need to know:

$\left\{ \begin{array}{l} \text{either } \mathbf{probability\ density\ function} \\ \text{or } \mathbf{mean\ and\ standard\ deviation} \end{array} \right\}$ to specify amplitude behaviour

and

$\left\{ \begin{array}{l} \text{either } \mathbf{power\ spectral\ density} \\ \text{or } \mathbf{autocorrelation\ function} \end{array} \right\}$ to specify frequency/time behaviour

Important relations between these different quantities can be derived by considering $R_{yy}(0)$, the autocorrelation coefficient at zero time delay. From eqns [6.26] and [6.30] we have

$$R_{yy}(0) = \lim_{T_o \rightarrow \infty} \frac{1}{T_o} \int_0^{T_o} y^2 \, dt = \int_0^\infty \phi(\omega) \, d\omega
 \tag{6.32}$$

From eqn [6.5], the first expression is equal to y_{RMS}^2 in the limit of infinitely long observation time T_o . From equation [6.23] the second expression is equal to W_{TOT} , the total power produced by the signal in a $1 \, \Omega$ resistor. Thus:

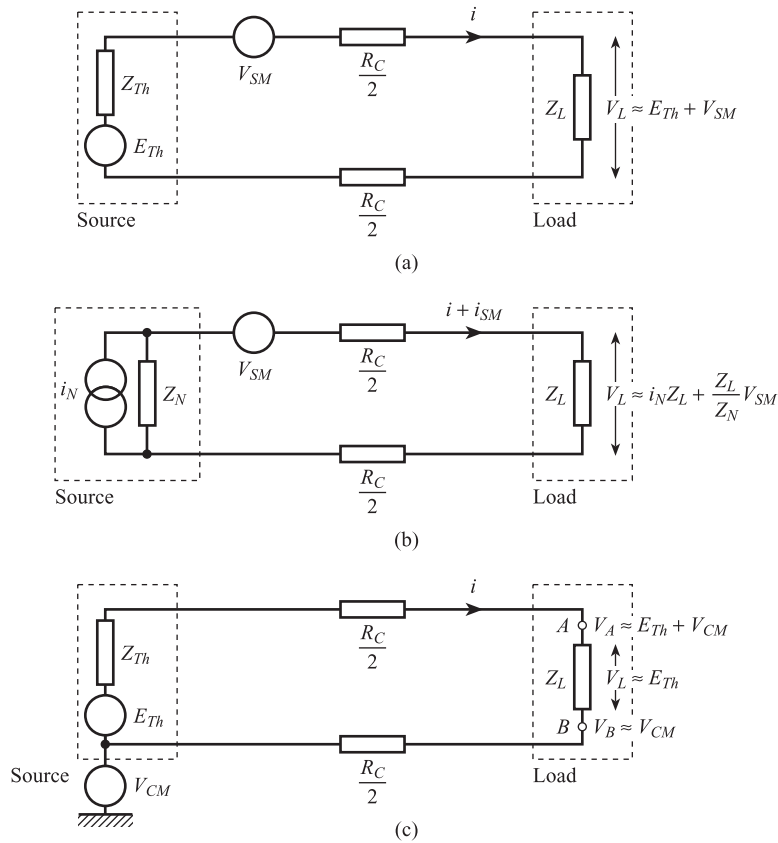
$R_{yy}(0) = y_{\text{RMS}}^2 = W_{\text{TOT}}$	[6.33]
---	--------

6.3

Effects of noise and interference on measurement circuits

In Section 5.1 we saw that the interconnection of two measurement system elements, e.g. a thermocouple and an amplifier, or a differential pressure transmitter and a recorder, could be represented by an equivalent circuit in which either a Thévenin voltage

Figure 6.7 Effects of interference on measurement circuit:
 (a) Voltage transmission – series mode interference
 (b) Current transmission – series mode interference
 (c) Voltage transmission – common mode interference.



source or a Norton current source is connected to a load. In industrial installations, source and load may be typically 100 metres apart and noise and/or interference voltages may also be present.

Figure 6.7(a) shows a **voltage transmission system** subject to **series mode interference**; here a noise or interference voltage V_{SM} is in series with the measurement signal voltage E_{Th} . The current i through the load is:

$$i = \frac{E_{Th} + V_{SM}}{Z_{Th} + R_C + Z_L}$$

and the corresponding voltage across the load is:

$$V_L = \frac{Z_L}{Z_{Th} + R_C + Z_L} (E_{Th} + V_{SM}) \quad [6.34]$$

Normally we make $Z_L \gg R_C + Z_{Th}$ to obtain maximum voltage transfer to the load (Section 5.1.1); under these conditions eqn [6.34] becomes:

$$V_L \approx E_{Th} + V_{SM} \quad [6.35]$$

This means that with a voltage transmission system all of V_{SM} is across the load; this affects the next element in the system and possibly results in a system measurement error. We define **signal-to-noise** or **signal to interference ratio** S/N in decibels by:

Signal-to-noise ratio

$$\frac{S}{N} = 20 \log_{10} \left(\frac{E_{Th}}{V_{SM}} \right) = 10 \log_{10} \left(\frac{W_S}{W_N} \right) \text{ dB} \quad [6.36]$$

where E_{Th} and V_{SM} are the r.m.s. values of the voltages, and W_S and W_N are the corresponding total signal and noise powers. Thus if $E_{Th} = 1 \text{ V}$ and $V_{SM} = 0.1 \text{ V}$, $S/N = +20 \text{ dB}$.

Figure 6.7(b) shows a **current transmission system** subject to the same series mode interference voltage V_{SM} . The Norton source current i_N divides into two parts, one part through the source impedance Z_N , the other part through Z_L . Using the current divider rule, the current through the load due to the source is:

$$i = i_N \frac{Z_N}{Z_N + R_C + Z_L}$$

In addition there is an interference current

$$i_{SM} = \frac{V_{SM}}{Z_N + R_C + Z_L}$$

through the load due to the interference voltage. The total voltage across the load is therefore:

$$\begin{aligned} V_L &= iZ_L + i_{SM}Z_L \\ &= i_N Z_L \cdot \frac{Z_N}{Z_N + R_C + Z_L} + V_{SM} \cdot \frac{Z_L}{Z_N + R_C + Z_L} \end{aligned} \quad [6.37]$$

Normally we make $R_C + Z_L \ll Z_N$ to obtain maximum current transfer to the load (Section 5.1.3); under these conditions eqn [6.37] becomes:

$$V_L \approx i_N Z_L + \frac{Z_L}{Z_N} V_{SM} \quad [6.38]$$

Since $Z_L/Z_N \ll 1$, this means that with a current transmission system only a small fraction of V_{SM} is across the load. Thus a current transmission system has far greater inherent immunity to series mode interference than a voltage transmission system. In a thermocouple temperature measurement system, therefore, it may be better to convert the thermocouple millivolt e.m.f. into a current signal (Section 9.4.1) prior to transmission, rather than transmit the e.m.f. directly.

Figure 6.7(c) shows a voltage transmission system subject to **common mode interference** in which the potentials of both sides of the signal circuit are raised by V_{CM} relative to a common earth plane. If, as above, $Z_L \gg R_C + Z_{Th}$, then current $i \rightarrow 0$ so that the potential drops $iR_C/2$, etc., can be neglected. Under these conditions:

$$\begin{aligned} \text{Potential at } B &= V_{CM} \\ \text{Potential at } A &= V_{CM} + E_{Th} \end{aligned}$$

and

$$V_L = V_B - V_A = E_{Th}$$

This means that the voltage across the load is unaffected by V_{CM} ; there is, however, the possibility of conversion of a common mode voltage to series mode.

6.4 Noise sources and coupling mechanisms

6.4.1 Internal noise sources

The random, temperature-induced motion of electrons and other charge carriers in resistors and semiconductors gives rise to a corresponding random voltage which is called thermal or Johnson noise. This has a power spectral density which is uniform over an infinite range of frequencies (white noise) but proportional to the absolute temperature θ K of the conductor, i.e.

$$\phi = 4Rk\theta \text{ W/Hz} \quad [6.39]$$

where $R\Omega$ is the resistance of the conductor and k is the Boltzmann constant $= 1.4 \times 10^{-23} \text{ J K}^{-1}$. From eqn [6.22] the total thermal noise power between frequencies f_1 and f_2 is:

$$W = \int_{f_1}^{f_2} 4Rk\theta \, df = 4Rk\theta(f_2 - f_1) \text{ W} \quad [6.40]$$

and from [6.33] the corresponding r.m.s. voltage is:

$$V_{\text{RMS}} = \sqrt{W} = \sqrt{4Rk\theta(f_2 - f_1)} \text{ V} \quad [6.41]$$

Thus if $R = 10^6 \Omega$, $f_2 - f_1 = 10^6 \text{ Hz}$ and $\theta = 300 \text{ K}$, $V_{\text{RMS}} = 130 \mu\text{V}$ and is therefore comparable with low-level measurement signals such as the output from a strain gauge bridge.

A similar type of noise is called **shot noise**; this occurs in transistors and is due to random fluctuations in the rate at which carriers diffuse across a junction. This is again characterised by a uniform power spectral density over a wide range of frequencies.

6.4.2 External noise and interference sources^[1]

The most common sources of external interference are nearby **a.c. power circuits** which usually operate at 240 V, 50 Hz. These can produce corresponding sinusoidal interference signals in the measurement circuit, referred to as **mains pick-up** or **hum**. Power distribution lines and heavy rotating machines such as turbines and generators can cause serious interference.

D.C. power circuits are less likely to cause interference because d.c. voltages are not coupled capacitively and inductively to the measurement circuit.

However, **switching** often occurs in both a.c. and d.c. power circuits when equipment such as motors and turbines is being taken off line or brought back on line. This causes sudden large changes in power, i.e. steps and pulses, which can produce corresponding **transients** in the measurement circuit.

The air in the vicinity of high voltage power circuits can become ionised and a **corona discharge** results. Corona discharge from d.c. circuits can result in random noise in the measurement circuit and that from a.c. circuits results in sinusoidal interference at the power frequency or its second harmonic.

Fluorescent lighting is another common interference source; arcing occurs twice per cycle so that most of the interference is at twice the power frequency.

Radio-frequency transmitters, welding equipment and electric arc furnaces can produce **r.f. interference** at frequencies of several MHz.

6.4.3 Coupling mechanisms to external sources

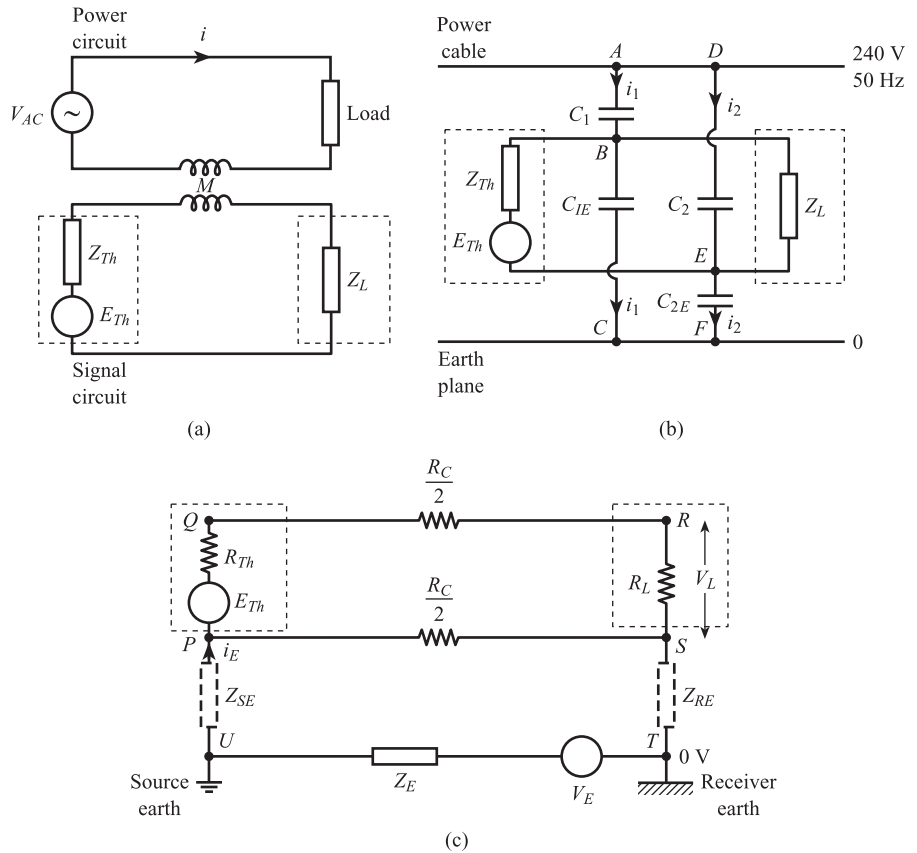
Inductive coupling^[2]

Figure 6.8(a) shows inductive or **electromagnetic coupling** between the measurement circuit and a nearby power circuit. If the circuits are sufficiently close together, then there may be a significant mutual inductance M between them. This means that an alternating current i in the power circuit induces a series mode interference voltage in the measurement circuit of magnitude

$$V_{SM} = M \frac{di}{dt} \quad [6.42]$$

Thus if $M \approx 1 \mu\text{H}$ and $di/dt \approx 10^3 \text{ A s}^{-1}$ (possible in a 1 horsepower motor) then $V_{SM} \approx 1 \text{ mV}$, which can be comparable with the measurement signal. The mutual inductance M depends on the geometry of the two circuits, namely on the overlapping length and separation, but is distributed over the entire length of the circuits rather than the 'lumped' equivalent value shown in Figure 6.8. Inductive coupling will occur even if the measurement circuit is completely isolated from earth.

Figure 6.8 Coupling mechanisms to external sources:
(a) Electromagnetic coupling
(b) Electrostatic coupling
(c) Multiple earths.



Capacitive coupling^[1,2]

Another important coupling mechanism is **capacitive** or **electrostatic coupling**, which is illustrated in Figure 6.8(b). The diagram shows the measurement circuit close to an a.c. power cable which is at a potential of 240 V (r.m.s.) relative to the earth plane. The power cable, earth plane and signal leads are all conductors, so that there may be some capacitance between the power cable and the signal leads and between the signal leads and the earth plane. These capacitances will be distributed over the entire length of the measurement circuit, but are represented by 'lumped' equivalents. C_1 and C_2 are the capacitances between the power cable and signal leads, and C_{1E} and C_{2E} the capacitances between the signal lead and the earth plane; all four capacitances will be proportional to the length of the measurement circuit, which could be tens of metres in an industrial installation. Ignoring the measurement signal voltage E_{Th} for the moment, the potentials at B and E are determined by the potential dividers ABC and DEF :

$$\begin{aligned} V_B &= 240 \left[\frac{1/(j\omega C_{1E})}{1/(j\omega C_{1E}) + 1/(j\omega C_1)} \right] = 240 \frac{C_1}{C_1 + C_{1E}} \\ V_E &= 240 \left[\frac{1/(j\omega C_{2E})}{1/(j\omega C_{2E}) + 1/(j\omega C_2)} \right] = 240 \frac{C_2}{C_2 + C_{2E}} \end{aligned} \quad [6.43]$$

Thus we have a common mode interference voltage $V_{CM} = V_E$ and a series mode interference voltage:

$$V_{SM} = V_B - V_E = 240 \left(\frac{C_1}{C_1 + C_{1E}} - \frac{C_2}{C_2 + C_{2E}} \right) \quad [6.44]$$

Thus series mode interference is zero only if there is perfect balance between the coupling capacitances, i.e. $C_1 = C_2$ and $C_{1E} = C_{2E}$; in practice small imbalances are present due to slightly different distances between each signal lead and the power cable/earth plane.

Multiple earths^[1]

The above explanation assumes an earth plane having a potential of 0 volts at every point on its surface. Heavy electrical equipment can, however, cause currents to flow through the earth, causing different potentials at different points. If the measurement circuit is completely isolated from the earth plane there is no problem. In practice, however, there may be a leakage path connecting the signal source to one earth point and another leakage path connecting the recorder or indicator to a different earth point, some distance away. If the two earth points are at different potentials, then common and series mode interference voltages are produced in the measurement circuit.

Figure 6.8(c) illustrates the general problem of **multiple earths**. The measurement signal source E_{Th} is connected via a resistive cable to a receiver represented by a resistive load R_L . Provided $R_L \gg R_C + R_{Th}$, the current flow in $PQRS$ is negligible and $V_L \approx E_{Th}$, provided the circuit is completely isolated from earth. However, leakage paths Z_{SE} and Z_{RE} exist between source/source earth and receiver/receiver earth. If

V_E is the difference in potential between source earth and receiver earth, then a current i_E flows in the circuit $UPST$, given by:

$$i_E = \frac{V_E}{Z_E + Z_{SE} + (R_C/2) + Z_{RE}} \quad [6.45]$$

Thus

$$\begin{aligned} \text{Potential at } P &= V_E - i_E(Z_E + Z_{SE}) \\ \text{Potential at } Q, R &= V_E - i_E(Z_E + Z_{SE}) + E_{Th} \\ \text{Potential at } S &= i_E Z_{RE} \end{aligned}$$

Thus there is a common mode interference voltage:

$$V_{CM} = V_S = V_E \frac{Z_{RE}}{Z_E + Z_{SE} + (R_C/2) + Z_{RE}} \quad [6.46]$$

To find the series mode interference voltage we need to calculate the voltage across R_L :

$$V_L = V_R - V_S = V_E - i_E(Z_E + Z_{SE} + Z_{RE}) + E_{Th} = E_{Th} + i_E R_C/2$$

i.e. there is a series mode interference voltage:

$$V_{SM} = V_E \frac{R_C/2}{Z_E + Z_{SE} + (R_C/2) + Z_{RE}} \quad [6.47]$$

Ideally we require both Z_{SE} and Z_{RE} to be as large as possible in order to minimise i_E and V_{SM} ; this, however, is not always possible in an industrial application. A common example is a thermocouple installation where in order to achieve as good a speed of response as possible the tip of the thermocouple touches the thermowell or sheath (Section 14.2). The thermowell is itself bolted to a metal vessel or pipe which is in turn connected to one point in the earth plane. Thus Z_{SE} will be very small, say $Z_{SE} = 10 \Omega$ (resistive), so that the receiver must be isolated from earth to minimise V_{SM} . Taking $Z_E = 1 \Omega$, $R_C/2 = 10 \Omega$, $V_E = 1 \text{ V}$ and $Z_{RE} = 10^6 \Omega$, we have:

$$V_{SM} = 1 \times \frac{10}{1 + 10 + 10 + 10^6} \text{ V} \approx 10 \mu\text{V}$$

The worst case is when the receiver is also directly connected to earth, i.e. $Z_{RE} \approx 0$, giving $V_{SM} = 0.48 \text{ V}$. Thus if the measurement circuit must be connected to earth, the connection must be made at one point only.

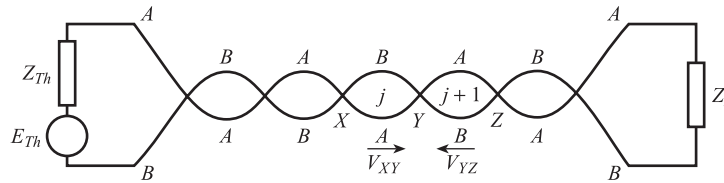
6.5

Methods of reducing effects of noise and interference

6.5.1 Physical separation

Since mutual inductances and coupling capacitances between measurement and power circuits are inversely proportional to the distance between them, this distance should be as large as possible.

Figure 6.9 Reduction of electromagnetic coupling by twisted pairs.



6.5.2 Electromagnetic shielding

The simplest way of reducing the effects of inductive coupling to an external interference source is shown in Figure 6.9. The two conductors *A* and *B* of the measurement circuit are twisted into loops of approximately equal area. This arrangement is commonly known as **twisted pairs** and is explained in ref. [2]. The magnitude of the interference voltage induced in a given loop is proportional to the area of the loop and the rate of change of the external magnetic field. The sign of the induced voltage depends on the orientation of conductors *A* and *B*. Thus if a voltage V_{XY} is induced in the *j*th loop between points *X* and *Y*, then an opposing voltage V_{YZ} is induced in the (*j* + 1)th loop between *Y* and *Z*. In the ideal case of both loops having the same area and experiencing the same magnetic fields, $|V_{XY}| = |V_{YZ}|$, i.e. there is a zero resultant induced voltage between *X* and *Z*. This process is repeated for the whole length of the twisted pair, giving a reduced overall interference voltage.

6.5.3 Electrostatic screening and shielding

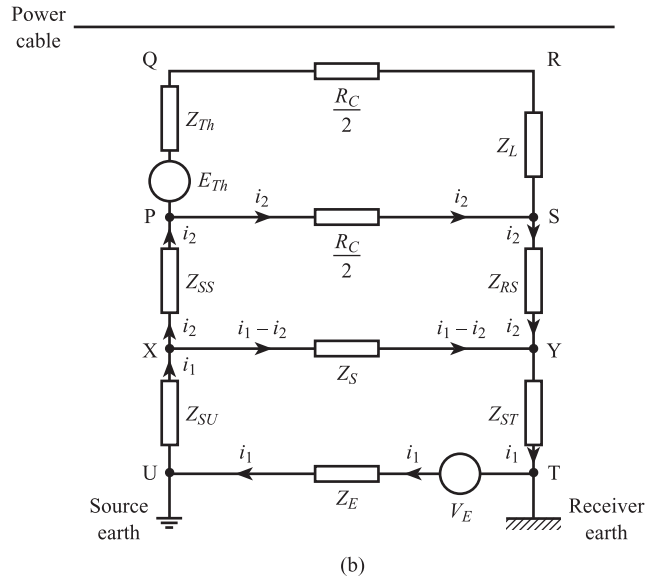
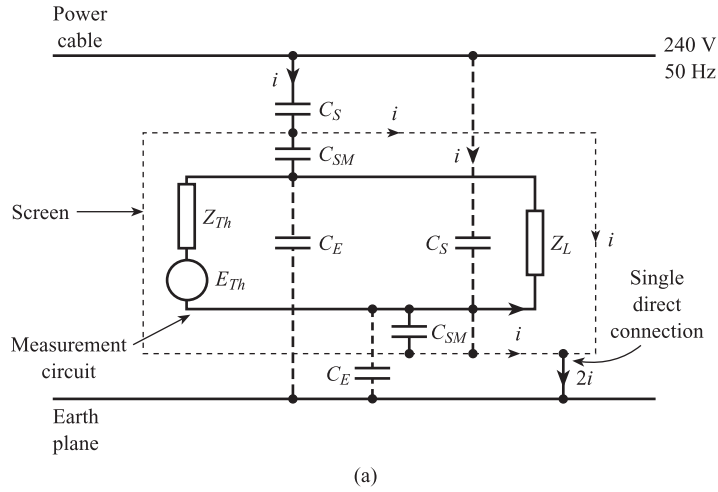
The best method of avoiding the problem of capacitive coupling to a power circuit (Section 6.4.3) is to enclose the entire measurement circuit in an earthed metal screen or shield. Figure 6.10(a) shows the ideal arrangement; the screen is connected directly to earth at a single point, at either the source or the receiver. There is no direct connection between the screen and the measurement circuit, only high impedance leakage paths via the small (screen/measurement circuit) capacitances C_{SM} . The screen provides a low impedance path to earth for the interfering currents *i*; the currents through C_{SM} and C_E are small, thus reducing series and common mode interference.

The above ideal of the measurement circuit completely insulated from the screen and the screen earthed at one point only may be difficult to achieve in practice for the following reasons:

- (a) The signal source may be directly connected to a local earth point via the structure on which it is mounted; an example is the thermocouple installation mentioned in Section 6.4.3.
- (b) The receiver may be directly connected to a local earth; an example is in a computer-based system where the receiver must be directly connected to the computer earth.
- (c) There may be indirect connections via leakage impedances.

Figure 6.10(b) illustrates the general problem. The measurement circuit PQRS is connected to the screen (impedance Z_S) via source/screen impedance Z_{SS} and receiver/screen impedance Z_{RS} . The screen is connected to earth point *U* at the source end via Z_{SU} and to earth point *T* at the receiver end via Z_{ST} . The measurement circuit can be affected by interference voltages from both V_E (potential difference between *U* and *T*) and nearby power circuits.

Figure 6.10 Reduction of electrostatic coupling using screening:
 (a) Ideal arrangement
 (b) Practical equivalent circuit.



Analysis of circuits UXYT and XPSY using Kirchhoff's laws gives:

$$\text{UXYT} \quad V_E = i_1 Z_E + i_1 Z_{SU} + (i_1 - i_2) Z_S + i_1 Z_{ST} \quad [6.48]$$

$$\text{XPSY} \quad 0 = -(i_1 - i_2) Z_S + i_2 Z_{SS} + i_2 R_C/2 + i_2 Z_{RS} \quad [6.49]$$

Solution of these equations gives:

$$i_1 = \frac{(Z_S + Z_{SS} + R_C/2 + Z_{RS}) V_E}{(Z_E + Z_{SU} + Z_S + Z_{ST})(Z_S + Z_{SS} + R_C/2 + Z_{RS}) - Z_S^2} \quad [6.50]$$

$$i_2 = \frac{Z_S V_E}{(Z_E + Z_{SU} + Z_S + Z_{ST})(Z_S + Z_{SS} + R_C/2 + Z_{RS}) - Z_S^2} \quad [6.51]$$

The series mode interference voltage in the measurement circuit PQRS is the voltage drop across PS, i.e.

$$V_{SM} = i_2 R_C / 2 = \frac{Z_S (R_C / 2) V_E}{(Z_E + Z_{SU} + Z_S + Z_{ST})(Z_S + Z_{SS} + R_C / 2 + Z_{RS}) - Z_S^2} \quad [6.52]$$

The common mode interference voltage is the voltage drop across ST, i.e.

$$\begin{aligned} V_{CM} = V_{ST} = V_{SY} + V_{YT} &= i_2 Z_{RS} + i_1 Z_{ST} \\ &= \frac{[Z_{RS} Z_S + Z_{ST}(Z_S + Z_{SS} + R_C / 2 + Z_{RS})] V_E}{(Z_E + Z_{SU} + Z_S + Z_{ST})(Z_S + Z_{SS} + R_C / 2 + Z_{RS}) - Z_S^2} \end{aligned} \quad [6.53]$$

To minimise V_{SM} and V_{CM} , we want the product term:

$$(Z_E + Z_{SU} + Z_S + Z_{ST})(Z_S + Z_{SS} + R_C / 2 + Z_{RS})$$

to be large. Since in practice the earth impedance Z_E , screen impedance Z_S and cable resistance $R_C / 2$ are all small, the above condition reduces to:

$$(Z_{SU} + Z_{ST})(Z_{SS} + Z_{RS}) \text{ to be large} \quad [6.54]$$

However, we cannot have *both* Z_{SU} and Z_{ST} large; either Z_{ST} or Z_{SU} must be small, otherwise the screen will not be earthed and there is therefore no low impedance path to earth for the capacitively coupled interference currents. Condition (6.54) therefore reduces to the two conditions:

$$\begin{aligned} Z_{SU}(Z_{SS} + Z_{RS}) &= \text{HIGH}; Z_{ST} = \text{LOW} \\ \text{OR} \\ Z_{ST}(Z_{SS} + Z_{RS}) &= \text{HIGH}; Z_{SU} = \text{LOW} \end{aligned} \quad [6.55]$$

which are satisfied if:

$$\begin{aligned} Z_{SU} &= \text{HIGH AND } (Z_{SS} \text{ OR } Z_{RS} \text{ OR both} = \text{HIGH}), Z_{ST} = \text{LOW} \\ \text{OR} \\ Z_{ST} &= \text{HIGH AND } (Z_{SS} \text{ OR } Z_{RS} \text{ OR both} = \text{HIGH}), Z_{SU} = \text{LOW} \end{aligned} \quad [6.56]$$

As mentioned above, in many practical situations it may be impossible to have the measurement circuit completely isolated from the screen, i.e. *both* Z_{SS} and Z_{RS} high. In this situation, possible confusion is avoided if Z_{SU} and Z_{SS} are *both* high, or Z_{ST} and Z_{RS} are *both* high.

In this situation the conditions become:

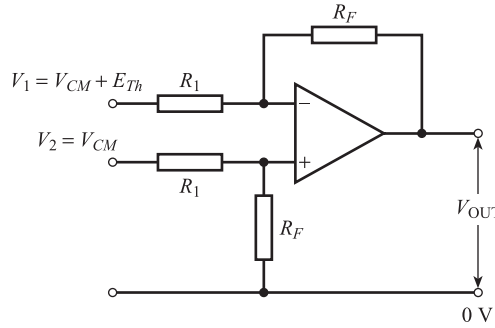
$$\begin{aligned} Z_{SU} &= \text{HIGH AND } Z_{SS} = \text{HIGH}, Z_{RS} = \text{LOW AND } Z_{ST} = \text{LOW} \\ &\quad (\text{Isolated source}) \\ \text{OR} \\ Z_{ST} &= \text{HIGH AND } Z_{RS} = \text{HIGH}, Z_{SS} = \text{LOW AND } Z_{SU} = \text{LOW} \\ &\quad (\text{Isolated receiver}) \end{aligned} \quad [6.57]$$

6.5.4 Use of differential amplifiers

Common mode interference voltages can be successfully rejected by the use of a differential amplifier (Figure 6.11 and Section 9.2). An ideal differential amplifier has an output:

$$V_{OUT} = \frac{R_F}{R_1} (V_2 - V_1) = -\frac{R_F}{R_1} E_{Th} \quad [6.58]$$

Figure 6.11 Use of differential amplifier.



i.e. only the sensor voltage E_{Th} is amplified. The output of a practical amplifier (Section 9.2.2) contains a contribution proportional to V_{CM} ; from eqn [9.39] we have:

$$V_{OUT} = -\frac{R_F}{R_1} E_{Th} + \left(1 + \frac{R_F}{R_1}\right) \frac{V_{CM}}{\text{CMRR}} \quad [6.59]$$

The common mode rejection ratio (CMRR) of the amplifier is the ratio of differential voltage gain to common mode voltage gain and should be as large as possible to minimise this effect. Thus if we have $E_{Th} = 1 \text{ mV}$, $R_1 = 1 \text{ k}\Omega$, $R_F = 1 \text{ M}\Omega$, $V_{CM} = 1 \text{ V}$ and $\text{CMRR} = 10^5$ (100 dB) then:

$$V_{OUT} \approx -1.0 + 0.01 \text{ V}$$

i.e. the resultant series mode interference is only 1%.

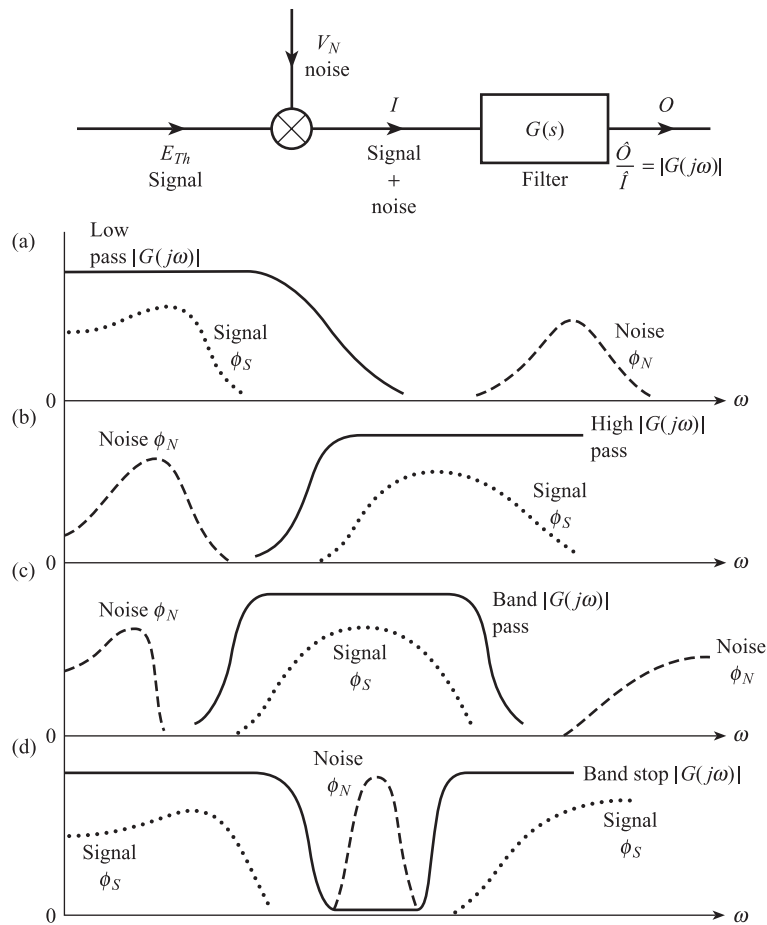
6.5.5 Filtering

A filter is an element which transmits a certain range (or ranges) of frequencies and rejects all other frequencies. An **analogue filter** is an electrical network, consisting usually of resistors, capacitors and operational amplifiers, which conditions continuous signals. A **digital filter** is usually a digital computer programmed to process sampled values of a signal (Chapter 10). Provided that the power spectrum of the measurement signal occupies a *different* frequency range from that of the noise or interference signal, then filtering improves the signal-to-noise ratio.

Figures 6.12(a)–(d) show the use of **low pass**, **high pass**, **band pass** and **band stop** filters in rejecting noise. In all cases the filter transmits the measurement signal but rejects the noise signal, which occupies a different frequency range. The diagrams show the amplitude ratio $|G(j\omega)|$ for each filter and the power spectral densities $\phi(\omega)$ for signal and noise. In order to transmit the measurement signal without distortion the transfer function $G(s)$ of the filter must, ideally, satisfy the conditions of Section 4.4, i.e. that $|G(j\omega)| = 1$ and $\arg G(j\omega) = 0$ for all the frequencies present in the measurement signal spectrum. Analogue filtering can be implemented at the signal conditioning stage; the a.c. amplifier of Figure 9.12 is an example of a band pass filter. Digital filtering can be implemented at the signal processing stage (Chapter 10).

If, however, measurement signal and noise spectra overlap, filtering has limited value. Figure 6.13(a) shows a measurement signal affected by wide band noise; a low-pass filter with bandwidth matched to the signal spectrum removes as much of the noise as possible, but the noise inside the filter bandwidth still remains. Figure 6.13(b)

Figure 6.12 Use of filtering to reject noise.



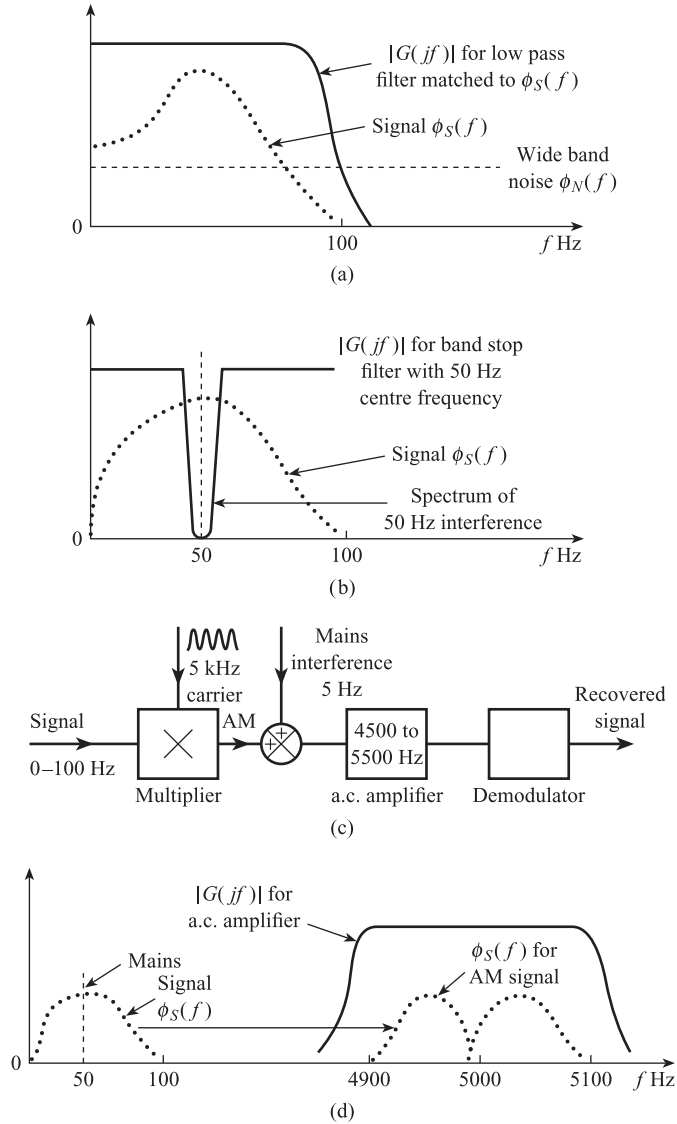
shows the measurement signal affected by 50 Hz interference; a narrow band-stop filter centred on 50 Hz rejects the interference but also rejects measurement signal frequencies around 50 Hz and causes amplitude and phase distortion over a wider range of frequencies.

6.5.6 Modulation

The problem of Figure 6.13(b) can be solved by modulating the measurement signal onto a higher frequency carrier signal, e.g. a 5 kHz sine wave as shown in Figure 6.13(c). The simplest form of modulation is **amplitude modulation**; this involves the multiplication of measurement and carrier signals and is discussed in detail in Section 9.3.

Modulation causes the spectrum of the measurement signal to be shifted to around 5 kHz (Figure 6.13(d)). If the 50 Hz interference is added *after* modulation, i.e. during transmission from sensor/modulator to a remote amplifier/demodulator, the interference spectrum is not shifted. The interference can then be easily rejected by an a.c. amplifier, i.e. a band pass filter with bandwidth matched to the spectrum of the amplitude modulated signal. Modulation, however, does not help the problem

Figure 6.13 Limitations of filtering and use of modulation.

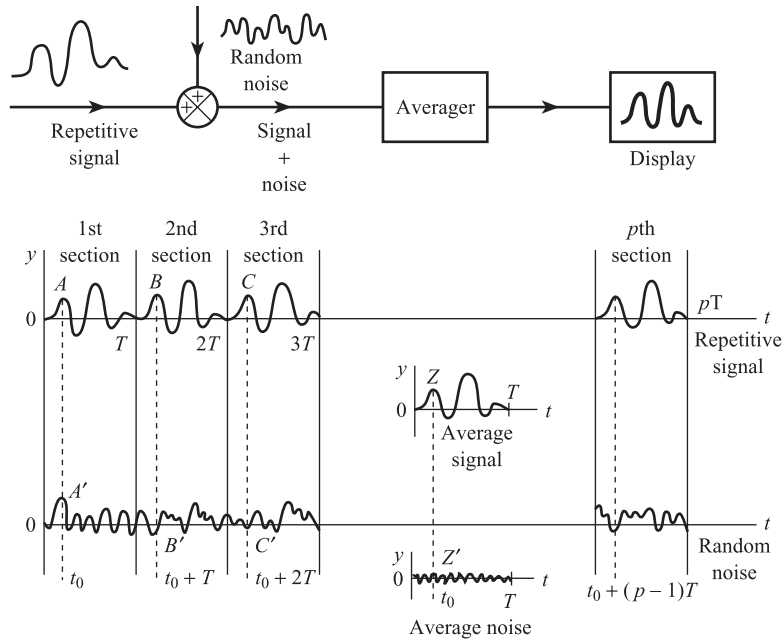


of Figure 6.13(a); the noise has a uniform power spectral density over a wide band of frequencies, so that moving the measurement signal to a different frequency range does not improve the signal-to-noise ratio.

6.5.7 Averaging

Signal averaging can be used to recover a **repetitive** measurement signal affected by random noise, even if the signal r.m.s. value is much less than that of the noise.^[3] The process is shown in Figure 6.14.

Suppose that T is the time for each complete cycle of the repetitive signal; p sections of the noise-affected signal, each of duration T , are fed into the averager. N samples from each section are taken and stored, giving pN samples in total; typically

Figure 6.14 Signal averaging.

we may have $p = 50$, $N = 100$. The sampling is exactly synchronised: i.e. if the i th sample of the 1st section is taken at time t_0 , the i th sample of the 2nd section is taken at $t_0 + T$, the i th sample of the 3rd at $t_0 + 2T$, and so on. Corresponding samples from each section are then averaged: e.g. the first sampled values from each of the p sections are added together and divided by p . Thus the average value of the i th sample is:

$$y_i^{\text{AV}} = \frac{1}{p}(y_{i1} + y_{i2} + \dots + y_{ip}), \quad i = 1, \dots, N \quad [6.60]$$

Each of these N average sample values are then displayed at the appropriate time to give the averaged signal. Corresponding sample values A, B, C, \dots of the signal component are approximately equal, so that the average value Z has a similar magnitude. Corresponding sample values A', B', C', \dots of the noise component are very different, some positive and some negative, so that the average value Z' is reduced in magnitude. Averaging therefore maintains the r.m.s. value of the measurement signal while reducing the r.m.s. value of the random noise.

This improvement in signal-to-noise ratio can be readily calculated for random noise with a normal probability density function. Suppose we have p normal signals $y_1(t)$ to $y_p(t)$, with standard deviations σ_1 to σ_p respectively; then from Section 2.3 the average signal

$$y_{\text{AV}}(t) = \frac{1}{p}[y_1(t) + y_2(t) + \dots + y_p(t)] \quad [6.61]$$

is also normal with standard deviation

$$\sigma_{\text{AV}} = \sqrt{\frac{\sigma_1^2}{p^2} + \frac{\sigma_2^2}{p^2} + \dots + \frac{\sigma_p^2}{p^2}} \quad [6.62]$$

If $\sigma_1 = \sigma_2 = \sigma_p = \sigma$, then

Reduction in noise
standard deviation
due to averaging

$$\sigma_{AV} = \sqrt{\frac{p\sigma^2}{p^2}} = \frac{\sigma}{\sqrt{p}} \quad [6.63]$$

Thus if we average 50 sections $\sigma_{AV} = \sigma/\sqrt{50} \approx \sigma/7$, i.e. the noise r.m.s. value is reduced by a factor of 7, giving an increase in signal-to-noise ratio of 17dB.

6.5.8 Autocorrelation

Autocorrelation can be used to *detect* the presence of a sinusoidal or any periodic signal buried in random noise. The actual waveform of the measurement signal cannot be recovered because phase information is lost in correlation, but we can measure the amplitude and period of the signal from the autocorrelation function (ACF) of the noise-affected signal. The ACF for the (signal + noise) is the sum of the signal ACF and noise ACF, i.e.

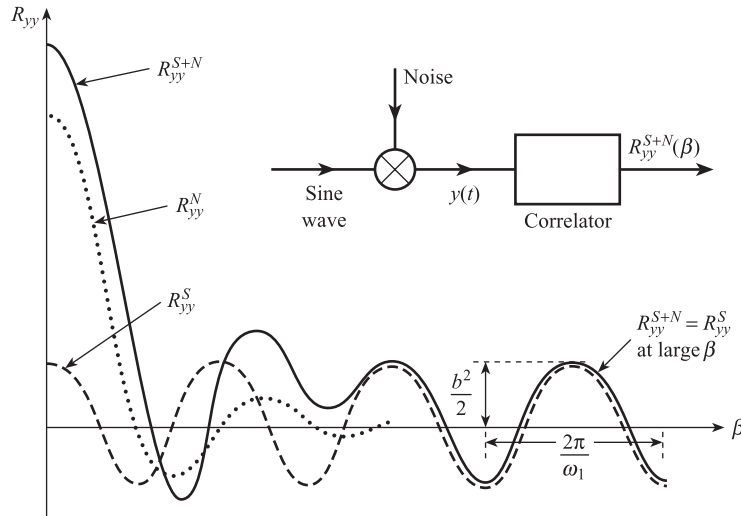
$$R_{yy}^{S+N}(\beta) = R_{yy}^S(\beta) + R_{yy}^N(\beta) \quad [6.64]$$

Thus using eqns [6.27] and [6.31] the ACF for a sinusoidal signal affected by band-limited white noise is:

$$R_{yy}^{S+N}(\beta) = \frac{b^2}{2} \cos \omega_1 \beta + A \frac{\sin \omega_c \beta}{\beta} \quad [6.65]$$

The form of $R_{yy}^{S+N}(\beta)$ is shown in Figure 6.15; at large values of β the $A(\sin \omega_c \beta)/\beta$ term due to the noise decays to zero, leaving the $(b^2/2) \cos \omega_1 \beta$ term due to the signal. Thus the amplitude b and period $2\pi/\omega_1$ of the original signal can be found from the amplitude and period of the autocorrelation function at large values of time delay. This method can be used in the vortex flowmeter (Chapter 12) to measure the vortex frequency in the presence of random flow turbulence.

Figure 6.15
Autocorrelation detection
of periodic signal buried
in noise.



Conclusion

The chapter began by defining **random signals** and **deterministic signals** and explained that in many practical situations the wanted signal may be random. Unwanted signals may also be present in the measurement circuit; these can be classified as either **interference** (deterministic) or **noise** (random).

The chapter then explained how random signals can be quantified using the following statistical functions: **mean**, **standard deviation**, **probability density function**, **power spectral density** and **autocorrelation function**.

The effects of noise and interference voltage on measurement circuits using both voltage and current transmission were then discussed. In the following section internal noise and external interference sources were discussed and the mechanisms whereby external sources are coupled to the measurement circuit were explained. The chapter concluded by explaining methods of reducing the effects of noise and interference, including **electromagnetic shielding**, **electrostatic screening**, **filtering**, **modulation**, **averaging** and **autocorrelation**.

References

- [1] OLIVER F J 1972 *Practical Instrumentation Transducers*. Pitman, London, pp. 290–333.
- [2] COOK B E 1979 'Electronic noise and instrumentation', *Journal of Instrumentation Measurement and Control*, vol. 12, no. 8.
- [3] Hewlett Packard, Technical Literature on Model 3721A Correlator.

Problems

6.1 Table Prob. 1 gives 50 sample values of a random signal.

- (a) Estimate the mean and standard deviation of the signal.
- (b) Using an interval $\Delta y = 0.5$ V, draw the P_j and C_j discrete probability distributions for the signal.

Table Prob. 1.

−0.59	1.02	−0.25	−0.34	0.95	1.24	−0.30	0.21	−0.89
−1.00	1.36	0.03	0.04	−0.13	−0.71	−1.23	0.03	−1.00
0.65	0.11	0.99	0.17	0.39	2.61	−0.08	−0.33	0.99
2.15	0.91	0.89	1.43	−1.69	−0.25	2.47	−1.97	−2.26
0.42	0.05	0.26	0.33	−0.42	0.79	−0.07	−0.32	−0.66
−0.63	−0.06	−0.61	0.77	1.90				

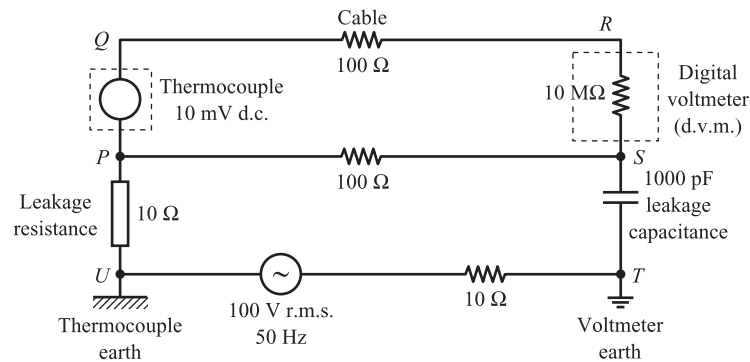
6.2 Two complete periods of a square wave can be represented by the following 20 sample values:

$$+1+1+1+1+1 \quad -1-1-1-1-1 \quad +1+1+1+1+1 \quad -1-1-1-1-1$$

Find the autocorrelation function of the signal over one complete period by evaluating the coefficients $R_{yy}(m\Delta T)$ for $m = 0, 1, 2, \dots, 10$.

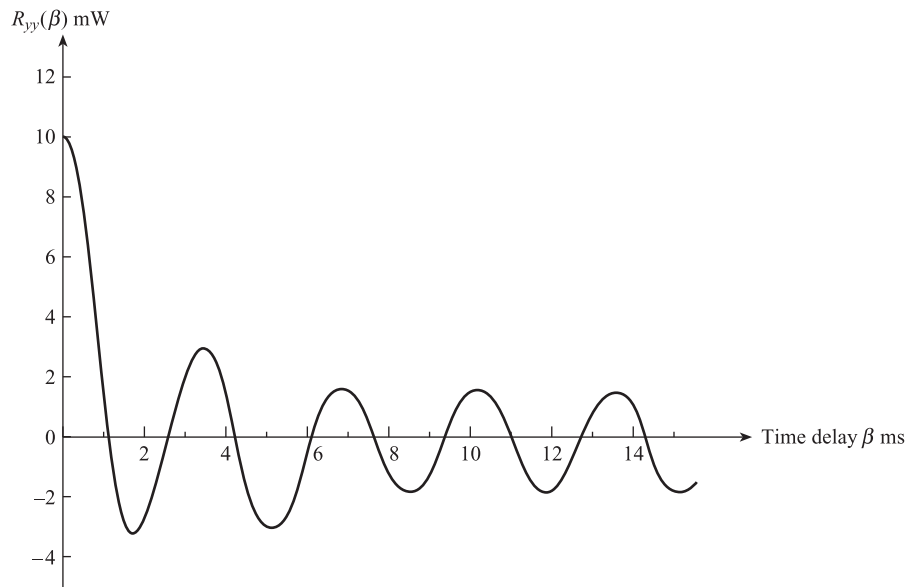
- 6.3 A sinusoidal signal of amplitude 1.4 mV and frequency 5 kHz is ‘buried’ in Gaussian noise with zero mean value. The noise has a uniform power spectral density of 100 pW Hz^{-1} up to a cut-off frequency of 1 MHz.
- Find the total power, r.m.s. value and standard deviation for the noise signal.
 - What is the signal-to-noise ratio in dB?
 - Sketch the autocorrelation function for the combined signal and noise.
 - The combined signal is passed through a band-pass filter with centre frequency 5 kHz and bandwidth 1 kHz. What improvement in signal-to-noise ratio is obtained?
 - The filtered signal is then passed through a signal averager which averages corresponding samples of 100 sections of signal. What further improvement in signal-to-noise ratio is obtained?
- 6.4 A thermocouple giving a 10 mV d.c. output voltage is connected to a high impedance digital voltmeter some distance away. A difference in potential exists between earth at the thermocouple and earth at the voltmeter. Using the equivalent circuit given in Figure Prob. 4.
- Calculate the r.m.s. values of the series mode and common mode interference voltages at the voltmeter input.
 - If the digital voltmeter has a common mode rejection ratio of 100 dB, find the minimum and maximum possible measured voltages.

Figure Prob. 4.



- 6.5 A sinusoidal signal is transmitted over a noisy transmission link to a remote correlator acting as a receiver. Figure Prob. 5 shows a typical autocorrelation function. Use the figure to estimate the following quantities:
- Signal power
 - Noise power
 - Signal-to-noise ratio in decibels
 - Signal amplitude
 - Signal frequency
 - Noise standard deviation (assume zero mean).

Hint: use eqns [6.27] and [6.33].

Figure Prob. 5.

7

Reliability, Choice and Economics of Measurement Systems

In Chapters 3 and 4 we defined the accuracy of a measurement system and explained how measurement error can be calculated, under both steady-state and dynamic conditions. **Reliability** is another important characteristic of a measurement system; it is no good having an accurate measurement system which is constantly failing and requiring repair. The first section of this chapter deals with the reliability of measurement systems, first explaining the fundamental principles of reliability and the reliability of practical systems, then failure rate data, and finally examining ways of improving reliability. The following section examines the problems of how to choose the most appropriate measurement system, for a given application, from several competing possibilities. Initially a specification for the required application can be drawn up: this will be a list of important parameters such as accuracy, reliability, etc., each with a desired value. This can then be compared with the manufacturer's specification for each of the competing measurement systems and the system with the closest specification is chosen. Even if all the required information is available this procedure is far from satisfactory because it takes no account of the relative importance of each parameter. A better method, explained in the final section, is to choose the system with minimum total lifetime operating cost.

7.1

Reliability of measurement systems

7.1.1 Fundamental principles of reliability

Probability P

If a large number of random, independent trials are made, then the probability of a particular event occurring is given by the ratio:

$$P = \frac{\text{number of occurrences of the event}}{\text{total number of trials}} \quad [7.1]$$

in the limit that the total number of trials tends to infinity. Thus the probability of a tossed coin showing heads tends to the theoretical value of $\frac{1}{2}$ over a large number of trials.

Reliability $R(t)$

The reliability of a measurement element or system can be defined as: ‘the probability that the element or system will operate to an agreed level of performance, for a specified period, subject to specified environmental conditions’. In the case of a measurement system ‘agreed level of performance’ could mean an accuracy of $\pm 1.5\%$. If the system is giving a measurement error outside these limits, then it is considered to have failed, even though it is otherwise working normally. The importance of environmental conditions on the reliability of measurement systems will be discussed more fully later. Reliability decreases with time; a measurement system that has just been checked and calibrated should have a reliability of 1 when first placed in service. Six months later, the reliability may be only 0.5 as the probability of survival decreases.

Unreliability $F(t)$

This is ‘the probability that the element or system will *fail* to operate to an agreed level of performance, for a specified period, subject to specified environmental conditions’. Since the equipment has either failed or not failed the sum of reliability and unreliability must be unity, i.e.

$$R(t) + F(t) = 1 \quad [7.2]$$

Unreliability also depends on time; a system that has just been checked and calibrated should have an unreliability of zero when first placed in service, increasing to, say, 0.5 after six months.

7.1.2 Practical reliability definitions

Since $R(t)$ and $F(t)$ are dependent on time, it is useful to have measures of reliability which are independent of time. We will consider two cases: in the first the items are non-repairable and in the second the items are repairable.

Non-repairable items

Suppose that N individual items of a given non-repairable component are placed in service and the times at which failures occur are recorded during a test interval T . We further assume that all the N items fail during T and that the i th failure occurs at time T_i , i.e. T_i is the survival time or **up time** for the i th failure. The total up time for N failures is therefore $\sum_{i=1}^N T_i$ and the **mean time to failure** is given by

$$\text{Mean time to fail} = \frac{\text{total up time}}{\text{number of failures}}$$

i.e.

$$\text{MTTF} = \frac{1}{N} \sum_{i=1}^{i=N} T_i \quad [7.3]$$

The **mean failure rate** $\bar{\lambda}$ is correspondingly given by:

$$\text{Mean failure rate} = \frac{\text{number of failures}}{\text{total up time}}$$

i.e.

$$\bar{\lambda} = \frac{N}{\sum_{i=1}^{i=N} T_i} \quad [7.4]$$

i.e. mean failure rate is the reciprocal of MTTF.

There are N survivors at time $t = 0$, $N - i$ at time $t = T_i$, decreasing to zero at time $t = T$; Figure 7.1(a) shows how the probability of survival, i.e. reliability, $R_i = (N - i)/N$ decreases from $R_i = 1$ at $t = 0$, to $R_i = 0$ at $t = T$. The i th rectangle has height $1/N$, length T_i and area T_i/N . Therefore from eqn [7.3] we have:

$$\text{MTTF} = \text{total area under the graph}$$

In the limit that $N \rightarrow \infty$, the discrete reliability function R_i becomes the continuous function $R(t)$. The area under $R(t)$ is $\int_0^T R(t) dt$ so that we have in general:

$$\text{MTTF} = \int_0^{\infty} R(t) dt \quad [7.5]$$

The upper limit of $t = \infty$ corresponds to N being infinite.

Repairable items

Figure 7.1(b) shows the failure pattern for N items of a repairable element observed over a test interval T . The **down time** T_{Dj} associated with the j th failure is the total time that elapses between the occurrence of the failure and the repaired item being put back into normal operation. The total down time for N_F failures is therefore $\sum_{j=1}^{j=N_F} T_{Dj}$ and the **mean down time** is given by

$$\text{Mean down time} = \frac{\text{total down time}}{\text{number of failures}}$$

i.e.

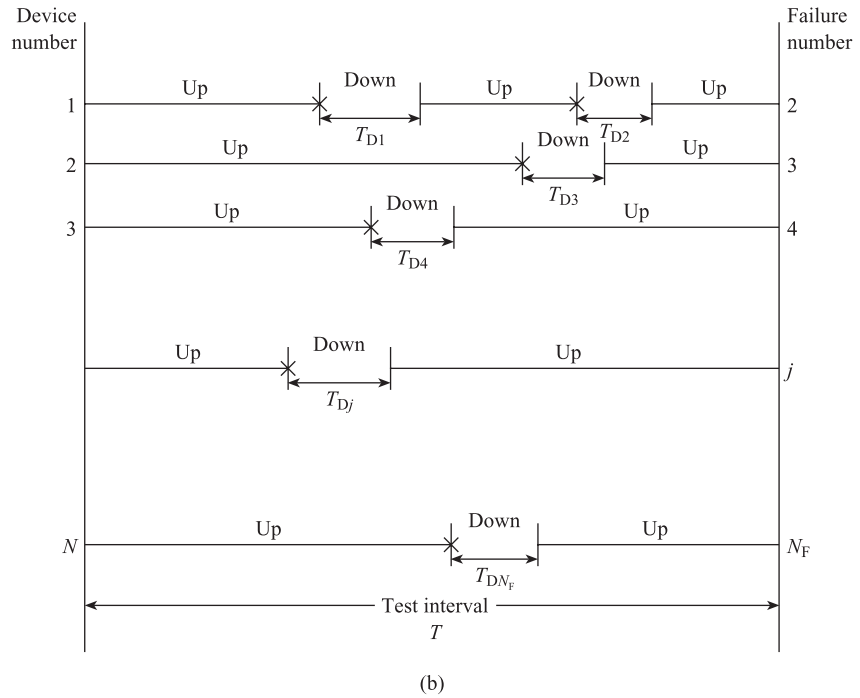
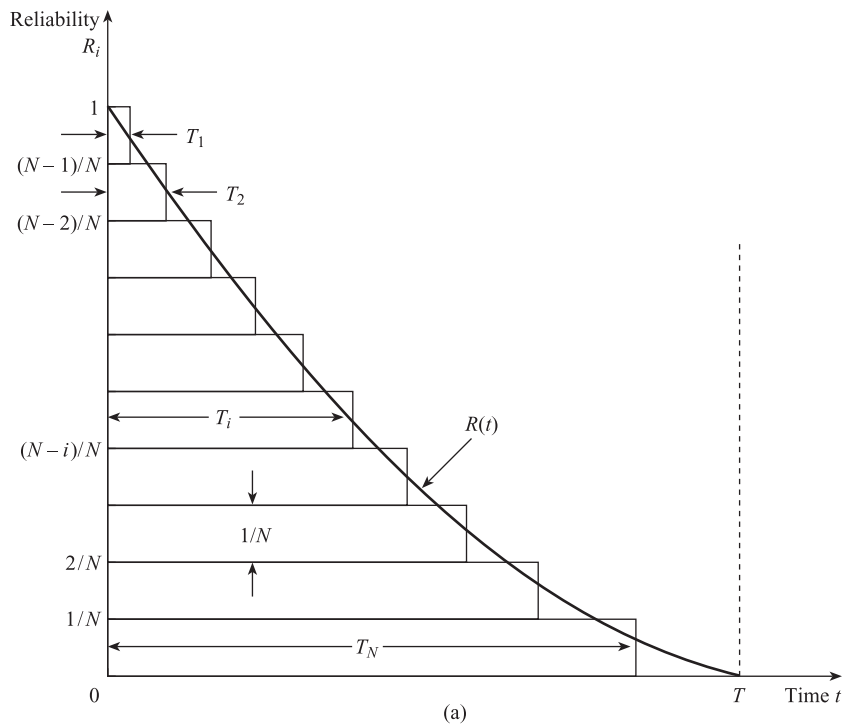
$$\text{MDT} = \frac{1}{N_F} \sum_{j=1}^{j=N_F} T_{Dj} \quad [7.6]$$

Figure 7.1

Failure patterns:

(a) Non-repairable items

(b) Repairable items.



The **total up time** can be found by subtracting the total down time from NT , i.e.:

$$\begin{aligned}\text{Total up time} &= NT - \sum_{j=1}^{N_F} T_{Dj} \\ &= NT - N_F \text{MDT}\end{aligned}$$

The mean up time or the **mean time between failures** (MTBF) is therefore given by:

$$\text{Mean time between failures} = \frac{\text{total up time}}{\text{number of failures}}$$

i.e.

$$\text{MTBF} = \frac{NT - N_F \text{MDT}}{N_F} \quad [7.7]$$

The **mean failure rate** $\bar{\lambda}$ is correspondingly given by:

$$\text{Mean failure rate} = \frac{\text{number of failures}}{\text{total up time}}$$

i.e.

$$\bar{\lambda} = \frac{N_F}{NT - N_F \text{MDT}} \quad [7.8]$$

Again mean failure rate is the reciprocal of MTBF.

Thus if 150 faults are recorded for 200 transducers over 1.5 years with a mean down time of 0.002 years, then the observed MTBF is 1.998 years and the mean failure rate is 0.5005 yr^{-1} .

The **availability** A of the element is the fraction of the total test interval over which it is performing within specification, i.e. up; thus we have:

$$\begin{aligned}\text{Availability} &= \frac{\text{total up time}}{\text{test interval}} \\ &= \frac{\text{total up time}}{\text{total up time} + \text{total down time}} \\ &= \frac{N_F \times \text{MTBF}}{N_F \times \text{MTBF} + N_F \times \text{MDT}}\end{aligned}$$

i.e.

$$A = \frac{\text{MTBF}}{\text{MTBF} + \text{MDT}} \quad [7.9]$$

Using the above data of MTBF = 1.998 years and MDT = 0.002 years gives $A = 0.999$.

Unavailability U is similarly defined as the fraction of the total test interval over which it is not performing to specification, i.e. failed or down; thus we have:

$$\text{Unavailability} = \frac{\text{total down time}}{\text{test interval}}$$

giving:

$$U = \frac{\text{MDT}}{\text{MTBF} + \text{MDT}} \quad [7.10]$$

It follows from eqns [7.9] and [7.10] that:

$$A + U = 1 \quad [7.11]$$

7.1.3 Instantaneous failure rate and its relation to reliability

We assume to begin with that n items of an element survive up to time $t = \xi$ and that Δn items fail during the small time interval $\Delta \xi$ between ξ and $\xi + \Delta \xi$. The probability of failure during interval $\Delta \xi$ (given survival to time ξ) is therefore equal to $\Delta n/n$. Assuming no repair during $\Delta \xi$ the corresponding **instantaneous failure rate** or **hazard rate** at time ξ is, from eqn [7.8], given by:

$$\lambda(\xi) = \frac{\Delta n}{n \Delta \xi} = \frac{\text{failure probability}}{\Delta \xi} \quad [7.12]$$

The unconditional probability ΔF that an item fails during the interval $\Delta \xi$ is:

$$\Delta F = \text{probability that item survives up to time } \xi$$

AND

$$\text{probability that item fails between } \xi \text{ and } \xi + \Delta \xi \text{ (given survival to } \xi \text{)}.$$

The first probability is given by $R(\xi)$ and from eqn [7.12] the second probability is $\lambda(\xi)\Delta \xi$. The combined probability ΔF is the product of these probabilities:

$$\Delta F = R(\xi)\lambda(\xi)\Delta \xi$$

i.e.

$$\frac{\Delta F}{\Delta \xi} = R(\xi)\lambda(\xi)$$

Thus in the limit that $\Delta \xi \rightarrow 0$, we have:

$$\frac{dF}{d\xi} = R(\xi)\lambda(\xi) \quad [7.13]$$

Also since $F(\xi) = 1 - R(\xi)$, $dF/d\xi = -(dR/d\xi)$, giving:

$$-\frac{dR}{d\xi} = R(\xi)\lambda(\xi)$$

i.e.

$$\int_{R(0)}^{R(t)} \frac{dR}{R} = - \int_0^t \lambda(\xi) d\xi \quad [7.14]$$

In eqn [7.14], the left-hand integral is with respect to R and the right-hand integral with respect to ξ . Since at $t = 0$, $R(0) = 1$, we have:

$$[\log_e R]_1^{R(t)} = - \int_0^t \lambda(\xi) d\xi$$

$$\log_e R(t) = - \int_0^t \lambda(\xi) d\xi$$

i.e.

*Relation between
reliability and
instantaneous
failure rate*

$$R(t) = \exp \left[- \int_0^t \lambda(\xi) d\xi \right] \quad [7.15]$$

7.1.4 Typical forms of failure rate function

In the previous section instantaneous failure rate or hazard rate $\lambda(t)$ was defined. Figure 7.2 shows the most general form of $\lambda(t)$ throughout the lifetime of an element. This is the so-called **bathtub curve** and consists of three distinct phases: early failure, useful life and wear-out failure. The **early failure region** is characterised by $\lambda(t)$ decreasing with time. When items are new, especially if the element is of a new design, early failures can occur due to design faults, poor quality components, manufacturing faults, installation errors, operator and maintenance errors; the latter may be due to unfamiliarity with the product. The hazard rate falls as design faults are rectified, weak components are removed, and the user becomes familiar with installing, operating and maintaining the element. The **useful life region** is characterised by a low,

Figure 7.2 Typical variation in instantaneous failure rate (hazard rate) during the lifetime of element – ‘bathtub curve’.

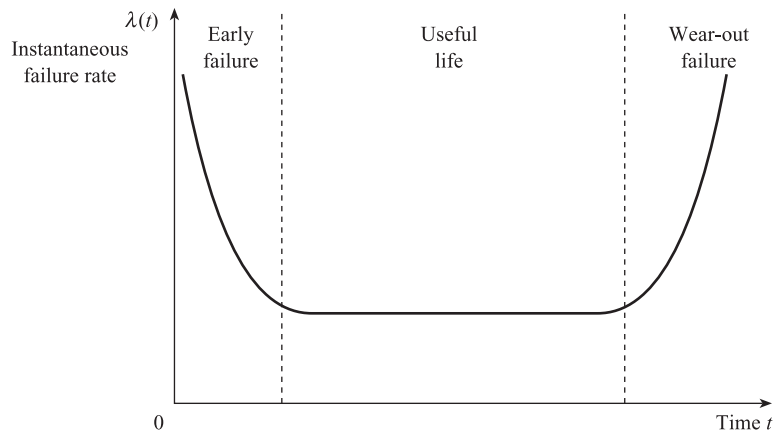
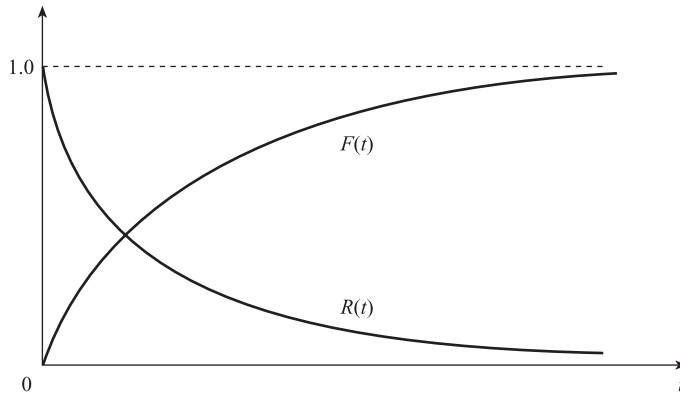


Figure 7.3 Reliability and unreliability with constant failure rate model.



constant failure rate. Here all weak components have been removed: design, manufacture, installation, operating and maintenance errors have been rectified so that failure is due to a variety of unpredictable lower-level causes. The **wear-out region** is characterised by $\lambda(t)$ increasing with time as individual items approach the end of the design life for the product; long-life components which make up the element are now wearing out.

Many measurement elements have a useful life region lasting many years, so that a **constant failure rate** model is often a good approximation. Here we have:

$$\lambda(t) = \lambda(\xi) = \lambda = \text{constant} \quad [7.16]$$

so that:

$$R(t) = \exp \left[-\lambda \int_0^t \xi \right] = \exp(-\lambda t) \quad [7.17]$$

$$F(t) = 1 - \exp(-\lambda t)$$

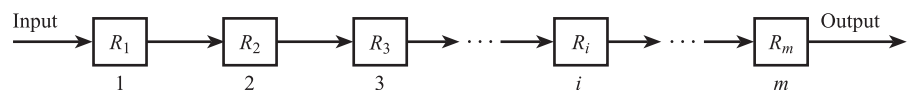
Thus a constant failure or hazard rate gives rise to an **exponential reliability** time variation or distribution as shown in Figure 7.3.

7.1.5 Reliability of systems

Series systems

We saw in Chapter 1 that a complete measurement system consists of several elements usually in series or cascade. Figure 7.4 shows a series system of m elements with individual reliabilities $R_1, R_2, \dots, R_i, \dots, R_m$ respectively. The system will only survive if every element survives; if one element fails then the system fails.

Figure 7.4 Reliability of series system.



Assuming that the reliability of each element is independent of the reliability of the other elements, then the probability that the system survives is the probability that element 1 survives *and* the probability that 2 survives *and* the probability that 3 survives, etc. The system reliability R_{SYST} is therefore the product of the individual element reliabilities, i.e.

*Reliability of
series system*

$$R_{\text{SYST}} = R_1 R_2 \dots R_i \dots R_m \quad [7.18]$$

If we further assume that each of the elements can be described by a constant failure rate λ (Section 7.1.4), and if λ_i is the failure rate of the i th element, then R_i is given by the exponential relation (eqn [7.17]):

$$R_i = e^{-\lambda_i t} \quad [7.19]$$

Thus

$$R_{\text{SYST}} = e^{-\lambda_1 t} e^{-\lambda_2 t} \dots e^{-\lambda_i t} \dots e^{-\lambda_m t} \quad [7.20]$$

so that if λ_{SYST} is the overall system failure rate:

$$R_{\text{SYST}} = e^{-\lambda_{\text{SYST}} t} = e^{-(\lambda_1 + \lambda_2 + \dots + \lambda_i + \dots + \lambda_m)t} \quad [7.21]$$

and

*Failure rate of system
of m elements in series*

$$\lambda_{\text{SYST}} = \lambda_1 + \lambda_2 + \dots + \lambda_i + \dots + \lambda_m \quad [7.22]$$

This means that the overall failure rate for a series system is the sum of the individual element or component failure rates. Equations [7.18] and [7.22] show the importance of keeping the number of elements in a series system to a minimum; if this is done the system failure rate will be minimum and the reliability maximum. A measurement system consisting of a thermocouple ($\lambda_1 = 1.1$), a millivolt to current converter ($\lambda_2 = 0.1$) and a recorder ($\lambda_3 = 0.1$) in series will therefore have a failure rate $\lambda_{\text{SYST}} = 1.3$.

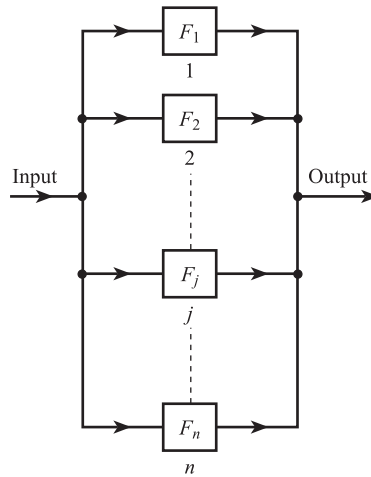
Parallel systems

Figure 7.5 shows an overall system consisting of n individual elements or systems in parallel with individual unreliabilities $F_1, F_2, \dots, F_j, \dots, F_n$ respectively. Only one individual element or system is necessary to meet the functional requirements placed on the overall system. The remaining elements or systems increase the reliability of the overall system; this is termed **redundancy**. The overall system will only fail if every element/system fails; if one element/system survives the overall system survives. Assuming that the reliability of each element/system is independent of the reliability of the other elements, then the probability that the overall system fails is the probability that element/system 1 fails *and* the probability that 2 fails *and* the probability that 3 fails, etc. The overall system unreliability F_{SYST} is therefore the *product* of the individual element system unreliabilities, i.e.

*Unreliability of
parallel system*

$$F_{\text{SYST}} = F_1 F_2 \dots F_j \dots F_n \quad [7.23]$$

Figure 7.5 Reliability of parallel system.



Comparing eqns [7.18] and [7.23] we see that, for series systems, system reliability is the product of element reliabilities, whereas for parallel systems system unreliability is the product of element unreliabilities. Often the individual elements/systems are identical, so that $F_1 = F_2 = \dots = F_i = \dots = F_n = F$, giving:

$$F_{\text{SYST}} = F^n \quad [7.24]$$

The temperature measurement system of the previous section has a failure rate $\lambda_{\text{SYST}} = 1.3 \text{ yr}^{-1}$; the corresponding unreliability F is given by

$$F = 1 - e^{-\lambda_{\text{SYST}} t}$$

Thus if $t = 0.5$ year then $F = 0.478$. Figure 7.6 shows a redundant system consisting of three single temperature measurement systems in parallel. The overall system unreliability is therefore:

$$F_{\text{OVERALL}} = F^3 = 0.109$$

so that the probability of a failure with the overall system is less than a quarter of that of a single system.

The above parallel system, while reliable, is expensive. Since the thermocouple failure rate is 11 times greater than the converter and recorder failure rates, a more

Figure 7.6 Reliability of three thermocouple temperature measurement systems in parallel.

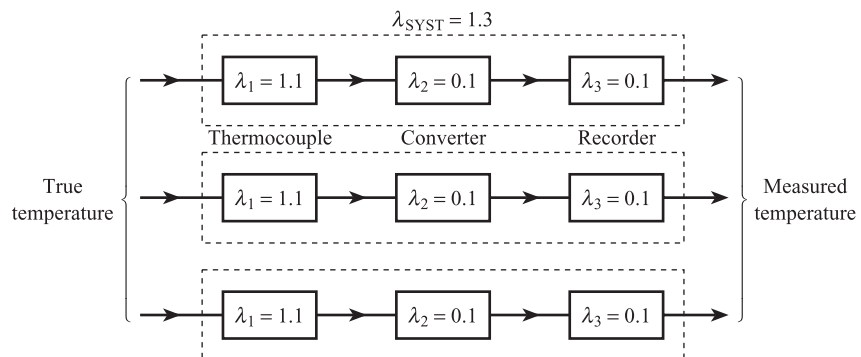
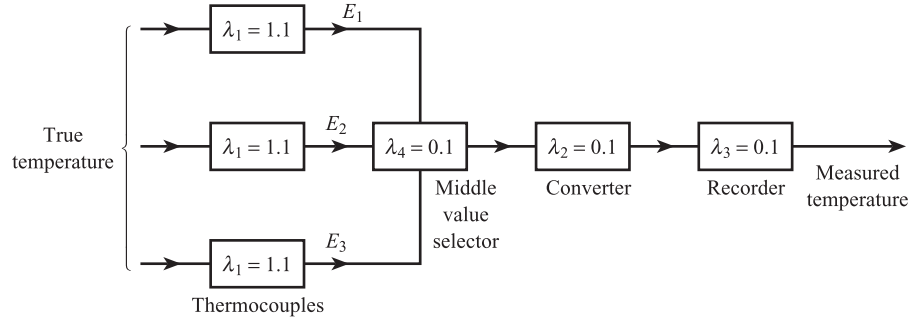


Figure 7.7 Reliability of system with three thermocouples and middle value selector.



cost-effective redundant system would have three thermocouples in parallel and only one converter and recorder. One possible system is shown in Figure 7.7. The three thermocouple e.m.f.'s E_1 , E_2 and E_3 are input into a middle value selector element. The selector output signal is that input e.m.f. which is neither the lowest nor the highest; thus if $E_1 = 5.0$ mV, $E_2 = 5.2$ mV and $E_3 = 5.1$ mV, the output signal is E_3 . If, however, thermocouple 3 fails so that $E_3 = 0$ mV, the selector output signal is E_1 . The reliability of this system can be analysed by replacing the three thermocouples by a single element of unreliability

$$F_1 = (1 - e^{-\lambda_1 t})^3 = (1 - e^{-0.55})^3 = 0.076$$

or reliability $R_1 = 1 - 0.076 = 0.924$. The reliability of the other elements with $\lambda = 0.1$ is:

$$R_2 = R_3 = R_4 = e^{-\lambda t} = e^{-0.05} = 0.951$$

Using [7.18], the overall system reliability is:

$$R_{\text{OVERALL}} = R_1 R_2 R_3 R_4 = 0.924(0.951)^3 = 0.795$$

i.e. $F_{\text{OVERALL}} = 0.205$. This is almost twice the unreliability of the parallel system but less than half that of a single system.

7.1.6 Failure rate data and models

A distinction must now be made between **components** and **elements**. A component is defined as a 'non-repairable' device, i.e. when it fails it is removed and thrown away. Examples are a resistor or an integrated circuit. An element, however, is a repairable part of a system, which is usually made up of several components. Examples are a pressure sensor, a temperature transmitter and a recorder.

Failure rate data for both components and elements can be found experimentally by direct measurements of the frequency of failure of a number of items of a given type. Equation [7.4] can be used to find the observed failure rate of non-repairable components and eqn [7.8] to find $\bar{\lambda}$ for repairable elements.

Table 7.1 gives observed average failure rates for typical instruments. These data have been taken from the UK data bank operated by the Systems Reliability Service (SRS).^[1] The table specifies the environment in which each type of instrument is located. For an element located in the process fluid, the environment is determined by the nature of the fluid, e.g. temperature, corrosion properties, presence of dirt or solid particles.

Table 7.1 Observed average failure rates for instruments.

Instrument	Environment	Experience (item-years)	No. of failures	Failure rate (failures/yr)
Chemical analyser, Oxygen	Poor, chemical/ship	4.34	30	6.92
pH meter	Poor, chemical/ship	28.08	302	10.75
Conductivity indicator	Average, industrial	7.53	18	2.39
Fire detector head	Average, industrial	1 470	128	0.09
Flow transmitter, pneumatic	Average, industrial	125	126	1.00
Level indicator, pneumatic	Average, industrial	898	201	0.22
Pressure controller	Average, industrial	40	63	1.58
Pressure indicator, dial, mechanical	Average, industrial	575	178	0.31
Pressure sensor, differential, electronic	Poor, chemical/ship	225	419	1.86
Pressure transmitter	Average, industrial	85 045	806	0.01
Recorder, pen	Average, industrial	26.02	7	0.27
Temperature indicator and alarm	Fair, laboratory	47.2	101	2.14
Temperature indicator, resistance thermometer	Fair, laboratory	212.3	68	0.32
Temperature indicator, bimetal	Average, industrial	165	215	1.30
Temperature trip unit	Average, industrial	120	70	0.58
Thermocouple	Poor, chemical/ship	317	127	0.40
Valve, gate	Poor, chemical/ship	11 564	841	0.07
non-return	Poor, chemical/ship	1 530	101	0.07
solenoid	Poor, chemical/ship	1 804	66	0.04

Source: after Wright^[1].

For an element located in the atmosphere, the environment is determined by atmospheric conditions, e.g. temperature, humidity, salinity, presence of dust. The failure rate of a given type of element will depend on the environment in which it is located: an iron–copper thermocouple will have a higher failure rate in a corrosive acid than in water.

Table 7.2 shows the observed failure rates for given types of elements at three works A, B, C which process different materials and fluids and have different background environments.^[2] The observed failure rates can be regarded as the product of a **base failure rate** λ_B and an **environmental correction factor** π_E :

Element failure rate model

$$\lambda_{\text{OBS}} = \pi_E \times \lambda_B \quad [7.25]$$

Here λ_B corresponds to the best environmental conditions and π_E has values 1, 2, 3 or 4, the highest figure corresponding to the worst environment.

The failure rate of elements can alternatively be calculated from the failure rate data/models for the basic components which make up the element.

Table 7.3 shows the calculation of the overall failure rate, from basic component data, for an electronic square root extractor module.^[3] The module gives an output voltage signal in the range 1–5 V, proportional to the square root of the input signal with range 4–20 mA; this type of module is commonly used in fluid flow rate control systems. The module is made up from basic electronic components of various types, all connected in series. Several components of each type are present. From

Table 7.2 Observed failure rates for instruments in different chemical plant environments.

Instrument (p = pneumatic)	Observed failure rate, faults/year	Environmental correction factor	Base failure rate, faults/year
Control valve (p)			
—	0.25	1	0.25
Works A	0.57	2	0.29
Works B	2.27	4	0.57
Works C	0.127	2	0.064
Differential pressure transmitter (p)			
—	0.76	1	0.76
Works A (flow)	1.86	3	0.62
Works A (level)	1.71	4	0.43
Works B (flow)	2.66	4	0.67
Works C (flow)	1.22	2	0.61
Variable area flowmeter transmitter (p)			
—	0.68	1	0.68
Works A	1.01	3	0.34
Thermocouple			
Works A	0.40	3	0.13
Works B	1.34	4	0.34
Works C	1.00	4	0.25
Controller			
—	0.38	1	0.38
Works A	0.26	1	0.26
Works B	1.80	1	1.80
Works C	0.32	1	0.32
Pressure switch			
—	0.14	1	0.14
Works A	0.30	2	0.15
Works B	1.00	4	0.25

Source: after Lees^[2].

eqn [7.22] the failure rate λ of a module containing m different component types in series with failure rates $\lambda_1, \lambda_2, \dots, \lambda_i, \dots, \lambda_m$, and one of each type present is:

$$\lambda = \lambda_1 + \lambda_2 + \dots + \lambda_i + \dots + \lambda_m \quad [7.26]$$

If there are multiple components of each type, all connected in series, then the module failure rate is given by:

$$\lambda = N_1\lambda_1 + N_2\lambda_2 + \dots + N_i\lambda_i + \dots + N_m\lambda_m \quad [7.27]$$

where $N_1, N_2, \dots, N_i, \dots, N_m$ are the quantities of each component type. The failure rate of each component type is calculated using the model equation:

$$\lambda_i = (F_{1i} + F_{2i} + F_{3i}) \times K_{1i} \times K_{2i} \times K_{3i} \times K_{4i} \quad [7.28]$$

Table 7.3 gives values of $F_1, F_2, F_3, K_1, K_2, K_3, K_4$ and failure rate λ_i for each component. Each failure rate is then multiplied by the appropriate quantity N_i and the $N_i\lambda_i$ values are added together to give a total module failure rate of 3.01×10^{-6} per hour.

Module failure rate – multiple components of each type

Table 7.3 Calculation of overall failure rate for electronic square root module.^a

Component	Failure rates per 10 ¹⁰ hours								Qty	Value
	F_1	F_2	F_3	K_1	K_2	K_3	K_4	Rate ^b		
RESISTORS										
Carbon film										
0 < R ≤ 100 K	100	0	0	1	1	1	1	100	17	1700
100 K < R ≤ 1 M	100	0	0	1	1.1	1	1	110	2	220
1 M < R ≤ 10 M	100	0	0	1	1.6	1	1	160	3	480
Metal film										
0 < R ≤ 100 K	150	0	0	1	1	1	1	150	17	2550
100 K < R ≤ 1 M	150	0	0	1	1.1	1	1	165	3	495
POTENTIOMETERS										
0 < R ≤ 50 K	700	0	0	1	1	1	1	700	8	5600
50 K < R ≤ 100 K	700	0	0	1	1	1.1	1	770	1	770
CAPACITORS										
Metal film										
0 < C ≤ 33 nF	200	0	0	1	1	1	1	200	3	600
33 nF < C ≤ 1 μF	200	0	0	1	1	1.3	1	260	2	520
1 μF < C ≤ 10 μF	200	0	0	1	1	1.5	1	300	1	300
Ceramic										
0 < C ≤ 3.3 nF	150	0	0	1	1	1	1	150	1	150
Electrolytic										
3.2 < C ≤ 62 μF	500	0	0	0.29	1	0.7	1	102	1	102
DIODES										
Silicon LP	200	0	0	0.55	1	1	1	110	2	220
Zener	1000	0	0	1.3	1	1	1	1300	1	1300
TRANSISTORS										
NPN LP	400	0	0	1.4	1	1	1	560	2	1120
INTEGRATED CIRCUITS										
OP AMP	160	50	600	1	1	1	1	810	9	7290
Quad switch	38	320	560	1	1	1	1	918	1	918
OTHERS										
Edge connectors	300	0	0	1	1	1	1	300	8	2400
Soldered joints	20	0	0	1	1	1	1	20	167	3340
PCB	60	0	0	1	1	1	1	60	1	60
Total rate: 3.01 × 10 ⁻⁶ per hour										
MTBF: 3.32 × 10 ⁵ hours										

^a Data sources:1: *Electronic Reliability Data*, National Centre of Systems Reliability, Application Code 2, 25C2: *Reliability Prediction Manual for Guided Weapon Systems*, MOD

3: Component supplier's information.

^b Rate = $(F_1 + F_2 + F_3) \times K_1 \times K_2 \times K_3 \times K_4$.Source: after Hellyer^[3].

7.1.7 Design and maintenance for reliability

Design for reliability

The following general principles should be observed.

Element selection. Only elements with well-established failure rate data/models should be used. Furthermore some technologies are inherently more reliable than others. Thus an inductive LVDT displacement sensor (Chapter 8) is inherently more reliable than a resistive potentiometer; the latter involves a contact sliding over a wire track, which will eventually become worn. A vortex flowmeter (Chapter 12) involves no moving parts and is therefore likely to be more reliable than a turbine flowmeter which incorporates a rotor assembly.

Environment. The environment in which the element is to be located should first be defined and the element should consist of components and elements which are capable of withstanding that environment. Thus the diaphragm of a differential pressure transmitter on a sulphuric acid duty should be made from a special alloy, e.g. Hastelloy C, which is resistant to corrosion.

Minimum complexity. We saw above that, for a series system, the system failure rate is the sum of the individual component/element failure rates. Thus the number of components/elements in the system should be the minimum required for the system to perform its function.

Redundancy. We also saw that the use of several identical elements/systems connected in parallel increases the reliability of the overall system. Redundancy should be considered in situations where either the complete system or certain elements of the system have too high a failure rate.

Diversity. In practice faults can occur which cause either more than one element in a given system, or a given element in each of several identical systems, to fail simultaneously. These are referred to as **common mode failures** and can be caused by incorrect design, defective materials and components, faults in the manufacturing process, or incorrect installation. One common example is an electronic system where several of the constituent circuits share a common electrical power supply; failure of the power supply causes all of the circuits to fail. This problem can be solved using **diversity**; here a given function is carried out by two systems in parallel, but each system is made up of different elements with different operating principles. One example is a temperature measurement system made up of two subsystems in parallel, one electronic and one pneumatic.

Maintenance

The **mean down time**, MDT, for a number of items of a repairable element has been defined as the mean time between the occurrence of the failure and the repaired element being put back into normal operation. It is important that MDT is as small as possible in order to minimise the financial loss caused by the element being out of action.

There are two main types of maintenance strategy used with measurement system elements. **Breakdown maintenance** simply involves repairing or replacing the element when it fails. Here MDT or **mean repair time**, T_R , is the sum of the times taken for a number of different activities. These include **realisation** that a fault has occurred, **access** to the equipment, **fault diagnosis**, **assembly** of repair equipment, components and personnel, **active repair/replacement** and finally **checkout**. **Preventive maintenance** is the servicing of equipment and/or replacement of components at regular fixed intervals; the corresponding **maintenance frequency** is m times per year. Here MDT or **mean maintenance time**, T_M , is the sum of times for access, **service/replacement** and checkout activities and therefore should be significantly less than mean repair time with breakdown maintenance.

7.2 Choice of measurement systems

The methods to be used and problems involved in choosing the most appropriate measurement system for a given application can be illustrated by a specific example. The example used will be the choice of the best system to measure the volume flow rate of a clean liquid hydrocarbon, range 0 to 100 m³ h⁻¹, in a 0.15 m (6 inch) diameter pipe. The measured value of flow rate must be presented to the observer in the form of a continuous trend on a chart recorder. The first step is to draw up a specification for the required flow measurement system. This will be a list of all important parameters for the complete system such as measurement error, reliability and cost, each with a desired value or range of values. The first two columns of Table 7.4 are an example of such a 'job specification'. As explained in Chapter 3, system measurement error in the steady state can be quantified in terms of the mean \bar{E} and standard deviation σ_E of the error probability distribution $p(E)$. These quantities depend on the imperfections, e.g. non-linearity and repeatability, of every element in the system. System failure rate λ and repair time T_R were defined in Section 7.1. Initial cost C_I is the cost of purchase, delivery, installation and commissioning of the complete system. C_R is the average cost of materials for each repair.

Table 7.4 Comparison table for selection of flow measurement system.

Parameter	Job specification	System 1 Orifice plate	System 2 Vortex	System 3 Turbine	System 4 Electromagnetic
Measurement error (at 50 m ³ h ⁻¹)	$\bar{E} \leq 0.25$ $\sigma_E \leq 0.8$ m ³ h ⁻¹	0.2 0.7	0.1 0.3	0.03 0.1	} Not technically feasible
Initial cost	$C_I \leq \text{£}4000$	3500	3000	4200	
Annual failure rate	$\lambda \leq 2.0$ failures yr ⁻¹	1.8	1.0	2.0	
Average repair time	$T_R \leq 8$ h	6	5	7	
Material repair cost	$C_R \leq \text{£}200$	100	100	300	

In this example the choice could be between four competing systems based on the orifice plate, vortex, turbine and electromagnetic primary sensing elements. The principles and characteristics of all four elements are discussed in Chapter 12. The configuration of the four systems could be:

1. Orifice plate – electronic D/P transmitter – square rooter – recorder.
2. Vortex element – frequency to voltage converter – recorder.
3. Turbine element – frequency to voltage converter – recorder.
4. Electromagnetic element – recorder.

The next step is to decide whether all the competing systems are technically feasible. The electromagnetic device will not work with electrically non-conducting fluids such as hydrocarbons, so that system 4 is technically unsuitable. Systems 1, 2 and 3 are feasible and the specification for each competing system must then be written down to see whether it satisfies the job specification. Table 7.4 gives possible specifications for the orifice plate, vortex and turbine systems. This data is entirely fictitious and is given only to illustrate the problems of choice. In practice a prospective user may not have all the information in Table 7.4 at his disposal. The manufacturer will be able to give estimates of initial cost C_i and the limits of measurement error, e.g. $\pm 2\%$ of full scale, for the orifice plate system at $50 \text{ m}^3 \text{ h}^{-1}$. He will not, however, be able to give values of mean error \bar{E} , failure rates and repair times. The last two quantities will depend on the environment of the user's plants and the maintenance strategy used. This information may be available within the user's company if adequate maintenance records have been kept. From Table 7.4 we see that the turbine flowmeter system 3 does not satisfy the job specification; both initial cost and material repair cost are outside the limits set. This would appear to rule out system 3, leaving 1 and 2. Both these systems satisfy the job specification but the vortex system 2 is cheaper, more accurate and more reliable than the orifice plate system 1. Thus, based on a straightforward comparison of job and system specification, the vortex measurement system 2 would appear to be the best choice for this application.

Under certain circumstances, however, the above conclusion could be entirely wrong. The turbine system is more expensive and less reliable than the vortex system, but is three times more accurate. We must now ask how much this increased accuracy is worth. Suppose the market value of the hydrocarbon is $\text{£}100 \text{ m}^{-3}$. A measurement error of one standard deviation in the turbine system, where $\sigma_E = 0.1 \text{ m}^3 \text{ h}^{-1}$, represents a potential cash loss of $\text{£}10$ per hour or approximately $\text{£}80\,000$ per annum. A corresponding error in the vortex system, where $\sigma_E = 0.3 \text{ m}^3 \text{ h}^{-1}$, represents an approximate potential loss of $\text{£}240\,000$ per annum. The difference between these two figures far outweighs the extra initial and maintenance costs, so that the turbine system 3 is the best choice in this case. We can conclude, therefore, that in order to choose the correct system for a given application, the financial value of each parameter in the job specification must be taken into account. In a costing application of this type, a digital printout of flow rate is more suitable than an analogue trend record.

7.3

Total lifetime operating cost

The total lifetime operating costing (TLOC) of a measurement system is the total cost penalty, incurred by the user, during the lifetime of the system. The TLOC is given by

$$\begin{aligned}
\text{TLOC} = & \text{initial cost of system (purchase, delivery, installation and commissioning)} \\
& + \text{cost of failures and maintenance over lifetime of the system} \\
& + \text{cost of measurement error over lifetime of the system} \quad [7.29]
\end{aligned}$$

and therefore takes account of the financial value of each parameter in the job specification. The best system for a given application is then the one with minimum TLOC. This method also enables the user to decide whether a measurement system is necessary at all. If no system is installed, TLOC may still be very large because no measurement implies a large measurement error. A measurement system should be purchased if it produces a significant reduction in TLOC.

Using eqn [7.29], we can derive an algebraic expression for TLOC using the parameters listed in Table 7.4. The initial cost of the system is $\pounds C_f$. If the system lifetime is T years and average failure rate λ faults yr^{-1} , then the total number of faults is λT . Since the average repair time is T_R hours then the total 'downtime' due to repair is $\lambda T T_R$ hours. The total lifetime cost of failures is the sum of the repair cost (materials and labour) and the process cost, i.e. the cost of lost production and efficiency while the measurement system is withdrawn for repair. If we define

$$\begin{aligned}
\pounds C_R &= \text{average materials cost per repair} \\
\pounds C_L &= \text{repair labour cost per hour} \\
\pounds C_P &= \text{process cost per hour}
\end{aligned}$$

then the total repair cost is $(C_R \lambda T + C_L T_R \lambda T)$ and the total process cost is $C_P T_R \lambda T$, giving:

$$\text{Total lifetime cost of failures} = [C_R + (C_L + C_P) T_R] \lambda T \quad [7.30]$$

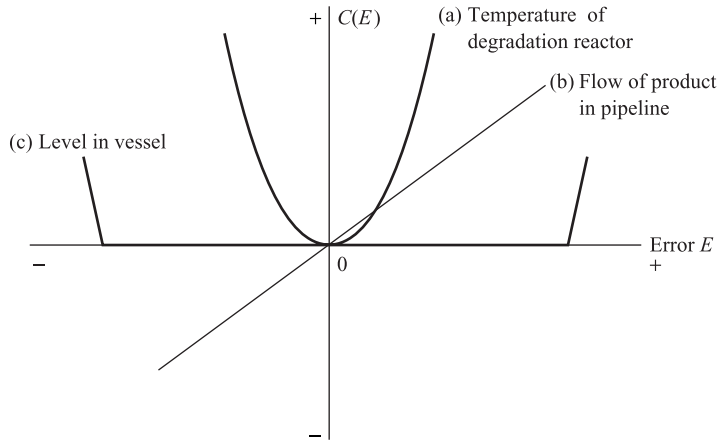
The above costs only apply to breakdown maintenance; many users also practise preventive maintenance in order to reduce failure rates. Suppose preventive maintenance is carried out on a measurement system m times yr^{-1} , the average maintenance time is T_M hours and the materials cost per service is $\pounds C_M$. The total number of services is mT and the total time taken for preventive maintenance is $m T T_M$ hours. Usually preventive maintenance of measurement systems is carried out at a time when the process or plant itself is shut down for repair and maintenance. This means that no process costs are incurred during preventive maintenance, giving:

$$\text{Total lifetime maintenance cost} = (C_M + C_L T_M) m T \quad [7.31]$$

The last term in eqn [7.29] involves the total lifetime cost of measurement error. In order to evaluate this we first need to evaluate the cost penalty function $C(E)$ ($\pounds \text{yr}^{-1}$) associated with a given steady-state measurement system error E . The form of $C(E)$ depends on the economics of the process on which the measurement is being made. A good example is temperature measurement in a chemical reactor where a degradation reaction is taking place.^[4] Here two reactions occur simultaneously: the feedstock A is converted into a desired product B but B is also degraded to an undesired product C. The rates of both reactions increase sharply with temperature, the rate of B to C being more temperature sensitive than the rate of A to B.

There is an optimum temperature at which the yield of B is maximum. If the reactor is operated at either above or below this optimum temperature, then the yield of B is sharply reduced and a cost penalty is incurred. This situation will occur if there is a measurement system error E between measured and true values of reactor temperature: the system tells the operator that the reactor is at optimum temperature

Figure 7.8 Error cost penalty function $C(E)$ for different processes.



when it is not. Figure 7.8(a) shows the form of the cost penalty function $C(E)$ in this case. We see that when $E = 0$, $C(E) = 0$ corresponding to optimum temperature; but $C(E)$ increases rapidly with positive and negative values of E as the yield of B decreases.

In Figure 7.8(b) $C(E)$ represents the cost penalty, due to imperfect flow measurement, incurred by a customer receiving a fluid by pipeline from a manufacturer. If E is positive, the customer is charged for more fluid than he actually receives and so is penalised, i.e. $C(E)$ is positive. If E is negative, the customer is charged for less fluid than was actually received and $C(E)$ is negative. Figure 7.8(c) refers to a non-critical liquid level measurement in a vessel. The vessel should be about half full, but plant problems will occur if the vessel is emptied or completely filled. Thus a cost penalty is incurred only if there is gross measurement error, i.e. the measurement system shows the vessel to be half full when almost empty.

We saw in Chapter 3 that the exact value of measurement error E , for a given measurement system at a given time, cannot be found. We can, however, find the probability that the system will have a certain error. This is quantified using a normal probability density function $p(E)$, with mean \bar{E} and standard deviation σ_E (Table 3.1). The probability of getting a measurement error between E and $E + dE$ is $p(E) dE$; the corresponding cost penalty is $C(E)p(E) dE$ per year, or $TC(E)p(E) dE$ throughout the system lifetime. The total lifetime cost of measurement error is then found by integrating the above expression over all possible values of E , i.e.

$$\text{Total lifetime cost of measurement error} = T \int_{-\infty}^{\infty} C(E)p(E) dE \quad [7.32]$$

The integral has a finite value, because the value of $p(E)$ becomes negligible for $|E|$ greater than 3 or 4 standard deviations; it can be evaluated numerically^[4] using values of the normalised Gaussian distribution.^[5]

From eqns [7.29]–[7.32] we have

$$\begin{aligned} \text{TLOC} = & C_I + [C_R + (C_L + C_P)T_R]\lambda T + (C_M + C_M T_M)mT \\ & + T \int_{-\infty}^{\infty} C(E)p(E) dE \end{aligned} \quad [7.33]$$

The relative importance of the terms in the above equation will depend on the application. In the chemical reactor $C(E)$ and C_p will be the major factors so that accuracy and reliability will be far more important than initial cost. In the tank level application, measurement error is unimportant and minimum TLOC will be obtained by the best trade-off between initial cost, reliability, and maintainability.

Conclusion

The first section of this chapter discussed the reliability of measurement systems. The fundamental principles and practical definitions of reliability were first explained and the relationship between reliability and instantaneous failure rate was derived. The typical variation in instantaneous failure rate throughout the lifetime of an element was then discussed and the reliability of series and parallel systems examined. The section concluded by looking at failure rate data and models and general strategies in design and maintenance for reliability.

The second section dealt with the problem of choice of measurement systems approached by comparing the job specification with those of the competing systems. This method does not take account of the financial value of each item in the specification. A better method, discussed in the final section, is to choose the systems with minimum lifetime operating cost.

References

- [1] WRIGHT R I (SRD Warrington) 1984 'Instrument reliability', *Instrument Science and Technology*, Institute of Physics, Bristol, vol. 1, pp. 82–92.
- [2] LEES F P 1976 'The reliability of instrumentation', *Chemistry and Industry*, March, pp. 195–205.
- [3] HELLYER F G (Protech Instruments and Systems) 1985 'The application of reliability engineering to high integrity plant control systems', *Measurement and Control*, 18 June, pp. 172–6.
- [4] BENTLEY J P 1979 'Errors in industrial temperature measurement systems and their effect on the yield of a chemical degradation reaction', *8th IMEKO Congress of the International Measurement Confederation*, Moscow, May.
- [5] WHITE J, YEATS A and SKIPWORTH G 1974 *Tables for Statisticians*, Stanley Thornes, London, pp. 18–19.

Problems

- 7.1 A batch of 100 identical thermocouples were tested over a 12-week period. Twenty failures were recorded and the corresponding down times in hours were as follows:

5, 6, 7, 8, 4, 7, 8, 10, 5, 4, 8, 5, 4, 5, 6, 5, 4, 9, 8, 6

Calculate:

- (a) Mean down time
- (b) Mean time between failures
- (c) Mean failure rate
- (d) Availability.

7.2 A flow measurement system consists of an orifice plate ($\lambda = 0.75$), differential pressure transmitter ($\lambda = 1.0$), square root extractor ($\lambda = 0.1$) and recorder ($\lambda = 0.1$). Calculate the probability of losing the flow measurement after 0.5 year for the following:

- (a) A single flow measurement system
- (b) Three identical flow measurement systems in parallel
- (c) A system with three orifice plates, three differential pressure transmitters and a middle value selector relay ($\lambda = 0.1$). The selected transmitter output is passed to a single square root extractor and recorder.

Annual failure rate data are given in brackets; assume that all systems were initially checked and found to be working correctly.

7.3 Use the data given in Table Prob. 3 to decide which level measurement system should be purchased. Assume a breakdown maintenance only strategy is practised, each system has the same measurement error, and there is a 10-year total lifetime.

Table Prob. 3.

	Parameter	System 1	System 2
Initial cost	£	1000	2000
Materials cost per repair	£	20	15
Labour cost per hour	£	10	10
Process cost per hour	£	100	100
Repair time	h	8	12
Annual failure rate	yr ⁻¹	2.0	1.0

Part B

Typical Measurement System Elements

8 Sensing Elements

In Chapter 1 we saw that, in general, a measurement system consists of four types of element: sensing, signal conditioning, signal processing and data presentation elements. The sensing element is the first element in the measurement system; it is in contact with, and draws energy from, the process or system being measured. The input to this element is the true value of the measured variable; the output of the element depends on this value. The purpose of this chapter is to discuss the principles and characteristics of sensing elements in wide current use; more specialised elements are discussed in later chapters. Table 8.1 lists the sensing elements described in this book according to the physical principle involved, e.g. inductive or thermoelectric. The elements are classified according to whether the output signal is electrical, mechanical, thermal or optical. Elements with an electrical output are further divided into passive and active. Passive devices such as resistive, capacitive and inductive elements require an external power supply in order to give a voltage or current output signal; active devices, e.g. electromagnetic and thermoelectric elements, need no external power supply.

The table also lists the input measured variables which a given type of element is used to sense, by giving the relevant section number in the book. Thus capacitive elements can sense pressure, liquid level, displacement and humidity. Elastic elements can sense force, pressure torque, acceleration and density. Sensors with a mechanical output are commonly used as the primary sensing element in measurement systems for mechanical variables such as force or flow rate. In order to obtain an electrical signal, this primary element is followed by a secondary sensing element with an electrical output signal. Examples are a resistive strain gauge sensing the strain in an elastic cantilever in a force measurement system, and an electromagnetic tachogenerator sensing the angular velocity of a turbine in a flow measurement system.

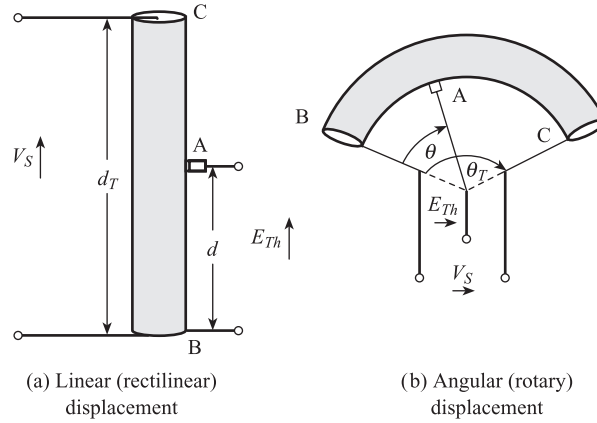
8.1 Resistive sensing elements

8.1.1 Potentiometers for linear and angular displacement measurement

Figure 8.1 shows potentiometers for the measurement of (a) linear (rectilinear) and (b) angular (rotary) displacement. They consist of a former with a cylindrical

Table 8.1 Sensing elements and measured variables.

Input measured variable													
Physical principle													
Electrical output passive	Resistive	8.1	8.6	8.6	8.6								Magnetic field
		15.5	15.5										Humidity
	Capacitive											8.1	
	Inductive		8.2									8.2	
	Piezoresistive		8.8										
	Photovoltaic		15.5										
Electrical output active	Photoconductive		15.5										
	FET												
	Hall effect											8.9	8.9
	Electromagnetic												8.10
	Thermoelectric	8.5											
		15.5	15.5										8.4
Mechanical output	Piezoelectric												
	Electrochemical		16.2	8.7									8.7
	Pyroelectric	15.5	15.5										8.9
	Elastic		8.6	4.1									
			9.4	8.6	8.6	9.4							
			9.5	9.5									8.6
Thermal output	Differential pressure												
	Turbine												
	Vortex												
	Pneumatic												
	Coriolis		13.1	13.1									13.1
	Heat transfer		15.5										14.4
Optical output	Various		15.6	15.6	15.6	15.6							15.6
													15.6

Figure 8.1 Potentiometer displacement sensors.

cross-section which is either a straight cylinder or an arc of a circle. Resistive material is then placed on the former so that the resistance per unit length is constant (the usual case). This means that resistance is proportional to the distance d travelled by the wiper between A and B.

From Figure 8.1(a), the ratio of open circuit voltage E_{Th} to supply voltage V_S is given by:

$$\frac{E_{Th}}{V_S} = \frac{\text{voltage across AB}}{\text{voltage across CB}} = \frac{\text{resistance across AB}}{\text{resistance across CB}}$$

where:

resistance of CB = total resistance of potentiometer = R_p

resistance of AB = fractional resistance = $R_p d/d_T = R_p x$

x = fractional displacement = d/d_T .

Therefore the open circuit voltage for a linear displacement potentiometer is:

$$E_{Th} = V_S x = V_S d/d_T \quad [8.1]$$

i.e. voltage is proportional to displacement.

From Figure 8.1(b), the open circuit voltage for an angular displacement potentiometer is:

$$E_{Th} = V_S \theta/\theta_T = V_S x \quad [8.2]$$

where $x = \theta/\theta_T$ is the fractional angular displacement.

In Section 5.1.2 the Thévenin resistance of the potentiometer was shown to be $R_{Th} = R_p x(1 - x)$. It was also shown that in general the relationship between the voltage across an external load R_L and fractional displacement x is non-linear (eqn [5.10]). The choice of a potentiometer for a given application involves four main parameters:

- **Maximum travel d_T , θ_T**
Depends on range of displacement to be measured, e.g. 0 to 5 cm, 0 to 300°.

- **Supply voltage V_S**
Set by required output range, e.g. for a range of 0 to 5 V d.c., we need $V_S = 5$ V d.c.
- **Resistance R_p**
For a given load R_L , choose R_p to be sufficiently small compared with R_L so that maximum non-linearity is acceptable (eqn [5.12]).
- **Power rating W_{\max}**
 W_{\max} should be greater than actual power V_S^2/R_p produced in R_p .

In **wire wound** potentiometers the resistive track, of total length d_T or θ_T , consists of n discrete turns of wire. The resistance between A and B therefore increases in a series of steps for a smooth continuous increase in displacement d or θ . The corresponding resolution error is therefore d_T/n , θ_T/n or $(100/n)\%$ (Section 2.1). A typical family of rectilinear precision potentiometers covers displacement spans from 12 to 2500 mm, non-linearity from $\pm 0.2\%$ and resolution from 0.008% with resistance values of 40 Ω /mm.

In **conductive plastic film** potentiometers the track is continuous so that there is zero resolution error and less chance of contact wear than with wire wound; the temperature coefficient of resistance is, however, higher. A family of rectilinear precision potentiometers covers displacement spans from 25 to 250 mm, non-linearities to $\pm 0.04\%$ and resistance values from 500 Ω to 80 k Ω . A typical angular (rotary) potentiometer has a diameter of 42 mm, an input range of 0 to 350°, a corresponding resistance range of 1 to 220 k Ω and non-linearity of $\pm 0.5\%$. The most modern development is the **hybrid** track potentiometer, which is manufactured by depositing a conductive film on a precision wire wound track and incorporates the best features of both types.

8.1.2 Resistive metal and semiconductor sensors for temperature measurement

The resistance of most **metals** increases reasonably linearly with temperature in the range -100 to $+800$ °C. The general relationship between the resistance R_T Ω of a metal element and temperature T °C is a power series of the form:

$$R_T = R_0(1 + \alpha T + \beta T^2 + \gamma T^3 + \dots) \quad [8.3]$$

where R_0 Ω is the resistance at 0 °C and α , β , γ are temperature coefficients of resistance. The magnitude of the non-linear terms is usually small. Figure 8.2(a) shows the variation in the ratio R_T/R_0 with temperature for the metals platinum, copper and nickel. Although relatively expensive, platinum is usually chosen for industrial resistance thermometers; cheaper metals, notably nickel and copper, are used for less demanding applications. Platinum is preferred because it is chemically inert, has linear and repeatable resistance/temperature characteristics, and can be used over a wide temperature range (-200 to $+800$ °C) and in many types of environments. It can be refined to a high degree of purity, which ensures that statistical variations in resistance, between similar elements at the same temperature (Section 2.3.2), are small. A typical platinum element has $R_0 = 100.0$ Ω , $R_{100} = 138.50$ Ω , $R_{200} = 175.83$ Ω , $\alpha = 3.91 \times 10^{-3}$ °C $^{-1}$ and $\beta = -5.85 \times 10^{-7}$ °C $^{-2}$. The change in resistance between

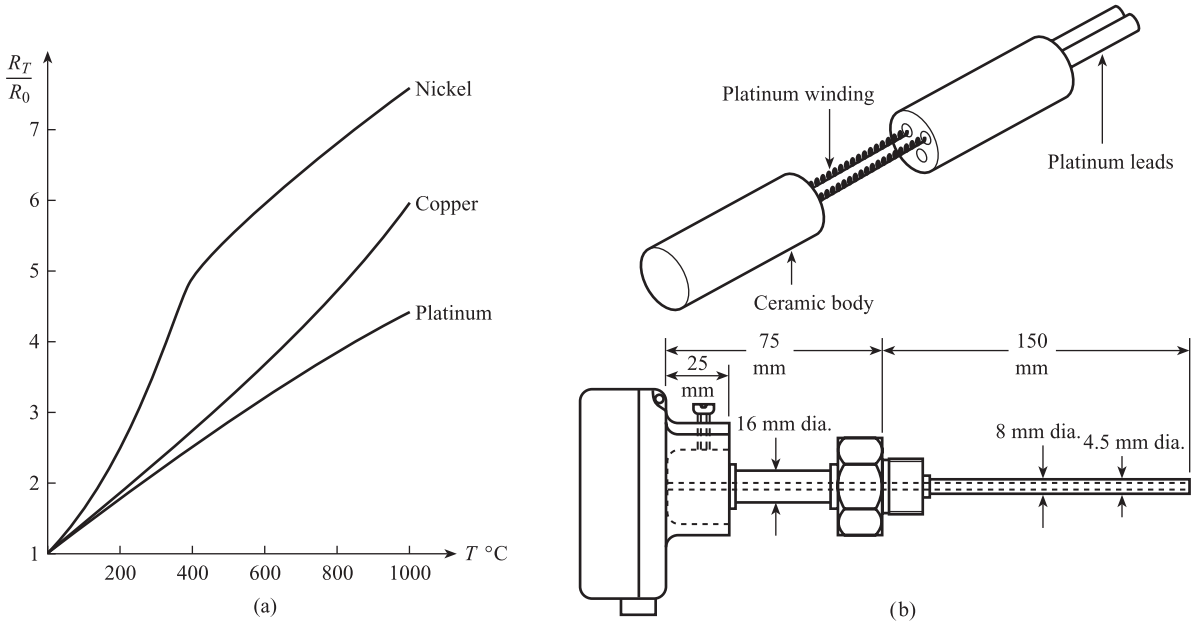


Figure 8.2
Metal resistive temperature sensors:
(a) Resistance/temperature characteristics of commonly used metals
(b) Typical construction of platinum element probe.^[1]

the ice point and the steam point, i.e. $R_{100} - R_0$, is called the **fundamental interval**; in the above element this is 38.5Ω . The maximum non-linearity as a percentage of f.s.d. (eqn [2.5]) between 0 and 200°C is $+0.76\%$.

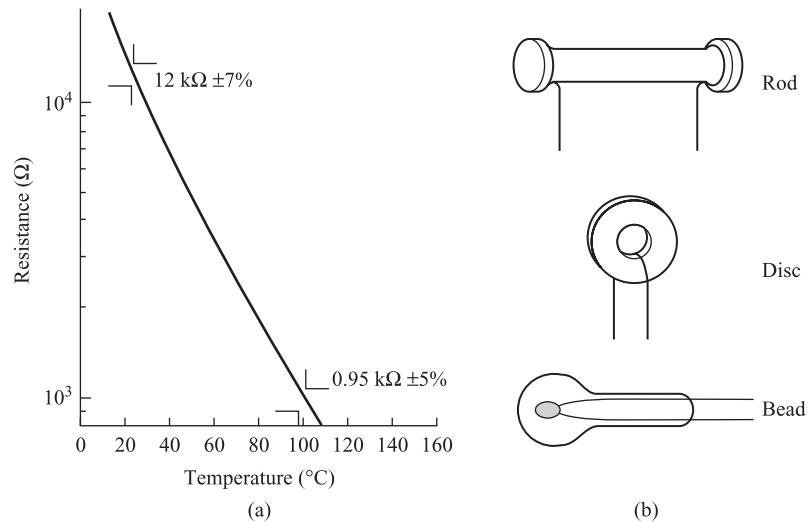
The standard IEC 751: 1983 (BS EN 60751: 1996)^[2] lays down tolerance limits on the maximum variation in resistance between platinum elements at a given temperature. For class A elements the tolerance limits are $\pm 0.06 \Omega$ at 0°C and $\pm 0.20 \Omega$ at 200°C ; for class B elements the tolerance limits are $\pm 0.12 \Omega$ at 0°C and $\pm 0.48 \Omega$ at 200°C . The amount of electrical power produced in the element should be limited in order to avoid self-heating effects (Chapter 14); in a typical element 10 mW of power causes a temperature rise of 0.3°C .

One type of element is constructed using the partially supported arrangement shown in Figure 8.2(b).^[1] Here fine platinum wire is wound into a very small spiral and is inserted into axial holes in a high purity alumina insulator. A small quantity of glass adhesive is introduced into the holes and the unit is fired, thus securely fixing a part of each turn onto the alumina; the remainder of the wire is free to move. The diagram also shows the element housed in a stainless steel protective sheath.

Resistive temperature elements made from **semiconductor** materials are often referred to as thermistors. The most commonly used type is prepared from oxides of the iron group of transition metal elements such as chromium, manganese, iron, cobalt and nickel. The resistance of these elements decreases with temperature – in other words there is a negative temperature coefficient (NTC) – in a highly non-linear way. Figure 8.3 shows typical thermistor resistance–temperature characteristics which can be described by the relationship:

$$R_{\theta} = K \exp \left(\frac{\beta}{\theta} \right) \quad [8.4]$$

Figure 8.3 Thermistor resistance–temperature characteristics and types (graph (a) after Mullard Ltd^[3]).



where R_θ is the resistance at temperature θ kelvin; K and β are constants for the thermistor. A commonly used alternative equation is:

$$R_\theta = R_{\theta_1} \exp \beta \left[\frac{1}{\theta} - \frac{1}{\theta_1} \right] \quad [8.5]$$

where R_{θ_1} Ω is the resistance at reference temperature θ_1 K, usually $\theta_1 = 25^\circ\text{C} = 298$ K. Thermistors are usually in the form of either beads, rods or discs (Figure 8.3); bead thermistors are enclosed in glass envelopes. A typical NTC thermistor has a resistance of 12 kΩ at 25 °C (298 K), falling to 0.95 kΩ at 100 °C (373 K), and $\beta = 3750$ K.^[3] The manufacturer's tolerance limits on the above figures are ±7%, i.e. ±840 Ω, at 25 °C, and ±5%, i.e. ±47.5 Ω, at 100 °C, which is far wider than for metal elements. The element time constant is 19 seconds in air and 3 seconds in oil, and the self-heating effect is 1 °C rise for every 7 mW of electrical power. Thermistors with positive temperature coefficients (P.T.C.) are also available; the resistance of a typical element increases from 100 Ω at −55 °C to 10 kΩ at 120 °C.

Thick-film polymers can be used as resistive sensors for temperature and humidity measurement.^[4] These are pastes consisting of a polymer matrix (usually epoxy, silicone or phenolic resin) that binds together the filler particles. If the filler material is metallic, e.g. silver flakes or copper particles, then the paste has similar resistive properties to a metal. If carbon particles are used as the filler material, then the paste has the resistive properties of a semiconductor. Solvents are then added to give the paste the thixotropic properties of an ink so it can be screen printed on to a substrate (often alumina). Following the printing process, the solvents are dried off and the pastes are cured at temperatures that do not affect the physical and chemical stability of the substrates. The printed patterns used for carbon and silver paste are shown in Figure 8.4(a).

Figure 8.4(b) shows the variation in resistances with temperature for silver and carbon polymers. Silver polymers exhibit a linear increase in resistance with temperature. This is described by a linear approximation to eqn [8.3], i.e.

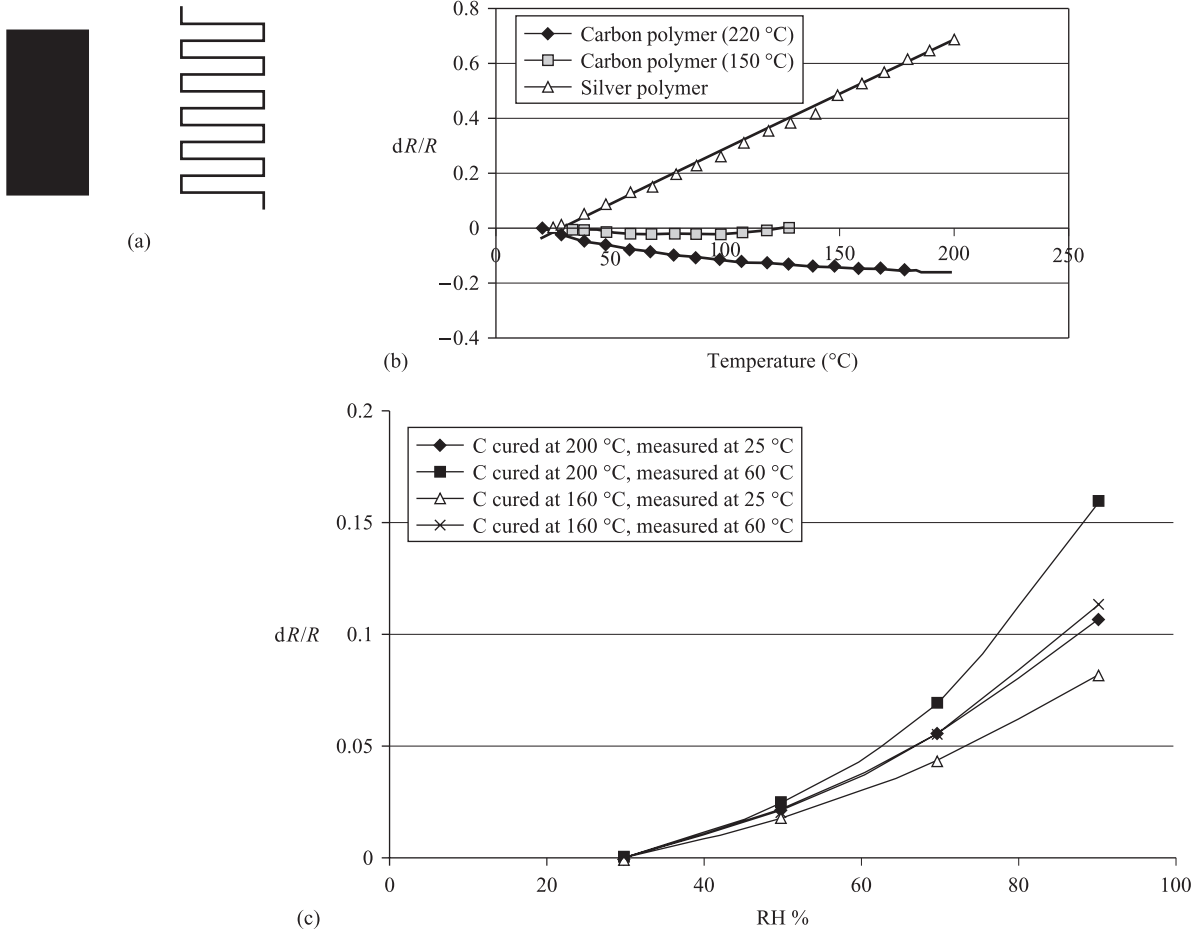


Figure 8.4 Thick-film polymer resistive sensors: (a) Printed patterns for carbon paste (left) and silver paste (right) (b) Changes in resistance of silver and carbon filled pastes with temperature (c) Changes in resistance of carbon polymer pastes with relative humidity (Figures 8.4(b) and (c) are reprinted by permissions of the Institute of Measurement and Control and the University of Southampton and N. M. White^[4]).

$$R_T = R_0(1 + \alpha T) \quad [8.6]$$

An alternative linear approximation for T between 25 and 200 $^{\circ}\text{C}$ is:

$$R_T = R_{25}[1 + \alpha(T - 25)] \quad [8.7]$$

where $\alpha = 3.732 \times 10^{-3} \text{ }^{\circ}\text{C}^{-1}$.^[4]

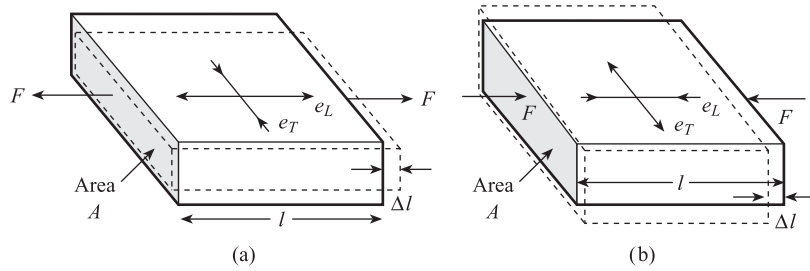
In contrast the carbon paste cured at 220 $^{\circ}\text{C}$ exhibits semiconductor or thermistor-like characteristics, described by eqns [8.4] and [8.5]: here the constant $\beta = 136 \text{ K}$.

Carbon polymers also show a variation in resistance with **humidity**. The polymer matrix absorbs water, causing it to swell. This causes the carbon particles embedded in the matrix to move further away from each other, thus reducing the number of conductive paths and consequently increasing the resistivity of the material. Figure 8.4(c) shows the variation in resistance with humidity in the range 30% to 90% for carbon polymers cured at 160 $^{\circ}\text{C}$ and 200 $^{\circ}\text{C}$ and operated at 25 $^{\circ}\text{C}$ and 60 $^{\circ}\text{C}$. The resistance–humidity characteristics are non-linear; the higher the curing temperature the greater the non-linearity.^[4]

Figure 8.5

Stress and strain:

- (a) Effect of tensile stress
 (b) Effect of compressive stress.



8.1.3 Metal and semiconductor resistive strain gauges

Before discussing strain gauges we must first briefly explain the concepts of stress, strain, elastic modulus and Poisson's ratio.

Stress is defined by force/area, so that in Figure 8.5(a) the stress experienced by the body is $+F/A$, the positive sign indicating a **tensile stress** which tends to increase the length of the body. In Figure 8.5(b) the stress is $-F/A$, the negative sign indicating a **compressive stress** which tends to reduce the length of the body. The effect of the applied stress is to produce a **strain** in the body which is defined by (change in length)/(original unstressed length). Thus in Figure 8.5(a) the strain is $e = +\Delta l/l$ (tensile), and in 8.5(b) the strain is $e = -\Delta l/l$ (compressive); in both cases the strain is **longitudinal**, i.e. along the direction of the applied stress. The relationship between strain and stress is linear for a given body over a certain range of values; the slope of the straight line is termed the **elastic modulus** of the body:

Elastic modulus

$$\text{Elastic modulus} = \frac{\text{stress}}{\text{strain}} \quad [8.8]$$

For linear tensile or compressive stress the elastic modulus is called **Young's modulus** E ; for shear stress the relevant elastic modulus is **shear modulus** S . Returning to Figure 8.5(a) we note that the increase in length of the body is accompanied by a decrease in cross-sectional area, i.e. a reduction in width and thickness. Thus in Figure 8.5(a) the longitudinal tensile strain is accompanied by a transverse compressive strain, and in Figure 8.5(b) the longitudinal compressive strain is accompanied by a transverse tensile strain. The relation between longitudinal strain e_L and accompanying transverse strain e_T is:

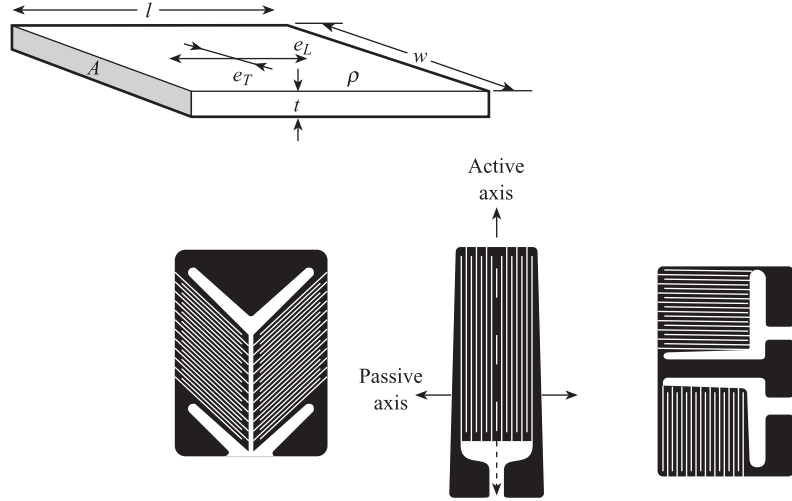
$$e_T = -\nu e_L \quad [8.9]$$

where ν is Poisson's ratio, which has a value between 0.25 and 0.4 for most materials.

A **strain gauge** is a metal or semiconductor element whose resistance changes when under strain. We can derive the relationship between changes in resistance and strain by considering the factors which influence the resistance of the element. The resistance of an element of length l , cross-sectional area A and resistivity ρ (Figure 8.6) is given by:

$$R = \frac{\rho l}{A} \quad [8.10]$$

Figure 8.6 Strain gauges.



In general with strain gauges ρ , l and A can change if the element is strained, so that the change in resistance ΔR is given by:

$$\Delta R = \left(\frac{\partial R}{\partial l} \right) \Delta l + \left(\frac{\partial R}{\partial A} \right) \Delta A + \left(\frac{\partial R}{\partial \rho} \right) \Delta \rho \quad [8.11]$$

i.e.

$$\Delta R = \frac{\rho}{A} \Delta l - \frac{\rho l}{A^2} \Delta A + \frac{l}{A} \Delta \rho$$

Dividing throughout by $R = \rho l / A$ yields

$$\frac{\Delta R}{R} = \frac{\Delta l}{l} - \frac{\Delta A}{A} + \frac{\Delta \rho}{\rho} \quad [8.12]$$

The ratio $\Delta l / l$ is the longitudinal strain e_L in the element. Since cross-sectional area $A = wt$ (Figure 8.6),

$$\frac{\Delta A}{A} = \frac{\Delta w}{w} + \frac{\Delta t}{t} = 2e_T$$

where e_T is the transverse strain in the element. From [8.9] and [8.12] we have:

$$\begin{aligned} \frac{\Delta R}{R} &= e_L - 2(-\nu e_L) + \frac{\Delta \rho}{\rho} \\ &= (1 + 2\nu)e_L + \frac{\Delta \rho}{\rho} \end{aligned} \quad [8.13]$$

We now define the **gauge factor** G of a strain gauge by the ratio (fractional change in resistance)/(strain), i.e.

$$G = \frac{\Delta R / R_0}{e}$$

Hence

*Resistance/strain
relationship for
a strain gauge*

$$\frac{\Delta R}{R_0} = Ge \quad [8.14]$$

where R_0 is the unstrained resistance of the gauge. From [8.13] the gauge factor is given by:

*Gauge factor of
a strain gauge*

$$G = 1 + 2\nu + \frac{1}{e} \frac{\Delta \rho}{\rho} \quad [8.15]$$

For most metals $\nu \approx 0.3$, and the term $(1/e) (\Delta \rho / \rho)$ representing strain-induced changes in resistivity (**piezoresistive effect**) is small (around 0.4), so that the overall gauge factor G is around 2.0. A popular metal for strain gauges is the alloy 'Advance'; this is 54% copper, 44% nickel and 1% manganese. This alloy has a low **temperature coefficient of resistance** ($2 \times 10^{-5} \text{ }^\circ\text{C}^{-1}$) and a low **temperature coefficient of linear expansion**. Temperature is both an interfering and a modifying input (Section 2.2), and the above properties ensure that temperature effects on zero values and sensitivity are small.

The most common strain gauges are of the bonded type, where the gauge consists of metal foil, cut into a grid structure by a photoetching process, and mounted on a resin film base. The film backing is then attached to the structure to be measured with a suitable adhesive. The gauge should be positioned so that its active axis is along the direction of the measured strain: the change in resistance, due to a given strain, along the passive axis is very small compared with that produced by the same strain along the active axis. A typical gauge has:

- Gauge factor 2.0 to 2.2
- Unstrained resistance $120 \pm 1 \text{ } \Omega$
- Linearity within $\pm 0.3\%$
- Maximum tensile strain $+2 \times 10^{-2}$
- Maximum compressive strain -1×10^{-2}
- Maximum operating temperature $150 \text{ }^\circ\text{C}$.

The change in resistance at maximum tensile strain is $\Delta R = +4.8 \text{ } \Omega$, and $\Delta R = -2.4 \text{ } \Omega$ at maximum compressive strain. A maximum gauge current between 15 mA and 100 mA, depending on area, is specified in order to avoid self-heating effects. Unbonded strain gauges consisting of fine metal wire stretched over pillars are used in some applications.

In semiconductor gauges the piezoresistive term $(1/e) (\Delta \rho / \rho)$ can be large, giving large gauge factors. The most common material is silicon doped with small amounts of p -type or n -type material. Gauge factors of between +100 and +175 are common for p -type silicon, and between -100 and -140 for n -type silicon. A negative gauge factor means a decrease in resistance for a tensile strain. Thus semiconductor gauges have the advantage of greater sensitivity to strain than metal ones, but have the disadvantage of greater sensitivity to temperature changes. Typically a rise in ambient temperature from 0 to $40 \text{ }^\circ\text{C}$ causes a fall in gauge factor from 135 to 120. Also the temperature coefficient of resistance is larger, so that the resistance of a typical unstrained gauge will increase from $120 \text{ } \Omega$ at $20 \text{ }^\circ\text{C}$ to $125 \text{ } \Omega$ at $60 \text{ }^\circ\text{C}$. Strain gauge elements are incorporated in deflection bridge circuits (Section 9.1).

8.1.4 Semiconductor resistive gas sensors

Metal oxide sensors have semiconducting properties which are affected by the presence of gases. The resistance of **chromium titanium oxide** is affected by **reducing** gases such as carbon monoxide (CO) and hydrocarbons. Here oxygen atoms near the surface react with reducing gas molecules; this reaction takes up conduction electrons so that fewer are available for conduction. This causes a decrease in electrical conductivity and a corresponding increase in resistance. The resistance of **tungsten oxide** is affected by **oxidising** gases such as oxides of nitrogen (NO_x) and ozone. Here atoms near the surface react with oxidising gas molecules; this reaction takes up conduction electrons, again causing a decrease in electrical conductivity and an increase in resistance with gas concentration. To aid the oxidation/reduction process, these sensors are operated at elevated temperatures well above ambient temperature.

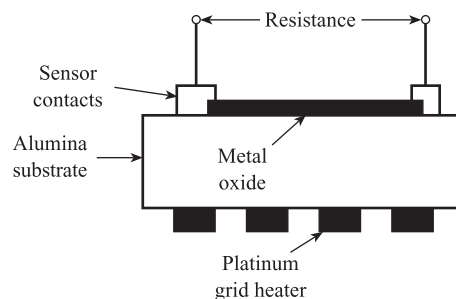
Figure 8.7 shows a typical construction of a metal oxide sensor using thick film technology. This consists of an alumina substrate with a film of oxide printed on one side and a platinum heater grid on the other. A typical NO_x sensor has an ambient temperature range of -20°C to $+60^\circ\text{C}$ and operating power of 650 mW. The resistance is typically 6 k Ω in air, 39 k Ω in 1.5 ppm NO_2 and 68 k Ω in 5.0 ppm NO_2 .^[5] A typical CO sensor has an ambient temperature range of -20°C to $+60^\circ\text{C}$ and an operating power of 650 mW. The resistance is typically 53 k Ω in air, 85 k Ω in 100 ppm CO and 120 k Ω in 400 ppm CO.^[5]

Gas sensing reactions occur at or near the surface of **organic polymer** semiconductors so that only a thin film of the material is required in a sensor. The metal phthalocyanines (MPc) have high sensitivities to certain gases. Thin films of MPc act as *p*-type semiconductors where electrical conductivity is due to positive holes. Electron acceptor gases such as chlorine and nitrogen dioxide are absorbed by the film and capture MPc electrons. This causes an increase in the population density of free holes and a corresponding increase in electrical conductivity, i.e. a decrease in resistance, with gas concentration. The metal M is chosen so that it has the greatest sensitivity to a particular gas. Thus lead has the highest sensitivity to nitrogen dioxide (NO_2) and copper the highest sensitivity to hydrogen chloride (HCl). For a lead phthalocyanine film detecting NO_2 , the relationship between resistance R and concentration $[\text{NO}_2]$ is approximately logarithmic, i.e.

$$\log_{10} R = -K \log_{10} [\text{NO}_2] + a \quad [8.16]$$

Here K and a are constants and concentrations are in the parts per billion (ppb) range (Figure 8.8(a)).^[6] A given metal phthalocyanine will also respond to other gases in addition to the one it has been selected for: thus copper has maximum response to

Figure 8.7 Typical construction of metal oxide gas sensor.



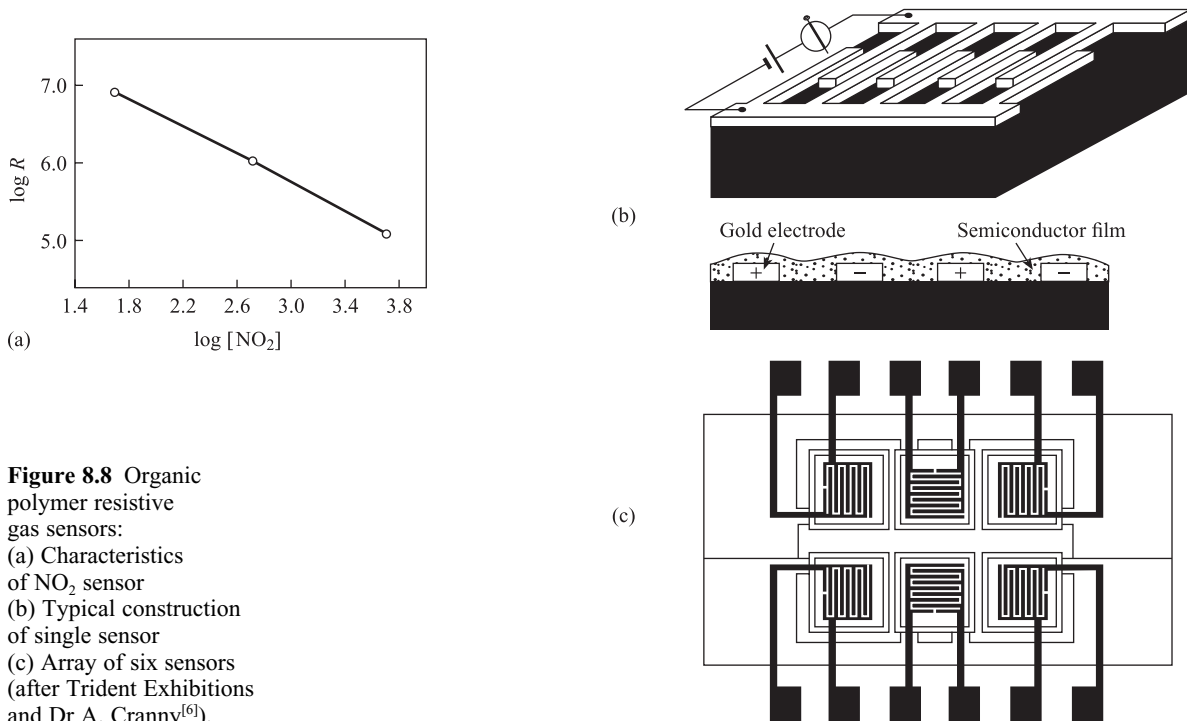


Figure 8.8 Organic polymer resistive gas sensors:
(a) Characteristics of NO_2 sensor
(b) Typical construction of single sensor
(c) Array of six sensors (after Trident Exhibitions and Dr A. Cranny^[6]).

HCl , but also responds to NO_2 , Cl_2 and H_2S .^[6] Thus the other gases act as **environmental modifying** and **interfering inputs** (Sections 2.1 and 19.2.4).

Figure 8.8(b) shows the construction of a typical individual sensor. Here a thin film of the metal phthalocyanine is deposited onto a planar configuration of gold electrodes deposited on an alumina substrate.^[6] Figure 8.8(c) shows an array of six sensors; each sensor is formed by depositing a thin film of a given MPC on a configuration of thick film platinum electrodes. By using a different metal M for each sensor, the concentration of each of six different gases in a mixture can in principle be found. Methods of compensation for modifying cross-sensitivity effects between the gases will need to be developed (Chapter 19).

8.2 Capacitive sensing elements

The simplest capacitor or condenser consists of two parallel metal plates separated by a dielectric or insulating material (Figure 8.9). The capacitance of this parallel plate capacitor is given by:

$$C = \frac{\epsilon_0 \epsilon A}{d} \quad [8.17]$$

where ϵ_0 is the permittivity of free space (vacuum) of magnitude 8.85 pF m^{-1} , ϵ is the relative permittivity or dielectric constant of the insulating material, $A \text{ m}^2$ is the area of overlap of the plates, and $d \text{ m}$ is their separation. From [8.17] we see that C

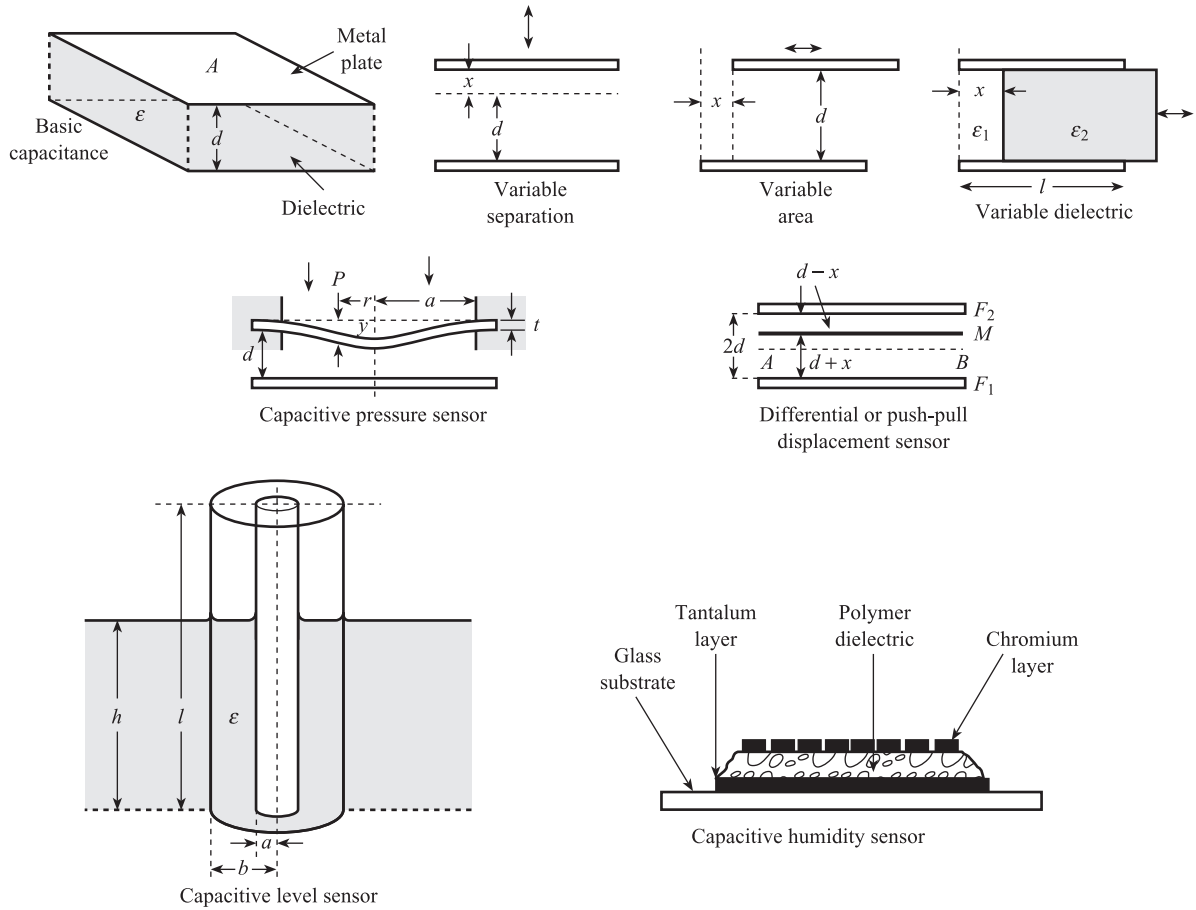


Figure 8.9 Capacitive sensing elements.

can be changed by changing either d , A or ϵ ; Figure 8.9 shows **capacitive displacement sensors** using each of these methods. If the displacement x causes the plate separation to increase to $d + x$ the capacitance of the sensor is:

$$C = \frac{\epsilon_0 \epsilon A}{d + x} \quad [8.18]$$

i.e. there is a non-linear relation between C and x . In the variable area type, the displacement x causes the overlap area to decrease by $\Delta A = wx$, where w is the width of the plates, giving:

$$C = \frac{\epsilon_0 \epsilon}{d} (A - wx) \quad [8.19]$$

In the variable dielectric type, the displacement x changes the amount of dielectric material ϵ_2 ($\epsilon_2 > \epsilon_1$) inserted between the plates. The total capacitance of the sensor

is the sum of two capacitances, one with area A_1 and dielectric constant ϵ_1 , and one with area A_2 and dielectric constant ϵ_2 , i.e.

$$C = \frac{\epsilon_0 \epsilon_1 A_1}{d} + \frac{\epsilon_0 \epsilon_2 A_2}{d}$$

Since $A_1 = wx$, $A_2 = w(l - x)$, when w is the width of the plates,

Variable dielectric displacement sensor

$$C = \frac{\epsilon_0 w}{d} [\epsilon_2 l - (\epsilon_2 - \epsilon_1)x] \quad [8.20]$$

A commonly used capacitive pressure sensor is shown in Figure 8.9. Here one plate is a fixed metal disc, the other is a flexible flat circular diaphragm, clamped around its circumference; the dielectric material is air ($\epsilon \approx 1$). The diaphragm is an elastic sensing element (Section 8.6) which is bent into a curve by the applied pressure P . The deflection y at any radius r is given by:

$$y = \frac{3}{16} \frac{(1 - \nu^2)}{Et^3} (a^2 - r^2)^2 P \quad [8.21]$$

where

a = radius of diaphragm

t = thickness of diaphragm

E = Young's modulus

ν = Poisson's ratio.

The deformation of the diaphragm means that the average separation of the plates is reduced. The resulting increase in capacitance ΔC is given by^[7]

Capacitive pressure sensor

$$\frac{\Delta C}{C} = \frac{(1 - \nu^2)a^4}{16Edt^3} P \quad [8.22]$$

where d is the initial separation of the plates and $C = \epsilon_0 \pi a^2 / d$ the capacitance at zero pressure.

The variable separation displacement sensor has the disadvantage of being non-linear (eqn [8.18]). This problem is overcome by using the three-plate differential or push-pull displacement sensor shown in Figure 8.9. This consists of a plate M moving between two fixed plates F_1 and F_2 ; if x is the displacement of M from the centre line AB , then the capacitances C_1 and C_2 formed by MF_1 and MF_2 respectively are:

Differential capacitive displacement sensor

$$C_1 = \frac{\epsilon \epsilon_0 A}{d + x}, \quad C_2 = \frac{\epsilon \epsilon_0 A}{d - x} \quad [8.23]$$

The relations between C_1 , C_2 and x are still non-linear, but when C_1 and C_2 are incorporated into the a.c. deflection bridge described in Section 9.1.3, the overall relationship between bridge output voltage and x is linear (eqn [9.23]).

The next sensing element shown in Figure 8.9 is a level sensor consisting of two concentric metal cylinders. The space between the cylinders contains liquid to the height h of the liquid in the vessel. If the liquid is non-conducting (electrical conductivity less than $0.1 \mu\text{mho cm}^{-3}$), it forms a suitable dielectric and the total capacitance of the sensor is the sum of liquid and air capacitances. The capacitance/unit length of two coaxial cylinders, radii b and a ($b > a$), separated by a dielectric ϵ is $2\pi\epsilon_0\epsilon/\log_e(b/a)$. Assuming the dielectric constant of air is unity, the capacitance of the level sensor is given by:

$$C_h = \frac{2\pi\epsilon_0\epsilon h}{\log_e\left(\frac{b}{a}\right)} + \frac{2\pi\epsilon_0(l-h)}{\log_e\left(\frac{b}{a}\right)}$$

Capacitive level sensor

$$C_h = \frac{2\pi\epsilon_0}{\log_e\left(\frac{b}{a}\right)} [l + (\epsilon - 1)h] \quad [8.24]$$

The sensor can be incorporated into the a.c. deflection bridge of Figure 9.5(a).

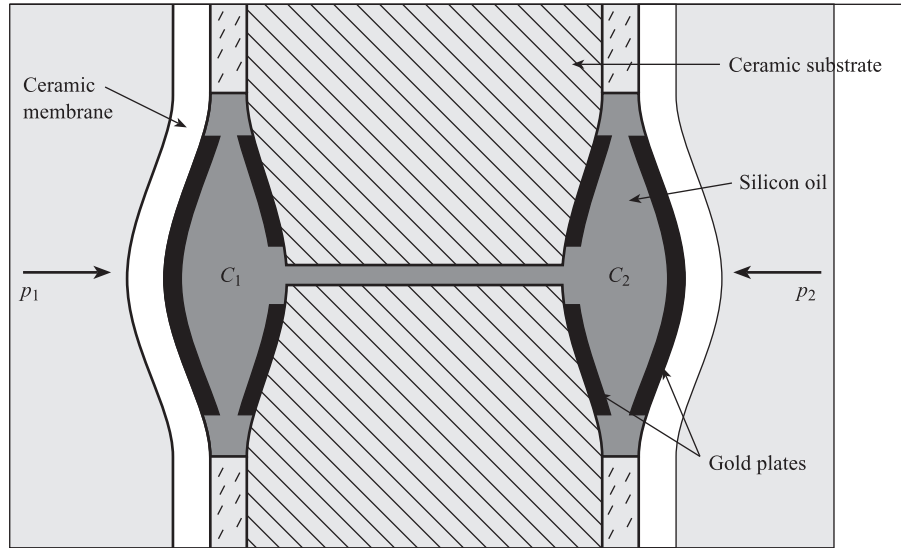
The final sensor shown in Figure 8.9 is a **thin-film capacitive humidity sensor**.^[8] The dielectric is a polymer which has the ability to absorb water molecules; the resulting change in dielectric constant and therefore capacitance is proportional to the percentage relative humidity of the surrounding atmosphere. One capacitor plate consists of a layer of tantalum deposited on a glass substrate; the layer of polymer dielectric is then added, followed by the second plate, which is a thin layer of chromium. The chromium layer is under high tensile stress so that it cracks into a fine mosaic which allows water molecules to pass into the dielectric. The stress in the chromium also causes the polymer to crack into a mosaic structure. A sensor of this type has a input range of 0 to 100% RH, a capacitance of 375 pF at 0% RH and a linear sensitivity of 1.7 pF/% RH. The capacitance–humidity relation is therefore the linear equation:

$$C = 375 + 1.7 \text{ RH pF}$$

The maximum departure from this line is 2% due to non-linearity and 1% due to hysteresis.

The basic capacitive pressure sensor shown in Figure 8.9 has some limitations. It consists of two circular metal plates or diaphragms, one flexible, one rigid, with air as dielectric. Because the dielectric constant ϵ for air is only 1, changes in capacitance ΔC caused by the applied pressure P will be very small. To increase ΔC , the thickness t of the flexible plate/diaphragm can be reduced; this gives greater deformation y for a given pressure P but reduces mechanical strength. Also many metals have limited resistance to corrosion. These problems can be largely overcome by using **liquid-filled ceramic membrane** sensors. Dielectric liquids such as silicon oil have a much higher ϵ than air, so that significant capacitance changes ΔC can be obtained with small membrane displacements of the order of $10 \mu\text{m}$. These small displacements, together with lower Young's modulus for ceramics than metals, mean that ceramic membranes can be made much thicker than metal diaphragms – between 0.25 and 1.5 mm is typical. This gives greater mechanical strength and ease

Figure 8.10 Ceramic liquid-filled differential pressure sensor (after Endress and Hauser Ltd.).



of maintenance; furthermore, ceramics such as aluminium oxide have excellent resistance to corrosion.

Figure 8.10 shows a **differential pressure** sensor using this technology. Process fluid at pressure p_1 in the left-hand chamber and at pressure p_2 in the right-hand chamber is in contact with the ceramic membrane. The membrane is supported on a ceramic substrate. Two capacitances C_1 and C_2 are formed using gold plates and silicon oil as dielectric. An increase in differential pressure $p_1 - p_2$ causes the left-hand membrane to move to the right, causing C_1 to increase by ΔC . The pressure change is transmitted through the fluid to the right, causing the right-hand membrane to move to the right and C_2 to decrease by ΔC . C_1 and C_2 are then incorporated in an a.c. bridge circuit (Sections 9.1.3 and 9.4.2).

Capacitive sensing elements are incorporated in either a.c. deflection bridge circuits (Section 9.1) or oscillator circuits (Section 9.5.1). Capacitive sensors are not pure capacitances but have an associated resistance R in parallel, to represent losses in the dielectric; this has an important influence on the design of circuits, particularly oscillator circuits. For example, a typical capacitive humidity sensor would have an approximate parallel dielectric loss resistance R of 100 k Ω at 100 kHz. The quality of a dielectric is often expressed in terms of its 'loss tangent' $\tan \delta$ where:

$$\tan \delta = \frac{1}{\omega CR}$$

In this example, if $C = 500$ pF then $\tan \delta \approx 0.03$. Figure 9.25(b) shows the capacitive sensor incorporated with a pure inductance into an oscillator circuit. The 'quality factor' Q of the circuit is given by

$$Q = R \sqrt{\frac{C}{L}} = \omega_n CR$$

and thus depends crucially on R . If the natural frequency f_n of the circuit with the above humidity sensor is $f_n = 10^5$ Hz, then the circuit Q factor is approximately 30.

Precautions should also be taken to minimise the effect of cable and stray capacitances on these circuits.

8.3 Inductive sensing elements

8.3.1 Variable inductance (variable reluctance) displacement sensors

In order to discuss the principles of these elements we must first introduce the concept of a **magnetic circuit**. In an electrical circuit an electromotive force (e.m.f.) drives a current through an electrical resistance and the magnitude of the current is given by

$$\text{e.m.f.} = \text{current} \times \text{resistance} \quad [8.25]$$

A simple magnetic circuit is shown in Figure 8.11(a): it consists of a loop or core of ferromagnetic material on which is wound a coil of n turns carrying a current i . By analogy we can regard the coil as a source of magnetomotive force (m.m.f.) which drives a flux ϕ through the magnetic circuit. The equation corresponding to [8.25] for a magnetic circuit is:

$$\text{m.m.f.} = \text{flux} \times \text{reluctance} = \phi \times \mathcal{R} \quad [8.26]$$

so that reluctance \mathcal{R} limits the flux in a magnetic circuit just as resistance limits the current in an electrical circuit. In this example m.m.f. = ni , so that the flux in the magnetic circuit is:

$$\phi = \frac{ni}{\mathcal{R}} \text{ weber} \quad [8.27]$$

This is the flux linked by a single turn of the coil; the total flux N linked by the entire coil of n turns is:

$$N = n\phi = \frac{n^2 i}{\mathcal{R}} \quad [8.28]$$

By definition the self-inductance L of the coil is the total flux per unit current, i.e.

*Self-inductance
of a coil*

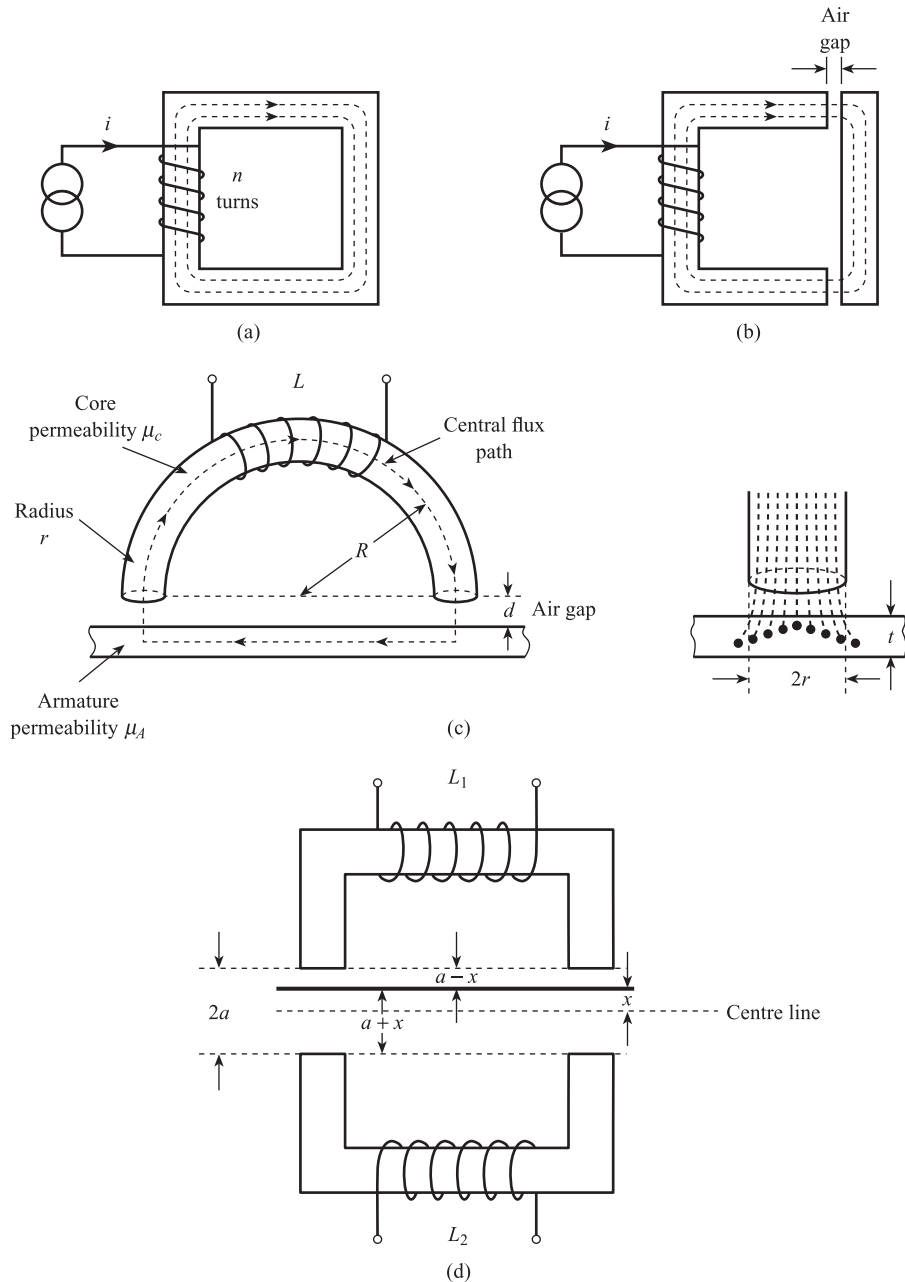
$$L = \frac{N}{i} = \frac{n^2}{\mathcal{R}} \quad [8.29]$$

The above equation enables us to calculate the inductance of a sensing element given the reluctance of the magnetic circuit. The reluctance \mathcal{R} of a magnetic circuit is given by:

$$\mathcal{R} = \frac{l}{\mu\mu_0 A} \quad [8.30]$$

where l is the total length of the flux path, μ is the relative permeability of the circuit material, μ_0 is the permeability of free space = $4\pi \times 10^{-7} \text{ H m}^{-1}$ and A is the

Figure 8.11 Variable reluctance elements:
 (a)(b) Basic principle of reluctance sensing elements
 (c) Reluctance calculation for typical element
 (d) Differential or push/pull reluctance displacement sensor.



cross-sectional area of the flux path. Figure 8.11(b) shows the core separated into two parts by an air gap of variable width. The total reluctance of the circuit is now the reluctance of both parts of the core together with the reluctance of the air gap. Since the relative permeability of air is close to unity and that of the core material many thousands, the presence of the air gap causes a large increase in circuit reluctance and a corresponding decrease in flux and inductance. Thus a small variation in air gap causes a measurable change in inductance so that we have the basis of an **inductive displacement sensor**.

Figure 8.11(c) shows a typical variable reluctance displacement sensor, consisting of three elements: a ferromagnetic core in the shape of a semitoroid (semicircular ring), a variable air gap and a ferromagnetic plate or armature. The total reluctance of the magnetic circuit is the sum of the individual reluctances, i.e.

$$\mathcal{R}_{\text{TOTAL}} = \mathcal{R}_{\text{CORE}} + \mathcal{R}_{\text{GAP}} + \mathcal{R}_{\text{ARMATURE}} \quad [8.31]$$

The length of an average, i.e. central, path through the core is πR and the cross-sectional area is πr^2 , giving:

$$\mathcal{R}_{\text{CORE}} = \frac{\pi R}{\mu_0 \mu_C \pi r^2} = \frac{R}{\mu_0 \mu_C r^2} \quad [8.32]$$

The total length of the flux path in air is twice the air gap, i.e. $2d$; also if there is little bending or fringing of the lines of flux in the air gap, then the cross-sectional area of the flux path in air will be close to that of the core. Assuming the relative permeability of air is unity,

$$\mathcal{R}_{\text{GAP}} = \frac{2d}{\mu_0 \pi r^2} \quad [8.33]$$

The length of an average central flux path in the armature is $2R$; the calculation of the appropriate cross-sectional area is more difficult. A typical flux distribution is shown in Figure 8.11(c) and for simplicity we assume that most of the flux is concentrated within an area $2rt$, giving

$$\mathcal{R}_{\text{ARMATURE}} = \frac{2R}{\mu_0 \mu_A 2rt} = \frac{R}{\mu_0 \mu_A rt} \quad [8.34]$$

Thus

$$\mathcal{R}_{\text{TOTAL}} = \frac{R}{\mu_0 \mu_C r^2} + \frac{2d}{\mu_0 \pi r^2} + \frac{R}{\mu_0 \mu_A rt}$$

i.e.

$$\mathcal{R}_{\text{TOTAL}} = \mathcal{R}_0 + kd \quad [8.35]$$

where

$$\mathcal{R}_0 = \frac{R}{\mu_0 r} \left[\frac{1}{\mu_C r} + \frac{1}{\mu_A t} \right] = \text{reluctance at zero air gap}$$

$$k = \frac{2}{\mu_0 \pi r^2}$$

A typical element with $n = 500$ turns, $R = 2$ cm, $r = 0.5$ cm, $t = 0.5$ cm, $\mu_C = \mu_A = 100$, has $\mathcal{R}_0 = 1.3 \times 10^7 \text{ H}^{-1}$, $k = 2 \times 10^{10} \text{ H}^{-1} \text{ m}^{-1}$. This gives $L = 19$ mH at $d = 0$ (zero air gap) and $L = 7.6$ mH at $d = 1$ mm. From [8.29] and [8.35] we have

*Inductance of
reluctance
displacement sensor*

$$L = \frac{n^2}{\mathcal{R}_0 + kd} = \frac{L_0}{1 + \alpha d} \quad [8.36]$$

where $L_0 = n^2/\mathcal{R}_0$ = inductance at zero gap and $\alpha = k/\mathcal{R}_0$. Equation [8.36] is applicable to any variable reluctance displacement sensor; the values of L_0 and α depend on core geometry and permeability. We see that the relationship between L and d is non-linear, but this problem is often overcome by using the push-pull or differential displacement sensor shown in Figure 8.11(d). This consists of an armature moving between two identical cores, separated by a fixed distance $2a$. From eqn [8.36] and Figure 8.11(d) we have:

Differential reluctance displacement sensor

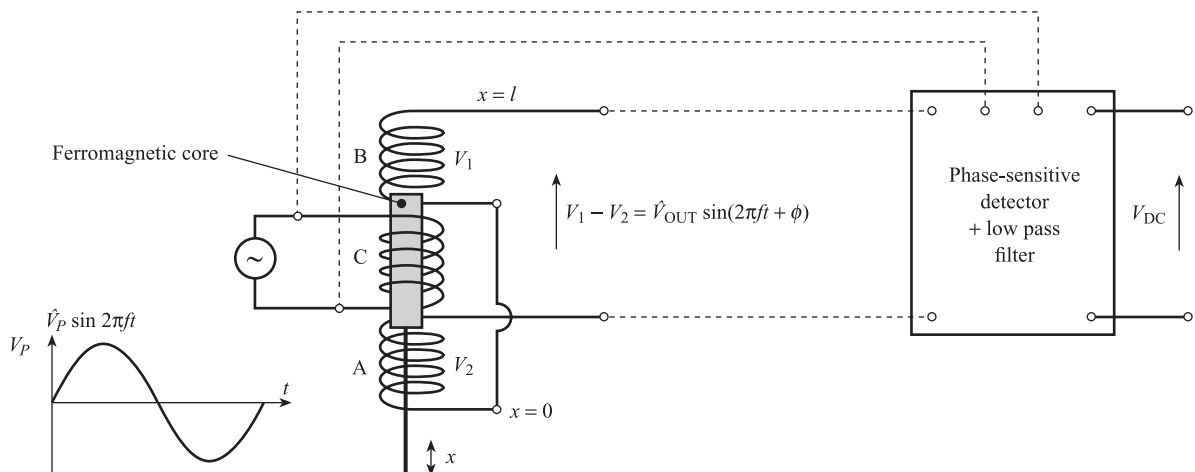
$$L_1 = \frac{L_0}{1 + \alpha(a - x)}, \quad L_2 = \frac{L_0}{1 + \alpha(a + x)} \quad [8.37]$$

The relationship between L_1 , L_2 and displacement x is still non-linear, but if the sensor is incorporated into the a.c. deflection bridge of Figure 9.5(b), then the overall relationship between bridge out of balance voltage and x is linear (eqn [9.25]). A typical sensor of this type would have an input span of 12 mm, a coil inductance (L_0) of 25 mH, a coil resistance of 70 Ω and a maximum non-linearity of 0.5%. Thus inductive sensors are not pure inductances but have an associated resistance R in series; this has an important influence on the design of oscillator circuits (Figure 9.25(a)).

8.3.2 Linear Variable Differential Transformer (LVDT) displacement sensor

This sensor is a transformer with a single primary winding and two identical secondary windings wound on a tubular ferromagnetic former (Figure 8.12). The primary winding is energised by an a.c. voltage of amplitude \hat{V}_p and frequency f Hz; the two secondaries are connected in series opposition so that the output voltage $\hat{V}_{OUT} \sin(2\pi ft + \phi)$ is the difference ($V_1 - V_2$) of the voltages induced in the secondaries. A ferromagnetic core or plunger moves inside the former; this alters the mutual inductance between the primary and secondaries. With the core removed the secondary voltages are ideally equal so that $\hat{V}_{OUT} = 0$. With the core in the former, V_1 and V_2 change with core position x , causing amplitude \hat{V}_{OUT} and phase ϕ to change.

Figure 8.12 LVDT and connections to phase-sensitive detector.



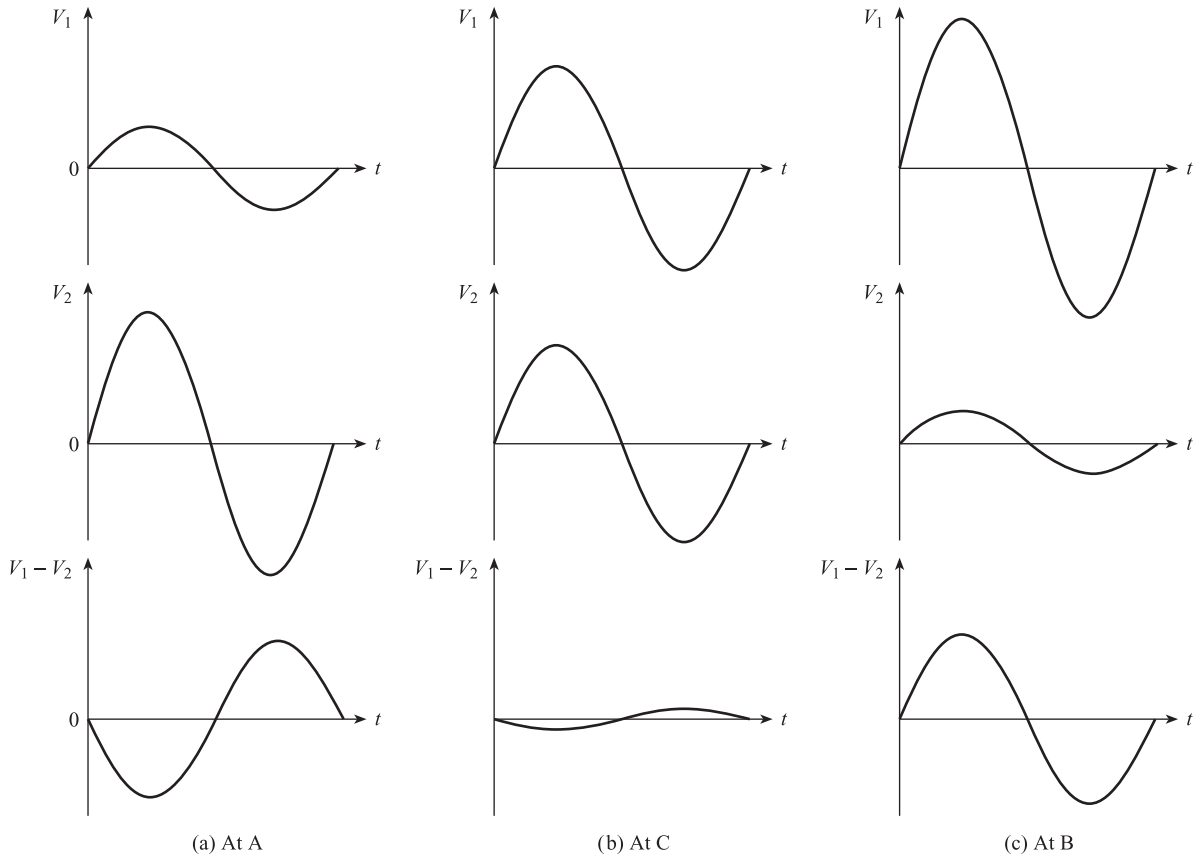
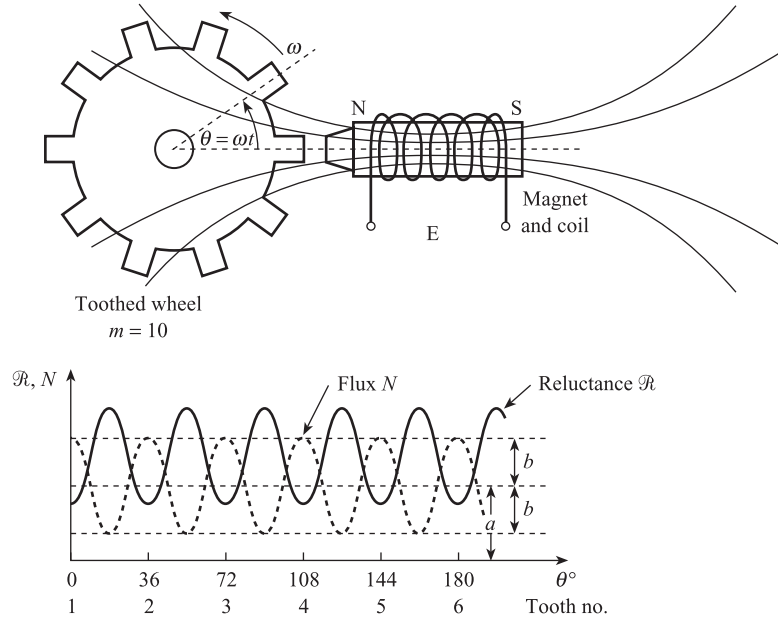


Figure 8.13 LVDT secondary waveforms.

Figure 8.13 shows a.c. waveforms for secondary voltages V_1 , V_2 and the difference $V_1 - V_2$ at three positions A, C and B. C is the halfway point at $x = \frac{1}{2}l$ and A and B are equidistant from C. Figure 8.13(a) shows the waveforms at A; here the lower secondary is strongly coupled to the primary and the upper secondary is weakly coupled to the primary; V_2 has therefore greater amplitude than V_1 and $V_1 - V_2$ is 180° out of phase with the primary voltage V_p . Figure 8.13(b) shows the waveforms at C; here the secondaries are equally coupled to the primary and V_1 and V_2 have approximately equal amplitudes; $V_1 - V_2$ has therefore minimum amplitude (ideally zero) and C is termed the **null point**. Figure 8.13(c) shows the waveforms at B; here the upper secondary is strongly coupled to the primary and the lower secondary is weakly coupled to the primary; V_1 has greater amplitude than V_2 and $V_1 - V_2$ is in phase with the primary voltage. Therefore $V_1 - V_2$ has the **same amplitude** at positions A and B but there is a **phase difference of 180°** .

The a.c. voltage $V_1 - V_2$ is converted to d.c. in a way which distinguishes between positions such as A and B either side of the null point C. This is done using a **phase sensitive detector or demodulator** (Section 9.3). This senses the 180° phase difference and gives a negative d.c. voltage at A and a positive d.c. voltage of equal magnitude at B. Figure 8.14 shows how the amplitude \hat{V}_{OUT} and phase ϕ of the a.c. output and the d.c. voltage V_{DC} vary with displacement x . The relationship between V_{DC} and x is linear over the central portion of the range 0 to l , but non-linear effects

Figure 8.15 Variable reluctance tachogenerator, angular variations in reluctance and flux.



piece but falls again as the next tooth approaches the pole piece. Figure 8.15 shows the resulting cyclic variation in reluctance \mathcal{R} with angular rotation θ . From eqn [8.26] the flux in the circuit is given by $\phi = \text{m.m.f.}/\mathcal{R}$, and the total flux N linked by a coil of n turns is:

$$N = n\phi = \frac{n \times \text{m.m.f.}}{\mathcal{R}} \quad [8.39]$$

so that $N \propto 1/\mathcal{R}$. The corresponding variation of flux N with θ is also shown in Figure 8.15. We see that a reluctance minimum corresponds to a flux maximum and vice versa. This relation may be approximated by

$$N(\theta) \approx a + b \cos m\theta \quad [8.40]$$

where a is the mean flux, b is the amplitude of the flux variation and m is the number of teeth. Using eqn [8.38] the induced e.m.f. is given by:

$$E = -\frac{dN}{dt} = -\frac{dN}{d\theta} \times \frac{d\theta}{dt} \quad [8.41]$$

where

$$\frac{dN}{d\theta} = -bm \sin m\theta$$

$$\frac{d\theta}{dt} = \omega_r \text{ (angular velocity of wheel)}$$

and

$$\theta = \omega_r t \text{ (assuming } \theta = 0 \text{ at } t = 0)$$

Thus

*Output signal for
variable reluctance
tachogenerator*

$$E = b m \omega_r \sin m \omega_r t \quad [8.42]$$

This is a sinusoidal signal of amplitude $\hat{E} = b m \omega_r$ and frequency $f = m \omega_r / (2\pi)$; i.e. both amplitude and frequency are proportional to the angular velocity of the wheel.

In principle ω_r can be found from either the amplitude or the frequency of the signal. In practice the amplitude measured by a distant recorder or indicator may be affected by loading effects (Section 5.1) and electrical interference (Section 6.3). A frequency system is therefore preferred (Chapter 10), where the number of cycles in a given time is counted to give a digital signal corresponding to the angular velocity. A variable reluctance tachogenerator is incorporated in the turbine flowmeter (Section 12.2) to give an accurate measurement of volume flow rate or total volume of fluid.

8.5

Thermoelectric sensing elements

Thermoelectric or thermocouple sensing elements are commonly used for measuring temperature. If two different metals A and B are joined together, there is a difference in electrical potential across the junction called the **junction potential**. This junction potential depends on the metals A and B and the temperature T °C of the junction, and is given by a power series of the form:

$$E_T^{AB} = a_1 T + a_2 T^2 + a_3 T^3 + a_4 T^4 + \dots \quad [8.43]$$

The values of constants a_1, a_2 , etc., depend on the metals A and B . For example, the first four terms in the power series for the e.m.f. of an iron v. constantan (Type J) junction are as follows,^[9] expressed in μV :

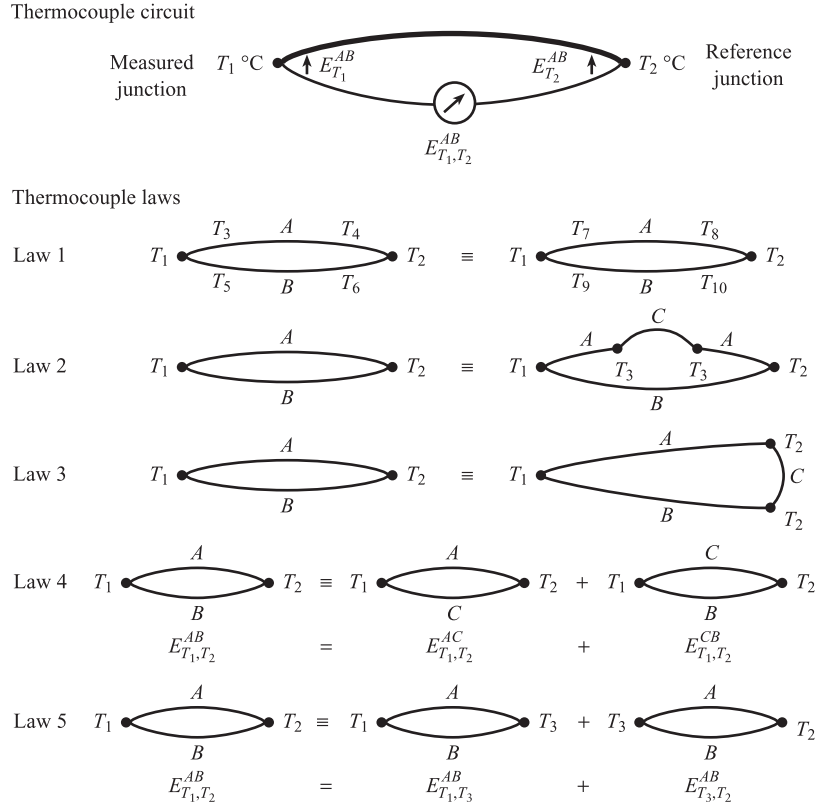
$$E_T^J = 5.037 \times 10^{-1} T + 3.043 \times 10^{-2} T^2 - 8.567 \times 10^{-5} T^3 + 1.335 \times 10^{-7} T^4 + \text{higher-order terms up to } T^7 \quad [8.44]$$

A thermocouple is a closed circuit consisting of two junctions (Figure 8.16), at different temperatures T_1 and T_2 °C. If a high-impedance voltmeter is introduced into the circuit, so that current flow is negligible, then the measured e.m.f. is, to a close approximation, the difference of the junction potentials, i.e.

$$\begin{aligned} E_{T_1, T_2}^{AB} &= E_{T_1}^{AB} - E_{T_2}^{AB} \\ &= a_1(T_1 - T_2) + a_2(T_1^2 - T_2^2) + a_3(T_1^3 - T_2^3) + \dots \end{aligned} \quad [8.45]$$

Thus the measured e.m.f. depends on the temperatures T_1, T_2 of both junctions. In the following discussion T_1 will be the temperature to be measured, i.e. the temperature of the measurement junction, and T_2 will be the temperature of the reference

Figure 8.16
Thermocouple principles.



junction. In order to accurately infer T_1 from the measured e.m.f., the reference junction temperature T_2 must be known.

Figure 8.16 summarises five ‘laws’ of thermocouple behaviour which are vital in temperature measurement.^[10] Law 1 states that the e.m.f. of a given thermocouple depends only on the temperatures of the junctions and is independent of the temperatures of the wires connecting the junctions. This is important in industrial installations, where the leads connecting measurement and reference junctions may be exposed to large changes in ambient temperature.

Law 2 states that if a third metal C is introduced into A (or B) then, provided the two new junctions are at the same temperature (T_3), the e.m.f. is unchanged. This means that a voltmeter can be introduced into the circuit without affecting the voltage produced.

If a third metal C is inserted between A and B at either junction, then Law 3 states that, provided the two new junctions AC and CB are both at the same temperature (T_1 or T_2), then the e.m.f. is unchanged. This means that at the measurement junction, wires A and B can be soldered or brazed together with a third metal without affecting the e.m.f. A voltage measuring device can be introduced at the reference junction again without affecting the measurement.

Law 4 (**law of intermediate metals**) can be used, for example, to deduce the e.m.f. of a copper–iron (AB) thermocouple, given the e.m.f. values for copper–constantan (AC) and constantan–iron (CB) thermocouples.

The fifth law (**law of intermediate temperatures**) is used in interpreting e.m.f. measurements. For a given pair of metals we have:

Law of intermediate temperatures

$$E_{T_1, T_2} = E_{T_1, T_3} + E_{T_3, T_2} \quad [8.46]$$

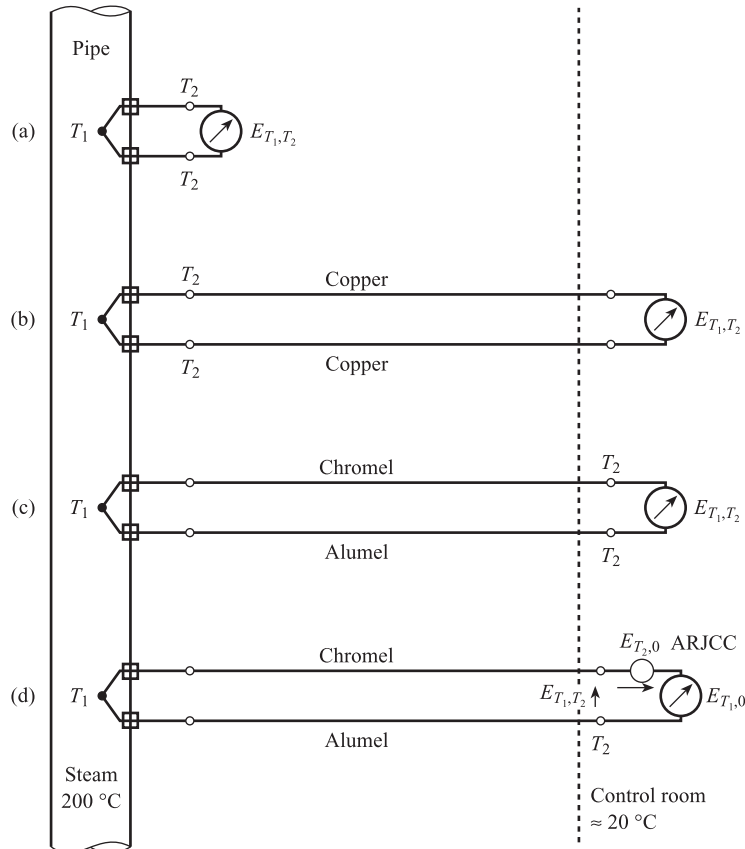
where T_3 is the intermediate temperature. If $T_2 = 0^\circ\text{C}$, then

$$E_{T_1, 0} = E_{T_1, T_3} + E_{T_3, 0} \quad [8.47]$$

Suppose that we wish to measure the temperature $T_1^\circ\text{C}$ of a liquid inside a vessel with a chromel v. alumel thermocouple. The measurement junction is inserted in the vessel and the reference junction is outside the vessel, where the temperature is measured to be 20°C , i.e. $T_3 = 20^\circ\text{C}$. The measured e.m.f. is 5.3 mV using a voltmeter inserted at the reference junction, i.e. $E_{T_1, T_3} = E_{T_1, 20} = 5.3$ mV. The value of $E_{T_3, 0} = E_{20, 0}$ is found to be 0.8 mV using thermocouple tables.^[9] These tables give the e.m.f. $E_{T, 0}$ for a particular thermocouple, with measured junction at $T^\circ\text{C}$ and reference junction at 0°C . From eqn [8.47], we have $E_{T_1, 0} = 5.3 + 0.8 = 6.1$ mV; T_1 is then found to be 149°C by looking up the temperature corresponding to 6.1 mV.

The importance of correct installation of thermocouples can be illustrated by the problem shown in Figure 8.17. Here we wish to measure the temperature of high-pressure steam in a pipe, at around 200°C , with a chromel v. alumel thermocouple, for which $E_{200, 0} = 8.1$ mV.

Figure 8.17
Thermocouple
installations.



Installation (a) with the meter located just outside the pipe is completely useless. The reference junction temperature T_2 can vary widely from sub-zero temperatures in cold weather to possibly $+50^\circ\text{C}$ if a steam leak occurs; the measured e.m.f. is therefore meaningless. Installation (b) with the meter located in the control room and connected to the thermocouple with copper leads is equally useless – the reference junction is still located outside the pipe.

In installation (c), the thermocouple is extended to the control room using extension or compensation leads made of chromel and alumel. This is an improvement because the reference junction is now in the control room where the variation in ambient temperature is smaller, possibly 10°C at most. However, this is still not satisfactory for most applications, and one obvious solution is to place the reference in a temperature-controlled environment, e.g. a refrigerator at 0°C .

An alternative solution which utilises the law of intermediate temperatures is shown in installation (d). The thermocouple e.m.f. is E_{T_1, T_2} for a measured junction temperature of $T_1^\circ\text{C}$ and a reference junction temperature of $T_2^\circ\text{C}$ (T_2 around 20°C). If we introduce a second source of e.m.f. of magnitude $E_{T_2, 0}$ into the circuit in series with E_{T_1, T_2} , then the voltmeter measures $E_{T_1, T_2} + E_{T_2, 0}$ which is equal to $E_{T_1, 0}$. Thus the voltmeter measures an e.m.f. relative to an apparent fixed reference temperature of 0°C , even though the actual reference temperature is varying about a mean of 20°C .

The e.m.f. source producing $E_{T_2, 0}$ is known as an **automatic reference junction compensation circuit** (ARJCC). From eqn [8.45] we have:

$$E_{T_2, 0} = a_1 T_2 + a_2 T_2^2 + a_3 T_2^3 + \dots \quad [8.48]$$

but since T_2 is small, we can approximate by $E_{T_2, 0} \approx a_1 T_2$. Thus we require a circuit giving a millivolt output signal proportional to reference temperature T_2 . This can be obtained with a metal resistance temperature sensor incorporated into a deflection bridge circuit, with a large value of R_3/R_2 (Section 9.1). The output voltage of the bridge must be equal to $E_{T_2, 0}$, so that using eqn [9.15] we require:

$$E_{T_2, 0} = a_1 T_2 = V_S \frac{R_2}{R_3} \alpha T_2$$

i.e.

*Automatic reference
junction compensation
bridge*

$$V_S \frac{R_2}{R_3} = \frac{a_1}{\alpha} \quad [8.49]$$

Thus any change in T_2 which causes the thermocouple e.m.f. to alter is sensed by the metal resistive sensor, producing a compensating change in bridge output voltage. The thermocouple signal $E_{T_1, 0}$ is at a low level, typically a few millivolts, and often requires amplification prior to processing and presentation. The open-loop temperature transmitter described in Section 9.4.2 is often used to convert a thermocouple e.m.f. to a current signal in a standard range, e.g. 4 to 20 mA.

In order to find an accurate estimate of T_1 from $E_{T_1, 0}$ an **inverse** equation of the form

$$T_1 = a'_1 E_{T_1, 0} + a'_2 E_{T_1, 0}^2 + a'_3 E_{T_1, 0}^3 + a'_4 E_{T_1, 0}^4 + \dots \quad [8.50]$$

should be solved using a microcontroller (Section 3.3 and Chapter 10).

Table 8.2 Thermocouple data and characteristics.

Type	Temperature ranges (°C)	e.m.f. values (μV) ^a	Tolerances	Extension leads	Characteristics
Iron v. constantan Type J	–20 to +700	$E_{100,0} = 5\,269$ $E_{200,0} = 10\,779$ $E_{300,0} = 16\,327$ $E_{500,0} = 27\,393$	Class 1 –40 °C to +375 °C ± 1.5 °C	As for thermocouple	Reducing atmospheres have little effect. Should be protected from moisture, oxygen and sulphur-bearing gases
Copper v. constantan Type T	–185 to +400	$E_{-100,0} = -3\,379$ $E_{+100,0} = 4\,279$ $E_{200,0} = 9\,288$ $E_{400,0} = 20\,872$	Class 1 –40 °C to +125 °C ± 0.5 °C	As for thermocouple	Recommended for low and sub-zero temperatures. Resists oxidising and reducing atmospheres up to approximately 350 °C. Requires protection from acid fumes
Nickel–chromium v. nickel–aluminium Chromel v. alumel Type K	0 to +1100	$E_{100,0} = 4\,096$ $E_{250,0} = 10\,153$ $E_{500,0} = 20\,644$ $E_{1000,0} = 41\,276$	Class 1 –40 °C to +375 °C ± 1.5 °C	As for thermocouple	Recommended for oxidising and neutral conditions. Rapidly contaminated in sulphurous atmospheres. Not suitable for reducing atmospheres
Platinum v. platinum–13% rhodium Type R	0 to +1600	$E_{300,0} = 2\,401$ $E_{600,0} = 5\,583$ $E_{900,0} = 9\,205$ $E_{1200,0} = 13\,228$	Class 1 0 to 1100 °C ± 1.0 °C	Copper Copper–nickel	High resistance to oxidation and corrosion. Particularly susceptible to many metal vapours, therefore important that non-metal sheaths are used

^a e.m.f. values are after International Standard IEC 584.1: 1995^[9].

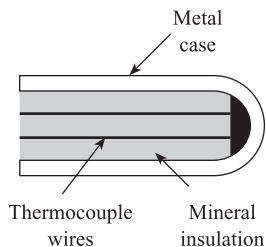
**Figure 8.18** Mineral insulated thermocouple.

Table 8.2 summarises the measurement range, e.m.f. values, tolerances and characteristics of four thermocouples in common industrial use. The table can be used to quantify non-linearity: for example, a copper v. constantan thermocouple, used between 0 and +400 °C, has an e.m.f. of 9288 μV at 200 °C compared with an ideal straight line value of 10 436 μV . Thus the non-linearity at 200 °C is –1 148 μV or –5.5% of f.s.d. Typical tolerances are of the order of $\pm 1\%$, i.e. about 10 times greater than for platinum resistance thermometers. For base metal thermocouples (types J, T and K), the extension or compensation leads are made of the same metals as the thermocouple itself. For rare metal thermocouples (e.g. type R), the metals in the extension leads are copper and copper–nickel, which have similar thermoelectric properties to platinum and platinum–rhodium but are far cheaper. In order to give mechanical and chemical protection, the thermocouple is often enclosed in a thermowell or sheath (Figure 14.1). An alternative is the mineral insulated thermocouple (Figure 8.18). This is a complete package, where the space between the thermocouple wires and metal case is filled with material which is both a good heat conductor and an electrical insulator. The dynamic characteristics of both types of installation are discussed in Section 14.3.

8.6

Elastic sensing elements

If a force is applied to a spring, then the amount of extension or compression of the spring is approximately proportional to the applied force. This is the principle of elastic sensing elements which convert an input force into an output displacement. Elastic elements are also commonly used for measuring torque, pressure and acceleration, which are related to force by the equations:

$$\text{torque} = \text{force} \times \text{distance}$$

$$\text{pressure} = \frac{\text{force}}{\text{area}} \quad [8.51]$$

$$\text{acceleration} = \frac{\text{force}}{\text{mass}}$$

In a measurement system an elastic element will be followed by a suitable secondary displacement sensor, e.g. potentiometer, strain gauge or LVDT, which converts displacement into an electrical signal. The displacement may be translational or rotational.

Elastic sensing elements have associated mass (inertance) and damping (resistance) as well as spring characteristics. In Section 4.1.2 the dynamics of a mass–spring–damper force sensor were analysed, and shown to be represented by the second-order transfer function:

$$G(s) = \frac{1}{\frac{1}{\omega_n^2} s^2 + \frac{2\xi}{\omega_n} s + 1}$$

Figure 8.19 shows dynamic models of elastic elements for measuring linear acceleration, torque, pressure and angular acceleration. The dynamics of all four elements are represented by second-order differential equations and transfer functions. The figure gives the values of steady-state gain K , natural frequency ω_n and damping ratio ξ for each type of sensor. The differential equation for a torque sensor is an analogue of eqn [4.14] for a force sensor; the torque equation involves rotational motion whereas the force equation involves translational motion. Here an input torque T is opposed by the spring torque $c\theta$ and damping torque $b\dot{\theta}$; the resultant unbalanced torque is equal to the product of moment of inertia I and angular acceleration $\ddot{\theta}$. In the pressure sensor, the input pressure P produces a force AP over the area A of the bellows which is opposed by the bellows spring force kx and damping force $\lambda\dot{x}$.

The conceptual model of an accelerometer, shown in Figure 8.19, is a casing containing a ‘seismic’ mass which moves on frictionless guide rails against a spring. If the casing is given an acceleration a , then the mass m experiences an inertia force ma in an opposite direction. This is the same force a car driver experiences when he is thrown back against his seat as the car accelerates, or thrown forwards during sudden braking. This force is opposed by the spring force kx , where x is the displacement of the mass relative to the casing. Under steady conditions at $t = 0$ – these two forces are in equilibrium, thus:

$$ma_{0-} = kx_{0-} \quad [8.52]$$

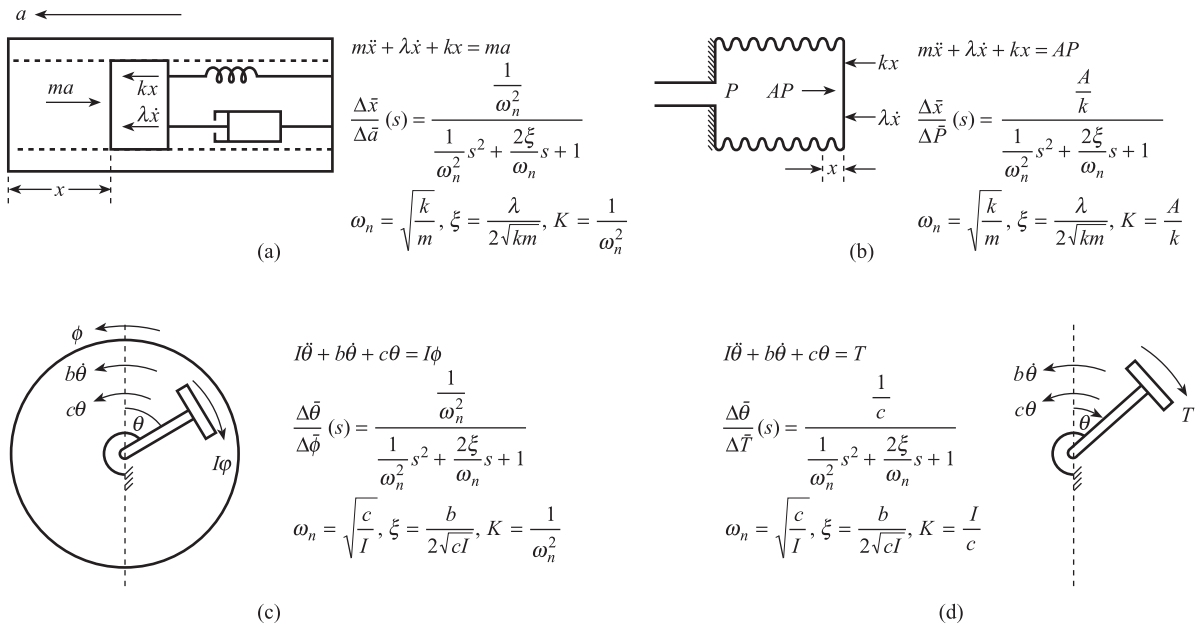


Figure 8.19 Dynamic models of elastic elements:

- (a) Linear accelerometer
 (b) Pressure sensor
 (c) Angular accelerometer
 (d) Torque sensor.

i.e. steady-state sensitivity

$$K = \frac{x_{0-}}{a_{0-}} = \frac{m}{k} = \frac{1}{\omega_n^2}$$

If the input acceleration is suddenly increased to a at time $t = 0-$, then the forces acting on the mass are no longer in equilibrium and the mass moves relative to the casing, i.e. velocity \dot{x} and acceleration \ddot{x} are non-zero. The resultant unbalanced force is $ma - kx - \lambda\dot{x}$, giving:

$$ma - kx - \lambda\dot{x} = m\ddot{x}$$

i.e.

$$m\ddot{x} + \lambda\dot{x} + kx = ma \quad [8.53]$$

where we note that the acceleration \ddot{x} of the mass relative to the casing is completely different from the acceleration a of the casing itself. By defining deviation variables Δx and Δa , we can use eqns [8.52] and [8.53] to derive the element transfer function (see Section 4.1). The differential equation for an angular acceleration sensor is the rotational analogue of [8.53]; here the inertia torque $I\phi$, due to the input acceleration ϕ , is opposed by spring torque $c\theta$ and damping torque $b\dot{\theta}$.

In Chapter 4 we saw that the optimum value of damping ratio ξ is 0.7; this ensures minimum settling time for step response and $|G(j\omega)|$ closest to unity for the frequency response. Many practical force sensors and accelerometers incorporate liquid or electromagnetic damping in order to achieve this value. However, elements such as diaphragm or bellows pressure sensors with only air damping have a very low damping ratio, typically $\xi = 0.1$ or less. In this case, the natural frequency ω_n of the sensor must be several times greater than the highest signal frequency ω_{MAX} , in order to limit the variation in $|G(j\omega)|$ to a few per cent.

Suppose we wish to measure pressure fluctuations containing frequencies up to 10 Hz, keeping the dynamic error within $\pm 2\%$, using an elastic pressure element with $\xi = 0.1$. We thus require:

$$0.98 \leq |G(j\omega)| \leq 1.02 \quad \text{for} \quad \omega \leq 62.8 \quad [8.54]$$

Since ξ is small and $\omega < \omega_n$, eqn [4.40] for $|G(j\omega)|$ can be approximated to:

$$|G(j\omega)| \approx \frac{1}{1 - \omega^2/\omega_n^2} \quad (\xi \text{ small, } \omega/\omega_n \ll 1) \quad [8.55]$$

In this situation $|G(j\omega)|$ cannot be less than unity, so that the above condition simplifies to:

$$\frac{1}{1 - \omega^2/\omega_n^2} \leq 1.02 \quad \text{for} \quad \omega \leq 62.8 \quad [8.56]$$

Thus

$$\frac{\omega}{\omega_n} \leq 0.14 \quad \text{for} \quad \omega \leq 62.8, \quad \text{i.e.} \quad \omega_n \geq 450$$

Since $\omega_n = \sqrt{k/m}$, ω_n can be increased by increasing the ratio k/m , giving a high stiffness, low mass sensor. However, increasing k reduces the steady-state sensitivity $K = A/k$ of the pressure element, so that a more sensitive secondary displacement sensor is required. The design of any elastic sensing element is therefore a compromise between the conflicting requirements of high steady-state sensitivity and high natural frequency.

Figure 8.20 shows four practical elastic sensing elements. All four elements are fairly stiff, i.e. k and ω_n are high, but steady-state sensitivity K and displacement x are small, so that strain gauges are used as secondary displacement sensors. In the cantilever force element or load cell, the applied force F causes the cantilever to bend so that the top surface experiences a tensile strain $+e$ and the bottom surface an equal compressive strain $-e$. The magnitude of strain e is given by:

$$e = \frac{6(l - x)}{wt^2E} F \quad [8.57]$$

where E is Young's modulus for the cantilever material and the other quantities are defined in Figure 8.20.

Strain gauges 1 and 3 sense a tensile strain $+e$ so that their resistance increases by ΔR . Gauges 2 and 4 sense a compressive strain $-e$ so that their resistance decreases by an equal amount. From eqn [8.14],

$$\Delta R = GR_0 e \quad [8.58]$$

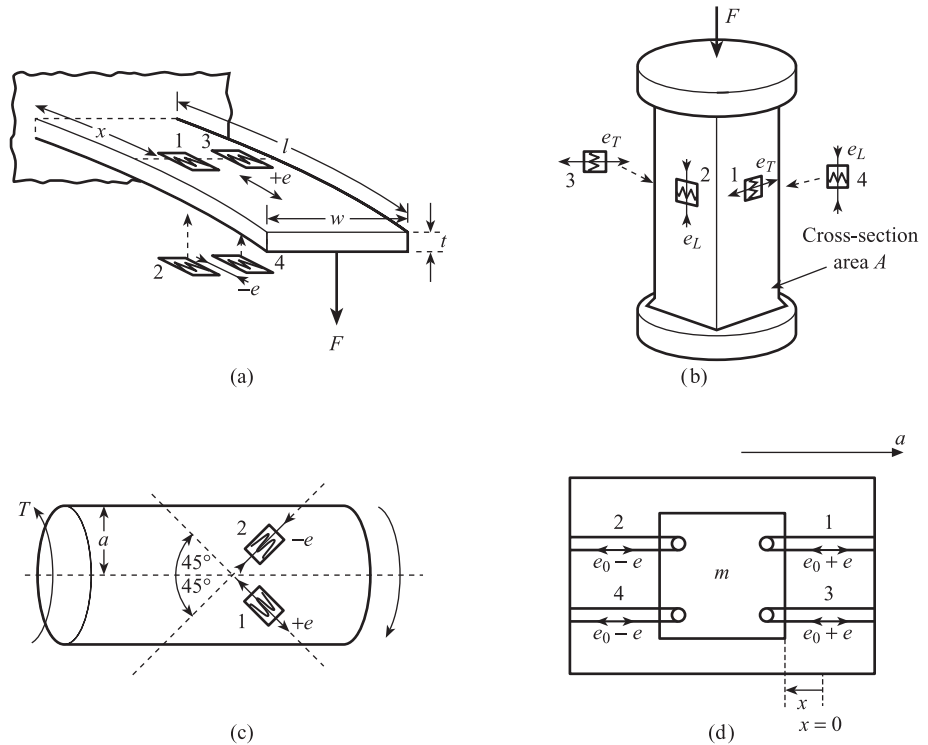
where G is the gauge factor and R_0 the unstrained resistance of the gauges. This gives:

$$\begin{aligned} R_1 &= R_3 = R_0 + \Delta R = R_0(1 + Ge) \\ R_2 &= R_4 = R_0 - \Delta R = R_0(1 - Ge) \end{aligned} \quad [8.59]$$

The four gauges are connected into a deflection bridge (see Figure 9.4(b) and eqn [9.18]).

Figure 8.20 Practical elastic sensing elements using strain gauges:

- (a) Cantilever load cell
(b) Pillar load cell
(c) Torque sensor
(d) Unbonded strain gauge accelerometer.



In the pillar load cell the applied force F causes a compressive stress $-F/A$, where A is the cross-sectional area of the pillar. This produces a longitudinal, compressive strain:

$$e_L = -\frac{F}{AE} \quad [8.60]$$

which is accompanied by a transverse, tensile strain (eqn [8.9]):

$$e_T = -\nu e_L = \frac{\nu F}{AE} \quad [8.61]$$

where E and ν are respectively Young's modulus and Poisson's ratio for the pillar material. Strain gauges are bonded onto the pillar so that gauges 1 and 3 sense e_T and gauges 2 and 4 sense e_L ; thus

$$\begin{aligned} R_1 = R_3 &= R_0 + R_0 G e_T = R_0 \left(1 + \frac{G \nu F}{AE} \right) \\ R_2 = R_4 &= R_0 + R_0 G e_L = R_0 \left(1 - \frac{G F}{AE} \right) \end{aligned} \quad [8.62]$$

The output voltage of the deflection bridge is given by eqn [9.19].

Figure 8.20(c) shows a cylindrical shaft acting as a torque sensing element. The applied torque T produces a shear strain ϕ in the shaft and corresponding linear tensile and compressive strains on the shaft surface. Gauge 1 is mounted with its active axis at $+45^\circ$ to the shaft axis, where the tensile strain has a maximum value $+e$, and

gauge 2 at -45° to the shaft axis where the compressive strain has a maximum value $-e$. Gauges 3 and 4 are mounted at similar angles on the other side of the shaft and experience strains $+e$ and $-e$ respectively. This maximum strain is given by:

$$e = \frac{T}{\pi S a^3} \quad [8.63]$$

where S is the shear modulus of the shaft material and a is the radius of the shaft. The resistances of the gauges are $R_1 = R_3 = R_0(1 + Ge)$ and $R_2 = R_4 = R_0(1 - Ge)$ and the corresponding bridge output voltage is given by eqn [9.18].

A simplified diagram of a practical accelerometer using four unbonded strain gauges is shown in Figure 8.20(d). The space between the seismic mass and casing is filled with liquid to provide damping. The unbonded strain gauges are stretched fine metal wires, which provide the spring restoring force as well as acting as secondary displacement sensors. The gauges are prestressed, so that at zero acceleration each gauge experiences a tensile strain e_0 and has a resistance $R_0(1 + Ge_0)$. If the casing is given an acceleration a , then the resultant displacement of the seismic mass m relative to the casing is (eqn [8.52]):

$$x = \frac{m}{k} a = \frac{1}{\omega_n^2} a \quad [8.64]$$

where k is the effective stiffness of the strain gauges. Gauges 1 and 3 increase in length from L to $L + x$, and gauges 2 and 4 decrease in length from L to $L - x$. The tensile strain in gauges 1 and 3 increases to $e_0 + e$, and that in gauges 2 and 4 decreases to $e_0 - e$, where:

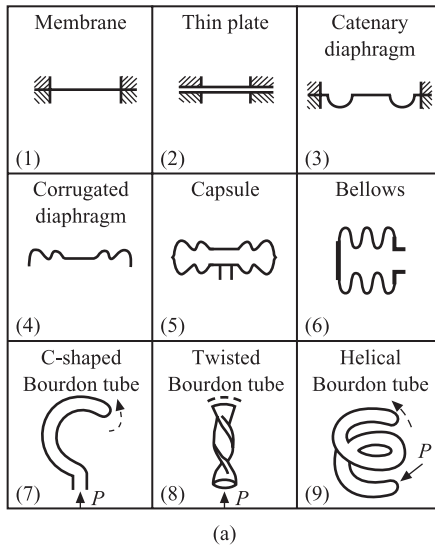
$$e = \frac{x}{L} = \frac{a}{\omega_n^2 L} \quad [8.65]$$

The four gauges are connected into a deflection bridge circuit with out of balance voltage given by eqn [9.20]. In order to ensure that all four gauges are kept in tension over the whole range of movement of the mass, the maximum acceleration induced strain is only one-half of the initial strain, i.e.

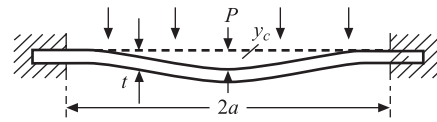
$$e_{\text{MAX}} = \frac{a_{\text{MAX}}}{\omega_n^2 L} = \frac{e_0}{2} \quad \text{or} \quad a_{\text{MAX}} = \frac{e_0 L \omega_n^2}{2} \quad [8.66]$$

Thus the acceleration input span is proportional to the square of the natural frequency. A family of accelerometers of this type, using $350 \, \Omega$ gauges, cover the ranges $\pm 5 \, g$ to $\pm 500 \, g$ with natural frequencies between 300 and 3000 Hz and a damping ratio of 0.7 ± 0.1 .^[11]

Figure 8.21(a) shows elastic pressure elements in current use. The bourdon tubes (7)–(9) are characterised by low stiffness and low natural frequency but large displacement sensitivity. A typical C-shaped tube of 50 mm bending diameter has a typical displacement travel of up to 4 mm, and is used with a potentiometer displacement sensor. C-shaped tubes have an approximately rectangular cross-section, are usually made from brass or phosphor-bronze, and cover pressure ranges from 35 kPa up to 100 MPa. The membranes, diaphragms and capsules (1)–(5) are far stiffer devices with higher natural frequency but lower displacement sensitivity. These elements are used with capacitive (Section 8.2) or strain gauge elements which are capable of sensing small displacements of 0.1 mm or less.



(a)



$$P = \frac{16 Et^3}{3a^4(1 - \nu^2)} y_c \left[1 + 0.5 \left(\frac{y_c}{t} \right)^2 \right] \quad \text{Accurate steady-state relation}$$

if $\left(\frac{y_c}{t} \right) \ll 1$ then

$$\text{Steady-state sensitivity } K = \frac{y_c}{P} \approx \frac{3a^4(1 - \nu^2)}{16Et^3} = \frac{1}{16t\gamma}$$

and

$$\text{Natural frequency } f_n = \frac{2.56}{\pi} \sqrt{\frac{Et^2}{3a^4(1 - \nu^2)\rho}} = \frac{2.56}{\pi} \sqrt{\frac{\gamma}{\rho}} \text{ Hz}$$

(b)

E = Young's modulus
 ν = Poisson's ratio
 ρ = density
 $\gamma = \frac{Et^2}{3a^4(1 - \nu^2)}$

Figure 8.21 Elastic pressure sensing elements:

(a) Different types (after Neubert^[12])
 (b) Flat circular diaphragm.

The performance equations for a flat circular diaphragm, clamped around its circumference, are summarised in Figure 8.21(b). We see that the relation between applied pressure P and centre deflection y_c is in general non-linear, but this non-linearity can be minimised by keeping the ratio y_c/t small. Thus if the non-linearity is to be limited to 1% maximum we require:

$$0.5 \left(\frac{y_c}{t} \right)^2 \leq \frac{1}{100} \quad \text{or} \quad y_c \leq 0.14t \quad [8.67]$$

The equations demonstrate that high steady-state sensitivity K and high natural frequency f_n cannot both be achieved. A higher sensitivity can be achieved by reducing the effective stiffness $\gamma = Et^2/[3a^4(1 - \nu^2)]$, but since f_n is proportional to $\sqrt{\gamma}$ this has the effect of reducing the natural frequency.

8.7 Piezoelectric sensing elements

If a force is applied to any crystal, then the crystal atoms are displaced slightly from their normal positions in the lattice. This displacement x is proportional to the applied force F : i.e., in the steady state,

$$x = \frac{1}{k} F \quad [8.68]$$

The stiffness k of the crystal is large, typically $2 \times 10^9 \text{ N m}^{-1}$. The dynamic relation between x and F can be represented by the second-order transfer function:

$$\frac{\Delta \bar{x}}{\Delta \bar{F}}(s) = \frac{1/k}{\frac{1}{\omega_n^2} s^2 + \frac{2\xi}{\omega_n} s + 1} \quad [8.69]$$

where $\omega_n = 2\pi f_n$ is large, typically $f_n = 10$ to 100 kHz, and ξ is small, typically $\xi \approx 0.01$.

In a piezoelectric crystal, this deformation of the crystal lattice results in the crystal acquiring a net charge q , proportional to x , i.e.

$$q = Kx \quad [8.70]$$

Thus from [8.68] and [8.70] we have

Direct piezoelectric effect

$$q = \frac{K}{k} F = dF \quad [8.71]$$

where $d = K/k \text{ C N}^{-1}$ is the charge sensitivity to force. Thus a piezoelectric crystal gives a direct electrical output, proportional to applied force, so that a secondary displacement sensor is not required. The piezoelectric effect is reversible; eqn [8.71] represents the direct effect where an applied force produces an electric charge. There is also an inverse effect where a voltage V applied to the crystal causes a mechanical displacement x , i.e.

Inverse piezoelectric effect

$$x = dV \quad [8.72]$$

The inverse effect is important in ultrasonic transmitters (Chapter 16). The dimensions of d in eqn [8.71], i.e. C N^{-1} , are identical with the dimensions m V^{-1} of d in eqn [8.72].

In order to measure the charge q , metal electrodes are deposited on opposite faces of the crystal to give a capacitor. The capacitance of a parallel plate capacitor formed from a rectangular block of crystal of thickness t (Figure 8.9 and eqn [8.17]) is given by:

$$C_N = \frac{\epsilon_0 \epsilon A}{t} \quad [8.73]$$

The crystal can therefore be represented as a charge generator q in parallel with a capacitance C_N , or alternatively by a Norton equivalent circuit (Section 5.1.3) consisting of a current source i_N in parallel with C_N . The magnitude of i_N is:

$$i_N = \frac{dq}{dt} = K \frac{dx}{dt} \quad [8.74]$$

or, in transfer function form:

$$\frac{\Delta \tilde{i}_N}{\Delta \tilde{x}}(s) = Ks \quad [8.75]$$

where d/dt is replaced by the Laplace operator s . We note that for a steady force F , F and x are constant with time, so that dx/dt and i_N are zero.

If the piezoelectric sensor is connected directly to a recorder (assumed to be a pure resistive load R_L) by a cable (assumed to be a pure capacitance C_C) then the complete equivalent circuit is shown in Figure 5.11. The transfer function relating recorder voltage V_L to current i_N is shown to be:

$$\frac{\Delta \bar{V}_L(s)}{\Delta \bar{i}_N(s)} = \frac{R_L}{1 + R_L(C_N + C_C)s} \quad [5.16]$$

The overall system transfer function relating recorder voltage V_L to input force F is:

$$\frac{\Delta \bar{V}_L(s)}{\Delta \bar{F}} = \frac{\Delta \bar{V}_L}{\Delta \bar{i}_N} \frac{\Delta \bar{i}_N}{\Delta \bar{x}} \frac{\Delta \bar{x}}{\Delta \bar{F}} \quad [8.76]$$

From [8.69], [8.75] and [5.16] we have:

$$\begin{aligned} \frac{\Delta \bar{V}_L(s)}{\Delta \bar{F}} &= \frac{R_L}{1 + R_L(C_N + C_C)s} Ks \frac{1/k}{\frac{1}{\omega_n^2} s^2 + \frac{2\xi}{\omega_n} s + 1} \\ &= \frac{K}{k} \frac{1}{(C_N + C_C)} \frac{R_L(C_N + C_C)s}{1 + R_L(C_N + C_C)s} \frac{1}{\frac{1}{\omega_n^2} s^2 + \frac{2\xi}{\omega_n} s + 1} \end{aligned}$$

*Transfer function for
basic piezoelectric
force measurement
system*

$$\frac{\Delta V_L(s)}{\Delta \bar{F}} = \frac{d}{(C_N + C_C)} \frac{\tau s}{(1 + \tau s)} \frac{1}{\left(\frac{1}{\omega_n^2} s^2 + \frac{2\xi}{\omega_n} s + 1 \right)} \quad [8.77]$$

where $\tau = R_L(C_N + C_C)$.

The above transfer function emphasises the two disadvantages of this basic system:

- The steady-state sensitivity is equal to $d/(C_N + C_C)$. Thus the system sensitivity depends on the cable capacitance C_C , i.e. on the length and type of cable.
- The dynamic part of the system transfer function (ignoring recorder dynamics) is:

$$G(s) = \frac{\tau s}{(\tau s + 1)} \frac{1}{\left(\frac{1}{\omega_n^2} s^2 + \frac{2\xi}{\omega_n} s + 1 \right)} \quad [8.78]$$

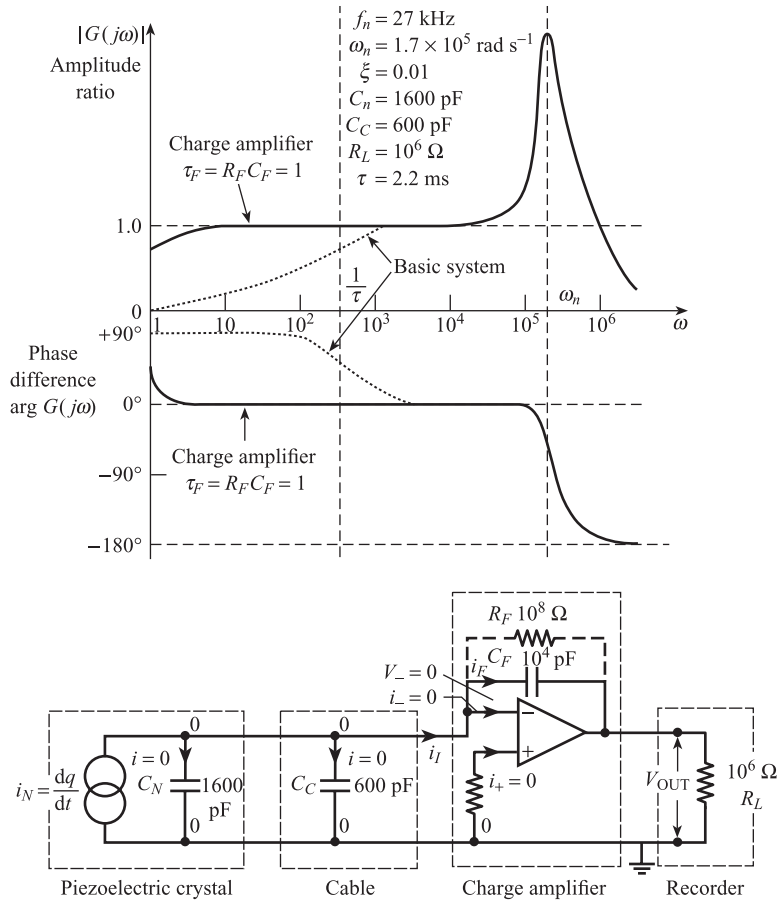
The second term is characteristic of all elastic elements and cannot be avoided; however, it causes no problems if the highest signal frequency ω_{MAX} is well below ω_n . The first term $\tau s/(\tau s + 1)$ means that the system cannot be used for measuring d.c. and slowly varying forces.

To illustrate this we can plot the frequency response characteristics $|G(j\omega)|$ and $\arg G(j\omega)$ for a typical system (Figure 8.22). Here

$$\text{Amplitude ratio } |G(j\omega)| = \frac{\tau\omega}{\sqrt{1 + \tau^2\omega^2}} \frac{1}{\sqrt{\left(1 - \frac{\omega^2}{\omega_n^2}\right)^2 + 4\xi^2 \frac{\omega^2}{\omega_n^2}}} \quad [8.79]$$

$$\text{Phase difference } \arg G(j\omega) = 90^\circ - \tan^{-1}(\omega\tau) - \tan^{-1}\left(\frac{2\xi(\omega/\omega_n)}{1 - (\omega^2/\omega_n^2)}\right)$$

Figure 8.22 Approximate frequency response characteristics and equivalent circuit for a piezoelectric measurement system.



The $\tau\omega/\sqrt{1+\tau^2\omega^2}$ term causes a low frequency roll-off so that $|G(j\omega)| = 0$ at $\omega = 0$ and the system cannot be used for frequencies much below $1/\tau$.

Using the values of Figure 5.11, i.e. $C_N = 1600 \text{ pF}$, $C_C = 600 \text{ pF}$, $R_L = 1 \text{ M}\Omega$, $\tau = 2.2 \times 10^{-3} \text{ s}$ and $1/\tau = 455 \text{ rad s}^{-1}$ or 72 Hz , we find there is a useful operating range between $3/\tau$ and $0.2\omega_n$, i.e. 216 Hz and 5.4 kHz , where $0.95 \leq |G(j\omega)| \leq 1.05$ and ϕ is close to zero. This is, however, insufficient for many applications.

These disadvantages are largely overcome by introducing a charge amplifier into the system, as shown in Figure 8.22. This is an integrator which ideally gives an output proportional to $\int i_N dt$, i.e. an output proportional to charge q , since $i_N = dq/dt$. Thus the system gives a non-zero output for a steady-force input. From Figure 8.22 we have:

$$i_1 = i_F + i_- \quad [8.80]$$

and the charge on feedback capacitor C_F is

$$q_F = C_F(V_- - V_{OUT}) \quad [8.81]$$

For an ideal operational amplifier (Section 9.2) we have $i_+ = i_- = 0$ and $V_- = V_+$. In this case we have $V_- = V_+ = 0$ and $i_F = dq_F/dt$, so that:

$$i_1 = i_F = \frac{dq_F}{dt} = -C_F \frac{dV_{OUT}}{dt} \quad [8.82]$$

Since there is zero potential drop across C_N and C_C , there is no current flow through either capacitor, so that:

$$i_1 = i_N = \frac{dq}{dt} \quad [8.83]$$

Thus from [8.82] and [8.83] we have:

Transfer characteristics of ideal charge amplifier

$$\frac{dV_{OUT}}{dt} = -\frac{1}{C_F} \frac{dq}{dt} \quad \text{i.e.} \quad V_{OUT} = -\frac{q}{C_F} \quad [8.84]$$

assuming that $V_{OUT} = 0$ when $q = 0$.

From eqns [8.84], [8.70] and [8.69], the overall transfer function for the force measurement system with a charge amplifier is:

Transfer function for piezoelectric system with ideal charge amplifier

$$\frac{\Delta \bar{V}_{OUT}}{\Delta \bar{F}}(s) = \frac{d}{C_F} \frac{1}{\left(\frac{1}{\omega_n^2} s^2 + \frac{2\xi}{\omega_n} s + 1 \right)} \quad [8.85]$$

The steady-state sensitivity is now d/C_F , i.e. it depends only on the capacitance C_F of the charge amplifier and is independent of transducer and cable capacitance. In the ideal case the $\tau_F s/(1 + \tau_F s)$ term is not present, so that $|G(j\omega)| = 1$ at $\omega = 0$. In practice a resistor R_F must be connected across feedback capacitor C_F to provide a path for d.c. current. This reintroduces a $\tau_F s/(1 + \tau_F s)$ term into the system transfer function, where $\tau_F = R_F C_F$. By making R_F and C_F large, the frequency response of the charge amplifier will extend down to well below 1 Hz. For example if $R_F = 10^8 \Omega$, $C_F = 10^4$ pF and $\tau_F = 1.0$ s, then $|G(j\omega)| = 0.95$ at $\omega = 3$ rad s^{-1} , i.e. at $f \approx 0.5$ Hz.

Table 8.3 (based on Table 16.1) shows properties of four commonly used piezoelectric materials. All figures are approximate and may depend on the direction of the applied force. Quartz occurs naturally in rocks and is piezoelectric when cut along certain directions. PZT and barium titanate are man-made ceramics possessing ferroelectric properties. If a strong electric field (typically 500–1000 kV/cm) is applied

Table 8.3 Properties of piezoelectric materials.

Material	Charge sensitivity d pC N ⁻¹	Dielectric constant ϵ	Voltage sensitivity $g \times 10^{-3}$ V m N ⁻¹	Young's modulus $E \times 10^9$ N m ⁻²	Damping ratio ξ
Quartz	2.3	4.5	50	80	2×10^{-5}
PZT	110	1200	10	80	7×10^{-3}
BaTi ₂ O ₃	78	1700	5.2	80	1×10^{-3}
PVDF	23	12	230	2	5×10^{-2}

to the crystal, at elevated temperatures (typically 80–110 °C), then the molecular dipoles remain aligned after the removal of the electric field. The material is then said to be **poled** and possesses piezoelectric and pyroelectric (Section 15.5.1) properties. Polyvinylidene fluoride (PVDF) is a long chain semi-crystalline polymer of the repeat unit $\text{CH}_2\text{--CF}_2$. After poling, this again possesses piezoelectric properties and is available in thin sheets with thickness between 10 and 1000 μm .^[13] From the table we see that the charge sensitivity d for PZT and BaTi_2O_3 is high; this is, however, offset for some applications by a high dielectric constant and therefore capacitance. This means that both ceramics have only moderate electric field sensitivity to force g . In contrast PVDF has a lower value of d but a much lower value of ϵ , giving the highest value of g of the four materials. Also PVDF has a much lower value of Young's modulus E and therefore elastic stiffness k than the other materials, giving greater displacement for the same force. The damping ratio ξ is also much greater for PVDF, giving a much flatter frequency response. The natural frequency f_n of PVDF film can vary from low MHz to GHz frequencies depending on film thickness.

Piezoelectric elements are commonly used for the measurement of acceleration and vibration. Here the piezoelectric crystal is used in conjunction with a seismic mass m . If the accelerometer casing is given an acceleration a , then there is a resulting inertia force $F = ma$ acting on the seismic mass and the piezoelectric crystal. This results in the crystal acquiring a charge $q = dF$, where $d \text{ C N}^{-1}$ is the crystal charge sensitivity to force. The resulting steady-state charge sensitivity of the piezoelectric accelerometer is:

$$\frac{\Delta q}{\Delta a} = dm \quad \text{C m}^{-1} \text{ s}^2 \quad [8.86]$$

Usually charge sensitivity is expressed in C g^{-1} , where $1 \text{ g} = 9.81 \text{ m s}^{-2}$, i.e.

$$\frac{\Delta q}{\Delta a} = 9.81dm \quad \text{C g}^{-1} \quad [8.87]$$

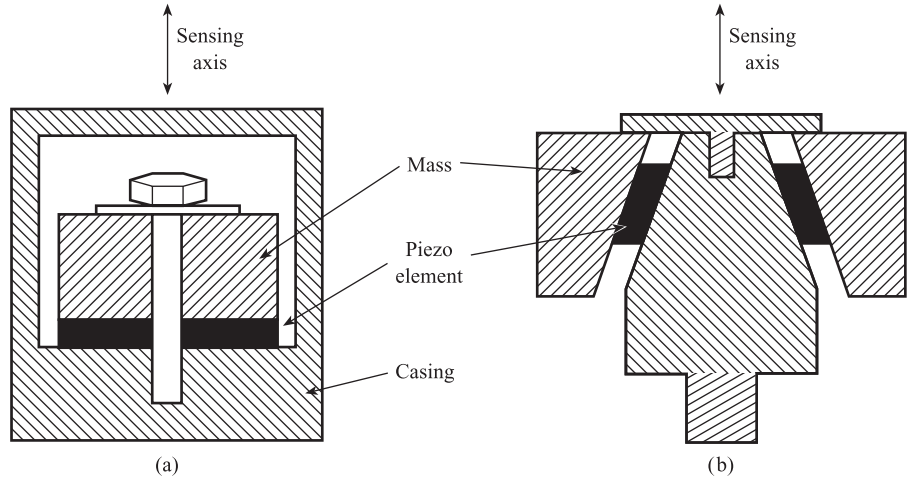
If the accelerometer is used with a charge amplifier with feedback capacitance C_F , the corresponding steady-state system voltage sensitivity is:

$$\frac{\Delta V}{\Delta a} = \frac{9.81dm}{C_F} \quad \text{V g}^{-1} \quad [8.88]$$

The dynamic and frequency response characteristics of piezoelectric accelerometers, with and without charge amplifiers, are as described earlier in this section.

Figure 8.23(a) shows a compression mode accelerometer, in which a crystal disc is sandwiched between the seismic mass and the accelerometer casing. The whole is bolted together to produce a large static pre-load compression force on the crystal. Depending on direction, the acceleration to be measured causes the compression force on the crystal to be greater or less than the static pre-load value. Figure 8.23(b) shows a shear-type accelerometer; here a piezoelectric element in the shape of a truncated conical tube is sandwiched between a tapered central pillar and the outer seismic mass.^[14] The acceleration to be measured causes corresponding shear forces in the piezoelectric element. A general purpose shear-mode accelerometer of this type has a charge sensitivity of 25 pC g^{-1} , a capacitance C_N of 1600 pF, a natural frequency f_n of 27 kHz and a weight of 18 g.

Figure 8.23 Piezoelectric accelerometers:
(a) Compression mode
(b) Shear mode
(after Purdy^[14]).



Consider a body, e.g. a part of a machine such as the casing of a pump or a compressor, which is executing sinusoidal vibrations with displacement amplitude \hat{x} at frequency f Hz, i.e.

$$\text{displacement } x = \hat{x} \sin 2\pi ft \quad \text{m} \quad [8.89]$$

$$\begin{aligned} \text{velocity } \dot{x} &= 2\pi f \hat{x} \cos 2\pi ft \quad \text{m s}^{-1} \\ &= \hat{v} \cos 2\pi ft, \text{ where } \hat{v} = 2\pi f \hat{x} \end{aligned} \quad [8.90]$$

$$\begin{aligned} \text{acceleration } \ddot{x} &= -4\pi^2 f^2 \hat{x} \sin 2\pi ft \quad \text{m s}^{-2} \\ &= -\hat{a} \sin 2\pi ft, \text{ where } \hat{a} = 4\pi^2 f^2 \hat{x} \end{aligned} \quad [8.91]$$

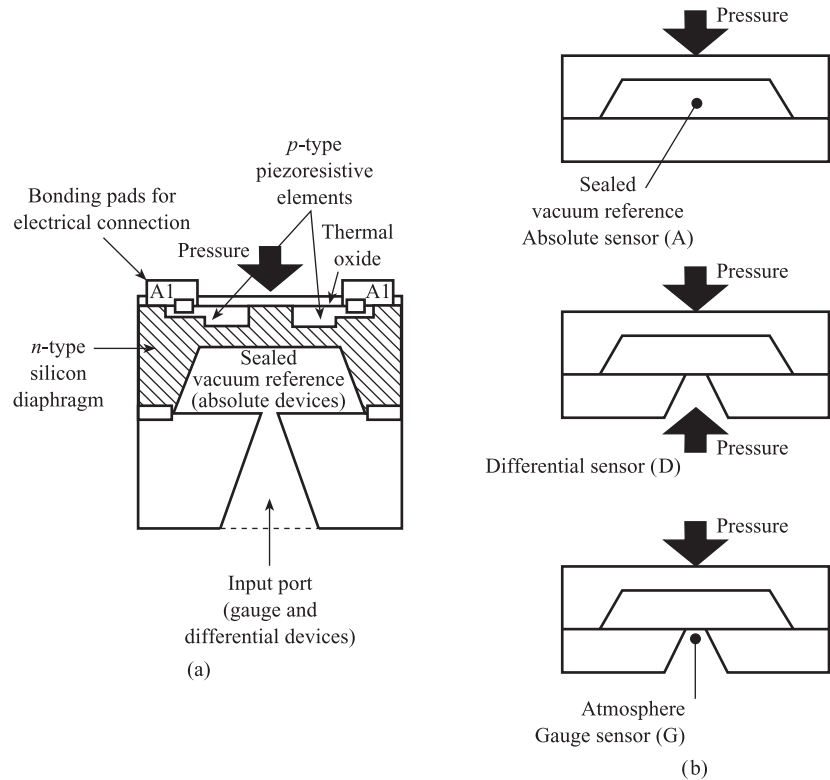
In the monitoring of machine vibration it is important to measure at least one of the amplitudes \hat{x} , \hat{v} , \hat{a} of displacement, velocity and acceleration respectively. This is especially so where the machine has certain resonant frequencies; here the above amplitudes may be large. It is possible to use a displacement transducer, differentiating the output once to obtain velocity information and twice to obtain acceleration information. However, displacement transducers often have insufficient sensitivity, inadequate frequency response or too large a mass for these applications; moreover the operation of differentiation amplifies unwanted high frequency noise. A better solution is to use a piezoelectric accelerometer, which has sufficient sensitivity, adequate frequency response and low mass; the accelerometer output can be integrated once for velocity information and twice for displacement information. The operation of integration tends to attenuate high frequency noise.

8.8

Piezoresistive sensing elements

In Section 8.1 the piezoresistive effect was defined as the change in resistivity ρ of a material with applied mechanical strain e , and is represented by the term $(1/e)(\Delta\rho/\rho)$ in the equation for gauge factor of a strain gauge. We saw that silicon doped with

Figure 8.24
Piezoresistive pressure
sensors (after Noble^[16]).



small amounts of *n*- or *p*-type material exhibits a large piezoresistive effect and is used to manufacture strain gauges with high gauge factors. The traditional way of making diaphragm pressure sensors is to cement metal foil strain gauges onto the flat surface of a metal diaphragm.

In piezoresistive pressure sensors the elastic element is a flat silicon diaphragm. The distortion of the diaphragm is sensed by four piezoresistive strain elements made by introducing doping material into areas of the silicon, where the strain is greatest.

One method of introducing the doping material is **diffusion** at high temperatures; the resulting four strain gauges are connected into a deflection bridge circuit in the normal way. A typical sensor of this type has an input range of 0 to 100 kPa, a sensitivity of around 3 mV/kPa (for a 10 V bridge supply voltage), a natural frequency of 100 kHz and combined non-linearity and hysteresis of $\pm 0.5\%$.^[15]

Figure 8.24(a) shows a piezoresistive pressure sensor where *p*-type doping material is introduced into an *n*-type silicon diaphragm using **ion implantation** technology.^[16] Four piezoresistive strain elements are thus produced (two in tension, two in compression), which are connected into a deflection bridge circuit. Figure 8.24(b) shows how the element may be used to measure absolute, differential and gauge pressures. A typical sensor of this type has an input range of 0 to 100 kPa, a sensitivity of around 1 mV/kPa (for a 12 V bridge supply voltage), a 10% to 90% rise time of 100 μ s and typical combined non-linearity and hysteresis of $\pm 0.1\%$.

8.9 Electrochemical sensing elements

8.9.1 Ion selective electrodes

Ion selective electrodes (ISEs) are sensors which directly measure the activity or concentration of ions in solution. They could, for example, be used to measure the concentration of lead, sodium or nitrate ions in drinking water. When an ISE is immersed in a solution, a reaction takes place between the charged species in the solution and those on the sensor surface. An equilibrium is then established between these species: there is a corresponding equilibrium potential difference between the sensor and solution, which depends mainly, but not entirely, on the activity of a single ion. This output signal depends also, to some extent, on the activity of other ions present in the solution; the electrodes are therefore *selective* rather than *specific*. For example, the output signal of a potassium electrode depends not only on the activity of potassium (K^+) ions in solution, but on some fraction of the sodium (Na^+) ions also present.

The Thévenin or open circuit e.m.f. of ISEs for monovalent ions is given by the modified Nernst equation:

Thévenin e.m.f. for monovalent ion ISE

$$E_{Th} = E_0 + \frac{R\theta}{F} \log_e(a_X + K_{X/Y} a_Y) \quad [8.92]$$

where E_0 = constant depending on electrode composition

R = universal gas constant (8.314 J K^{-1})

θ = absolute temperature (K)

F = Faraday number ($96\,493 \text{ C}$)

a_X = activity of ion X in solution, e.g. K^+

a_Y = activity of ion Y in solution, e.g. Na^+

$K_{X/Y}$ = selectivity coefficient of X electrode to Y ($0 < K < 1$)

The smaller the value of $K_{X/Y}$ the more selective the electrode is to X; typically $K_{K^+/Na^+} \approx 2.6 \times 10^{-3}$. The above equation is applicable to any monovalent ion, i.e. where a single electron is involved in the reaction. If n electrons are involved in the reaction then eqn [8.92] should be modified by replacing $R\theta/F$ with $R\theta/nF$.

The activity a_A of an ion A in solution depends on, but is not proportional to, the concentration C_A of that ion. The activity of an ion of particular concentration in a given solution is a function not only of its own concentration, but also of the concentration of all other ions and species. The relation between a_A and C_A is of the form:

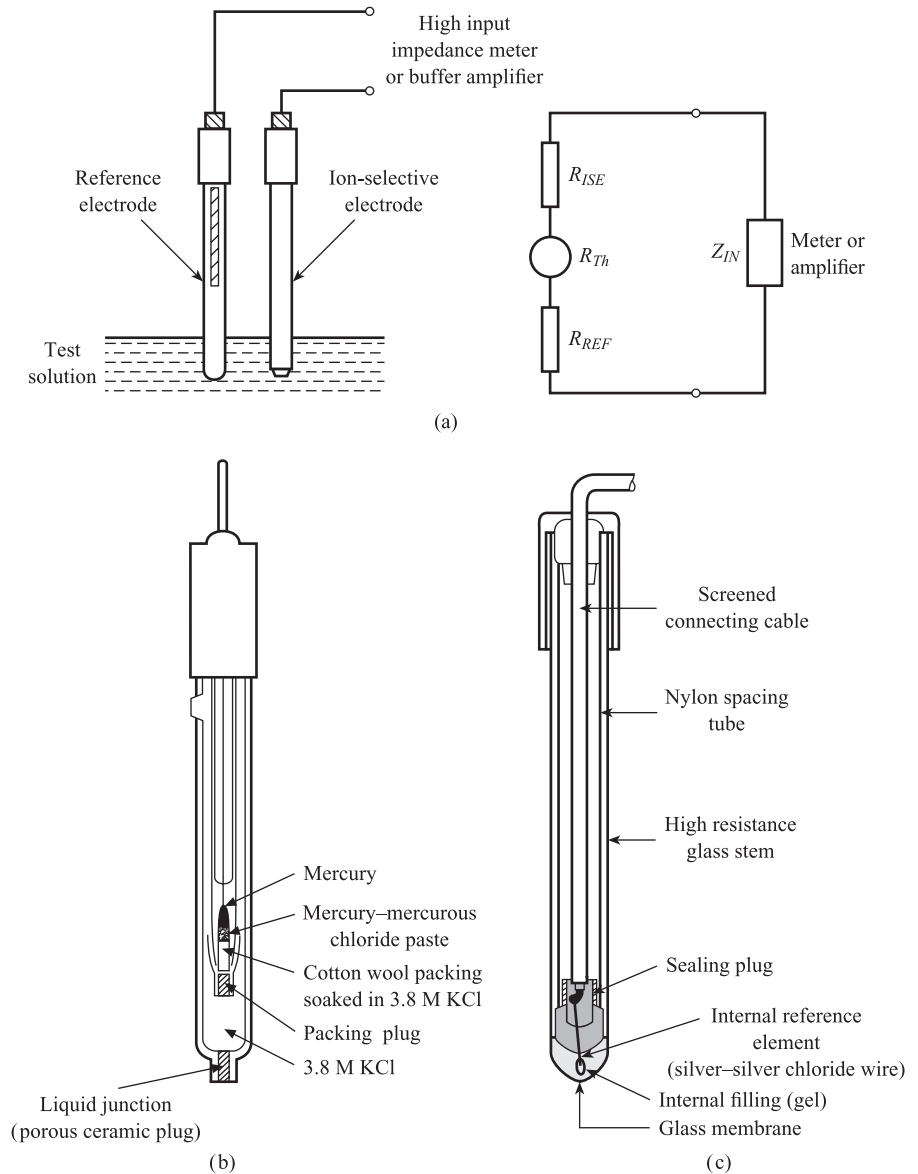
$$a_A = f_A C_A \quad [8.93]$$

where f_A is the activity coefficient for the ion A. In general $f_A < 1$ and is a non-linear function of C_A . At low concentrations ($< 10^{-4} \text{ mole litre}^{-1}$), $f_A \approx 1$ and $a_A \approx C_A$.

Figure 8.25(a) shows the basic system for measuring the activity or concentration of an ion in solution. Because an ion-selective electrode is only a single electrode and therefore only one half of a complete electrochemical cell, it must be used with a suitable standard reference electrode, immersed in the same test solution.

Figure 8.25

Ion-selective electrodes:
 (a) Basic system for ion concentration measure and equivalent circuit
 (b) Calomel reference electrode (after Bailey^[17],
 © P. L. Bailey 1980.
 Reprinted by permission
 of John Wiley &
 Sons Ltd)
 (c) Practical pH sensor
 (after Thompson^[18]).



Reference electrodes are electrochemical half-cells whose potential is held at a constant value by the chemical equilibrium maintained inside them. Figure 8.25(a) also shows the Thévenin equivalent circuit for the system; the Thévenin resistance R_{Th} is made up of the resistance of the ISE in series with the resistance of the reference electrode and can be as high as $10^9 \Omega$. This high resistance means that the potential difference E_{Th} between ion selective and reference electrodes must be measured using either a high input impedance millivoltmeter or a buffer amplifier with $Z_{IN} \approx 10^{12} \Omega$ (Section 5.1). One commonly used reference electrode is the calomel electrode shown in Figure 8.25(b).^[17] This consists of a mercury-mercurous chloride (Hg/Hg_2Cl_2)

electrode system which is in contact with a saturated solution of potassium chloride (KCl). The glass container has a porous ceramic plug; this provides a liquid junction, which allows ions to diffuse between the KCl and test solutions.

An important industrial application of ISEs is the measurement of the activity of hydrogen ions in solution. Acidity and alkalinity are quantified using pH where:

$$\text{pH} = -\log_{10} a_{\text{H}^+} = -\frac{1}{2.303} \log_e a_{\text{H}^+} \quad [8.94]$$

where a_{H^+} is the activity of the H^+ ion in solution. Hydrogen ion activity can vary from 10^0 for a strong acid, through 10^{-7} for a neutral solution (e.g. pure water), to 10^{-14} for a strong alkali. The corresponding pH values are 0, 7 and 14.

A typical pH sensor is shown in Figure 8.25(c).^[18] Here the ISE is a membrane of a specially formulated glass. A thin layer (10^{-7} m thick) of hydrated silica forms on the wetted surface of the glass. An equilibrium is set up between the activities of H^+ ions in this layer and those in the test solution; an increase in acidity causes more H^+ ions to be deposited in the layer which raise its potential relative to the bulk solution. Because the H^+ ion is the only positive ion small enough to fit into the silica lattice, the glass electrode is highly selective to H^+ and the selectivity coefficient K to other positive ions can usually be assumed to be zero. The corresponding Thévenin e.m.f. for the sensor is:

$$E_{\text{Th}} = E_0 + \frac{R\theta}{F} \log_e a_{\text{H}^+} \quad [8.95]$$

Using eqn [8.94], at $\theta = 298$ K (25 °C) we have:

$$E_{\text{Th}} = E_0 - \frac{8.314 \times 298 \times 2.303}{96\,493} \text{pH}$$

*Thévenin e.m.f.
for glass ISE*

$E_{\text{Th}} = E_0 - 0.0592 \text{ pH V}$	[8.96]
---	--------

Thus the sensor output voltage is proportional to pH with a sensitivity of -59.2 mV/pH at 25 °C. The constant E_0 depends on the construction of the glass electrode and the choice of the reference electrode; the sensor shown has an internal reference electrode consisting of a silver wire coated with silver chloride immersed in a potassium chloride/silver gel. The Thévenin resistance R_{Th} of the sensor is made up of the glass electrode resistance (100 to 300 M Ω) in series with the reference electrode resistance (10 k Ω).^[18]

Table 8.4 gives the type and concentration range of 19 ISEs in common use.^[19] Many of these are **solid-state electrodes**, where the membrane is either a single crystal or a compacted disc of a highly insoluble inorganic salt. Other ISEs use **neutral carriers** as the active material; these are non-ionic organic molecules which are incorporated into an inert matrix of PVC or silicone rubber. ISEs for sensing soluble gases such as ammonia and sulphur dioxide are also available. The gas diffuses through a **gas-permeable membrane** and then dissolves in an internal filling solution; the resulting change in the activity of a given ion in the solution (e.g. H^+) is measured using an ion selective and a reference electrode in the usual way.

Table 8.4

Ion-selective electrodes.

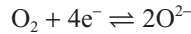
Model no.	Electrode	Type	Concentration range
ISE 301	Chloride	Solid-state	$10^0 - 5 \times 10^{-5}$ M
ISE 302	Bromide	Solid-state	$10^0 - 5 \times 10^{-6}$ M
ISE 303	Iodide	Solid-state	$10^0 - 10^{-6}$ M
ISE 304	Cyanide	Solid-state	$10^{-2} - 10^{-6}$ M
ISE 305	Sulphide	Solid-state	$10^0 - 10^{-7}$ M
ISE 306	Copper	Solid-state	$10^0 - 10^{-6}$ M
ISE 307	Lead	Solid-state	$10^{-1} - 10^{-4}$ M
ISE 308	Silver	Solid-state	$10^0 - 10^{-6}$ M
ISE 309	Cadmium	Solid-state	$10^{-1} - 10^{-5}$ M
ISE 310	Calcium	PVC membrane	$10^0 - 10^{-5}$ M
ISE 311	Nitrate	PVC membrane	$10^0 - 10^{-5}$ M
ISE 312	Barium	PVC membrane	$10^0 - 10^{-4}$ M
ISE 313	Water hardness	PVC membrane	$10^0 - 10^{-4}$ M (as $\text{Ca}^{2+} + \text{Mg}^{2+}$)
ISE 314	Potassium	PVC membrane	$10^0 - 10^{-5}$ M
ISE 315	Sodium	PVC membrane	$10^{-1} - 10^{-5}$ M
ISE 321	Ammonia	Gas-permeable membrane	$10^{-1} - 10^{-5}$ M
ISE 322	Sulphur dioxide	Gas-permeable membrane	$5 \times 10^{-2} - 5 \times 10^{-5}$ M
ISE 323	Carbon dioxide	Gas-permeable membrane	$10^{-2} - 10^{-4}$ M
ISE 324	Nitrogen oxides	Gas-permeable membrane	$10^{-2} - 5 \times 10^{-6}$ M

Source: adapted from Ref. [19].

8.9.2 Electrochemical gas sensors

Some solid-state materials give an electrochemical response to certain gases. An example is **zirconia**, which is sensitive to oxygen. Zirconia is based on zirconium oxide (ZrO_2) with small amounts of other metal oxides present. These atoms replace Zr atoms at lattice sites and enable the material to conduct both electrons and oxygen O^{2-} ions. Opposite surfaces of a slab of zirconia are coated with a thin layer of platinum, which is porous to oxygen molecules, to give two electrodes. If a surface is exposed to a gas containing oxygen, then oxygen molecules diffuse into the zirconia.

If the sensor is heated to around 600 to 700 °C, the following reversible electrochemical reaction takes place between oxygen molecules and electrons:



The electrons and oxygen ions migrate between the electrodes until an equilibrium is established; there will be a corresponding electrochemical voltage across the electrodes.

A practical sensor consists of a small hollow cone of zirconia, coated on both the inside and outside with a layer of porous platinum and held at a constant temperature of 640 °C.^[20] A sample of the gas to be analysed is present on the inside of the cone and a reference gas (often air) is present on the outside. Under these conditions, the open circuit (Thévenin) e.m.f. of the sensor is given by the Nernst equation:

*Thévenin e.m.f. for
zirconia oxygen sensor*

$$E_{Th} = E_0 + \frac{R\theta}{nF} \log_e \left(\frac{P_{\text{O}_2}^{\text{REF}}}{P_{\text{O}_2}^{\text{SAM}}} \right) \quad [8.97]$$

where $E_0 = \text{constant}$

$n = \text{number of electrons (4) involved in reaction}$

$P_{\text{O}_2}^{\text{REF}} = \text{partial pressure of oxygen in reference gas (cone outside)}$

$P_{\text{O}_2}^{\text{SAM}} = \text{partial pressure of oxygen in sample gas (cone inside)}$.

Provided both the sensor temperature θ and the partial pressure $P_{\text{O}_2}^{\text{REF}}$ of the reference gas outside the sensor are held constant, then E_{Th} depends only on the partial pressure of oxygen in the sample gas inside the sensor. Typically, the sensitivity of the sensor is 60 mV/%O₂ at 640 °C.

8.9.3 Chemically sensitive field effect transistors (CHEMFET)

Figure 8.26(a) shows the construction of an n -channel enhancement-mode MOSFET (metal oxide semiconductor field effect transistor).^[21] It is a chip of silicon crystal with impurities added to create areas of n -type and p -type material. The device has four terminals. The source S and drain D are regions of enriched n -type material, the body or substrate (B) is p -type material and the gate G is metal or polysilicon material. The body is often connected to the source to give a three-terminal device. The gate is insulated from the substrate by a thin layer of silicon dioxide so that negligible current is drawn through the gate terminal.

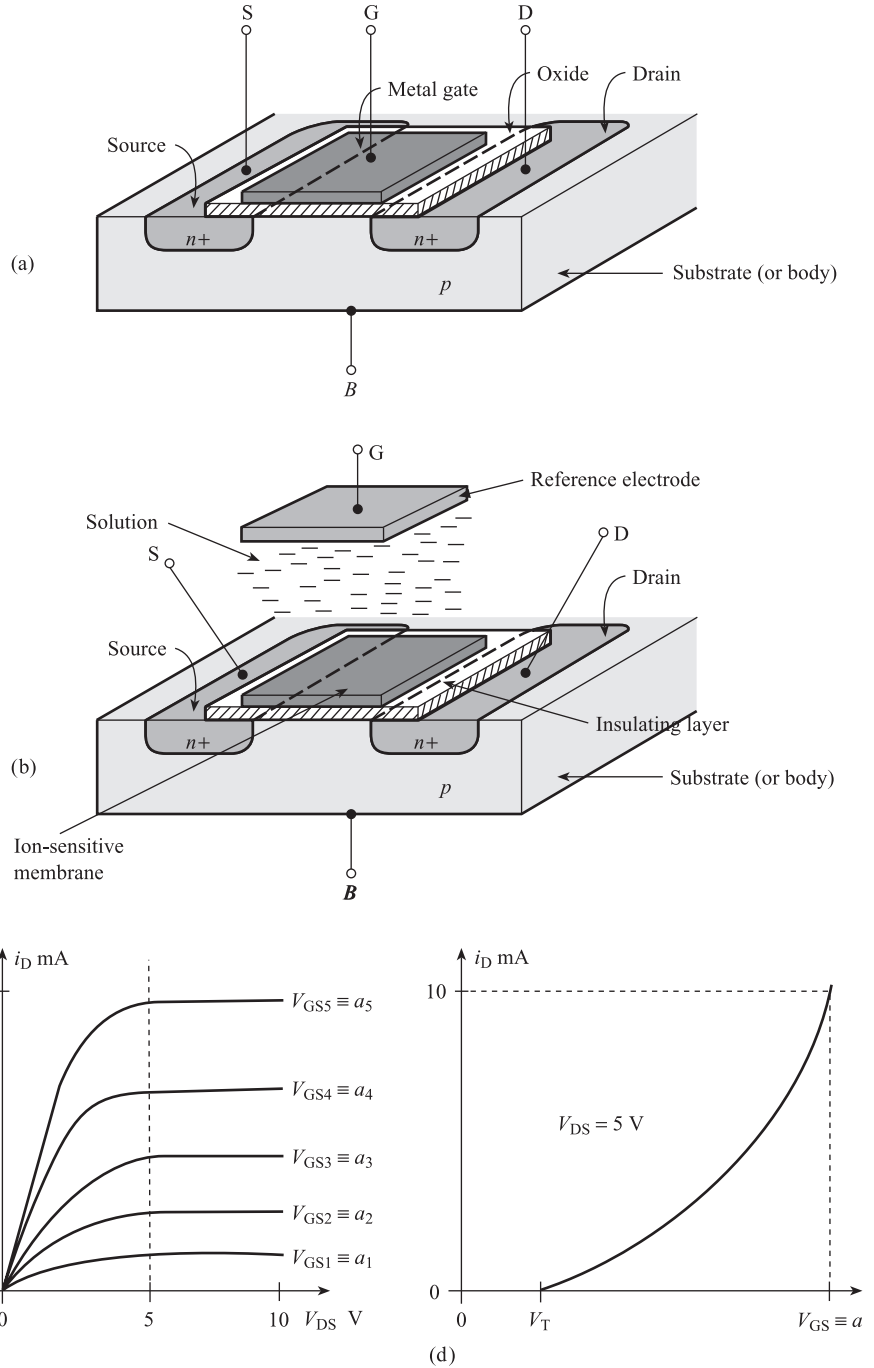
Figures 8.26(c) and (d) show typical characteristics for the device. If the voltage V_{GS} between gate and source is greater than a threshold value V_T , then electrons are attracted to the region under the gate, and a channel of n -channel material is induced between the drain and source. The thickness of this channel increases as V_{GS} is increased. Suppose that a given voltage $V_{GS2} (>V_T)$ is applied between gate and source and the voltage V_{DS} , between drain and source, is increased from zero. There is now a flow of electrons from source to drain, i.e. a current flow i_D from drain to source. Initially i_D increases linearly with V_{DS} , but increased i_D causes the voltage in the drain area to rise and a tapering of the channel towards the drain. This means that as V_{DS} increases further, the increase in i_D gets smaller until it reaches a saturation value which is independent of V_{DS} (Figure 8.26(c)). Figure 8.26(d) shows how the saturation current i_D increases with V_{GS} for a fixed value of $V_{DS} = 5 \text{ V}$, for $V_{GS} > V_T$; the relationship is non-linear. In many applications V_{GS} is the input signal and i_D the output signal, so that Figure 8.26(d) is the input–output characteristic for the device. Because the gate current is negligible, FETs have extremely high-input impedance and are used as the input stage of **buffer amplifiers**, which are used with high impedance sensors such as **ion-selective electrodes** (Section 8.9.1).

The metal gate G is normally inert, but by using a layer which is sensitive to a given gas, a **gas-sensitive FET (gasFET)** sensor can be produced. One example uses a platinum or palladium layer on the gate to detect the presence of hydrogen. Here the gate–source voltage V_{GS} will be the equilibrium potential between the gas and this layer and will depend on the gas concentration a via a Nernst equation similar to eqn [8.97]. The relationship between drain current i_D and a will be broadly similar to that shown in Figure 8.26(d).

Figure 8.26(b) shows the general construction of an **ion-sensitive FET (ISFET)**. ISFETs have been developed from **ion-selective electrodes**; instead of connecting an ion-selective electrode to the FET input stage of an amplifier, the FET is used directly as a sensor for ion concentration. There is now no metal gate but a reference

Figure 8.26 Chemically sensitive field effect transistors:

(a) Construction of n -channel enhancement MOSFET (Figure 8.26(a) is reprinted from *Electrical Engineering Principles and Applications 2/E* by ALLAN R. HAMBLEY by permission of Pearson Education Inc., Upper Saddle River, NJ, USA^[21])
 (b) Construction of ion-sensitive FET (ISFET) (Figure 8.26(b) adapted from Hambley^[21])
 (c), (d) Typical characteristics.



electrode separate from the transistor. The solution to be analysed is introduced into the space between the reference electrode and the gate area. In a pH sensor the gate is simply a silicon nitride layer which is both an electrical insulator and sensitive to H^+ ions. By depositing an ion-sensitive layer on top of the silicon nitride layer, sensors for a range of ions can be made. For example, a layer of sodium aluminosilicate glass will be sensitive to Na^+ ion concentration. The gate–source voltage will be the sum of the reference electrode bias potential and the equilibrium potential between the solution and the membrane. This equilibrium potential will depend on ion activity a via a Nernst equation similar to eqn [8.92]; i_D will correspondingly depend on a .

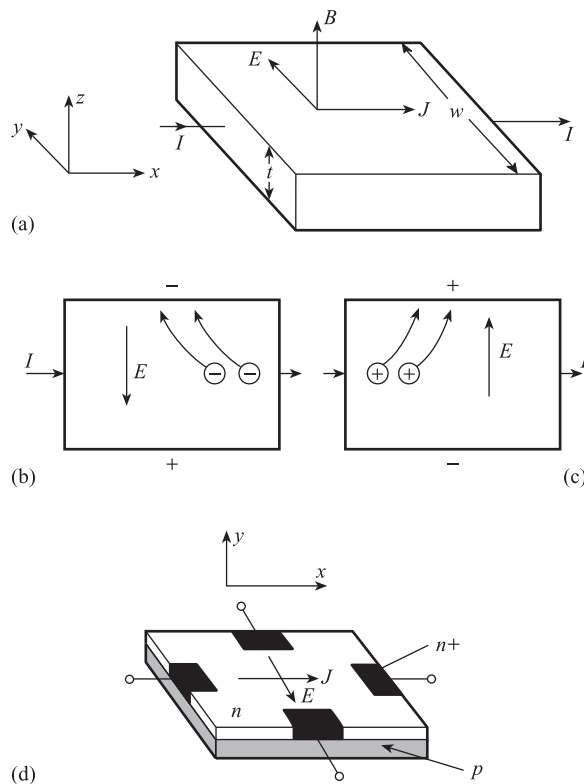
8.10 Hall effect sensors

Figure 8.27(a) shows a rectangular slab of metal or semiconductor material and a corresponding xyz coordinate system. A current I flows through the slab in the x -direction, producing a corresponding current density J . A magnetic field of flux density B is applied to the slab in the z -direction. In a metal there are electron (n) charge carriers only; in a semiconductor there may be both electron and hole (p) charge carriers. Figure 8.27(b) shows the motion of electrons in the xy -plane; the magnetic field is perpendicular to the plane of the paper. The electrons experience a force in the positive y -direction, due to the magnetic field, causing them to be deflected as shown. The top of the slab becomes negatively charged and the bottom positively

Figure 8.27

Hall effect sensors:

- (a) Geometry
- (b) Motion of electrons
- (c) Motion of holes
- (d) Typical sensor.



charged, resulting in an electric field E in the negative y -direction. The force on the electrons due to this electric field is in the opposite direction to the magnetic force and an equilibrium is established, with the two forces equal.

In this equilibrium situation, E is given by:

$$E = -(1/ne)JB = -R_H JB \quad [8.98]$$

where: E = Hall electric field = V/w V/m

V = Hall voltage V

w = width of slab m

J = current density = I/wt Am^{-2}

t = slab thickness m

B = magnetic flux density T (tesla)

R_H = Hall coefficient = $1/ne$

n = density of electrons m^{-3}

e = charge on the electron C.

The Hall voltage V is therefore given by:

$$V = +(R_H/t)IB \quad [8.99]$$

Figure 8.27(c) shows the motion of holes through the slab in the xy -plane; the magnetic field is again in the plane of the paper. The top of the slab becomes positively charged, the bottom negatively charged, with a resulting electric field E in the positive y -direction. The corresponding Hall voltage is given by:

$$V = +(R_H/t)IB \quad [8.100]$$

where: $R_H = 1/pe$

p = density of holes m^{-3} .

An important application of Hall devices is as **magnetic field** sensors; from eqns [8.99] and [8.100] we see that, for a constant current I , V is proportional to B . Silicon, doped with n - and p -type material, has a high Hall coefficient and is a suitable material. A typical sensor, shown in Figure 8.27(d), consists of an n -type conducting layer on a p -type substrate. There are two pairs of electrodes, one pair for current, one pair for Hall voltage, formed by diffusing highly doped and therefore highly conducting regions of n -type material into the n layer. A typical device has thickness t of 1 mm and Hall coefficient R_H of 3×10^{-2} ; if current $I = 10$ mA then $V = 30$ mV for a magnetic field B of 0.1 tesla.

Conclusion

This chapter has discussed the principles, characteristics and applications of a wide range of sensing elements.

References

- [1] BENTLEY J P 1984 'Temperature sensor characteristics and measurement system design', *J. Phys. E: Scientific Instruments*, vol. 17, pp. 430–9.
- [2] IEC 751: 1983 (BS EN 60751: 1996) *Industrial Platinum Resistance Detector Elements*, International Electrotechnical Commission.
- [3] Mullard Ltd 1974 *Technical Information on Two-point NTC Thermistors*.
- [4] PAPAIOSTAS T V and WHITE N M 2000 'Thick-film polymer sensors for physical variables', *Measurement and Control*, vol. 33, no. 4, pp. 105–8.
- [5] VAN EWYK R 1996 'Flammable gas sensors and sensing', *Measurement and Control*, vol. 29, no. 1, pp. 13–16.
- [6] JEFFEREY P D *et al.* 1998 'Thick film chemical sensor array allows flexibility in specification', *Sensor and Transducer Conf.*, NEC Birmingham.
- [7] NEUBERT H K P 1975 *Instrument Transducers: An Introduction to their Performance and Design* (2nd edn), Oxford University Press, London, pp. 237–8.
- [8] LEE-INTEGER 1985 'Advanced relative humidity sensor', *Electronic Product Review*, June.
- [9] IEC 584.1: 1995 *International Thermocouple Reference Tables*, International Electrotechnical Commission.
- [10] DOEBELIN E O 1975 *Measurement Systems: Application and Design* (2nd edn), McGraw-Hill, New York, pp. 520–1.
- [11] Consolidated Electrodynamics, *Bulletin 4202B/1167 on Type 4-202 Strain Gauge Accelerometer*.
- [12] NEUBERT H K P *Instrument Transducers*, p. 56 (see Ref. 4).
- [13] CHATIGNY J V and ROBB L E 1986 'Sensors: making the most of piezo film', *Sensor Review*, vol. 7, no. 1, pp. 15–20.
- [14] PURDY D 1981 'Piezoelectric devices. A step nearer problem-free vibration measurement', *Transducer Technology*, vol. 4, no. 1.
- [15] Endevco 1980 *Product Development News*, vol. 16, issue 3.
- [16] NOBLE M 1985 'IC sensors boost potential of measurement systems', *Transducer Technology*, vol. 8, no. 4.
- [17] BAILEY P L 1976 *Analysis with Ion Selective Electrodes*, Heyden.
- [18] THOMPSON W 'pH facts – the glass electrode', *Kent Technical Review*, pp. 16–22.
- [19] E.D.T. Research 1984 Technical Data on Ion Selective Electrodes.
- [20] Sirius Instruments Ltd 1983 in *Technical Bulletin on Zirconia Oxygen Analysers*.
- [21] HAMBLEY A R 2002 *Electrical Engineering: Principles and Applications* (2nd edn), Prentice-Hall, Englewood Cliffs, NJ, pp. 521–8.

Problems

- 8.1 A platinum resistance sensor is to be used to measure temperatures between 0 and 200 °C. Given that the resistance R_T Ω at T °C is given by $R_T = R_0(1 + \alpha T + \beta T^2)$ and $R_0 = 100.0$, $R_{100} = 138.50$, $R_{200} = 175.83$ Ω , calculate:

- (a) the values of α and β ;
 (b) the non-linearity at 100 °C as a percentage of full-scale deflection.

8.2 Four strain gauges are bonded onto a cantilever as shown in Figure 8.20(a). Given that the gauges are placed halfway along the cantilever and the cantilever is subject to a downward force of 0.5 N, use the data given below to calculate the resistance of each strain gauge:

Cantilever data		Strain gauge data	
Length	$l = 25 \text{ cm}$	Gauge factor	$G = 2.1$
Width	$w = 6 \text{ cm}$	Unstrained resistance	$R_0 = 120 \Omega$
Thickness	$t = 3 \text{ mm}$		
Young's modulus	$E = 70 \times 10^9 \text{ Pa}$		

8.3 A variable dielectric capacitive displacement sensor consists of two square metal plates of side 5 cm, separated by a gap of 1 mm. A sheet of dielectric material 1 mm thick and of the same area as the plates can be slid between them as shown in Figure 8.9. Given that the dielectric constant of air is 1 and that of the dielectric material 4, calculate the capacitance of the sensor when the input displacement $x = 0.0, 2.5$ and 5.0 cm .

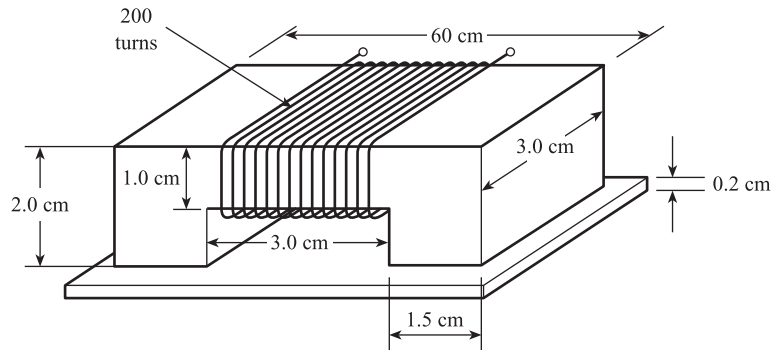
8.4 A variable reluctance sensor consists of a core, a variable air gap and an armature. The core is a steel rod of diameter 1 cm and relative permeability 100, bent to form a semi-circle of diameter 4 cm. A coil of 500 turns is wound onto the core. The armature is a steel plate of thickness 0.5 cm and relative permeability 100. Assuming the relative permeability of air = 1.0 and the permeability of free space = $4\pi \times 10^{-7} \text{ H m}^{-1}$, calculate the inductance of the sensor for air gaps of 1 mm and 3 mm.

8.5 By taking a central flux path, estimate the inductance of the sensor shown in Figure Prob. 5

- (a) for zero air gap;
 (b) for a 2 mm air gap.

Assume the relative permeability of core and armature is 10^4 and that of air is unity.

Figure Prob. 5.



8.6 A variable reluctance tachogenerator consists of a ferromagnetic gear wheel with 22 teeth rotating close to a magnet and coil assembly. The total flux N linked by the coil is given by:

$$N(\theta) = 4.0 + 1.5 \cos 22\theta \text{ milliwebers}$$

where θ is the angular position of the wheel relative to the axis of the magnet. Calculate the amplitude and frequency of the output signal when the angular velocity of the wheel is 1000 and 10 000 r.p.m.

8.7 An iron v. constantan thermocouple is to be used to measure temperatures between 0 and 300 °C. The e.m.f. values are as given in Table 8.2.

- Find the non-linearity at 100 °C and 200 °C as a percentage of full scale.
- Between 100 °C and 300 °C the thermocouple e.m.f. is given by $E_{T0} = a_1T + a_2T^2$. Calculate a_1 and a_2 .
- The e.m.f. is 12 500 μV relative to a reference junction of 20 °C and the corresponding reference junction circuit voltage is 1000 μV . Use the result of (b) to estimate the measured junction temperature.

8.8 An accelerometer consisting of an elastic element and a potentiometric displacement sensor has to meet the following specification:

Input range = 0 to 5g	Damping ratio = 0.8
Output range = 0 to 10 V	Maximum non-linearity = 2% of f.s.d.
Natural frequency = 10 Hz	Seismic mass = 0.005 kg

- Calculate the required spring stiffness and damping constant.
- What should the input displacement range of the potentiometer be? ($g = 9.81 \text{ m s}^{-2}$)
- If the accelerometer is to be used with a recorder of 10 k Ω resistance, what is the maximum allowable potentiometer resistance?

8.9 An accelerometer is to measure the angular acceleration of a rotating mixing vessel. The angular position of the vessel varies sinusoidally with time with amplitude 2.5 rad and period 2 s. The rotating seismic mass is equivalent to a mass of 0.1 kg on a weightless arm of length 5 cm. The stiffness of the spring is $2.5 \times 10^{-2} \text{ N m rad}^{-1}$ and the damping ratio is $1/\sqrt{2}$. The angular position of the seismic mass is measured with a secondary potentiometric sensor. What should the input range of this sensor be?

8.10 A flat circular diaphragm of density $6 \times 10^3 \text{ kg m}^{-3}$ is to be used as a pressure sensor. The element should fulfil the following specification:

Input range = 0 to 10 ⁴ Pa
Maximum non-linearity = 1% of f.s.d
Amplitude ratio to be flat with $\pm 3\%$ up to 100 Hz

Using the equations given in Figure 8.21, and assuming a damping ratio of 0.01, calculate:

- the thickness t of the diaphragm;
- the output displacement range of the sensor.

8.11 A piezoelectric crystal, acting as a force sensor, is connected by a short cable of negligible capacitance and resistance to a voltage detector of infinite bandwidth and purely resistive impedance of 10 M Ω .

- Use the crystal data below to calculate the system transfer function and to sketch the approximate frequency response characteristics of the system.
- The time variation in the thrust of an engine is a square wave of period 10 ms. Explain carefully, but without performing detailed calculations, why the above system is unsuitable for this application.
- A charge amplifier with feedback capacitance $C_F = 1000 \text{ pF}$ and feedback resistance $R_F = 100 \text{ M}\Omega$ is incorporated into the system. By sketching the frequency response characteristics of the modified system, explain why it is suitable for the application of part (b).

<i>Crystal data</i>	Charge sensitivity to force = 2 pC N^{-1}
	Capacitance = 100 pF
	Natural frequency = 37 kHz
	Damping ratio = 0.01

- 8.12 (a) The casing of a compressor is executing sinusoidal vibrations with a displacement amplitude of 10^{-4} m and a frequency of 500 Hz . Calculate the amplitude of the acceleration of the casing in units of g ($g = 9.81 \text{ m s}^{-2}$).
- (b) A piezoelectric crystal accelerometer has a steady-state sensitivity of 2.0 pC/g , a natural frequency of 20 kHz , a damping ratio of 0.1 and a capacitance of 100 pF . It is connected to an oscilloscope (a resistive load of $10 \text{ M}\Omega$) by a cable of capacitance 100 pF .
- (i) Without performing detailed calculations, sketch magnitude and phase frequency response characteristics for the accelerometer. Using these characteristics:
- (ii) Estimate the amplitude of the voltage measured by the oscilloscope when the accelerometer is mounted on the casing described in (a).
- (iii) Explain why this system is unsuitable for measuring vibrations at 20 Hz . How should the system be modified to make these measurements possible?

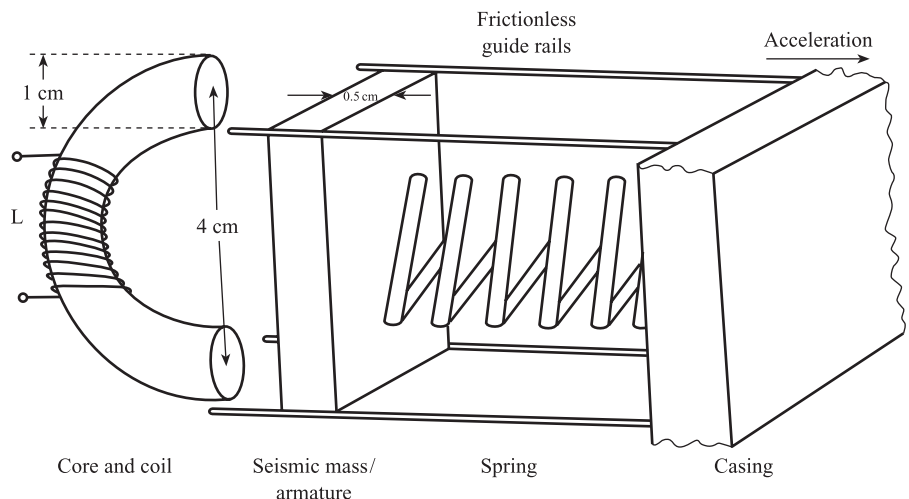
- 8.13 A seismic mass accelerometer with a variable reluctance displacement sensor is shown in Figure Prob. 13. The undamped natural frequency of the accelerometer is to be 25 Hz and the range of the acceleration input is to be 0 to $5g$. Using the data given below, calculate:

- (a) the required spring stiffness;
- (b) the air gap at maximum acceleration;
- (c) the range of variation of the coil inductance.

Data

Relative permeability of armature and coil material	= 100
Relative permeability of air	= 1
Permeability of free space	= $4\pi \times 10^{-7} \text{ H/m}$
Effective mass of armature and spring	= 0.025 kg
Acceleration of gravity g	= 9.81 m/s^2
Number of coil turns	= 500
Air gap at zero acceleration	= 3 mm

Figure Prob. 8.13.



Basic problems

- 8.14 A platinum resistance sensor has a resistance of $100.0\ \Omega$ at $0\ ^\circ\text{C}$ and a temperature coefficient of resistance α of $4 \times 10^{-3}\ ^\circ\text{C}^{-1}$. If the resistance of the sensor is $125\ \Omega$, find the corresponding temperature of the sensor.
- 8.15 A platinum resistance sensor has a resistance of $100\ \Omega$ at $0\ ^\circ\text{C}$ and a temperature coefficient of resistance of $4 \times 10^{-3}\ ^\circ\text{C}^{-1}$. Find the resistance of the sensor at $-100\ ^\circ\text{C}$.
- 8.16 A thermistor has constants $K = 0.1\ \Omega$, $\beta = 3200\ \text{K}$. Find the resistance at the ice point.
- 8.17 A steel bar has a cross-sectional area of $10^{-3}\ \text{m}^2$, Young's modulus of $2 \times 10^{11}\ \text{Pa}$ and Poisson's ratio of 0.4. If the bar is subject to a compressive force of $10^5\ \text{N}$, find the corresponding longitudinal and transverse strains.
- 8.18 Two strain gauges, each with an unstrained resistance of $120\ \Omega$ and a gauge factor of 2.0, are bonded onto the steel bar of Problem 8.17 so that one measures the longitudinal strain and one the transverse strain. Find the corresponding gauge resistances for the longitudinal and transverse strains.
- 8.19 A parallel plate capacitive displacement sensor consists of two square metal plates $8\ \text{cm} \times 8\ \text{cm}$, separated by a gap of $2\ \text{mm}$. The space between the plates is completely filled by a slab with a dielectric constant of 6.0. If the permittivity of free space is $8.85\ \text{pF/m}$, find the capacitance of the sensor.
- 8.20 A parallel plate capacitance pressure sensor consists of two circular plates of diameter $2\ \text{cm}$ separated by an air gap of $1\ \text{mm}$. If the dielectric constant of air is 1.0 and the permittivity of free space is $8.85\ \text{pF/m}$, find the capacitance of the sensor.
- 8.21 A strain gauge having an unstrained resistance of $120\ \Omega$ and a gauge factor of 2.1 is bonded onto a steel girder so that it experiences a tensile stress of $10^8\ \text{Pa}$. If Young's modulus for steel is $2 \times 10^{11}\ \text{Pa}$, calculate the strained resistance of the gauge.
- 8.22 Table Prob. 22 gives values for the e.m.f. of a Type T thermocouple relative to a reference junction temperature of $0\ ^\circ\text{C}$. Use the table to calculate:
- (a) the percentage non-linearity at $150\ ^\circ\text{C}$ if the temperature range is 0 to $300\ ^\circ\text{C}$;
 - (b) the temperature inside a vessel if an e.m.f. of $11.5\ \text{mV}$ is measured relative to a reference junction of $20\ ^\circ\text{C}$.
- 8.23 The e.m.f. of a type T thermocouple is measured to be $8.561\ \text{mV}$ relative to a reference junction temperature of $20\ ^\circ\text{C}$. Use the table provided in Problem 8.22 to find the temperature of the measured junction.
- 8.24 A variable reluctance tachogenerator consists of a ferromagnetic wheel with 20 teeth rotating close to a bar magnet and coil. If the wheel is rotating at $6000\ \text{rpm}$, what is the frequency of the a.c. voltage induced in the coil?
- 8.25 A force sensor includes an elastic spring with a stiffness of $10^6\ \text{N m}^{-1}$. If the force input has a range of 0 to $5\ \text{kN}$, find the corresponding displacement output range.
- 8.26 A doped silicon wafer has a thickness of $0.5\ \text{mm}$ and a Hall coefficient of 2×10^{-2} . If the current through the wafer is $7.5\ \text{mA}$, find the Hall voltage for a magnetic flux density of $0.2\ \text{T}$.

Table Prob. 22 e.m.f. in mV for type T thermocouple (measured junction at T °C, reference junction at 0 °C).

Temp. °C	0	1	2	3	4	5	6	7	8	9	10
0	0.000	0.039	0.078	0.117	0.156	0.195	0.234	0.273	0.312	0.351	0.391
10	0.391	0.430	0.470	0.510	0.549	0.589	0.629	0.669	0.709	0.749	0.789
20	0.789	0.830	0.870	0.911	0.951	0.992	1.032	1.073	1.114	1.155	1.196
30	1.196	1.237	1.279	1.320	1.361	1.403	1.444	1.486	1.528	1.569	1.611
40	1.611	1.653	1.695	1.738	1.780	1.822	1.865	1.907	1.950	1.992	2.035
50	2.035	2.078	2.121	2.164	2.207	2.250	2.294	2.337	2.380	2.424	2.467
60	2.467	2.511	2.555	2.599	2.643	2.687	2.731	2.775	2.819	2.864	2.908
70	2.908	2.953	2.997	3.042	3.087	3.131	3.176	3.221	3.266	3.312	3.357
80	3.357	3.402	3.447	3.493	3.538	3.584	3.630	3.676	3.721	3.767	3.813
90	3.813	3.859	3.906	3.952	3.998	4.044	4.091	4.137	4.184	4.231	4.277
100	4.277	4.324	4.371	4.418	4.465	4.512	4.559	4.607	4.654	4.701	4.749
110	4.749	4.796	4.844	4.891	4.939	4.987	5.035	5.083	5.131	5.179	5.227
120	5.227	5.275	5.324	5.372	5.420	5.469	5.517	5.566	5.615	5.663	5.712
130	5.712	5.761	5.810	5.859	5.908	5.957	6.007	6.056	6.105	6.155	6.204
140	6.204	6.254	6.303	6.353	6.403	6.452	6.502	6.552	6.602	6.652	6.702
150	6.702	6.753	6.803	6.853	6.903	6.954	7.004	7.055	7.106	7.156	7.207
160	7.207	7.258	7.309	7.360	7.411	7.462	7.513	7.564	7.615	7.666	7.718
170	7.718	7.769	7.821	7.872	7.924	7.975	8.027	8.079	8.131	8.183	8.235
180	8.235	8.287	8.339	8.391	8.443	8.495	8.548	8.600	8.652	8.705	8.757
190	8.757	8.810	8.863	8.915	8.968	9.021	9.074	9.127	9.180	9.233	9.286
200	9.286	9.339	9.392	9.446	9.499	9.553	9.606	9.659	9.713	9.767	9.820
210	9.820	9.874	9.928	9.982	10.036	10.090	10.144	10.198	10.252	10.306	10.360
220	10.360	10.414	10.469	10.523	10.578	10.632	10.687	10.741	10.796	10.851	10.905
230	10.905	10.960	11.015	11.070	11.125	11.180	11.235	11.290	11.345	11.401	11.456
240	11.456	11.511	11.566	11.622	11.677	11.733	11.788	11.844	11.900	11.956	12.011
250	12.011	12.067	12.123	12.179	12.235	12.291	12.347	12.403	12.459	12.515	12.572
260	12.572	12.628	12.684	12.741	12.797	12.854	12.910	12.967	13.024	13.080	13.137
270	13.137	13.194	13.251	13.307	13.364	13.421	13.478	13.535	13.592	13.650	13.707
280	13.707	13.764	13.821	13.879	13.936	13.993	14.051	14.108	14.166	14.223	14.281
290	14.281	14.339	14.396	14.454	14.512	14.570	14.628	14.686	14.744	14.802	14.860
300	14.860	14.918	14.976	15.034	15.092	15.151	15.209	15.267	15.326	15.384	15.443
310	15.443	15.501	15.560	15.619	15.677	15.736	15.795	15.853	15.912	15.971	16.030
320	16.030	16.089	16.148	16.207	16.266	16.325	16.384	16.444	16.503	16.562	16.621
330	16.621	16.681	16.740	16.800	16.859	16.919	16.978	17.038	17.097	17.157	17.217
340	17.217	17.277	17.336	17.396	17.456	17.516	17.576	17.636	17.696	17.756	17.816

9

Signal Conditioning Elements

As stated in Chapter 1, signal conditioning elements convert the output of sensing elements into a form suitable for further processing. This form is usually a d.c. voltage, a d.c. current or a variable frequency a.c. voltage.

9.1

Deflection bridges

Deflection bridges are used to convert the output of resistive, capacitive and inductive sensors into a voltage signal.

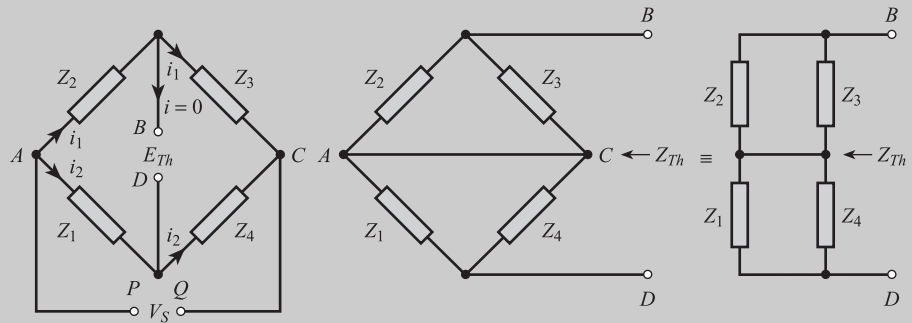
9.1.1 Thévenin equivalent circuit for a deflection bridge

In Chapter 5 we saw that any linear network can be represented by a Thévenin equivalent circuit consisting of a voltage source E_{Th} together with a series impedance Z_{Th} . Figure 9.1 shows a general deflection bridge network. E_{Th} is the open-circuit output voltage of the bridge, i.e. when current i in $BD = 0$. Using Kirchhoff's laws:

$$\text{Loop } PABCQ \quad V_S = i_1 Z_2 + i_1 Z_3 \quad \text{i.e.} \quad i_1 = \frac{V_S}{Z_2 + Z_3} \quad [9.1]$$

$$\text{Loop } PADCQ \quad V_S = i_2 Z_1 + i_2 Z_4 \quad \text{i.e.} \quad i_2 = \frac{V_S}{Z_1 + Z_4} \quad [9.2]$$

Figure 9.1 Calculation of Thévenin equivalent circuit for a deflection bridge.



Assuming Q is at earth potential, then:

Potential at P and $A = V_S$

Potential at $B = V_S - i_1 Z_2$

Potential at $D = V_S - i_2 Z_1$

E_{Th} is equal to the potential difference between B and D , i.e.

$$\begin{aligned} E_{Th} &= (V_S - i_1 Z_2) - (V_S - i_2 Z_1) \\ &= i_2 Z_1 - i_1 Z_2 \end{aligned}$$

Using [9.1] and [9.2] we have

*Thévenin voltage for
general deflection
bridge*

$$E_{Th} = V_S \left(\frac{Z_1}{Z_1 + Z_4} - \frac{Z_2}{Z_2 + Z_3} \right) \quad [9.3]$$

Z_{Th} is the impedance, looking back into the circuit, between the output terminals BD , when the supply voltage V_S is replaced by its internal impedance. Assuming the internal impedance of the supply is zero, then this is equivalent to a short circuit across AC (see Figure 9.1). We see that Z_{Th} is equal to the parallel combination of Z_2 and Z_3 in series with the parallel combination of Z_1 and Z_4 , i.e.

*Thévenin impedance
for general deflection
bridge*

$$Z_{Th} = \frac{Z_2 Z_3}{Z_2 + Z_3} + \frac{Z_1 Z_4}{Z_1 + Z_4} \quad [9.4]$$

If a load, e.g. a voltmeter or amplifier, of impedance Z_L is connected across the output terminals BD , then the current through the load is $i = E_{Th} / (Z_{Th} + Z_L)$. The corresponding voltage across the load is $V_L = E_{Th} Z_L / (Z_{Th} + Z_L)$. Thus in the limit that $|Z_L| \gg |Z_{Th}|$, $V_L \rightarrow E_{Th}$.

9.1.2 Design of resistive deflection bridges

In a resistive or Wheatstone bridge all four impedances Z_1 to Z_4 are pure resistances R_1 to R_4 . From [9.3] we have

*Output voltage for
resistive deflection
bridge*

$$E_{Th} = V_S \left(\frac{R_1}{R_1 + R_4} - \frac{R_2}{R_2 + R_3} \right) \quad [9.5]$$

We first consider the case when only one of the resistances is a sensing element. Here R_1 depends on the input measured variable I , i.e. $R_1 = R_I$, and R_2 , R_3 and R_4 are fixed resistors. This gives

$$E_{Th} = V_S \left(\frac{1}{1 + R_4/R_I} - \frac{1}{1 + R_3/R_2} \right) \quad [9.6]$$

from which we see that to design a single element bridge we need to specify the three parameters V_s , R_4 and R_3/R_2 . The individual values of R_2 and R_3 are not critical; it is their ratio which is crucial to the design. The three parameters can be specified by considering the range and linearity of the output voltage and electrical power limitations for the sensor. Thus if I_{\min} and I_{\max} are minimum and maximum values of the measured variable, and $R_{I_{\min}}$ and $R_{I_{\max}}$ are the corresponding sensor resistances, then in order for the bridge output voltage to have a range from V_{\min} to V_{\max} the following conditions must be obeyed:

$$V_{\min} = V_s \left(\frac{1}{1 + R_4/R_{I_{\min}}} - \frac{1}{1 + R_3/R_2} \right) \quad [9.7]$$

$$V_{\max} = V_s \left(\frac{1}{1 + R_4/R_{I_{\max}}} - \frac{1}{1 + R_3/R_2} \right) \quad [9.8]$$

Often we require $V_{\min} = 0$, i.e. the bridge to be balanced when $I = I_{\min}$; in this case [9.7] reduces to:

Relationship between resistances in a balanced Wheatstone bridge

$$\frac{R_4}{R_{I_{\min}}} = \frac{R_3}{R_2} \quad [9.9]$$

A third condition is required to complete the design. One important consideration is the need to limit the electrical power $i_s^2 R_I$ in the sensor to a level which enables it to be dissipated as heat flow to the surrounding fluid; otherwise the temperature of the sensor rises above that of the surrounding fluid, thereby affecting the sensor resistance (Chapter 14). Thus if \hat{w} watts is the maximum power dissipation, using [9.2] we require:

$$V_s^2 \frac{R_I}{(R_I + R_4)^2} \leq \hat{w} \quad [9.10]$$

for $I_{\min} \leq I \leq I_{\max}$.

Another requirement which is often important is the need to keep the non-linearity of the overall relationship between E_{Th} and I within specified limits. Assuming $V_{\min} = 0$, then the ideal relationship between V and I is the ideal straight line:

$$V_{\text{IDEAL}} = \left(\frac{V_{\max}}{I_{\max} - I_{\min}} \right) I - \left(\frac{V_{\max}}{I_{\max} - I_{\min}} \right) I_{\min} \quad [9.11]$$

From Chapter 2, the non-linear function $N(I) = E_{Th} - V_{\text{IDEAL}}$. Suppose we require the non-linearity as a percentage of full scale to be less than \hat{N} per cent over the measurement range; we then have the condition:

$$\frac{E_{Th} - V_{\text{IDEAL}}}{V_{\max}} \times 100 \leq \hat{N} \quad [9.12]$$

for $I_{\min} \leq I \leq I_{\max}$, where E_{Th} and V_{IDEAL} are given by [9.6] and [9.11] respectively.

The value of ratio R_3/R_2 varies according to the type of resistive sensor used; it is useful to have a graph which gives some insight into this. From [9.9] we have $R_4 = (R_3/R_2)R_{I_{\min}}$. Substituting for R_4 in [9.6] gives:

$$\frac{E_{Th}}{V_S} = \frac{1}{1 + (R_3/R_2)(R_{I_{MIN}}/R_I)} - \frac{1}{1 + R_3/R_2}$$

or

$$v = \frac{1}{1 + r/x} - \frac{1}{1 + r} = \frac{x}{x + r} - \frac{1}{1 + r} \quad [9.13]$$

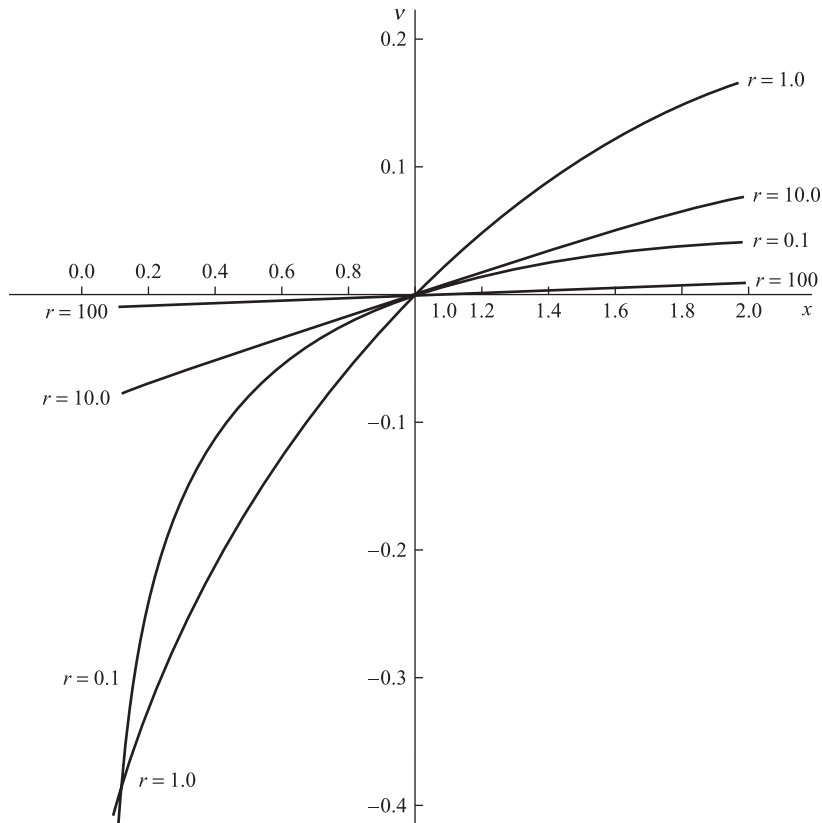
where

$$v = \frac{E_{Th}}{V_S}, \quad r = \frac{R_3}{R_2}, \quad x = \frac{R_I}{R_{I_{MIN}}}$$

Figure 9.2 shows graphs of v versus x , for x in the range 0.1 to 2.0, and for $r = 0.1, 1.0, 10.0$ and 100 . We note that v is always zero at $x = 1$, corresponding to the bridge being balanced at $I = I_{MIN}$; also that $v(x)$ is in general non-linear, the degree of non-linearity depending on r .

For a strain gauge (Section 8.1) the change in resistance $\Delta R = R_0 Ge$ is very small; this means that x is very close to 1. We require the sensitivity of the bridge to be as high as possible, i.e. $(\partial v / \partial x)_{x=1}$ to be maximum. From Figure 9.2 we see that this occurs when $r = R_3/R_2 = 1$, i.e. $R_3 = R_2$. Using eqn [9.9], this means that $R_4 = R_{I_{MIN}} = R_0$. Thus for a bridge with a single strain gauge, we require R_2, R_3 and R_4 to all equal the unstrained

Figure 9.2 The deflection bridge function $v(x) = x/(x + r) - 1/(1 + r)$.



gauge resistance R_0 . The value of V_S is determined by the power condition [9.10]. Putting $r = 1$ in [9.13] gives:

$$v(x) = \frac{x-1}{2(x+1)} \approx \frac{1}{4}(x-1)$$

so that:

$$\frac{E_{Th}}{V_S} = \frac{1}{4} \left(\frac{R_I}{R_{I_{MIN}}} - 1 \right) = \frac{1}{4} \left(\frac{R_I - R_{I_{MIN}}}{R_{I_{MIN}}} \right) = \frac{1}{4} \frac{\Delta R}{R_0} = \frac{1}{4} Ge$$

Thus:

*Output voltage for
single-element strain
gauge bridge*

$$E_{Th} = \frac{V_S}{4} Ge \quad [9.14]$$

i.e. the relationship between E_{Th} and e is linear.

The resistance R_T Ω of a metal resistance sensor, e.g. platinum, at T °C is given approximately by (Section 8.1) $R_T = R_0(1 + \alpha T)$. Typically x varies between 1 and 2 ($R_0 = 100 \Omega$, $R_{250} \approx 200 \Omega$). Since this device has only a small non-linearity (less than 1%) a linear bridge is required. From Figure 9.2 we see this means a large value of r , e.g. $r \approx 100$, linearity being obtained at the expense of low sensitivity. For large r (i.e. $r \gg 1$) eqn [9.13] approximates to:

$$v \approx \frac{1}{r}(x-1) \quad \text{i.e.} \quad \frac{E_{Th}}{V_S} = \frac{R_2}{R_3} \left(\frac{R_T}{R_{T_{MIN}}} - 1 \right)$$

If $T_{MIN} = 0$ °C, then since $R_T/R_0 = 1 + \alpha T$:

*Output voltage for
metal resistance
sensor bridge (large r)*

$$E_{Th} = V_S \frac{R_2}{R_3} \alpha T \quad [9.15]$$

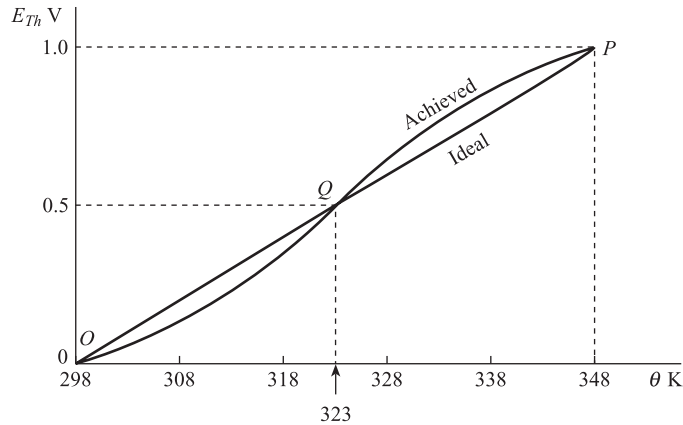
i.e. a linear relationship between E_{Th} and T .

For given V_S (satisfying [9.10]), R_3/R_2 can be found from [9.15] and R_4 from [9.9]. Figure Prob. 16 in this chapter shows an accurate arrangement for temperature measurement involving a platinum resistance sensor with four-lead connection to a deflection bridge. With a copper or nickel resistance sensor, this circuit provides the voltage source $E_{T_{2,0}}$ necessary for automatic reference junction compensation of a thermocouple e.m.f. (see Section 8.5 and Problem 9.2).

The resistance R_θ of a thermistor varies non-linearly with absolute temperature θ K according to the relationship $R_\theta = K \exp(\beta/\theta)$ (Section 8.1). A typical thermistor has a resistance of 12 k Ω at 298 K (25 °C) falling to 2 k Ω at 348 K (75 °C); i.e. x varies from 1.0 to 0.17 over this measurement range. By choosing a suitable value of r , usually between 0.25 and 0.30, it is possible to use the bridge non-linearity to partially compensate for the thermistor non-linearity; this means the overall relationship between E_{Th} and θ is reasonably linear over this range (see Figures 9.2 and 9.3). Supposing we require an output range of 0 to 1.0 V, corresponding to a temperature range of 298 to 348 K; then almost minimum non-linearity is obtained if we design

Figure 9.3

Design conditions and characteristics for thermistor bridge.



the bridge so that $E_{Th} = 0.5$ V at $\theta = 323$ K (Figure 9.3). The bridge is then designed by solving the following three equations for V_S , R_4 and R_3/R_2 :

$$0.0 = V_S \left(\frac{1}{1 + R_4/R_{298}} - \frac{1}{1 + R_3/R_2} \right) \quad (\text{point } O)$$

$$0.5 = V_S \left(\frac{1}{1 + R_4/R_{323}} - \frac{1}{1 + R_3/R_2} \right) \quad (\text{point } Q) \quad [9.16]$$

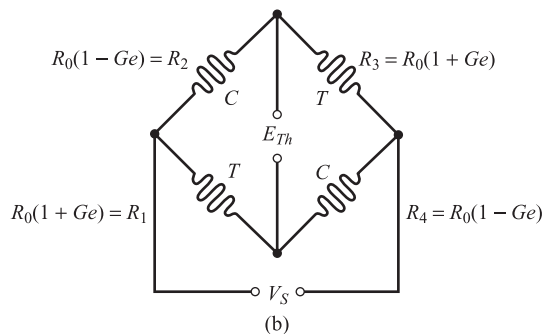
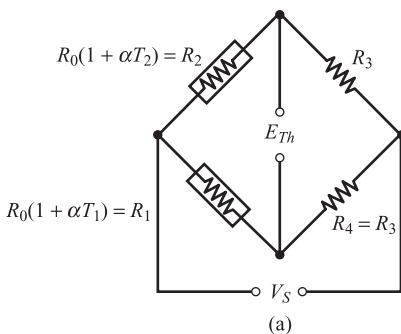
$$1.0 = V_S \left(\frac{1}{1 + R_4/R_{348}} - \frac{1}{1 + R_3/R_2} \right) \quad (\text{point } P)$$

A bridge with two metal resistance sensor elements can be designed to give an output voltage approximately proportional to temperature differences $T_1 - T_2$. The bridge incorporates one element at T_1 °C and another at T_2 °C so that $R_1 = R_0(1 + \alpha T_1)$ and $R_2 = R_0(1 + \alpha T_2)$, as shown in Figure 9.4(a). In order to balance the bridge when $T_1 - T_2 = 0$, we require $R_4/R_1 = R_3/R_2$ when $T_1 = T_2$; this implies $R_4/R_0 = R_3/R_0$, i.e. $R_4 = R_3$. Using [9.6], we have:

Figure 9.4

(a) Two-element resistance sensor bridge
(b) Four-element strain gauge bridge.

$$E_{Th} = V_S \left\{ \frac{1}{1 + \frac{R_3}{R_0} \left(\frac{1}{1 + \alpha T_1} \right)} - \frac{1}{1 + \frac{R_3}{R_0} \left(\frac{1}{1 + \alpha T_2} \right)} \right\}$$



and if we choose R_3 so that $R_3/R_0 \gg 1$, this approximates to:

$$E_{Th} \approx V_s \left(\frac{1 + \alpha T_1}{R_3/R_0} - \frac{1 + \alpha T_2}{R_3/R_0} \right)$$

i.e.

*Output voltage for
two-element resistance
sensor bridge*

$$E_{Th} = V_s \frac{R_0}{R_3} \alpha (T_1 - T_2) \quad [9.17]$$

which has a similar form to [9.15]. This bridge has several applications, including the measurement of humidity with wet and dry bulb sensors and as a detector in a thermal radiation measurement system (Section 15.2).

Bridges with four active strain gauges, mounted on elastic elements, are commonly used for the measurement of force, torque, acceleration and pressure. Provided the gauges are correctly connected into the bridge, so that one opposite pair (e.g. R_1, R_3) are in tension and the other opposite pair (e.g. R_2, R_4) are in compression, then the sensitivity is greater than for a single-element bridge. This bridge also compensates for changes in gauge resistance due to temperature. For metal strain gauges the effect of temperature is to multiply each gauge resistance by the factor $(1 + \alpha T)$; this cancels out in the output voltage eqn [9.5]. The only design decision to be made is the value of supply voltage; V_s is determined either by the maximum power condition [9.10] or by the maximum specified gauge current (Section 8.1).

For the cantilever load cell and torque element of Section 8.6 (Figures 8.20(a) and (c)), we have $R_1 = R_3 = R_0(1 + Ge)$ and $R_2 = R_4 = R_0(1 - Ge)$, where R_0 is the unstrained gauge resistance. Here

$$e = \frac{6(l-x)F}{wt^2E}$$

for the cantilever and

$$e = \frac{T}{\pi S a^3}$$

for the torque element. Using [9.5] the output voltage of the bridge (Figure 9.4) is thus given by:

$$\begin{aligned} E_{Th} &= V_s \left\{ \frac{R_0(1 + Ge)}{R_0(1 + Ge) + R_0(1 - Ge)} - \frac{R_0(1 - Ge)}{R_0(1 - Ge) + R_0(1 + Ge)} \right\} \\ &= V_s \left(\frac{1 + Ge}{2} - \frac{1 - Ge}{2} \right) \end{aligned}$$

i.e.

*Output voltage for
cantilever and torque
elements*

$$E_{Th} = V_s Ge \quad [9.18]$$

Here the output voltage is four times that of the single gauge bridge (eqn [9.14]). For the pillar load cell (Figure 8.20(b)):

$$R_1 = R_3 = R_0 \left(1 + \frac{GF}{AE} \right) \quad \text{and} \quad R_2 = R_4 = R_0 \left(1 - \frac{GF}{AE} \right)$$

Using eqn [9.5] and assuming $(GF/AE) \ll 1$, the approximate bridge output voltage is:

*Output voltage for
pillar load cell*

$$E_{Th} \approx \frac{V_s}{2} (1 + \nu) \frac{GF}{AE} \quad [9.19]$$

Finally for the unbonded strain gauge accelerometer (Figure 8.20(d)), we have

$$R_1 = R_3 = R_0 [1 + G(e_0 + e)] \quad \text{and} \quad R_2 = R_4 = R_0 [1 + G(e_0 - e)]$$

where e_0 = strain due to prestressing which is present at zero acceleration and e is the acceleration-induced strain $= a/\omega_n^2 L$. The output voltage of the bridge is given by:

*Output voltage for
strain gauge
accelerometer*

$$E_{Th} = \frac{V_s G e}{1 + G e_0} \quad [9.20]$$

The output voltage of these bridges is usually small and requires high amplification; typically if $V_s = 15$ V, $G = 2$ and $e = 10^{-5}$, then $E_{Th} \approx V_s G e = 300$ μ V. Because of the problems in amplifying low-level d.c. signals (see following section), an a.c. supply voltage $V_s = \hat{V}_s \sin \omega_s t$ is often used to give an a.c. output voltage; a.c. carrier systems are discussed fully in Section 9.3.

9.1.3 Design of reactive deflection bridges

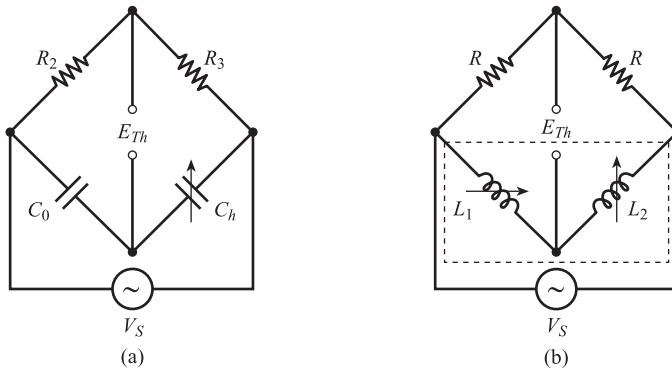
A reactive bridge has an a.c. supply voltage; two arms are usually reactive impedances and two arms resistive impedances. Figure 9.5(a) shows the bridge to be used with the capacitance level transducer of Section 8.2; here we have

$$C_h = \frac{2\pi\epsilon_0}{\log_e(b/a)} [l + (\epsilon - 1)h]$$

Also $Z_1 = 1/(j\omega C_0)$, $Z_2 = R_2$, $Z_3 = R_3$ and $Z_4 = 1/(j\omega C_h)$.

Figure 9.5

(a) Bridge for capacitive level sensor
(b) Bridge for inductive push-pull displacement sensor.



This gives

$$E_{Th} = V_s \left(\frac{1}{1 + C_0/C_h} - \frac{1}{1 + R_3/R_2} \right)$$

Thus in order to get $\hat{E}_{Th} = 0$ at minimum level h_{\min} , we require $C_0 = C_{h_{\min}}(R_3/R_2)$, giving:

Output voltage for capacitance level bridge

$$E_{Th} = V_s \left(\frac{1}{1 + \frac{C_{h_{\min}}}{C_h} \frac{R_3}{R_2}} - \frac{1}{1 + \frac{R_3}{R_2}} \right) \quad [9.21]$$

Again if R_3/R_2 is made large compared with 1, this approximates to the linear form:

$$E_{Th} \approx V_s \frac{R_2}{R_3} \left(\frac{C_h}{C_{h_{\min}}} - 1 \right)$$

The most common two-element reactive bridges incorporate either capacitive or inductive push-pull displacement sensors (Sections 8.2 and 8.3). The capacitive sensor (Figure 8.9) has $C_1 = \epsilon \epsilon_0 A/(d+x)$ and $C_2 = \epsilon \epsilon_0 A/(d-x)$; if this is connected into an a.c. bridge so that $Z_1 = 1/(j\omega C_1)$, $Z_2 = Z_3 = R$, $Z_4 = 1/(j\omega C_2)$ we have:

$$E_{Th} = V_s \left(\frac{C_2}{C_1 + C_2} - \frac{1}{2} \right) \quad [9.22]$$

This gives:

Output voltage for capacitance push-pull bridge

$$E_{Th} = \frac{V_s}{2d} x \quad [9.23]$$

i.e. the relationship between E_{Th} and x is linear and independent of frequency ω . We note that the alternative way of connecting the sensor into the bridge so that $Z_1 = 1/(j\omega C_1)$ and $Z_2 = 1/(j\omega C_2)$ gives an output voltage which is non-linearly related to x and dependent on the supply frequency ω . A similar result is obtained with the variable reluctance push-pull displacement sensor (Figure 8.11). This has:

$$L_1 = \frac{L_0}{1 + \alpha(a-x)}, \quad L_2 = \frac{L_0}{1 + \alpha(a+x)}$$

and from Figure 9.5(b) we have $Z_1 = j\omega L_1$, $Z_2 = Z_3 = R$, $Z_4 = j\omega L_2$, giving:

$$E_{Th} = V_s \left(\frac{L_1}{L_1 + L_2} - \frac{1}{2} \right) \quad [9.24]$$

from which

Output voltage for inductive push-pull bridge

$$E_{Th} = \frac{V_s \alpha x}{2(1 + \alpha a)} \quad [9.25]$$

Again the relationship between E_{Th} and x is linear and frequency independent. In practice, however, these sensors will have associated resistance so that eqns [9.23] and [9.25] are only approximate.

9.2

Amplifiers

Amplifiers are necessary in order to amplify low-level signals, e.g. thermocouple or strain gauge bridge output voltages, to a level which enables them to be further processed.

9.2.1 The ideal operational amplifier and its applications

Ideal operational amplifier characteristics

The operational amplifier can be regarded as the basic building block for modern amplifiers. It is a high gain, integrated circuit amplifier designed to amplify signals from d.c. up to many kHz. It is not normally used by itself but with external feedback networks to produce precise transfer characteristics which depend almost entirely on the feedback network. Usually there are two input terminals and one output terminal, the voltage at the output terminal being proportional to the difference between the voltages at the input terminals. Figure 9.6 shows the circuit symbol and a simplified equivalent circuit for an operational amplifier. Table 9.1 summarises the main characteristics of an ideal operational amplifier together with those of a typical practical amplifier OPA27.^[1]

Figure 9.6 Circuit symbol and simplified equivalent circuit for operational amplifier.

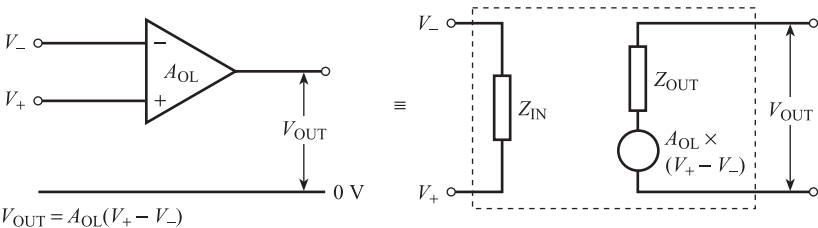


Table 9.1 Ideal and typical operational amplifier characteristics.

Parameter	Ideal op-amp	OPA27 ^[1]
D.C. open-loop gain A_{OL}	∞	120 dB (10^6)
Input impedance Z_{IN}	∞	6 M Ω
Output impedance Z_{OUT}	0	70 Ω
Input offset voltage V_{OS}	0	25 μ V
Temp. coeff. of input offset voltage γ	0	0.6 μ V $^{\circ}$ C $^{-1}$
Input bias current i_B	0	40 nA
3 dB bandwidth 0 to f_B	0 to ∞	0 to 10 Hz
Common mode rejection ratio, CMMR	∞	114 dB

*Summing point
conditions for ideal
operational amplifier
with negative feedback*

$$\begin{aligned} i_- = i_+ &= 0 \\ V_- &= V_+ \end{aligned} \quad [9.26]$$

The first condition results from assuming input impedance $Z_{IN} = \infty$. The second condition results from assuming that $A_{OL} \rightarrow \infty$: since $V_{OUT} = A_{OL}(V_+ - V_-)$ and V_{OUT} is finite, then the differential voltage $(V_+ - V_-) \rightarrow 0$ i.e. $V_+ = V_-$.

We now derive the transfer characteristics for six voltage amplifier circuits.

Inverting amplifier

Figure 9.7 shows a signal source V_{IN} , R_{IN} connected to an inverting amplifier. Since $V_+ = V_- = 0$:

$$i_{IN} = \frac{V_{IN}}{R_{IN}}, \quad i_F = \frac{V_{OUT}}{R_F}$$

Also

$$i_{IN} + i_F = i_- = 0$$

giving

$$\frac{V_{IN}}{R_{IN}} + \frac{V_{OUT}}{R_F} = 0$$

$$V_{OUT} = \frac{-R_F V_{IN}}{R_{IN}} \quad [9.27]$$

Thus the output voltage V_{OUT} is proportional to the input voltage V_{IN} with gain $-R_F/R_{IN}$. The resistance R is set equal to the resistance of R_{IN} in parallel with R_F , i.e. $R = \frac{R_{IN} R_F}{R_{IN} + R_F}$. This is to balance the d.c. bias currents to inverting and non-inverting inputs.

Figure 9.7
Inverting amplifier.

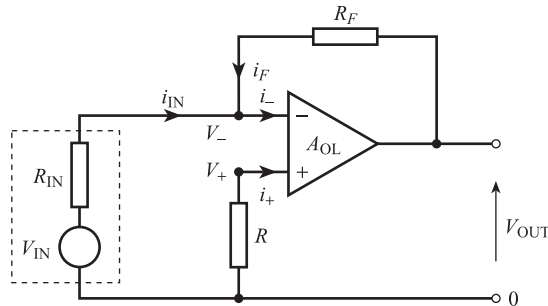


Figure 9.8

Non-inverting amplifier.

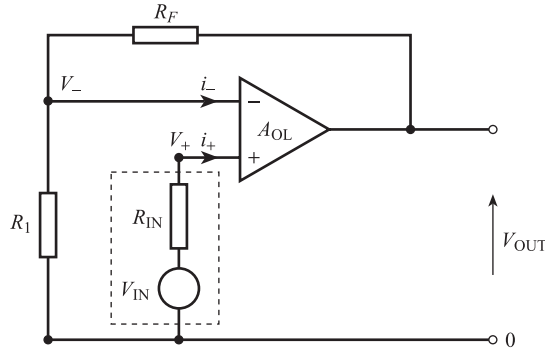
**Non-inverting amplifier**

Figure 9.8 shows a non-inverting amplifier circuit. Since $i_+ = 0$, $V_+ = V_{IN}$; also R_F and R_1 form a potential divider so that:

$$V_- = V_{OUT} \left(\frac{R_1}{R_1 + R_F} \right)$$

Also since $V_+ = V_-$

$$V_{OUT} \left(\frac{R_1}{R_1 + R_F} \right) = V_{IN}$$

$$V_{OUT} = \left(1 + \frac{R_F}{R_1} \right) V_{IN} \quad [9.28]$$

Thus output voltage V_{OUT} is proportional to input voltage V_{IN} with gain $\left(1 + \frac{R_F}{R_1} \right)$.

Voltage follower

Figure 9.9 shows a signal source V_{IN} , R_{IN} connected to a voltage follower circuit. Here $V_- = V_{OUT}$, and since $i_+ = 0$, $V_+ = V_{IN}$. Since $V_- = V_+$ then:

$$V_{OUT} = V_{IN} \quad [9.29]$$

This circuit has unity gain, high input impedance and low output impedance and is used as a buffer amplifier to connect a voltage signal source with high output impedance to a low impedance load.

Differential amplifier

Figure 9.10 shows two voltage sources V_1 , R_{IN} and V_2 , R_{IN} connected to a differential amplifier. V_2 , R_{IN} and R_F form a potential divider, so that:

Figure 9.9
Voltage follower.

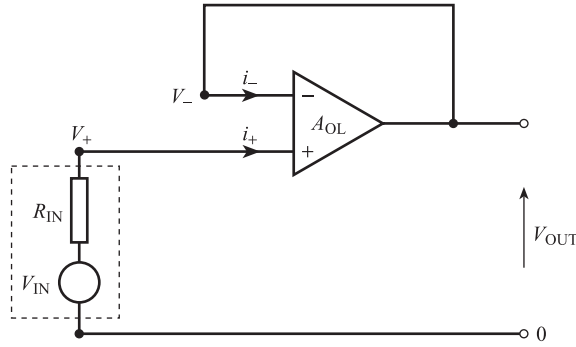
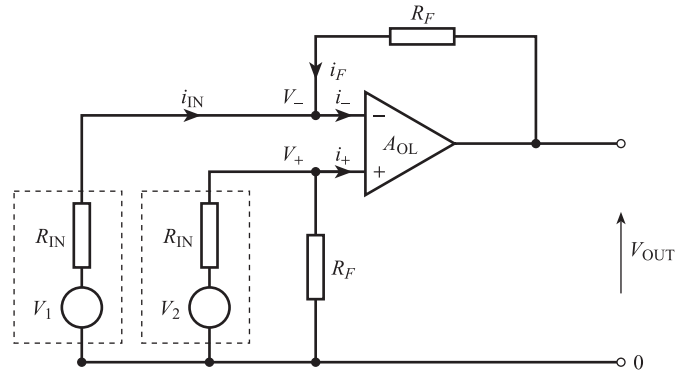


Figure 9.10
Differential amplifier.



$$V_+ = V_2 \left(\frac{R_F}{R_F + R_{IN}} \right)$$

Also:

$$i_{IN} + i_F = i_- = 0$$

where

$$i_{IN} = \frac{(V_1 - V_-)}{R_{IN}}, \quad i_F = \frac{(V_{OUT} - V_-)}{R_F}$$

giving:

$$\frac{(V_1 - V_-)}{R_{IN}} + \frac{(V_{OUT} - V_-)}{R_F} = 0$$

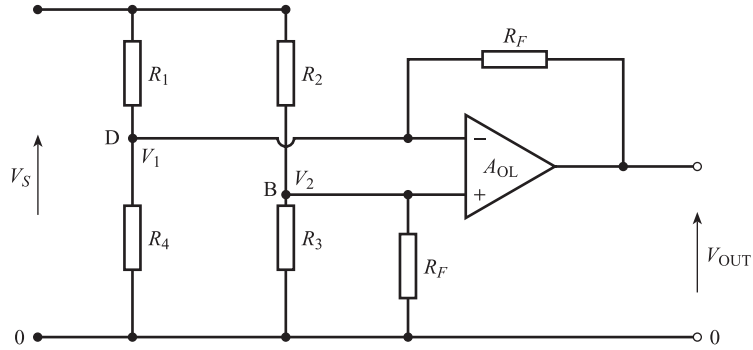
and

$$V_- = \frac{R_{IN} \cdot V_{OUT}}{(R_F + R_{IN})} + \frac{R_F V_1}{(R_F + R_{IN})}$$

Since $V_- = V_+$

$$\frac{R_{IN} V_{OUT}}{(R_F + R_{IN})} + \frac{R_F V_1}{(R_F + R_{IN})} = \frac{R_F V_2}{(R_F + R_{IN})}$$

Figure 9.11 Strain gauge bridge connected to differential amplifier.



giving:

$$V_{\text{OUT}} = \frac{R_F}{R_{\text{IN}}} (V_2 - V_1) \quad [9.30]$$

The output voltage V_{OUT} is therefore proportional to the voltage *difference* ($V_2 - V_1$), and the closed-loop gain is R_F/R_{IN} .

Figure 9.11 shows a strain gauge bridge connected to a differential amplifier. Here R_1 and R_3 experience tensile strain $+e$ so that:

$$R_1 = R_3 = R_0(1 + Ge)$$

while R_2 and R_4 experience compressive strain $-e$ so that:

$$R_2 = R_4 = R_0(1 - Ge)$$

R_{IN} is the Thévenin resistance of the potential divider R_1, R_4 (also R_2, R_3): R_{IN} is therefore equal to the resistance of R_1 and R_4 in parallel (Figure 5.7). Since the strain e is much less than 1, we have:

$$R_{\text{IN}} \approx R_0/2$$

V_2 is the potential at B and is set by the potential divider R_3, R_2 giving:

$$V_2 = V_S \left(\frac{R_3}{R_3 + R_2} \right) = \frac{V_S}{2} (1 + Ge)$$

V_1 is the potential at D and is set by the potential divider R_4, R_1 giving:

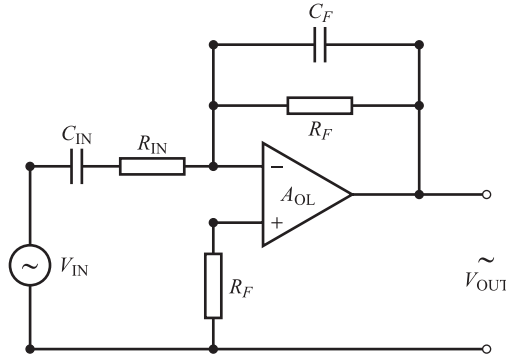
$$V_1 = V_S \left(\frac{R_4}{R_4 + R_1} \right) = \frac{V_S}{2} (1 - Ge)$$

Since

$$V_{\text{OUT}} = \frac{R_F}{R_{\text{IN}}} (V_2 - V_1)$$

we obtain:

Figure 9.12
A.C. amplifier.



$$V_{OUT} = 2 \frac{R_F}{R_0} V_S G e \quad [9.31]$$

Typically $V_S = 15 \text{ V}$, $e = 10^{-5}$, $R = 120 \text{ } \Omega$ and $G = 2$; therefore to give $V_{OUT} = 5 \text{ V}$, R_F must be $1 \text{ M}\Omega$.

A.C. amplifier

Figure 9.12 shows an a.c. signal source V_{IN} connected to an inverting amplifier with input resistance R_{IN} , capacitance C_{IN} , feedback resistance R_F and capacitance C_F . The circuit can be analysed using eqn [9.27] with R_{IN} and R_F replaced by complex impedances Z_{IN} and Z_F to give:

$$V_{OUT} = -\frac{Z_F}{Z_{IN}} V_{IN}$$

Here Z_{IN} is the series combination of R_{IN} and C_{IN} , i.e.:

$$Z_{IN} = R_{IN} + (1/C_{IN}s)$$

where s is the Laplace operator.

Z_F is the parallel combination of R_F and C_F , i.e.:

$$Z_F = \frac{R_F}{R_F C_F s + 1}$$

From these equations, the transfer function relating output voltage V_{OUT} to input voltage V_{IN} , for the a.c. amplifier, is:

$$\frac{\tilde{V}_{OUT}}{\tilde{V}_{IN}} = -\frac{R_F}{R_{IN}} \left(\frac{1}{R_F C_F s + 1} \right) \left(\frac{R_{IN} C_{IN} s}{R_{IN} C_{IN} s + 1} \right) \quad [9.32]$$

Figure 9.13 shows the amplitude frequency response characteristics of the amplifier. It has a mid-band gain of R_F/R_{IN} , and a bandwidth between f_1 and f_2 and can be used in a.c. carrier systems (Section 9.3).

Figure 9.13 Ideal frequency response characteristics of a.c. amplifier.

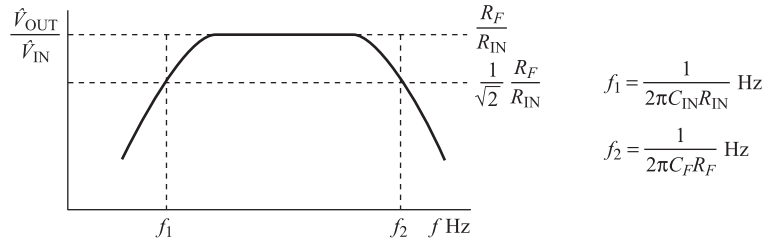
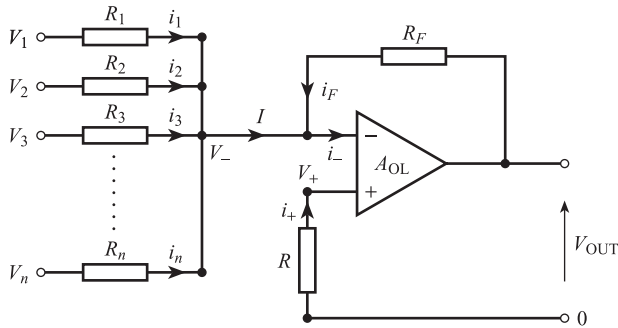


Figure 9.14 Voltage adder.



Voltage adder

Figure 9.14 shows a set of voltages V_1, V_2, \dots, V_n connected into a summing amplifier. Here:

$$V_- = V_+ = 0$$

and

$$i_1 = \frac{V_1}{R_1}, i_2 = \frac{V_2}{R_2}, \dots, i_n = \frac{V_n}{R_n}$$

giving:

$$I = i_1 + i_2 + \dots + i_n = \frac{V_1}{R_1} + \frac{V_2}{R_2} + \dots + \frac{V_n}{R_n}$$

Also

$$i_F = \frac{V_{OUT}}{R_F}, I + i_F = i_- = 0, i_F = -I$$

giving:

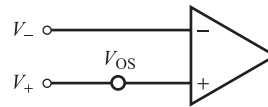
$$V_{OUT} = -R_F \left(\frac{V_1}{R_1} + \frac{V_2}{R_2} + \frac{V_3}{R_3} + \dots + \frac{V_n}{R_n} \right) \quad [9.33]$$

The output voltage V is the sum of the voltages V_1, V_2, \dots, V_n ; each voltage is weighted by a factor R_F/R . This voltage adder forms the basis of an analogue-to-digital converter (Section 10.1). R is set equal to the resistance of $R_1, R_2, \dots, R_n, R_F$ in parallel in order to balance the d.c. bias currents to inverting and non-inverting inputs.

9.2.2 Limitations of practical operational amplifiers

Table 9.1 summarises the characteristics of the practical OPA27 operational amplifier. The parameters V_{OS} , γ , i_B and CMRR influence the d.c. performance of the amplifier and are discussed first.

The existence of input offset voltage V_{OS} means that V_{OUT} is unequal to zero when both V_- and $V_+ = 0$ volts, i.e.



$$V_{OUT} = A_{OL}(V_+ - V_-) + A_{OL}V_{OS} \quad [9.34]$$

Some operational amplifiers have facilities for adjusting V_{OS} to zero, i.e. for obtaining $V_{OUT} = 0$ when $V_+ = V_- = 0$. However, V_{OS} is dependent on the temperature T_E °C of the amplifier environment, where γ is the appropriate temperature coefficient. Thus supposing V_{OS} is set to zero at $T_E = 15$ °C; then if T_E subsequently increases to 25 °C, the resulting input offset voltage is $\gamma(25 - 15)$, i.e. $\approx 6 \mu\text{V}$, which causes a change of approximately $0.6 \times 10^6 \mu\text{V}$, i.e. 0.6 V in the output of the open-loop operational amplifier. The effect on a closed-loop amplifier is considerably reduced but may be still important. For an inverting amplifier we have:

$$V_{OUT} = -\frac{R_F}{R_{IN}}V_{IN} + \left(1 + \frac{R_F}{R_{IN}}\right)V_{OS} \quad [9.35]$$

With a thermocouple temperature sensor, $V_{IN} \approx 40T \mu\text{V}$, i.e. $40 \mu\text{V}$ change for every 1 °C change in measured temperature T . The above variation in V_{OS} with environmental temperature therefore causes the output of the inverting amplifier to drift significantly.

Ideally the output voltage should depend only on the differential voltage ($V_+ - V_-$) and should be independent of the common mode voltage $V_{CM} = (V_+ + V_-)/2$. For a practical operational amplifier, however, we have:

$$V_{OUT} = A_{OL}(V_+ - V_-) + A_{CM}V_{CM} \quad [9.36]$$

where A_{CM} is the common mode gain. A more commonly used term is Common Mode Rejection Ratio (CMRR), where:

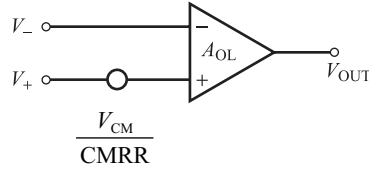
$$\text{CMRR} = \frac{A_{OL}}{A_{CM}}$$

or in decibels

$$(\text{CMRR})_{\text{dB}} = 20 \log_{10} \left(\frac{A_{OL}}{A_{CM}} \right) \quad [9.37]$$

This gives:

$$V_{OUT} = A_{OL} \left[(V_+ - V_-) + \frac{V_{CM}}{CMRR} \right] \quad [9.38]$$



i.e. the equivalent circuit for an open-loop amplifier.

Typically $(CMRR)_{dB} = 110$ dB, i.e. $CMRR \approx 3 \times 10^5$. For a closed-loop differential amplifier (Figure 9.10), we have:

$$V_{OUT} \approx \frac{R_F}{R_{IN}} (V_2 - V_1) + \left(1 + \frac{R_F}{R_{IN}} \right) \frac{V_{CM}}{CMRR} \quad [9.39]$$

If the differential amplifier is used with the strain gauge bridge described in Section 9.2.1 (Figure 9.11), then we have:

$$V_2 - V_1 = V_S G e = 300 \mu V$$

Also $V_{CM} = 7.5$ V, so that $V_{CM}/CMRR = 25 \mu V$.

Thus the common mode voltage can have a significant effect. However, much greater errors can occur in a differential amplifier if there is any mismatch between the values of the two input resistances R_{IN} and the two R_F resistances.

The a.c. performance of a practical operational amplifier is determined by its dynamic characteristics. These are adequately represented by a first-order lag, i.e.

$$\frac{\Delta V_{OUT}}{\Delta(V_+ - V_-)}(s) = \frac{A_{OL}}{1 + \tau s} \quad [9.40]$$

where A_{OL} is the d.c. open-loop gain, τ is the time constant, and $\Delta(V_+ - V_-)$ and ΔV_{OUT} are corresponding small changes in input and output. The variation in open-loop amplifier gain with frequency f is thus given by:

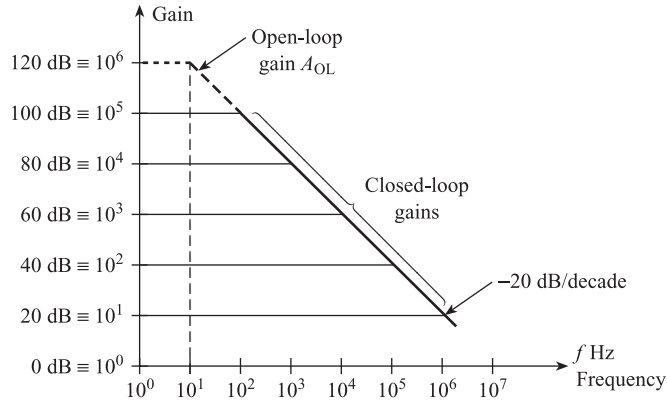
*Gain-frequency
relation for open-loop
amplifier*

$$A_{OL}(f) = \frac{\hat{V}_{OUT}}{(V_+ - V_-)}(f) = \frac{A_{OL}}{\sqrt{1 + (f/f_B)^2}} \quad [9.41]$$

where $f_B = 1/2\pi\tau$ is the -3 dB cut-off frequency.

The open-loop gain-bandwidth product $A_{OL} \times f_B$ is typically $\approx 10^6 \times 10 = 10^7$ Hz. Figure 9.15 shows the variation in gain with frequency for both open- and closed-loop amplifiers. We note that the lower the gain of the closed-loop amplifier the greater the bandwidth. This is because the gain-bandwidth product of a closed-loop amplifier is also equal to the open-loop value of $A_{OL} f_B$. The frequency response of a practical a.c. amplifier (Figures 9.12 and 9.13) depends, to some extent, on the frequency characteristics of the operational amplifier as well as on those of the external components.

Figure 9.15 Typical gain–frequency characteristics for operational amplifier.



9.2.3 Instrumentation amplifiers

An instrumentation amplifier is a high-performance differential amplifier system consisting of several closed-loop operational amplifiers. An ideal instrumentation amplifier gives an output voltage which depends *only* on the difference of two input voltages V_1 and V_2 , i.e.

$$V_{\text{OUT}} = K(V_2 - V_1) \quad [9.42]$$

where the gain K is precisely known and can be varied over a wide range. A practical instrumentation amplifier should have a gain which can be set by a single external resistor and should combine the following:

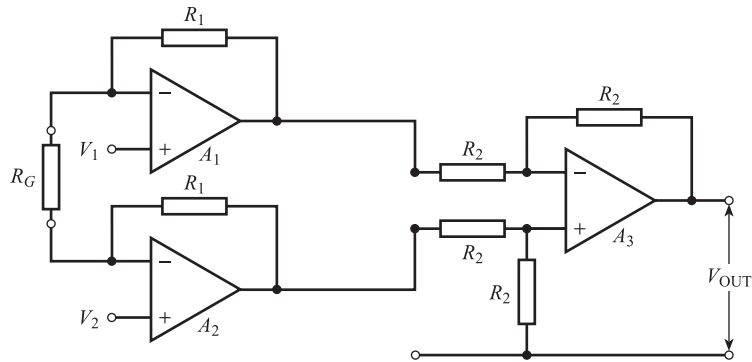
- High input impedance
- High common mode rejection ratio
- Low input offset voltage
- Low temperature coefficient of offset voltage.

The differential amplifier already discussed (Figure 7.4(d)), which uses a single operational amplifier, is inadequate: in order to obtain high gain, R_{IN} must be low. This means low input impedance; also the differential amplifier is highly susceptible to any mismatch in resistance values.

Figure 9.16 shows a typical instrumentation amplifier system consisting of three operational amplifiers, A_1 , A_2 and A_3 . The two input non-inverting amplifiers A_1 and A_2 provide an overall differential gain of $(1 + 2R_1/R_G)$ and a common mode gain of unity. The output amplifier A_3 is a unity gain differential amplifier. A typical precision instrumentation amplifier, INA 115, has:^[2]

- $Z_{\text{IN}} \approx 10^{10} \Omega$ in parallel with 6 pF.
- $(\text{CMRR})_{\text{dB}} \approx 115 \text{ dB min.}$
- Offset voltage $V_{\text{OL}} \approx 50 \mu\text{V max.}$
- Temperature coefficient of offset voltage $\gamma \approx 0.25 \mu\text{V } ^\circ\text{C}^{-1}$.

Figure 9.16 Typical instrumentation amplifier.



9.3 A.C. carrier systems

Two of the most difficult problems in conditioning low-level d.c. signals from sensors are external interference in the signal circuit (Section 6.4) and amplifier drift (Section 9.2.2). These problems can be avoided if the signal is converted into a.c. form, amplified and then reconverted into d.c.

The initial or primary elements in an a.c. carrier system are usually of one of the following types:

- (a) R , L , C sensors in a suitable deflection bridge (Section 9.1)
- (b) An LVDT sensor (Section 8.3).

The output voltage of a four-element strain gauge bridge with a cantilever load cell is given by $E_{Th} = GV_S e$ (eqn [9.18]), i.e. the output signal is proportional to the *product* of the supply voltage V_S and the strain signal e . Similar results are obtained with other bridge circuits (eqns [9.15], [9.17], [9.19], [9.20], [9.23] and [9.25]); in each case the bridge output voltage is proportional to the product of the supply voltage and the measured variable. The output voltage of the LVDT sensor (Section 8.3) is also approximately proportional to the product of supply voltage and displacement x of the core from the null point. In an a.c. carrier system the supply voltage is a.c., i.e. $V_S = \hat{V}_S \sin 2\pi f_s t$, with a frequency f_s of typically a few kHz. The measured variable is also a function of time; in the case of a step change in force on the cantilever, the strain variation $e(t)$ is a damped sine wave. In the general case $e(t)$ is a complicated function of time which can be expressed as a sum of many sine waves (Sections 4.3 and 6.2):

$$e(t) = \sum_{i=1}^m \hat{e}_i \sin 2\pi f_i t$$

Figure 9.17 shows a typical measurement signal frequency spectrum containing frequencies from $f_1 = 0$ Hz up to f_m (often only a few Hz).

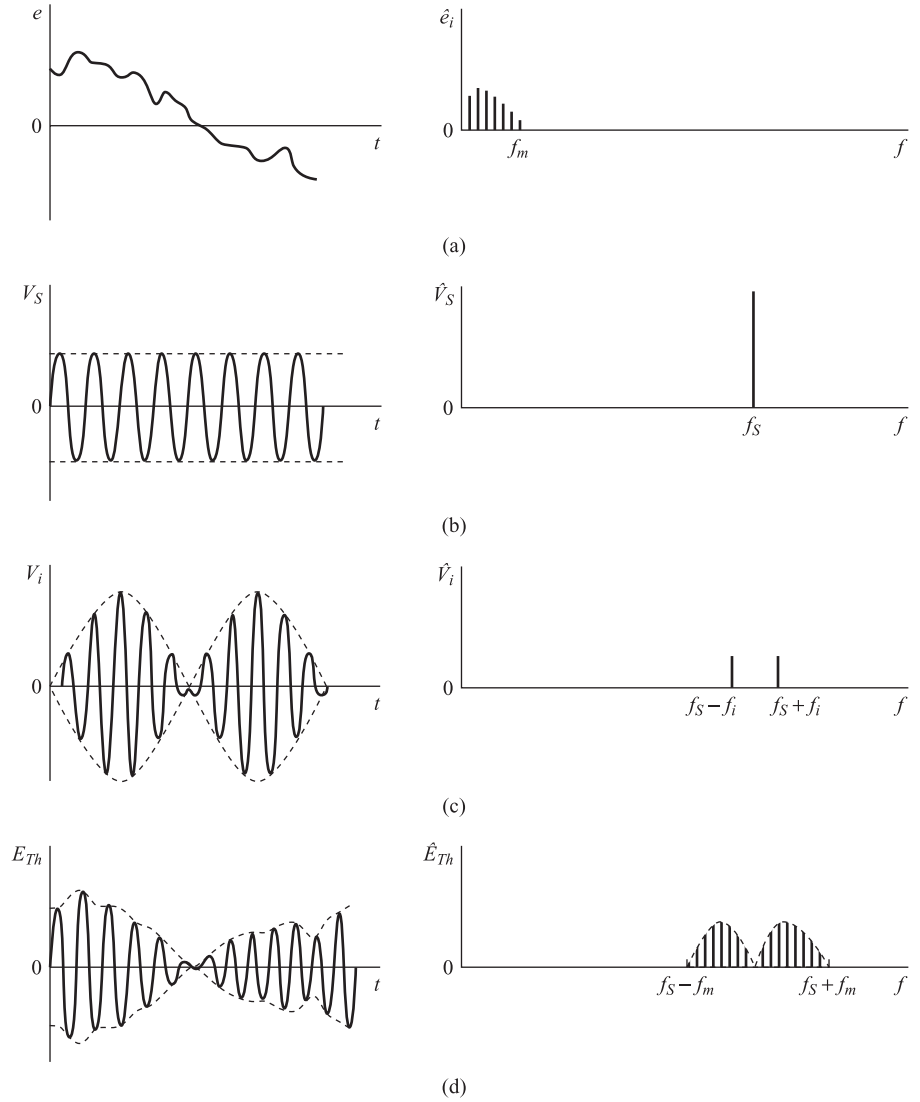
The bridge output voltage is thus given by:

$$E_{Th} = \sum_{i=1}^m \hat{V}_i \sin 2\pi f_i t \sin 2\pi f_s t \quad [9.43]$$

Figure 9.17

Corresponding waveforms and frequency spectra for amplitude modulation:

- (a) Measurement signal
(b) Supply voltage
(c) AM with sinusoidal modulating signal
(d) Complete AM waveform.



where $\hat{V}_i = G\hat{V}_S\hat{e}_i$. If we, for the moment, consider only the i th component:

$$V_i = \hat{V}_i \sin 2\pi f_i t \sin 2\pi f_S t$$

then we have a sine wave of frequency f_S and amplitude $\hat{V}_i \sin 2\pi f_i t$. This is amplitude modulation (AM); here the amplitude of the carrier signal frequency f_S is being altered according to the instantaneous value of the modulating signal frequency f_i (Figure 9.17). Using the identity:

$$\sin A \sin B = \frac{1}{2} \cos(A - B) - \frac{1}{2} \cos(A + B)$$

the amplitude modulated signal

$$V_i = \hat{V}_i \sin 2\pi f_S t \sin 2\pi f_i t$$

can be expressed in the form:

$$V_i = \frac{\hat{V}_i}{2} \cos 2\pi(f_s - f_i)t - \frac{\hat{V}_i}{2} \cos 2\pi(f_s + f_i)t \quad [9.44]$$

Thus the AM signal is the sum of two cosinusoidal signals with frequencies $f_s - f_i$ and $f_s + f_i$; the corresponding frequency spectrum (Figure 9.17) contains two lines. This form of amplitude modulation is called **balanced amplitude modulation**, because when $\hat{e}_i = 0$, $\hat{V}_i = 0$, i.e. the bridge is balanced. This means also that the frequency spectrum does not contain the carrier frequency f_s ; there are only two lines at the sideband frequencies $f_s \pm f_i$. Hence the alternative name is **double sideband carrier suppressed amplitude modulation**. We see that each frequency f_i in the modulating signal spectrum contributes two lines to the AM spectrum, e.g. if $f_s = 1$ kHz, then $f_i = 1$ Hz gives lines at 999 and 1001 Hz. The AM spectrum corresponding to the total modulating signal (0 to f_m Hz) consists therefore of frequencies between $f_s - f_m$ and $f_s + f_m$, e.g. between 995 and 1005 Hz if $f_s = 1$ kHz and $f_m = 5$ Hz.

We see therefore that the operation of multiplication and thence modulation has the effect of shifting the spectrum of the measurement signal from low frequencies to higher frequencies. The amplitudes \hat{V}_i are small but an a.c. amplifier (Figures 9.12 and 9.13) can now be used. The bandwidth frequencies f_1 and f_2 are chosen so that they include the measurement signal between $f_s - f_m$ and $f_s + f_m$ (Figure 9.17), but exclude low frequency drift voltages and 50 Hz mains interference.

In the above example, an amplifier with $f_1 = 900$ Hz and $f_2 = 1100$ Hz will successfully amplify the measurement signal and reject drift and interference. It is important to realise that this system only rejects drift and interference signals which are introduced *after* the modulator; for example, drift in bridge output voltage due to drift in bridge supply voltage will be regarded as part of the measurement signal.

The AM signal must now be demodulated in order to obtain an output voltage which is proportional to the strain signal $e(t)$. Figure 9.18 shows corresponding waveforms for $e(t)$ and supply voltage $V_s(t)$; we see that at time interval t_1 , $e(t_1) = +e_1$ and at time interval t_2 , $e(t_2) = -e_1$. Thus at time t_1 the cantilever is below the neutral position and gauges 1 and 3 are in tension. At time t_2 the cantilever is above the neutral position and gauges 1 and 3 are in compression. The corresponding bridge output voltages are:

$$E_{Th} = +Ge_1 \hat{V}_s \sin 2\pi f_s t \quad \text{at } t_1$$

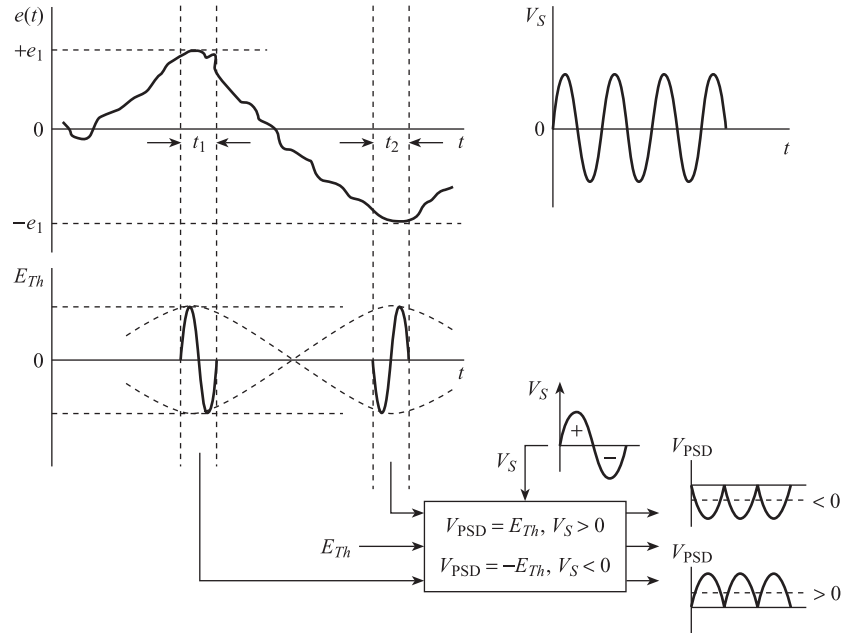
and

$$E_{Th} = -Ge_1 \hat{V}_s \sin 2\pi f_s t = Ge_1 \hat{V}_s \sin(2\pi f_s t + 180) \quad \text{at } t_2$$

i.e. the signals have equal amplitude but are 180° out of phase (Figure 9.18).

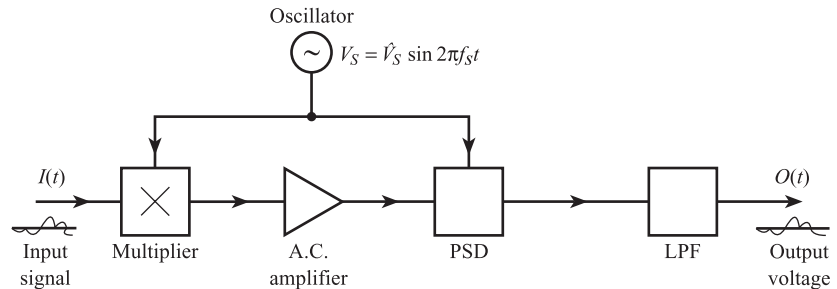
Thus in order to distinguish between the situations at t_1 and t_2 , we need a demodulator which detects this phase difference and gives a positive output voltage when e is positive and a negative voltage when e is negative. Such a demodulator is called a **phase-sensitive demodulator** (PSD). The simplest form of PSD is an amplifier with a gain of ± 1 according to the sign of the supply voltage; that is,

$$\left. \begin{aligned} V_{\text{PSD}} &= E_{Th} & \text{when } V_s > 0 \\ V_{\text{PSD}} &= -E_{Th} & \text{when } V_s < 0 \end{aligned} \right\} \quad [9.45]$$

Figure 9.18 Phase-sensitive demodulation.

The action of this element is shown in Figure 9.18. We see that a low-pass filter (Section 6.5) is required to give the mean value of the output signal. The bandwidth of this filter should be less than f_s in order to filter out carrier frequencies, but greater than f_m in order not to filter out measurement signal frequencies. The complete a.c. carrier system is shown in Figure 9.19.

We have seen above that an a.c. bridge can be used to generate an a.c. voltage from a resistive, capacitive or inductive sensor. This raises the question of how to convert a low-level d.c. voltage signal, e.g. a thermocouple e.m.f., into a.c. form. The usual solution here is to sample the signal at high speed, around 1000 times per second, using a transistor switch or 'chopper' driven by an oscillator. The resulting 'chopped' signal is a series of pulses whose amplitudes correspond to the instantaneous value of the d.c. voltage; this is pulse amplitude modulation (PAM). The PAM signal can be processed by an a.c. amplifier and phase-sensitive demodulator so that the chopper simply replaces the multiplier in Figure 9.19. The resulting **chopper-stabilised amplifier** has excellent drift characteristics.

Figure 9.19 Complete a.c. carrier system.

9.4 Current transmitters

In Section 5.1 we saw that sensing elements could be represented by either a Thévenin voltage source or a Norton current source. In Section 6.3 we saw that a current transmission system rejects series interference more efficiently than a voltage transmission system. In this section we discuss transmitters used in the process industries to give an output d.c. current signal in the standard range 4 to 20 mA proportional to the input measured variable. The output has a **live zero** of 4 mA: this enables a distinction to be made between a zero input situation (output = 4 mA) and a fault situation (output = 0 mA).

These transmitters were initially **closed-loop systems** with **high-gain negative feedback** (Section 3.3). Here the overall transmitter sensitivity depends mainly on the sensitivity of the elements in the feedback path and is largely unaffected by changes in the characteristics of forward path elements, for example amplifier drift. The zero and span of these transmitters can be adjusted but, in the case of force balance systems, the adjustments have to be made mechanically, for example by adjusting the position of a pivot. Closed-loop transmitters have now been largely replaced by **open-loop transmitters**. Here the overall transmitter sensitivity depends on the sensitivity of every element in the system; these element sensitivities can change due to modifying inputs and/or non-linear effects. However, by using precision mechanical components and high-performance electronic integrated circuits, the above effects are minimised and open-loop transmitters are now widely used. They have the advantage that zero and span adjustments can be made electronically, which is more convenient than mechanical adjustment. The most recent development is that of **intelligent** or **'smart' transmitters**: here a microcontroller is incorporated into an open-loop transmitter.^[3] This results in an improvement in overall accuracy and enhanced flexibility and versatility.

9.4.1 Closed-loop transmitters

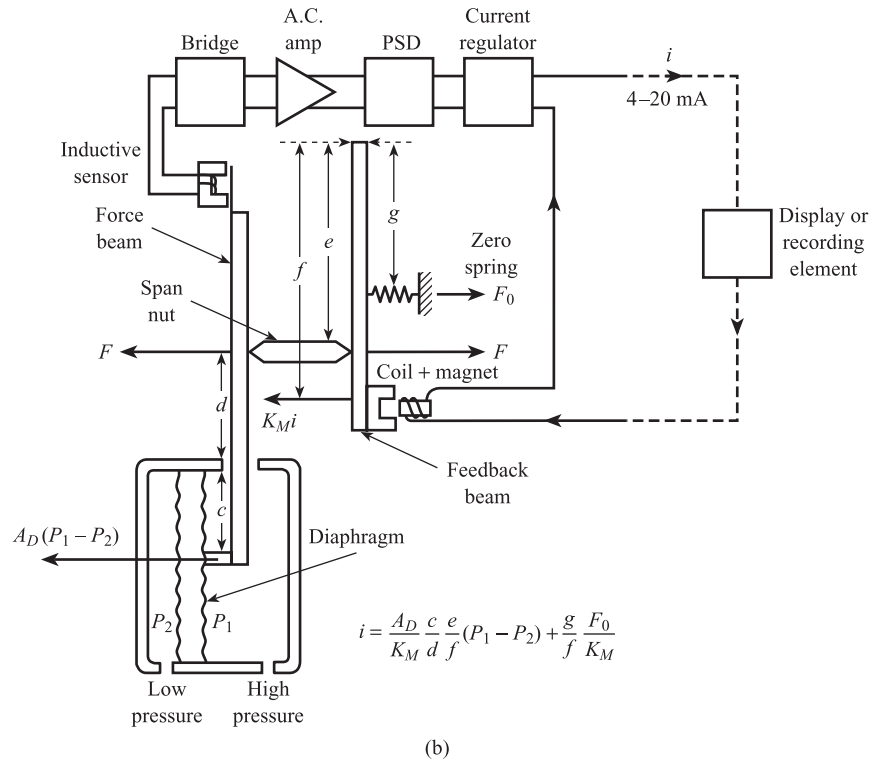
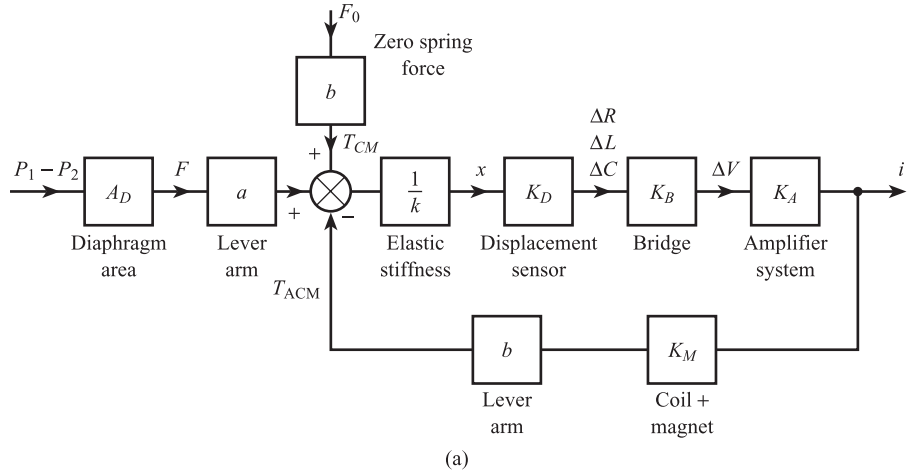
Figure 9.20(a) shows a simplified block diagram of a closed-loop differential pressure transmitter operating on the force balance or, more accurately, torque balance principle. The diaphragm force $(P_1 - P_2)A_D$ produces a clockwise torque $A_D(P_1 - P_2)a$ on the lever arm, which is supported by a clockwise torque F_0b due to the zero spring. The output current i is fed back to a coil, inside a permanent magnet; this produces a force $K_M i$ on the lever arm and a corresponding anticlockwise torque $K_M i b$. Any imbalance of these torques causes the lever to rotate; the resulting displacement x is measured by a sensor–bridge–amplifier system. The resulting change in output current is fed back to the coil and magnet to adjust the anticlockwise torque until an approximate torque balance is again obtained.

Inspection of Figure 9.20(a) gives

$$i = \frac{K_D K_B K_A / k}{1 + K_D K_B K_A b K_M / k} [a A_D (P_1 - P_2) + b F_0] \quad [9.46]$$

If the gain K_A of the amplifier system is high so that $\frac{K_D K_B K_A b K_M}{k}$ is very much greater than 1, then eqn [9.46] reduces to:

Figure 9.20 Closed-loop differential pressure transmitters:
(a) Simplified block diagram
(b) Simplified schematic diagram.



$$i = \frac{a}{b} \frac{A_D}{K_M} (P_1 - P_2) + \frac{F_0}{K_M} \quad [9.47]$$

From eqn [9.47] we see that transmitter sensitivity = $(a/b)(A_D/K_M)$ and zero bias = F_0/K_M . The closed-loop transmitter has the advantage, therefore, that the overall sensitivity is independent of diaphragm stiffness, displacement sensor sensitivity and amplifier gain, so that once set it should remain constant and not drift. The main disadvantage of this type of transmitter is that sensitivity (input span) and zero adjustments must be made mechanically; the input span is adjusted by altering the

ratio a/b and the zero by altering F_0 . For example, suppose $A_D = 10^{-2} \text{ m}^2$ (circular diaphragm approximately 11 cm in diameter) and $K_M = 10^3 \text{ N A}^{-1}$. Then in order to obtain an output range of 4 to 20 mA, corresponding to 0 to 10^4 Pa (0 to 1 metre water), we require $a/b = 0.16, f_0 = 4 \text{ N}$.

Figure 9.20(b) shows a simplified schematic diagram of a two-lever torque balance differential pressure transmitter using an inductive displacement sensor.

9.4.2 Open-loop transmitters

Open-loop differential pressure transmitters

Figure 9.21(a) shows a general simplified block diagram for an open-loop differential pressure transmitter. The input differential pressure $(P_1 - P_2)$ acting over the area A_D of the sensing diaphragm produces a deflecting force $A_D(P_1 - P_2)$ which is opposed by the elastic spring force kx . The resulting diaphragm deformation x is small ($\approx 10^{-5} \text{ m}$) and approximately proportional to $(P_1 - P_2)$. This displacement can be measured using variable capacitance, variable reluctance or resistive strain gauge sensors. Another possibility is to use a piezoresistive sensor consisting of a silicon diaphragm with diffused p - or n -type material to give four strain gauges. With strain gauge elements, a d.c. four-element strain gauge bridge is used; the amplifier system consists of an instrumentation amplifier and output current regulator. With capacitive or inductive sensors, an a.c. bridge is used with a carrier amplifier system consisting of an a.c. amplifier, phase sensitive demodulator, d.c. amplifier and output current regulator. Span and zero adjustments are made electronically via the amplifier system.

Figure 9.21(b) shows a **differential capacitance displacement sensor**. The input differential pressure causes the sensing diaphragm to be displaced a small distance x to the left. This in turn causes C_1 to fall from C_0 to $C_0 - \Delta C$ and C_2 to increase from C_0 to $C_0 + \Delta C$, where ΔC is the change in capacitance proportional to $(P_1 - P_2)$. The capacitances are incorporated in an a.c. bridge circuit, similar to Figure 9.5(a), which has:

$$Z_1 = \frac{1}{j\omega C_1}, Z_2 = Z_3 = R, Z_4 = \frac{1}{j\omega C_2}$$

The bridge output voltage is therefore given by:

$$\begin{aligned} \Delta V &= V_s \left(\frac{C_2}{C_1 + C_2} - \frac{1}{2} \right) \\ &= V_s \left(\frac{C_0 + \Delta C}{C_0 - \Delta C + C_0 + \Delta C} - \frac{1}{2} \right) \end{aligned} \quad [9.48]$$

which simplifies to:

$$\Delta V = \frac{V_s}{2C_0} \Delta C \quad [9.49]$$

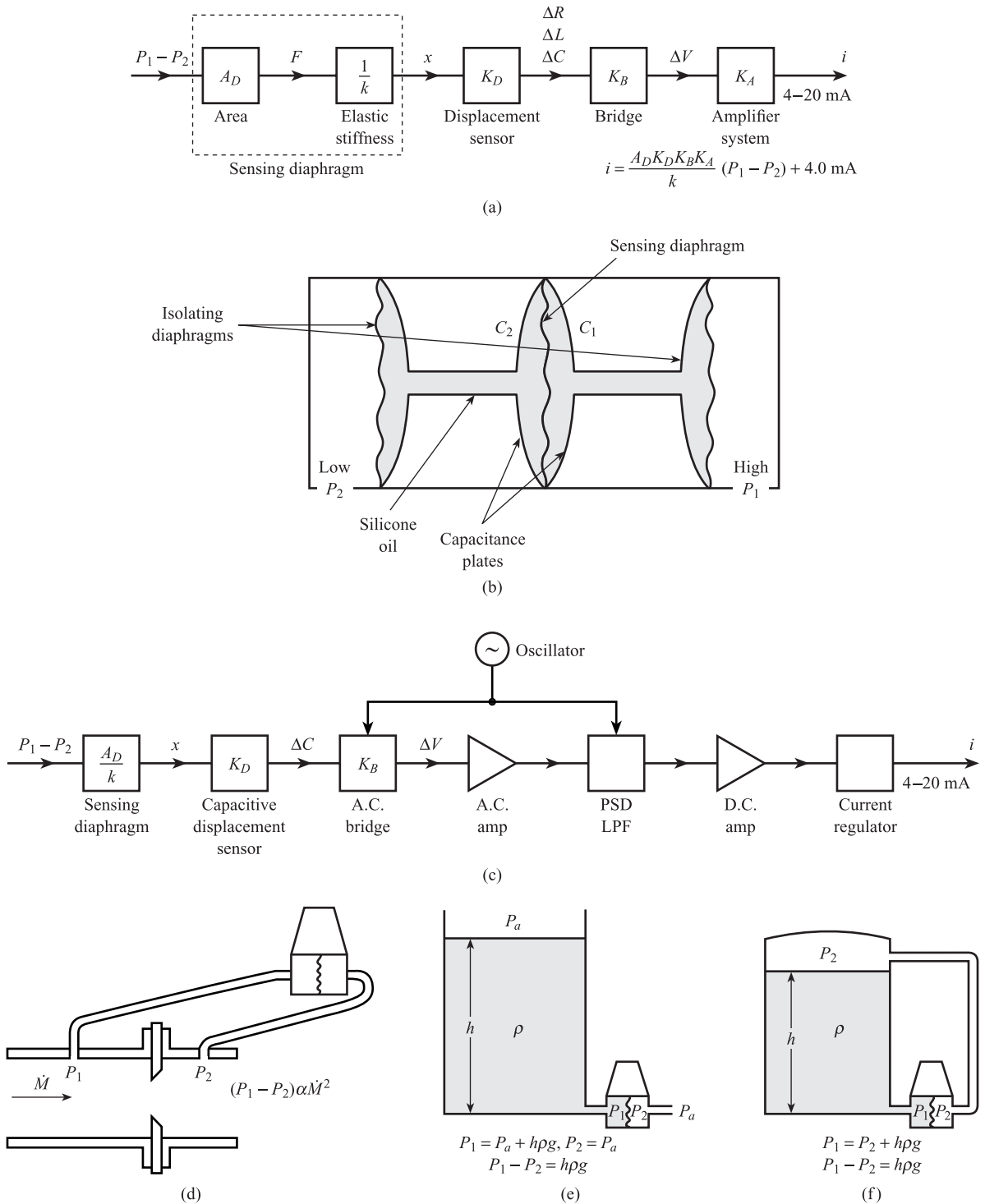


Figure 9.21 Open-loop differential pressure transmitters: (a) General block diagram; (b) Differential capacitance – principle; (c) Differential capacitance – block diagram; (d) Application – flow measurement; (e) Application – level measurement open vessel; (f) Application – level measurement closed vessel.

Thus ΔV is proportional to ΔC and the bridge sensitivity K_B is equal to $V_S/2C_0$. Figure 9.21(c) shows a block diagram of the complete transmitter; typically the overall accuracy is $\pm 0.25\%$.

This type of transmitter is widely used in the process industries for measuring pressure, flow rate and liquid level. The transmitter can be used for measuring gauge pressure (pressure relative to atmosphere) by opening the low pressure chamber to atmosphere, i.e. setting P_2 equal to atmospheric pressure P_a . By evacuating and sealing the low pressure chamber, i.e. setting P_2 equal to zero, the transmitter can be used for measuring absolute pressure (pressure relative to vacuum).

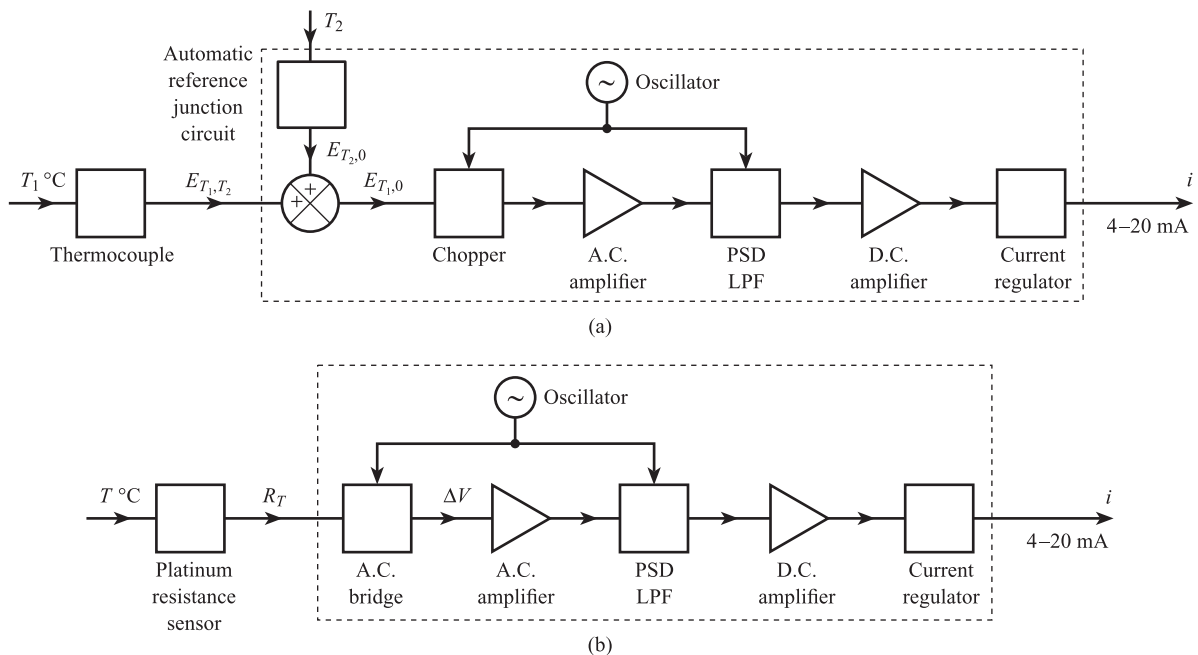
Figure 9.21(d) shows the use of the transmitter with a differential pressure flowmeter to measure mass flow rate \dot{M} of a fluid in a pipe; here differential pressure $(P_1 - P_2)$ is proportional to \dot{M}^2 (Section 12.3.1). Figures 9.21(e) and (f) show the application of the transmitter to the measurement of liquid level in open and closed vessels; in both cases differential pressure is proportional to the height h of liquid.

Open-loop temperature transmitters

Figure 9.22 shows block diagrams for two types of open-loop transmitter. Both use an a.c. carrier amplifier system (Section 9.3) and give a 4–20 mA d.c. current output.

In the millivolt input type, Figure 9.22(a), the input is a thermocouple e.m.f. E_{T_1, T_2} . The automatic reference junction circuit provides an e.m.f. equal to $E_{T_2, 0}$; this is added to E_{T_1, T_2} to give a compensated e.m.f. $E_{T_1, 0}$ which is relative to a fixed reference junction temperature of 0°C (Section 8.5). This e.m.f. is then ‘chopped’ to give the a.c. voltage necessary for the carrier system. This type of transmitter can be located close to the process so that the signal is transmitted to a remote control room as a 4–20 mA current using normal leads. This is simpler and less prone to

Figure 9.22 Open-loop temperature transmitters:
(a) Millivolt input
(b) Resistance input.



external interference than the alternative of transmitting the basic millivolt e.m.f. E_{T_1, T_2} using extension leads as in Figure 8.17(d).

In the resistance input type, Figure 9.22(b), the input is the resistance R_T of a resistance sensor. This is incorporated into a deflection bridge circuit which gives a voltage output ΔV proportional to temperature T (Section 9.1.1 and eqn [9.15]). Problem 9.16 shows a four-lead resistance sensor with two sensor leads and two dummy leads, incorporated into a deflection bridge circuit. Here the bridge output voltage is independent of the lead resistance R_C and therefore the temperature of the plant environment. The a.c. bridge output voltage necessary for the carrier system is obtained either by using an a.c. bridge supply or by using a d.c. bridge supply and ‘chopping’ the resulting d.c. bridge output voltage.

9.4.3 Intelligent or smart transmitters

By incorporating a microcontroller into the basic open-loop transmitter, not only is the accuracy of the transmitter increased but flexibility and versatility are enhanced. An intelligent or smart transmitter can perform the following functions.

Computer calculation of measured value (Section 3.3). Here the microcontroller solves the **inverse equation** to calculate an accurate value of the measured variable from the sensor output signal. This means that non-linear, hysteresis and environmental effects in the sensor can be compensated for. The overall accuracy of a smart transmitter is therefore typically $\pm 0.1\%$ of span compared with $\pm 0.25\%$ for a conventional transmitter. This accurate measured value in engineering units is then converted into a standard 4–20 mA current output.

Remote diagnosis of faults. Signals at different points in the transmitter are continuously monitored and the actual values compared with expected values. Both the existence and the nature of a fault can be detected in this way.

Remote re-ranging. Span and zero adjustments can be made remotely from the control room rather than at the transmitter itself.

Remote identification. The transmitter identification number and maintenance records are stored in the computer memory; this information can again be accessed remotely.

Digital communications. A digital communications signal can be superimposed on the 4–20 mA analogue current signal.

Local indication of measured value. An analogue indication or digital display of measured value is available at the transmitter.

Figure 9.23 is a block diagram of a smart differential pressure transmitter.^[3] The differential capacitance pressure sensor of Figure 9.21(b) gives a change in capacitance ΔC which depends on input differential pressure $(P_1 - P_2)$. This is converted into a d.c. voltage V_1 by the signal conditioning system of Figure 9.21(c). The relationship between $(P_1 - P_2)$ and V_1 is non-linear and is also affected by changes in the temperature of the sensor. ΔT is the deviation in temperature from standard conditions.

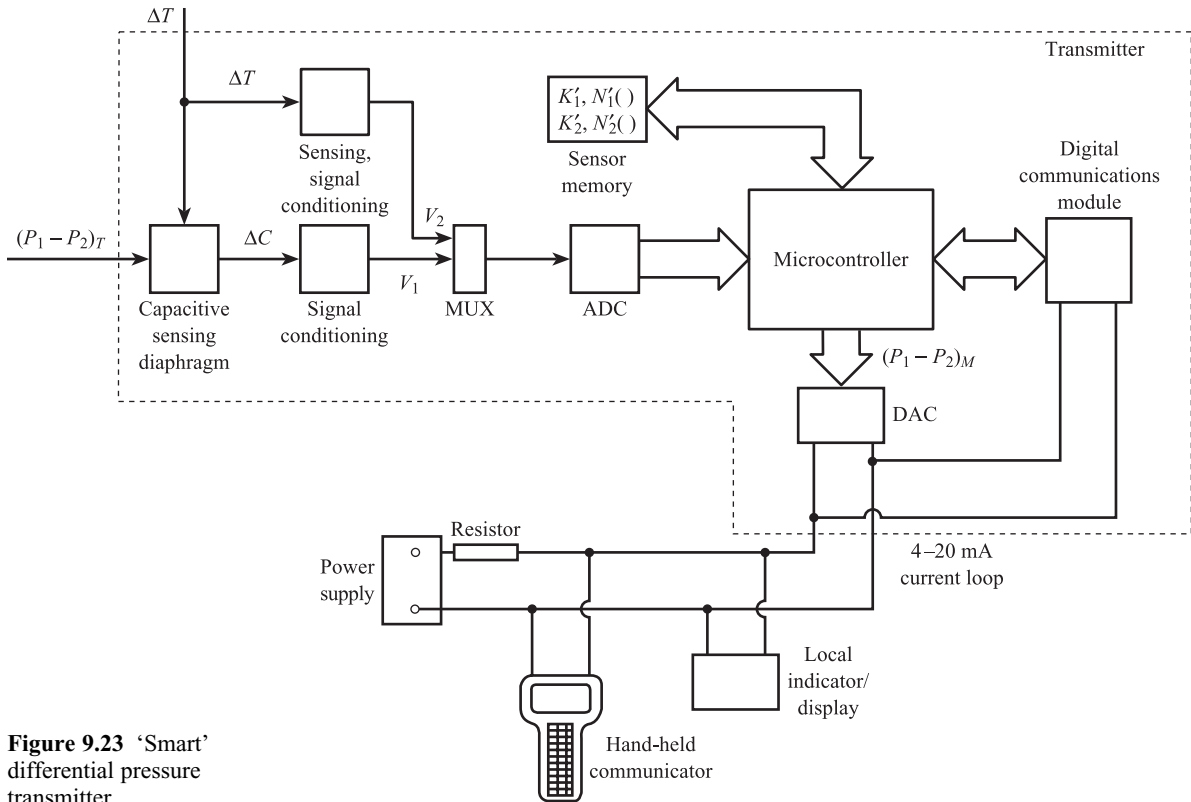


Figure 9.23 ‘Smart’ differential pressure transmitter.

Calibration of a given sensor/signal conditioning element gives corresponding values of $(P_1 - P_2)$, V_1 and ΔT and an inverse equation of the form (eqn [3.17]):

$$P_1 - P_2 = K'_1 V_1 + N'_1(V_1) + a'_1 + K'_M \Delta T V_1 + K'_I \Delta T \quad [9.50]$$

The coefficients K'_1 , a'_1 , etc., are specific to an individual element. Similarly ΔT is measured with a temperature sensor and appropriate signal conditioning element to give a d.c. output voltage V_2 . Here the inverse equation is:

$$\Delta T = K'_2 V_2 + N'_2(V_2) + a'_2 \quad [9.51]$$

where again K'_2 , $N'_2()$ and a'_2 are specific to an individual element. The coefficients K'_1 , $N'_1()$, K'_2 , $N'_2()$, etc., are stored in a sensor memory which is identified with the individual differential pressure and temperature sensors.

The voltages V_1 and V_2 are then input to a **time division multiplexer** (Section 18.1) which transfers them one at a time to an analogue-to-digital converter (ADC) (see Section 10.1). The ADC gives a parallel digital output signal proportional to V_1 or V_2 . This is fed to a microcontroller along with the inverse equation coefficients from the sensor memory. The microcontroller solves eqns [9.51] and [9.50] to give an accurate measured value of the differential pressure $(P_1 - P_2)$ in engineering units. If the transmitter is being used to measure flow rate or liquid level, the measured value of flow rate or level is calculated in engineering units from $(P_1 - P_2)$. This measured value is then output from the microcontroller to a digital-to-analogue converter (DAC) (see Section 10.1). The DAC forms a 4–20 mA current loop with a d.c. power

supply and a series resistor; an analogue indicator and/or recorder is connected into the loop to display the measured value of $(P_1 - P_2)$.

The measured value of $(P_1 - P_2)$ is also transferred from the computer to a digital communications module. This gives a serial digital signal corresponding to $(P_1 - P_2)$ using **frequency shift keying** (FSK) (see Section 18.6). This is a sinusoidal signal at two distinct frequencies, one corresponding to a binary '1' and the other to binary '0'. The FSK signal (typical amplitude of 0.5 mA) is then superimposed on the 4–20 mA analogue signal; this means that no d.c. component is added to the 4–20 mA signal (Section 18.7). Communication between the transmitter and the outside world is via a hand-held communicator which is connected into the current loop. There is two-way communication between the communicator and the microcontroller via the digital communications module. Thus a technician can transmit information requesting a range change and receive information back confirming that the change has been implemented.

9.5

Oscillators and resonators

In Section 9.3 we studied a.c. carrier systems, where the amplitude of a sinusoidal voltage depends on the magnitude of the measured variable – **amplitude modulation** (AM); these systems reject external interference added after the modulator. An alternative is **frequency modulation** (FM), where the frequency of a sinusoidal voltage depends on the magnitude of the measured variable. FM systems also reject interference and have the following advantages over AM systems:

- (a) The external interference affects signal amplitude more than it affects signal frequency; FM is therefore inherently more resistant to interference than AM.
- (b) By counting pulses over a fixed time interval, a frequency signal can easily be converted to digital form (Section 10.1.4).

Examples of sensors which directly generate frequency signals are the variable reluctance tachogenerator (Section 8.4), the turbine flowmeter (Section 12.3.2) and the vortex flowmeter (Section 12.3.3). Because of the advantages of frequency signals, however, we need general methods for producing them. These are **oscillators**, which are purely electrical, and **resonators**, which are electromechanical. Oscillators and resonators are feedback systems which rely on the dynamic property of a closed-loop system, consisting of elements with dynamic characteristics, to sustain continuous oscillations, if certain conditions are satisfied.

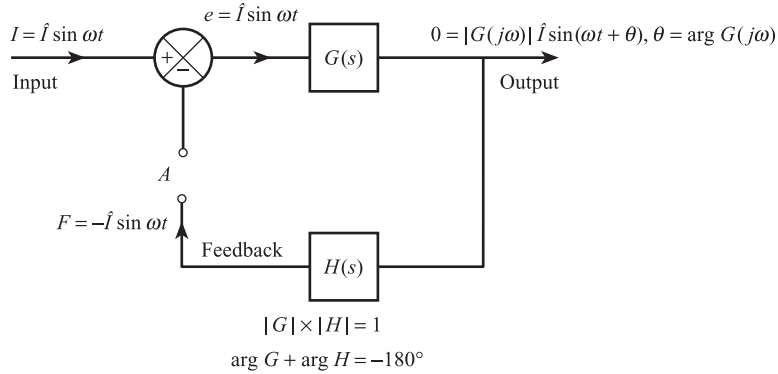
Figure 9.24 shows a closed-loop system consisting of a forward path element with transfer function $G(s)$ and a feedback path element with transfer function $H(s)$. Suppose that an input signal $I = \hat{I} \sin \omega t$ is applied to the system with the feedback link broken at A . The corresponding feedback signal F is also sinusoidal and is given by (Section 4.2):

$$F = |G(j\omega)| |H(j\omega)| \hat{I} \sin(\omega t + \phi) \quad [9.52]$$

where:

$$\phi = \arg G(j\omega) + \arg H(j\omega) \quad [9.53]$$

If we make the product of magnitudes $|G| \times |H|$ equal to 1 and the sum of arguments (phase angles) equal to -180° , then $F = -\hat{I} \sin \omega t$, i.e. F has the same amplitude as

Figure 9.24 Principle of oscillator/resonator.

the input signal but is 180° out of phase. If the feedback link is now closed, then $e = 2\hat{I} \sin \omega t$, but if $I(t)$ is reduced to zero, then $e = \hat{I} \sin \omega t$ and the system remains in continuous oscillation at frequency ω . The conditions for continuous oscillation at ω are therefore:

*Conditions for
continuous
oscillation at ω*

$ G(j\omega) \times H(j\omega) = 1$ $\arg G(j\omega) + \arg H(j\omega) = -180^\circ$	[9.54]
---	--------

Under these conditions there is a sinusoidal output signal at frequency ω for no input signal.

9.5.1 Oscillators

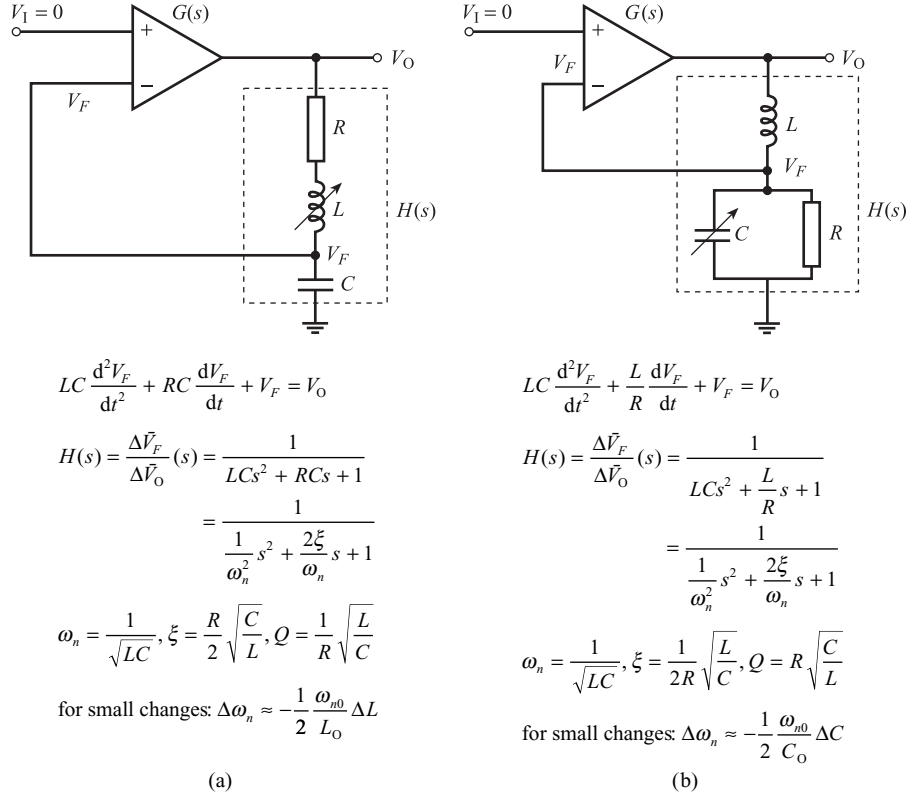
Here the feedback element $H(s)$ is an L – C – R circuit and $G(s)$ is an amplifier (maintaining amplifier). In Figure 9.25(a) the L – C – R circuit consists of an inductive sensor (pure inductance with series loss resistance) in series with a fixed pure capacitance; in Figure 9.25(b) the L – C – R circuit consists of a capacitive sensor (pure capacitance with parallel loss resistance) in series with a fixed pure inductance. From Figure 9.25 we see that each circuit is described by a second-order differential equation and a corresponding second-order transfer function of the form:

$$H(s) = \frac{1}{\frac{1}{\omega_n^2} s^2 + \frac{2\xi}{\omega_n} s + 1} \quad [9.55]$$

The figure also gives expressions for the natural frequency ω_n , the damping ratio ξ and the Q factor for the circuits. Since $\omega_n = 1/\sqrt{LC}$ for both circuits, a change in L for the inductive sensor or a change in C for the capacitive sensor both result in a change in circuit natural frequency. We therefore design the system to oscillate at ω_n . From eqn [9.55] we have:

$$H(j\omega) = \frac{1}{\left(1 - \frac{\omega^2}{\omega_n^2}\right) + j2\xi \frac{\omega}{\omega_n}} \quad \text{and} \quad H(j\omega_n) = \frac{1}{j2\xi} \quad [9.56]$$

Figure 9.25 Oscillators:
(a) Inductive sensor
(b) Capacitive sensor.



From eqns [9.54], in order to sustain oscillations at $\omega = \omega_n$, the gain and phase of the maintaining amplifier must satisfy the conditions:

Gain and phase conditions for maintaining amplifier in oscillator

$$|G(j\omega_n)| = \frac{1}{|H(j\omega_n)|} = 2\xi = \frac{1}{Q} \quad [89.57]$$

$$\arg G(j\omega_n) = -180^\circ - \arg H(j\omega_n) = -90^\circ$$

over the range of ω_n corresponding to the range of variation of either L or C .

Figure 9.26 shows a frequency system for measuring sinusoidal variations in pressure. The capacitive pressure sensor of Figure 8.9 is used; for small changes, the

Figure 9.26 Frequency pressure measurement system.

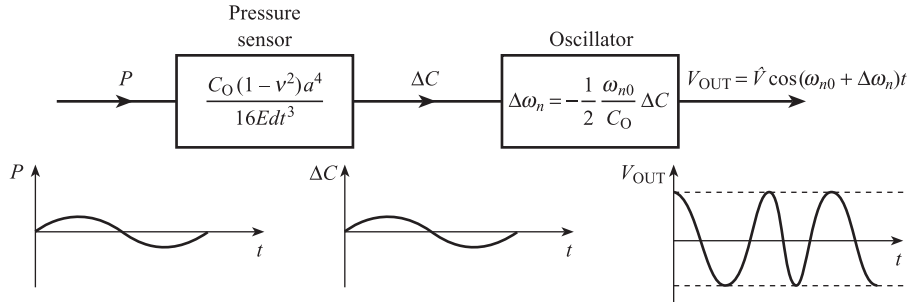
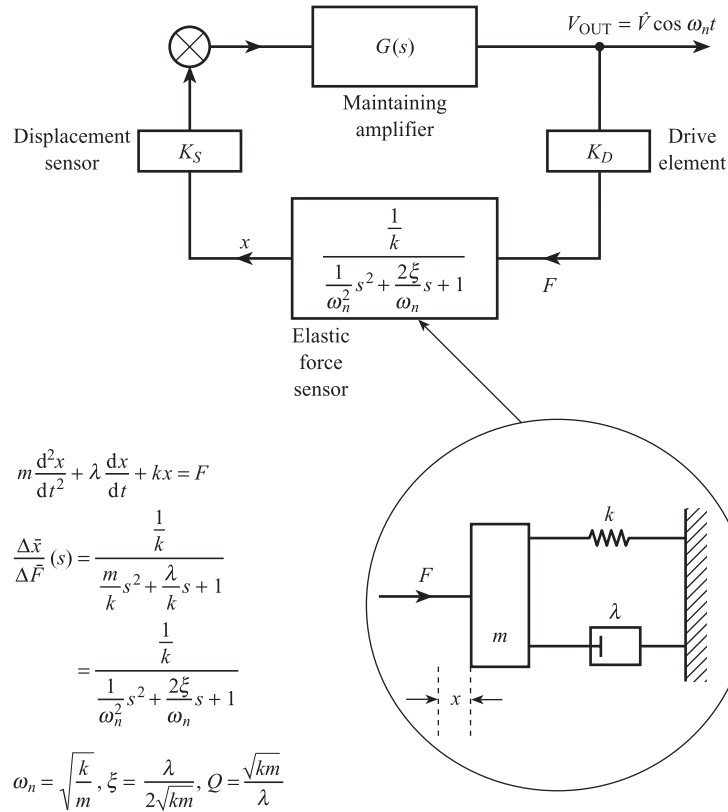


Figure 9.27 Block diagram of resonator.



increase in capacitance ΔC is proportional to the applied pressure P (eqn [8.22]). The sensor is incorporated in the oscillator circuit of Figure 9.25(b); the change $\Delta \omega_n$ in circuit natural frequency is approximately proportional to ΔC . The frequency of the oscillator output signal varies sinusoidally with time, giving rise to the **frequency modulated signal** shown.

9.5.2 Resonators

Figure 9.27 shows the block diagram for a resonator.^[4] The forward path element $G(s)$ is again an amplifier; the feedback element $H(s)$ consists of:

- A drive element to convert voltage to force
- An elastic force sensor to convert force to displacement
- A displacement sensor to convert displacement into voltage.

From Figure 9.27 we have:

$$H(s) = \frac{K_S K_D}{k} \frac{1}{\frac{1}{\omega_n^2} s^2 + \frac{2\xi}{\omega_n} s + 1} \quad [9.58]$$

The figure also gives expressions for natural frequency ω_n , damping ratio ξ and Q factor. Since $\omega_n = \sqrt{k/m}$, changes in either effective stiffness k or effective mass

m cause corresponding changes in ω_n . Thus provided the system is designed to oscillate at ω_n , it could be used, for example, to sense force variations (affecting k) or density variations (affecting m). From eqns [9.54] and [9.58], in order to sustain oscillations at $\omega = \omega_n$, the gain and phase of the maintaining amplifier must satisfy the conditions:

Gain and phase conditions for maintaining oscillations in a resonator

$$|G(j\omega_n)| = \frac{1}{|H(j\omega_n)|} = \frac{2\xi k}{K_S K_D} = \frac{\lambda}{K_S K_D} \sqrt{\frac{k}{m}} \quad [9.59]$$

$$\arg G(j\omega_n) = -180^\circ - \arg H(j\omega_n) = -90^\circ$$

over the range of ω_n , corresponding to the range of variation in either m or k .

Figure 9.28(a) shows a vertical section through a resonant sensor for measuring absolute pressure. The sensor uses a vibrating flat circular plate. If the plate is clamped around the circumference and subject to a radial tensile force F , then the fundamental frequency ω_n of transverse vibration is given by:

$$\omega_n = 2\pi f_n = K \sqrt{\frac{F}{\sigma}} \quad [9.60]$$

where σ is the mass per unit area of the disc and K is a constant. Therefore if F is changed, f_n changes. The flat plate is a circular silicon wafer which is clamped around its circumference by pier supports; these form part of a silicon structure. The

Figure 9.28
Examples of resonators:
(a) Vibrating plate element
(b) Vibrating tube element.

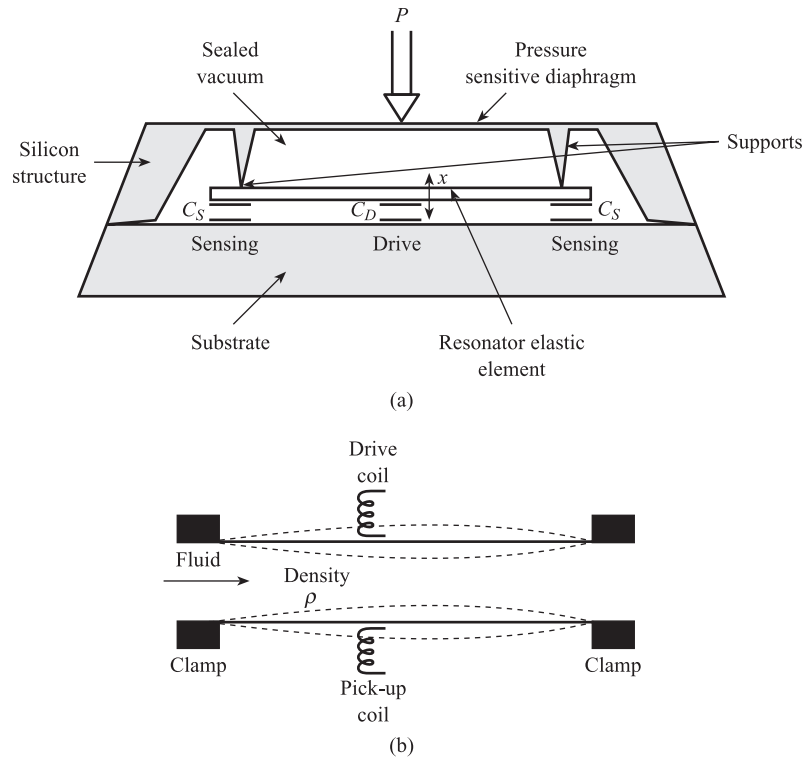


plate is enclosed in a sealed vacuum chamber. An increase in the downward pressure P applied to the pressure sensitive diaphragm at the top produces an increase in the tensile force F on the plate and a corresponding increase in natural frequency f_n . Two metal electrodes, an inner circular electrode and an outer annular electrode, are deposited on the bottom surface of the plate. Corresponding and concentric electrodes are deposited on the upper surface of the substrate to form two capacitances. The outer capacitance C_s is the sensor capacitance, which detects the transverse displacement x of the plate. Changes in C_s are converted into a d.c. voltage signal using an a.c. bridge, an a.c. amplifier and a phase sensitive detector.

The inner capacitance C_D provides the drive element; if a voltage V is applied across the plates then the plates acquire equal and opposite charges, causing an attractive force between the plates. The drive force per unit voltage K_D is given by:

$$K_D = \frac{\epsilon_0 AV}{d^2} \quad [9.61]$$

where ϵ_0 is the permittivity of free space, A the area of the plates and d their separation.

The relationship between pressure P and natural frequency f_n is non-linear and is also affected by the temperature T of the plate. Temperature is measured using a forward-biased diode within the substrate; the relationship between output voltage V and T is again non-linear. The overall inverse equation for pressure is:^[5]

$$P = \sum_{i=0}^3 \sum_{j=0}^3 K_{ij} f_n^i V^j \quad [9.62]$$

This equation involves powers of f_n , powers of V and cross-terms such as $f_n V^2$; there are 16 calibration constants K_{ij} .

Figure 9.28(b) shows a vibrating thin-walled tube element, inside which a fluid is flowing.^[6] The tube is clamped at each end and a transverse force is applied to the tube using a drive coil connected to the maintaining amplifier. This causes transverse deflection of the tube centre, which is sensed by a pick-up coil and fed back to the amplifier. By correct choice of amplifier gain and phase characteristics, the tube is continuously maintained in transverse oscillation at a fundamental frequency $f_n = (1/2\pi)(\sqrt{k/m})$. The total vibrating mass m and therefore f_n depend on the fluid density ρ , as well as on the mass of the tube itself. The inverse equation for density is:

$$\rho = \frac{A}{f_n^2} + \frac{B}{f_n} + C \quad [9.63]$$

where A , B and C are constants. This tube arrangement is particularly useful for liquids and liquid–solid mixtures.

Conclusion

This chapter has studied methods of converting the output of sensing elements into a form suitable for further processing; this is usually a d.c. voltage, d.c. current or variable frequency a.c. voltage. The chapter began by examining the principles of **bridge circuits**, which convert a change in resistance, capacitance or inductance into a d.c. or a.c. voltage. It then went on to study the principles and characteristics of ideal and practical **operational amplifiers**. The third section looked at **a.c. carrier**

systems where **amplitude modulation** is used to reject external interference. In the fourth section three types of **current transmitter** were studied: **closed-loop**, **open-loop** and **intelligent**; these give a standard 4 to 20 mA output signal. The final section examined **oscillators** and **resonators**, which give a variable frequency signal, i.e. **frequency modulation**.

References

- [1] Burr-Brown 1999 *I C Data Book – Linear Products*, OPA27: ultra low noise precision operational amplifier.
- [2] Burr-Brown 1999 *I C Data Book – Linear Products*, INA115: precision instrumentation amplifier.
- [3] Rosemount Ltd 1989 *Technical Information on Model 3051C Smart Differential Pressure Transmitter*.
- [4] LANGDON R M 1985 'Resonator sensors – a review', *J. Phys. E: Scientific Instruments*, vol. 18, pp. 103–15.
- [5] FROST D (Druck Ltd) 1999 'Resonant silicon pressure transducers', *Sensors and Transducers Conf.*, NEC Birmingham.
- [6] Sarasota Automation Instrumentation Division 1985 *Technical Information on FD 800 Series Density Meters*.

Problems

- 9.1 A platinum resistance sensor has a resistance of $100\ \Omega$ at $0\ ^\circ\text{C}$ and a temperature coefficient of resistance of $4 \times 10^{-3}\ ^\circ\text{C}^{-1}$. Given that a 15 V supply is available, design a deflection bridge giving an output range of 0 to 100 mV for an input range of 0 to $100\ ^\circ\text{C}$:
- (a) using the procedure summarised by eqns [9.7] and [9.8];
 - (b) using the linear approximation of eqn [9.15].

Give values for all circuit components and assume a high impedance load.

- (c) How should the circuit be altered if the input range is changed to 50 to $150\ ^\circ\text{C}$?
- 9.2 A thermocouple has an e.m.f. of 4.1 mV at $100\ ^\circ\text{C}$ and 16.4 mV at $400\ ^\circ\text{C}$ relative to a cold junction of $0\ ^\circ\text{C}$. A deflection bridge incorporating a nickel metal resistance sensor is to be used as the voltage source $E_{T_{2,0}}$ necessary for automatic reference compensation of the thermocouple e.m.f. The nickel sensor has a resistance of $10\ \Omega$ at $0\ ^\circ\text{C}$ and a temperature coefficient of resistance of $6.8 \times 10^{-3}\ ^\circ\text{C}^{-1}$. Design the deflection bridge assuming a 1 V supply is available. (*Hint*: eqns [8.49] and [9.15].)

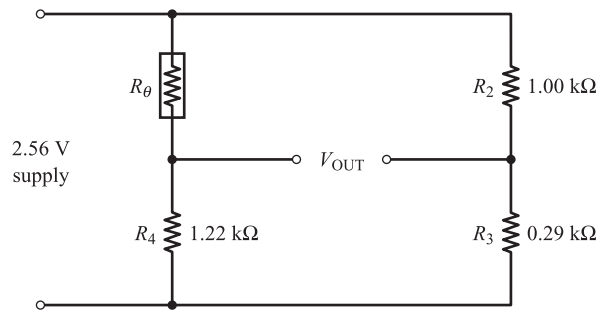
- 9.3 The resistance $R_\theta\ \text{k}\Omega$ of a thermistor at $\theta\ \text{K}$ is given by:

$$R_\theta = 1.68 \exp \left[3050 \left(\frac{1}{\theta} - \frac{1}{298} \right) \right]$$

The thermistor is incorporated into the deflection bridge circuit shown in Fig. Prob. 3.

- (a) Assuming that V_{OUT} is measured with a detector of infinite impedance, calculate:
 - (i) the range of V_{OUT} corresponding to an input temperature range of 0 to $50\ ^\circ\text{C}$;
 - (ii) the non-linearity at $12\ ^\circ\text{C}$ as a percentage of full-scale deflection.
- (b) Calculate the effect on the range of V_{OUT} of reducing the detector impedance to $1\ \text{k}\Omega$.

Figure Prob. 3.



- 9.4 The resistance $R_\theta \Omega$ of a thermistor varies with temperature $\theta \text{ K}$ according to the following equation:

$$R_\theta = 0.0585 \exp\left(\frac{3260}{\theta}\right)$$

Design a deflection bridge, incorporating the thermistor, to the following specification:

- Input range 0 to 50 °C
- Output range 0 to 1.0 V
- Relationship between output and input to be approximately linear.

- 9.5 Four strain gauges, with specification given below, are available to measure the torque on a cylindrical shaft 4 cm in diameter connecting a motor and load.

- (a) Draw clearly labelled diagrams showing:
- (i) the arrangement of the gauges on the shaft;
 - (ii) the arrangement of the gauges in the bridge circuit, for optimum accuracy and sensitivity.
- (b) Calculate the maximum achievable bridge out-of-balance voltage for an applied torque T of 10^3 N m given the following:

Tensile and compressive strains $= \pm T/\pi S a^3$ where $S = 1.1 \times 10^{11} \text{ N m}^{-2}$ is the shear modulus of the shaft material and a is the radius of the shaft in metres.

Strain gauge data:

Resistance	= 120 Ω
Gauge factor	= 2.1
Maximum current	= 50 mA

- 9.6 A load cell consists of a domed vertical steel cylinder 20 cm high and 15 cm in diameter. Four flat surfaces, at right angles to each other, are cut on the vertical surface so as to form 10 cm squares. Resistance strain gauges are attached to these flat surfaces so that two gauges (on opposite faces) suffer longitudinal compression and two gauges (on the other pair of opposite faces) suffer transverse tension. The strain gauges have the following specification:

Resistance	= 100 Ω
Gauge factor	= 2.1
Maximum gauge current	= 30 mA

The gauges are connected in a temperature-compensated bridge and the out-of-balance signal is input to a differential amplifier. Calculate the minimum amplifier gain if the amplifier output voltage is to be 1 V for a compressive force of 10^5 N.

Young's modulus for steel	$= 2.1 \times 10^{11} \text{ N m}^{-2}$
Poisson's ratio for steel	$= 0.29$

- 9.7 The unbonded strain gauge accelerometer of Figure 8.20 and Section 9.1.2 has a natural frequency of 175 Hz and an input range of 0 to 5g. Given that the strain due to prestressing is twice the maximum acceleration-induced strain, use the strain gauge data given below to calculate the range of the bridge output voltage.

Resistance	$= 120 \Omega$
Gauge factor	$= 2.1$
Maximum current	$= 50 \text{ mA}$
Length at zero acceleration	$= 2.3 \text{ cm}$

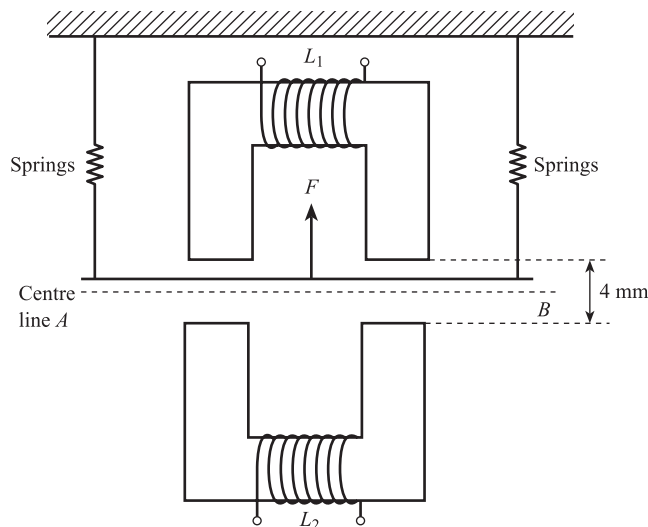
- 9.8 The capacitance level transducer of Section 8.2 and Figure 8.9 is to be used to measure the depth h of liquid in a tank between 0 and 7 m. The total length l of the transducer is 8 m and the ratio b/a of the diameters of the concentric cylinders is 2.0. The dielectric constant ϵ of the liquid is 2.4 and the permittivity of free space ϵ_0 is 8.85 pF m^{-1} . The transducer is incorporated into the deflection bridge of Figure 9.5(a) with $R_2 = 100 \Omega$, $R_3 = 10 \text{ k}\Omega$ and $V_s = 15 \text{ V}$.

- Calculate the value of C_0 so that the amplitude \hat{E}_{Th} is zero when the tank is empty.
- Using this value of C_0 calculate \hat{E}_{Th} at maximum level.
- Explain why the relationship between \hat{E}_{Th} and h is non-linear and calculate the non-linearity at $h = 3.5 \text{ m}$ as a percentage of full-scale deflection.

- 9.9 Figure Prob. 9 shows a variable reluctance force sensor which is incorporated into the bridge circuit of Figure 9.5(b). When the applied force is zero the armature is positioned along the centre line AB .

- Explain why the sensor would be suitable for measuring force signals containing frequencies between 0 and 10 Hz.

Figure Prob. 9.



- (b) Sketch the frequency spectrum of the bridge output voltage.
- (c) Use the data given below to calculate the form of the bridge output voltage when $F = +1.0 \text{ N}$ and $F = -1.0 \text{ N}$.
- (d) Using the results of (c), explain how to demodulate the bridge output voltage.

Overall spring stiffness = 10^3 N m^{-1}

Effective mass of spring and armature = $25 \times 10^{-3} \text{ kg}$

Damping ratio = 0.7

Inductance of each coil = $\frac{20}{1 + 2d} \text{ mH}$ (d = air gap in mm)

Amplitude of bridge supply = 1 V

Frequency of bridge supply = 1000 Hz

- 9.10** A strain in the range 0 to 10^{-3} is to be measured using a four-strain-gauge bridge connected to a differential amplifier (Figure 9.11). The strain gauges have resistance 120Ω and gauge factor 2.1, and the supply voltage is 15 V. Find the value of the amplifier feedback resistance if the output signal range is 0 to 1.0 V.
- 9.11** Design an a.c. amplifier system which incorporates an ideal operational amplifier, to meet the following specification:
- Midband input impedance = $10 \text{ k}\Omega$
 - Midband gain = 100
 - Bandwidth = 100 to 1000 Hz.
- 9.12** The electronic torque balance D/P transmitter of Figure 9.20(a) is to have an output range of 4 to 20 mA for input ranges between 0 to 0.5 m of water and 0 to 5.0 m of water. The diaphragm has a diameter of 10 cm and the maximum value of a/b is 2.0. Take $g = 9.81 \text{ m s}^{-2}$, and the density of water = 10^3 kg m^{-3} .
- (a) Complete the design by calculating the electromagnetic force constant and the zero spring force.
- (b) Find the values of a/b corresponding to input ranges of 0 to 1 m and 0 to 5 m.
- 9.13** The variable reluctance displacement transducer of Problem 8.4 is incorporated into an electrical oscillator circuit with a fixed capacitance of 500 pF. Find the variation in frequency of the oscillator output signal corresponding to a variation in air gap of between 1 and 3 mm.
- 9.14** The natural frequency f_n Hz of a thin-walled tube executing circumferential vibrations in a fluid of density $\rho \text{ kg m}^{-3}$ is given by:

$$f_n^2 = \frac{1.25 \times 10^{10}}{\rho + 350}$$

The stiffness of the tube is 10^9 N m^{-1} and the damping ratio $\xi = 0.1$. The tube is incorporated in a closed-loop system which also includes a drive coil of sensitivity 10^4 N V^{-1} and a displacement sensing coil of sensitivity 10^3 V m^{-1} . The system is required to give a sinusoidal voltage output signal whose frequency changes with fluid density in the range $\rho = 250$ to 1500 kg m^{-3} . Find the gain and phase characteristics of the maintaining amplifier. What is the effect of changes in fluid viscosity on the system?

- 9.15** A solid-state capacitive humidity sensor has a capacitance given by:

$$C = 1.7 \text{ RH} + 365 \text{ pF}$$

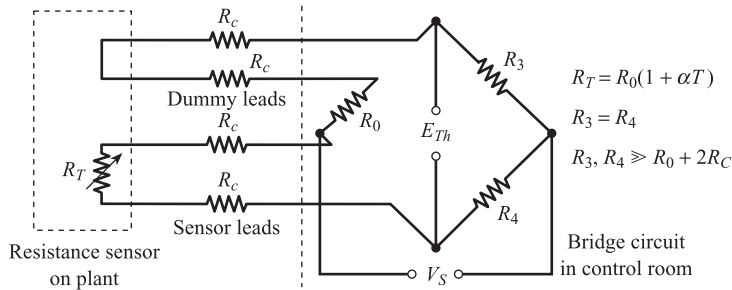
where RH is the percentage relative humidity. The sensor has an associated parallel resistance of $100 \text{ k}\Omega$. The sensor is incorporated into a feedback oscillator system with a pure inductance

and a maintaining amplifier. The oscillator is to give a sinusoidal output voltage at the natural frequency of the L - C circuit for a relative humidity between 5 and 100%.

- Draw a diagram of a suitable oscillator system.
- If the frequency of the output signal is to be 100 kHz at RH = 100%, calculate the required inductance.
- Find the gain and phase characteristics of the maintaining amplifier.

9.16 Figure Prob. 16 shows a four-lead bridge circuit; R_c is the resistance of the leads connecting the sensor to the bridge circuit. Show that $E_{Th} \approx V_S(R_0/R_3)\alpha T$, i.e. the bridge output voltage is unaffected by changes in R_c .

Figure Prob. 16.



9.17 A resonant pressure sensor consists of a vibrating circular silicon plate. The natural frequency f_n Hz of the plate is given by:

$$P = 10^4 - 30f_n + 0.12f_n^2$$

where P Pa is the input pressure. The stiffness of the plate is 10^7 N/m and the damping ratio is 0.01. The sensitivity of the capacitance displacement sensor is 2×10^2 V/m and the sensitivity of the drive element is 5 N/V.

- If the sensor is to have an output frequency range of 1.0 to 3.0 kHz, what is the input pressure range?
- What are the gain and phase characteristics of the maintaining amplifier?

Basic problems

9.18 A deflection bridge has a supply voltage of 10 V. Find the bridge output voltage when:

- $R_1 = 101 \Omega$, $R_2 = 99 \Omega$, $R_3 = 101 \Omega$, $R_4 = 99 \Omega$
- $R_1 = 100.1 \Omega$, $R_2 = 99.9 \Omega$, $R_3 = 100.1 \Omega$, $R_4 = 99.9 \Omega$.

9.19 A platinum resistance sensor has a resistance of 100Ω at 0°C and a temperature coefficient of resistance of $4 \times 10^{-3} ^\circ\text{C}^{-1}$.

- The above sensor is incorporated into a bridge circuit which has $R_3/R_2 = 100$. Find the value of R_4 such that $V_{OUT} = 0$ at 0°C .
- Complete the bridge design by calculating the supply voltage required to give $V_{OUT} = 100$ mV at 100°C .

9.20 A simple weight sensor consists of a steel cantilever clamped at one end with the free end subject to a downward force F .

- If $F = 10^2$ N, use the data given below to calculate the strain halfway along the cantilever.

- (b) Four identical strain gauges (specified below) are to be bonded onto the cantilever halfway along its length as shown in Figure 8.20(a). Use the data given below to calculate the bridge output voltage corresponding to the above conditions.

$$\text{Strain } e = \frac{6(l-x)F}{wt^2E}$$

Cantilever: length $l = 150 \text{ mm}$

width $w = 50 \text{ mm}$

thickness $t = 3 \text{ mm}$

Young's modulus $E = 2 \times 10^{11} \text{ N m}^{-2}$

Gauge factor $G = 2.0$

Bridge supply voltage $V_s = 15 \text{ V}$

10 Signal Processing Elements and Software

The output signal from the conditioning elements is usually in the form of a d.c. voltage, d.c. current or variable frequency a.c. voltage. In many cases calculations must be performed on the conditioning element output signal in order to establish the value of the variable being measured. Examples are the calculation of temperature from a thermocouple e.m.f. signal, and the calculation of total mass of product gas from flow rate and density signals. These calculations are referred to as **signal processing** and are usually performed digitally using a computer. The first section of this chapter discusses the principles of **analogue-to-digital conversion** and the operation of typical analogue-to-digital converters. The following section explains the structure and operation of typical **computer systems**. The various forms of computer **software**, both low- and high-level languages, are discussed in the next section. The final section looks at the two main types of signal processing calculation in measurement systems: steady-state calculation of measured value, and dynamic digital **compensation** and **filtering**.

10.1 Analogue-to-digital (A/D) conversion

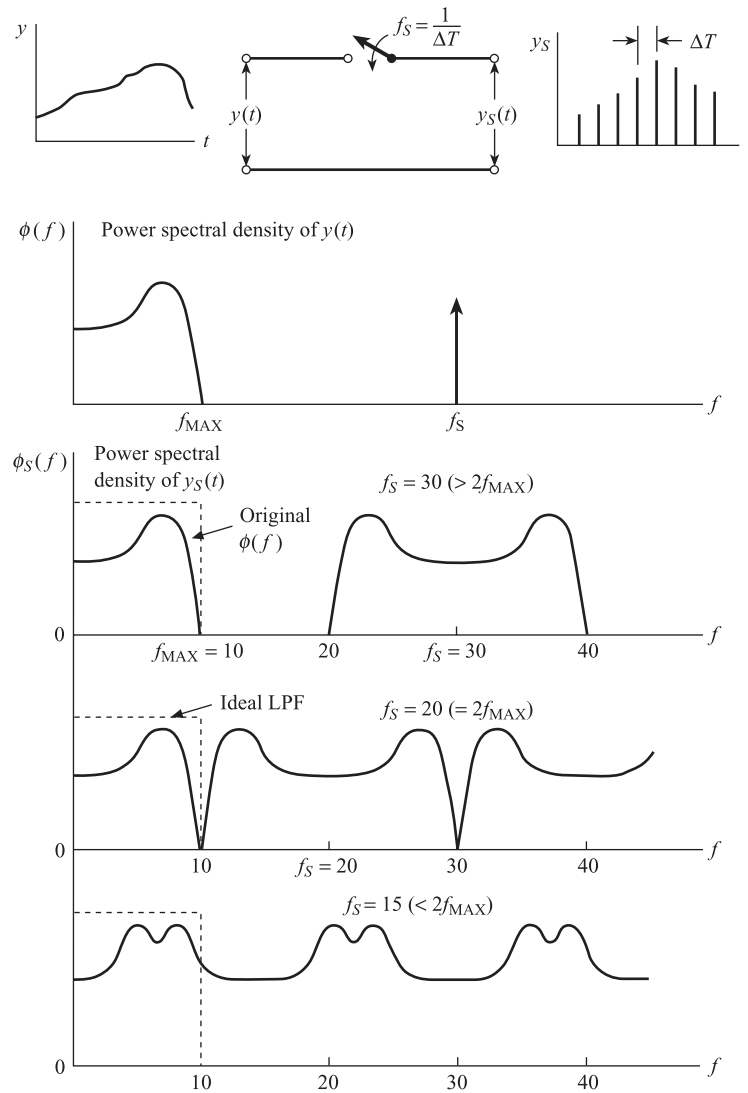
This section commences by discussing the three operations involved in A/D conversion: these are **sampling**, **quantisation** and **encoding**. The first operation is performed by a **sample-and-hold device**; the second and third are combined in an **analogue-to-digital converter**.

10.1.1 Sampling

In Chapter 6 we saw that a continuous signal $y(t)$ could be represented by a set of samples y_i , $i = 1, \dots, N$, taken at discrete intervals of time ΔT (sampling interval). The operation is shown in Figure 10.1; the switch is closed f_s times per second, where **sampling frequency** $f_s = 1/(\Delta T)$. In order for the sampled signal $y_s(t)$ to be an adequate representation of $y(t)$, f_s should satisfy the conditions of the Nyquist sampling theorem, which can be stated as follows:

A continuous signal can be represented by, and reconstituted from, a set of sample values provided that the number of samples per second is at least twice the highest frequency present in the signal.

Figure 10.1
Time waveform and frequency spectrum of sampled signal.



Mathematically we require:

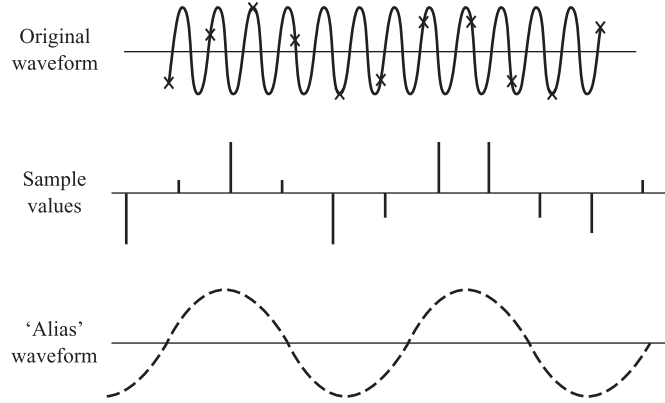
Nyquist sampling theorem

$$f_s \geq 2f_{MAX}$$

[10.1]

where f_{MAX} is the frequency beyond which the continuous signal power spectral density $\phi(f)$ becomes negligible (Chapter 6 and Figure 10.1).

The above result can be explained by examining the power spectral density $\phi_s(f)$ of the sampled signal. Because the sampled signal is a series of sharp pulses, $\phi_s(f)$ contains additional frequency components which are centred on multiples of the sampling frequency. Figure 10.1 shows $\phi_s(f)$ in the three situations $f_s > 2f_{MAX}$, $f_s = 2f_{MAX}$ and $f_s < 2f_{MAX}$. If $f_s > 2f_{MAX}$, then the additional frequency components

Figure 10.2 Aliasing.

can easily be filtered out with an ideal low-pass filter of bandwidth 0 to f_{MAX} and the original signal reconstituted. If $f = 2f_{\text{MAX}}$, it is just possible to filter out the sampling components and reconstitute the signal. If $f < 2f_{\text{MAX}}$, the sampling components occupy the same frequency range as the original signal and it is impossible to filter them out and reconstitute the signal.

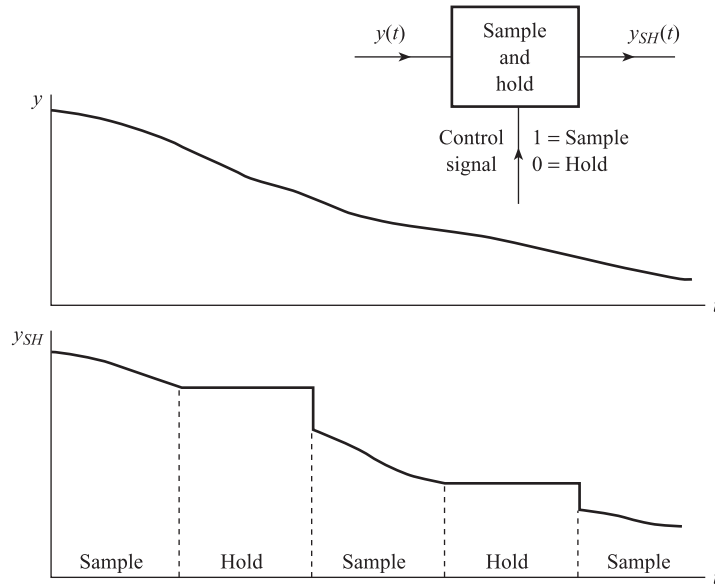
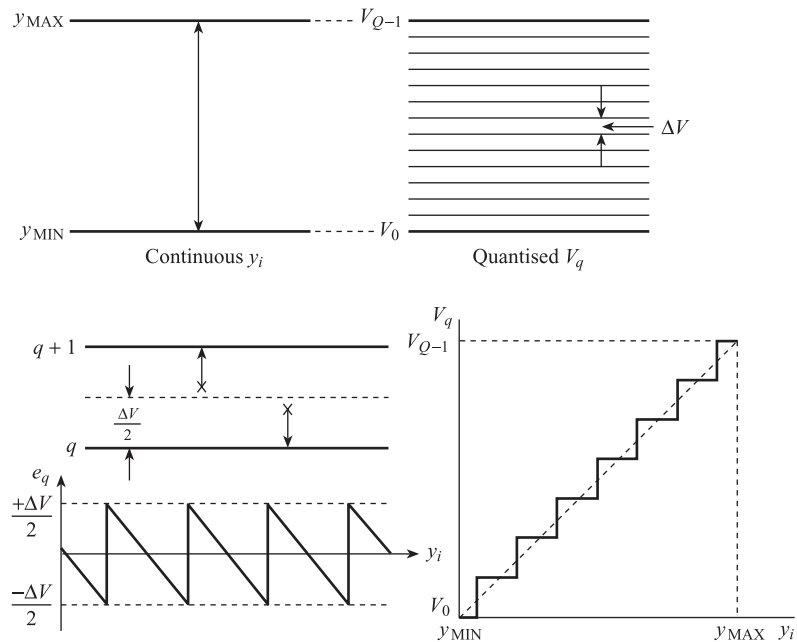
The effect of sampling at too low a frequency is shown in Figure 10.2. Here a sine wave of period 1 s, i.e. frequency 1 Hz, is being sampled approximately once every second, i.e. the sampling frequency is below the Nyquist minimum of 2 samples/second. The diagram shows that it is possible to reconstruct an entirely different sine wave of far lower frequency from the sample values. This is referred to as the 'alias' of the original signal; it is impossible to decide whether the sample values are derived from the original signal or its alias. The phenomenon of two different signals being constructed from a given set of sample values is referred to as **aliasing**.

The operation of analogue-to-digital conversion can take up to a few milliseconds; it is necessary therefore to hold the output of the sampler constant at the sampled value while the conversion takes place. This is done using a **sample-and-hold device** as shown in Figure 10.3. In the **sample** state the output signal follows the input signal; in the **hold** state the output signal is held constant at the value of the input signal at the instant of time the **hold** command is sent. The sample-and-hold waveform shown is ideal; in practice errors can occur due to the finite time for the transition between sample-and-hold states (aperture time) and reduction in the hold signal (droop).

10.1.2 Quantisation

Although the above sample values are taken at discrete intervals of time, the values y_i can take any value in the signal range y_{MIN} to y_{MAX} (Figure 10.4). In quantisation the sample voltages are rounded either up or down to one of Q quantisation values or levels V_q , where $q = 0, 1, 2, \dots, Q - 1$. These quantum levels correspond to the Q decimal numbers $0, 1, 2, \dots, Q - 1$. If $V_0 = y_{\text{MIN}}$ and $V_{Q-1} = y_{\text{MAX}}$, then there are $(Q - 1)$ spacings occupying a span of $y_{\text{MAX}} - y_{\text{MIN}}$. The spacing width or quantisation interval ΔV is therefore:

$$\Delta V = \frac{y_{\text{MAX}} - y_{\text{MIN}}}{Q - 1} \quad [10.2]$$

Figure 10.3 Sample and hold.**Figure 10.4** Quantisation.

The operation of quantisation produces an error $e_q = V_q - y_i$ termed the **quantisation error**. Normally if y_i is above the halfway point between two levels $q, q + 1$ it is rounded up to V_{q+1} ; if y_i is below halfway it is rounded down to V_q (Figure 10.4). The maximum quantisation error e_q^{MAX} is therefore $\pm \Delta V/2$, or expressed as a percentage of span $y_{\text{MAX}} - y_{\text{MIN}}$:

Maximum percentage
quantisation error

$$e_q^{\text{MAX}} = \pm \frac{\Delta V}{2(y_{\text{MAX}} - y_{\text{MIN}})} \times 100\% = \pm \frac{100}{2(Q-1)} \% \quad [10.3]$$

We see that the relationship between V_q and y_i is characterised by a series of discrete steps or jumps; this is an example of resolution errors discussed in Chapter 2. Obviously the greater the number of levels Q , the lower the quantisation errors.

10.1.3 Encoding

The encoder converts the quantisation values V_q into a parallel digital signal corresponding to a binary coded version of the decimal numbers $0, 1, 2, \dots, Q-1$. The commonly used decimal or denary number system uses a **base** or **radix** of 10, so that any positive integer is expressed as a series of powers of 10 (decades):

$$d_n \times 10^n + d_{n-1} \times 10^{n-1} + \dots + d_i \times 10^i + \dots + d_1 \times 10^1 + d_0 \times 10^0 \quad [10.4]$$

where the d_i are the respective weights or digits, which take the values 0 to 9. In digital computers the **binary number system** is used. This has a base of 2 so that any positive integer can be expressed as a series of powers of 2:

$$\begin{array}{c} b_n \times 2^n + b_{n-1} \times 2^{n-1} + \dots + b_i \times 2^i + \dots + b_1 \times 2^1 + b_0 \times 2^0 \\ \uparrow \qquad \qquad \qquad \qquad \qquad \qquad \qquad \qquad \qquad \qquad \qquad \qquad \qquad \uparrow \\ \text{MSB} \qquad \qquad \qquad \qquad \qquad \qquad \qquad \qquad \qquad \qquad \text{LSB} \\ \text{(Most significant bit)} \qquad \qquad \qquad \qquad \qquad \qquad \qquad \text{(Least significant bit)} \end{array} \quad [10.5]$$

where the weightings b_i are referred to as bits or digits. A bit can take only the values 0 or 1 so that calculations on binary numbers are easily performed by logic circuits which distinguish between two states – on or off, true or false. In order to convert the decimal number 183 to binary, we express it in the form:

$$1 \times (128) + 0 \times (64) + 1 \times (32) + 1 \times (16) + 0 \times (8) + 1 \times (4) + 1 \times (2) + 1 \times (1)$$

i.e.

$$1 \times 2^7 + 0 \times 2^6 + 1 \times 2^5 + 1 \times 2^4 + 0 \times 2^3 + 1 \times 2^2 + 1 \times 2^1 + 1 \times 2^0$$

giving the 8-bit binary number 10110111. To produce an electrical signal corresponding to this number we require eight wires in parallel, the voltage on each wire being typically 5 V for a '1' and 0 V for a '0'; this signal is an 8-bit parallel digital signal. The number of binary digits n required to encode Q decimal numbers is given by:

$$Q = 2^n$$

i.e.

Number of digits in
binary code

$$n = \log_2 Q = \frac{\log_{10} Q}{\log_{10} 2} \quad [10.6]$$

Thus if $Q = 200$, $n = \log_{10} 200 / \log_{10} 2 = 2.301 / 0.301 = 7.64$. Since, however, n must be an integer, we require eight bits, which corresponds to $Q = 2^8 = 256$. From eqn [10.3], the corresponding maximum quantisation error is $\pm 100 / 2(255)\% = \pm 0.196\%$. If the

Table 10.1.

Analogue input (V)	Decimal number	Digital output
0	0	00 000 000
1.2	$\frac{1.2}{5.0} \times 255 = 61.2 \approx 61$	00 111 101
3.7	$\frac{3.7}{5.0} \times 255 = 188.7 \approx 189$	10 111 101
5	255	11 111 111

input range of the converter is 0 to 5 V, then the corresponding analogue input, decimal numbers and digital output signals are as shown in Table 10.1.

Other codes are as follows.

Binary coded decimal (b.c.d.)

Here each decade of the decimal number is *separately* coded into binary. Since $2^3 = 8$ and $2^4 = 16$, four binary digits DCBA are required to encode the 10 numbers 0 to 9 in each decade. In 8:4:2:1 b.c.d. $A \equiv 2^0 = 1$, $B \equiv 2^1 = 2$, $C \equiv 2^2 = 4$, $D \equiv 2^3 = 8$; thus the decimal number 369 becomes

DCBA	DCBA	DCBA
0011	0110	1001
3	6	9

The number of decades p of b.c.d. required to encode Q decimal numbers is given by $Q = 10^p$, i.e. $p = \log_{10} Q$, and the corresponding total number of binary digits is:

Number of digits
in b.c.d.

$$4p = 4 \log_{10} Q$$

[10.7]

The input signal to character displays (Chapter 11) is normally in b.c.d. form; since the signal is already separated into decades the conversion into seven segment or 7×5 dot matrix code is easier than with pure binary.

Octal code

Here a base of 8 is used so that the weights take the values 0 to 7. In order to convert 183 decimal, i.e. $(183)_{10}$, into octal we express it in the form:

$$2(64) + 6(8) + 7(1)$$

i.e.

$$2 \times 8^2 + 6 \times 8^1 + 7 \times 8^0$$

i.e.

$$267 \text{ octal or } (267)_8$$

A binary number is easily coded into octal by arranging the digits in groups of 3, where for each group $A \equiv 2^0 = 1$, $B \equiv 2^1 = 2$, $C \equiv 2^2 = 4$. Thus 010110111 (binary code for $(183)_{10}$) becomes:

CBA	CBA	CBA		
010	110	111		
2	6	7	i.e.	267 octal

Hexadecimal code (hex)

Here a base of 16 is used and the digits are the ten numbers 0 to 9 and the six letters ABCDEF. Since $2^4 = 16$, each hexadecimal digit corresponds to four binary digits:

Binary	0000	0001	0010	0011	0100	0101	0110	0111
Hex	0	1	2	3	4	5	6	7
Binary	1000	1001	1010	1011	1100	1101	1110	1111
Hex	8	9	A	B	C	D	E	F

Some corresponding decimal, binary and hexadecimal numbers are

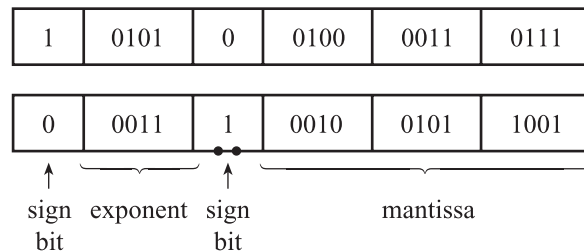
Decimal	Binary	Hexadecimal
94	01011110	5E
167	10100111	A7
238	11101110	EE

Floating point representation

Here a number is expressed in the form aN^b where a is the **mantissa**, b the **exponent** and N the **base** of the number system. Thus for a denary or decimal system with $N = 10$, we have:

$$\begin{aligned}-43\,700 &= -.437 \times 10^{+5} \\ +0.000\,259 &= +.259 \times 10^{-3}\end{aligned}$$

Both the mantissa and the exponent, each with a corresponding sign bit, can then be separately represented inside a computer using either binary, b.c.d. or hexadecimal code. Thus if three-decade b.c.d. is used for the mantissa and four-digit binary for the exponent, with 0 corresponding to $-$ and 1 to $+$, the above numbers can be represented by:



This representation is used when the range of numbers in a given computation is very wide. For example, the above format covers the range from 0.001×10^{-15} to $0.999 \times 10^{+15}$. Arithmetic operations are performed on exponent and mantissa separately.

According to the IEEE standard 754-1985, the standard floating-point representation is:

23-bit mantissa, 8-bit exponent, 1-bit sign (single precision)

52-bit mantissa, 11-bit exponent, 1-bit sign (double precision)

10.1.4 Frequency to digital conversion

In several cases the output signal from primary sensing or signal conditioning elements is an a.c. voltage with a frequency which depends on the measured variable. Examples are:

- The variable reluctance tachogenerator (Section 8.4)
- Electrical and electromechanical oscillators for displacement, density and differential pressure measurement (Section 9.4)
- Turbine, vortex and Doppler flow meters (Sections 12.2 and 16.4).

There are two main methods of converting a variable frequency sinusoidal signal into a parallel digital output signal. The sine wave must first be converted into a square wave signal with sharp edges using a Schmitt trigger circuit.

In the first method the **frequency** f_s of the signal is measured by counting the number of pulses during a fixed time interval T . The principle is shown in Figure 10.5(a). The number N_s of positive-going edges during T is counted, giving:

$$f_s = \frac{N_s}{T}, \quad \text{i.e.} \quad N_s = f_s T \quad [10.8]$$

Figure 10.5 Frequency to digital conversion:

(a) Frequency measurement – principle
(b) Frequency measurement – system

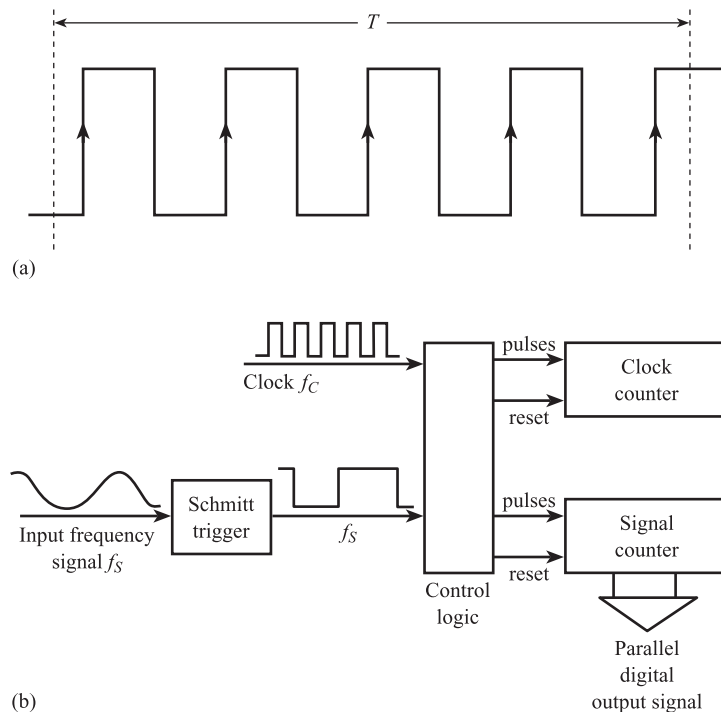
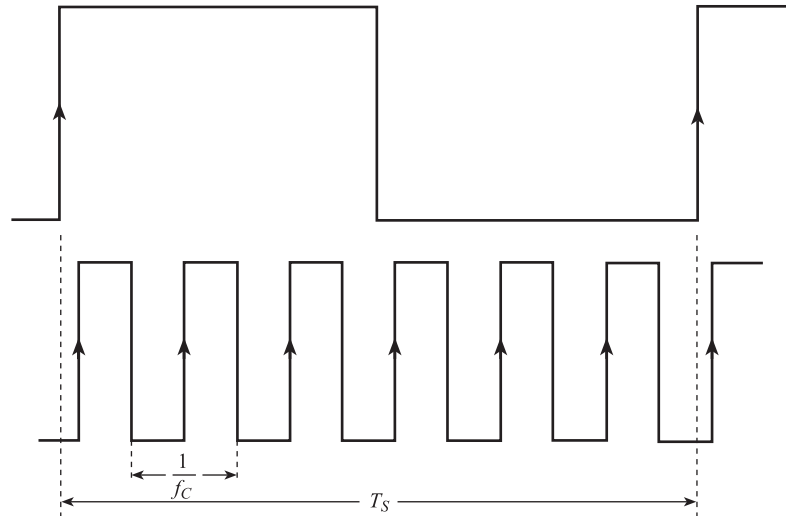
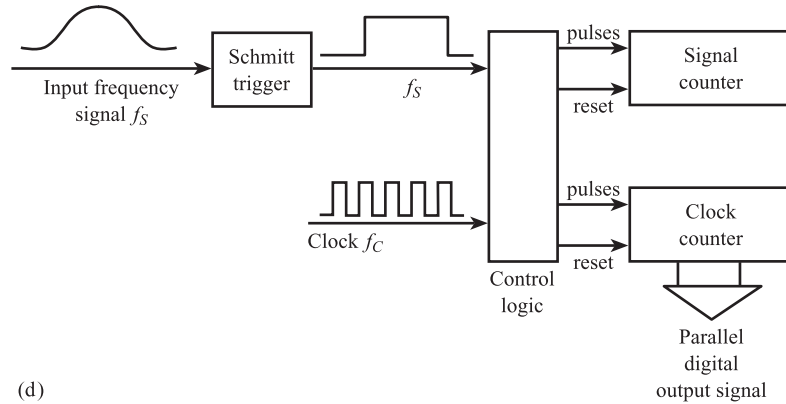


Figure 10.5 (cont'd)
 (c) Period measurement – principle
 (d) Period measurement – system.



(c)



(d)

Figure 10.5(b) shows one possible system for implementing this method. Both counters are initially reset to zero. The number N_C is then loaded into the clock counter; this sets the counting interval T to be:

$$T = \frac{N_C}{f_C} \quad [10.9]$$

where f_C is the clock frequency. Clock pulses are input to the clock counter, which then counts down to zero. Signal pulses are input to the signal counter; this counts up until the clock counter reaches zero, when the count is stopped. The signal count is then:

$$N_S = \frac{N_C}{f_C} \cdot f_S \quad [10.10]$$

The parallel digital output signal corresponds to signal count N_S , which is proportional to input signal frequency f_S .

The resolution of this method is limited to ± 1 signal count; this can mean poor percentage resolution at low frequencies. If we consider the example when $f_S = 20$ Hz

and $f_C = 10$ kHz, then to get $T = 1$ s, $N_C = 10^4$, giving $N_S = 20 \pm 1$, i.e. a percentage resolution of $\pm 5\%$. Percentage resolution can be increased by increasing the counting interval, but this is only possible if T is small compared with the time scale of the dynamic variations in the measurement signal.

This problem can be solved using the second method. Here the **period** T_S of the signal is measured by counting the number of clock pulses within T_S . The principle is shown in Figure 10.5(c). The number N_C of positive-going edges is counted, giving:

$$T_S = \frac{N_C}{f_C}, \quad \text{i.e.} \quad N_C = f_C T_S \quad [10.11]$$

where $1/f_C$ is the clock period. Figure 10.5(d) shows one possible system for implementing this method. Both counters are initially set to zero; clock pulses are input to the clock counter and signal pulses to the signal counter. The clock counter counts up until a count of 1 is registered in the signal counter; the count then stops. The clock count N_C is then given by eqn [10.11] and is proportional to T_S . The parallel digital output signal is proportional to this clock count.

The resolution of this method is ± 1 clock count. Using the above example with $f_S = 20$ Hz, $T_S = 0.05$ s and $f_C = 10$ kHz, $N_C = 500 \pm 1$, i.e. a percentage resolution of $\pm 0.002\%$.

However, some frequency signals are subject to random fluctuations which cause the signal period to vary, even though the input true value of the measured variable is constant. For example, the period of a nominal 20 Hz signal from a vortex flow meter may vary randomly between 0.04 s and 0.06 s about a mean value of 0.05 s. It is therefore essential to measure the **mean frequency** or **mean period** of the signal. The first method gives the mean frequency of 20 cycles measured over 1 second; the second method gives the period of one cycle only. This problem is solved using the second method but now the clock counter counts up until a count of 20 is registered in the signal counter. The mean clock count N_C for one signal cycle is then the total clock count divided by 20; the mean signal period T_S is then given by eqn [10.11].

10.1.5 Digital-to-analogue converters (DACs)

A DAC gives an analogue output voltage which is proportional to an input parallel digital signal, e.g. an 8-bit binary signal $b_7b_6 \dots b_1b_0$. In Figure 10.6 an operational amplifier is used to sum a number of currents which are either zero or non-zero depending on whether the corresponding bit is 0 or 1. The current corresponding to the most significant bit is twice that corresponding to the next significant bit and so on. This is achieved in Figure 10.6(a) by using a network of binary-weighted resistors 2^0R , 2^1R , 2^2R , \dots , 2^7R . The problem with this arrangement is that a very large range of resistance values is required. A better alternative is the ladder network shown in Figure 10.6(b); the advantage of this circuit is that the required current distribution can be obtained with only two values of resistance, R and $2R$.

10.1.6 Analogue-to-digital converters (ADCs)

One commonly used type of analogue to digital converter is the **dual-slope** converter. Here the input is a continuous voltage V_{IN} rather than sample values; dual slope

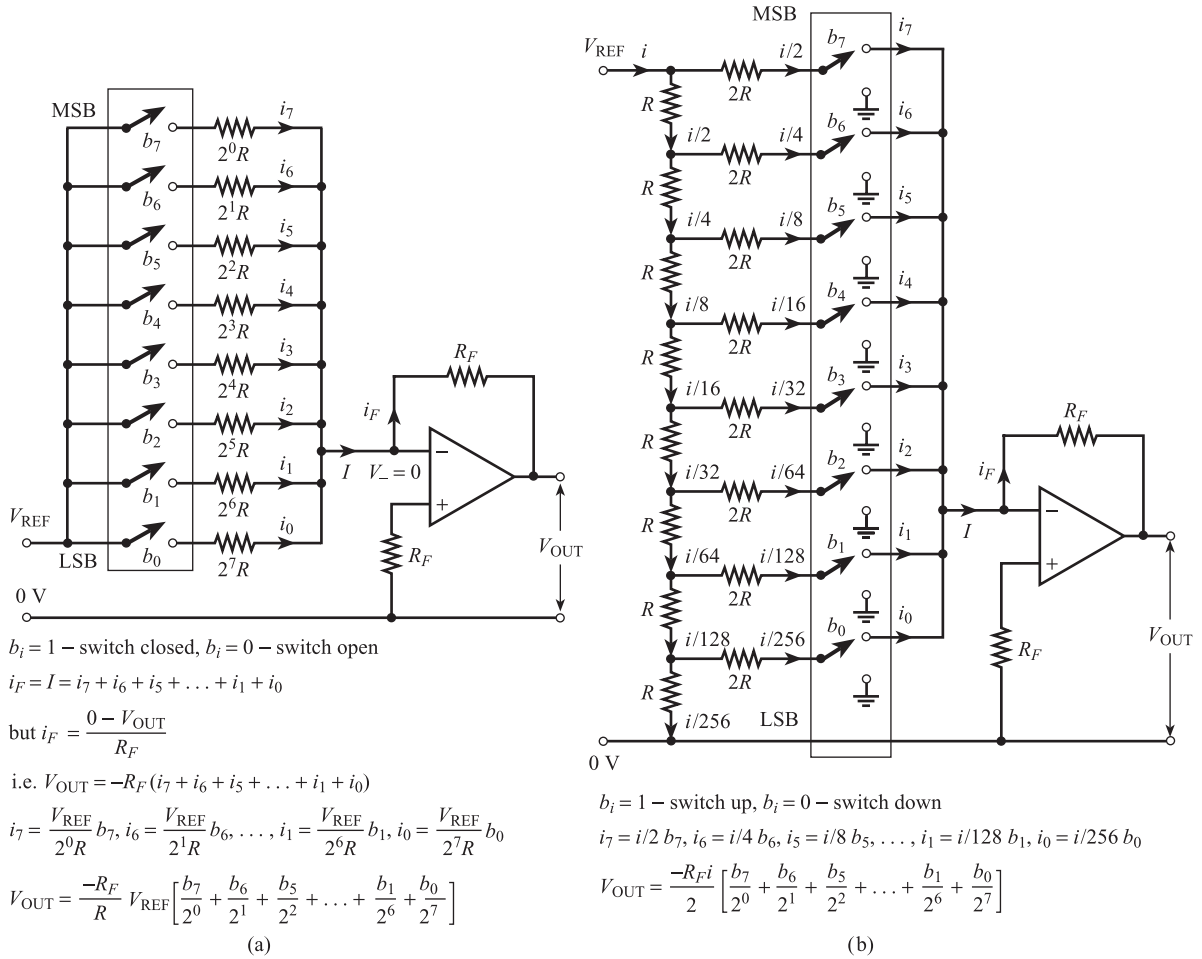


Figure 10.6 Summing amplifier DACs:
(a) Binary weighted resistor network
(b) R-2R ladder network.

converters are used in digital voltmeters and indicators. Figures 10.7(a) and (b) show a schematic diagram of the system and the principle of operation.

Firstly the control logic switches V_{IN} onto the integrator input for a fixed time interval. During this time interval the integrator output V_I is a positive ramp with a slope proportional to V_{IN} (Figure 10.7(b)) so that the output V_C of the comparator is 0. At the end of the fixed time interval V_I is proportional to V_{IN} (voltages V_1, V_2, V_3). At this point the control logic switches the reference voltage $-V_{REF}$ onto the integrator and resets the counter to zero. The integrator output is then a negative ramp with a fixed rate of decrease. This means that the time taken for V_I to decrease to zero is proportional to V_{IN} . During this time the control logic routes clock pulses to the counter and the counter increments. When V_I falls to zero the comparator output V_C changes to 1 and the count is stopped. The count is proportional to the fall time and therefore to V_{IN} : the parallel digital output signal is proportional to the count. This method has the advantage that integration tends to average out the effects of mains interference voltages.

Figure 10.7(c) shows a schematic diagram of a **successive approximation** analogue-to-digital converter. This method involves making successive guesses at the binary code corresponding to the input voltage y_i . The trial code is converted into an analogue voltage using a DAC, and a comparator is used to decide whether the guess

Figure 10.7 Analogue-to-digital converters:
 (a) Dual slope – system
 (b) Dual slope – principle
 (c) Successive approximation.

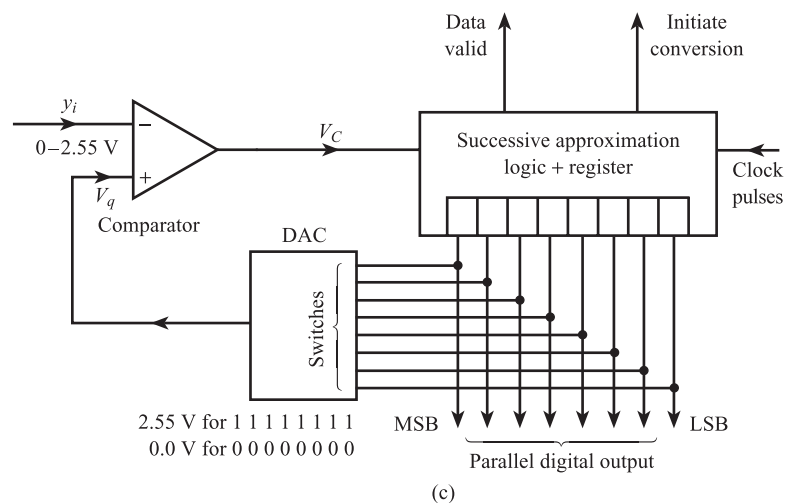
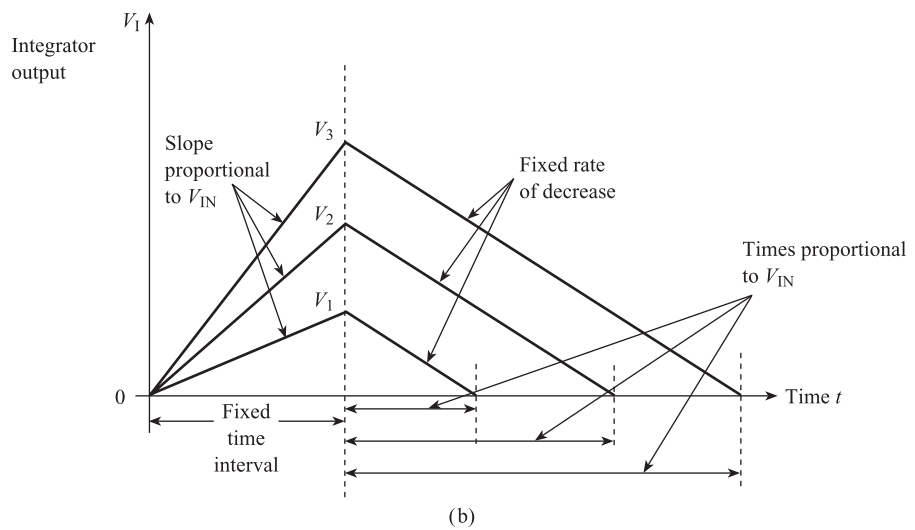
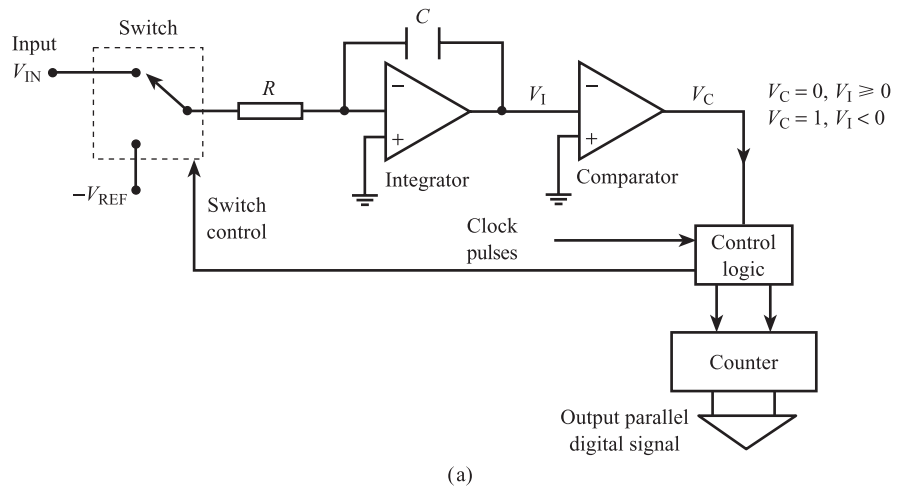


Table 10.2 Typical sequence of guesses in successive approximation ADC.

		Input voltage $y_i = 0.515$ V			
		Clock pulse	DAC input	DAC V_q output (volts)	Comparator output V_C
Initiate conversion →		1 Clear register	00000000	0	0
	2 First guess		01111111 (127) ₁₀	1.27	1 HIGH $b_7 = 0$
	3 Next guess		00111111 (63) ₁₀	0.63	1 HIGH $b_6 = 0$
	4		00011111 (31) ₁₀	0.31	0 LOW $b_5 = 1$
	5		00101111 (47) ₁₀	0.47	0 LOW $b_4 = 1$
	6		00110111 (55) ₁₀	0.55	1 HIGH $b_3 = 0$
	7		00110011 (51) ₁₀	0.51	0 LOW $b_2 = 1$
	8		00110101 (53) ₁₀	0.53	1 HIGH $b_1 = 0$
	9 Final guess		00110100 (52) ₁₀	0.52	1 HIGH $b_0 = 0$
Data valid →		Output digital signal = 00110100			

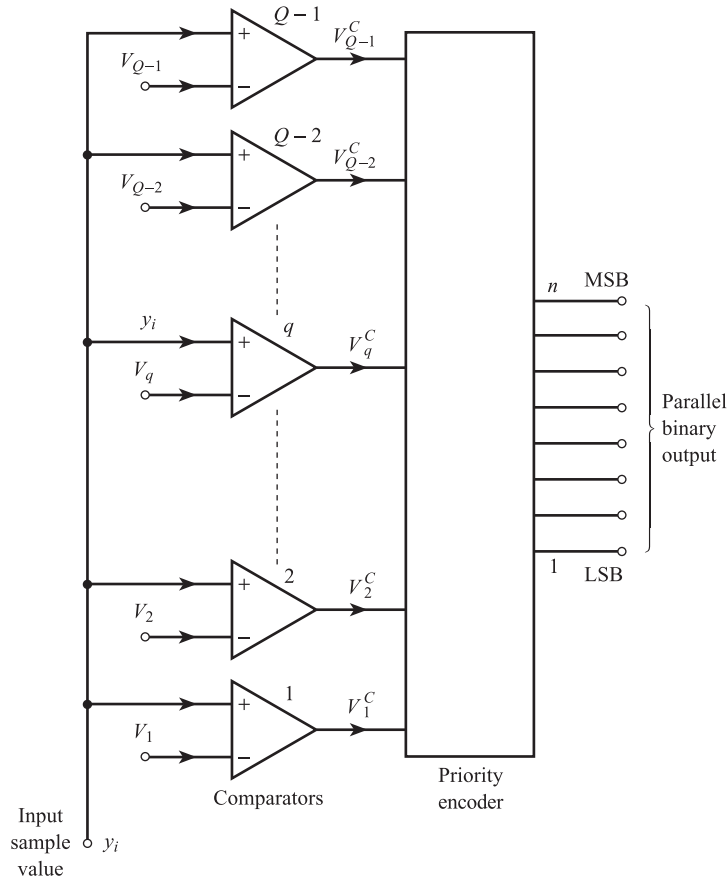
is too high or too low. On the basis of this result another guess is made, and the process is repeated until V_q is within half a quantisation interval of y_i .

Table 10.2 shows a series of guesses for an 8-bit binary converter with an input range of 0 to 2.55 V. The first guess is always 01111111 corresponding to (127)₁₀, i.e. approximately half full scale: this guess is high so that b_7 is set to 0; if the guess had been low b_7 would be set to 1. The next guess is 00111111 corresponding to (63)₁₀, i.e. approximately one-quarter full scale; this guess is also high so that b_6 is confirmed as 0. The process continues until all the remaining bits have been confirmed; the DATA VALID signal then changes state.

Successive approximation converters (SAC) can be used for sample rates up to over 10^6 samples/s; even 16-bit types can be used up to over 10^5 samples/s. For the fastest applications up to 10^9 samples/s, such as video digitisation, flash converters are used. SAC converters can be linked to microcontrollers using two-way serial communication over a pair of wires. Here the successive approximation logic is provided by the microcontroller; the SAC consists only of a DAC and a comparator. The microcontroller sends out clock pulses to operate the DAC switches and receives the digital code in serial form.

Figure 10.8 shows a general schematic diagram of a **flash or parallel analogue-to-digital converter**.^[1] In any n -digit binary ADC there are Q quantisation voltage levels V_0 to V_{Q-1} , where $Q = 2^n$. In a flash ADC there are $Q - 1$ comparators in parallel and $Q - 1$ corresponding voltage levels V_1 to V_{Q-1} . There is no need to provide the V_0 voltage level. In each comparator q , the input sample value y_i is compared with the corresponding voltage level V_q . If y_i is less than or equal to V_q , the output is zero corresponding to 0. If y_i is greater than V_q , the output is non-zero corresponding to a 1, i.e.

Figure 10.8 Flash analogue-to-digital converter.



$$V_q^C = 0, \quad y_i \leq V_q$$

$$V_q^C = 1, \quad y_i > V_q$$

[10.12]

Thus if y_i lies between V_q and V_{q+1} , i.e. $V_q < y_i \leq V_{q+1}$, the output of the lowest q comparators 1 to q will all be 1 and the output of the remaining comparators $q+1$ to $Q-1$ will all be 0 . Thus the comparators provide a $Q-1$ digit parallel input code to a **priority encoder** which generates an n -digit binary parallel output code corresponding to the value of q . The main advantage of the flash converter is the short conversion time; the main disadvantage is that the large number of comparators required to give acceptable resolution mean that it is relatively expensive.

10.2

Computer and microcontroller systems

10.2.1 The general computer system

Figure 10.9 is a block diagram of a general computer system; the system is made up of the following elements.

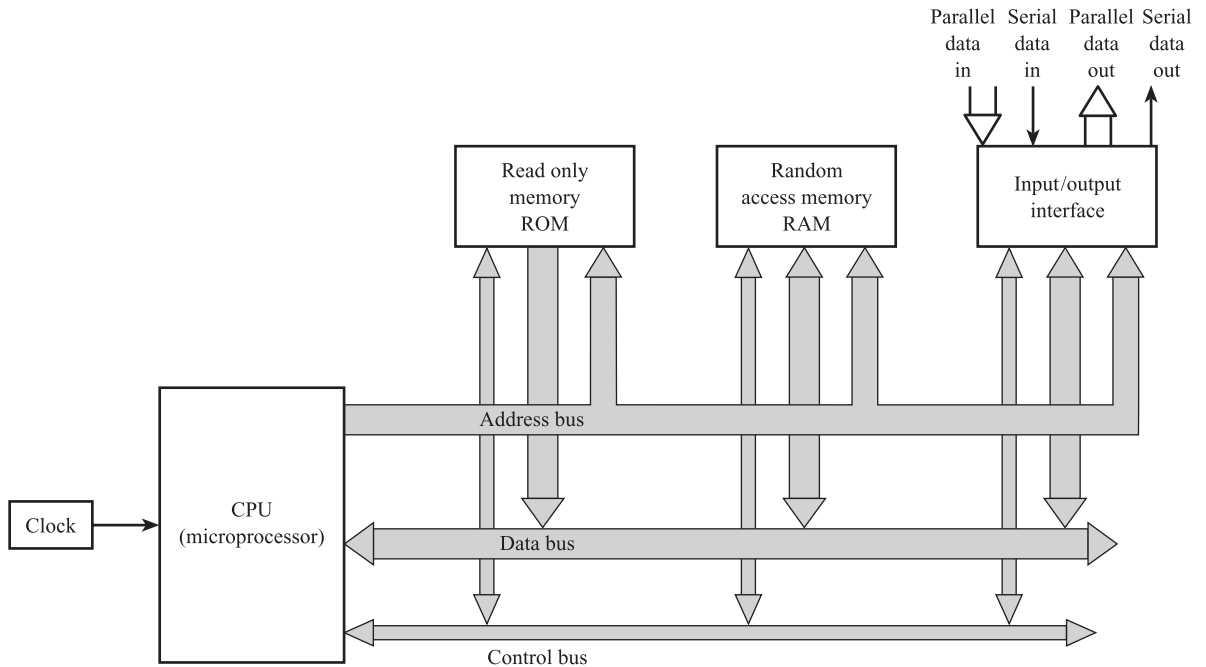


Figure 10.9 General computer system.

The **microprocessor** consists of three main parts. The control unit controls the processing of **instructions** by providing the necessary control and timing signals. The **arithmetic logic unit** carries out arithmetic operations such as addition and subtraction and logic operations such as NOT, AND, OR. The **register array** is a collection of registers required to temporarily store instructions, addresses and data during the execution of an instruction.

The **read only memory (ROM)** consists of a large number of permanent storage elements, each specified by a unique **address**. Information can only be read from ROM; no information can be written into ROM. Reading is an operation whereby a copy of a data word or instruction is transferred from a given storage location to another device without changing the contents of the store. Writing is an operation whereby a data word or instruction is placed in a given storage location. Instructions are normally stored in ROM.

The **random access memory (RAM)** consists of a large number of non-permanent storage elements, each specified by a unique address. Information can both be read from and written into RAM. Both instructions and data can be stored in RAM.

The **input/output interface** consists of a number of **ports** to which external devices can be physically connected. The ports can be configured to accept input data in parallel and/or serial format and output data in parallel and/or serial format. For example, data from an ADC can be received at the parallel input port and data transmitted to a display or printer at the parallel output port.

The **address bus** has a one-way flow of information; the microprocessor sends out address codes to memory locations and input/output ports.

The **data bus** has a two-way flow of information. Here, for example, data is transferred from the input port or RAM to the microprocessor, and instructions are

transferred from the ROM to the microprocessor. The results of calculations or operations are transferred from the microprocessor to RAM or the output port.

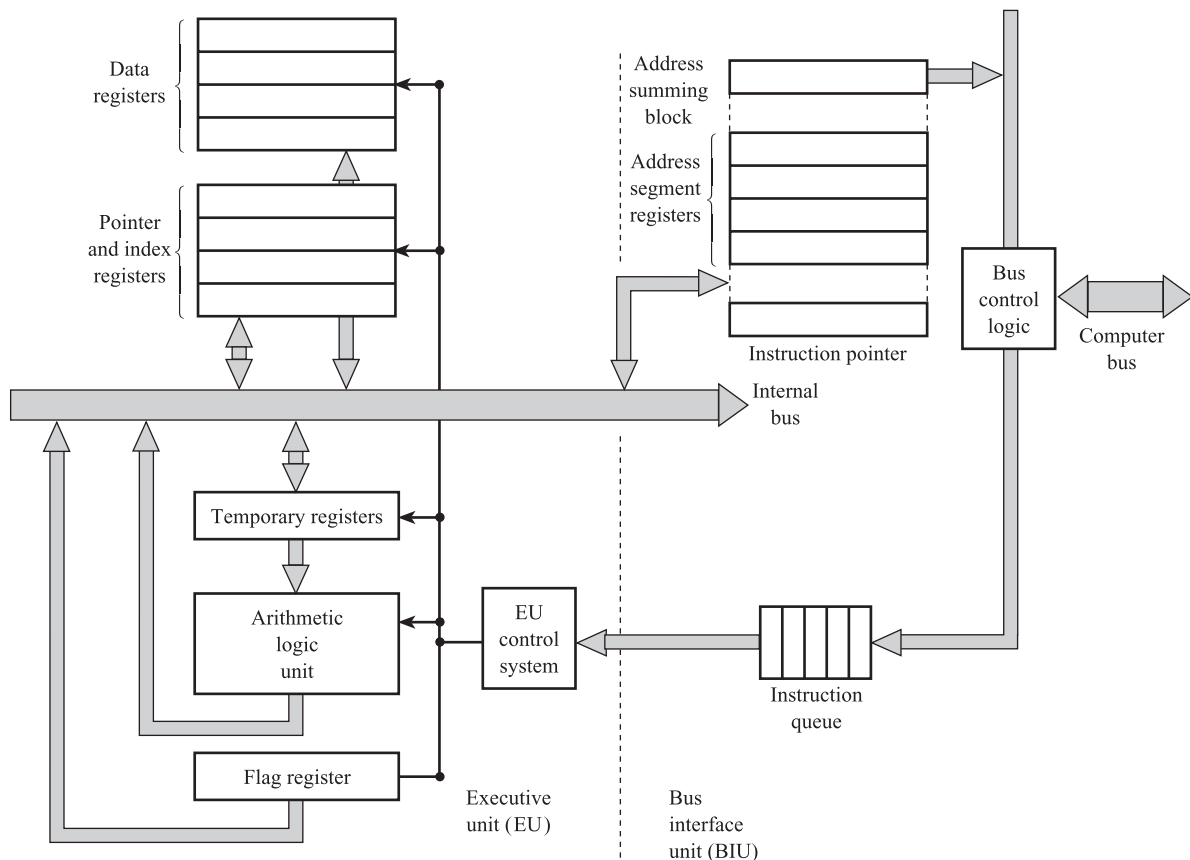
The **control bus** also has a two-way flow of information. The microprocessor sends out enable and clock signals to all elements in the system to achieve the coordination and synchronisation necessary for the above information transfers to take place. It receives information back on the status of each element.

A small-scale computer system based on an 8-bit microprocessor will correspondingly have an 8-bit data bus. A 16-bit address bus will enable $2^{16} = 65\,536$ different locations to be addressed. A typical system would have two 4 K ROMs, each capable of storing 4096 8-bit bytes, and two RAMs, each capable of storing 128 8-bit bytes.

The computer operates sequentially by executing a series of steps; the timing of these steps is determined by the clock. Each step is performed as a result of an instruction; the sequence of instructions is called a **program**. The first step in the execution of an instruction is for the CPU to address the memory location in which the instruction is stored. The instruction is then fetched and decoded; any data required by the instruction is also fetched. The instruction is then executed and the results of the instruction are transferred to memory or an output port. After completing the instruction the CPU moves on to the next one.

Figure 10.10 Layout of typical microprocessor.^[1]

Figure 10.10 shows the layout of a typical microprocessor. The processor is divided into two separate units. The **executive unit (EU)** executes the instructions;



the **bus interface unit (BIU)** interfaces with the computer buses, fetches instructions, reads operands and writes results.^[1]

The **EU control system** fetches an instruction from the **instruction queue**, decodes it and sends out control signals to execute the instruction. The **arithmetic logic unit (ALU)** performs all arithmetic and logic operations; the **data registers** are used to store data before and after these operations. The **flag register** contains status flags associated with arithmetic operations such as *zero*, *sign*, *carry*. The **pointer** and **index registers** are used to create an address in the BIU; the result of the instruction is then transferred to this temporary address.

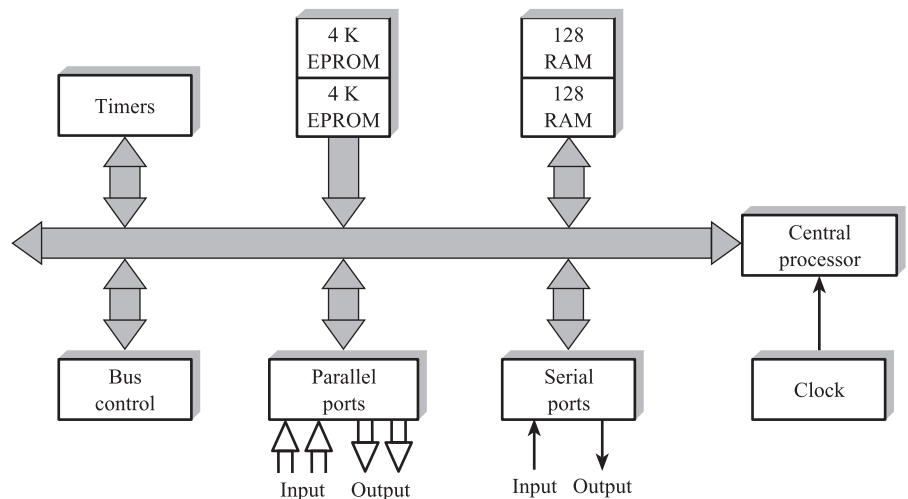
While a given instruction is being executed in the EU, the **bus control logic** fetches the next instructions from memory via the computer bus and places them in the instruction queue. The **address segment registers** and **instruction pointer** are used to create parts of the instruction address. These are then combined in the **address summing block** to create the full address of the next instruction to be fetched.

10.2.2 Microcontrollers

In a **microcontroller** the processor, memory and input/output are all combined on a single chip. Microcontrollers are widely used for signal processing in measurement systems.

Figure 10.11 shows the layout of a typical microcontroller.^[2] This is an 8-bit system with CPU, memory, four parallel ports, two serial ports, 12 MHz clock and a single bus. There are two 4 K EPROMs (Electrically Programmable Read Only Memory). This memory is non-volatile and programmed electrically; once programmed it cannot be changed, but memory contents are unchanged when the electrical power is switched off. Program instructions are stored in EPROM. There are two 128-byte RAMs, which are used to store data; this is volatile memory whose contents are lost when the power is switched off. An alternative to RAM is EEPROM (Electrically Erasable PROM); this will hold data without a continuous power supply, and program instructions can be changed or updated in the field.

Figure 10.11 Layout of a typical microcontroller.



10.3

Microcontroller and computer software

10.3.1 Assembly language for microcontrollers

Microcontrollers are programmed in **assembly** language. Here each instruction is of the form:

operator operand

The operator specifies the instruction to be carried out and is defined by a three- to six-letter mnemonic called an **opcode**. A typical microcontroller has a set of about 35 instructions, which are stored in EEPROM. Table 10.3 lists some typical instructions.

The working register W is at the heart of the microcontroller CPU. It is used to perform arithmetic and logic operations. This means that data must first be transferred from a file register to W; the operation is then performed in W and the result transferred from W to another register. Consequently several instructions involve the W register.

The operand is either data or an address location. In an 8-bit microcontroller the basic data or address word is eight bits or one byte long; this is referred to as a **file**. A single file can therefore cover the range of numbers 0 to 255 decimal, 0000 0000 to 1111 1111 binary or 00 to FF hexadecimal. Typically there are 16 special-purpose registers, specified by the hex addresses 00 to 0F. These include, for example, timer/counter, program counter, status, file select, input and output port registers. In addition there are typically 70 general-purpose registers, specified by the hex addresses 10 to 5F. These are within the RAM and are used to store user data files; they are referred to as file registers or simply files. To accommodate data numbers greater than 255, two 8-bit data files are combined; this allows numbers up to 2^{16} , i.e. 65 536. These two files are then stored in two adjacent file registers.

Table 10.3 Typical microcontroller instructions.

Opcode	Description
ADDLW	Adds a number to contents of W
ADDWF	Adds contents of W to contents of file
CALL	Calls a subroutine
CLRF	Clears file F
CLRW	Clears the W register
DECF	Subtracts 1 from file
GOTO	Unconditional jump to specified location in program
INCF	Adds 1 to file
MOVF	Moves contents of file into W
MOVLW	Moves data file directly into W
MOVWF	Moves contents of W to file
RETURN	Returns from a subroutine to main program
SUBLW	Subtracts contents of W from a number
SUBWF	Subtracts contents of W from contents of file

Table 10.4 Typical microcontroller program.

Opcode	Operand	Description
CLRW		Clears W register
MOVF	2C	Moves contents of file 2C to W
ADDLW	\$1A	Adds the number 1A (hex) to W
SUBWF	2D	Subtracts contents of W from contents of file 2D
MOVWF	result	Moves contents of W to reserved register with name 'result'

Table 10.4 shows a typical assembler program for a microcontroller. The contents of file register 2C are transferred to the W register, the hex number 1A is added to W, and the contents of W are then subtracted from the contents of file register 2D. The final result is then transferred from W to a reserved register with the name 'result'.

10.3.2 Higher-level languages

Assembly language programs generally take less time to execute and require less memory than those written in other languages; they also support any type of input, output and peripheral device. However, assembly programming is far more difficult; we can see from the example in Table 10.4 that several lines of code are necessary to perform a simple arithmetic operation. Several types of error are possible in assembly programming which are much less likely in a high-level language. If we assume that it takes about the same time, per line of code, to write, debug, test, execute and comment irrespective of the language, then assembly language implementation will be far more expensive. Another disadvantage of assembly language is that it is specific to one type of processor and is therefore not **portable** to other microprocessors or microcontrollers. Assembly code written for one type of processor cannot be moved to another processor with a different instruction set.

High-level languages have the following characteristics:

1. They include **procedures**: a procedure is a sequence of operations which defines exactly how a task is to be performed.
2. The control of program flow is determined by the way the program is **structured**, i.e. by the sequential ordering of operations or by explicit linkages between them.
3. They include **assignment statements**; an assignment statement assigns a new value to a variable, usually by computing the numerical value of an algebraic expression specified in the statement. Examples are:

$$A = B + C$$

$$Y = 5.0 * \sin T$$

$$Y = \exp(-7.2 * X)$$

4. Several **data types** are possible; examples are *integer*, *real* and *Boolean*. High-level languages are processor-independent and use a **compiler** to translate the complete high-level language program into the assembly code for a given processor. They therefore require more memory (the compiler is itself a large program) and take more time to execute. However, high-level programs are easier to write and correct.

Table 10.5 Typical BASIC statements and operators.

Statements	Operators
BAUD	ADD (+)
CALL	DIVIDE (/)
CLEAR	EXPONENTIATION (**)
CLEAR(S&I)	MULTIPLY (*)
CLOCK(1&0)	SUBTRACT(—)
DATA	LOGICAL AND (.AND.)
READ	LOGICAL OR (.OR.)
RESTORE	LOGICAL X-OR (. XOR.)
DIM	LOGICAL NOT (.OR.)
DO-WHILE	ABS()
DO-UNTIL	INT()
END	SGN()
FOR-TO-STEP	SQR()
NEXT	RND
GOSUB	LOG()
RETURN	EXP()
GOTO	SIN()
ON-GOTO	COS()
ON-GOSUB	TAN()
IF-THEN-ELSE	ATN()
INPUT	=, >, >=, <, <=, <>
LET	ASC()
ONERR	CHR()
ONEX1	CBY()
ONTIME	DBY()
PRINT	XBY()
PRINT#	GET

BASIC is a very popular, easy-to-learn language. It began as an interpreted rather than a compiled language. This means that it is translated and executed statement-by-statement, using a program called an **interpreter**, instead of being fully translated into machine code before execution. There are several ‘dialects’ of BASIC which are specific to a given processor; this makes it less portable than other high-level languages. Table 10.5 shows some typical BASIC statements and operators. These include input/output statements, program sequence control statements and arithmetic operators. Control of flow is obtained by attaching a numerical label (line number) to each statement and then executing the resulting program in an ascending sequence of these statement labels. An assignment statement would therefore read:

```
10 LET I = J + 50
```

Subroutines are called with GOSUB N statements, where N is the line number of the first statement of the subroutine. Return to the main program is then via a RETURN statement at the end of the subroutine. Program sequence is controlled by IF, THEN, ELSE, GOTO N statements. This reliance on line numbers can lead to a lack of program structure, making programs difficult to follow, and can lead to errors if the wrong line number is given.

Because BASIC is an interpretive language, it is decoded and error-checked line by line during operation and so is far too slow and inefficient for the processing of

measurement signals. **C** is the chosen language for fast, efficient signal processing in measurement systems by **embedded** microcontrollers and computers. C is a relatively low-level language operating fairly close to assembly instructions. It has a highly modular simple structure which uses **functions** as sub-programs; a function is a self-contained unit of code. Before any variable is used as a function, it has to be **declared**, i.e. given a name and type. The general term for a name is an **identifier**. C permits the following data types:

float	floating point	3.4×10^{38} to 1.2×10^{-38}
int	integer	-32 768 to +32 767
char	up to 256 characters (e.g. upper/lower case letters)	

The **assignment operator** = assigns to the variable on the left-hand side a value given by the expression on the right-hand side. Thus to convert Celsius temperature into Fahrenheit we have:

```
temp_f = temp_c * 9.0/5.0 + 32
```

The basic **arithmetic operators** + (add), - (subtract), * (multiply) and / (divide) are available; higher-level arithmetic is provided by **standard library functions**. Some of these are shown in Figure 10.12(a). **Relational operators** pose a question to which the answer is either yes or no. These are:

$a > b$	Is a greater than b ?
$a < b$	Is a less than b ?
$a == b$	Is a equal to b ?
$a >= b$	Is a greater than or equal to b ?

There are also the **logical operators** && for AND and || for OR. The **increment operator** ++ increases the value of variable i by 1; the **decrement operator** i-- decreases it by 1. Functions are defined by enclosing the code that the function is to contain in braces { }. Standard library functions are used to provide high-level facilities, e.g. graphics, input/output and arithmetic; examples are:

clrscr ()	Clear screen
printf ("message")	Print 'message'

The 'message' contained in the parentheses is termed the **argument**. Program sequence is controlled by the **if-else**, **while** and **do-while** constructs. For example, the if-else construct has the form:

```
if (test condition)
{
    Block of code to be executed if test condition is TRUE
}
else {
    Block of code to be executed if test condition is FALSE
}
```

In C, loops can be implemented using the **for** construct, which has the form:

```
for (initialisation; test condition; action at end)
{
    Code to be executed while test condition is TRUE
}
```

Floating-point maths	String-to-number conversion
acos	atof
asin	atoi
atan	atol
cos	strtod
cosh	Bit manipulation
deg	BIT
exp	RES
mod	SET
log	Arithmetic
log10	abs
rad	Input/output
rand	printf
sin	sprintf
sinh	putch
sqrt	getch
tan	puts
tanh	putchar

(a)

```
main ( )
{
    float temp_c = 0.0;
    float temp_f;
    int i;
    clrscr ( );
    for (i = 0; i <= 20; i ++ )
    {
        temp_c = (float) i;
        temp_f = temp_c * 9.0/5.0 + 32.0;
        printf ("%5.1 f degrees C is % 5.1 f degrees F
                |r\n", temp_c, temp_f);
    }
    wait ( );
}
```

(b)

Figure 10.12
C programming language:
(a) Typical functions
(b) Typical program.

Figure 10.12(b) shows a typical C program; this displays a table of Fahrenheit temperatures for the Celsius temperatures 0, 1, 2, 3, . . . , 20.

10.3.3 Virtual instrument software

The languages discussed above are suitable for programming **embedded** micro-controllers which carry out basic signal processing operations within the measurement system. If more advanced signal processing and data presentation operations are required, for example displaying the frequency spectrum of a measurement signal, then **applications** software is required. This type of software is more suitable for **personal computers** (PCs) operating in a windowed environment than for smaller microcontroller systems. **Graphical programming languages** are an important example of applications software. Here the program consists of a number of standard functions, represented by icons or block diagram symbols; the relationship between the functions is represented by lines drawn between the symbols. The program block diagram is shown on the computer monitor screen and the programmer develops the program by selecting symbols representing standard functions and drawing inter-connecting lines between them using keyboard and mouse. Once the program has been completed and tested it can be run; the screen display format is then changed in order to present measured values to the observer. Many data presentation formats are possible, for example analogue-type pointer scale indicators, digital character displays to present numerical values, and graphics displays to show signal waveforms (Chapter 11). The completed system is called a **virtual instrument** because many of the measurement system functions have been performed in software rather than hardware.

Typical virtual instrumentation software will have a comprehensive library of standard functions.^[3] Arithmetic functions will include add, subtract, multiply, divide, square root and reciprocal. Logical functions include AND, OR, NOT, NOT AND.

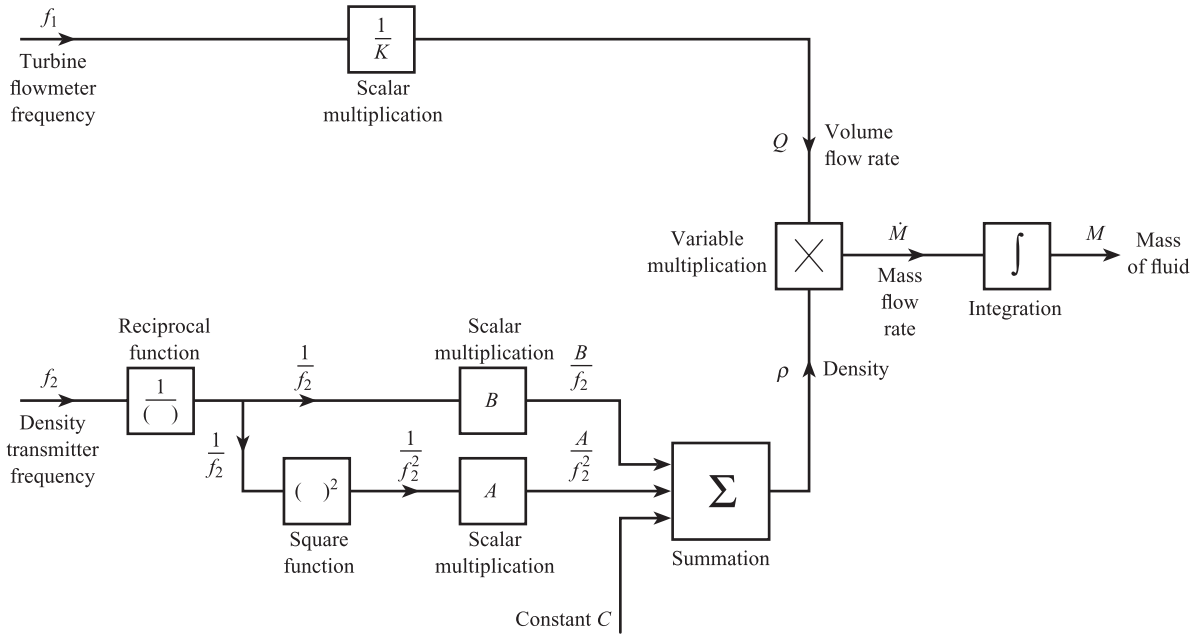


Figure 10.13 Virtual instrument graphical program for measurement of mass of fluid.

Trigonometric and logarithmic functions include sine, cosine, tangent, exponential, powers of 10, powers of the variable, and natural logarithms. Comparison functions give a logical 1 or 0 output depending on whether two variables are equal, or one is greater than the other, or one is less than the other. There are also a number of functions involving **arrays**. If, for example, values of a variable at different sampling intervals are stored in an array and then the elements of the array are added together, the **time integral** of the variable can be found.

Figure 10.13 shows a graphical program for calculating the total mass of fluid transferred down a pipeline during a time interval T (Section 12.4.1). The inputs to the program are the frequency f_1 from a turbine flowmeter (Section 12.3.2) and the frequency f_2 from a vibrating tube density resonator (Section 9.5.2). The volume flow rate Q of fluid is given by:

$$Q = \frac{1}{K} f_1 \quad [10.13]$$

where K is the meter factor of the turbine flowmeter. The density of the fluid is given by:

$$\rho = \frac{A}{f_2^2} + \frac{B}{f_2} + C \quad [10.14]$$

where A , B and C are constants. The mass flow rate \dot{M} is then:

$$\dot{M} = \rho Q \quad [10.15]$$

and finally the total mass of fluid transferred during time T is the time integral:

$$M = \int_0^T \dot{M} dt \quad [10.16]$$

10.4 Signal processing calculations

10.4.1 Steady-state compensation

Computer calculation of measured value in the steady state has already been discussed in Section 3.3. Here the output U of the uncompensated system (normally comprising sensing, signal conditioning and ADC elements) is input to the computer. The computer then solves the steady-state inverse model equation:

$$I = K'U + N'(U) + a' + K'_M I_M U + K'_I I_I \quad [10.17]$$

which obtains an estimate I' of model input I and thus compensates for non-linearity and environmental effects in the uncompensated system. The computer requires estimates I'_M, I'_I of the modifying and interfering inputs I_M, I_I and values of the model parameters $K', N'(), a'$, etc. We now consider examples of the computer solution of the inverse equation in both linear and non-linear cases.

Linear case

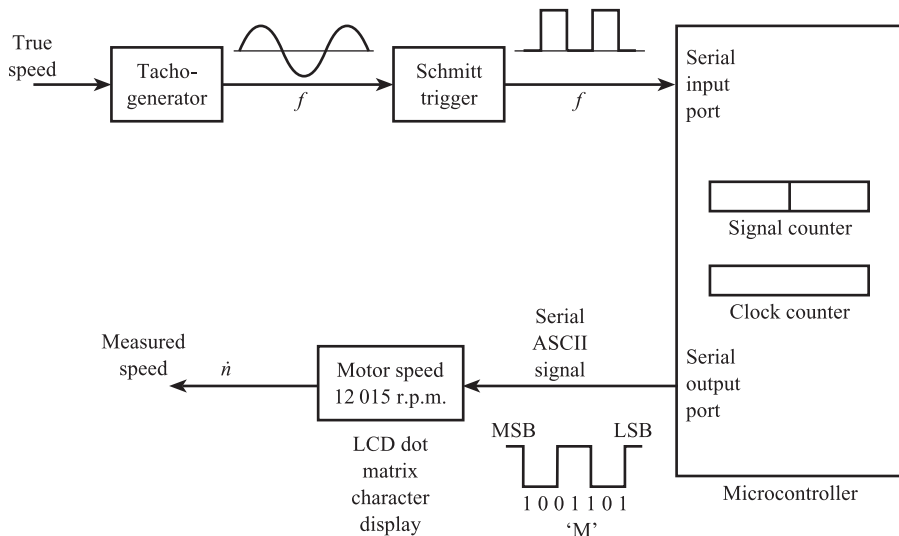
In this case the system input I is exactly proportional to the output U , i.e.

$$I = K'U \quad [10.18]$$

As an example of the solution of this equation we consider a speed measurement system (Figure 10.14) using an 8-bit microcontroller programmed in assembly language.

In this system the angular speed of a motor is sensed by a variable reluctance tachogenerator and the measured speed in rpm is displayed on a LCD dot matrix character display (Section 11.6). The tachogenerator (Section 8.4) gives an approximately sinusoidal output voltage with frequency f Hz proportional to angular speed n rev/s. This voltage is input to a Schmitt trigger circuit to give a train of

Figure 10.14 Angular speed measurement system using microcontroller.



sharp-edged pulses at frequency f . This pulse train is input to a serial input port of the microcontroller and then can be transferred to a 16-bit signal counter within the microcontroller. This signal counter is configured from two adjacent 8-bit (single byte) general-purpose file registers. There is also a 16-bit clock counter using the dedicated counter/timer register. The microcontroller calculates the measured speed \dot{n} from frequency f and converts it into ASCII code (see later notes). This code is transferred to a microcontroller output serial port and the serial ASCII signal transferred to the LCD display to present the measured speed.

From Section 8.4, the frequency f Hz of the tachogenerator output voltage is given by:

$$f = \frac{m\omega_r}{2\pi} \quad [10.19]$$

where ω_r rad/s is the angular velocity of the wheel and m the number of teeth. If \dot{n} is the angular speed in rpm then:

$$\frac{\dot{n}}{60} = \frac{\omega_r}{2\pi}$$

giving:

$$f = \frac{m\dot{n}}{60} \quad [10.20]$$

Thus if $m = 12$ and the range of \dot{n} is 0 to 18 750 rpm, then the corresponding range of f is 0 to 3750 Hz. If the signal counting interval $T = 1$ s, then the corresponding signal count $N_s = fT$ (Section 10.1.4) has a range between 0 and 3750. This can be accommodated by the 16-bit signal counter, which can count up to 65 535 ($2^{16} - 1$). From eqn [10.20], we now have:

$$\dot{n} = 5N_s \quad [10.21]$$

which has the linear form of eqn [10.18].

Thus in order to measure \dot{n} , the pulses are counted over 1 s and the count multiplied by 5. The main stages in the microcontroller program are therefore:

- Stage A – Count signal pulses for 1 second
- Stage B – Multiply count by 5
- Stage C – Convert hexadecimal count to decimal
- Stage D – Convert decimal count to ASCII for display.

Each of these stages will now be discussed in more detail.

Stage A. Here the frequency measurement method of Figures 10.5(a) and (b) is used; the signal pulses are input to the signal counter and the clock pulses to the clock counter. Assuming a clock frequency of 10 kHz, the hexadecimal equivalent of 10 000 decimal is initially loaded into the clock counter; each clock pulse causes the counter to decrement by 1. The signal counter starts at zero and increments by 1 for each signal pulse until the clock counter reaches zero, when the count is stopped to give the required signal count N_s .

Stage B. The count N_s in the signal counter (maximum count 3750 decimal) is multiplied by 5 to give the speed \dot{n} (maximum value 18 750) and the result transferred

to another two-byte register. The multiply instruction is available in larger micro-controllers: **MUL A,B** multiplies the numbers A and B together. In smaller micro-controllers the multiplication instruction is not available; here the signal count is added to itself five times.

Stage C. The measured speed n is in the form of a four-digit hexadecimal number PQRS; this must be converted into a five-digit decimal number JKNVW before it can be displayed. In principle this conversion first involves division by 100 decimal (64 hex) to obtain the number of hundreds and then division of both quotient and remainder by 10 decimal (A hex) to find the number of thousands, hundreds, tens and units. The resulting five digits J, K, N, V and W are then stored in five separate locations. In practice the division instruction is unlikely to be available in a micro-controller. The procedure here is to repeatedly subtract 10 000 decimal until the number just goes negative, then step back one; the number of subtractions is the value of the first digit J. Then repeatedly subtract 1000 decimal to find the second digit K and so on for N, V and W.

Stage D. The LCD character display controller/driver accepts input data in American Standard Code for Information Interchange (**ASCII**). This code is in either seven-digit binary (an eighth digit is added as a parity check) or hexadecimal form and is shown in Table 10.6.

There are 128 possible codes of which 96 are used for the display of characters; these include the numerals 0 to 9, the letters A to Z (upper and lower case), punctuation marks and other symbols. The remaining 32 codes are used for **control** of the display; these include LF (line feed), which moves the display to the next line, and CR (carriage return), which moves the display to the first position on the same line.

From Table 10.6 we see that the decimal numbers 0 to 9, which are represented by the four-digit binary codes 0000 to 1001, can be converted by adding 48 decimal, i.e. adding the three more significant digits 011, to give the seven-digit ASCII code. Each of the five decimal numbers JKNVW is thus converted into ASCII, and this information together with caption information is passed to the serial output interface. Here it is converted into binary **serial** form, i.e. a series of 1's and 0's, which are transmitted, one bit at a time, along a single wire to the display unit. Figure 10.14 shows the transmission of the letter 'M' in the binary ASCII coded form 1001101.

The above calculation would have been significantly simpler using floating-point numbers and a high-level language with multiplication and ASCII conversion operations.

Non-linear case

If the effects of environmental inputs can be neglected, eqn [10.17] simplifies to:

$$I = K'U + N'(U) + a' \quad [10.22]$$

In an 8-bit microcontroller programmed in assembly language, numbers can be in 16-bit, i.e. two-byte, form but the multiplication operation may not be available. This means that the non-linear function $N'(U)$ may not be realised using a polynomial in U , and a **look-up table** is normally used. We will consider the example of temperature measurement in the range 0 to 250 °C using a copper–constantan thermocouple.

Table 10.6 American Standard Code for Information Interchange (ASCII).

	ASCII character set (7-bit code)							
	More significant							
	0	1	2	3	4	5	6	7
Less significant	000	001	010	011	100	101	110	111
0	NUL	DLE	SP	0	@	P	'	p
0000								
1	SOH	DC1	1	1	A	Q	a	q
0001								
2	STX	DC2	"	2	B	R	b	r
0010								
3	ETX	DC3	#	3	C	S	c	s
0011								
4	EOT	DC4	\$	4	D	T	d	t
0100								
5	ENQ	NAK	%	5	E	U	e	u
0101								
6	ACK	SYN	&	6	F	V	f	v
0110								
7	BEL	ETB	'	7	G	W	g	w
0111								
8	BS	CAN	(8	H	X	h	x
1000								
9	HT	EM)	9	I	Y	i	y
1001								
A	LF	SUB	*	:	J	Z	j	z
1010								
B	VT	ESC	+	;	K	[k	{
1011								
C	FF	FS	,	<	L	\	l	:
1100								
D	CR	GS	—	=	M]	m	}
1101								
E	SO	RS	●	>	N	↑	n	~
1110								
F	SI	VS	/	?	O	↓	o	DEL
1111								

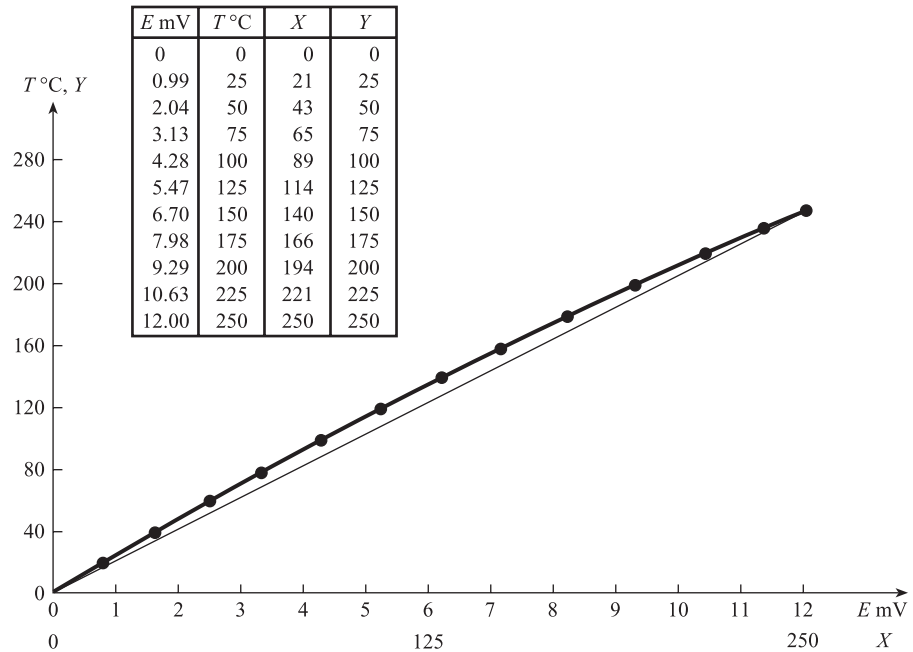
Figure 10.15 shows the graph of the inverse relation between temperature T °C and e.m.f. E mV (relative to a reference junction at temperature 0 °C). Here the vertical axis corresponds to the dependent variable T and the horizontal axis to the independent variable E . The table assumes 8-bit representation and shows some corresponding values of E , T , X and Y , where X and Y are integer variables scaled to take values between 0 and 250 and defined by the equations:

$$X = \frac{250}{12} E, Y = T \quad [10.23]$$

Thus a change in X of 1 corresponds to a change in E of 0.048 mV and a change in Y of 1 corresponds to a change in T of 1 °C. There are 251 pairs of values of X and

Figure 10.15

Temperature/e.m.f. relationship and look-up table for copper–constantan thermocouple.



Y , and 251 adjacent storage locations are used to store the value of Y corresponding to each value of X . The computer reads the value of input X and adds to it the address of the first storage location. This gives the address of the location where the corresponding value of Y is stored; this value is then fetched.

The importance of using scaled variables can be illustrated by the example of a 16-bit computer where high-level arithmetic operations are available but the numbers are in 16-bit integer form rather than floating point. Here a square root operation is available which is used to calculate the volume flow rate Q m³/h of liquid in a pipe from a measurement of the differential pressure ΔP created across an orifice plate flowmeter (Section 12.3.1). The range of integer variables is 0 to 65 535, but since $\sqrt{65\,535} = 256$, the square root operation could limit the number of calculated values of Q to 256. The problem is again solved by introducing scaled variables. Suppose the ranges of Q and ΔP are respectively 0 to 10 m³/h and 0 to 10⁴ Pa and they are related by the equation:

$$Q = 0.1\sqrt{\Delta P} \quad [10.24]$$

We now introduce integer variables X and Y scaled to take values between 0 and 65 535 and defined by the equations:

$$X = \frac{65\,535}{10^4} \Delta P, \quad Y = \frac{65\,535}{10} Q \quad [10.25]$$

The computer then solves the corresponding scaled equation:

$$Y = 256\sqrt{X} \quad [10.26]$$

In cases where both high-level arithmetic operations and floating-point representation of numbers are available then the non-linear function can be realised using a polynomial and the inverse equation solved without using scaled variables. If we

consider again the example of a copper–constantan thermocouple, this time measuring temperature T between 0 and 400 °C, the corresponding range of values of e.m.f. E will be 0 to 21 mV. If a 12-bit ADC is used, then the input to the computer can be regarded as a 12-bit integer decimal number X proportional to E , with range between 0 and 4095. Since 4095 corresponds to 21 mV, E is first calculated using:

$$E = \frac{21}{4095}X = 0.5128 \times 10^{-2}X \quad [10.27]$$

T is then calculated using the inverse equation:

$$T = 0.2555 \times 10^2 E - 0.5973 \times 10^0 E^2 + 0.2064 \times 10^{-1} E^3 - 0.3205 \times 10^{-3} E^4 \quad [10.28]$$

The coefficients in both equations can be expressed in floating-point form, and the operations of exponentiation, multiplication and addition can be used to solve eqn [10.28].

10.4.2 Dynamic digital compensation and filtering

Dynamic compensation has already been discussed in Section 4.4. Given an uncompensated element with transfer function $G_u(s)$, a compensating element $G_c(s)$ is introduced into the system such that the overall transfer function $G(s) = G_u(s)G_c(s)$ satisfies a given frequency response specification. The compensating transfer function $G_c(s)$ can be implemented using analogue signal conditioning elements; for example a lead-lag circuit (Figure 9.12) can be used to extend the frequency response of a thermocouple. In this section we see how a computer can be used as a **digital signal processor** to give a compensating z -transfer function $G_c(z)$. Also in Section 6.5.5 we saw how filtering can be used to reduce the effects of noise and/or interference on a signal. This improvement in signal-to-noise ratio can only be achieved if the signal spectrum occupies a frequency range which is substantially different from that of the noise/interference spectrum. In Section 9.2.1 we saw how an **analogue filter** $G(j\omega)$ for continuous signals can be implemented using an operational amplifier circuit. For example, the a.c. amplifier of Figure 9.12 is a band-pass filter. In this section we see how a **digital filter** $G(z)$ for sampled signals can be implemented using a digital signal processor.

Principles of digital signal processing^[4]

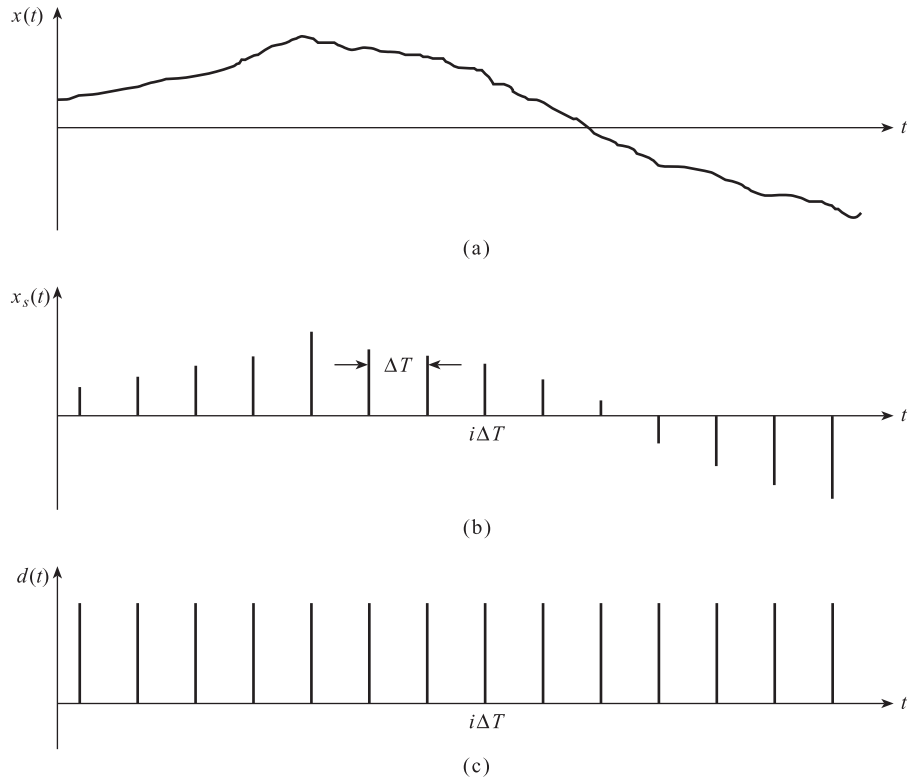
Figures 10.16(a) and (b) show a continuous signal $x(t)$ and the corresponding sampled signal $x_s(t)$; the sample interval is ΔT so that the i th sample occurs at time $i\Delta T$. Figure 10.16(c) shows an infinite train $d(t)$ of unit impulses; the i th impulse occurs at time $i\Delta T$ and is denoted by $\delta(t - i\Delta T)$ where $\delta(\cdot)$ is the **Dirac δ function**. We therefore have:

$$d(t) = \sum_{i=0}^{\infty} \delta(t - i\Delta T) \quad [10.29]$$

We can now regard $x_s(t)$ as the product of $x(t)$ and $d(t)$, i.e.:

$$x_s(t) = \sum_{i=0}^{\infty} x(t) \delta(t - i\Delta T) \quad [10.30]$$

Figure 10.16 Signal conversion:
 (a) Continuous signal
 (b) Sampled signal
 (c) Infinite impulse train.



The products $x(t)\delta(t - i\Delta T)$ are only non-zero at times $i\Delta T$ so that we have:

$$x_s(t) = \sum_{i=0}^{\infty} x(i\Delta T)\delta(t - i\Delta T) \quad [10.31]$$

We now calculate the **Laplace transform** $\bar{x}_s(s)$ of $x_s(t)$ (Section 4.1.1):

$$\bar{x}_s(s) = \mathcal{L}\left\{\sum_{i=0}^{\infty} x(i\Delta T)\delta(t - i\Delta T)\right\} = \sum_{i=0}^{\infty} x(i\Delta T)\mathcal{L}\{\delta(t - i\Delta T)\}$$

But

$$\mathcal{L}\{\delta(t - i\Delta T)\} = \exp(-i\Delta Ts)$$

(Laplace transform of a delayed unit impulse), giving:

*Laplace transform
of sampled signal*

$$\bar{x}_s(s) = \sum_{i=0}^{\infty} x(i\Delta T) \exp(-i\Delta Ts) \quad [10.32]$$

We now introduce the **z-transform** $\bar{x}_s(z)$ of $x_s(t)$ by defining:

$$z = \exp(\Delta Ts) \quad [10.33]$$

so that $z^{-1} = \exp(-\Delta Ts)$ corresponds to a time delay of one sampling interval and $z^{-i} = \exp(-i\Delta Ts)$ corresponds to a time delay of i sampling intervals. We therefore have:

*z-transform of
sampled signal*

$$\bar{x}_s(z) = \sum_{i=0}^{i=\infty} x(i)z^{-i} \quad [10.34]$$

The **frequency spectrum** of any signal $x(t)$ can be found by calculating the **Fourier transform** $\bar{x}(j\omega)$. To convert the Laplace transform $\bar{x}(s)$ into $\bar{x}(j\omega)$ we simply replace s by $j\omega$ (Section 4.2.2). Correspondingly to convert the z -transform $\bar{x}(z)$ into $\bar{x}(j\omega)$ we replace z by $\exp(j\omega\Delta T)$. The Fourier transform of the sampled signal $x_s(t)$ is therefore:

*Fourier transform of
sampled signal*

$$\bar{x}_s(j\omega) = \sum_{i=0}^{i=\infty} x(i\Delta T) \exp(-j\omega i\Delta T) \quad [10.35]$$

In Section 4.1.1 we defined the **transfer function** $G(s)$ of an element as the ratio of the Laplace transform of the output signal to that of the input signal. Here we can similarly define the z -transform $G(z)$ of a digital signal processor as the ratio of the z -transform of the output signal $\bar{y}(z)$ to that of the input signal $\bar{x}(z)$, i.e.

*z-transfer function
of an element*

$$G(z) = \frac{\bar{y}(z)}{\bar{x}(z)} \quad [10.36]$$

so that

$$\bar{y}(z) = G(z)\bar{x}(z)$$

Figure 10.17 shows a digital signal processor with transfer function $G(z)$ converting a sampled signal $x_s(t)$, with z -transform $\bar{x}(z)$, into a sampled signal $y_s(t)$ with z -transform $\bar{y}(z)$.

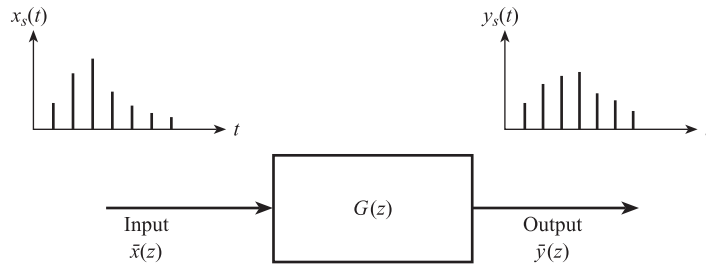
Types of digital filter

There are two main types of digital filter. The first is the **non-recursive filter**. Here $G(z)$ is of the form:

Non-recursive filter

$$G(z) = g_0 + g_1z^{-1} + g_2z^{-2} + \dots + g_nz^{-n} \quad [10.37]$$

Figure 10.17 Processing of sampled signals.



so that

$$\begin{aligned}\bar{y}(z) &= G(z)\bar{x}(z) \\ &= (g_0 + g_1z^{-1} + g_2z^{-2} + \dots + g_nz^{-n})\bar{x}(z)\end{aligned}$$

The **inverse transform** of $\bar{y}(z)$ is the value y_i of $y_s(t)$ at the i th sampling interval $i\Delta T$. This can be found by recalling that the operator z^{-1} corresponds to a time delay of one sampling interval. This means the inverse transform of $z^{-1}\bar{x}(z)$ is $x(i-1)$, i.e. the value of $x_s(t)$ one sampling interval earlier; similarly the inverse transform of $z^{-2}\bar{x}(z)$ is $x(i-2)$, etc. Thus we have:

Inverse transform of non-recursive filter

$$y_i = g_0x(i) + g_1x(i-1) + g_2x(i-2) + \dots + g_nx(i-n) \quad [10.38]$$

The inverse transform is often referred to as a **difference equation**. From eqn [10.38] we see that in a non-recursive filter, a given output sample value depends on input sample values only, i.e. it does not depend on output sample values, so there is no feedback from the output.

Figure 10.18 shows the implementation of a non-recursive filter using the operations of time shifting, coefficient multiplication and addition.

The second main type of digital filter is the **recursive filter**. Here $G(z)$ is of the form:

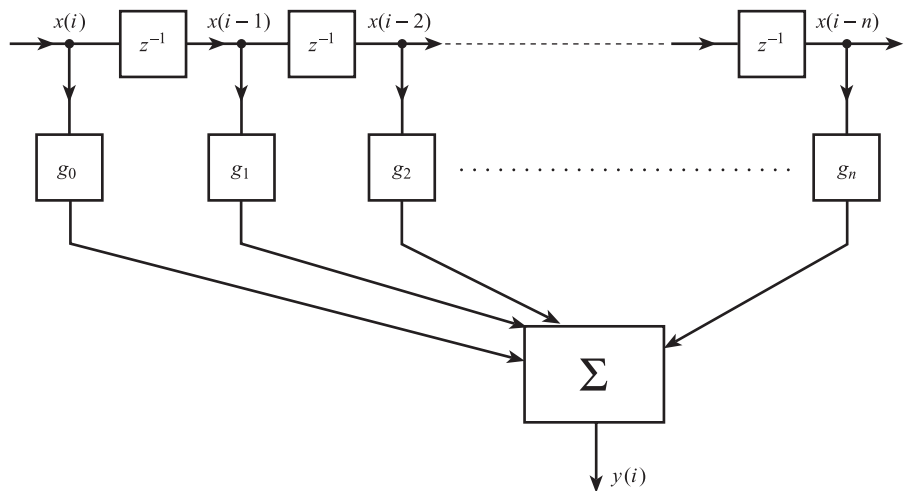
Recursive filter

$$G(z) = \frac{a_0 + a_1z^{-1} + a_2z^{-2} + \dots + a_nz^{-n}}{1 + b_1z^{-1} + b_2z^{-2} + \dots + b_mz^{-m}} = \frac{\bar{y}(z)}{\bar{x}(z)} \quad [10.39]$$

i.e.

$$\begin{aligned}(a_0 + a_1z^{-1} + a_2z^{-2} + \dots + a_nz^{-n})\bar{x}(z) \\ = (1 + b_1z^{-1} + b_2z^{-2} + \dots + b_mz^{-m})\bar{y}(z)\end{aligned}$$

Figure 10.18
Implementation of non-recursive filter.



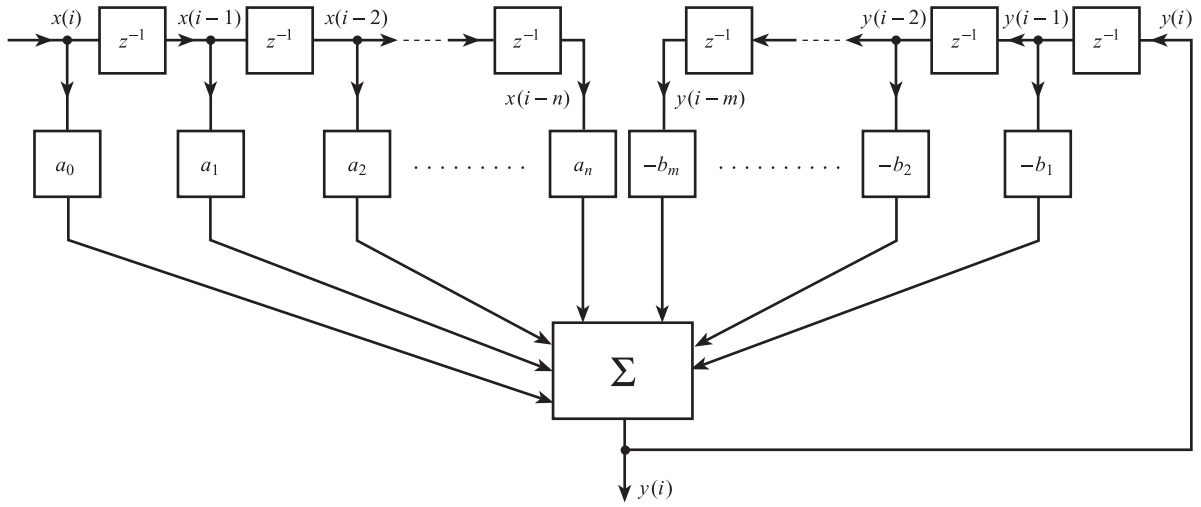


Figure 10.19 Implementation of a recursive filter.

Using the same procedure as above, the corresponding inverse transform or difference equation is:

$$y(i) + b_1 y(i-1) + b_2 y(i-2) + \dots + b_m y(i-m) = a_0 + a_1 x(i-1) + a_2 x(i-2) + \dots + a_n x(i-n)$$

giving:

*Inverse transform
of recursive filter*

$$y_i = [a_0 x(i) + a_1 x(i-1) + \dots + a_n x(i-n)] - [b_1 y(i-1) + b_2 y(i-2) + \dots + b_m y(i-m)] \quad [10.40]$$

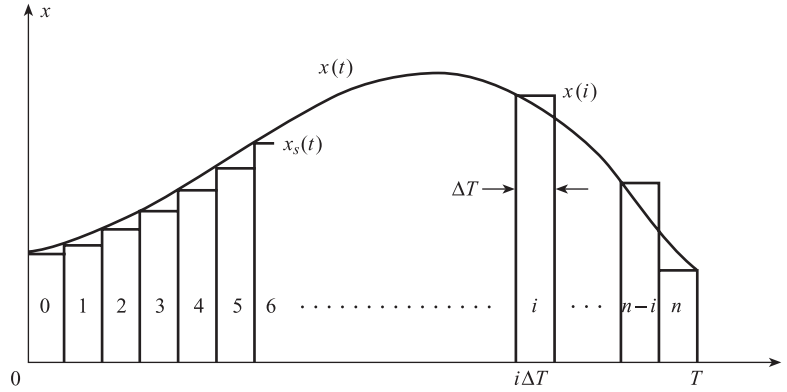
From eqn [10.40] we see that in a recursive filter, a given output sample value depends on both input and output sample values, meaning there is feedback from the output. Figure 10.19 shows the implementation of a recursive filter.

Examples of digital filters and compensators

Integration. There are several situations where a signal must be integrated in order to obtain the required measured value. Two common examples are the calculation of the total mass of fluid delivered in a given time interval and the determination of the composition of a gas from the areas under the peaks in a gas chromatograph. Figure 10.20 shows how the definite integral $\int_0^T x(t) dt$, the area under the continuous function $x(t)$, may be approximated by the area under the sampled signal $x_s(t)$. The area of the rectangle associated with the i th sample value is $x(i)\Delta T$. Thus the integral:

$$y(T) = \int_0^T x(t) dt$$

Figure 10.20
Approximate evaluation
of definite integral.



may be approximated by the difference equation:

*Sampled approximation
to integral*

$$y(T) \approx y(n) = \Delta T \sum_{i=0}^{i=n} x(i) \quad [10.41]$$

where $(n + 1)\Delta T = T$.

Differentiation. There are also situations where a signal must be differentiated to obtain the required measured value. Examples are the calculation of the rate of change of temperature in a reactor or the rate of change of flow rate in a pipe. In some situations the derivative:

$$\dot{x}(t) = \frac{dx}{dt}$$

may be approximated by the difference equation:

*Sampled approximation
to derivative*

$$\dot{x}(i) = \frac{1}{\Delta T} [x(i + 1) - x(i)] \quad [10.42]$$

However, for this method to be valid, there should be sufficient binary digits to ensure a large number of quantisation levels and small quantisation errors.

Band pass filter. We consider the example of a band pass filter which is used to improve the signal-to-noise ratio for a sinusoidal vortex flowmeter signal affected by wide-band random turbulence (Section 12.3.3). A suitable filter has the z -transform:

$$G(z) = \frac{1 - z^{-2}}{1 - 2r \cos(\omega_0 \Delta T) z^{-1} + r^2 z^{-2}} \quad [10.43]$$

where ω_0 rad/s is the centre frequency of the filter, ΔT s the sampling interval and r a dimensionless parameter between 0 and 1 which determines the bandwidth of the filter. If we require f_0 to be 40 Hz, use a sampling frequency f_s of 300 samples/s and choose r to be 0.95, we have:

$$\omega_0 = 2\pi \times 40 \text{ rad/s}$$

$$\Delta T = \frac{1}{f_s} = 3.33 \times 10^{-3} \text{ s}$$

$$\omega_0 \Delta T = 0.837$$

$$\cos \omega_0 \Delta T = 0.670$$

giving

$$G(z) = \frac{\bar{y}(z)}{\bar{x}(z)} = \frac{1 - z^{-2}}{1 - 1.272z^{-1} + 0.903z^{-2}} \quad [10.44]$$

The frequency response $G(j\omega)$ of the filter can be found by replacing z^{-1} by $e^{-j\omega\Delta T}$ and z^{-2} by $e^{-2j\omega\Delta T}$ to give:

$$G(j\omega) = \frac{1 - e^{-2j\omega\Delta T}}{1 - 1.272e^{-j\omega\Delta T} + 0.903e^{-2j\omega\Delta T}} \quad [10.45]$$

If ω_s rad/s is the angular sampling frequency, then $\Delta T = 2\pi/\omega_s$, giving:

$$G(j\omega) = \frac{1 - \exp(-j4\pi\omega/\omega_s)}{1 - 2.272 \exp(-j2\pi\omega/\omega_s) + 0.903 \exp(-j4\pi\omega/\omega_s)} \quad [10.46]$$

Figure 10.21(a) shows the magnitude $|G(j\omega)|$ and argument $\arg G(j\omega)$ of $G(j\omega)$ plotted against normalised frequency ω/ω_s .

Rearranging eqn [10.44] gives:

$$(1 - 1.272z^{-1} + 0.903z^{-2})\bar{y}(z) = (1 - z^{-2})\bar{x}(z)$$

and taking the inverse transform gives the difference equation:

$$y(i) - 1.272y(i-1) + 0.903y(i-2) = x(i) - x(i-2)$$

i.e.

$$y(i) = x(i) - x(i-2) + 1.272y(i-1) - 0.903y(i-2) \quad [10.47]$$

Figure 10.21(b) shows the flowsheet for a program which solves eqn [10.47] to implement the digital filter.

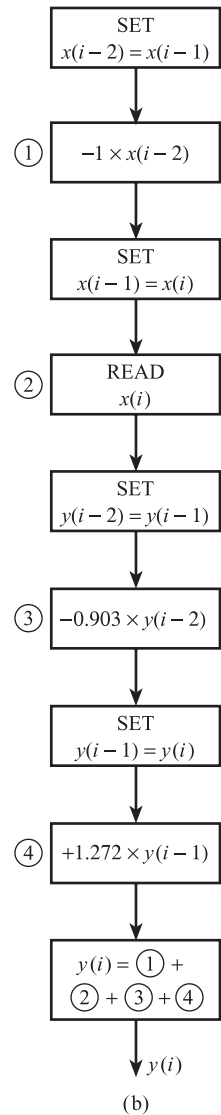
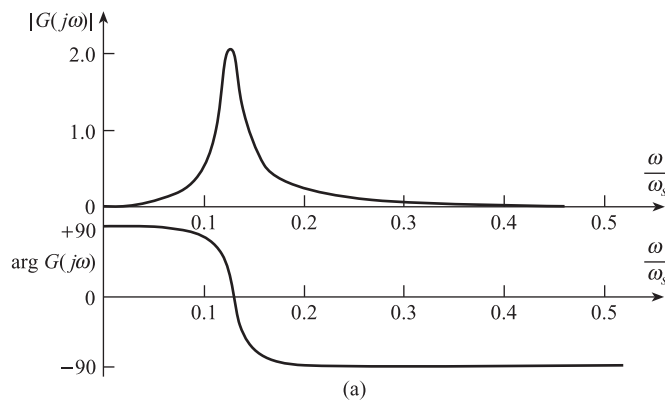
We see that in order to implement recursive and non-recursive filters the operations of multiplication and addition/subtraction are continually required. This has led to the development of microprocessors with highly optimised architecture and instruction sets for specialised digital signal processing (DSP) operations.

Conclusion

This chapter has discussed the conversion of analogue signals into digital form. It has examined the structure of computers and microcontrollers, their operation and software. The use of computers and microcontrollers to perform steady-state and dynamic digital calculations to establish the measured value of a variable has been discussed.

Figure 10.21

Band-pass digital filter:
(a) Frequency response
(b) Implementation.



References

- [1] Intel Corporation 2000 *Technical Information on Intel 8088 Microprocessors*.
- [2] Intel Corporation 2001 *Technical Information on Intel 8052 Microcontrollers*.
- [3] National Instruments 1998 *Functional Reference Manual for LabVIEW Graphical Programming Language*.
- [4] BROOK D and WYNNE R J 1988 *Signal Processing – Principles and Applications*, Edward Arnold, London.

Problems

- 10.1 An analogue-to-digital converter has an input range of 0 to 5 V and incorporates a 12-bit encoder.
- Assuming a binary encoder, find:
 - the maximum percentage quantisation error;
 - the digital output signals corresponding to input voltages of 0.55 V and 2.63 V.
 - Convert the binary codes of (a) (ii) into hexadecimal form.
 - Repeat (a) assuming a three-decade, 8:4:2:1 binary-coded decimal (b.c.d.) encoder.

- 10.2 The digital-to-analogue converter of Figure 10.6(a) is required to give an output voltage in the range 0 to 2.55 V, corresponding to an 8-bit digital input signal 00000000 to 11111111.
- Assuming $V_{\text{REF}} = -15$ V, $R = 1$ k Ω , calculate the value of R_F required.
 - Find the output voltage corresponding to an input signal of 11000101.

- 10.3 An analogue first-order low-pass filter has the transfer function

$$G(s) = \frac{1}{1 + \tau s}$$

where τ is the time constant of the filter.

- What is the 3 dB bandwidth of the analogue filter?
- Use the bilinear transformation

$$s = \frac{2}{\Delta T} \left(\frac{1 - z^{-1}}{1 + z^{-1}} \right)$$

where ΔT is the sampling interval, to show that an equivalent digital filter has the z -transfer function:

$$G(z) = \frac{\bar{y}(z)}{\bar{x}(z)} = \frac{a_0 + a_1 z^{-1}}{1 - b z^{-1}}$$

where

$$a_0 = a_1 = \frac{1}{\left(\frac{2\tau}{\Delta T} + 1 \right)}, \quad b_1 = \frac{\left(\frac{2\tau}{\Delta T} - 1 \right)}{\left(\frac{2\tau}{\Delta T} + 1 \right)}$$

- Hence show that the corresponding difference equation is:

$$y(i) = a_0 x(i) + a_1 x(i-1) + b_1 y(i-1)$$

- In the special case that $2\tau/\Delta T = 1$ show that:

$$G(z) = \frac{1}{2}(1 + z^{-1})$$

and that:

$$|G(j\omega)| = \cos \frac{\omega \Delta T}{2}, \quad \arg G(j\omega) = -\frac{1}{2} \omega \Delta T$$

What is the 3 dB bandwidth of this filter?

- 10.4 The output signal of a vortex flowmeter has a frequency range between 5 and 50 Hz. The mean period of the signal is to be measured using a signal counter and a clock counter. The signal is input to the signal counter, which increments until N_s cycles have been counted. The clock counter is 16-bit binary and has a clock input of frequency 10 kHz. The clock counter increments until a count of N_c is registered on the signal counter. What is the maximum possible value of N_s ?

11 Data Presentation Elements

The data presentation element is the final element in the measurement system, its function being to communicate the measured value of the variable to a human observer. It is important that the measured value is presented as clearly and easily as possible, otherwise the value registered by the observer may be different. Consider an accurate flow measurement system where the true value of flow rate is $11.3 \text{ m}^3 \text{ h}^{-1}$ and the measured value $11.5 \text{ m}^3 \text{ h}^{-1}$, i.e. a **measurement system error** of $11.5 - 11.3 = 0.2 \text{ m}^3 \text{ h}^{-1}$. If the observed value is $12.0 \text{ m}^3 \text{ h}^{-1}$, then the **observation error** is $12.0 - 11.5 = 0.5 \text{ m}^3 \text{ h}^{-1}$. This is greater than the measurement error and means that the high system accuracy is wasted.

Observation error depends on many factors:

- Distance of the element from the observer
- Ambient lighting
- Eyesight, patience and skill of the observer.

However, a clear presentation is of major importance. This chapter begins by reviewing **data presentation** elements in current use, and goes on to examine their principles and characteristics in detail.

11.1

Review and choice of data presentation elements

Figure 11.1 classifies data presentation elements in wide current use, showing the relevant section in the chapter where the device is covered. It begins by classifying elements into **displays** and **recorders/printers**.

If no permanent record of measured variables is required, then displays can be used. A choice must first be made between **analogue pointer-scale indicators** and **digital displays**. With the pointer-scale indicator, the observer must **interpolate** if the pointer lies between two scale marks: thus if the pointer lies between 9 and 10 the observer must decide whether the measured value is say 9.4, 9.5 or 9.6. Thus an observation error of up to ± 0.5 units is possible. This problem is avoided with a two-decade digital display, which presents the number directly as 9.5.

Section 11.3 discusses the principles of **character** displays, which display numerals and letters of the alphabet, and **graphic** displays, which can also show line diagrams, graphs and waveforms, etc.

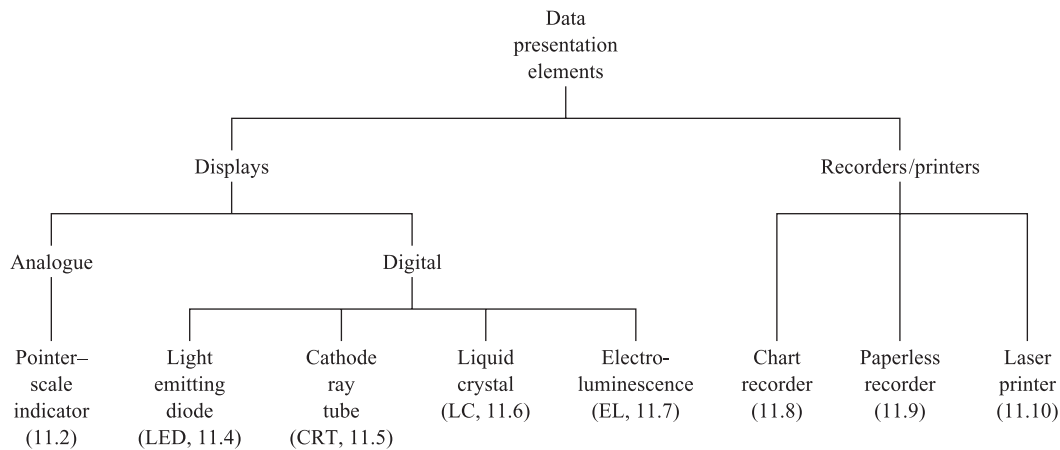


Figure 11.1
Classification of data
presentation elements.

There are four types of digital display technology in wide current use: **light emitting diodes (LED)**, **cathode ray tubes (CRT)**, **liquid crystal displays (LCD)** and **electroluminescent displays (EL)**. LEDs have high power consumption, which makes them only suitable for small-scale character displays; they are not used in graphic displays. CRTs are used for character and graphics displays, monochrome and colour, but have the disadvantage of high operating voltages and are high-volume bulky devices. LCDs are used for both character and graphics displays. LCD character displays, usually monochrome, have much lower power consumption than equivalent LED displays. LCD graphics displays, monochrome and colour, are **flat screen** panels and have lower operating voltages and power consumption than equivalent CRT devices. Electroluminescent displays are also flat screen and are used for both character and graphics monochrome displays. They have higher operating voltages and power consumption than equivalent LCD devices but greater contrast ratio and viewing angle.

A record of the time variation of the measured variables would be essential, for example, in the following situations:

- High-speed events, e.g. a human heartbeat, which are too fast to be followed by a human observer. Changes in the recorded blood pressure waveform will then show clearly any irregular or abnormal behaviour.
- The monitoring of a complex process such as a gas compressor which has a number of associated measured variables. If the compressor breaks down, then the exact sequence of events *drop in lubricating oil pressure – rise in bearing temperature – drop in delivery pressure* can be found and the cause of failure established.
- Large amounts of data which are to be used in numerical calculations. Examples are the calculations of the yield and efficiency of a chemical reactor from composition, temperature, pressure and flow-rate data, and the value of gas transferred from supplier to customer in a given month.

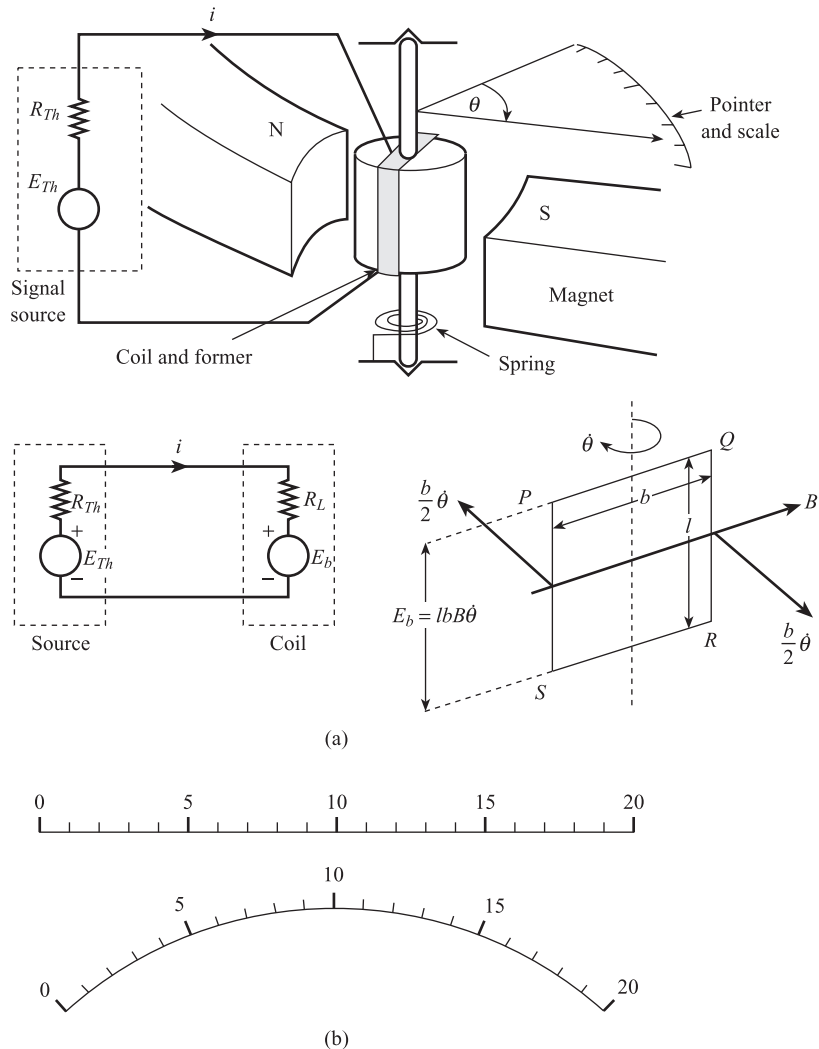
Chart recorders give a record, on paper, of the time variation of a measured variable; these can be analogue or digital and the record can be either a continuous line or a series of dots. They can record up to six variables but have limited speed of response; they also require regular replacement of paper and pens. A chart recorder could be

satisfactorily used in situation (b). **Paperless** recorders use LCD displays and digital archive memory; these typically can record four measured variables and have less maintenance requirements than chart recorders. They also have a fast speed of response and could be satisfactorily used in situation (a). **Laser printers** can print large amounts of data, in character or graphics form, on paper. A laser printer would therefore be ideal in situation (c) where large tables of numerical data need to be printed out for checking and calculation.

11.2 Pointer-scale indicators

These are analogue display devices. Figure 11.2(a) shows simplified diagrams and an equivalent circuit for a moving coil indicator connected to a Thévenin signal source

Figure 11.2
Pointer-scale indicators: principle and recommended scale format:
(a) Mechanical arrangement and circuit
(b) Scales.



E_{Th} , R_{Th} . The coil is situated in a radial magnetic field of flux density B , so that a current i through the coil produces a deflecting torque:

$$T_D = BnAi \quad [11.1]$$

where A is the cross-sectional area of the coil and n the number of turns. This deflecting torque is opposed by the spring restoring torque:

$$T_R = c\theta \quad [11.2]$$

where c is the spring stiffness and θ the angular deflection. Assuming negligible frictional torque, the resultant unbalanced torque on the coil is $T_D - T_R$. This is equal to the product of moment of inertia I and angular acceleration $d^2\theta/dt^2$, i.e.

$$BnAi - c\theta = I \frac{d^2\theta}{dt^2} \quad [11.3]$$

The current i is given by:

$$i = \frac{E_{Th} - E_b}{R_{Th} + R_L} \quad [11.4]$$

where R_L is the resistance of the coil and E_b is the back e.m.f. induced in the coil due to its motion in the magnetic field. E_b can be calculated using Faraday's law of electromagnetic induction as shown in Figure 11.1(a). If we consider one turn $PQRS$ of the coil, then the voltage induced in PS , with length l moving with translational velocity $(b/2)(d\theta/dt)$ perpendicular to the magnetic field B , is $Bl(b/2)(d\theta/dt)$. An equal and opposite voltage is induced in QR , so that the resultant voltage in $PQRS$ is $Blb(d\theta/dt)$, i.e. $BA(d\theta/dt)$ since $A = lb$. The total back e.m.f. for a coil of n turns is:

$$E_b = nAB \frac{d\theta}{dt} \quad [11.5]$$

From [11.3]–[11.5] we have:

$$BnA \left[\frac{E_{Th} - nAB(d\theta/dt)}{R_{Th} + R_L} \right] - c\theta = I \frac{d^2\theta}{dt^2} \quad [11.6]$$

i.e.

*Differential equation
for pointer-scale
indicator*

$$\frac{I}{c} \frac{d^2\theta}{dt^2} + \frac{(nAB)^2}{c(R_{Th} + R_L)} \cdot \frac{d\theta}{dt} + \theta = \frac{nAB}{c(R_{Th} + R_L)} E_{Th} \quad [11.7]$$

By defining $\Delta\theta$ and ΔE_{Th} to be deviations from initial steady conditions $\theta(0-)$, $E_{Th}(0-)$ (Section 4.1.2) we can derive the transfer function for the indicator. This can be expressed in the standard second-order form:

*Transfer function for
pointer-scale indicator*

$$\frac{\Delta\tilde{\theta}}{\Delta\tilde{E}_{Th}}(s) = \frac{K}{\frac{1}{\omega_n^2} s^2 + \frac{2\xi}{\omega_n} s + 1} \quad [11.8]$$

where

$$\text{Steady-state sensitivity} \quad K = \frac{nAB}{c(R_{th} + R_L)} \text{ rad V}^{-1}$$

$$\text{Natural frequency} \quad \omega_n = \sqrt{\frac{c}{I}} \text{ rad s}^{-1}$$

$$\text{Damping ratio} \quad \xi = \frac{(nAB)^2}{2\sqrt{cI(R_{th} + R_L)}}$$

From eqn [11.8] we see that the steady-state sensitivity K depends on magnetic flux density B , spring stiffness c and total circuit resistance $R_{th} + R_L$. Reducing c gives a larger K but a lower ω_n ; similarly increasing n and A also increases K but this gives a larger moment of inertia I and again reduced ω_n . The value of K is affected by stray magnetic fields, ferrous instrument panels (altering B), temperature and ageing (altering c). Departures from the ideal steady-state relation $\theta = (nAB/c)i$ are quantified using error bands (Section 2.1); there are typically nine classes of accuracy, ranging from $\pm 0.05\%$ to $\pm 5\%$ of f.s.d.

A typical meter has a coil resistance of 75Ω , $\pm 2.5\%$ error bands, input range 0 to 1 mA, and output range 0 to $\pi/2$ radians, i.e. a current sensitivity of $1.57 \times 10^3 \text{ rad A}^{-1}$. The moment of inertia I of the coil-former-pointer assembly is fairly large, so that ω_n is small, typically $f_n \approx 0.5$ to 1.5 Hz . The damping ratio ξ depends on the total circuit resistance $R_{th} + R_L$; a value for ξ of around 0.7 is ideal (Section 4.3). If ξ is greater than 0.7 (with a given R_{th} and R_L), it can be reduced by connecting an additional resistance in *series* with R_L . This causes a corresponding reduction in sensitivity. If ξ is less than 0.7, it can be increased by connecting a resistance in *parallel* with R_L . This causes a corresponding increase in sensitivity. The scale corresponds to the range of the measured variable, e.g. 0 to 200°C , 0 to $50 \text{ m}^3 \text{ h}^{-1}$. In order to reduce observation error it is important that the scale should be legible, clear and not overcrowded with scale marks.

Experiments show that observers are able to mentally subdivide a scale division into five equal parts with reasonable accuracy. To achieve an observation error of 1% of f.s.d., each part should be about 1% of the scale range. This means a scale with 20 minor divisions, usually grouped into four or five major divisions as shown in Figure 11.2(b).

11.3

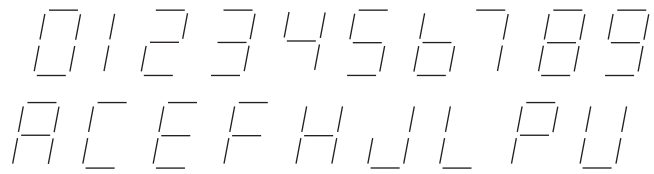
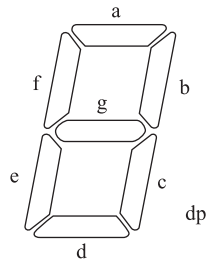
Digital display principles

11.3.1 Character displays

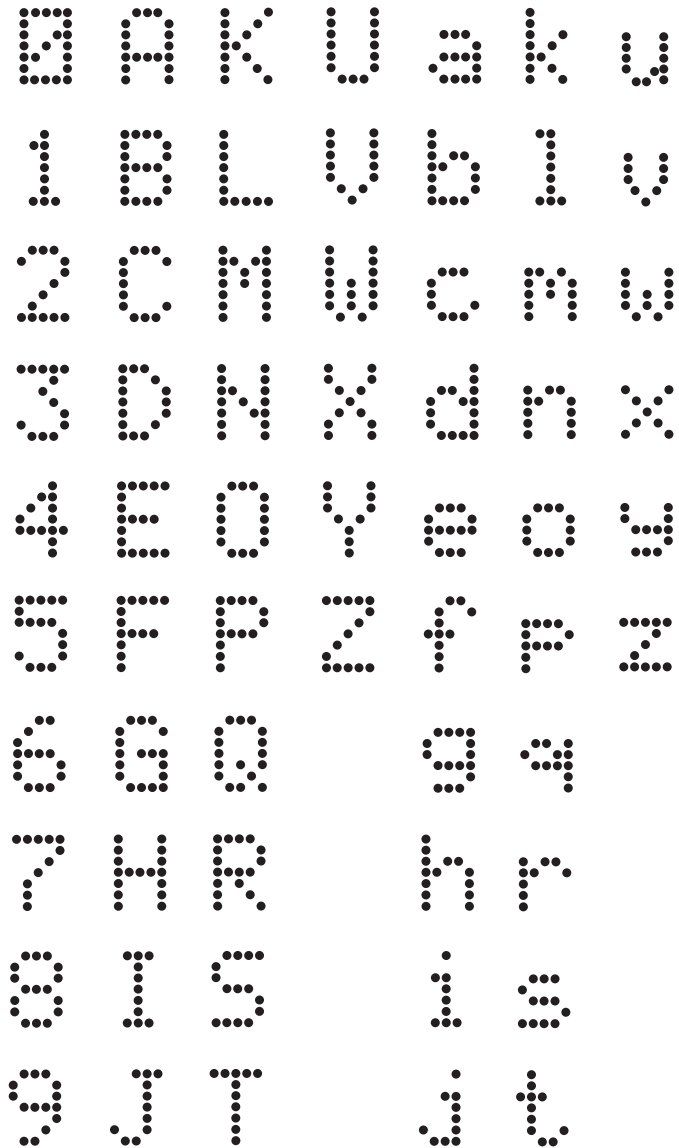
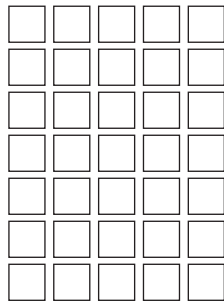
These are used to display the numerals 0 to 9, the letters of the alphabet A to Z in either upper or lower case format, and a few other symbols such as punctuation marks. Displays showing alphabetical and numerical information are often referred to as **alphanumeric**.

Figure 11.3 shows two character formats in widespread use: seven-segment and 7×5 dot-matrix. Figure 11.3(a) shows seven segments a to g arranged in a figure-of-eight configuration and the corresponding character set. This is limited to the ten numerals and nine upper case letters. The 7×5 dot-matrix format enables a far larger

Figure 11.3 Character formats for displays:
 (a) Seven-segment character format
 (b) 7×5 dot-matrix character format.



(a)

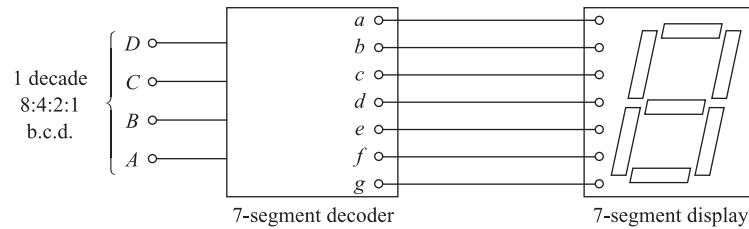


(b)

set of typically 192 characters to be obtained; this includes all the numerals, upper and lower case letters (Figure 11.3(b)), together with Greek letters and other symbols. A 9×7 dot-matrix format gives a better representation of lower case letters.

Each character format is an array of segments or dots; these elements are referred to as **pixels**. To display a character each pixel must be separately switched 'on' and 'off' independently of the other pixels. When a pixel is switched on, either it is a source emitting light or it is modulating light from other sources. When a pixel is switched off it is either not emitting light or not modulating light. As an example, suppose we wish to display the numerals 0 to 9 using the seven-segment format (Figure 11.4). Each of the pixels *abcdefg* can be switched individually on or off using a seven-digit parallel binary code where a '1' corresponds to 'on' and a '0' to 'off'. Figure 11.4 shows the seven-segment codes corresponding to the numerals 0 to 9. A seven-segment decoder is used to convert the input parallel digital signal, usually in binary coded decimal (b.c.d.) or ASCII format, into seven-segment code. Figure 11.4 shows

Figure 11.4 Display of numerals using seven-segment format.



Denary number	b.c.d. code D C B A	7-segment code							Displayed numeral
		<i>a</i>	<i>b</i>	<i>c</i>	<i>d</i>	<i>e</i>	<i>f</i>	<i>g</i>	
0	0 0 0 0	1	1	1	1	1	1	0	
1	0 0 0 1	0	1	1	0	0	0	0	
2	0 0 1 0	1	1	0	1	1	0	1	
3	0 0 1 1	1	1	1	1	0	0	1	
4	0 1 0 0	0	1	1	0	0	1	1	
5	0 1 0 1	1	0	1	1	0	1	1	
6	0 1 1 0	0	0	1	1	1	1	1	
7	0 1 1 1	1	1	1	0	0	0	0	
8	1 0 0 0	1	1	1	1	1	1	1	
9	1 0 0 1	1	1	1	0	0	1	1	

the table to convert the DCBA code, representing one decade of 8421 b.c.d., to the seven-segment *abcdefg* code. Decoders are also used to convert input data in parallel b.c.d. or ASCII format into 7×5 or 9×7 format for dot-matrix displays; the logic is normally implemented using a read only memory (ROM).

11.3.2 Graphic displays

Graphic displays are used to show line diagrams, graphs, waveforms, bar charts, etc., and consist of a large number of pixels arranged in rows (along the y -axis) and columns (along the x -axis). A typical graphic display consists of 320×240 , i.e. 76 800, pixels each of area $0.33 \text{ mm} \times 0.33 \text{ mm}$, giving a total viewing area of $120 \text{ mm} \times 92 \text{ mm}$. To make electrical contact with each individual pixel would require 76 800 electrical connections occupying an area of a few square metres! Since this is clearly impossible, some method of multiplexing must be found.

The principle of **pixel matrix multiplexing** is based on **time division multiplexing**, where one pair of conductors can serve many pixels by suitable timing of the voltage across the conductors. The pixels are arranged in a matrix of columns (x) and rows (y). Each column (x) and each row (y) has an electrical conductor giving a corresponding matrix of conductors. Each pixel, with position coordinates (x, y), is connected across the corresponding x and y conductors at their point of intersection (Figure 11.5(a)). The voltage applied to a column conductor will be present at all of the pixels in that column; the voltage applied to a row conductor will be present at all of the pixels in that row. The minimum voltage to turn a pixel 'on', i.e. to emit or modulate light, is V_s . The column voltages V_x switch between 0 and $+V_s/2$; there will be m transitions during each repetition period T , where m is the number of pixels in each column. The row voltages V_y switch between 0 and $-V_s/2$; there will be n transitions during each repetition period T , where n is the number of pixels in each row. A pixel at position (x, y) is switched on during a time interval when the column voltage V_x is $+V_s/2$ and the row voltage V_y is $-V_s/2$.

Figure 11.5(a) shows a 3×3 matrix of pixels and Figure 11.5(b) the corresponding column voltage waveforms V_x and row voltage waveforms V_y . The pixel (2, 1) is switched on during time interval 0 to $T/3$. The pixels (1, 1), (2, 1), (1, 3) and (2, 3) are switched on during the time interval $T/3$ to $2T/3$. Pixel (3, 2) is switched on during time interval $2T/3$ to T . In this example there are six electrical conductors for nine pixels so that the saving in external connections is small. However, in the above example of a 320×240 matrix, $320 + 240 = 560$ external connections are required to address 76 800 pixels. All waveforms are repeated every repetition period T ; this is to refresh the display. Provided T is sufficiently short, the brightness of the screen remains reasonably constant without flicker.

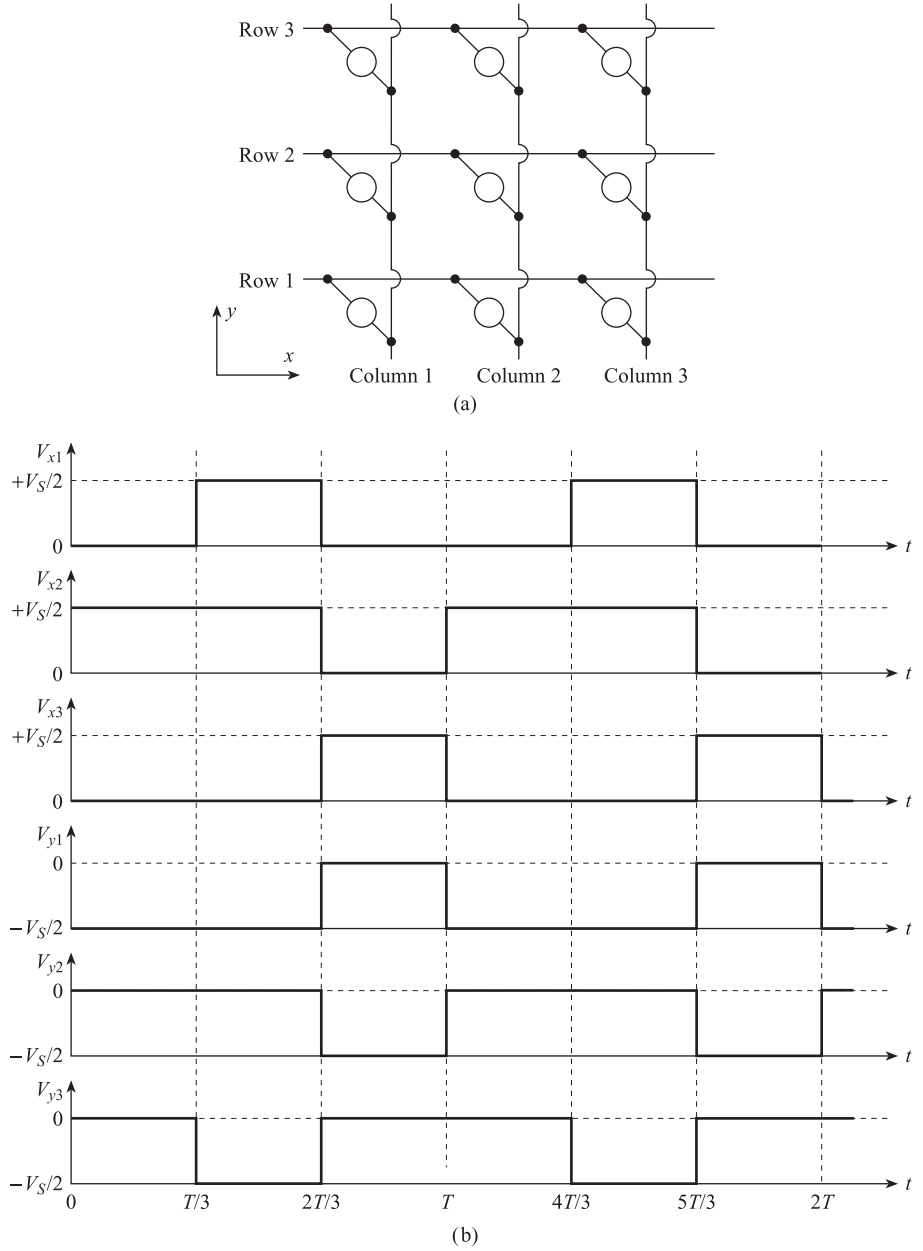
11.4

Light-emitting diode (LED) displays

When a semiconductor diode is forward biased, as shown in Figure 11.6(a), a current i_F flows, which depends exponentially on the forward voltage V_F :

$$i_F = i_s \exp\left(\frac{qV_F}{k\theta}\right) \quad [11.9]$$

Figure 11.5
Pixel multiplexing:
(a) 3×3 pixel matrix
(b) Voltage waveforms.



where i_s is the reverse saturation current, q the electron or hole charge, k Boltzmann's constant and θ K the absolute temperature. Taking natural logarithms we have:

$$\log_e i_F = \frac{q}{K\theta} V_F + \log_e i_s \quad [11.10]$$

i.e. there is an approximately linear relation between $\log_e i_F$ and V_F as shown in Figure 11.6(b).

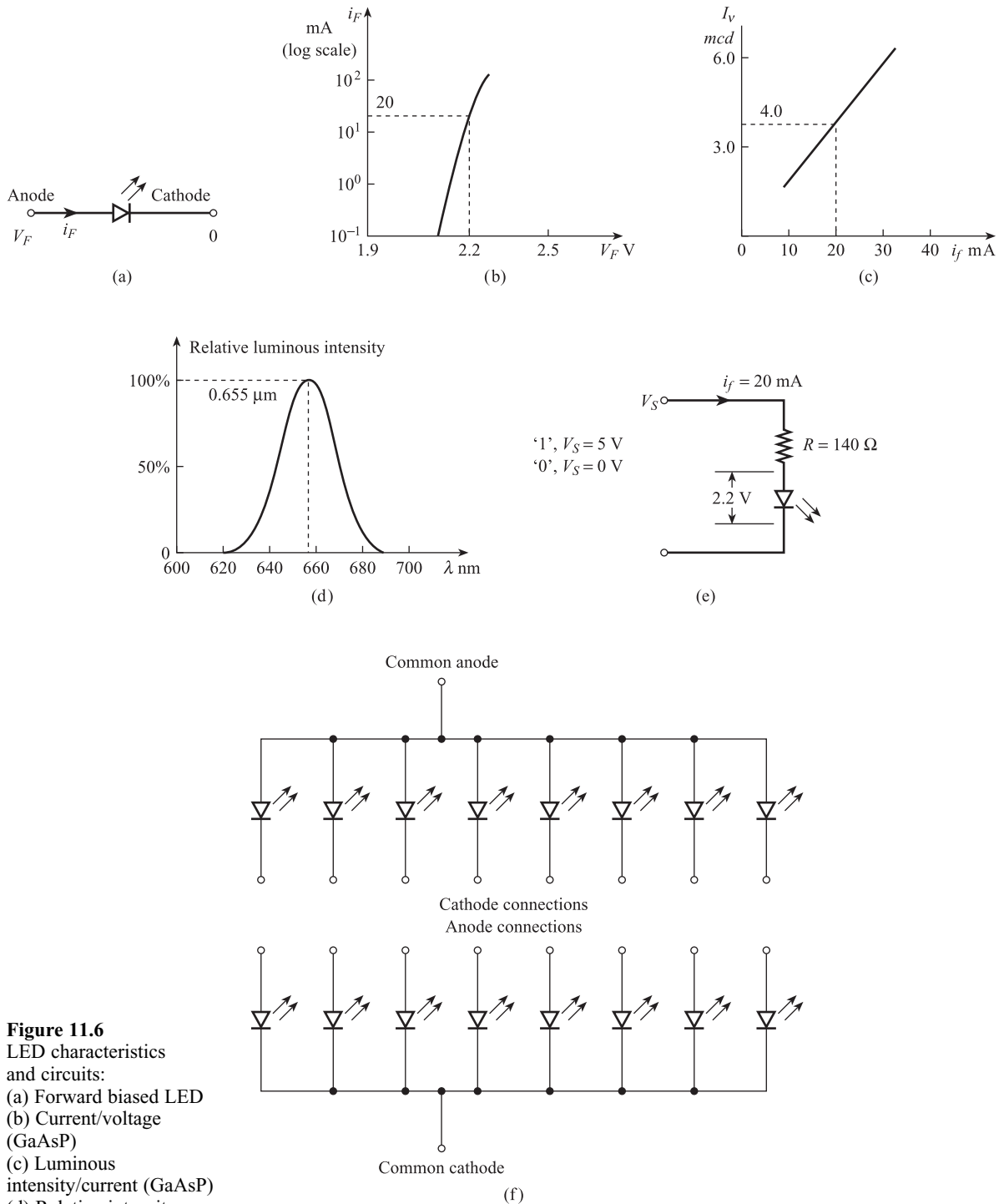


Figure 11.6
LED characteristics
and circuits:
(a) Forward biased LED
(b) Current/voltage
(GaAsP)
(c) Luminous
intensity/current (GaAsP)
(d) Relative intensity
wavelength (GaAsP)
(e) Series resistor
(f) Interconnection
methods.

Light-emitting diodes have the special property that when forward biased they emit electromagnetic radiation over a certain band of wavelengths. Two commonly used LED materials are gallium arsenide phosphide (GaAsP), which emits red light, and gallium phosphide (GaP), which emits green or yellow light. In both cases the luminous intensity I_v of the diode light source increases with current i_F ; for GaAsP diodes the relationship is approximately linear (Figure 11.6(c)). The light emitted by a GaAsP (red) diode is distributed over a narrow band of wavelengths centred on $0.655 \mu\text{m}$. Figure 11.6(d) shows the relationship between relative luminous intensity and wavelength λ . Similarly the light emitted by a GaP (green) diode is distributed over a narrow band of wavelengths centred on $0.560 \mu\text{m}$. The human eye is far more sensitive to green light than red, so a green LED of low radiant power may appear as bright as a red LED of much higher radiant power. The response of LEDs to step changes in i_F is extremely fast; turn-on and turn-off times of 10 ns are typical.

When switched 'on', a typical GaAsP diode requires a forward current i_F of around 20 mA corresponding to a luminous intensity I_v of 4.0 mcd (millicandela), and a forward voltage V_F of 2.2 V. When used as a display pixel the diode should be switched 'on' by a logic signal in the '1' state, and switched 'off' when the signal is in the '0' state. Figure 11.6(e) shows a simple circuit for achieving this, using a series resistor R of 140Ω . For a '1' input, $V_S \approx 5 \text{ V}$, $i_F = (5 - 2.2)/140 = 20 \text{ mA}$ and the diode is 'on'. For a '0' input, $V_S \approx 0 \text{ V}$, i_F is negligible and the diode is 'off'. Alternatively a 20 mA constant current source may be switched in and out by the logic signal.

A seven-segment LED display device consists of eight individual LEDs, one for each segment and one for the decimal point. There are two possible methods of interconnection, common anode or common cathode (Figure 11.6(f)).

Using the above data, the power consumption of an individual pixel is $2.2 \times 20 \times 10^{-3} \text{ W}$, i.e. 44 mW; the total power consumption of the seven-segment display is therefore around 320 mW. This high power consumption means that LEDs are only suitable for character displays and are unsuitable for graphics displays.

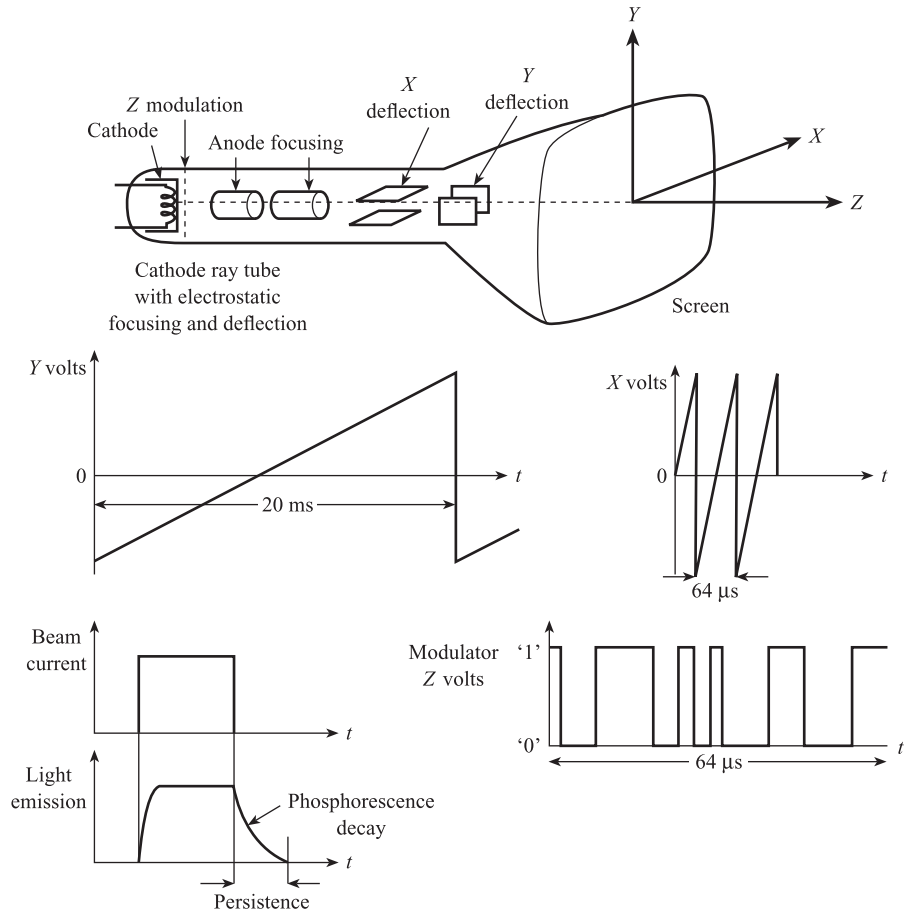
11.5

Cathode ray tube (CRT) displays

Cathode ray tubes are used to create large-scale displays. These devices are often referred to as **monitors**. A **visual display unit (VDU)** is a combination of a CRT display and a keyboard.

Figure 11.7 shows a basic CRT: electrons are emitted at the cathode and accelerated towards the anode. A third electrode, called a grid or modulator, is placed between cathode and anode: by altering the potential of the modulator the number of electrons in the beam, i.e. the beam current, can be adjusted. The beam then passes through a focusing system followed by X and Y deflection systems: the focusing and deflection systems can be electromagnetic (EM), or electrostatic (ES) as shown in the diagram. The electron beam is brought to a focus on the inside surface of the screen, which is coated with a large number of **phosphor dots**. These dots form the pixels. Phosphors are semiconductor materials which emit visible radiation in response to the impact of electrons: a spot of light therefore appears on the screen. In response to a pulse change in beam current, i.e. a sudden increase followed by a sudden decrease, the light emission does not fall instantaneously but there is a gradual

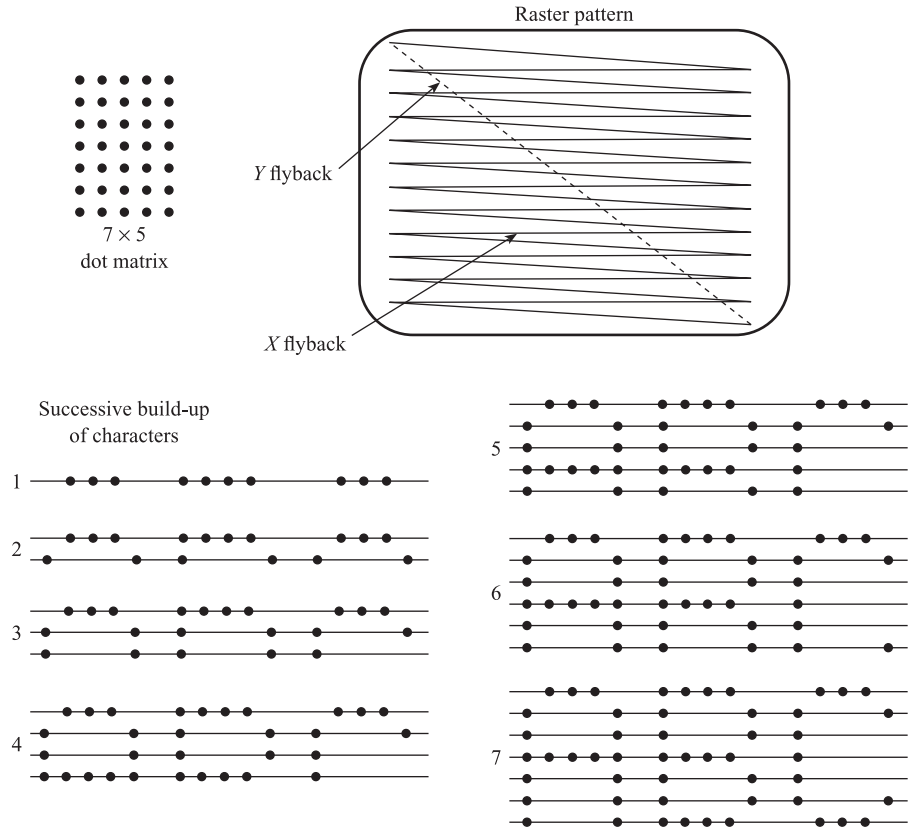
Figure 11.7 Cathode ray construction and waveforms.



reduction called **phosphorescence decay** (Figure 11.7). The corresponding decay time is called the **persistence** of the phosphor; phosphors with a wide range of persistences are available, ranging from less than 1 μ s (very short) to greater than 1 s (very long). In **refresh displays** the phosphors must be 'refreshed' or re-energised every time the phosphorescence decays to a certain level: this is necessary to obtain a stationary pattern on the screen with minimum **flicker**. In the more expensive **storage displays**, the display is retained on the screen and refreshment is not necessary.

A **monochrome** display is obtained with a non-storage CRT and a standard 312-line **raster**. In a raster-type display constant amplitude sawtooth deflection voltages are applied to both X and Y plates (Figure 11.7). The period of the Y voltage, i.e. the time taken for the display to move from the top to the bottom of the screen, is relatively long. A typical period is 20 ms, corresponding to a refreshment rate of 50 frames or pictures per second. This is suitable for a phosphor with a medium persistence of say 50 ms. The period of the X voltage, i.e. the time for each traverse across the screen, is 312 times shorter, i.e. 64 μ s. The resulting motion of the spot on the screen is shown in Figure 11.8. 312 horizontal 'lines' are traced out during the movement of the spot from top to bottom of the screen.

Figure 11.8 Raster display and character generation using 7×5 dot-matrix format.



Suppose we wish to generate a fixed format of 2000 alphanumeric characters arranged in 25 lines of 80 characters per line. If a 9×7 character format is used, then each character space occupies 10×8 pixels. Thus there are $25 \times 10 = 250$ horizontal lines of pixels with $80 \times 8 = 640$ pixels on each horizontal line. To create the characters on the screen, the electron beam is switched on and off to produce the required pattern. A high frequency pulse waveform is applied to the modulator electrode, which causes the electron beam current to be switched on and off many times during the $64 \mu\text{s}$ required for each horizontal traverse (**z modulation**). During each traverse the electron beam moves across a single line of pixels, causing them to be switched either 'on' or 'off' depending on whether the modulator signal is a '1' or a '0'. Since there are nine lines of pixels for each character, nine complete horizontal traverses are required to build up each complete line of characters. Figure 11.8 shows how the characters build up in a 7×5 format. The entire display of 25 lines, using a character space of 10×8 , is completed in 20 ms using 250 horizontal line scans. This is less than the theoretical number of 312, partly because of the time required for vertical flyback, and partly because the top and bottom of the CRT screen are not used, to avoid image distortion.

The input measurement data to the monitor is usually in serial ASCII digital form (Chapter 10) and must be converted into the serial pulse video signal required by the modulator to energise the pixels. Each horizontal sweep takes $64 \mu\text{s}$ but only about $40 \mu\text{s}$ is available for character generation; since 640 pixels must be energised during

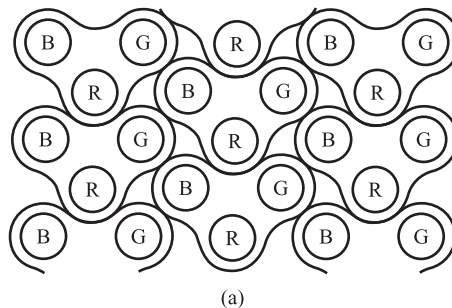
this time, the video signal has 16×10^6 pulses or bits per second. The monitor is normally operated under computer control, and an observer/operator can enter information and instructions via a keyboard. This facility enables the operator to request different display formats, e.g. the values of the most important measured variables for the complete process, or the values of all the measured variables associated with a particular part of the process.

A **colour display** produces images containing a wide range of colours. The screen of a colour CRT is coated with dots of three different types of phosphor: one type of phosphor emits red light, the second green light, the third blue light. Dots of each type are arranged in equilateral triangles called triads (Figure 11.9(a)). The monitor has three electron guns, one for each type of phosphor. The corresponding electron beams are deflected horizontally and vertically to produce a raster display as in a monochrome monitor. As the beams traverse the screens, the intensity of each beam is varied according to the voltage applied to the corresponding modulator electrode. This creates varying colour intensities at the triads and colour images on the screen.

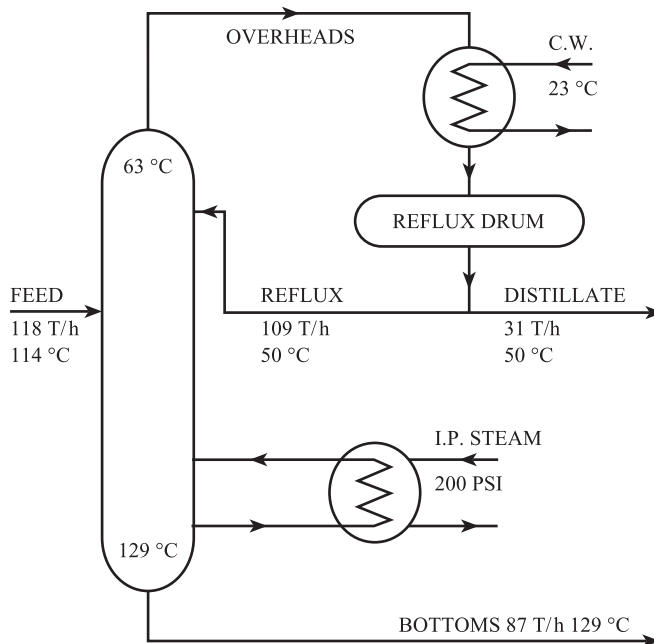
Figure 11.9

Colour displays:

- (a) Phosphor dot triads
(b) Chemical plant line diagram.



(a)



(b)

The above colour display system can be used to create **graphic displays**. In a fixed format alphanumeric display characters occupy fixed positions in a display and each character is built up using a fixed 7×5 or 9×7 dot-matrix format. In a graphic display the screen contains a full matrix of pixels, each of which can be turned on or off to produce graphical images or pictures, alphanumeric characters at any position on the screen or a combination of both. Figure 11.9(b) shows, in black-and-white, a colour line diagram of part of a chemical plant; alphanumeric data such as descriptions of process variables and their measured values can be displayed at any appropriate point on the diagram.

CRT displays have the disadvantage that they are not 'flat screen' technology and occupy more volume than comparable liquid crystal displays. They have much higher operating voltages (around 16 kV) than LCDs (around 15 V); power consumption is also higher in CRT than in LCD displays.

11.6

Liquid crystal displays (LCDs)

Liquid crystal displays (LCDs) do not emit light but use light incident on them from external sources. Consequently LCDs use significantly less power (microwatts) than LEDs (milliwatts). Liquid crystals flow under shear forces as in normal liquids but have some of the properties of solids. In **nematic** liquid crystals individual molecules have a rod-like shape. As the orientation of the molecules changes so there is a corresponding rotation of the plane of **polarisation** of the incident light. An applied electric field can alter both the orientation of the molecules and the plane of polarisation of the light, thus creating light and dark areas.

Figures 11.10(a) and (b) show the construction of a reflective **monochrome** display using **field effect** or **twisted nematic** (TN) liquid crystal material. The LC material is in contact with a pair of conducting electrodes which are transparent to light; a voltage is applied across these to create an electric field. There are glass plates above and below the electrodes. An x polarising filter is situated above the upper glass plate; this transmits only x polarised light. Similarly a y polarising filter below the lower glass plate transmits only y polarised light.

Figure 11.10(a) shows the situation when the applied voltage $V = 0$. The molecules near the top of the LC are lined up along the x -direction. Moving downwards through the liquid, their orientation gradually changes so that the molecules at the bottom are lined up along the y -direction. The light entering the liquid is x polarised; as it moves downwards the direction of polarisation rotates so that the light is y polarised on leaving the liquid. The light is therefore able to pass through the y polarising filter and is reflected back to the observer, the surface appearing pale grey or green.

Figure 11.10(b) shows the situation when the applied voltage V is non-zero. In this case the molecules remain aligned along the x direction throughout the liquid crystal: this means that the light remains x polarised as it moves downwards. The light cannot therefore pass through the lower y polarising filter and is absorbed; the surface appears black to an observer.

Figure 11.10(c) shows a seven-segment LCD which can display the numerals 0 to 9 and nine upper case letters. Typically the display has an operating voltage of 10 V and a total current of 10 μ A. The response time of the device, to turn on or turn

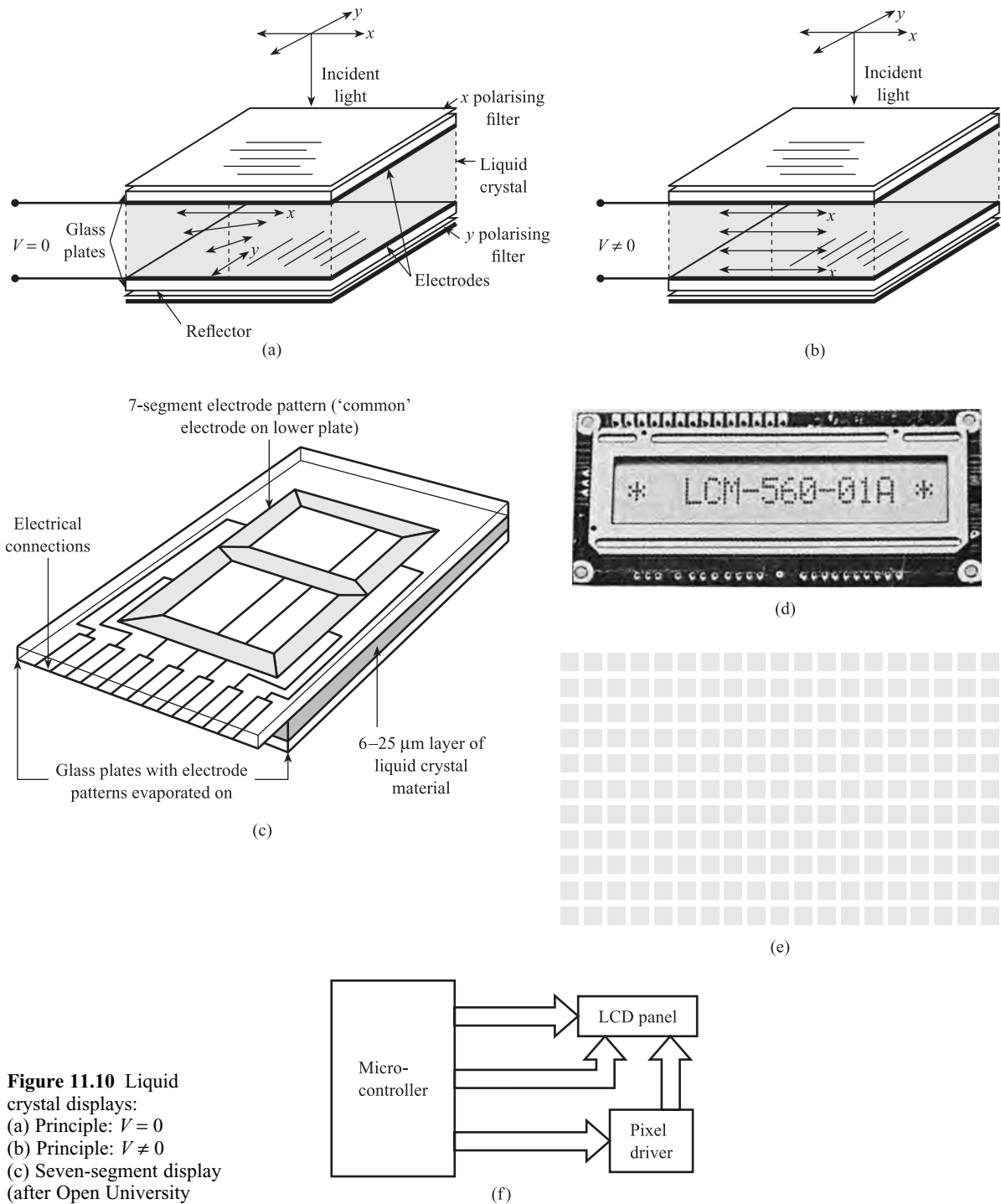


Figure 11.10 Liquid crystal displays:
 (a) Principle: $V = 0$
 (b) Principle: $V \neq 0$
 (c) Seven-segment display (after Open University T292 Instrumentation)
 (d) Character display
 (e) Graphics display
 (f) Character display system.

off signals, is typically 50 ms. The display is therefore driven by a pulse signal of r.m.s. voltage 10 V and frequency 60 Hz, i.e. a period of 17 ms. This enables the display to be continuously refreshed, giving a contrast ratio of 20:1 with no flicker. Pulsed operation reduces power consumption and avoids electrode deterioration due to electrolytic effects.

In order to display numerals, upper and lower case letters and other symbols, LCD **monochrome character** displays are used; here each character is displayed using the 7×5 dot matrix format (Section 11.3.1). Figure 11.10(d) shows a display for 16 characters on a single line, i.e. 16×1 format; formats range typically from 8×2 to 40×4 .

In order to display graphical information **monochrome graphics** displays are used. These consist of a matrix of pixels (Figure 11.10(e)); the pixel matrix multiplexing technique described in Section 11.3.2 is used. Display formats vary typically from 122×32 to 320×240 . A 128×64 graphics display has a view area of $62.5 \text{ mm} \times 43.5 \text{ mm}$ with **viewing angles** θ between -15° and $+45^\circ$ and ϕ between -35° and $+35^\circ$ respectively. The **contrast ratio** is typically 10, and **response times** for rise and fall are typically 250 ms and 300 ms respectively; the LCD supply voltage V is typically 13.0 V.^[1]

Figure 11.10(f) shows a typical system for an LCD character display.^[2] It consists of a microcontroller, segment/pixel driver and LCD panel. The input parallel digital signal will be in ASCII form; the microcontroller will, for each character, convert the input ASCII code into 7×5 dot matrix code and send this to the segment driver.

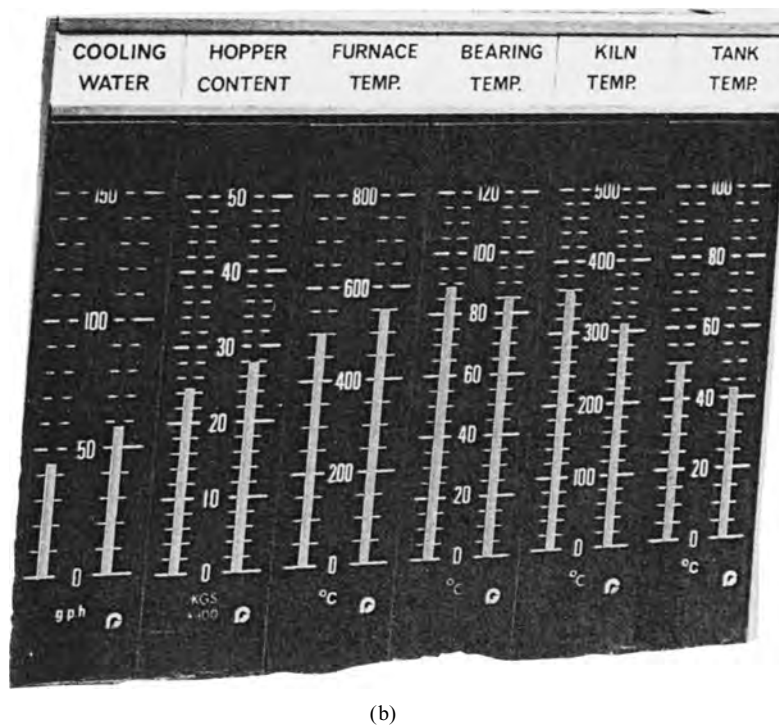
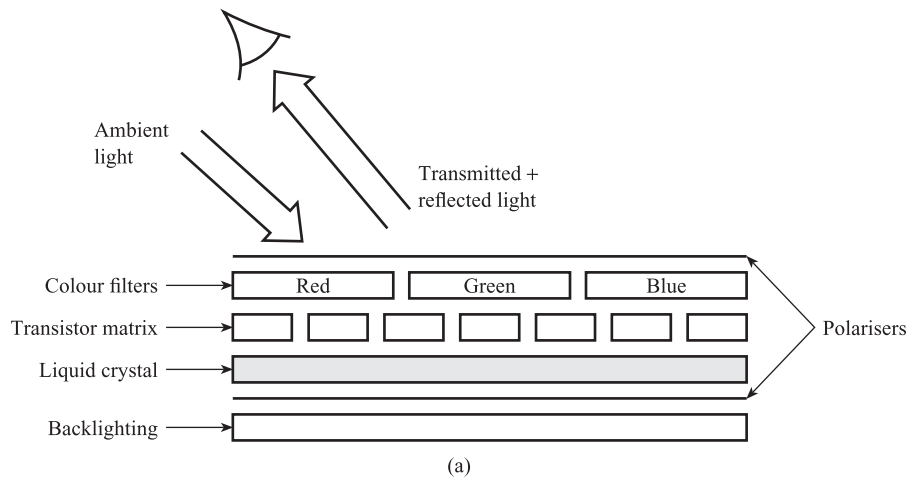
The basic liquid crystal element shown in Figure 11.10(a) can be used to produce **colour displays** by the addition of a matrix of red, green and blue filter elements between the upper electrode and the x polarising filter. However, in order to produce large area displays with sufficient brightness and contrast ratio to be read clearly at low ambient lighting levels, further developments have been made:

- (a) The addition of 'backlighting', a light source at the bottom underneath the y polarising filter. The observer now receives light both reflected back through the display from external sources and transmitted through the display from the backlight source.
- (b) The development of **super-twisted nematic** (STN) liquid crystals where the angle of twist, i.e. angle of rotation of the plane of polarisation of light, is greater than 90° .
- (c) A more recent development is **thin film transistor** (TFT) technology. Here there is a thin film of semiconductor providing a matrix of transistors, so that there is a drive transistor associated with each individual LC pixel. This gives more effective pixel multiplexing, with all pixels in a given row or column having the same voltage. Figure 11.11(a) shows the construction of a typical TFT display.^[3]

A typical compact STN colour display has a screen size of 8.2 inches, pixel format 640×480 , brightness 70 cd/m^2 and contrast ratio 50:1. A comparable TFT display has screen size 8.4 inches, pixel format 800×600 , brightness 130 cd/m^2 and contrast ratio 250:1. A larger area TFT display for industrial use has a screen size of 15 inches, pixel format 1024×768 , brightness 250 cd/m^2 and contrast ratio 400:1.^[4]

These displays can be used to show line diagrams of a section of a process or plant together with the measured values of process variables at an appropriate point on the diagram (Figure 11.9). Figure 11.11(b) shows a **bargraph** or **strip indicator** display

Figure 11.11 Colour liquid crystal displays:
 (a) Construction of TFT display
 (b) Strip indicator display.



of measured values. Large LCD displays have several advantages over comparable CRT displays; these include lower operating voltage, lower power consumption and flat screens/panels.

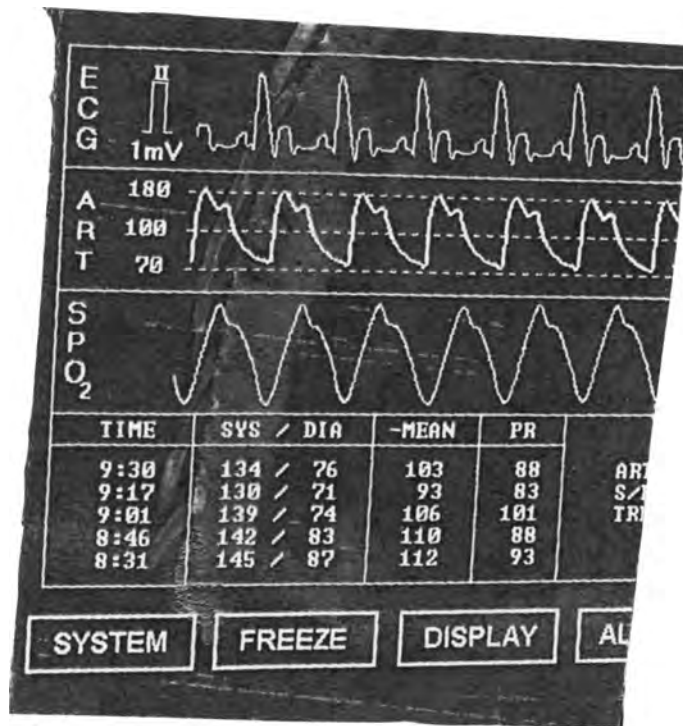
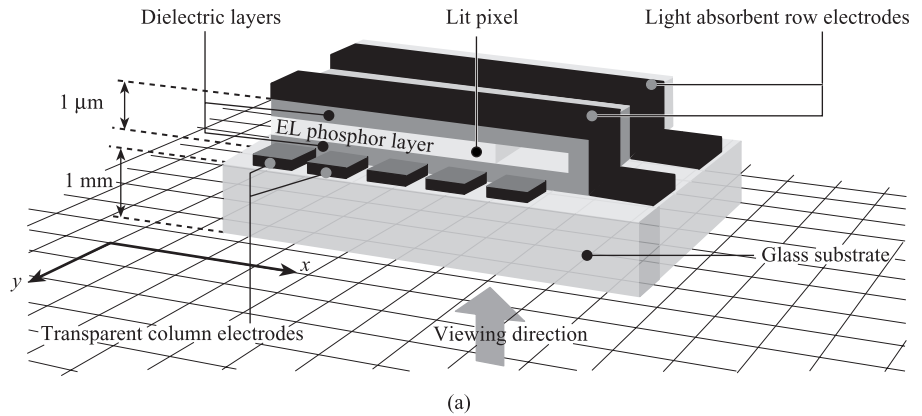
11. 7

Electroluminescence (EL) displays

When a voltage is applied across a **phosphor** material, light is emitted. This effect is called **electroluminescence**. A typical electroluminescent phosphor material is zinc sulphide doped with small amounts of metals, the metals being chosen according

Figure 11.12

Electroluminescence displays (after Trident Microsystems Ltd.^[5]):
 (a) Construction
 (b) Display of measured variable waveforms.



(b)

to the required colour. For example, an amber colour light with peak wavelength $\lambda = 580 \text{ nm}$ is emitted if the zinc sulphide is doped with manganese and copper. Electroluminescent displays consist of a matrix of pixels, where each pixel is a phosphor element which can be switched on and off by an applied voltage.

Figure 11.12(a) shows the construction of an EL display which consists of a number of layers deposited on a glass substrate.^[5] The first layer is a number of x -axis or column electrodes which are electrically conductive and transparent to light. Then there is the matrix of phosphor elements, which is sandwiched between two dielectric layers. Finally there are a number of y -axis or row electrodes which absorb light. Each pixel is located at an intersection of an x and a y electrode and connected across

them. The display is viewed through the glass substrate; with no voltage across the electrodes the pixel appears black. If a voltage pulse, typically of height 100 V and duration 10 μs , is applied across the electrodes, the pixel emits light. The luminance of the pixel decays from an initial value, just after the pulse, of around 1000 cd/m^2 , with a time constant of typically 500 μs . This means that the display must be continually refreshed to avoid flicker. The pulse is repeated approximately every 1000 μs , i.e. the pulse repetition frequency is 1 kHz; this enables a continuous luminance of at least 100 cd/m^2 to be obtained. Because the voltage is applied for only 1% of the time, the power required for each pixel is considerably reduced; around 100 μW per pixel is typical. The pulse repetition interval can be increased by adding memory to the pixel element.

To obtain graphic displays with a matrix of pixels, the multiplexing techniques described in Section 11.3.2 are used. A typical display with screen size of 3.1 inches has 160×120 pixels and an active display area of 62×42 mm; an 8.9-inch screen has 640×240 pixels and an active area of $211 \text{ mm} \times 79 \text{ mm}$.^[5] Figure 11.12(b) shows an electroluminescent screen used to display waveforms of three measured variables; the waveforms in amber show up clearly against the black background.^[5] Electroluminescent displays are flat screen-like liquid crystal displays but have a higher operating voltage and greater power consumption. However, EL displays are brighter, with a greater contrast ratio and viewing angle, than comparable LC displays.

11.8 Chart recorders

These provide a continuous record, on paper, of the time variation of measured variables.

Figures 11.13(a) and (b) show schematic and block diagrams of an **analogue** chart recorder. This is a **closed-loop** system using **position feedback**. The input voltage V_{IN} is opposed by the feedback voltage V_F to give an error voltage:

$$e = V_{\text{IN}} - V_F \quad [11.11]$$

This error voltage is amplified by an amplifier of gain K_A , and the amplifier output voltage V_A is input to a d.c. motor which drives the pen. The angular rotation θ of the motor is converted into the vertical displacement y of the pen by a pulley system. The pen writes on a chart which is driven at a constant speed along the x -direction, i.e. the x position of the pen is proportional to time. The motor angular position θ is sensed by a displacement sensor, often a potentiometer, to provide the feedback voltage V_F , thus closing the loop. An increase in input voltage V_{IN} will cause error e to increase in the short term, causing V_A , θ and y to increase. This causes a corresponding increase in V_F which reduces e ; the system settles out with the pen at a new position y such that V_F is as close as possible to V_{IN} .

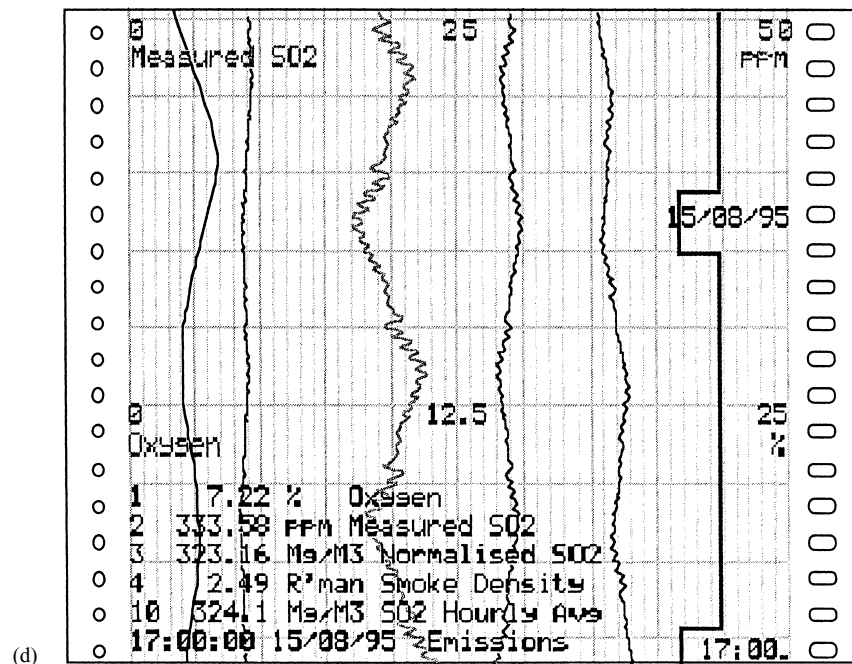
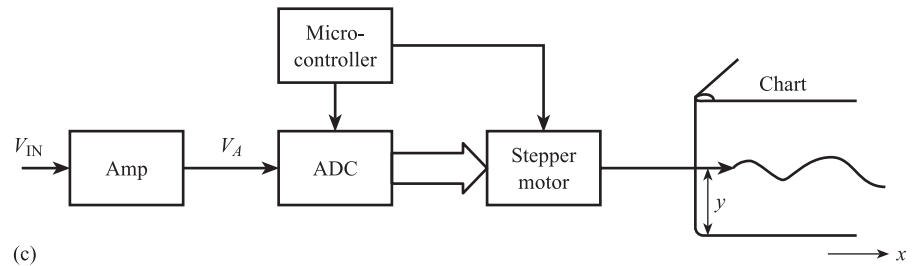
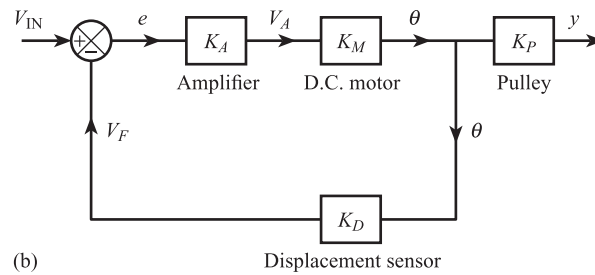
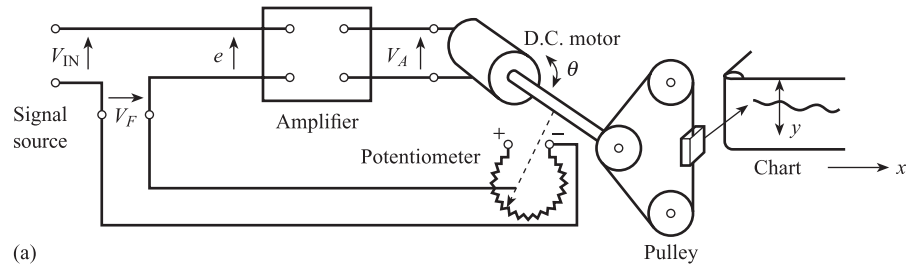
Using a similar analysis to that of eqns [3.11] to [3.19], the overall sensitivity of the closed-loop system is given by:

$$\frac{y}{V_{\text{IN}}} = \frac{K_A K_M K_P}{1 + K_A K_M K_D} \quad [11.12]$$

Figure 11.13

Chart recorders:

- (a) Schematic of analogue recorder
 (b) Block diagram of analogue recorder
 (c) Block diagram of digital recorder
 (d) Chart record of measured variables.



If the amplifier gain is large, so that $K_A K_M K_D \gg 1$, then $y/V_{IN} \approx K_p/K_D$. This means that the overall sensitivity is largely independent of K_A and K_M so that, for example, any changes in K_M due to non-linearity have negligible effect.

A typical analogue chart recorder has a displacement span y of 100 mm and an input range of 0 to 10 V or 4 to 20 mA d.c. The pen positioning accuracy is $\pm 0.2\%$, the input impedance 250 k Ω and the response time less than 2.0 s for 100% step change.

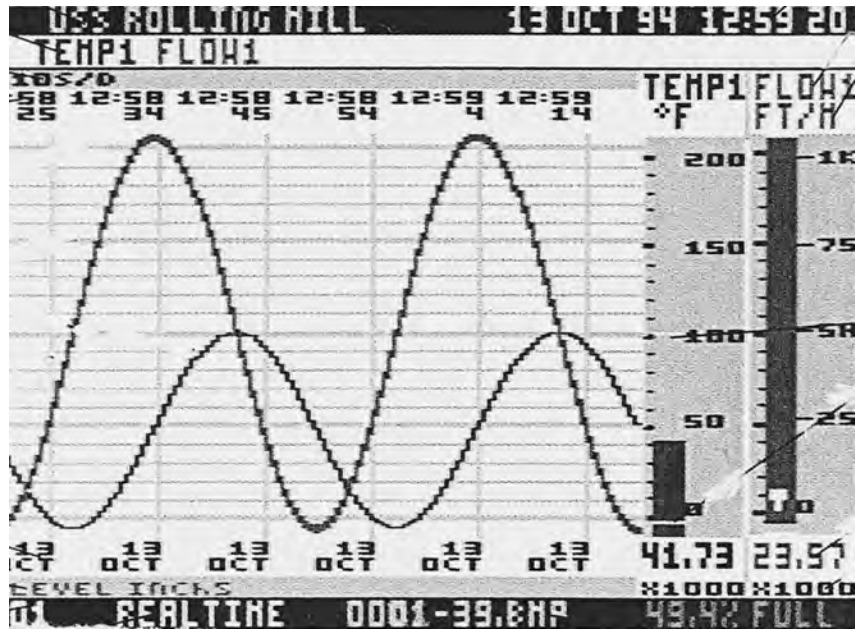
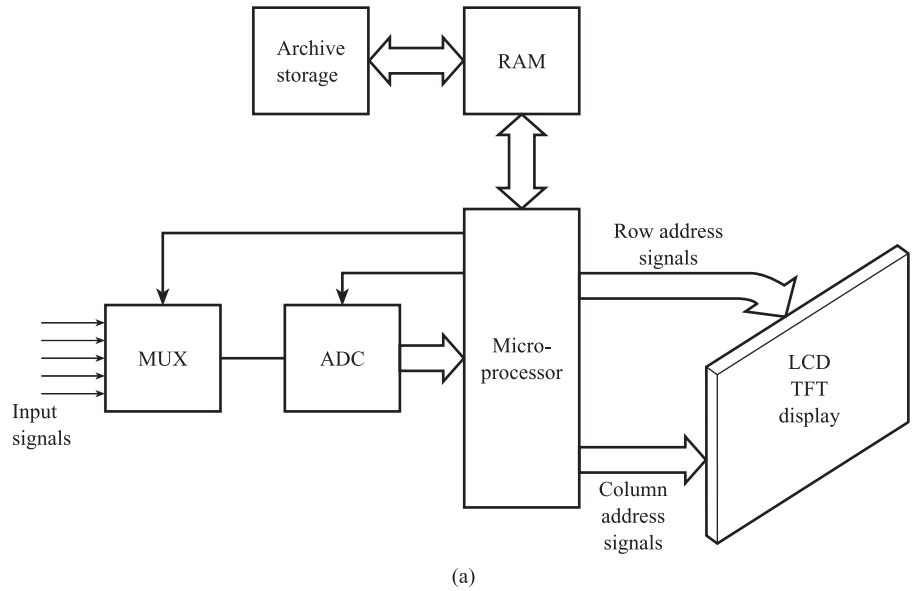
Figure 11.13(c) shows a block diagram of an open-loop **digital** chart recorder. Here the input voltage V_{IN} is amplified if necessary and the resulting voltage V_A input to an analogue-to-digital converter (ADC). The parallel digital output signal from the ADC is input to a digital stepper motor which moves the pen in the vertical y -direction. A typical recorder has a recording width (span of y) of 100 mm and an input range of 0 to 10 V d.c.^[6] The ADC has a resolution of $14\frac{1}{2}$ bits; the final motor output displacement has 10^5 steps, giving a pen positioning resolution of 0.1 mV. Input resistance is 100 k Ω , electrical measurement error within 0.4% and pen positioning error within 0.35%.

Several measured variables can be recorded using **multi-channel** recorders. There are two main types. In **continuous** or **line** recorders there is a separate motor and pen for each variable and the measured values are recorded as a continuous trace. Normally up to four pens are possible and in order for each pen to travel the full chart width and cross each other they must be offset from each other horizontally. Since horizontal displacement x is proportional to time, this can be done by creating a small time shift between the traces. In the **multi-point** type there is a single motor and pen which is switched sequentially between the input signals. The first variable is switched in and a dot printed on the chart, then the second and a dot printed, and so on for all the variables, returning to the first to repeat the process. The trace for each variable is therefore a series of dots in a given colour. Figure 11.13(d) is a continuous chart record of several variables.

11.9 Paperless recorders

The time variation of measured variables can be recorded without paper using a combination of LCD colour display and digital archive memory. Figure 11.14(a) shows a block diagram of a typical paperless recorder. The input measurement signals are input to a multiplexer and the selected signal is converted into parallel digital form by an analogue-to-digital converter for input to a microprocessor. The microprocessor generates the row and column address signals required for pixel matrix multiplexing in graphic displays (Section 11.3.2). Colour TFT liquid crystal displays are used (Section 11.6). Input data is stored initially in random access memory (RAM) and then transferred to archive memory; past data can then be retrieved from archive memory and displayed on the screen. A typical recorder of this type will accept up to 12 analogue input signals, d.c. voltage or current, and has a 144 mm \times 144 mm TFT LCD screen.^[7] The archive memory is either a 1.4 Mbyte floppy disk or a 300 Mbyte memory card. With the disk and four input variables, each sampled at one-minute intervals, approximately 110 days of record is obtained. Figure 11.14(b) shows continuous time and bar-graph recordings for two measured variables.

Figure 11.14 Paperless recorders:
(a) System block diagram
(b) Typical recording.

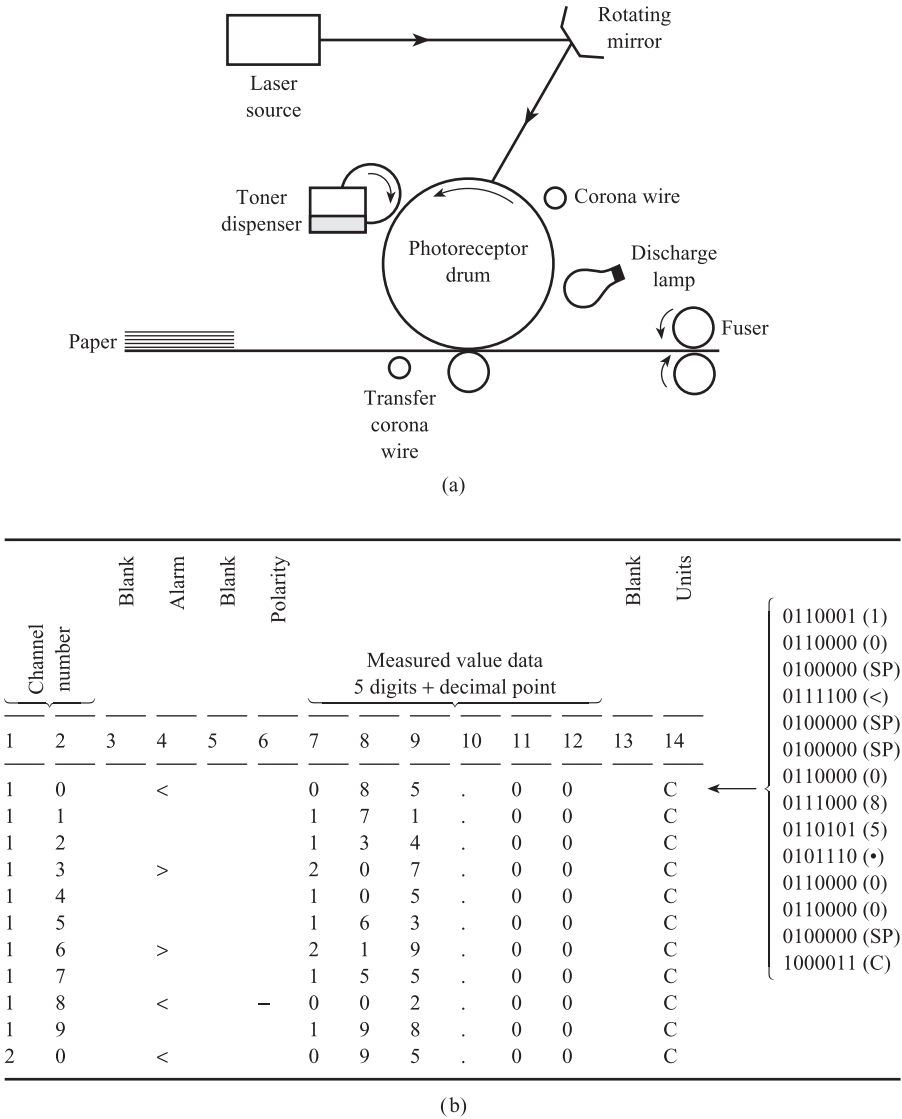


11.10

Laser printers

Figure 11.15(a) shows the basic layout of a laser printer. The printer receives input data in parallel digital form: for characters this could be in **ASCII** format (Section 10.4.1); for graphics it will be in **vector** format, where geometrical shapes are encoded into

Figure 11.15
Laser printers:
(a) Schematic diagram
(b) Typical table of data.



numerical values. The operation of the printer is controlled by a computer acting as a **print controller**. The controller converts this incoming data into **bitmap image** pages, each page corresponding to an array of black/white or coloured dots.

The **photoreceptor drum** is an array of photoconductive elements or pixels which correspond to the above bitmap image page. Initially all of the elements are given a positive charge; this is done by passing an electric current through the **corona wire**. The drum rotates and the controller directs a laser beam to move across the entire photoreceptor array in a raster pattern (Figure 11.8). The laser beam is moved by a rotating polygonal mirror and is switched on and off at high speed as it strikes each pixel. If light hits an element, its resistance falls sharply, causing the charge to fall to a negative value. If no light is incident, the pixel retains its positive charge.

The result is that the drum is an array of positively and negatively charged pixels, i.e. an **electrostatic image** of the bitmap page.

The drum is then coated with positively charged black powder toner. The toner clings to the negatively charged elements on the drum but not to the positively charged elements, thus creating a toner version of the bitmap. The sheet of paper is given a negative charge by the **transfer corona wire**; this charge is greater than the negative charge of the electrostatic image so that the paper can pull the toner powder away. The drum rolls over the sheet of paper and the paper picks up the toner to create an exact image on paper. The paper is then discharged so that it can be separated from the drum and finally passes to the **fuser**. This is a pair of heated rollers which melt any loose toner particles so that they fuse with the paper fibres. The printing process is now complete. The electrostatic image on the drum surface is then erased by passing it under the discharge lamp.

Laser printers can create tables of measurement data by printing numbers, letters and special characters on paper. Figure 11.15(b) shows an extract from a 14-column table of measured values of temperatures in a reactor. The table has 14 characters on each line which specify the channel number, the measured value and the units of measurement. By printing > or <, the table indicates that the temperature is either greater than a specified upper limit (say 200 °C) or less than a specified lower limit (say 100 °C).

The input data to the printer is in parallel ASCII digital form from a computer (Section 10.4.1 and Table 10.6). Figure 11.15(b) gives the 14 binary ASCII input code words corresponding to each of the 14 characters on the first line of the table.

Conclusion

The chapter began by reviewing types of data presentation elements in wide current use and the factors influencing choice. The principles and characteristics of analogue and digital displays, recorders and printers were then discussed.

References

- [1] DV³ Displays 2003 *Technical Data on Monochrome Graphics LCD Displays*.
- [2] Nicomatic Displays 2003 *Technical Data on LCD Character Displays*.
- [3] Sequoia Technology 2003 *Technical Data on Advanced Transflective TFT Displays*.
- [4] Trident Displays 2003 *Technical Data on Colour LCD Displays*.
- [5] Trident Displays 2003 *Technical Data on Electroluminescence Displays*.
- [6] Siemens 2001 *Catalog MP 20-2001, Process Recorders and Accessories*.
- [7] Eurotherm Controls 1997 *Technical Data on 4100G Paperless Recorder*.

Problems

11.1 A moving coil indicator is connected to a Thévenin signal source of resistance $125\ \Omega$. Use the data given below to answer the following questions.

- (a) Calculate the steady-state sensitivity (rad V^{-1}), natural frequency and damping ratio for the system.
- (b) What additional resistance must be connected into the circuit to give a damping ratio of 0.7? What is the sensitivity of the modified system?

Number of turns on coil = 100

Coil resistance = $75\ \Omega$

Coil area = $10^{-4}\ \text{m}^2$

Coil moment of inertia = $2.5 \times 10^{-5}\ \text{kg m}^2$

Magnetic flux density = $150\ \text{Wb m}^{-2}$

Spring stiffness = $10^{-3}\ \text{Nm rad}^{-1}$

11.2 A closed-loop chart recorder using position feedback consists of the following elements:

Amplifier – sensitivity = $10^3\ \text{V/V}$.

D.C. motor – sensitivity = $1.0\ \text{rad/V}$.

Displacement sensor – sensitivity = $5.0\ \text{V/rad}$.

Pulley – sensitivity = $0.15\ \text{m/rad}$.

- (a) Find the recorder output range for an input voltage range of 0 to 5 V.
- (b) Explain why a change in motor sensitivity to $0.9\ \text{rad/V}$ has negligible effect on pen position.

11.3 It is desired to display the numerals 0 to 9 and the letters ACEFJH using the seven-segment character format shown in Figure 11.3(a). Write down a table for the conversion of a four-input DCBA (8:4:2:1 b.c.d.) to the seven-segment output abcdefg code to drive the display.

Part C

Specialised Measurement Systems

12 Flow Measurement Systems

Measurement of the rate of flow of material through pipes is extremely important in a wide range of industries, including chemical, oil, steel, food and public utilities. There are a large and bewildering number of different flowmeters on the market and the user is faced with the problem of choice outlined in Chapter 7. This chapter explains the principles and characteristics of the more important flowmeters in current use. The chapter is divided into five sections: essential principles of fluid mechanics, measurement of velocity at a point in a fluid, volume flow rate, mass flow rate, and flow measurement in difficult situations.

12.1 Essential principles of fluid mechanics

12.1.1 Shear stress and viscosity

There are three states of matter: solid, liquid and gas. Liquids and gases are different in many respects but behave in the same way under the action of a deforming force. Liquids and gases, i.e. fluids, **flow** under the action of a deforming force, whereas a solid retains its shape. The effect is illustrated in Figure 12.1(a), which shows the effect of a shear force F on a rectangular block. The corresponding **shear stress** τ is the force per unit area F/A , where A is the area of the base of the block. The effect of τ is to deform the block as shown, and the resulting *shear strain* is quantified by the angle ϕ . In a solid ϕ will be constant with time and of magnitude proportional to τ . In a fluid ϕ will increase with time and the fluid will flow. In a Newtonian fluid the rate of change of shear strain $\phi/\Delta t$ is proportional to τ , i.e. $\tau = \text{constant} \times (\phi/\Delta t)$ where Δt is the time interval in which ϕ occurs. If ϕ is small and in radians, we have $\phi = \Delta x/y$; also if v is the velocity of the top surface of the block relative to the base, $v = \Delta x/\Delta t$. This gives:

$$\tau = \text{constant} \times \frac{v}{y}$$

where the constant of proportionality is the **dynamic viscosity** η of the fluid. Replacing the velocity gradient term v/y by its differential form dv/dy we have

$$\tau = \eta \frac{dv}{dy} \quad [12.1]$$

*Newton's Law of
Viscosity*

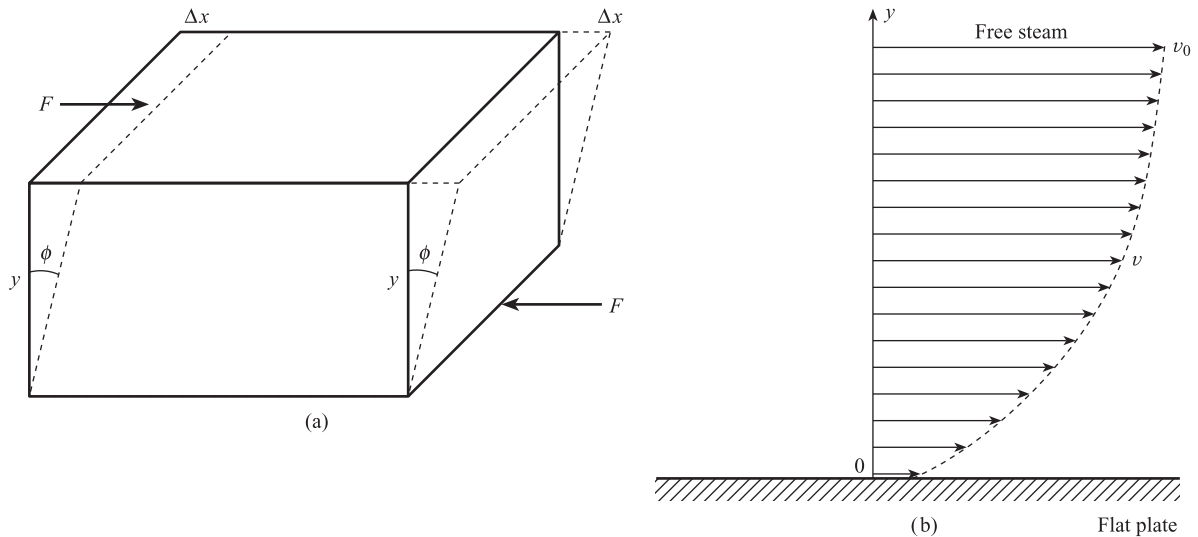


Figure 12.1 Shear stress and viscosity:

- (a) Deformation caused by shearing forces
 (b) Velocity distribution in boundary layers.

Figure 12.1(b) shows a fluid flowing over a solid boundary, e.g. a flat plate. The fluid in contact with the plate surface at $y = 0$ has zero velocity. As we move away from the plate, i.e. as y increases, the velocity v of the layers increases, until well away from the plate the layers have the free stream velocity v_0 . The layers between the free stream and the boundary are called *boundary layers* and are characterised by a velocity gradient dv/dy . From eqn [12.1] we see that frictional shear stresses are present in these boundary layers.

12.1.2 Liquids and gases

Although liquids and gases have the common properties of fluids, they have distinctive properties of their own. A liquid is difficult to compress, i.e. there is a very small decrease in volume for a given increase in pressure, and it may be regarded as incompressible, i.e. density ρ is independent of pressure (but will depend on temperature).

Gases are easy to compress, and density depends on both pressure and temperature. For an ideal gas we have:

Equation of state for ideal gas

$$PV = mR\theta, \text{ i.e. } P = \rho R\theta \quad [12.2]$$

where P = absolute pressure (Pa)
 θ = absolute temperature (K)
 V = volume (m^3)
 ρ = density (kg m^{-3})
 R = constant for the gas ($\text{J kg}^{-1} \text{K}^{-1}$).

For real gases the above equation must be corrected by introducing an experimental compressibility factor or gas law deviation constant.

The amount of heat required to raise the temperature of a gas by a given amount depends on whether the gas is allowed to expand, i.e. to do work, during the heating process. A gas therefore has two specific heats: specific heat at constant volume C_V and specific heat at constant pressure C_P . If the expansion or contraction of a gas is carried out **adiabatically**, i.e. no heat enters or leaves the system, the process is accompanied by a change in temperature and the corresponding relationship between pressure and volume (or density) is:

$$PV^\gamma = \frac{P}{\rho^\gamma} = \text{constant} \quad [12.3]$$

where γ is the specific heat ratio C_P/C_V .

12.1.3 Laminar and turbulent flow: Reynolds number

Experimental observations have shown that two distinct types of flow can exist. The first is **laminar flow**, or viscous or streamline flow; this is shown for a circular pipe in Figure 12.2(a). Here the particles move in a highly ordered manner, retaining the same relative positions in successive cross-sections. Thus laminar flow in a circular pipe can be regarded as a number of annular layers: the velocity of these layers increases from zero at the pipe wall to a maximum at the pipe centre with significant viscous shear stresses between each layer. Figure 12.2(a) shows the resulting velocity profile; this is a graph of layer velocity v versus distance r of layer from centre, and is parabolic in shape.

The second type of flow, **turbulent flow**, is shown in Figure 12.2(b). This is highly disordered; each particle moves randomly in three dimensions and occupies different relative positions in successive cross-sections. As a result, the velocity and pressure at a given point in the pipe are both subject to small random fluctuations with time about their mean values. The viscous friction forces which cause the ordered motion in laminar flow are much smaller in turbulent flow. Figure 12.2(b) shows a typical velocity profile for turbulent flow in a circular pipe. It is obtained by taking a point r in the pipe and measuring the time average v of the velocity component, along the direction of flow at that point.

The **Reynolds number** tells us whether the flow in a given situation is laminar or turbulent. It is the dimensionless number:

Reynolds number

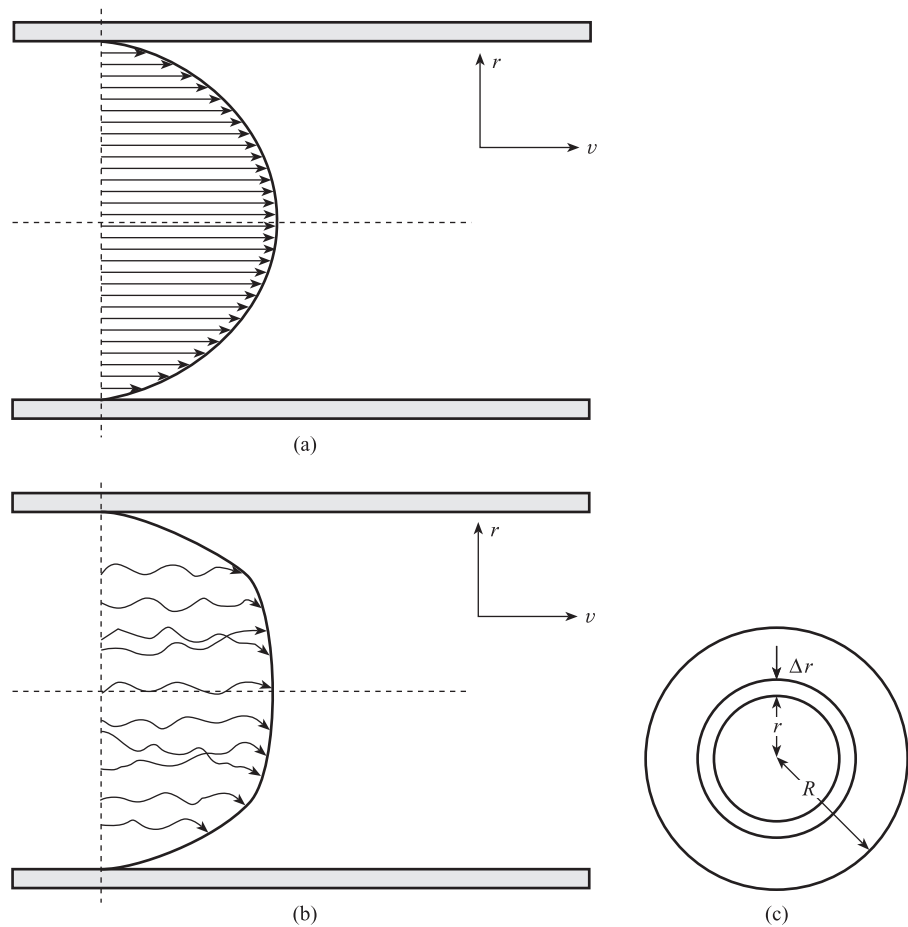
$$Re = \frac{v l \rho}{\eta} \quad [12.4]$$

where l is a characteristic length of the situation, e.g. pipe diameter. The Reynolds number represents the ratio of inertial forces (proportional to $v l \rho$) to viscous forces (proportional to η); thus a low value of Re implies laminar flow and a high value turbulent flow. The following is an approximate guide:

$$\begin{aligned} Re < 2 \times 10^3 & - \text{laminar flow} \\ 2 \times 10^3 < Re < 10^4 & - \text{transition region} \\ Re > 10^4 & - \text{turbulent flow} \end{aligned}$$

Figure 12.2 Types of flow and velocity profiles in a circular pipe:

- (a) Laminar
- (b) Turbulent
- (c) Calculation of volume flow rate.



12.1.4 Volume flow rate, mass, flow rate and mean velocity

Figures 12.2(a) and (b) show the velocity profiles $v(r)$ for both laminar and turbulent flow. If we consider an annular element radius r , thickness Δr , then this will have area $2\pi r\Delta r$ (Figure 12.2(c)). The corresponding volume flow rate ΔQ through the element is given by:

$$\begin{aligned}\Delta Q &= \text{area of element} \times \text{velocity} \\ &= 2\pi r\Delta r \times v(r)\end{aligned}$$

Hence the total **volume flow rate** through a circular pipe of radius R is:

Volume flow rate in a circular pipe

$$Q = 2\pi \int_0^R v(r)r \, dr \quad [12.5]$$

In many problems the variation in velocity over the cross-sectional area can be neglected and assumed to be constant and equal to the mean velocity \bar{v} , which is defined by:

Mean velocity

$$\bar{v} = \frac{Q}{A} \quad [12.6]$$

Here A is the cross-sectional area of the fluid normal to the direction of flow. Finally the corresponding mass flow rate \dot{M} is given by:

Mass flow rate

$$\dot{M} = \rho Q = \rho A \bar{v} \quad [12.7]$$

12.1.5 Continuity: conservation of mass and volume flow rate

Figure 12.3 shows a streamtube through which there is a steady flow; since conditions are steady the principle of conservation of mass means that:

$$\begin{aligned} \text{Mass of fluid entering in unit time} &= \text{mass of fluid leaving in unit time} \\ \text{i.e. mass flow rate in} &= \text{mass flow rate out} \end{aligned}$$

Using eqn [12.7] we have:

Conservation of mass flow rate

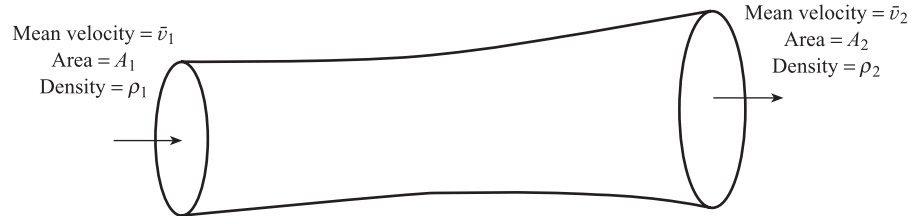
$$\rho_1 A_1 \bar{v}_1 = \rho_2 A_2 \bar{v}_2 = \dot{M} \quad [12.8]$$

If the fluid can be considered incompressible then $\rho_1 = \rho_2$ and eqn [12.8] reduces to the volume flow rate conservation equation:

Conservation of volume flow rate

$$A_1 \bar{v}_1 = A_2 \bar{v}_2 = Q \quad [12.9]$$

Figure 12.3
Conservation of mass flow rate in a streamtube.



12.1.6 Total energy and conservation of energy

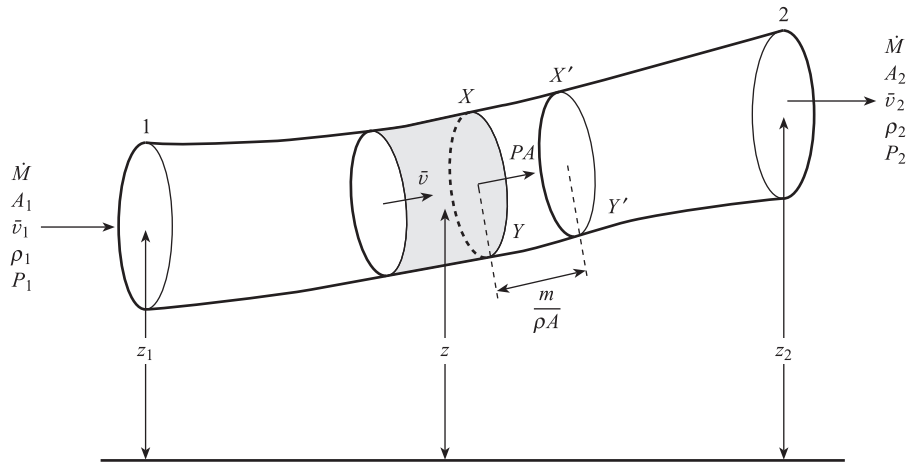
Figure 12.4 shows an element of an incompressible fluid flowing in a streamtube. Since the element is at a height z above the datum level it possesses **potential energy** given by:

$$\text{Potential energy} = mgz$$

where m is the mass of the element. The element is moving with a mean velocity \bar{v} and therefore also possesses **kinetic energy** given by:

$$\text{Kinetic energy} = \frac{1}{2} m \bar{v}^2$$

Figure 12.4 Total energy and energy conservation in a flowing fluid.



In addition the element of fluid can also do work because it is flowing under pressure. If the pressure acting over cross-section XY is P and the area of the cross-section is A , then:

$$\text{Force exerted on } XY = PA$$

If the entire element moves to occupy volume $XX'Y'Y$ then the magnitude of this volume is m/ρ , where ρ is the density of the fluid. The corresponding distance moved, XX' , is given by $m/\rho A$ and the work done by the fluid is:

$$\text{Flow work} = \text{force} \times \text{distance} = PA \times m/\rho A = mP/\rho$$

Flow work is often referred to as **pressure energy**; this is the energy possessed by a fluid when moving under pressure as part of a continuous stream.

The total energy of a flowing fluid is the sum of pressure, kinetic and potential energies, so that:

Fluid energy

$$\text{Total energy/unit mass} = \frac{P}{\rho} + \frac{1}{2} \bar{v}^2 + gz \quad [12.10]$$

Thus if we consider cross-sectional areas 1 and 2 in Figure 12.4, the principle of conservation of energy means that the total energy/unit mass is the same at both sections. This assumes that there is no energy inflow or outflow between sections 1 and 2, for example no energy lost in doing work against friction. Using eqn [12.10] we have:

*Conservation of energy
– incompressible fluid*

$$\frac{P_1}{\rho_1} + \frac{1}{2} \bar{v}_1^2 + gz_1 = \frac{P_2}{\rho_2} + \frac{1}{2} \bar{v}_2^2 + gz_2 \quad [12.11]$$

Equations [12.10] and [12.11] only apply to incompressible fluids where density ρ is independent of pressure P . For adiabatic expansion/contraction of a gas described by $P/\rho^\gamma = \text{constant}$, the flow work or pressure energy term must be modified to $[\gamma/(\gamma - 1)](P/\rho)$ so that:

Conservation of energy
– compressible fluid

$$\left(\frac{\gamma}{\gamma-1}\right)\frac{P_1}{\rho_1} + \frac{1}{2}\bar{v}_1^2 + gz_1 = \left(\frac{\gamma}{\gamma-1}\right)\frac{P_2}{\rho_2} + \frac{1}{2}\bar{v}_2^2 + gz_2 \quad [12.12]$$

12.2

Measurement of velocity at a point in a fluid

This is important in investigational work, such as studies of the velocity distribution around an aerofoil in a wind tunnel, or measurement of the velocity profile in a pipe prior to the installation of a permanent flowmeter. There are two main methods.

12.2.1 Pitot-static tube

Figure 12.5 shows the principle of the pitot-static tube. At the impact hole part of the fluid is brought to rest; this part has therefore no kinetic energy, only pressure energy. At the static holes the fluid is moving and therefore has both kinetic and pressure energy. This creates a pressure difference $P_I - P_S$ which depends on velocity v .

Incompressible flow

Assuming energy conservation and no frictional or heat losses, the sums of pressure, kinetic and potential energies at the impact and static holes are equal. Since kinetic energy at the impact hole is zero:

$$\frac{P_I}{\rho} + 0 + gz_I = \frac{P_S}{\rho} + \frac{v^2}{2} + gz_S \quad [12.13]$$

where z_I, z_S are the elevations of the holes above a datum line and $g = 9.81 \text{ m s}^{-2}$. If $z_I = z_S$ then

Pitot tube –
incompressible flow

$$v = \sqrt{\frac{2(P_I - P_S)}{\rho}} \quad [12.14]$$

Compressible flow

The above assumes that the fluid densities at the impact and static holes are equal. Since $P_I > P_S$ a compressible fluid has $\rho_I > \rho$. The energy balance equation is now:

$$\left(\frac{\gamma}{\gamma-1}\right)\frac{P_I}{\rho_I} + 0 = \left(\frac{\gamma}{\gamma-1}\right)\frac{P_S}{\rho} + \frac{v^2}{2} \quad [12.15]$$

where γ = ratio of specific heats at constant pressure and volume = C_p/C_v . Assuming the density changes are adiabatic, we have:

$$\frac{P_I}{\rho_I^\gamma} = \frac{P_S}{\rho^\gamma} \quad [12.16]$$

giving:

$$v = \sqrt{2 \left(\frac{\gamma}{\gamma - 1} \right) \frac{P_s}{\rho} \left[\left(\frac{P_t}{P_s} \right)^{(\gamma-1)/\gamma} - 1 \right]}$$

or, in terms of the pressure difference $\Delta P = P_t - P_s$:

*Pitot tube –
compressible flow*

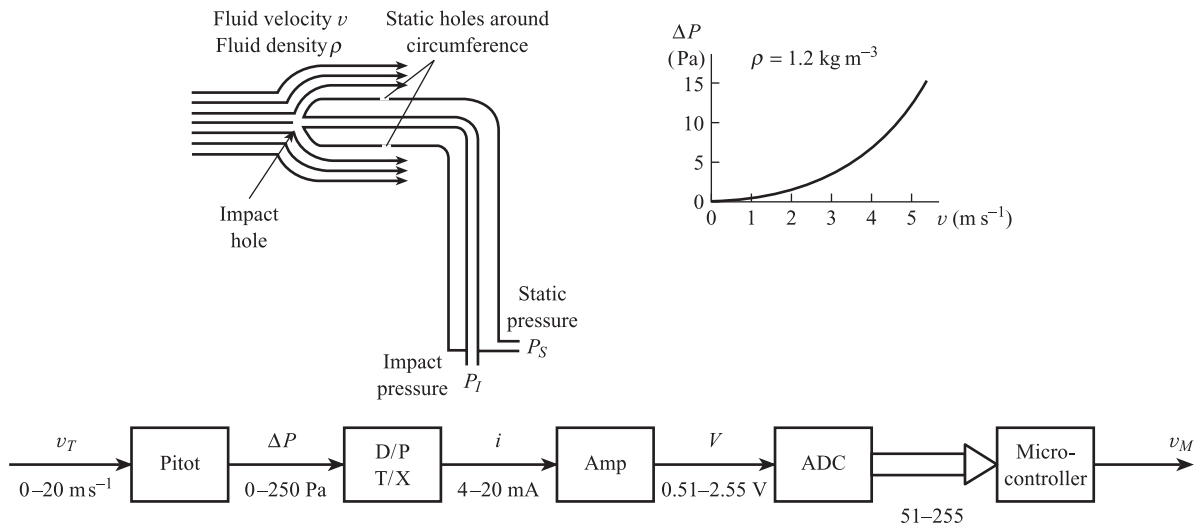
$$v = \sqrt{2 \left(\frac{\gamma}{\gamma - 1} \right) \frac{P_s}{\rho} \left[\left(1 + \frac{\Delta P}{P_s} \right)^{(\gamma-1)/\gamma} - 1 \right]} \quad [12.17]$$

Characteristics and systems

From the incompressible eqn [12.14] we have $\Delta P = \frac{1}{2} \rho v^2$, i.e. there is a square law relation between ΔP and v (see Figure 12.5). Applying the incompressible equation to air at standard temperature (20 °C) and pressure ($P_s = 10^5$ Pa), with $\rho = 1.2 \text{ kg m}^{-3}$, gives $\Delta P = 0.6 v^2$. Thus at $v = 5 \text{ m s}^{-1}$ we have $\Delta P = 15 \text{ Pa}$, $\Delta P/P_s = 1.5 \times 10^{-4}$; and at $v = 100 \text{ m s}^{-1}$, $\Delta P = 6 \times 10^3 \text{ Pa}$, $\Delta P/P_s = 6 \times 10^{-2}$. The small $\Delta P/P_s$ ratio means that for $v < 100 \text{ m s}^{-1}$, the difference in density between the air at the impact and static holes is negligible; the error introduced by using the incompressible equation is within 1%. Close examination of the compressible eqn [12.17] shows that it reduces to the incompressible eqn [12.14] if $\Delta P/P_s \ll 1$.

The above very low differential pressures mean that special pressure transmitters must be used. One such transmitter uses a linear variable differential transformer to sense the deformation of a diaphragm capsule with a large area; this gives a 4 to 20 mA current output proportional to input differential pressure in the range 0 to 250 Pa.^[1] Figure 12.5 shows a computer-based measurement system incorporating this transmitter for measuring air velocities in the range 0 to 20 m s⁻¹. The amplifier converts the transmitter output to a voltage signal between 0.51 and 2.55 V. The

Figure 12.5 Pitot-static tube.



analogue-to-digital converter gives an 8-bit parallel digital output signal corresponding to decimal numbers D between 51 and 255. The computer reads D and calculates ΔP using:

$$\Delta P = 1.2255(D - 51)$$

and the measured velocity v_M using $v_M = \sqrt{1.67 \Delta P}$.

The above system is only suitable for measuring the time average of the velocity at a point in a fluid. The system frequency response is insufficient for it to measure the rapid random velocity fluctuations present in turbulent flow.

12.2.2 Hot-wire and film anemometers

These are capable of measuring both average velocity and turbulence. A full account is given in Sections 14.2 and 14.3.

12.3

Measurement of volume flow rate

12.3.1 Differential pressure flowmeters

These are the most common industrial flowmeters for clean liquids and gases. Here a constriction is placed in the pipe and the differential pressure developed across the constriction is measured. The main problem is to accurately infer volume flowrate from the measured differential pressure (D/P).

Theoretical equation for incompressible flow through a D/P meter

The constriction causes a reduction in the cross-sectional area of the fluid. Figure 12.6(a) shows this reduction and defines relevant quantities. The following assumptions enable a theoretical calculation of pressure difference to be made.

1. Frictionless flow – i.e. no energy losses due to friction, either in the fluid itself or between the fluid and the pipe walls.
2. No heat losses or gains due to heat transfer between the fluid and its surroundings.
3. Conservation of total energy (pressure + kinetic + potential):

$$E_1 = \frac{P_1}{\rho_1} + \frac{1}{2} v_1^2 + g z_1 = E_2 = \frac{P_2}{\rho_2} + \frac{1}{2} v_2^2 + g z_2 \quad [12.18]$$

4. Incompressible fluid, i.e. $\rho_1 = \rho_2 = \rho$.
5. Horizontal pipe, i.e. $z_1 = z_2$. This means that eqn [12.18] reduces to:

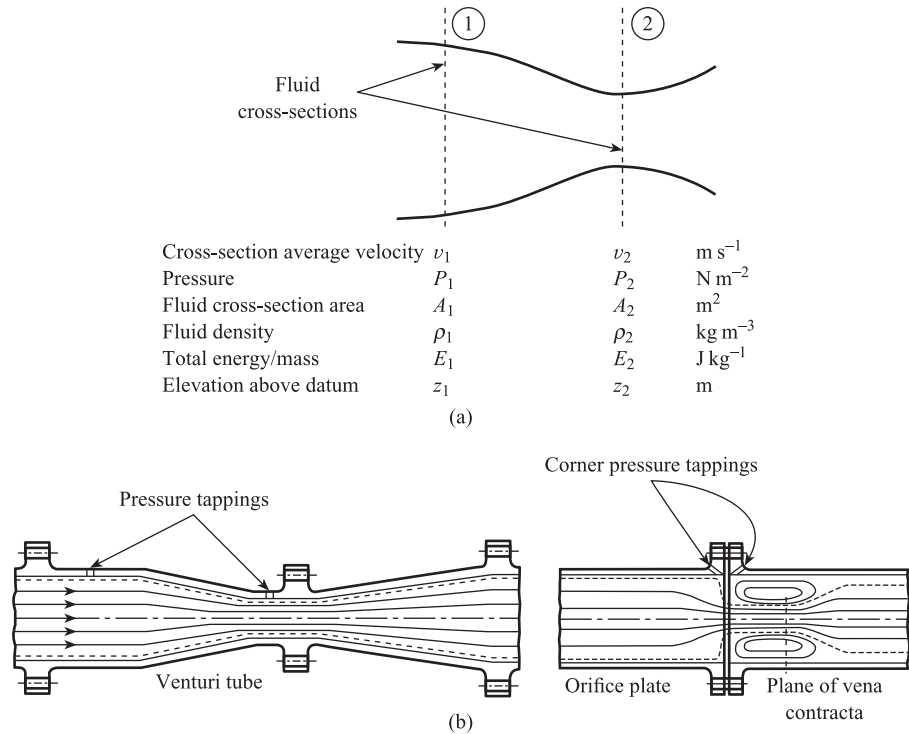
$$\frac{v_2^2 - v_1^2}{2} = \frac{P_1 - P_2}{\rho} \quad [12.19]$$

6. Conservation of volume flow rate, i.e.

$$Q_1 = Q_2 = Q \quad \text{where} \quad Q_1 = A_1 v_1 \quad \text{and} \quad Q_2 = A_2 v_2 \quad [12.20]$$

Figure 12.6

(a) Principle of differential pressure flowmeter
 (b) Effect of meter geometry on fluid cross-sectional area.



Since $A_2 < A_1$, it follows from the conservation of volume flow rate [12.20] that $v_2 > v_1$; i.e. fluid velocity and kinetic energy are greater at the constriction. Since total energy is conserved [12.19] then the pressure energy at the constriction must be reduced, i.e. $P_2 < P_1$. From [12.19] and [12.20] we have:

Theoretical equation for incompressible flow through a differential pressure flowmeter

$$Q_{Th} = \frac{A_2}{\sqrt{1 - \left(\frac{A_2}{A_1}\right)^2}} \sqrt{\frac{2(P_1 - P_2)}{\rho}} \quad [12.21]$$

Practical equation for incompressible flow

The above equation is not applicable to practice flowmeters for two main reasons:

- Assumption 1 of frictionless flow is not obeyed in practice. It is approached most closely by well-established turbulent flows in smooth pipes, where friction losses are small and constant but non-zero. Well-established turbulence is characterised by a Reynolds number greater than around 10^4 . Reynolds number specifies the ratio between inertial forces and viscous friction forces and is given by $Re_D = vD\rho/\eta$ where D is the pipe diameter and η the fluid viscosity.
- A_1 and A_2 are the cross-sectional areas of the fluid, which cannot be measured and which may change with flow rate. The cross-sectional area of the pipe is

$\pi D^2/4$ and the cross-sectional area of the meter is $\pi d^2/4$ where D and d are the respective diameters. At cross-section ① we have $A_1 = \pi D^2/4$ if the fluid fills the pipe. At cross-section ② we have $A_2 \approx 0.99\pi d^2/4$ for a Venturi, this being a gradual constriction which the fluid can follow (Figure 12.6(b)). However, the orifice plate is a sudden constriction, which causes the fluid cross-sectional area to have a minimum value of $0.6\pi d^2/4$ at the vena contracta.

For these reasons, the theoretical equation is corrected for practical use by introducing a correction factor termed the coefficient of discharge C . The modified equation is:

Practical equation for incompressible flow through a differential pressure flowmeter

$$Q_{\text{ACT}} = CE A_2^M \sqrt{\frac{2(P_1 - P_2)}{\rho}} \quad [12.22]$$

where C = discharge coefficient

E = velocity of approach factor $= 1/\sqrt{1 - \beta^4}$

β = flowmeter-pipe diameter ratio $= d/D$

A_2^M = flowmeter cross-sectional area $= \pi d^2/4$.

Values of C depend upon:

- (a) type of flowmeter, e.g. orifice plate or Venturi,
- (b) Reynolds number Re_D ,
- (c) diameter ratio β ,

i.e. $C = F(Re_D, \beta)$ for a given flowmeter.

Values of C have been measured experimentally, for several types of flowmeters, over a wide range of fluid conditions. Corresponding measurements of Q_{ACT} and $(P_1 - P_2)$ are made for a given fluid, pipe and meter. If d , D and ρ are known, C can be found from [12.22]. Important sources are BS 1042: Section 1.1: 1981^[2] and ISO 5167: 1980.^[3] These are identical and give discharge coefficient data for orifice plates, nozzles and Venturi tubes (Figure 12.7) inserted in circular pipes which are running full. The C data is given both in table form and as regression equations which are ideal for computer use. Table 12.1 summarises the data for orifice plates.

The table is in three parts: part (a) shows the Stolz equation, which expresses C in terms of Re_D and β . The equation also involves the parameters L_1 and L'_2 . These parameters have different values (part (b)) for the three different recommended types of tappings (Figure 12.7). Part (c) summarises the conditions which d , D , β and Re_D must satisfy if the Stolz equation is to be valid. The conditions on Re_D are especially complicated; the allowable range of Reynolds number depends on the value of β .

Compressible fluids

In order to accurately represent the behaviour of gases as well as liquids, restriction 4 above that $\rho_1 = \rho_2$ must be removed. Assuming adiabatic pressure/volume changes between cross-sections ① and ②, we have:

$$\frac{P_1}{\rho_1^\gamma} = \frac{P_2}{\rho_2^\gamma} \quad [12.23]$$

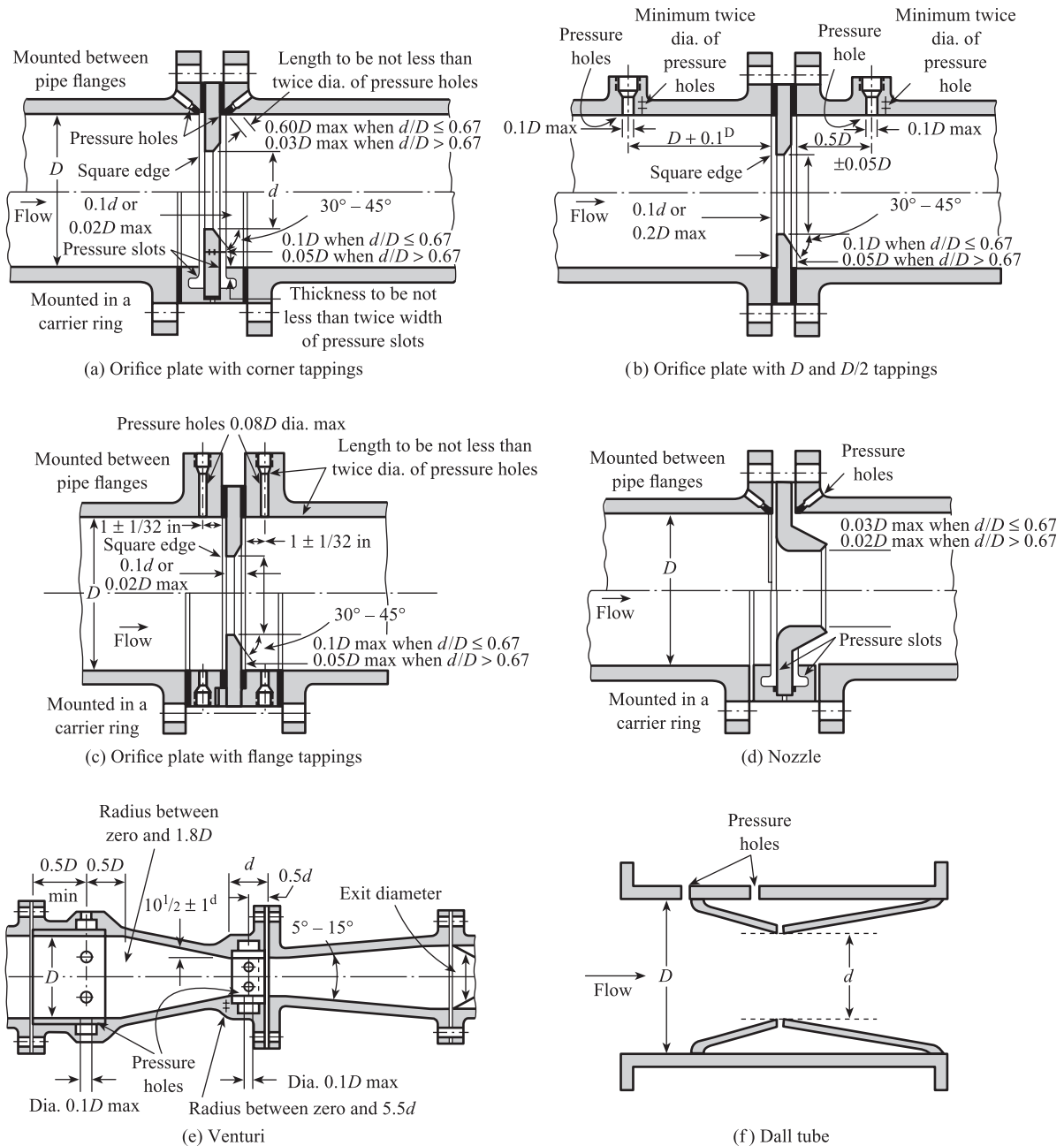


Figure 12.7 Differential pressure flowmeters ((a)–(e) after British Standards Institution^[2]).

where γ = specific heat ratio C_p/C_v ; since $P_1 > P_2$, $\rho_1 > \rho_2$. The energy balance eqn [12.7] must be modified to:

$$\left(\frac{\gamma}{\gamma - 1} \right) \frac{P_1}{\rho_1} + \frac{1}{2} v_1^2 = \left(\frac{\gamma}{\gamma - 1} \right) \frac{P_2}{\rho_2} + \frac{1}{2} v_2^2 \quad [12.24]$$

Table 12.1 Discharge coefficient data for orifice plate (from BS 1042: Section 1.1: 1981†).‡

(a) The Stolz equation

$$C = 0.5959 + 0.0312\beta^{2.1} - 0.184\beta^8 + 0.0029\beta^{2.5} \left(\frac{10^6}{Re_D} \right)^{0.75} + 0.0900L_1\beta^4(1 - \beta^4)^{-1} - 0.0337L_2'\beta^3$$

Note

If $L_1 \geq \frac{0.0390}{0.0900}$ ($= 0.4333$) use 0.0390 for the coefficient of $\beta^4(1 - \beta^4)^{-1}$.

(b) Values of L_1 and L_2'

Corner tapings	$L_1 = L_2' = 0$
D and $D/2$ tapings	$L_1 = 1,^* L_2' = 0.47$
Flange tapings	$L_1 = L_2' = 25.4/D^\dagger$

(c) Conditions of validity

	Corner taps	Flange taps	D and $D/2$ taps
d (mm)	$d \geq 12.5$	$d \geq 12.5$	$d \geq 12.5$
D (mm)	$50 \leq D \leq 1000$	$50 \leq D \leq 760$	$50 \leq D \leq 760$
β	$0.23 \leq \beta \leq 0.80$	$0.2 \leq \beta \leq 0.75$	$0.2 \leq \beta \leq 0.75$
Re_D	$5000 \leq Re_D \leq 10^8$ for $0.23 \leq \beta \leq 0.45$ $10\,000 \leq Re_D \leq 10^8$ for $0.45 < \beta \leq 0.77$ $20\,000 \leq Re_D \leq 10^8$ for $0.77 \leq \beta \leq 0.80$	$1260\beta^2 D^\dagger \leq Re_D \leq 10^8$	$1260\beta^2 D^\dagger \leq Re_D \leq 10^8$

* Hence coefficient of $\beta^4(1 - \beta^4)^{-1}$ is 0.0390.

† D expressed in mm.

‡ Extracts from BS 1042: Section 1.1: 1981 are reproduced by permission of BSI. Complete copies can be obtained from them at Linford Wood, Milton Keynes MK14 6LE, UK.

Since $\rho_2 < \rho_1$, i.e. the fluid expands, $Q_2 > Q_1$ and volume flow rate is not conserved. However, there is conservation of mass flow rate \dot{M} , i.e.

$$\dot{M}_1 = v_1 A_1 \rho_1 = \dot{M}_2 = v_2 A_2 \rho_2 \quad [12.25]$$

This underlines the greater significance of mass flow in gas metering. From [12.23]–[12.25] we have

Theoretical equation for compressible flow

$$\dot{M}_{Th} = \varepsilon \frac{A_2}{\sqrt{1 - \left(\frac{A_2}{A_1} \right)^2}} \sqrt{2\rho_1(P_1 - P_2)} \quad [12.26]$$

where:

ε = expansibility factor

$$= \sqrt{\left(\frac{\gamma}{\gamma - 1}\right) \left(\frac{P_2}{P_1}\right)^{2/\gamma} \left[\frac{1 - (P_2/P_1)^{(\gamma-1)/\gamma}}{1 - (P_2/P_1)} \right] \left[\frac{1 - (A_2/A_1)^2}{1 - (A_2/A_1)^2 (P_2/P_1)^{2/\gamma}} \right]}$$

i.e. ε is a function of the three dimensionless groups P_2/P_1 , γ , A_2/A_1 or $\Delta P/P_1$, γ , β ;
i.e. $\varepsilon = f(\Delta P/P_1, \gamma, \beta)$ where $\Delta P = P_1 - P_2$. The above equation for ε is never used in practice. In BS 1042 and ISO 5167, ε is given as a regression equation. For orifice plates this is:

$$\varepsilon = 1 - (0.41 + 0.35\beta^4) \left(\frac{1}{\gamma}\right) \left(\frac{\Delta P}{P_1}\right) \quad [12.27]$$

if $(P_2/P_1) \geq 0.75$. Note that $\varepsilon = 1.0$ for a liquid.

Summarising, the following equation is applicable to any practical differential pressure flowmeter, metering any clean liquid or gas:

*General, practical
equation for
differential pressure
flowmeter*

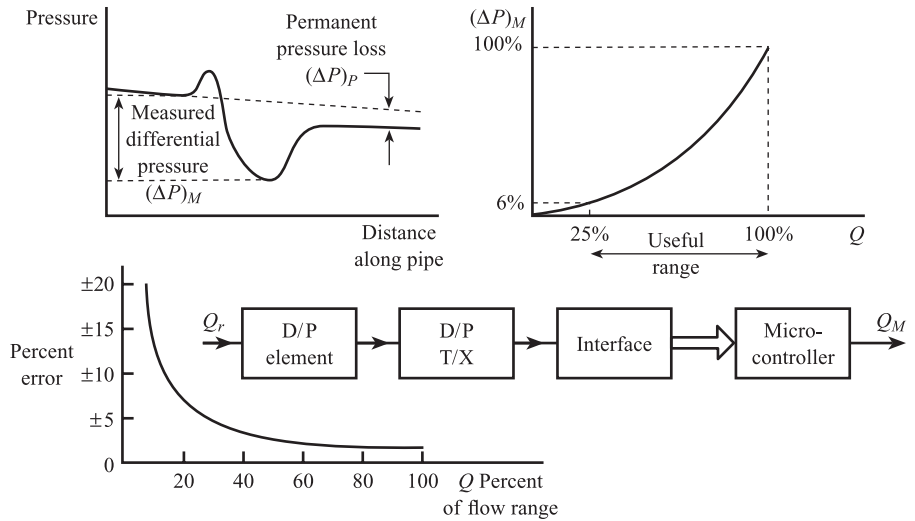
$$\dot{M}_{\text{ACT}} = C E \varepsilon A_2^M \sqrt{2\rho_1(P_1 - P_2)} \quad [12.28]$$

General characteristics

The following general characteristics of differential pressure flowmeters should be borne in mind when deciding on the most suitable meter for a given application.

1. No moving parts; robust, reliable and easy to maintain; widely established and accepted.
2. There is always a permanent pressure loss (ΔP_p) due to frictional effects (Figure 12.8). The cost of the extra pumping energy may be significant for large installations.
3. These devices are non-linear, i.e. $Q \propto \sqrt{\Delta P}$ or $\Delta P \propto Q^2$. This limits the useful range of a meter to between 25% and 100% of maximum flow. At lower flows the differential pressure measurement is below 6% of full scale and is clearly inaccurate.
4. Can only be used for clean fluids, where there is well-established turbulent flow, i.e. $Re_D > 10^4$ approximately. Not generally used if solids are present, except for Venturis with dilute slurries.
5. A typical flowmeter system (Figure 12.8) consists of the differential pressure sensing element, differential pressure transmitter (Chapter 9), interface circuit and microcontroller. For a transmitter giving a d.c. current output signal (typically 4 to 20 mA) the interface circuit consists of an amplifier acting as a current-to-voltage converter and an analogue-to-digital converter. For a resonator transmitter (Section 9.4) giving a sinusoidal output of variable frequency, the interface circuit consists of a Schmitt trigger and a binary counter (Figure 10.5). The computer reads the input binary number, converts it into differential pressure ΔP and then calculates the measured flow rate Q_M using eqn [12.22]. The calculation is based on values of ρ_1 , C , β , etc., stored in memory. The

Figure 12.8
Characteristics of
differential pressure
flowmeters and typical
system.



system measurement error $E = Q_M - Q_T$ is determined by the transmitter accuracy, quantisation errors and uncertainties in the values of the above parameters. A graph of percentage error versus flowrate is shown in Figure 12.8.

6. Considerable care must be taken with the installation of the meter. The standards give detailed information on the following:
 - (a) The geometry of the flowmeter itself (Figure 12.7). C values are only applicable to meters with the prescribed geometry.
 - (b) Minimum lengths of straight pipe upstream and downstream of the meter.
 - (c) The arrangement of the pressure pipes connecting the flowmeter to the differential pressure device.

Types of differential pressure flowmeter

The four elements in current use are the orifice plate, Venturi, Dall tube and nozzle (see Figure 12.7). Of these the orifice plate is by far the most widely used. It is cheap and available in a very wide range of sizes. The main disadvantages are the limited accuracy ($\pm 1.5\%$ at best) and the high permanent pressure loss $(\Delta P)_P$. There are three recommended arrangements of pressure tapplings to be used with orifice plates: corner, flange and $D - D/2$ (Figure 12.7). The values of C are given by Table 12.1 and are different for each arrangement. Table 12.2 summarises the main parameters

Table 12.2.

Parameter/meter	Venturi	Nozzle	Dall tube	Orifice plate
Approximate value of C	0.99	0.96	0.66	0.60
Relative values of measured differential pressure $(\Delta P)_M$	1.0	1.06	2.25	2.72
Permanent ΔP as % of $(\Delta P)_M$				
i.e. $\frac{(\Delta P)_P}{(\Delta P)_M} \times 100\%$	10–15%	40–60%	4–6%	50–70%

of the four elements. The Dall tube combines a high measured differential pressure $(\Delta P)_M$ (like the orifice plate) with a low permanent pressure loss $(\Delta P)_P$ (better than Venturi).

Calculation of orifice plate hole diameter d

To calculate d we need accurate values of C , E and ε . Since all three quantities are functions of d (via $\beta = d/D$), an iterative calculation is required. Figure 12.9 is a flowsheet for one possible calculation method; this is suitable for manual or computer implementation.

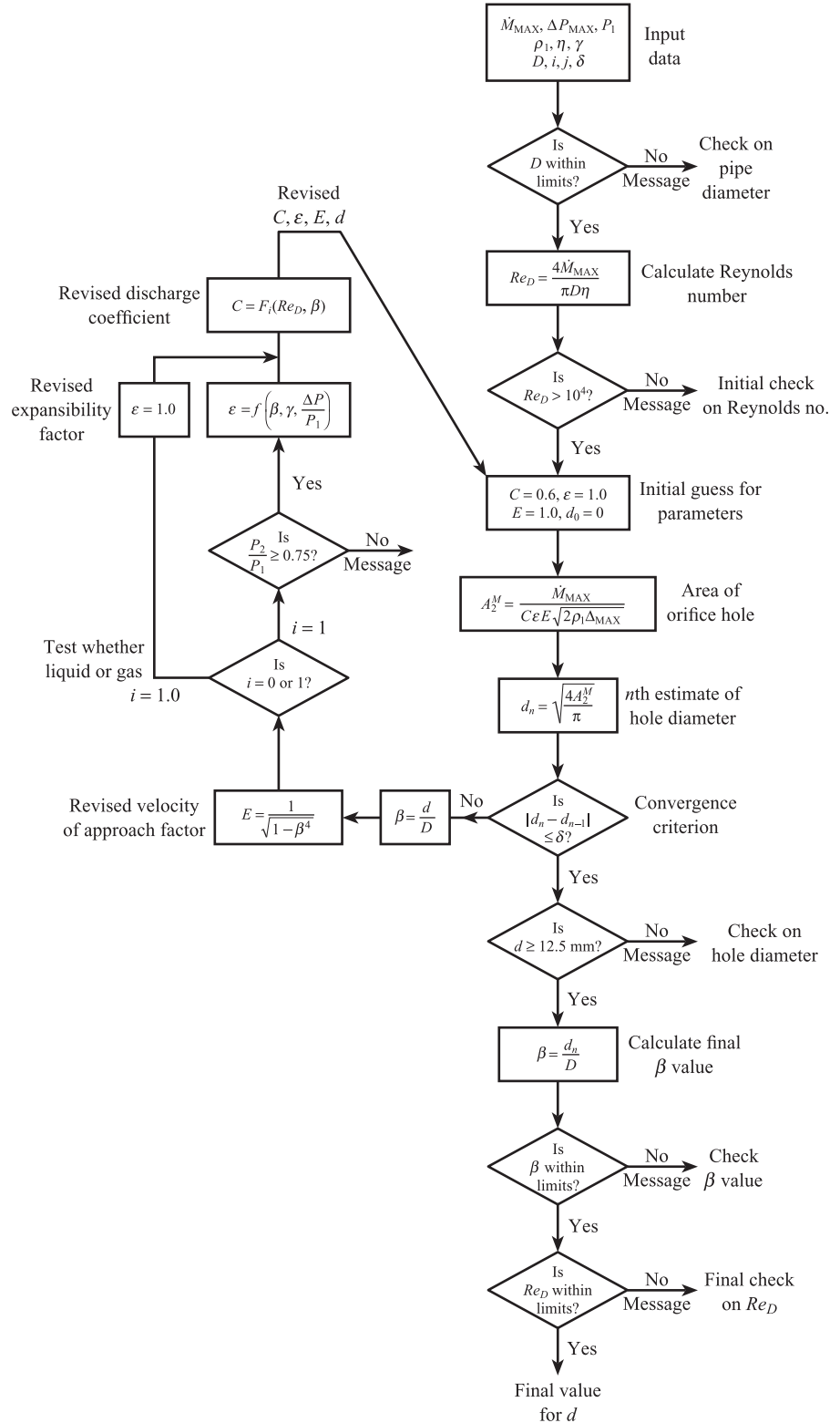
Notes on flowsheet

- The following input data are required:
 - \dot{M}_{MAX} Maximum mass flow rate (kg s^{-1})
 - ΔP_{MAX} Differential pressure at maximum flow (Pa)
 - P_1 Upstream pressure (Pa)
 - ρ_1 Fluid density at upstream conditions (kg m^{-3})
 - η Dynamic viscosity of fluid (Pa s)
 - γ Specific heat ratio
 - δ Machining tolerance (m)
 - D Pipe diameter (m)
 - i Fluid index: $i = 0$ for liquid, $i = 1$ for gas
 - j Tappings index: $j = 0$ for corner, $j = 1$ for flange, $j = 2$ for $(D - D/2)$.
- Calculation of Reynolds number uses \dot{M}_{MAX} and pipe diameter D . Since $Re_D = \rho(vD/\eta)$ and since $v = \dot{M}_{\text{MAX}}/(\rho\pi D^2/4)$, $Re_D = 4\dot{M}_{\text{MAX}}/(\pi D\eta)$.
- The values of d , D , β and Re_D must be checked against the conditions of validity of the Stolz equation (Table 12.1). An initial approximate check that Re_D is greater than 10^4 is followed by a final accurate check once β is established.
- There is no point in calculating d more accurately than the tolerance δ to which the hole can be machined. This provides a criterion for either continuing or concluding the calculation. Thus if d_{n-1} , d_n are respectively the $(n - 1)$ th and n th guesses for d , then:
 - if $|d_n - d_{n-1}| > \delta$ continue calculation,
 - if $|d_n - d_{n-1}| \leq \delta$ conclude calculation.
- Since final values of C , ε and E will be close to the initial guesses, the calculation should require no more than about six iterations.
- Since Venturi and Dall tubes are sold in standard sizes, a different approach is required. An approximate calculation will give the most suitable size; then an accurate calculation of $(\Delta P)_{\text{MAX}}$ is carried out for the size chosen.

12.3.2 Mechanical flowmeters

A mechanical flowmeter is a machine which is placed in the path of the flow, and made to move by the flow. The number of machine cycles per second f is proportional to volume flow rate Q , i.e. $f = KQ$, so that measurement of f yields Q . However, mechanical flowmeters are often used to measure the total volume of fluid

Figure 12.9 Flowsheet for orifice plate sizing.



$V = \int_0^T Q \, dt$ that has been delivered during a time interval T . The total number of machine cycles during T is:

$$N = \int_0^T f \, dt = K \int_0^T Q \, dt = KV$$

i.e. the total count is proportional to volume. A large number of mechanical flowmeters have been developed, but the most commonly used is the **axial flow turbine flowmeter**.

Principle of turbine flowmeter

A turbine flowmeter (see Figures 12.10 and 12.11) consists of a multi-bladed rotor suspended in the fluid stream; the axis of rotation of the rotor is parallel to the direction of flow. The fluid impinges on the blades and causes them to rotate at an angular velocity approximately proportional to flow rate. The blades, usually between four and eight in number, are made of ferromagnetic material, and each blade forms a magnetic circuit with the permanent magnet and coil in the meter housing. This gives a variable reluctance tachogenerator (Section 8.4); the voltage induced in the coil has the form of a sine wave whose frequency is proportional to the angular velocity of the blades.

Assuming that the drag torque due to bearing and viscous friction is negligible, the rotor angular velocity ω_r is proportional to Q , i.e.

$$\omega_r = kQ \quad [12.29]$$

where k is a constant which depends on the geometry of the blade system. An approximate value for k can be evaluated using Figure 12.10. If Q is the volume flow rate through the meter then the corresponding mean velocity \bar{v} is:

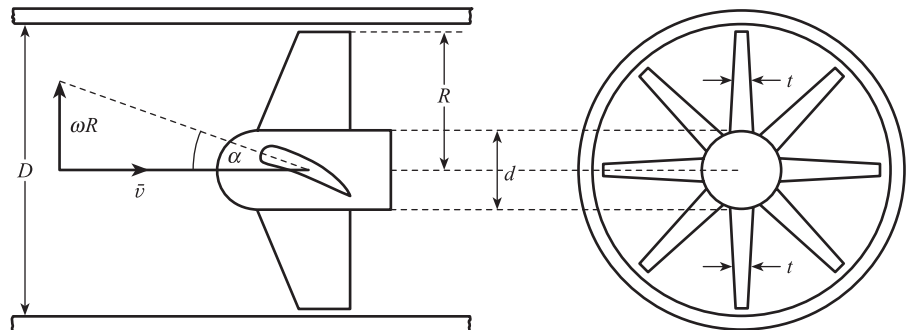
$$\bar{v} = \frac{Q}{A} \quad [12.30]$$

where A is the cross-sectional area of the fluid. Assuming the fluid fills the pipe, then:

$A = \text{area of pipe} - \text{area of hub} - \text{area of blades}$

$$= \frac{\pi}{4} D^2 - \frac{\pi}{4} d^2 - m \left(R - \frac{d}{2} \right) t \quad [12.31]$$

Figure 12.10 Turbine flowmeter – principles.



where m is the number of blades and t their average thickness. From the inlet velocity triangle shown in Figure 12.10 we have:

$$\frac{\omega_r R}{\bar{v}} = \tan \alpha$$

where ω_r is the angular velocity of the blades, $\omega_r R$ is the velocity of the blade tip perpendicular to the direction of flow and α is the inlet blade angle at tip. From eqns [12.29] and [12.30] we have:

$$k = \frac{\omega_r}{Q} = \frac{\tan \alpha}{AR} \quad [12.32]$$

The principle of the variable reluctance tachogenerator was explained in Section 8.4; from eqn [8.42] the voltage induced in the coil is:

$$E = bm\omega_r \sin m\omega_r t \quad [8.42]$$

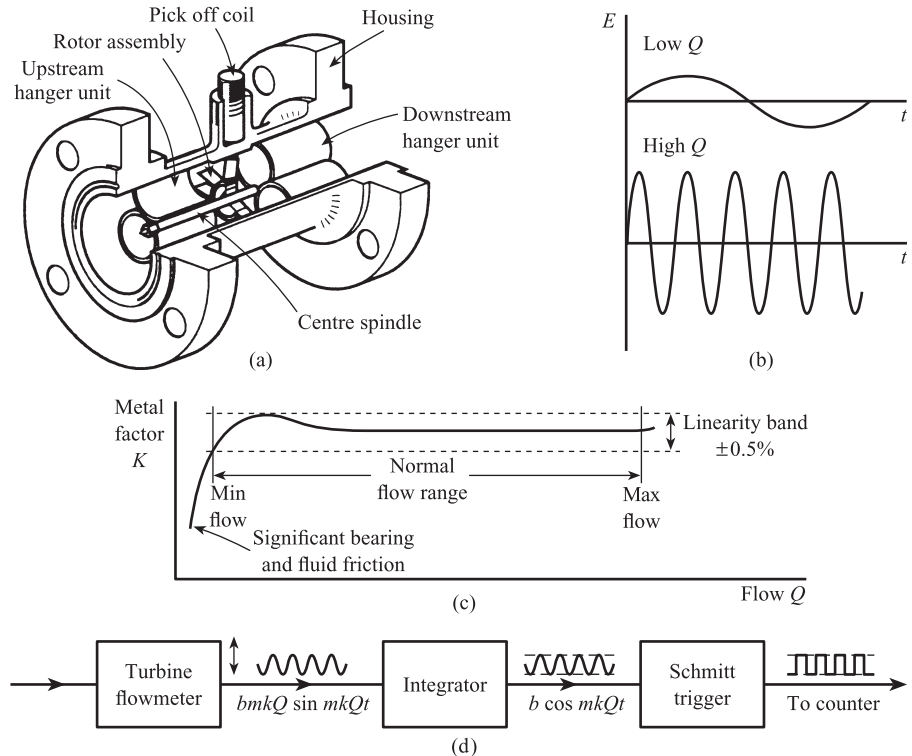
where m is the number of blades and b is the amplitude of the angular variation in magnetic flux. Thus:

Output signal from turbine flowmeter

$$E = bmkQ \sin mkQt \quad [12.33]$$

This is a sinusoidal signal of amplitude $\hat{E} = bmkQ$ and frequency $f = (mk/2\pi)Q$, i.e. both amplitude and frequency are proportional to flow rate (see Figure 12.11).

Figure 12.11
Turbine flowmeter:
(a) Construction (after Lomas, Kent Instruments, 1977, Institute of Measurement and Control Conference 'Flow-Con 77')
(b) Signals
(c) Characteristics
(d) System.



The flowmeter signal E is usually passed through an integrator and a Schmitt trigger circuit (Figure 12.11). The output is thus a constant amplitude, square wave signal of variable frequency f which can be successfully transmitted to a remote counter, even in the presence of considerable noise and interference. Since $f = (mk/2\pi)Q = KQ$, where K is the linear sensitivity or meter factor, the total count N is proportional to total volume V . Using eqn [12.32] the meter factor is given by $K = (m \tan \alpha)/2\pi AR$.

Characteristics

The meter factor K for a given flowmeter is found by direct calibration: typical results are shown in Figure 12.11. The normal flow range is usually from about 10% up to 100% of maximum rated flow. Over this range, the deviation of meter factor K from mean value is usually within $\pm 0.5\%$ and may be only $\pm 0.25\%$. Below 10% of maximum, bearing and fluid friction become significant and the relationship between f and Q becomes increasingly non-linear. Repeatability is quoted to be within $\pm 0.1\%$ of actual flow. A 5-inch meter with a range between 45 and 450 $\text{m}^3 \text{h}^{-1}$ and a meter factor of 1.17×10^3 pulses m^{-3} will give an output of between 15 and 150 pulses per second (with water).

Turbine flowmeters are available to fit a wide range of pipe diameters, typically between 5 and 500 mm. They tend to be more delicate and less reliable than competing flowmeters; blades and bearings can be damaged if solid particles are present in the fluid. They are relatively expensive, and there is a permanent pressure drop, typically between 0.1 and 1.0 bar, at maximum flow (with water). Modern turbine flowmeters have 'thrust compensation' where the thrust of the fluid impinging on the rotor is balanced by an opposing thrust, thus reducing bearing wear. Flow straightening vanes are positioned upstream of the meter to remove fluid swirl which would otherwise cause the rotor angular velocity to be too high or too low, depending on direction.

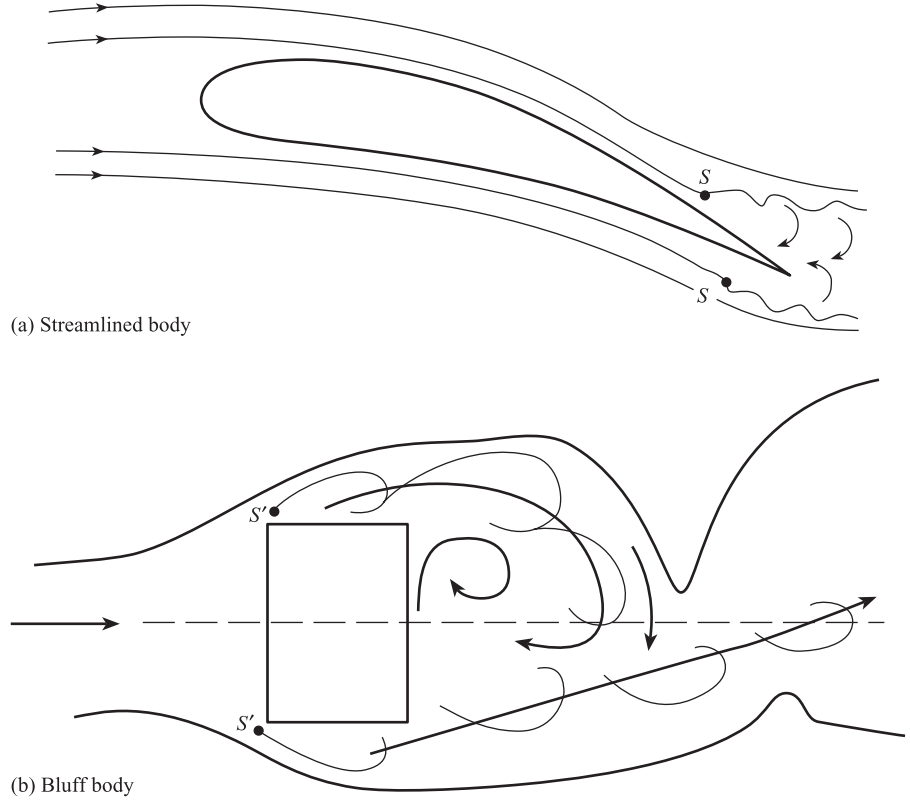
12.3.3 Vortex flowmeters

Principle

The operating principle of the vortex flowmeter is based on the natural phenomenon of **vortex shedding**. When a fluid flows over any body, boundary layers of slower moving fluid move over the surface of the body (Section 12.1.1). If the body is **streamlined**, as in an aerofoil (Figure 12.12(a)), then the boundary layers can follow the contours of the body and remain attached to the body over most of its surface. The boundary layers become detached at the separation points S , which are well to the rear of the body, and the resulting wake is small. If, however, the body is unstreamlined, i.e. **bluff**, e.g. a rectangular, circular or triangular cylinder (Figure 12.12(b)), then the boundary layers cannot follow the contours and become separated much further upstream (points S'). The resulting wake is now much larger.

Figure 12.12(b) shows the vortex growth region behind the bluff body. Separated boundary layers along the bottom surface of the bluff body are flowing into the developing lower vortex. Separated layers along the top surface roll up into a clockwise circulation, which will form the upper vortex. The figure also shows upper layers moving downwards towards the lower layers. The process continues with the clockwise circulation growing further and upper layers moving further downwards to cut

Figure 12.12 Principles of vortex shedding:
(a) Streamlined body
(b) Bluff body.



off the flow to the lower vortex. The lower vortex is then detached and moves downstream; the clockwise circulation also moves downstream to form the developing upper vortex. This process is continually repeated with vortices being produced and shed alternately from top and bottom surfaces of the bluff body.

The vortices shed from the bluff body form a wake known as a **von Karman vortex street**. This is shown in Figure 12.13 both in idealised form (a) and as a computer simulation of the flow behind the bluff body (b). This consists of two rows of vortices moving downstream, parallel to each other, at a fixed velocity. The distances l between each vortex and h between the rows are constant, and a vortex in one row occurs halfway between two vortices in another row. If d is the width of the bluff body, then:

$$h \approx d \quad \text{and} \quad l \approx 3.6h$$

The frequency of vortex shedding f is the number of vortices produced from each surface of the bluff per second. This is given by:

*Frequency of
vortex shedding*

$$f = S \frac{v_1}{d}$$

[12.34]

where v_1 is the mean velocity at the bluff body, d is the width of the bluff and S is a dimensionless quantity called the Strouhal number. Since S is practically constant, f is proportional to v_1 , thus providing the basis of a flowmeter.

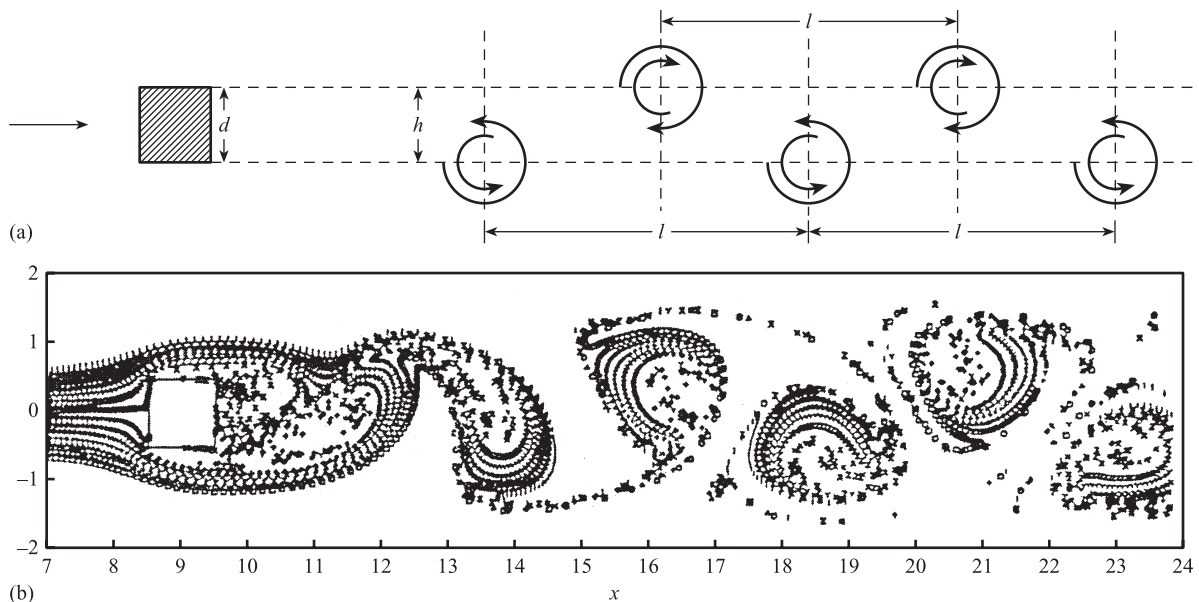


Figure 12.13 von Karman vortex street:
(a) Idealised
(b) Computer simulation.

We now derive the meter factor (sensitivity). If

- Q = volume flow rate ($\text{m}^3 \text{s}^{-1}$),
 A, A_1 = cross-sectional areas of the flow, upstream and at the bluff body respectively (m^2),
 v, v_1 = velocities of the flow, upstream and at the bluff body respectively (m s^{-1}),
 D = pipe diameter (m),

then assuming the flow is incompressible, conservation of volume flow rate gives

$$Q = Av = A_1 v_1 \quad [12.35]$$

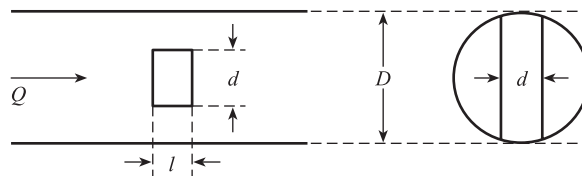
The frequency f of vortex shedding is given by

$$f = S \frac{v_1}{d} \quad [12.36]$$

where S is the Strouhal number and d is the width of the bluff body (Figure 12.14 shows a rectangular bluff body). Assuming the fluid fills the pipe:

$$A = \frac{\pi}{4} D^2 \quad [12.37]$$

Figure 12.14 Derivation of meter factor.



The fluid cross-section at the bluff body is approximately given by:

$$A_1 \approx \frac{\pi}{4} D^2 - Dd = \frac{\pi}{4} D^2 \left(1 - \frac{4}{\pi} \frac{d}{D} \right) \quad [12.38]$$

From [12.35]–[12.38], the theoretical equation for the meter factor $K = f/Q$ is:

$$K = \frac{f}{Q} = \frac{4S}{\pi D^3} \frac{1}{\frac{d}{D} \left(1 - \frac{4}{\pi} \frac{d}{D} \right)} \quad [12.39]$$

This equation is corrected, for practical use, by introducing a bluntness coefficient k ,^[4] thus:

*Practical equation
for meter factor*

$$K = \frac{f}{Q} = \frac{4S}{\pi D^3} \cdot \frac{1}{\frac{d}{D} \left(1 - \frac{4}{\pi} k \frac{d}{D} \right)} \quad [12.40]$$

k has different values for different bluff body shapes: e.g. $k = 1.1$ for a circle, and 1.5 for a rectangle and equilateral triangle.

Signal characteristics

The vortex mechanism produces approximately sinusoidal variations in fluid velocity and pressure, at the shedding frequency f , in the vicinity of the bluff body. Figures 12.15(a), (b) and (c) show vortex signal waveforms at approximate frequencies $f = 100, 200$ and 400 Hz. However, for pipe Reynolds numbers Re_D greater than about 10 000, the flow in the pipe is turbulent. This means that there are background random variations in fluid velocity and pressure with time, at any point in the pipe (Figure 12.15(d)). These random variations affect the vortex shedding mechanism, causing random variations in both the amplitude and frequency of the signal about a mean value. Because vortex frequency f is used to measure volume flow rate Q , random variations in f limit the **repeatability** of the meter. This effect can be quantified by measuring the random variation in the period T of individual cycles. If \bar{T} is the mean period and σ is the standard deviation of a set of individual periods, then a useful measure of repeatability is **percentage standard deviation, % σ** :

$$\% \sigma = \frac{\sigma}{\bar{T}} \times 100\% \quad [12.41]$$

Bluff body characteristics and geometry

Investigations show^[4] that the Strouhal number S is a constant for a wide range of Reynolds numbers (Figure 12.16(a)). This means that, for a given flowmeter in a given pipe, i.e. fixed D, d and k , the meter factor K is practically independent of flow rate, density and viscosity. Here Re_D is the body Reynolds number $vd\rho/\eta$.

The vortex shedding from a number of bluff body shapes has been investigated in order to establish which shape gives the most regular shedding. The power spectral density of the vortex signals for bluff bodies, of the same width d , with

Figure 12.15 Typical vortex flowmeter signals:
(a) $f = 100$ Hz
(b) $f = 200$ Hz
(c) $f = 400$ Hz
(d) Without bluff body – random turbulence.

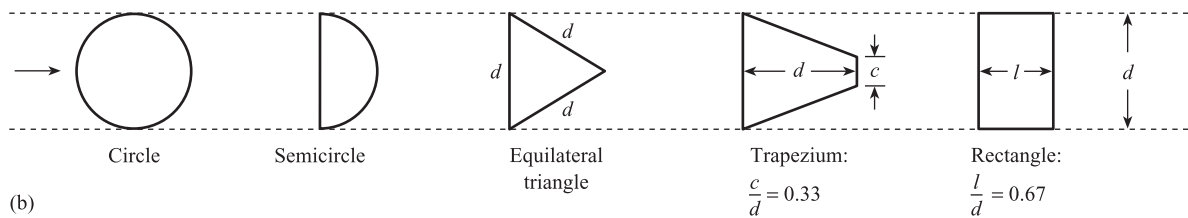
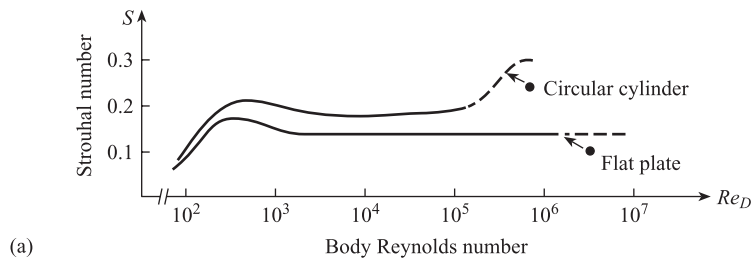
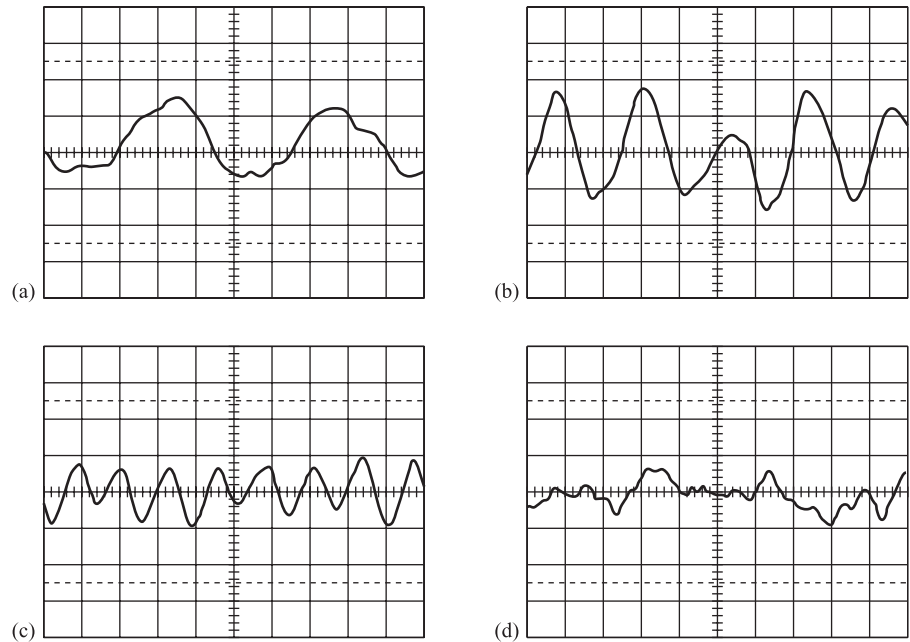
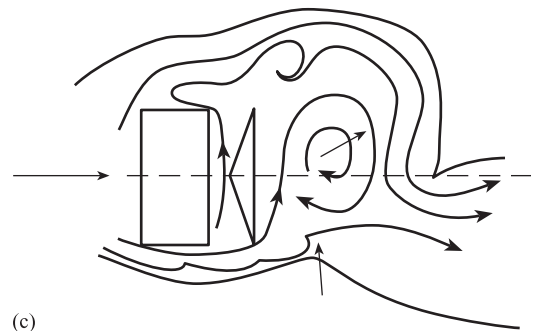


Figure 12.16 Bluff body characteristics and geometry:
(a) Strouhal number versus Reynolds number
(b) Bluff body shapes
(c) Dual bluff body.



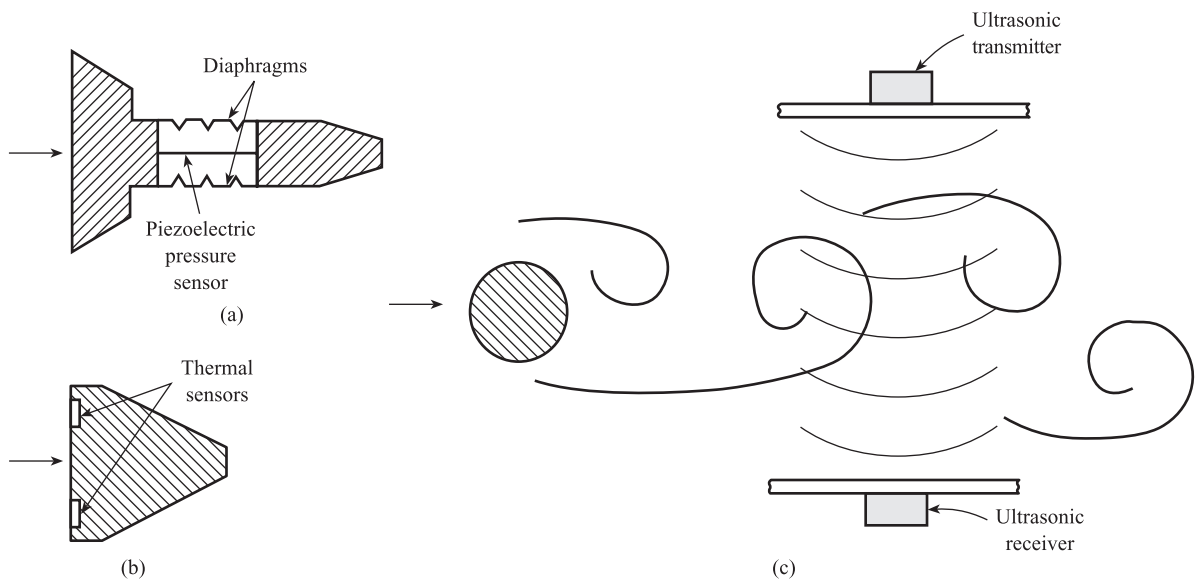
cross-sectional shapes in the form of a circle, semicircle, equilateral triangle, trapezium and rectangle (Figure 12.16(b)) have been measured at the same flow conditions.^[5] It was found that the rectangle with $l/d = 0.67$ gave the narrowest frequency spectrum, i.e. the lowest value of $\% \sigma$, of all the five shapes. Typically $\% \sigma$ for this optimum rectangle is between 9% and 25%, depending on the strength of the flow turbulence. Further single bluff body shapes have been developed; Figure 12.17 shows a T-shaped bluff body.

There have also been investigations of the vortex shedding from combinations of two bluff bodies separated by a narrow gap.^[6,7] Figure 12.16(c) shows the vortex mechanism in a dual combination consisting of a rectangle upstream and a triangle downstream. Boundary layers along the bottom surface are flowing into the developing lower vortex. A strong clockwise circulation is first established from upper boundary layers and lower boundary layers moving up through the gap. This grows sufficiently to directly entrain further lower layers. Upper and gap layers move around this circulation to join lower layers flowing into the lower vortex. The circulation moves upwards and further downstream to form the developing upper vortex. This causes lower layers to be pulled upwards to cut off the flow to the lower vortex, which then becomes detached. The stronger circulation and shedding mechanism result in $\% \sigma$ being significantly lower than for a single bluff body, typically 4–15% depending on the strength of the turbulence.

Vortex flowmeters can be used to measure the total volume $V = \int_0^T Q dt$ of fluid that has passed through the meter during time T . This is done by counting the number of vortex cycles N during T . Thus:

$$V = \int_0^T Q dt = \int_0^T (f/K) dt = (1/K) \int_0^T f dt = N/K \quad [12.42]$$

Figure 12.17 Bluff body shapes and detection systems.



deviation for the measurement of V , then the number of cycles N which must be collected to achieve %s will depend on both %s and % σ . If we assume a normal distribution of frequency values, then we have (Section 6.5.7):

$$N = \frac{\% \sigma^2}{\% s^2} \quad [12.43]$$

giving:

$$V = \frac{1}{K} \cdot \frac{\% \sigma^2}{\% s^2} \quad [12.44]$$

For volume measurements, the optimum vortex flowmeter will need minimum volume V to achieve desired repeatability %s; this means the optimum flowmeter will have minimum % σ^2/K . This can be achieved by:

- (a) Choosing the cross-sectional shape which has lowest % σ .
- (b) For this cross-sectional shape, choosing the blockage ratio d/D which minimises % σ^2/K . For a range of typical single and dual bluff bodies, optimum d/D is around 0.1 to 0.15.^[8]

Vortex detection systems and practical flowmeters

As explained above, vortex shedding is characterised by approximately sinusoidal changes in fluid velocity and pressure in the vicinity and downstream of the bluff body. Figure 12.17 shows three commonly used bluff body shapes; these use three different methods of vortex detection.

- (a) *Piezoelectric* (Section 8.7). Figure 12.17(a) shows a T-shaped bluff body; part of the tail is not solid but fluid filled. Flexible diaphragms in contact with the process fluid detect small pressure variations due to vortex shedding. These pressure changes are transmitted to a piezoelectric differential pressure sensor which is completely sealed from the process fluid.
- (b) *Thermal* (Sections 14.2 and 14.3). Figure 12.17(b) shows an approximately triangular-shaped bluff body with two semiconductor thermal sensors on the upstream face. The sensors are incorporated into constant-temperature circuits which pass a heating current through each sensor; this enables small velocity fluctuations due to vortices to be detected.
- (c) *Ultrasonic* (Chapter 16). Figure 12.17(c) shows a narrow circular cylinder which creates a von Karman vortex street downstream. An ultrasonic transmission link sends a beam of ultrasound through the vortex street. The vortices cause the received sound wave to be modulated in both amplitude and phase.

Vortex flowmeters give a frequency pulse output signal proportional to flow rate like turbine meters; however, they have no moving parts and are more reliable. The bluff body provides an obstruction to flow so that vortex meters can only be used with clean liquids and gases; there is also a permanent pressure loss. A typical range of vortex flowmeters covers pipe diameters of 15, 25, 40, 50, 100, 150 and 200 mm.^[9] The accuracy (including non-linearity, hysteresis and repeatability) for liquids is $\pm 0.65\%$ of flow rate for pipe Reynolds numbers greater than 20 000. For gases and steam, the accuracy is $\pm 1.35\%$ of flow rate for pipe Reynolds numbers greater than 15 000.

12.4

Measurement of mass flow rate

Liquids and gases such as crude oil, natural gas and hydrocarbon products are often transferred from one organisation to another by pipeline. Since these products are bought and sold in units of mass, it is essential to know accurately the mass M of fluid that has been transferred in a given time T . There are two main methods of measuring M : inferential and direct.

12.4.1 Inferential methods

Here mass flow rate \dot{M} and total mass M are computed from volume flow rate and density measurements using $\dot{M} = \rho Q$ and $M = \rho V$. For pure liquids density ρ depends on temperature only. If temperature fluctuations are small, then ρ can be assumed to be constant and M can be calculated using only measurements of total volume V obtained from a mechanical flowmeter. If the temperature variations are significant then the density ρ must also be measured. In liquid mixtures density depends on both temperature and composition and again ρ must be measured. The same is also true of pure gases, where density depends on pressure and temperature, and gas mixtures where density depends on pressure, temperature and composition.

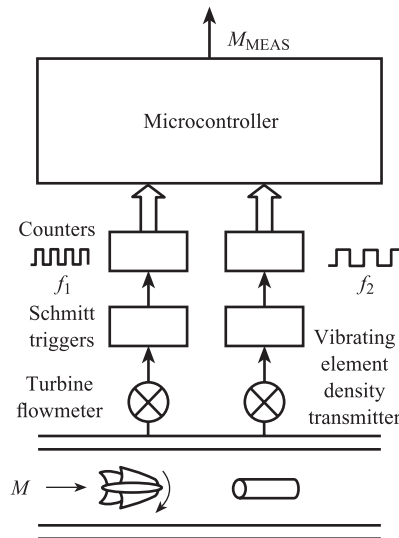
Figure 12.18 shows a typical system based on a turbine flowmeter and a vibrating element density transducer in conjunction with a digital microcontroller. The turbine flowmeter (Section 12.3.2) gives a pulse output signal, with frequency f proportional to volume flow rate Q , i.e.

$$f_1 = KQ \quad [12.45]$$

where K = meter factor for turbine flowmeter. The vibrating element density transducer (Section 9.5.2) also gives a pulse output signal, with frequency f_2 which depends on fluid density ρ via the non-linear equation:

$$\rho = \frac{A}{f_2^2} + \frac{B}{f_2} + C \quad [12.46]$$

Figure 12.18 Inferential measurement of mass flow.



Each pulse signal is input to a counter; the computer reads the state of each counter at the beginning and end of a fixed counting interval ΔT . The computer calculates frequencies f_1 and f_2 using:

$$f = \frac{N_{\text{NEW}} - N_{\text{OLD}}}{\Delta T} \quad [12.47]$$

where N_{OLD} and N_{NEW} are the counts at the beginning and end of ΔT . Q and ρ are then calculated from [12.45] and [12.46] using the transducer constants K , A , B and C stored in memory. The total mass M transferred during time T is then:

$$M = \Delta T \sum_{i=1}^n \rho_i Q_i \quad [12.48]$$

where ρ_i and Q_i are values of ρ and Q evaluated at the i th interval ΔT , and $n = T/\Delta T$.

12.4.2 Direct methods

In a direct or true mass flowmeter the output of the sensing element depends on the mass flow rate \dot{M} of fluid passing through the flowmeter. Such a flowmeter is potentially more accurate than the inferential type. One of the most popular and successful direct mass flowmeters in current use is based on the Coriolis effect.^[10]

Coriolis flowmeter

The Coriolis effect is shown in Figure 12.19(a). A slider of mass m is moving with velocity v along a rod; the rod itself is moving with angular velocity ω about the axis XY . The mass experiences a Coriolis force of magnitude:

$$F = 2m\omega v \quad [12.49]$$

and direction perpendicular to both linear and angular velocity vectors.

Figure 12.19(b) shows the flowmeter. Here the fluid flows through the U-tube $ABCD$, which is rotating with an angular velocity ω about the axis XY . Here ω varies sinusoidally with time at constant frequency f , i.e. $\omega = \hat{\omega} \sin 2\pi ft$. Consider an element of fluid of length Δx travelling with velocity v along the limb AB , which will have mass

$$\Delta m = \rho A \Delta x$$

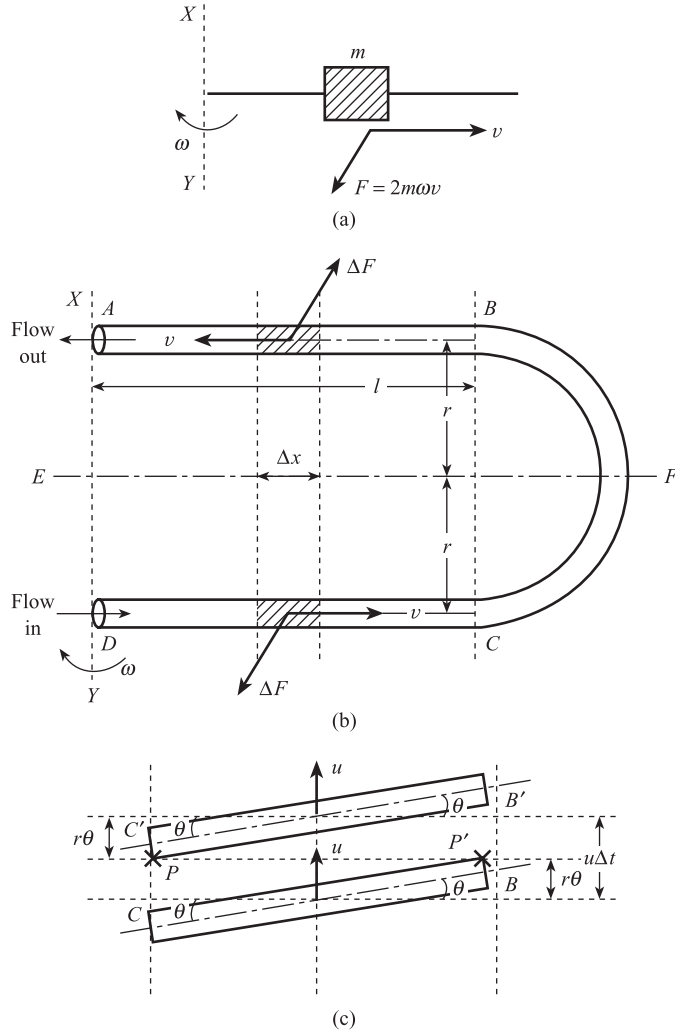
where ρ is the density of the fluid and A the internal cross-sectional area of the tube. The element experiences a Coriolis force:

$$\Delta F = 2\Delta m\omega v = 2\rho A\omega v\Delta x$$

in the direction shown. The total force on the limb AB of length l is:

$$F = 2\rho A\omega v \int_0^l dx = 2\rho A\omega vl \quad [12.50]$$

Figure 12.19 Coriolis mass flowmeter:
 (a) Coriolis effect
 (b) Flowmeter
 (c) Measurement of twist angle.



The limb CD experiences a force of equal magnitude F but in the opposite direction. In BC the velocity and angular velocity vectors are parallel, so the Coriolis force is zero. The U-tube therefore experiences a resultant deflecting torque $T = F2r = 4lr\omega\rho Av$ about the axis EF . Since the mass flow rate \dot{M} through the tube is equal to ρAv we have

$$T = 4lr\omega\dot{M} \quad [12.51]$$

i.e. the deflecting torque is proportional to mass flow rate. Under the action of T the U-tube is twisted through an angle given by:

$$\theta = \frac{T}{c} = \frac{4lr\omega}{c} \dot{M} \quad [12.52]$$

where c is the elastic stiffness of the U-tube. The twist angle θ varies sinusoidally with time, $\theta = \hat{\theta} \sin 2\pi ft$, in response to the sinusoidal variation in ω .

Figure 12.19(c) shows an optical method of measuring θ using optical sensors P and P' . At time t sensor P' detects the tube in position CB and emits a voltage pulse; at a later time $t + \Delta t$, sensor P detects the tube in position $C'B'$ and again emits a pulse. The time interval Δt is small compared with the period of oscillation $1/f$ of θ . The distance $BB' = CC'$ travelled by the tube in Δt is $u\Delta t$ where u is the velocity of the tube at BC . This depends on tube angular velocity ω according to:

$$u = \omega l$$

From the diagram we see that:

$$BB' = CC' = u\Delta t = 2r\theta$$

giving

$$\theta = \frac{\omega l}{2r} \Delta t \quad [12.53]$$

Eliminating θ between [12.52] and [12.53] gives:

*Equation for
Coriolis flowmeter*

$$\dot{M} = \frac{c}{8r^2} \Delta t \quad [12.54]$$

A typical range of seven meters covers pipe diameters between 0.1 and 4.0 inches and can be used for both liquid and gas flows.^[11] For liquid flows, the flow range for the 0.1-inch meter is 0 to 82 kg/h, increasing to 0 to 409 tonne/h for the 4.0-inch meter. Accuracy is $\pm 0.10\%$ of flow rate and repeatability $\pm 0.05\%$ of flow rate. For gas flows, a typical flow range for the 0.1-inch meter is 0 to 8 kg/h, increasing to 0 to 34 tonne/h for the 4.0-inch meter, based on air at 20 °C and 6.8 bar and a 0.68 bar pressure drop. Accuracy is $\pm 0.35\%$ and repeatability $\pm 0.20\%$ of flow rate.

12.5 Measurement of flow rate in difficult situations

The flowmeters discussed so far will be suitable for the vast majority, perhaps 90%, of measurement problems. There will, however, be a small number of situations where they cannot be used. These 'difficult' flowmetering problems are characterised by one or more of the following features:

- The flow is laminar or transitional ($Re < 10^4$).
- The fluids involved are highly corrosive or toxic.
- Multiphase flows, that is mixtures of solids, liquids and gases. Important industrial examples are sand/water mixtures, oil/water/gas mixtures and air/solid mixtures in pneumatic conveyors.
- No obstruction or pressure drop can be tolerated (e.g. measurement of blood flow).
- There is also a need for a portable 'clip-on' flowmeter to give a temporary indication, usually for investigational work. This is strapped onto the outside of the pipe, thus avoiding having to shut down the plant in order to break into the pipe.

This section outlines methods which should be considered for these problem areas.

12.5.1 Electromagnetic flowmeter

The principle is based on Faraday's law of electromagnetic induction. This states that if a conductor of length l is moving with velocity v , perpendicular to a magnetic field of flux density B (Figure 12.20), then the voltage E induced across the ends of the conductor is given by:

$$E = Blv \quad [12.55]$$

Thus if a conducting fluid is moving with average velocity \bar{v} through a cylindrical metering tube, perpendicular to an applied magnetic field B (Figure 12.20), then the voltage appearing across the measurement electrodes is:

$$E = BD\bar{v} \quad [12.56]$$

where D = separation of electrodes = metering tube diameter. The above equation assumes that the magnetic field is uniform across the tube. If we further assume that the fluid fills the tube, then $\bar{v} = Q/(\pi D^2/4)$, giving:

Equation for
electromagnetic
flowmeter

$$E = \frac{4B}{\pi D} Q \quad [12.57]$$

If the magnetic field coils are energised by normal direct current then several problems occur: polarisation (i.e. the formation of a layer of gas around the measuring electrodes), electrochemical and thermoelectric effects all cause interfering d.c.

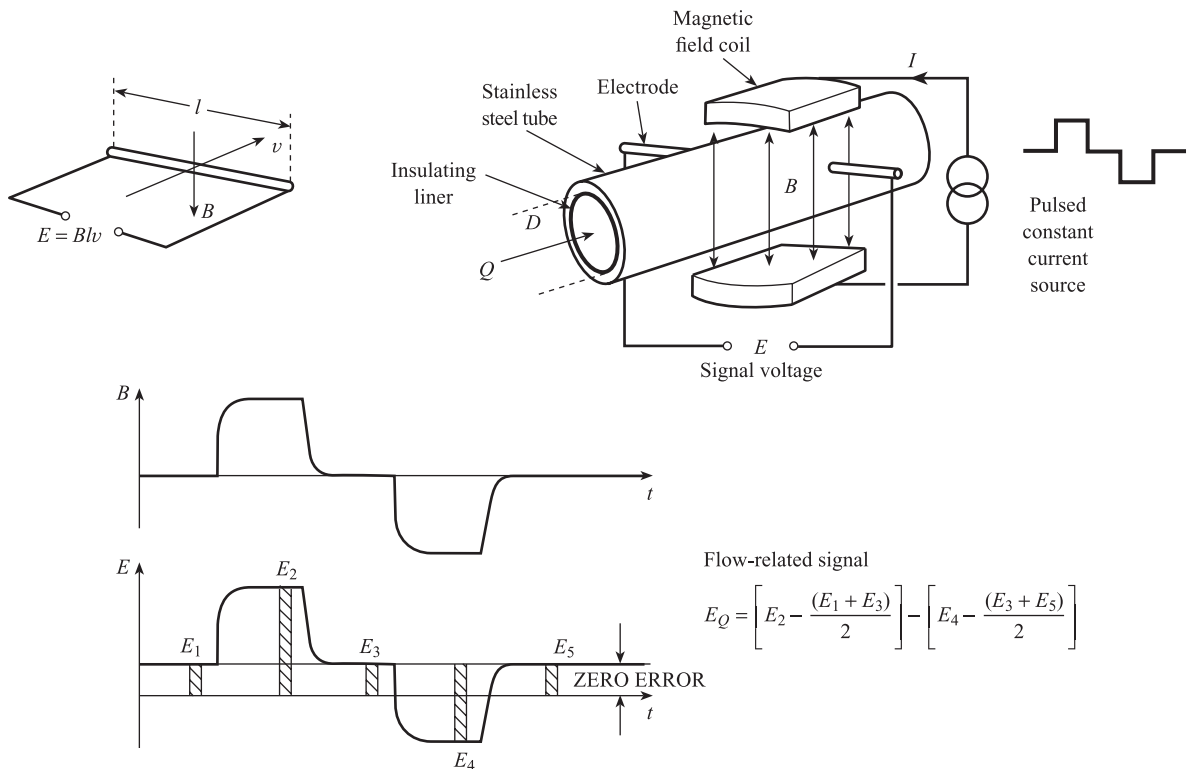


Figure 12.20 Electromagnetic flowmeter – principle, construction and signals.

voltages. These problems can be overcome by energising the field coils with alternating current at 50 Hz. The a.c. magnetic field induces a 50 Hz a.c. voltage across the electrodes with amplitude proportional to flow rate. However, this flow-generated voltage is subject to 50 Hz interference voltages generated by transformer action in a loop consisting of the signal leads and the fluid path. The above problems can be overcome by energising the field coils with direct current which is pulsed at a fixed period. Figure 12.20 shows typical waveforms of magnetic field B and induced signal voltage E .^[12] The signal is amplified and fed to a 12-bit analogue-to-digital converter and a microcontroller. The signal is sampled five times during each complete period of about 400 ms. By suitable processing of the five sample values E_1, E_2, E_3, E_4 and E_5 the zero error can be rejected and the flow-related signal measured.

The main features of the electromagnetic flowmeter are as follows:

1. The electrodes are flush with the inside of the insulating liner, which has the same diameter as the surrounding pipework. The meter therefore does not obstruct the flow in any way, and there is negligible pressure loss or chance of blockage.
2. The meter can only be used with fluids of electrical conductivity greater than $5 \mu\text{mho cm}^{-1}$; this rules out all gases and liquid hydrocarbons. It is suitable for slurries provided that the liquid phase has adequate conductivity.
3. A typical range of flowmeters covers pipe diameters between 15 and 900 mm and gives either a 4 to 20 mA d.c. current output or a variable frequency pulse output.^[13]
4. With the frequency output the system accuracy is typically $\pm 0.5\%$ of reading for flow velocities between 0.3 and 10.0 m/s, and repeatability is $\pm 0.1\%$ of reading.
5. Power consumption is typically 20 W.

12.5.2 Ultrasonic flowmeters

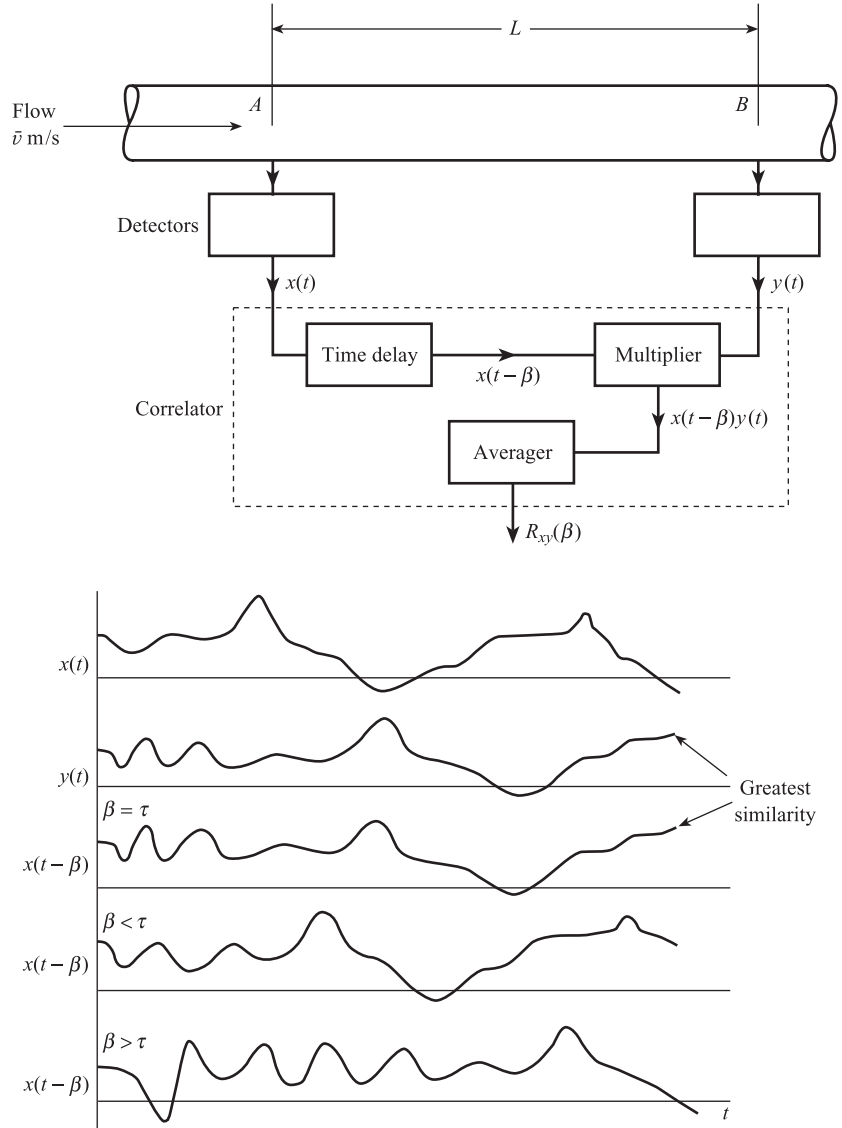
Ultrasonic flowmeters use sensors which are clamped on the outside of the pipe, i.e. do not intrude into the pipe; this makes them particularly useful for multiphase flows. Doppler, transit time and cross-correlation ultrasonic flowmeters are covered in Section 16.4.

12.5.3 Cross-correlation flowmeter

A schematic diagram of the flowmeter system is shown in Figure 12.21. This method assumes that some property of the fluid, e.g. density, temperature, velocity or conductivity, is changing in a random manner. This property is detected at two positions A and B on the pipe. The corresponding detector output voltages $x(t)$ and $y(t)$ are random signals. In Section 6.2 we defined the autocorrelation function $R_{yy}(\beta)$ of a single signal $y(t)$, in terms of the average value of the product $y(t) \cdot y(t - \beta)$ of the signal with a time-delayed version $y(t - \beta)$. The cross-correlation function $R_{xy}(\beta)$ between two random signals $x(t), y(t)$ is similarly defined in terms of the mean value $\overline{x(t - \beta) \cdot y(t)}$ of the product $x(t - \beta) \cdot y(t)$ of a delayed version $x(t - \beta)$ of the upstream signal with the undelayed downstream signal $y(t)$. Mathematically we have:

$$R_{xy}(\beta) = \lim_{T \rightarrow \infty} \frac{1}{T} \int_0^T x(t - \beta) \cdot y(t) dt \quad [12.58]$$

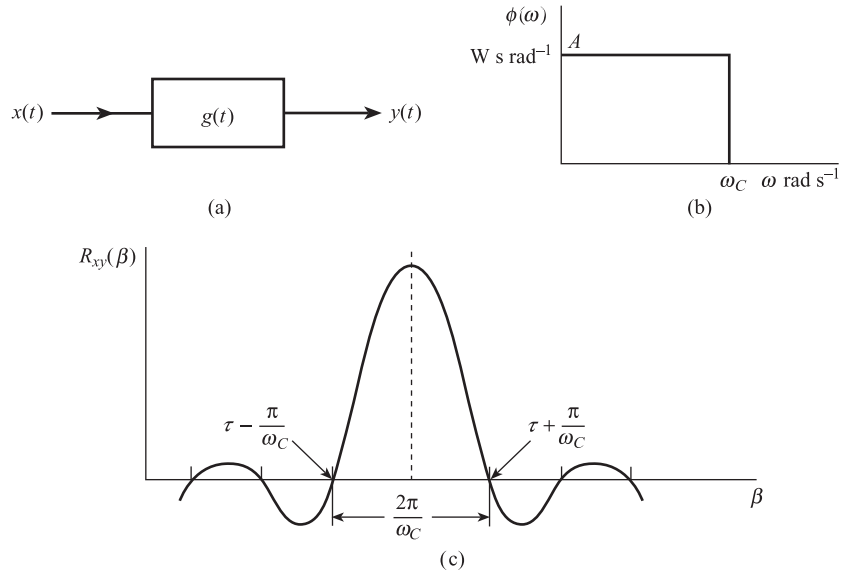
Figure 12.21 Cross-correlation flowmeter – schematic diagrams and typical signals.



where β is the variable time delay and T the observation time. Figure 12.21 shows typical waveforms of $x(t)$, $y(t)$ and the time-delayed version $x(t - \beta)$ for three different time delays β . It can be seen that $x(t - \beta)$ is most similar to $y(t)$ when $\beta = \tau$, the mean transit time between A and B. In other words the cross-correlation function $R_{xy}(\beta)$ has a maximum when $\beta = \tau$. Thus τ can be measured by finding the value of β at which $R_{xy}(\beta)$ is maximum. Since $\tau = L/\bar{v}$, where L is the distance between A and B, the average velocity \bar{v} and volume flow rate Q can then be found.

The above result can be proved more rigorously using random signal analysis. Since $x(t)$ and $y(t)$ are random signals, whose time behaviour is not known explicitly, eqn [12.58] cannot be used for evaluating $R_{xy}(\beta)$. Let us regard the length of pipe between A and B as a system with input $x(t)$, output $y(t)$ and impulse response

Figure 12.22 Theoretical cross-correlation function for flowmeter.



(weighting function) $g(t)$, as indicated in Figure 12.22. We can then express $y(t)$ in terms of $x(t)$ using the convolution integral:

$$y(t) = \int_0^t g(t')x(t-t') dt' \quad [12.59]$$

Using [12.58] and [12.59] it can be shown that:

$$R_{xy}(\beta) = \int_0^\infty g(t') R_{xx}(\beta-t') dt' \quad [12.60]$$

that is, the cross-correlation function can be expressed as a convolution integral involving $g(t)$ and the autocorrelation function R_{xx} . If we assume that the length of pipe can be represented by a pure time delay $\tau = L/\bar{v}$, then the corresponding system impulse response is simply a unit impulse delayed by τ , i.e.

$$g(t') = \delta(t' - \tau) \quad [12.61]$$

This gives:

$$R_{xy}(\beta) = R_{xx}(\beta - \tau) \quad [12.62]$$

so that the cross-correlation function is a time-shifted version of the autocorrelation function. We further assume that the signal $x(t)$ has a power spectral density $\phi(\omega)$ which is constant up to ω_C and zero for higher frequencies:

$$\begin{aligned} \phi(\omega) &= A \quad 0 \leq \omega \leq \omega_C \\ &= 0 \quad \omega > \omega_C \end{aligned} \quad [12.63]$$

The autocorrelation function is the Fourier transform of the power spectral density (Section 6.2.5), i.e.

$$R_{xx}(\beta) = \int_0^\infty \phi(\omega) \cos \omega\beta d\omega \quad [12.64]$$

Thus:

$$R_{xx}(\beta) = A \int_0^{\omega_c} \cos \omega \beta d\omega = A \frac{\sin \omega_c \beta}{\beta} \quad [12.65]$$

and

$$R_{xy}(\beta) = R_{xx}(\beta - \tau) = A \frac{\sin \omega_c(\beta - \tau)}{(\beta - \tau)} \quad [12.66]$$

We see from Figure 12.22(c) that $R_{xy}(\beta)$ has a maximum at $\beta = \tau$ as explained earlier. We note also that for accurate measurement of τ and \bar{v} a sharp maximum is required. This means that τ should be much greater than the width of the peak, i.e. $\tau \gg 2\pi/\omega_c$ or $\tau \gg 1/f_c$.

In many industrial situations, solids in bulk are conveyed through pipes by a gas phase such as air. In these applications it is extremely important to measure the mass flow rate of the solid phase; this depends on both the distribution of the solid material over the pipe cross-section and the mean velocity of the solid phase. Solids velocity can be measured using cross-correlation techniques; capacitance, ultrasonic, optical, radiometric and electrodynamic sensors have been used.^[14] Of these, **electrodynamic** sensors have proved the most useful. Here there is a pair of electrodes, at opposite ends of a pipe diameter, mounted flush with the pipe wall but electrically insulated from it. The electric charge carried on the solid particles induces charges on the electrodes which vary randomly with time. By having two pairs of electrodes and cross-correlating the signals, the solid's velocity can be found.^[15] This technique has been successfully used to measure the mass flow rate of pulverised coal in power stations.^[16]

Conclusion

The chapter first discussed the principles of **fluid mechanics** essential to an understanding of flow measurement. Methods for the measurement of **velocity at a point** in the fluid were then studied. The next section examined systems for the measurement of **volume flow rate** and included **differential pressure**, **mechanical** and **vortex flowmeters**. The following section explained systems for the measurement of **mass flow rate**, including both **inferential** and **direct flowmeters**, the **Coriolis meter** being an important example of the latter. The measurement of flow rate in difficult situations using **electromagnetic**, **ultrasonic** and **cross-correlation flowmeters** was finally discussed.

References

- [1] Bell and Howell Ltd, Electronics and Instruments Division 1981 *Technical Information on Very Low Range Pressure Transmitters*.
- [2] British Standards Institution BS 1042 1981 *Methods of Measurement of Fluid Flow in Closed Conduits – Section 1.1: Orifice Plates, Nozzles and Venturi Tubes in Circular Cross-section Conduits Running Full*.

- [3] International Organization for Standardization ISO 5167 1980 *Measurement of Fluid Flow by Means of Orifice Plate, Nozzles and Venturi Tubes Inserted in Circular Cross-section Conduits Running Full*.
- [4] ZANKER K J and COUSINS T 1975 'The performance and design of vortex meters', *Proc. Int. Conf. on Fluid Flow Measurement in the Mid 1970's*, National Engineering Laboratory, April 1975.
- [5] IGARISHI T 1985 'Fluid flow around a bluff body used for a Karman vortex flowmeter', *Proc. Int. Conf. FLUCOME '85*, Tokyo, 1985.
- [6] BENTLEY J P, BENSON R A and SHANKS A J 1996 'The development of dual bluff body vortex flowmeters', *Flow Measurement and Instrumentation*, vol. 7, no. 2, pp. 85–90.
- [7] BENTLEY J P and MUDD J W 2003 'Vortex shedding mechanisms in single and dual bluff bodies', *Flow Measurement and Instrumentation*, vol. 14, nos 1–2, pp. 23–31.
- [8] BENSON R A and BENTLEY J P 1994 'The optimisation of blockage ratio for optimal multiple bluff body vortex flowmeters', *Proc. Int. Conf. FLUCOME '94*, Toulouse, Sept. 1994.
- [9] Emmerson Process Management 2002 *Rosemount Comprehensive Product Catalogue 2002–2003 edn – Model 8800C Smart Vortex Flowmeter*.
- [10] PLACHE K O 1980 'Measuring mass flow using the Coriolis principle', *Transducer Technology*, vol. 2, no. 3.
- [11] Emmerson Process Management 2002 *Product Data Sheet on Micro Motion ELITE Mass Flow and Density Meters*.
- [12] Flowmetering Instruments Ltd 1985 *Technical Information on D.C. Field Electromagnetic Flowmeters*.
- [13] Emmerson Process Management 2002 *Rosemount Comprehensive Product Catalogue 2002–2003 edn – Series 8700 Magnetic Flowmeter Systems*.
- [14] YAN Y 1996 'Mass flow measurement of bulk solids in pneumatic pipelines', *Meas. Sci. Technol.*, vol. 7, pp. 1687–706.
- [15] YAN Y, BYRNE B, WOODHEAD S and COULTHARD J 1995 'Velocity measurement of pneumatically conveyed solids using electrodynamic sensors', *Meas. Sci. Technol.*, vol. 6, pp. 1–23.
- [16] Department of Trade and Industry 2002 *Project Summary 303 – Pulverised Fuel Measurement with Split Control*.

Problems

12.1

A pitot tube is used to measure the mean velocity of high pressure gas in a 0.15 m diameter pipe. At maximum flow rate the mean pitot differential pressure is 250 Pa. Use the data given below to:

- (a) calculate the mean velocity of the gas at maximum flow rate;
- (b) estimate the maximum mass flow rate;
- (c) estimate the Reynolds number at maximum flow;
- (d) explain why an orifice plate would be suitable to measure the mass flow rate of the gas.
- (e) Given that a differential pressure transmitter of range 0 to 3×10^4 Pa is available, estimate the required diameter of the orifice plate hole (assume coefficient of discharge = 0.6, expansibility factor and velocity of approach factor = 1.0).

Data

Density of gas = 5.0 kg m^{-3}

Viscosity of gas = $5.0 \times 10^{-5} \text{ Pa s}$

- 12.2 An orifice plate is to be used in conjunction with a differential pressure transmitter to measure the flow rate of water in a 0.15 m diameter pipe. The maximum flow rate is $50 \text{ m}^3 \text{ h}^{-1}$, the density of water is 10^3 kg m^{-3} and the viscosity is 10^{-3} Pa s .

- Explain why an orifice plate meter is suitable for this application.
- Estimate** the required orifice plate hole diameter if the transmitter has an input range of 0 to $1.25 \times 10^4 \text{ Pa}$.

- 12.3 A Venturi is to be used to measure the flow rate of water in a pipe of diameter $D = 0.20 \text{ m}$. The maximum flow rate of water is $1.5 \times 10^3 \text{ m}^3 \text{ h}^{-1}$, density is 10^3 kg m^{-3} , and viscosity is 10^{-3} Pa s . Venturis with throat diameters of 0.10 m, 0.14 m and 0.18 m are available from the manufacturer.

- Choose the most suitable Venturi for the application, assuming a differential pressure at maximum flow of approximately $3 \times 10^5 \text{ Pa}$.
- Calculate an accurate value for the differential pressure developed across the chosen Venturi, at maximum flow rate. (Use the following formula for the coefficient of discharge:

$$C = 0.9900 - 0.023 \left(\frac{d}{D} \right)^4 + 0.002 \left(\frac{10^6}{Re_D} \right)$$

where d = Venturi throat diameter, and Re_D = Reynolds number referred to pipe diameter.)

- 12.4 Oxygen at 100°C and 10^6 Pa is flowing down a pipe of diameter $D = 0.20 \text{ m}$. The maximum flow rate of oxygen is $3.6 \times 10^4 \text{ kg h}^{-1}$. It is proposed to measure this flow using an orifice plate in conjunction with a differential pressure transducer of range 0 to $5 \times 10^4 \text{ Pa}$. Using Table 12.1, eqn [12.27], and the data given below:

- explain why an orifice meter is suitable for this application;
- make an initial estimate of the diameter d of the orifice plate hole;
- calculate a more accurate value of hole diameter d , using one iteration only.

Data

Density of oxygen = 10.0 kg m^{-3}

Viscosity of oxygen = $2.40 \times 10^{-5} \text{ Pa s}$

Tappings: corner

Specific heat ratio = 1.4

- 12.5 A turbine flowmeter consists of an assembly of four ferromagnetic blades rotating at an angular velocity $\omega \text{ rad s}^{-1}$ given by:

$$\omega = 4.5 \times 10^4 Q$$

where $Q \text{ m}^3 \text{ s}^{-1}$ is the volume flow rate of the fluid. The total flux N linked by the coil of the magnetic transducer is given by:

$$N = 3.75 + 0.88 \cos 4\theta \text{ milliwebers}$$

where θ is the angle between the blade assembly and the transducer. The range of the flowmeter is 0.15×10^{-3} to $3.15 \times 10^{-3} \text{ m}^3 \text{ s}^{-1}$. Calculate the amplitude and frequency of the transducer output signal at minimum and maximum flows.

- 12.6 A vortex flowmeter consisting of a rectangular bluff body is used to measure liquid flow rates in the range 0.1 to $1.0 \text{ m}^3/\text{s}$. Use the data given below to find the following:

- (a) The range of vortex frequencies.
- (b) The number of cycles that must be collected to achieve a volume repeatability standard deviation of 0.1% (assuming a normal distribution).
- (c) The volume of liquid collected corresponding to (b).

Data

Pipe diameter = 0.15 m

Bluff body width = 0.015 m

Strouhal number = 0.15

Bluffness coefficient = 1.5

Percentage standard deviation for individual cycles = 10%

12.7 A turbine flowmeter has a bore of internal diameter 150 mm. The rotor consists of eight blades, each of mean thickness 5 mm, mounted on a hub of mean diameter 35 mm. The clearance between each blade tip and the bore is 1 mm, and the inlet blade angle at tip is 20° . Estimate the meter factor K in pulses/m³.

12.8 A cross-correlation flowmeter consists of two transducers, spaced 0.15 m apart, detecting random fluctuations in density. The velocity of flow is 1.0 m s^{-1} and the fluctuations contain frequencies up to 100 Hz. State whether the flowmeter is suitable for this application.

12.9 Steam at $P_1 = 20 \times 10^5 \text{ Pa}$ absolute and 250°C is flowing down a circular pipe of diameter $D = 0.150 \text{ m}$. An orifice plate with hole diameter $d = 0.080 \text{ m}$ and corner taps is used to measure the steam flow rate. If the measured differential pressure ΔP is $2.5 \times 10^4 \text{ Pa}$, using the data given below:

- (a) **Estimate** the steam mass flow rate in kg h^{-1} .
- (b) Estimate the value of Reynolds number for the pipe.
- (c) Discuss the nature of the flow and the suitability of the orifice plate flowmeter.
- (d) Calculate an **accurate** value of the steam mass flow rate in kg h^{-1} .

Data

Steam density = 9.0 kg m^{-3}

Steam dynamic viscosity = $1.8 \times 10^{-5} \text{ Pa s}$

Steam specific heat ratio $k = 1.3$

Discharge coefficient

$$C = 0.5959 + 0.0312\beta^2 - 0.184\beta^8$$

Expansibility factor

$$\varepsilon = 1 - (0.41 + 0.35\beta^4) \frac{1}{k} \cdot \frac{\Delta P}{P_1}$$

where $\beta = d/D$.

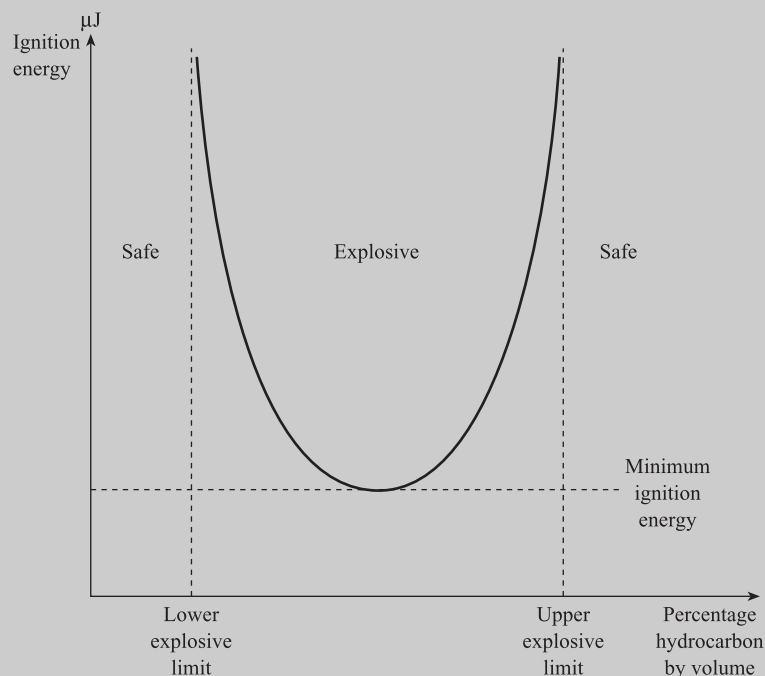
12.10 A Coriolis flowmeter consists of a U tube. The distance between the limbs is 15 cm and the stiffness is 10^3 Nm rad^{-1} . If the range of flow rate is 1.0 to 10.0 kg s^{-1} , what is the corresponding range of time intervals for measuring the angle of twist of the tube?

13 Intrinsically Safe Measurement Systems

Many oil, gas and chemical plants process chemicals which are potentially explosive: common examples are hydrocarbons, i.e. compounds containing carbon and hydrogen. Any small leakage from the plant means that the atmosphere surrounding the plant will be a mixture of hydrocarbon and air; because air contains oxygen, this mixture is potentially explosive or **flammable**.

Under certain conditions, this mixture may be ignited by an electrical spark or a hot surface. Figure 13.1 shows the general relationship between the ignition energy of a hydrocarbon–air mixture and the percentage of hydrocarbon present by volume. We see that a potentially explosive mixture is one where the concentration of hydrocarbon is between the **lower explosive limit (LEL)** and **upper explosive limit (UEL)**. The graph also defines the **minimum ignition energy (MIE)** for a mixture. The values of these parameters are different for different hydrocarbons: hydrogen has LEL = 4%, UEL = 75% and MIE = 19 μJ ; propane has LEL = 2.2%, UEL = 10%

Figure 13.1 Relationship between ignition energy and percentage of hydrocarbon for hydrocarbon–air mixture.



and $MIE = 250 \mu J$. This shows that a hydrogen–air mixture is far easier to ignite than a propane–air mixture. The ignition energy increases asymptotically as the hydrocarbon concentration is reduced towards LEL and as the concentration is increased towards UEL.

There are three separate factors which determine the overall probability of an explosion, which leads to three different types of hazard classification:

1. Probability of explosive gas–air mixture being present: **area classification**.
2. The electrical spark energy required to ignite the mixture: **gas classification**.
3. The surface temperature required to ignite the mixture: **temperature classification**.

The area classification recommended by the **International Electrotechnical Commission** (IEC) and adopted by European countries is based on three zones:

- Zone 0: explosive gas–air mixture is continuously present or present for long periods;
Zone 1: explosive gas–air mixture is likely to occur in normal operation;
Zone 2: explosive gas–air mixture is not likely to occur, and if it occurs, it will exist only for a short time.

The USA and Canada use a system based on two divisions: Division 1 corresponds to Zones 0 and 1; Division 2 corresponds to Zone 2.

Since a gas–air mixture can be ignited by an electrical spark, the **maximum spark energy** under fault conditions must not exceed the **minimum ignition energy** for that mixture. Since all hydrocarbon gases have different MIEs, the IEC recommends a gas classification for equipment based on five representative (test) gases. In order of increasing ease of ignition, these are methane (Group I), propane (Group IIA), ethylene (Group IIB) and hydrogen/acetylene (Group IIC). This classification means, for example, that ethylene–air cannot be ignited by Group IIB equipment since the maximum spark energy, under fault conditions, is less than the minimum ignition energy for that mixture. In the USA and Canada, the four gases propane, ethylene, hydrogen and acetylene are used in the classification, and suitable equipment is designed D, C, B and A respectively.

Since gas–air mixtures can also be ignited directly by hot surfaces, the maximum surface temperature of any equipment located in a given gas–air mixture must not exceed the ignition temperature of the gas. Equipment to be installed in a potentially explosive atmosphere is therefore also classified according to the maximum surface temperature that can be produced under fault conditions. There are six classes of equipment ranging from least safe, T1 (450 °C), through T2 (300 °C), T3 (200 °C), T4 (135 °C) and T5 (100 °C), to the most safe, T6 (85 °C). The user must ensure that the temperature class of the equipment is below the ignition temperature of any gas–air mixture that may arise.

It is therefore imperative that any measurement system which is installed in a potentially explosive gas mixture cannot ignite the gas mixture under any possible fault condition. One possible solution is to use **pneumatic measurement systems** which use compressed air as a signalling medium rather than electrical energy. Since there is no possibility of a spark at all with pneumatic equipment, they are **intrinsically safe**; the principles and characteristics of pneumatic measurement systems are discussed in the first section of this chapter. However, it is more difficult and expensive to interface pneumatic transducers to electronic signal processing and data

presentation elements, so ways of making electrical transducers safe in explosive atmospheres must be found.

One method is to enclose the electrical device in a **flame-proof enclosure** which is capable of withstanding the explosion inside it and so prevent the ignition of the flammable mixture surrounding it. Other methods include pressurising or purging the enclosure with air, filling the enclosure with sand, immersing the equipment in oil, or taking special precautions to ensure that sparks do not occur. However, the most universally acceptable method is to limit the electrical energy produced during any possible fault condition, so that it is below the minimum ignition energy of the gas mixture. This is referred to as **intrinsic safety**. The second section of this chapter looks at **intrinsically safe electronic** measurement systems.

13.1

Pneumatic measurement systems

Pneumatic measurement systems use compressed air as a signalling medium rather than electrical energy. The standard pneumatic signal range is 0.2 to 1.0 bar (1 bar = 10^5 Pa), i.e. 3 to 15 lb wt in⁻² (p.s.i.g.); these pressures are gauge pressures, i.e. pressures relative to atmospheric pressure. Thus a simple pneumatic temperature measurement system consists of a temperature transmitter giving an output of 0.2 to 1.0 bar, corresponding to an input of 0 to 100 °C, connected by copper, nylon or plastic tubing to an indicator. The indicator is a pressure gauge, incorporating a Bourdon tube elastic sensing element, with a scale marked in degrees Celsius; this means there is an indication of 0 °C for 0.2 bar input and 100 °C for 1.0 bar input. The transmitter must be supplied with clean, dry air at 1.4 bar (\approx 20 p.s.i.g.). Pneumatic measurement systems are simple, robust, reliable and easy to maintain and are not affected by electrical interference.

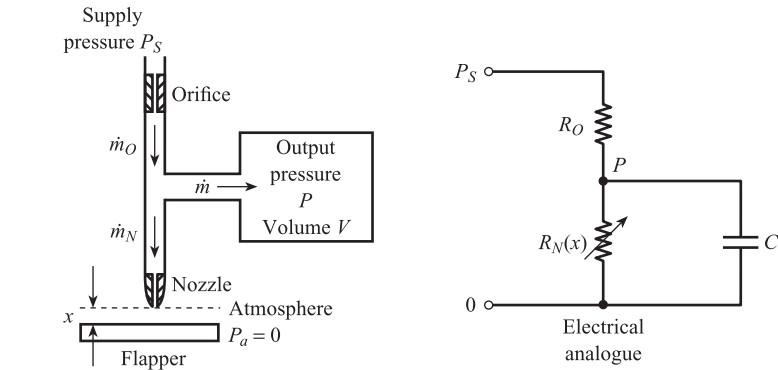
One disadvantage of pneumatic systems is the time delay or lag in transmitting a change in pressure from transmitter to receiver. This delay can be several seconds and increases with tube length so that problems can occur with transmission distances over 150 m. Transmission distances over 300 m are not recommended, unless booster equipment is used. Another disadvantage is the possibility of condensed moisture in the pipework freezing at sub-zero ambient temperatures with open-air installations. Obviously it is more difficult and expensive to interface pneumatic transmitters to digital computers and data loggers than the corresponding electrical devices.

This section begins by studying the characteristics of the flapper/nozzle displacement sensor, discusses the need for and principles of relays, explains the principles of operation and applications of torque balance transmitters, and concludes by discussing pneumatic transmission and data presentation.

13.1.1 Flapper/nozzle displacement sensing element

The flapper/nozzle displacement sensor forms the basis of all pneumatic transmitters. It consists (Figure 13.2) of a fixed restrictor (orifice) in series with a variable restrictor (flapper and nozzle). Altering the separation x of the flapper and nozzle alters the resistance to air flow and the output pressure P : an increase in x causes a reduction in resistance and a fall in pressure. The volume V represents the capacity of the

Figure 13.2 Principle of flapper/nozzle displacement sensor.



Parameters

Molecular weight of air	$w = 29$
Volume	$V = 3.2 \times 10^{-3} \text{ m}^3$ (100 m of 1/4 inch (6.4 mm) OD tubing)
Ideal gas constant	$R = 8.314 \text{ J K}^{-1} \text{ mol}^{-1}$
Absolute ambient temperature	$\theta = 293 \text{ K}$
Coefficient of discharge	$C_D = 0.6$
Density of air	$\rho = 1.0 \text{ kg m}^{-3}$
Diameter of orifice	$d_O = 2 \times 10^{-4} \text{ m}$
Diameter of nozzle	$d_N = 8 \times 10^{-4} \text{ m}$
Supply pressure	$P_S = 1.4 \times 10^5 \text{ Pa (gauge)}$
Atmospheric pressure	$P_a = 0 \text{ (gauge)}$

transmission line connecting the sensor to an indicator. The equivalent electrical circuit (Figure 13.2) is a potentiometer consisting of a fixed resistor in series with a variable resistor and a capacitive load across the variable resistor.

The relevant equations are:

$$\dot{m} = \dot{m}_O - \dot{m}_N \quad [13.1]$$

$$\dot{m} = \frac{wV}{1000R\theta} \frac{dP}{dt} \quad [13.2]$$

$$\dot{m}_O = C_D \frac{\pi}{4} d_O^2 \sqrt{2\rho(P_S - P)} \quad [13.3]$$

$$\dot{m}_N = C_D \pi d_N x \sqrt{2\rho(P - P_a)} \quad [13.4]$$

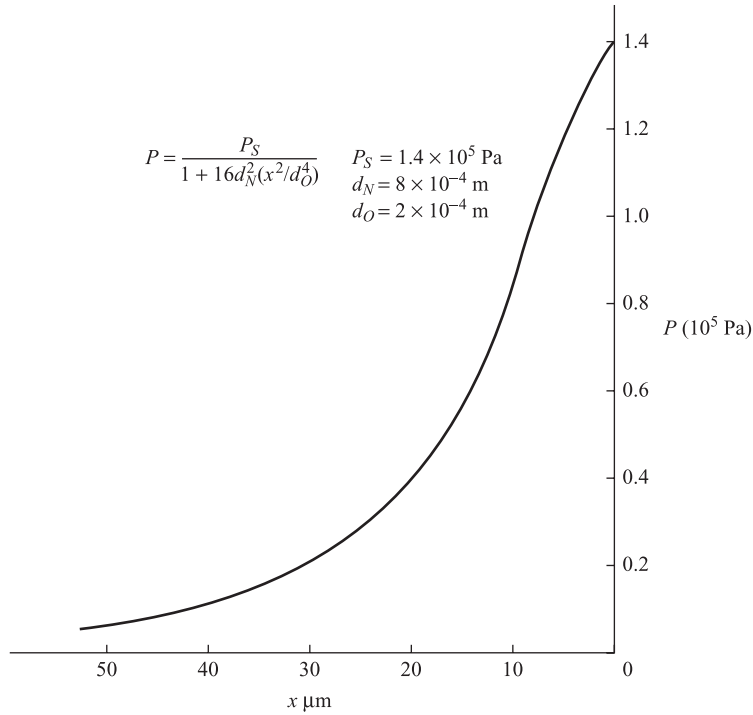
Figure 13.2 also explains the meaning and gives typical values of the element parameters. Equation [13.2] is based on the ideal gas law $PV = nR\theta$ for n moles of an ideal gas occupying volume V at absolute temperature θ . Since $n = (\text{mass in g/molecular weight}) = (\text{mass in kg} \times 10^3/\text{molecular weight}) = (1000 m/w)$, then

$$\text{mass } m = (wV/1000R\theta)P$$

$$\text{mass flow rate } \dot{m} = (wV/1000R\theta)(dP/dt)$$

Equations [13.3] and [13.4] giving the mass flow rate of air through orifice and nozzle are based on eqn [12.28]. The velocity of approach factor E and expansibility factor ϵ are both assumed to be unity. The area of the orifice hole is $\pi d_O^2/4$ and the effective area of the nozzle is assumed to be the surface area of a cylinder of diameter d_N and length x . This assumption is true only for small displacements x .

Figure 13.3 Steady-state characteristics of flapper–nozzle displacement sensor.



In the steady state dP/dt and \dot{m} are zero, so that $\dot{m}_O = \dot{m}_N$, i.e.

$$(d_O^2/4)\sqrt{P_s - P} = d_N x \sqrt{P} \quad [13.5]$$

since $P_a = 0$. This gives:

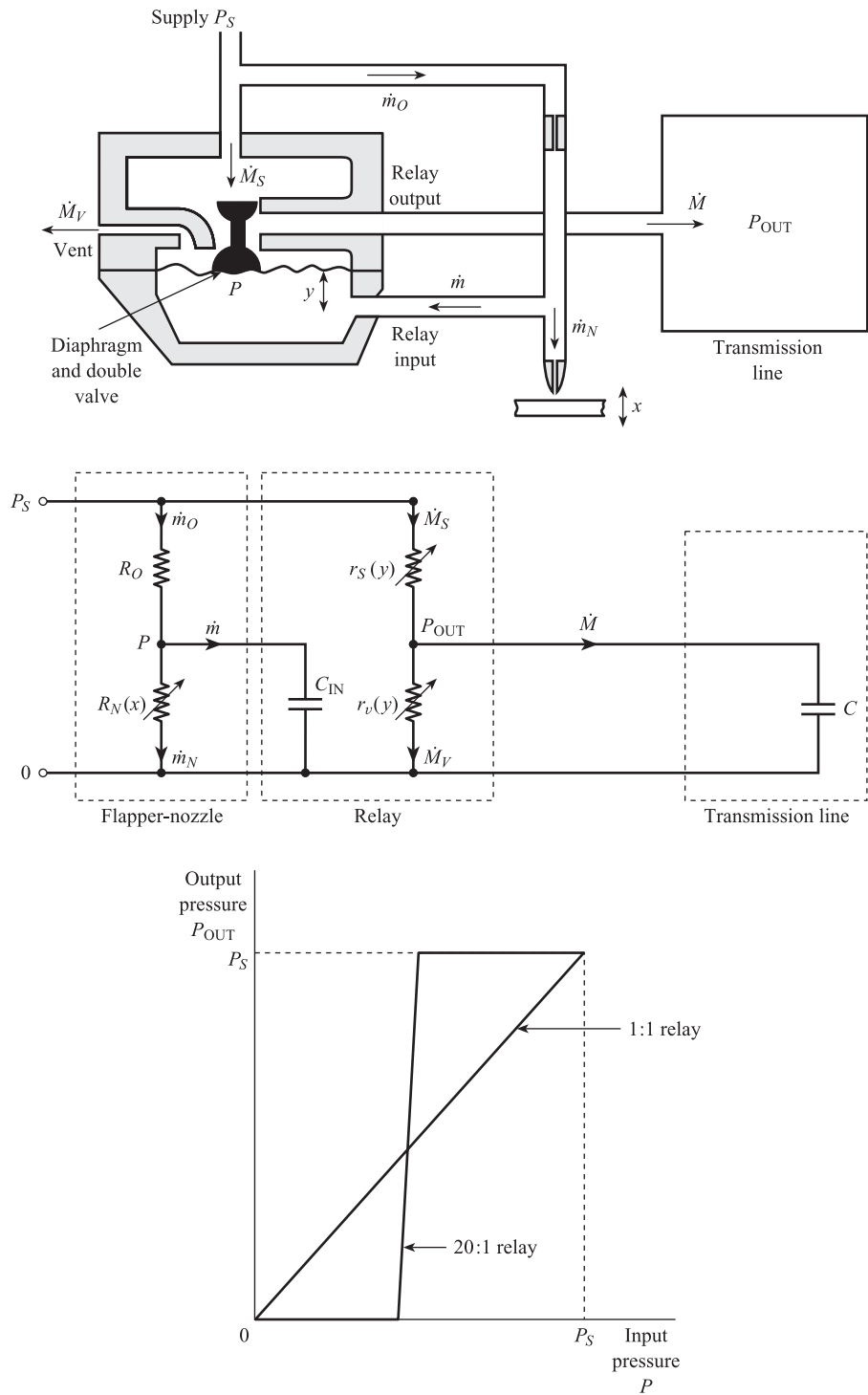
Steady-state relation between pressure and displacement for flapper/nozzle

$$P = \frac{P_s}{1 + 16(d_N^2 x^2 / d_O^4)} \quad [13.6]$$

This relationship is plotted in Figure 13.3; we see that it is characterised by non-linearity and very high sensitivity – typically $dP/dx \approx -5 \times 10^9 \text{ Pa m}^{-1}$. Because of these characteristics the flapper/nozzle itself is unsuitable for use as a sensing element in a measurement system. It is usually incorporated into a closed-loop torque-balance transmitter where it detects small movements due to any imbalance of torques.

The relation between dynamic changes in input displacement and output pressure can be approximately described by a first-order transfer function. The corresponding time constant τ is extremely long, typically several minutes. This is because the orifice and nozzle diameters are very small so that they present a high resistance to flow. If x decreases, air must be brought in via the orifice to increase P ; the mass flow rate \dot{m}_O and rate of increase in pressure dP/dt are small. Similarly if x increases, air must be vented via the nozzle to decrease P ; the mass flow rate \dot{m}_N and rate of decrease in pressure are small. This means that the flapper/nozzle sensor cannot be connected directly onto a pneumatic transmission line, but only via a device which gives increased air flows and therefore a reduced time constant.

Figure 13.4 Relay, equivalent circuit and steady-state characteristics.



13.1.2 Principle of relay amplifier

Figure 13.4 shows a relay amplifier connecting a flapper/nozzle to a transmission line. The nozzle back-pressure P is the input to the relay and the transmission line is connected to the relay output. Air can now flow from supply to the transmission line via the double valve. This is a low-resistance path which bypasses the orifice and allows a high flow rate of air into the line. There is also a low-resistance path, again via the double valve, connecting the transmission line to a vent port. This bypasses the nozzle and allows a high flow rate of air out of the line when the line is being depressured. A change in nozzle back-pressure P causes the centre of the diaphragm and the double valve to move; this adjusts the relative values of supply flow \dot{M}_S and vent flow \dot{M}_V , thus changing the relay output pressure P_{OUT} . For example if P increases, the diaphragm and double valve move upwards; this reduces \dot{M}_V but increases \dot{M}_S and the net flow \dot{M} into the line. The output pressure P_{OUT} rises until equilibrium is re-established.

Figure 13.4 also shows an approximate electrical equivalent circuit for the flapper/nozzle, relay and transmission line. The input capacitance C_{IN} of the relay is small and corresponds to the volume of the input chamber below the diaphragm. The resistances r_S and r_V of the supply and vent paths are small compared with the resistances R_O and R_N of orifice and nozzle. The supply and vent flows \dot{M}_S and \dot{M}_V are therefore large compared to the corresponding orifice and nozzle flows \dot{m}_O and \dot{m}_N . The resistances r_S and r_V are variable and depend on the displacement y of the diaphragm and double valve. The pressure underneath the diaphragm is the nozzle back-pressure P ; the pressure above the diaphragm is atmospheric, i.e. a gauge pressure of zero. The resultant deflecting force on the diaphragm is $A_{RD}P$ newtons, where A_{RD} is the area of the diaphragm. If $k \text{ N m}^{-1}$ is the effective stiffness of the diaphragm, then the spring restoring force is ky newtons, so that at equilibrium:

$$A_{RD}P = ky \quad \text{and} \quad y = \frac{A_{RD}}{k} P \quad [13.7]$$

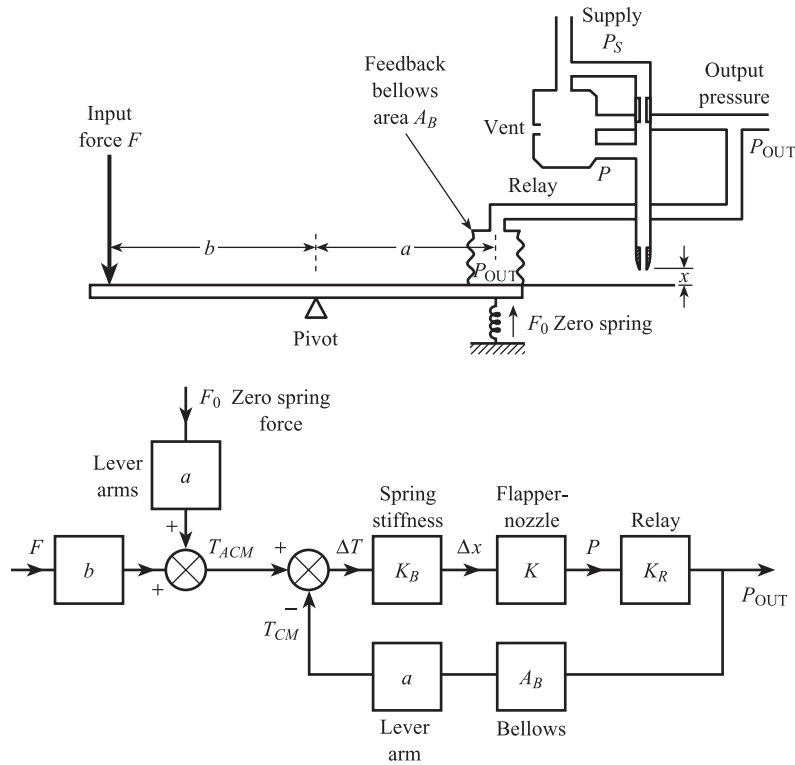
i.e. y is proportional to P .

The relationships between r_S , r_V and y will depend on the shape of the double valve and will in general be non-linear. An increase in P and y causes an increase in r_V , a decrease in r_S , and increase in P_{OUT} . In the steady state, when $dP_{OUT}/dt = \dot{M} = 0$, the output pressure is determined by the potentiometer r_S , r_V . The value of P_{OUT} can be calculated by a detailed analysis based on equations similar to [13.5]. By careful design it is possible to produce an overall linear relationship between P_{OUT} and P . The steady-state sensitivity $K_R = \Delta P_{OUT}/\Delta P$ of relays in common use usually varies from unity up to 20 (Figure 13.4). A typical relay has a steady-state air consumption $\dot{M}_S = \dot{M}_V$ of around 1 kg h^{-1} . These higher air flows mean that the time constant $(r_S + r_V)C$ describing dynamic pressure variations is now only a few seconds.

13.1.3 Torque-balance transmitters

Figure 13.5 shows a flapper/nozzle and relay incorporated into a basic torque-balance transmitter. The transmitter is a closed-loop, negative feedback device and gives a pneumatic output signal, in the standard range, proportional to an input force F . An increase in F increases the anticlockwise moment on the beam, causing it to rotate in an anticlockwise direction. This reduces the flapper/nozzle separation x ,

Figure 13.5 Schematic and block diagrams of basic torque balance transmitter.



causing an increase in nozzle back-pressure P and relay output pressure P_{OUT} . This increase in pressure is fed to the transmission line – but also to the feedback bellows, causing an increase in the feedback force $A_B P_{OUT}$. This gives an increased clockwise moment to oppose the increased anticlockwise moment due to F . The beam will rotate and the output pressure will change until clockwise and anticlockwise moments are again equal. The flapper/nozzle and relay detect small rotations of the beam due to any imbalance of torques.

From Figure 13.5 we have:

$$\text{Anticlockwise moments} \quad T_{ACM} = Fb + F_0a$$

$$\text{Clockwise moment} \quad T_{CM} = P_{OUT}A_Ba$$

Assuming perfect torque balance we have:

$$P_{OUT}A_Ba = Fb + F_0a$$

i.e.

*Simple model for
basic torque-balance
transmitter*

$$P_{OUT} = \frac{b}{aA_B}F + \frac{F_0}{A_B} \quad [13.8]$$

Thus the output pressure is proportional to the input force. According to this simple theory, the sensitivity of the transmitter is $b/(aA_B)$; i.e. sensitivity depends only on

the lever arm ratio b/a and feedback bellows area A_B . Thus sensitivity is independent of flapper/nozzle, relay characteristics and supply pressure. A transmitter with $b/a = 1$, $A_B = 5 \times 10^{-4} \text{ m}^2$ (circular bellows approximately 2.5 cm in diameter), and zero spring force $F_0 = 10 \text{ N}$ will give an output pressure between 0.2 and 1.0 bar for an input force between 0 and 40 N. Adjusting the position of the pivot alters the ratio b/a and the sensitivity of the transmitter. This means that it is possible to adjust the input range of the transmitter while maintaining an output range of 0.2 to 1.0 bar. Thus the input range of the above transmitter can be changed from 0 to 40 N, down to 0 to 4 N, by increasing the b/a ratio from 1 to 10.

The above theory assumes that there is perfect torque balance; this is obviously an oversimplification. Figure 13.5 shows a block diagram of the system; this allows for a difference ΔT between clockwise and anticlockwise moments. K_B is the stiffness of the beam/spring arrangement, i.e. the change in flapper/nozzle separation x for unit change in torque. K is the sensitivity of the flapper/nozzle at the prevailing operating conditions, and K_R is the relay sensitivity. Using Figure 13.5 we have:

$$\left. \begin{aligned} T_{\text{ACM}} &= bF + aF_0 \\ T_{\text{CM}} &= aA_B P_{\text{OUT}} \\ \Delta T &= T_{\text{ACM}} - T_{\text{CM}} \\ P_{\text{OUT}} &= K_B K K_R \Delta T \end{aligned} \right\} \quad [13.9]$$

giving:

*Accurate model for
torque-balance
transmitter*

$$P_{\text{OUT}} = \frac{K_B K K_R}{1 + K_B K K_R a A_B} (bF + aF_0) \quad [13.10]$$

In this more accurate model the output pressure depends on the flapper/nozzle sensitivity K and therefore on the supply pressure P_S (eqn [13.6]). Typical values are:

$$K_B = 6 \times 10^{-5} \text{ m/Nm}^{-1}$$

$$K = 5 \times 10^9 \text{ Pa m}^{-1}$$

$$K_R = 20$$

$$a = b = 5 \times 10^{-2} \text{ m}$$

$$A_B = 5 \times 10^{-4} \text{ m}^2$$

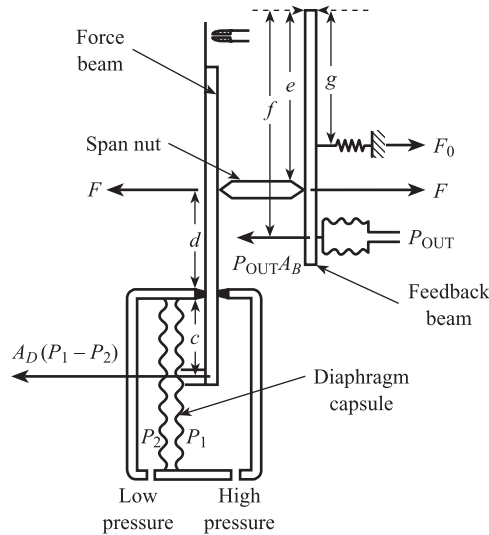
$$F_0 = 10 \text{ N}$$

$$K_B K K_R a A_B = 150$$

Since $K_B K K_R a A_B$ is large compared with 1, the effect of supply pressure variations is small: typically an increase in supply pressure of 10^4 Pa (1.5 p.s.i.) causes an increase in output pressure of only 0.2%.

This characteristic is important in large pneumatic installations, where variations in compressor delivery pressure and load changes can cause fluctuations in supply pressure of up to $\pm 0.2 \text{ bar}$ ($\pm 3 \text{ p.s.i.}$). The torque balance transmitter is an example of the use of high-gain negative feedback in reducing non-linearity and modifying input effects (Section 3.3).

Figure 13.6 Principle of pneumatic D/P transmitter.



A common example of the torque/balance principle is the pneumatic differential pressure (D/P) transmitter; this is shown in simplified schematic form in Figure 13.6. It consists of two levers, the force beam and the feedback beam (or span lever). The resultant force on the diaphragm capsule is $A_D(P_1 - P_2)$, where $P_1 - P_2$ is the differential pressure and A_D is the cross-sectional area of the capsule. This produces a clockwise moment $A_D(P_1 - P_2)c$ on the force beam, which is opposed by the anticlockwise moment Fd due to the action of the span nut on the force beam. Thus at equilibrium:

$$\text{Force beam: } A_D(P_1 - P_2)c = Fd \quad [13.11]$$

The span nut also produces an anticlockwise moment Fe on the feedback beam, which is supported by anticlockwise moment F_0g , due to the zero spring force. These are opposed by the clockwise moment $P_{OUT}A_Bf$ due to the output pressure acting on the feedback bellows. Thus at equilibrium:

$$\text{Feedback beam: } Fe + F_0g = P_{OUT}A_Bf \quad [13.12]$$

Eliminating F between [13.11] and [13.12] gives:

Simple model for pneumatic differential pressure transmitter

$$P_{OUT} = \frac{A_D}{A_B} \frac{c}{f} \frac{e}{d} (P_1 - P_2) + \frac{g}{f} \frac{F_0}{A_B} \quad [13.13]$$

i.e.

$$\text{Sensitivity} = \frac{A_D}{A_B} \frac{c}{f} \frac{e}{d} \quad \text{and} \quad \text{zero pressure} = \frac{g}{f} \frac{F_0}{A_B}$$

Therefore adjusting the position of the span nut alters the ratio e/d and the sensitivity. This means that for an output range of 0.2 to 1.0 bar, the input range of a typical transmitter can be adjusted from 0 to 1 m of water (maximum sensitivity, span

nut at bottom), to 0 to 10 m of water (minimum sensitivity, span nut at top). The zero spring force F_0 is adjusted to obtain a zero pressure of 0.2 bar. Equation [13.13] can be corrected to take imperfect torque balance into account.

The pneumatic differential pressure transmitter has a similar torque/balance principle to the closed-loop electronic current transmitter discussed in Section 9.4.1.

The applications of the pneumatic transmitter are similar to those of current transmitters detailed in Section 9.4.2.

13.1.4 Pneumatic transmission and data presentation

In Sections 13.1.1 and 13.1.2 we represented the transmission line connecting transmitter and receiver as a single fluidic capacitance $C = wV/R\theta$. This is a considerable oversimplification, because the transmission line has both fluidic resistance and fluidic inductance (fluid analogue of electrical inductance). The resistance is due to fluid friction, and the inductance is due to the mass of the air in the pipe. Moreover the transmission line cannot adequately be represented by a single fluidic $L-C-R$ circuit. This is because the inductance, capacitance and resistance are distributed along the transmission line and therefore cannot be 'lumped' together into single values.^[1]

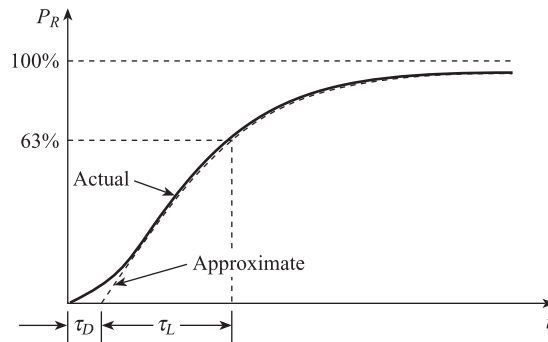
Figure 13.7 shows the response of transmission line output pressure to a step increase in input pressure. The response is the S-shaped curve characteristic of elements or systems with multiple transfer lags. The diagram shows the response approximated by a pure time delay of length τ_D , together with a single first-order transfer lag of time constant τ_L . The corresponding approximate transfer function for the transmission line is:

$$\frac{\Delta P_R}{\Delta P_{OUT}} = \frac{e^{-\tau_D S}}{1 + \tau_L S} \quad [13.14]$$

Both τ_D and τ_L increase with the length of the transmission line, but the ratio between the two times is constant: $\tau_D/\tau_L \approx 0.24$.^[2] Thus for piping of 6 mm outside diameter, a 150 m line has $\tau_D = 0.77$ s, $\tau_L = 3.2$ s; a 300 m line has $\tau_D = 2.3$ s, $\tau_L = 9.7$ s; and a 600 m line has $\tau_D = 7.4$ s, $\tau_L = 31$ s.

A pressure gauge consisting of a C-shaped Bourdon tube elastic element (Figure 8.21) linked mechanically to a pointer moving over a scale is commonly used as a data presentation element in pneumatic measurement systems.

Figure 13.7
Equivalent network
and step response
for pneumatic
transmission line.



13.2 Intrinsically safe electronic systems

13.2.1 The Zener barrier

In intrinsically safe electronic systems **Zener barrier devices** are used to limit the amount of electrical energy produced in the hazardous area under any possible fault condition. Figure 13.8 shows a basic Zener barrier circuit which will be located in a safe area such as a control room. A signal conditioning, processing or data presentation element such as an amplifier, computer or recorder will be connected across terminals 1 and 2. Terminals 3 and 4 will be connected via a cable to a sensor, transducer or transmitter located in the hazardous area.

The barrier is designed so that if, under fault conditions, a high voltage up to 250 V r.m.s. is applied across terminals 1 and 2 then the resulting electrical energy in the hazardous area is limited to less than the minimum ignition energy of the mixture. The fuse F of resistance R_F is present to protect the Zener diodes D_1 and D_2 . The surge current rating of the fuse is significantly less than the surge current rating of the diodes, so that if the fault current is increasing rapidly, F blows before either D_1 or D_2 burns out. D_1 provides a safe path to earth for the a.c. fault current; the corresponding r.m.s. voltage across D_1 is limited to the Zener **breakdown** or **avalanche voltage** V_z of the diode. A second diode D_2 is connected in parallel with D_1 for increased reliability, so that even if D_1 fails, the r.m.s. voltage across D_2 , and therefore across terminals 3 and 4, is again limited to V_z . The resistor R_2 limits the fault current in the external hazardous area circuit to a maximum value of V_z/R_2 . Thus under the above fault condition, the Zener barrier can be regarded as a Thévenin voltage source of V_z with series resistance R_2 across terminals 3 and 4. V_z and R_2 are the most important parameters in the barrier specification. The resistance R_1 between the diodes allows both diodes to be tested separately.

In normal operation D_1 and D_2 do not conduct and the barrier has a total or 'end-to-end' resistance of $R_F + R_1 + R_2$ together with the inherent capacitance of the Zener diodes. Provided that the usual conditions for maximum voltage transfer in a Thévenin signal circuit (Section 5.1.1) or maximum current transfer in a Norton

Figure 13.8 Basic Zener barrier circuit.

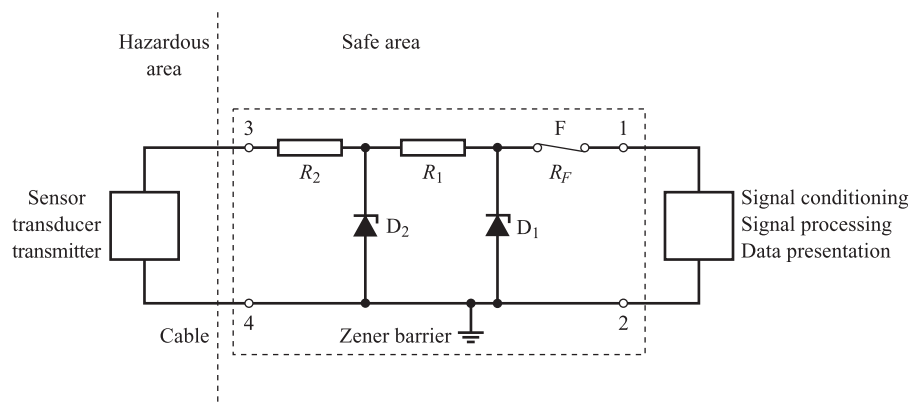
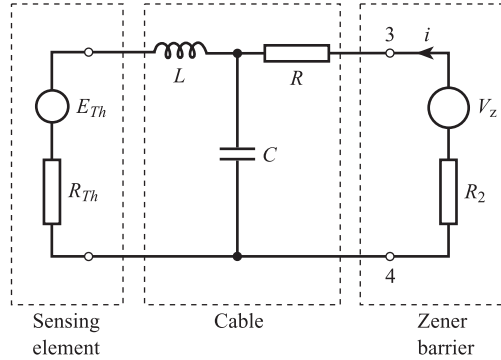


Figure 13.9 Equivalent circuit of Zener barrier fault conditions.



signal circuit (Section 5.1.3) are obeyed, the barrier will introduce no error into the measurement system.

13.2.2 Energy storage calculation for fault conditions

The cable which connects terminals 3 and 4 of the Zener barrier to the sensor, transducer or transmitter in the hazardous area will have inductance and capacitance as well as resistance. Figure 13.9 shows a simplified approximate equivalent circuit for the cable using single lumped values L , C and R ; in practice inductance, capacitance and resistance are distributed along the entire length of the cable. The diagram also shows the sensing element represented by a Thévenin equivalent circuit E_{Th} , R_{Th} (a Norton equivalent circuit i_N , R_N is also possible) and the Zener barrier under fault conditions as a Thévenin equivalent circuit V_z , R_2 . The energy stored in the cable capacitance C therefore has a maximum value of $\frac{1}{2}CV_z^2$. The energy stored in the cable inductance L is $\frac{1}{2}Li^2$, where $i = V_z/R_2$, the maximum current that can flow in the circuit. The maximum total stored energy in the circuit is therefore:

Maximum stored energy in circuit

$$E_{MAX} = \frac{1}{2}CV_z^2 + \frac{1}{2}L(V_z/R_2)^2 \quad [13.15]$$

Since E_{MAX} is the maximum energy available to create a spark, it must be less than the minimum ignition energy (MIE) for the gas–air mixture.

Consider the example of the chromel–alumel thermocouple used in a hydrogen–air atmosphere with a MTL 160 barrier.^[3] The barrier has $V_z = 10$ V, $R_2 = 50$ Ω . The maximum permissible cable capacitance and inductance for safe operation with hydrogen (group IIC) are 4 μ F and 1.2 mH. The actual cable used is 100 m of standard chromel–alumel extension lead with $R = 28$ Ω , $C = 1.85$ nF and $L = 60$ μ H. This gives

$$\begin{aligned} E_{MAX} &= \frac{1}{2} \times 1.85 \times 10^{-9} \times 10^2 + \frac{1}{2} \times 60 \times 10^{-6} (10/50)^2 \text{ J} \\ &= 1.3 \text{ } \mu\text{J} \end{aligned}$$

This is well below 19 μ J, the minimum ignition energy for hydrogen–air, so the system is safe to use in this application.

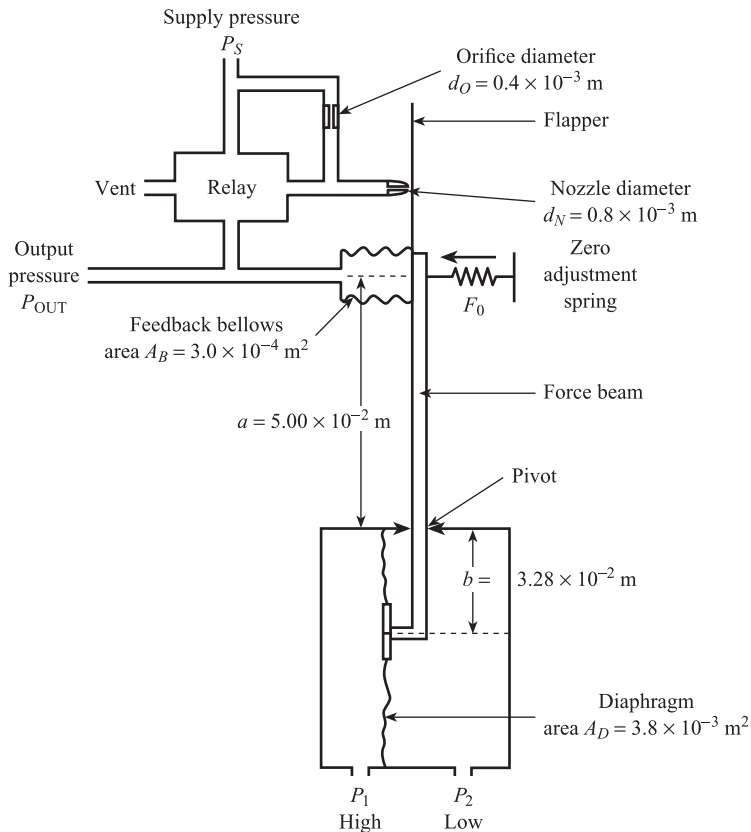
Conclusion

The chapter began by explaining that the atmosphere surrounding certain plants and processes may be potentially explosive, a common example being hydrocarbon–air mixtures. It then went on to define three types of **hazard classification: area, gas and temperature**. Equipment can then be classified according to the hazardous environment in which it can be safely used. The chapter then described two types of measurement systems which are **intrinsically safe**, i.e. cannot ignite the explosive mixture. The first are **pneumatic measurement systems** where there is no possibility of a spark. The second are **intrinsically safe electronic systems** where **Zener barriers** are used to limit the electrical energy available under fault conditions to a safe value.

References

- [1] ROHMANN C P and GROGAN E C 1956 'On the dynamics of pneumatic transmission lines', *Transactions of the A.S.M.E.*, Cleveland, Ohio, p. 866.

Figure Prob. 1.



- [2] SCHINSKEY F G 1979 *Process Control Systems*, 2nd edition, pp. 38–9. McGraw-Hill, New York.
- [3] Measurement Technology Ltd 1991 *Making the World Intrinsically Safe*. Technical Publication.

Problems

13.1 Figure Prob. 1 shows a pneumatic, torque/balance transmitter to be used for measuring differential pressures in the range 0 to 10^4 Pa.

- Draw a labelled block diagram of the transmitter.
- Using the data given, calculate the range of the transmitter output signal:
 - when the supply pressure P_s is 1.40 bar,
 - when the supply pressure P_s is 1.75 bar.

Comment briefly on the practical significance of these results.

Data

Zero spring force	$F_0 = 6.24 \text{ N}$
Flapper/nozzle sensitivity	$K = \frac{2.0d_N P_s}{d_o^2} \text{ Pa m}^{-1}$
Displacement of flapper for unit torque	$K_B = 6.0 \times 10^{-5} \text{ m (Nm)}^{-1}$
Relay pressure gain	$K_R = 20.0 \text{ Pa}^{-1}$

13.2 A Zener barrier for use with a platinum resistance sensor has $V_z = 5 \text{ V}$, $R_z = 10 \Omega$. The two-conductor cable connecting the sensor to the barrier has a capacitance of $0.05 \mu\text{F}$ and an inductance of 0.01 mH . Is this system safe to use with hydrogen–air atmosphere with a minimum ignition energy of $19 \mu\text{J}$?

14 Heat Transfer Effects in Measurement Systems

14.1 Introduction

The temperature of a sensing element at any instant of time depends on the rate of transfer of heat both to and from the sensor. Heat transfer takes place as a result of one or more of three possible types of mechanism – **conduction**, **convection** and **radiation**. Conduction is the main heat transfer mechanism inside solids. A solid may be regarded as a chain of interconnected atoms, each vibrating about a fixed position. An increase in temperature at one end of a solid bar causes an increase in the vibrational energy and amplitude of the atoms at that end of the chain. This energy increase is transmitted from one atom to the next along the chain, so that ultimately the temperature increase is transmitted to the other end of the bar. This chapter is concerned with **heat transfer** between a sensing element and the fluid in which it is situated. In this situation the main heat transfer mechanism is convection. Here heat is transferred to and from the sensor by the random, highly disordered motion of molecules of fluid past the sensor. This random motion and corresponding heat transfer occur even when the average velocity of the bulk fluid past the sensor is zero. This is known as **natural convection**. If the bulk fluid is made to move so that the average velocity past the sensor is no longer zero, then there is a corresponding increase in rate of heat transfer. This is referred to as **forced convection**. Heat transfer by means of radiation involves the transmission of electromagnetic waves and will be discussed in Chapter 15.

From Newton's law of cooling the convective heat flow W watts between a sensor at T °C and fluid at T_F °C is given by:

$$W = UA(T - T_F) \quad [14.1]$$

where U W m⁻² °C⁻¹ is the convection heat transfer coefficient and A m² is the heat transfer area. Heat transfer coefficients are calculated using the correlation:

$$Nu = \phi(Re, Pr) \quad [14.2]$$

between the three dimensionless numbers:

$$\begin{aligned}\text{Nusselt} \quad Nu &= \frac{Ud}{k} \\ \text{Reynolds} \quad Re &= \frac{\nu d \rho}{\eta} \\ \text{Prandtl} \quad Pr &= \frac{c \eta}{k}\end{aligned}\quad [14.3]$$

where:

$$\begin{aligned}d \text{ m} &= \text{sensor diameter} \\ \nu \text{ m s}^{-1} &= \text{fluid velocity} \\ \rho \text{ kg m}^{-3} &= \text{fluid density} \\ \eta \text{ Pa s} &= \text{fluid viscosity} \\ c \text{ J }^{\circ}\text{C}^{-1} &= \text{fluid heat capacity} \\ k \text{ W m}^{-1} ^{\circ}\text{C}^{-1} &= \text{fluid thermal conductivity}\end{aligned}$$

The function ϕ is determined experimentally; its form depends on the shape of the sensor, the type of convection and the direction of fluid flow in relation to the sensor. For example, a correlation for forced convection cross-flow over a cylinder is:

$$Nu = 0.48(Re)^{0.5}(Pr)^{0.3} \quad [14.4]$$

From [14.3] and [14.4] we have:

$$U = 0.48 \frac{k^{0.7} \rho^{0.5} c^{0.3} \nu^{0.5}}{d^{0.5} \eta^{0.2}} \quad [14.5]$$

For two-dimensional, natural and forced convection from a cylinder, the approximate correlation is^[1,2]

$$Nu = 0.24 + 0.56Re^{0.5} \quad [14.6]$$

giving

$$U = \frac{0.24k}{d} + 0.56k \left(\frac{\rho \nu}{d \eta} \right)^{0.5} \quad [14.7]$$

From [14.5] and [14.7] we see that the convection heat transfer coefficient for a given sensor depends critically on the physical properties and velocity of the surrounding fluid.

The following three sections of this chapter explain how convective heat transfer has three important applications in measurement systems. These are:

- (a) in understanding and calculating the dynamic characteristics of thermal sensors;
- (b) in hot wire and film systems for fluid velocity measurements;
- (c) in the katharometer for gas thermal conductivity and composition measurement.

Table 14.1.

Fluid conditions	Typical U_{FW} $W m^{-2} ^\circ C^{-1}$	Typical τ for sensor in thermowell (min)	Typical τ for mineral insulated thermocouple (s)
Fast liquid	625	1.0	0.7
Slow liquid	250	1.5	1.5
Fast gas	125	2	10
Medium gas	63	4	20
Slow gas	25	8	30

14.2

Dynamic characteristics of thermal sensors

14.2.1 Bare temperature sensor

The transfer function for a bare (unenclosed) temperature sensor has already been found to be (Section 4.1):

*Transfer function for
bare temperature
sensor*

$$\frac{\Delta \bar{T}_S(s)}{\Delta \bar{T}_F(s)} = \frac{1}{1 + \tau_s s} \quad [14.10a]$$

where $\Delta T_S, \Delta T_F$ $^\circ C$ = deviations in sensor and fluid temperatures from equilibrium

τ_s = sensor time constant = MC/UA

M kg = sensor mass

C $J kg^{-1} ^\circ C^{-1}$ = sensor specific heat

U $W m^{-2} ^\circ C^{-1}$ = convection heat transfer coefficient between fluid and sensor

A m^2 = sensor heat transfer area

Since τ_s depends on U , the time constant of a given sensor will depend critically on the nature and velocity of the fluid surrounding the sensor (see Table 14.1).

14.2.2 Temperature sensor enclosed in a thermowell or sheath

A temperature sensor such as a thermocouple or resistance thermometer is usually enclosed in a sheath or thermowell to give chemical and mechanical protection. Figure 14.1(a) shows a typical thermocouple installation and Figure 14.1(b) is a simplified model where sensor and thermowell are represented by single ‘lumped’ masses M_S and M_W respectively.

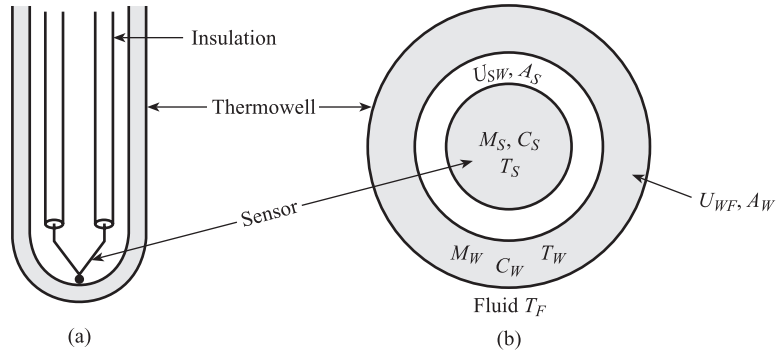
Ignoring the thermal capacity of the space between sensor and well, the heat balance equations are:

$$\text{Sensor: } M_S C_S \frac{dT_S}{dt} = U_{SW} A_S (T_W - T_S) \quad [14.8]$$

$$\text{Well: } M_W C_W \frac{dT_W}{dt} = -U_{SW} A_S (T_W - T_S) + U_{WF} A_W (T_F - T_W) \quad [14.9]$$

Figure 14.1 Sensor in thermowell:

(a) Typical thermowell installation
(b) Simplified model.



which become

$$\tau_1 \frac{dT_S}{dt} = T_W - T_S \quad [14.10]$$

$$\tau_2 \frac{dT_W}{dt} = -\delta(T_W - T_S) + (T_F - T_W) \quad [14.11]$$

$$\text{where } \tau_1 = \frac{M_S C_S}{U_{SW} A_S}, \quad \tau_2 = \frac{M_W C_W}{U_{WF} A_W}, \quad \delta = \frac{U_{SW} A_S}{U_{WF} A_W} \quad [14.12]$$

and

A_S, A_W = sensor/thermowell heat transfer areas

C_S, C_W = sensor/thermowell specific heats

U_{SW} = sensor/thermowell heat transfer coefficient

U_{WF} = fluid/thermowell heat transfer coefficient

Defining ΔT_F , ΔT_W and ΔT_S to be deviations from initial steady conditions, the Laplace transforms of [14.10] and [14.11] are:

$$[1 + \tau_1 s] \Delta \bar{T}_S = \Delta \bar{T}_W \quad [14.13]$$

$$[(1 + \delta) + \tau_2 s] \Delta \bar{T}_W = \Delta \bar{T}_F + \delta \Delta \bar{T}_S \quad [14.14]$$

Eliminating \bar{T}_W between these equations gives the overall transfer function:

*Transfer function for
temperature sensor
in sheath*

$$\frac{\Delta \bar{T}_S}{\Delta \bar{T}_F}(s) = \frac{1}{\tau_1 \tau_2 s^2 + (\tau_1 + \tau_2 + \delta \tau_1) s + 1} \quad [14.15]$$

This is a second-order model and is a good representation of an incorrect installation where the tip of the sensing element does not touch the sheath. The effective heat transfer coefficient U_{SW} between sensor and well is now very small; this means that τ_1 is very large and the system response extremely sluggish. A correct normal installation with the sensor tip touching the sheath has a far higher U_{SW} and lower τ_1 . In the limit of perfect heat transfer between sensor and well, both elements are at the same temperature T_S and the heat balance equation is now:

$$(M_S C_S + M_W C_W) \frac{dT_S}{dt} = U_{FW} A_W (T_F - T_S) \quad [14.16]$$

giving the first-order transfer function:

$$\frac{\Delta \tilde{T}_S}{\Delta \tilde{T}_F}(s) = \frac{1}{1 + \tau s}, \quad \tau = \frac{M_S C_S + M_W C_W}{U_{FW} A_W} \quad [14.17]$$

This model is a good representation of installations where special steps have been taken to improve heat transfer, namely filling the sheath with oil or mercury or using a crimped metal sleeve to increase the heat transfer area. Table 14.1 gives typical time constants for elements in thermowells under different fluid conditions.

Even with a good installation, the time constant for a sensor in a thermowell is considerably longer than that of the sensor itself. If a fast response is required and the sensor must be protected, then a mineral insulated thermocouple would be used. This is shown in Figure 8.18 and consists of a fine wire thermocouple inside a narrow thin-walled tube; the tube is filled with mineral material which is a good heat conductor but an electrical insulator. This device is described by the transfer function of eqn [14.17]; in this case M_S and M_W are small, giving time constants 100 times shorter than thermowell installations (see Table 14.1).

14.2.3 Fluid velocity sensor with self-heating current

If a current i is passed through a resistive element, like a fine metal wire or semiconductor film, then the element is heated to a temperature T which is greater than T_F , the temperature of the surrounding fluid. The element temperature T and resistance R_T depend on the balance between electrical power $i^2 R_T$ and the rate of overall convective heat transfer between element and fluid. Since convective heat transfer depends on the velocity v of the fluid, the element is used as a fluid velocity sensor (see following section). The heat balance equation is:

$$i^2 R_T - U(v)A(T - T_F) = MC \frac{dT}{dt} \quad [14.18]$$

where $U(v)$ is the convective heat transfer coefficient between sensor and fluid. If i_0 , R_{T_0} , T_0 and v_0 represent steady equilibrium conditions, then:

$$i_0^2 R_{T_0} - U(v_0)A(T_0 - T_F) = 0 \quad [14.19]$$

Defining Δi , ΔR_T , Δv and ΔT to be small deviations from the above equilibrium values, we have:

$$i = i_0 + \Delta i, \quad T = T_0 + \Delta T \quad [14.20]$$

$$R_T = R_{T_0} + \Delta R_T, \quad U(v) = U(v_0) + \sigma \Delta v$$

In [14.20] $\sigma = (\partial U / \partial v)_{v_0}$, i.e. the rate of change of U with respect to v , evaluated at equilibrium velocity v_0 . From [14.18] and [14.20] we have:

$$\begin{aligned} & (i_0 + \Delta i)^2 (R_{T_0} + \Delta R_T) - [U(v_0) + \sigma \Delta v]A(T_0 + \Delta T - T_F) \\ &= MC \frac{d}{dt} (T_0 + \Delta T) \end{aligned} \quad [14.21]$$

Neglecting all terms involving the product of two small quantities gives:

$$\begin{aligned} & (i_0^2 + 2i_0 \Delta i)R_{T_0} + i_0^2 \Delta R_T - U(v_0)A(T_0 - T_F) - U(v_0)A\Delta T - \sigma A(T_0 - T_F)\Delta v \\ &= MC \frac{d\Delta T}{dt} \end{aligned} \quad [14.22]$$

Subtracting [14.19] from [14.22] gives:

$$2i_0 R_{T_0} \Delta i + i_0^2 \Delta R_T - U(v_0) A \Delta T - \sigma A (T_0 - T_F) \Delta v = MC \frac{d\Delta T}{dt} \quad [14.23]$$

ΔT can be eliminated by setting $K_T = \Delta R_T / \Delta T$, i.e. $\Delta T = (1/K_T) \Delta R_T$, where K_T is the slope of the element resistance–temperature characteristics; thus

$$\left(\frac{U(v_0) A}{K_T} - i_0^2 \right) \Delta R_T + \frac{MC}{K_T} \frac{d\Delta R_T}{dt} = 2i_0 R_{T_0} \Delta i - \sigma A (T_0 - T_F) \Delta v \quad [14.24]$$

which reduces to:

$$\Delta R_T + \tau_v \frac{d\Delta R_T}{dt} = K_I \Delta i - K_v \Delta v \quad [14.25]$$

where

$$\tau_v = \frac{MC}{U(v_0) A - i_0^2 K_T}, \quad K_I = \frac{2K_T i_0 R_{T_0}}{U(v_0) A - i_0^2 K_T}, \quad K_v = \frac{K_T \sigma A (T_0 - T_F)}{U(v_0) A - i_0^2 K_T} \quad [14.26]$$

Taking the Laplace transform of [14.26] gives:

$$(1 + \tau_v s) \Delta \bar{R}_T = K_I \Delta \bar{i} - K_v \Delta \bar{v}$$

i.e.

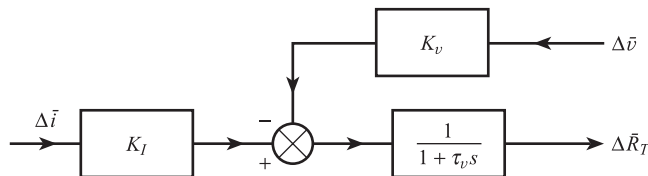
*Transfer function for
fluid velocity sensor*

$$\Delta \bar{R}_T = \left(\frac{K_I}{1 + \tau_v s} \right) \Delta \bar{i} - \left(\frac{K_v}{1 + \tau_v s} \right) \Delta \bar{v} \quad [14.27]$$

The corresponding block diagram for the sensing element is shown in Figure 14.2.

From eqn [14.27] and Figure 14.2 we note that the resistance of the element can be altered by either a change in current Δi or a change in fluid velocity Δv ; the time constant for both processes is τ_v . For a metal resistance element we have $R_T \approx R_0(1 + \alpha T)$, giving $K_T = dR_T/dT = R_0 \alpha$, where R_0 = resistance of the element at 0 °C, and α °C⁻¹ is the temperature coefficient of resistance. For a semiconductor resistance element (thermistor) we have $R_\theta = K e^{\beta/\theta}$, i.e.

Figure 14.2 Block diagram for thermal velocity sensor.



$$K_\theta = \frac{dR_\theta}{d\theta} = \frac{-\beta}{\theta^2} K e^{\beta/\theta} = \frac{-\beta}{\theta^2} R_\theta$$

so that here K_θ is negative and depends on thermistor temperature θ kelvin as well as the characteristic constant β . We can now calculate τ_v in a typical situation, e.g. for a thin film of semiconductor material 1 cm square, deposited on the surface of a probe inserted in a slow-moving gas stream. Typically we have:

$$\begin{aligned} \theta_0 &= 383 \text{ K (110 } ^\circ\text{C)} & R_{\theta_0} &= 150 \Omega \\ MC &= 2.5 \times 10^{-5} \text{ J } ^\circ\text{C}^{-1} & A &= 10^{-4} \text{ m}^2 \\ U(v_0) &= 25 \text{ W m}^{-2} ^\circ\text{C}^{-1} & i_0 &= 25 \times 10^{-3} \text{ A} \\ K_\theta &= -4.0 \Omega ^\circ\text{C}^{-1} \end{aligned}$$

giving

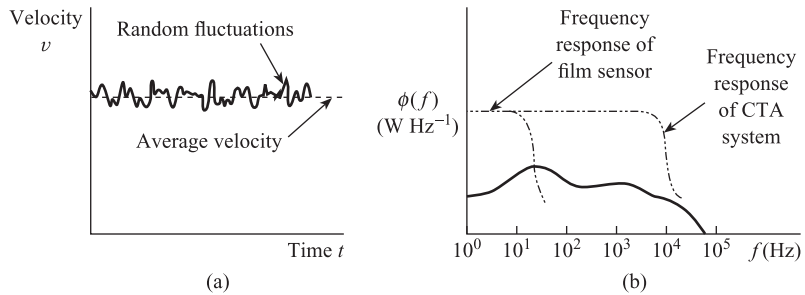
$$\tau_v = \frac{MC}{U(v_0)A - i_0^2 K_\theta} = \frac{2.5 \times 10^{-5}}{50 \times 10^{-4}} = 5.0 \text{ ms}$$

From Section 4.4 we can see that the bandwidth of the probe is between 0 and $1/(2\pi \times 5 \times 10^{-3})$, i.e. between 0 and 32 Hz. Lower time constants can be obtained with probes of a lower mass/area ratio in fluids with a higher heat transfer coefficient. It is not usually possible to reduce τ_v much below 1 ms, i.e. to increase the bandwidth much above 160 Hz.

There are, however, several potential applications of thermal velocity sensors which require a far higher bandwidth. In the testing of aircraft in wind tunnels it is important to measure the power spectral density $\phi(f)$ (Section 6.2) of the turbulence associated with air flow over the aircraft surfaces. Turbulence refers to the small random fluctuations in velocity at a point in a fluid occurring at high Reynolds numbers (Figure 14.3(a)). The corresponding power spectral density can extend up to around 50 kHz (Figure 14.3(b)).

Another potential application is the detection of vortices in the vortex-shedding flowmeter (Section 12.2), where vortex frequencies up to around 1 kHz are possible. This difficulty is solved by incorporating the sensor into a constant temperature anemometer system. We will see in the following section that the CTA system time constant is considerably less than τ_v . Note that in the limit $i_0 \rightarrow 0$, i.e. negligible self-heating current, and $\tau_v \rightarrow MC/UA$, i.e. the time constant of a velocity sensor tends to that of a bare temperature sensor.

Figure 14.3 Flow turbulence and sensor frequency response.



14.3

Constant-temperature anemometer system for fluid velocity measurements

14.3.1 Steady-state characteristics

From the previous section the steady-state equilibrium equation for a fluid velocity sensor with self-heating current is:

$$i^2 R_{T_0} = U(v) A (T_0 - T_F) \quad [14.19a]$$

In a constant-temperature anemometer system the resistance R_{T_0} and temperature T_0 of the sensor are maintained at constant values (within limits). From [14.19a] we see that if the fluid velocity v increases, causing an increase in $U(v)$, then the system must increase the current i through the sensor in order to restore equilibrium. Since sensor resistance R_{T_0} remains constant, the voltage drop $i R_{T_0}$ across the element increases, thus giving a voltage signal dependent on fluid velocity v .

The correlation of eqn [14.6] for two-dimensional, convective heat transfer from a narrow cylinder in an incompressible fluid is the one most appropriate to fluid velocity sensors.^[3] This is:

$$Nu = 0.24 + 0.56 Re^{0.5} \quad [14.6]$$

giving

$$U = \frac{0.24k}{d} + 0.56k \left(\frac{\rho v}{d\eta} \right)^{0.5} \quad [14.7]$$

i.e.

$$U = a + b\sqrt{v} \quad [14.28]$$

where

$$a = \frac{0.24k}{d}, \quad b = 0.56k \left(\frac{\rho}{d\eta} \right)^{0.5} \quad [14.29]$$

We see that since a and b depend on the sensor dimensions d and the fluid properties k , ρ and η , they are constants only for a *given sensor* in a *given fluid*. This means that if a sensor is calibrated in a certain fluid, the calibration results will not apply if the sensor is placed in a different fluid. Figure 14.4 shows a typical hot wire velocity sensor.

Figure 14.5(a) is a schematic diagram of a constant-temperature anemometer system. This is a self-balancing bridge which maintains the resistance R_T of the sensor at a constant value R . An increase in fluid velocity v causes T and R_T to fall in the short

Figure 14.4 Hot wire velocity sensor.

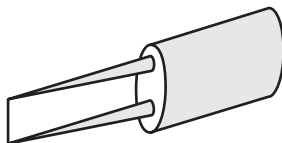
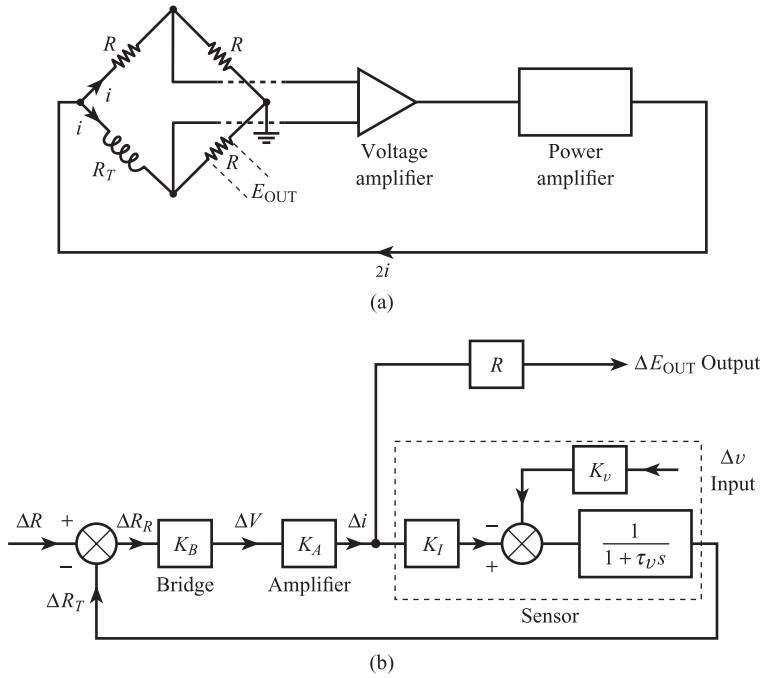


Figure 14.5 Constant-temperature anemometer system:
(a) Schematic diagram
(b) Block diagram.



term, thus unbalancing the bridge; this causes the amplifier output current and current through the sensor to increase, thereby restoring T and R_T to their required values. Since $R_T = R$ and $R_T = R_0(1 + \alpha T)$ for a metallic sensor, then the constant temperature T of the sensor is:

$$T = \frac{1}{\alpha} \left(\frac{R}{R_0} - 1 \right) \quad [14.30]$$

From [14.19], [14.28] and [14.30] we have:

$$i^2 R = A(a + b\sqrt{v}) \left[\frac{1}{\alpha} \left(\frac{R}{R_0} - 1 \right) - T_F \right] \quad [14.31]$$

and since $E_{OUT} = iR$:

$$E_{OUT}^2 = AR(a + b\sqrt{v}) \left[\frac{1}{\alpha} \left(\frac{R}{R_0} - 1 \right) - T_F \right] \quad [14.321]$$

giving

$$E_{OUT} = (E_0^2 + \gamma\sqrt{v})^{1/2} \quad [14.33]$$

where

$$E_0^2 = ARa \left[\frac{1}{\alpha} \left(\frac{R}{R_0} - 1 \right) - T_F \right], \quad \gamma = ARb \left[\frac{1}{\alpha} \left(\frac{R}{R_0} - 1 \right) - T_F \right] \quad [14.34]$$

Steady-state relationship between output voltage and velocity for constant temperature anemometer

Figure 14.6 Steady-state CTA characteristics for tungsten filament in air.

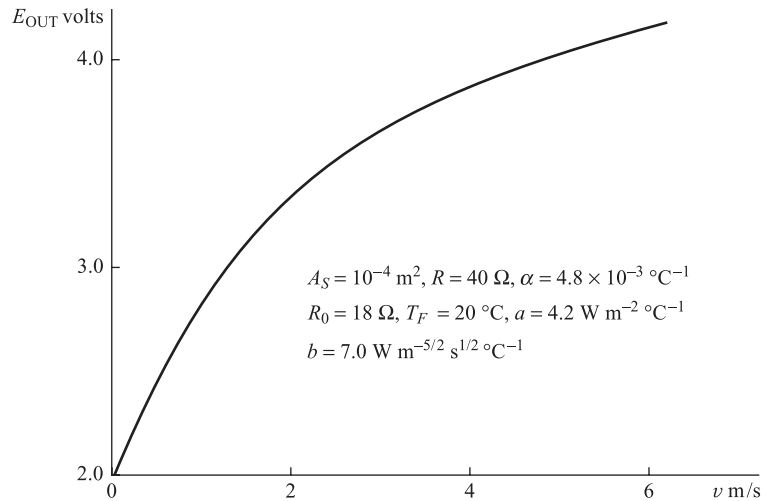


Figure 14.6 shows a typical relationship between E_{OUT} and v ; these characteristics were found experimentally for a tungsten filament CTA system in air. We note that when $v = 0$, $E_{\text{OUT}} = E_0 \approx 2.0 \text{ V}$ (natural convection) and that the relationship is highly non-linear. The slope of this relationship, that is the sensitivity of the system, is greatest at the lowest velocities. A CTA system can therefore be used for measuring low fluid velocities of the order of a few metres per second; this is in contrast to the pitot tube (Section 12.1), which has a very low sensitivity at low fluid velocities.

In order to measure velocity we need an inverse equation which expresses v in terms of measured voltage E_{OUT} . This can be found by rearranging eqn [14.33] to give:

$$v = \left[\frac{1}{\gamma} (E_{\text{OUT}}^2 - E_0^2) \right]^2$$

E_{OUT} is input to a microcontroller in which experimentally determined values of E_0 and γ are stored, and v can then be calculated. Since E_0 and γ are dependent on fluid properties, the system must be recalibrated if the fluid is changed. From eqns [14.34] we see that if the fluid temperature T_F changes, then E_0 , γ and the system calibration changes. One method of compensating for this is to incorporate a second unheated element at temperature T_F into the self-balancing bridge circuit. At higher velocities ($v \gtrsim 10 \text{ m/s}$) the CTA system can be calibrated using a pitot tube; at lower velocities one possibility is to use the cross-correlation method (Section 12.4) using two thermal velocity sensors.

14.3.2 Dynamic characteristics

We now calculate the transfer function of the constant-temperature anemometer system to see whether the frequency response is sufficient to detect rapid velocity fluctuations due to turbulence and vortex shedding. A block diagram of the system is shown in Figure 14.5(b); this incorporates the block diagram of a thermal velocity sensor derived in Section 14.2.3. The system equations are:

$$\text{Sensor} \quad \Delta R_T = \left(\frac{K_I}{1 + \tau_v s} \right) \Delta i - \left(\frac{K_v}{1 + \tau_v s} \right) \Delta v \quad [14.27]$$

$$\text{Bridge} \quad \Delta V = K_B \Delta R_R \quad [14.35]$$

$$\text{Amplifier} \quad \Delta i = K_A \Delta V \quad [14.36]$$

$$\text{Output voltage} \quad \Delta E_{\text{OUT}} = R \Delta i \quad [14.37]$$

$$\begin{aligned} \text{Resultant change in} \quad \Delta R_R &= \Delta R - \Delta R_T \\ \text{bridge resistance} \quad &= -\Delta R_T \text{ (since } \Delta R = 0) \end{aligned} \quad [14.38]$$

From [14.35]–[14.38]:

$$\Delta R_T = \frac{-1}{R K_A K_B} \Delta E_{\text{OUT}}, \quad \Delta i = \frac{\Delta E_{\text{OUT}}}{R} \quad [14.39]$$

Substituting [14.39] in [14.27] gives:

$$\frac{-1}{R K_A K_B} \Delta E_{\text{OUT}} = \left(\frac{1}{1 + \tau_v s} \right) \left(\frac{K_I}{R} \Delta E_{\text{OUT}} - K_v \Delta v \right)$$

Rearranging, we have:

$$[(1 + K_I K_A K_B) + \tau_v s] \Delta E_{\text{OUT}} = K_\theta K_A K_B R \Delta v$$

giving

*Transfer function
for CTA system*

$$\frac{\Delta \bar{E}_{\text{OUT}}}{\Delta \bar{v}}(s) = \frac{K_{CTA}}{1 + \tau_{CTA} s} \quad [14.40]$$

where

$$K_{CTA} = \frac{K_v K_A K_B R}{1 + K_I K_A K_B}, \quad \tau_{CTA} = \frac{\tau_v}{1 + K_I K_A K_B} \quad [14.41]$$

We can now calculate τ_{CTA} for a typical system incorporating the semiconductor element discussed in Section 14.2.3. Using the data previously given, we have:

$$\tau_v = 5.0 \text{ ms}, \quad K_I = \frac{2K_\theta i_0 R_{\theta_0}}{U(V_0)A - i_0^2 K_\theta} = -6 \times 10^3 \Omega \text{ A}^{-1}$$

For a 150Ω bridge with supply voltage $V_S = 7.5 \text{ V}$,

$$K_B = \frac{\Delta V}{\Delta R_R} = \frac{1}{4} \frac{V_S}{R} = \frac{1}{4} \times \frac{7.5}{150} = 1.25 \times 10^{-2} \text{ V } \Omega^{-1}$$

In the typical case of a voltage amplifier of gain 10^3 followed by an emitter-follower power amplification stage, $K_A \approx -4 \text{ A V}^{-1}$. From [14.41] we have:

$$\tau_{CTA} = \frac{5.0}{1 + 6 \times 10^3 \times 1.25 \times 10^{-2} \times 4} \text{ ms} = \frac{5.0}{301} \text{ ms} = 17 \mu\text{s}$$

Thus the bandwidth of the system is between 0 and $1/(2\pi \times 17 \times 10^{-6})$ Hz, i.e. between 0 and 10 kHz, which is easily sufficient for vortex detection and is adequate for most turbulence measurement applications (see Figure 14.3(b)).

14.4

Katharometer systems for gas thermal conductivity and composition measurement

The convective heat transfer coefficient U between a sensor and a moving gas depends on the thermal conductivity k of the gas as well as the average gas velocity (eqn [14.7]). In a katharometer the velocity of the gas past the element is maintained either constant or small (preferably both), so that U depends mainly on the thermal conductivity of the gas. A constant self-heating current i_0 is passed through the element. Thus from the steady-state heat balance equation,

$$i_0^2 R_T = U(k)A(T - T_F) \quad [14.19b]$$

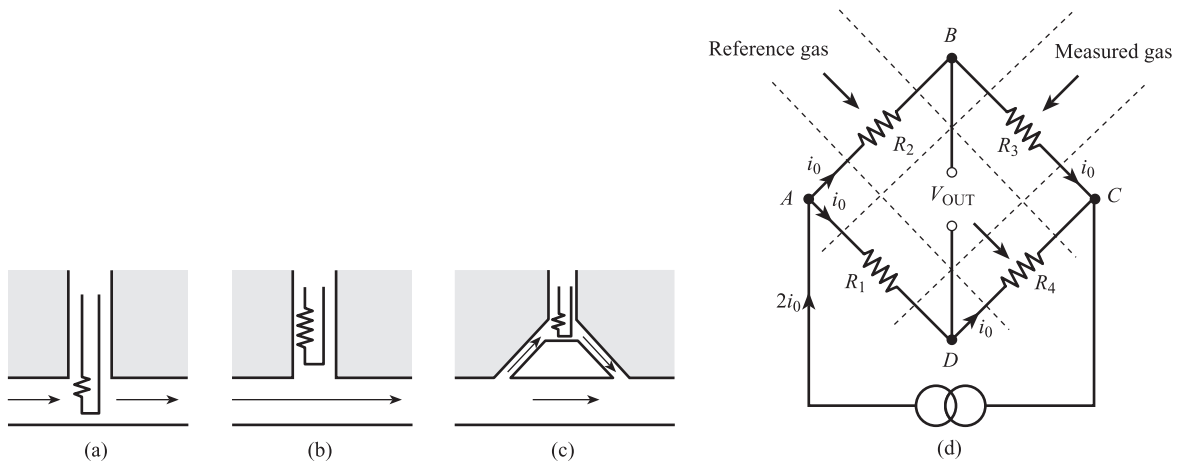
we see that if gas thermal conductivity k increases, causing $U(k)$ to increase, then the temperature T of the element falls.

Typical katharometer element configurations are shown in Figures 14.7(a)–(c) where the element is either a metal filament or a thermistor. A system normally consists of four such elements, each element being located in a separate cavity inside a metal block. The gas to be measured passes over one pair of elements and a reference gas passes over the other pair. In Figure 14.7(a) all of the gas flow passes over the element, whereas in Figure 14.7(b) there is only a small gas circulation around the element. Figure 14.7(d) shows the arrangement of the four elements in a deflection bridge with a constant current supply; note that measured and reference gas elements are arranged in opposite arms of the bridge.

In order to find the relationship between the resistance R_T of an element and gas thermal conductivity k , we need to eliminate T from eqn [14.19b]. For a metal filament we have:

$$R_T = R_0(1 + \alpha T), \quad R_{T_F} = R_0(1 + \alpha T_F)$$

Figure 14.7
Katharometer elements and deflection bridge.



where R_{T_F} is the resistance of the filament at the temperature T_F of the fluid ($T_F < T$). Thus:

$$\frac{R_T}{R_{T_F}} = \frac{1 + \alpha T}{1 + \alpha T_F} \approx 1 + \alpha(T - T_F) \quad [14.42]$$

assuming that terms involving $(\alpha T_F)^2$ etc. are negligible. Rearranging gives:

$$T - T_F = \frac{1}{\alpha} \left(\frac{R_T}{R_{T_F}} - 1 \right) \quad [14.43]$$

Substituting [14.43] in [14.19b], we have:

$$i_0^2 R_T = \frac{UA}{\alpha} \left(\frac{R_T}{R_{T_F}} - 1 \right) \quad [14.44]$$

i.e.

$$BR_T = U(R_T - R_{T_F}) \quad [14.45]$$

where $B = i_0^2 \alpha R_{T_F} / A$ is a constant if gas temperature T_F is constant. Rearranging gives:

Relationship between filament resistance and fluid heat transfer coefficient for constant current

$$R_T = \frac{R_{T_F}}{1 - \frac{B}{U}} \quad [14.46]$$

In the bridge circuit of Figure 14.7(d) we have:

$$R_1 = R_3 = \frac{R_{T_F}}{1 - (B/U_M)} \quad \text{for measured gas} \quad [14.47]$$

and

$$R_2 = R_4 = \frac{R_{T_F}}{1 - (B/U_R)} \quad \text{for reference gas}$$

The bridge output voltage (potential difference between B and D) is thus:

$$\begin{aligned} V_{\text{OUT}} &= i_0(R_1 - R_2) = i_0 R_{T_F} \left\{ \frac{1}{1 - (B/U_M)} - \frac{1}{1 - (B/U_R)} \right\} \\ &= i_0 R_{T_F} B \frac{(1/U_M) - (1/U_R)}{(1 - B/U_M)(1 - B/U_R)} \end{aligned} \quad [14.48]$$

For a typical system

$$\begin{aligned} \alpha &= 4 \times 10^{-3} \text{ } ^\circ\text{C}^{-1}, \quad 2i_0 = 100 \text{ mA}, \quad R_{T_F} = 10 \text{ } \Omega \\ A &= 10^{-4} \text{ m}^2, \quad U \approx 25 \text{ W m}^{-2} \text{ } ^\circ\text{C}^{-1} \end{aligned}$$

giving

$$B = \frac{i_0^2 \alpha R_{T_F}}{A} = 1.0 \quad \text{and} \quad \frac{B}{U} \approx \frac{1}{25}$$

Since B/U is small compared with 1, eqn [14.48] can be approximated by

*Output voltage from
katharometer system*

$$V_{\text{OUT}} = \frac{i_0^3 R_{T_F}^2 \alpha}{A} \left(\frac{1}{U_M} - \frac{1}{U_R} \right) \quad [14.49]$$

From [14.49] we see that the output voltage is proportional to the cube of the sensor current and also depends non-linearly on the heat transfer coefficients U_M and U_R . Using [14.7] we have $U_M = k_M f(v)$ and $U_R = k_R f(v)$, where

$$f(v) = \frac{0.24}{d} + 0.56 \left(\frac{\rho v}{d \eta} \right)^{0.5}$$

and k_M and k_R are the thermal conductivities of the measured and reference gases respectively. If the flow rates of measured and reference gases are equal, then the velocity v is the same for both gases. The element of Figure 14.7(a) is situated directly in the gas stream. This means that there is substantial forced convection, i.e. the $0.56 (\rho v / d \eta)^{0.5}$ term is large. Thus V_{OUT} depends critically on the gas flow rates: elements of this type need tight control of gas flow but respond rapidly to sudden changes in thermal conductivity. The element of Figure 14.7(b) is situated out of the main gas stream where velocity and forced convection are much smaller. In the limit that v is negligible we have $f(v) = 0.24/d$ and:

*Output voltage for
katharometer with
negligible gas velocity*

$$V_{\text{OUT}} = D \left(\frac{1}{k_M} - \frac{1}{k_R} \right) \quad [14.50]$$

where $D = i_0^3 R_{T_F}^2 \alpha d / (0.24 A)$. This type of element is not sensitive to changes in gas flow rate, i.e. tight control of gas flow rates is not necessary, but responds slowly to sudden changes in thermal conductivity. Most elements in current use are of the type shown in Figure 14.7(c); here a fraction of the gas flow is passed over the filament. These have an adequate speed of response and a low sensitivity to flow changes.

The main use of the katharometer is as a detector in a gas chromatograph system for measuring the composition of gas mixtures (Chapter 17). Here an inert gas such as nitrogen, helium or argon, referred to as the carrier, sweeps a sample of gas to be analysed through a packed column. In this application the katharometer reference gas is pure carrier; the katharometer measured gas is the gas leaving the column. Initially, while the components of the sample are inside the column, the gas leaving the column is pure carrier. Pure carrier gas flows over all four elements: therefore each arm of the bridge has the same resistance and the bridge output voltage is zero. The components then emerge from the column one at a time; as each component emerges the katharometer measured gas is a mixture of carrier gas and that component. This causes corresponding changes in thermal conductivity k_M and resistances R_1 and R_3 so that the bridge output voltage is no longer zero. The thermal conductivities of the reference and measured gases are now given by:

$$k_R = k_C, \quad k_M = x_i k_i + (1 - x_i) k_C \quad [14.51]$$

where

k_C = thermal conductivity of carrier

k_i = thermal conductivity of i th component in sample

x_i = molar fraction of i th component in mixture of carrier and i th component.

The second equation assumes a linear relation between mixture thermal conductivity and composition. Substituting in eqn [14.50] gives:

$$V_{\text{OUT}} = D \left[\frac{1}{x_i k_i + (1 - x_i) k_C} - \frac{1}{k_C} \right]$$

which simplifies to:

$$V_{\text{OUT}} = D \frac{(k_C - k_i) x_i}{k_C [x_i k_i + (1 - x_i) k_C]} \quad [14.52]$$

Usually x_i is small, so that this reduces to:

*Approximate
output voltage for
katharometer detector
in gas chromatograph
system*

$$V_{\text{OUT}} \approx D \left(\frac{k_C - k_i}{k_C^2} \right) x_i \quad [14.53]$$

This application of the katharometer is discussed further in Chapter 17 and reference [4].

Conclusion

The chapter began by discussing the principles of **convective heat transfer**. It then explained three important applications of these principles to measurement systems. These are:

- In understanding and calculating the **dynamic characteristics of thermal sensors**.
- In **hot wire** and **film systems** for fluid velocity measurements.
- In the **katharometer** for **gas thermal conductivity** and **composition measurement**.

References

- [1] KING L V 1914 'On the convection of heat from small cylinders in a stream of fluid', *Philosophical Transactions of Royal Society*, series A, vol. 214.
- [2] COLLIS D C and WILLIAMS M J 1959 'Two-dimensional convection from heated wires at low Reynolds numbers', *Journal of Fluid Mechanics*, vol. 6.
- [3] GALE B C *An Elementary Introduction to Hot Wire and Hot Film Anemometry*. DISA Technical Publication.
- [4] W. G. Pye and Co. *Technical Literature on Series 104 Chromatographs*.

Problems

14.1 A tungsten filament has a resistance of $18\ \Omega$ at $0\ ^\circ\text{C}$, a surface area of $10^{-4}\ \text{m}^2$ and a temperature coefficient of resistance of $4.8 \times 10^{-3}\ ^\circ\text{C}^{-1}$. The heat transfer coefficient between the filament and air at $20\ ^\circ\text{C}$ is given by $U = 4.2 + 7.0\sqrt{\nu}\ \text{W m}^{-2}\ ^\circ\text{C}^{-1}$, where $\nu\ \text{m s}^{-1}$ is the velocity of the air relative to the filament. The filament is incorporated into the constant temperature anemometer system of Figure 14.5, which maintains the filament resistance at $40\ \Omega$. Plot a graph of system output voltage versus air velocity in the range 0 to $10\ \text{m s}^{-1}$.

14.2 A heated tungsten filament is to be used for velocity measurements in a fluid of temperature $20\ ^\circ\text{C}$. With a constant current of $50\ \text{mA}$ through the filament, the voltage across the filament was $2.0\ \text{V}$ when the fluid was stationary and $1.5\ \text{V}$ when the fluid velocity was $36\ \text{m s}^{-1}$. Use the data below to:

- identify the heat transfer characteristics of the system;
- decide whether the system is suitable for measuring small velocity fluctuations, containing frequencies up to $10\ \text{kHz}$, about a steady velocity of $16\ \text{m s}^{-1}$.

Explain *briefly* why a constant temperature system would give a better performance in (b).

Filament data

Surface area	$= 10^{-4}\ \text{m}^2$
Resistance at $0\ ^\circ\text{C}$	$= 18\ \Omega$
Temperature coefficient of resistance	$= 4.8 \times 10^{-3}\ ^\circ\text{C}^{-1}$
Heat capacity	$= 1.3\ \mu\text{J}\ ^\circ\text{C}^{-1}$

14.3 A miniature thermistor with appreciable heating current is to be used to measure the flow turbulence in a slow-moving gas stream. The frequency spectrum of the turbulence extends up to $10\ \text{Hz}$ and the gas temperature is $90\ ^\circ\text{C}$. With a constant current of $23.4\ \text{mA}$, the steady-state voltage across the thermistor was $3.5\ \text{V}$. Starting from first principles, and using the thermistor data given below, show that a constant current system is unsuitable for this application. Explain briefly how the turbulence measurements can be made successfully with a modified system.

Thermistor data

Mass	$= 10^{-4}\ \text{kg}$
Specific heat	$= 1.64 \times 10^2\ \text{J kg}^{-1}\ ^\circ\text{C}^{-1}$

Temperature $T\ ^\circ\text{C}$	88	100	105	108	110	112	118	125
Resistance $R_T\ \Omega$	240	185	170	155	150	140	130	116

14.4 A temperature sensor has a mass of $0.05\ \text{kg}$ and a surface area of $10^{-3}\ \text{m}^2$ and is made of material of specific heat $500\ \text{J kg}^{-1}\ ^\circ\text{C}^{-1}$. It is placed inside a thermowell of mass $0.5\ \text{kg}$, surface area $10^{-2}\ \text{m}^2$ and specific heat $800\ \text{J kg}^{-1}\ ^\circ\text{C}^{-1}$. The heat transfer coefficient between sensor and thermowell is $25\ \text{W m}^{-2}\ ^\circ\text{C}^{-1}$ and between thermowell and fluid is $625\ \text{W m}^{-2}\ ^\circ\text{C}^{-1}$.

- Calculate the system transfer function and thus decide whether it can follow temperature variations containing frequencies up to $10^{-3}\ \text{Hz}$.
- What improvement is obtained if the heat transfer coefficient between sensor and thermowell is increased to $1000\ \text{W m}^{-2}\ ^\circ\text{C}^{-1}$?

14.5 A katharometer system is to be used to measure the percentage of hydrogen in a mixture of hydrogen and methane. The percentage of hydrogen can vary between 0 and 10% . The system consists of four identical tungsten filaments arranged in the deflection bridge circuit of Figure 14.7(d). The gas mixture, at $20\ ^\circ\text{C}$, is passed over elements 1 and 3; pure methane, also

at 20 °C, is passed over elements 2 and 4. Assuming a linear relation between mixture thermal conductivity and composition, use the data given below to:

- find the range of the open circuit bridge output voltage;
- plot a graph of bridge output voltage versus percentage hydrogen.

Data

Temperature coefficient of resistance of tungsten	$= 5 \times 10^{-3} \text{ }^{\circ}\text{C}^{-1}$
Resistance of filament at 20 °C	$= 10 \text{ } \Omega$
Total bridge current	$= 200 \text{ mA}$
Filament surface area	$= 10^{-5} \text{ m}^2$
Heat transfer coefficient between filament and gas	$= 5 \times 10^4 k$
where k = gas thermal conductivity	
Thermal conductivity of hydrogen	$= 17 \times 10^{-2} \text{ W m}^{-1} \text{ }^{\circ}\text{C}^{-1}$
Thermal conductivity of methane	$= 3 \times 10^{-2} \text{ W m}^{-1} \text{ }^{\circ}\text{C}^{-1}$

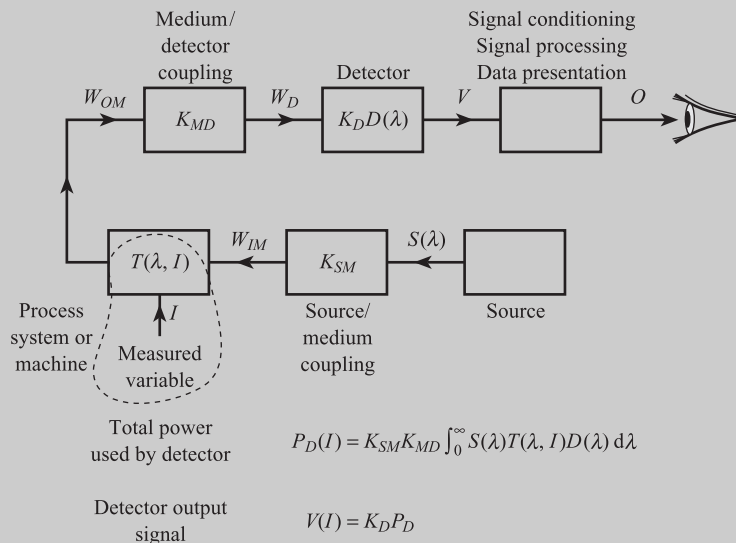
15 Optical Measurement Systems

15.1 Introduction: types of system

Light is a general title which covers radiation in the ultraviolet (UV), visible and infrared (IR) portions of the **electromagnetic spectrum**. **Ultraviolet radiation** has wavelengths between $0.01\ \mu\text{m}$ and $0.4\ \mu\text{m}$ (1 micron or micrometre (μm) = 10^{-6} m), **visible radiation** wavelengths are between $0.4\ \mu\text{m}$ and $0.7\ \mu\text{m}$ and **infrared wavelengths** are between 0.7 and $100\ \mu\text{m}$. Most of the systems discussed in this chapter use radiation with wavelengths between 0.3 and $10\ \mu\text{m}$, i.e. visible and infrared radiation.

Figures 15.1 and 15.2 show two important general types of optical measurement system. Both types include a basic optical transmission system which is made up of a **source**, a **transmission medium** and a **detector**. The function $S(\lambda)$ describes how the amount of radiant power emitted by the source varies with wavelength λ . $T(\lambda)$ describes how the efficiency of the transmission medium varies with λ . The detector converts the incoming radiant power into an electrical signal. The sensitivity or responsivity K_D is the change in detector output (ohms or volts) for 1 watt change in incident power. $D(\lambda)$ describes how the detector responds to different wavelengths λ . It is important that the three functions $S(\lambda)$, $T(\lambda)$ and $D(\lambda)$ are compatible with

Figure 15.1 Fixed source, variable transmission medium system.



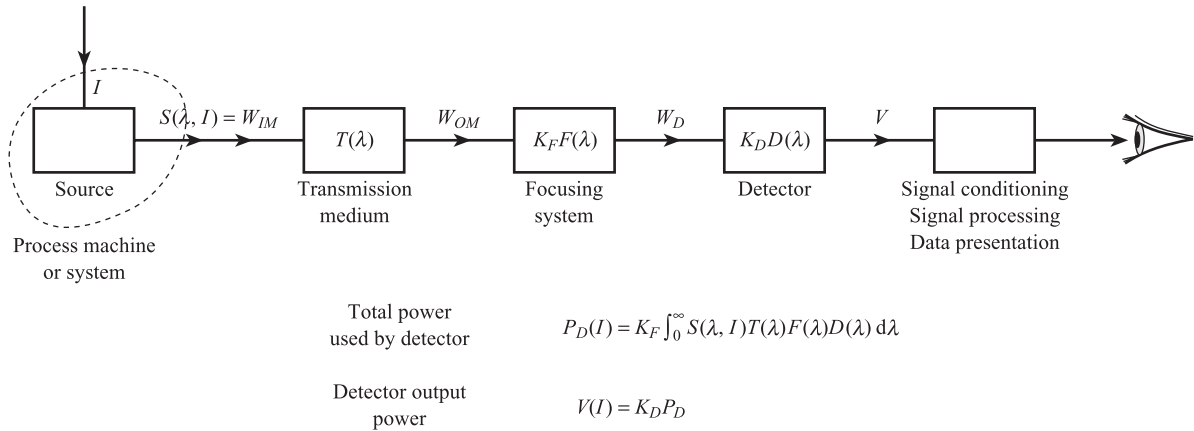


Figure 15.2 Variable source, fixed transmission medium system.

each other. This means that the values of all three functions must be reasonably large over the wavelengths of interest, otherwise these wavelengths will not be transmitted. Both systems also include signal conditioning, signal processing and data presentation elements.

Fixed source, variable transmission medium

The system shown in Figure 15.1 has a fixed source, i.e. constant total power; typical sources are a tungsten lamp, a light-emitting diode or a laser. However, the characteristics T of the transmission medium are not fixed but can vary according to the value of the measured variable I . In one example, the transmission medium consists of two optical fibres and the displacement to be measured changes the coupling between the fibres. In another, where the transmission medium is a tube filled with gas, changes in gas composition vary the fraction of infrared power transmitted through the tube. Systems of this type normally use a **narrow band** of wavelengths. The constant K_{SM} describes the efficiency of the geometrical coupling of the source to the transmission medium (e.g. optical fibre) and the constant K_{MD} the coupling of the medium to the detector. Optical measurement systems of this type have the following advantages over equivalent electrical systems:

- (a) No electromagnetic coupling to external interference voltages.
- (b) No electrical interference due to multiple earths.
- (c) Greater safety in the presence of explosive atmospheres. Here the source, detector, signal conditioning elements, etc., with their associated power supplies, are located in a safe area, e.g. a control room. Only the transmission fibre is located in the hazardous area, so that there is no possibility of an electrical spark causing an explosion.
- (d) Greater compatibility with optical communication systems.
- (e) Optical fibres may be placed close together without crosstalk.

Variable source, fixed transmission medium

The system shown in Figure 15.2 has a variable source in that the source power S varies according to the value of the measured variable I . The most common example is a

temperature measurement system where the total amount of radiant power emitted from a hot body depends on the temperature of the body. In this system the transmission medium is usually the atmosphere with fixed characteristics $T(\lambda)$. Since a hot body emits power over a wide range of wavelengths, systems of this type are usually **broadband** but may be made **narrowband** by the use of optical filters. Unlike optical fibres, the atmosphere cannot contain a beam of radiation and prevent it from diverging. A focusing system is usually necessary to couple the source to the detector. The constant K_F specifies the efficiency of this coupling and the function $F(\lambda)$ the wavelength characteristics of the focusing system. In temperature measurement systems of this type, the radiation receiver can be remote from the hot body or process. This means they can be used in situations where it is impossible to bring conventional sensors, e.g. thermocouples and resistance thermometers, into physical contact with the process. Examples are:

- (a) High temperatures at which a normal sensor would melt or decompose.
- (b) Moving bodies, e.g. steel plates in a rolling mill.
- (c) Detailed scanning and imaging of the temperature distribution over a surface; the number of conventional sensors required would be prohibitively large.

15.2

Sources

15.2.1 Principles

All of the sources used in optical measurement systems and described in this section emit radiation over a continuous band of wavelengths rather than at a single wavelength λ . The intensity of a source is specified by the **spectral exitance** function $S(\lambda)$ which is defined via the following:

The amount of energy per second emitted from 1 cm^2 of the projected area of the source, into a unit solid angle, between wavelengths λ and $\lambda + \Delta\lambda$ is $S(\lambda)\Delta\lambda$.

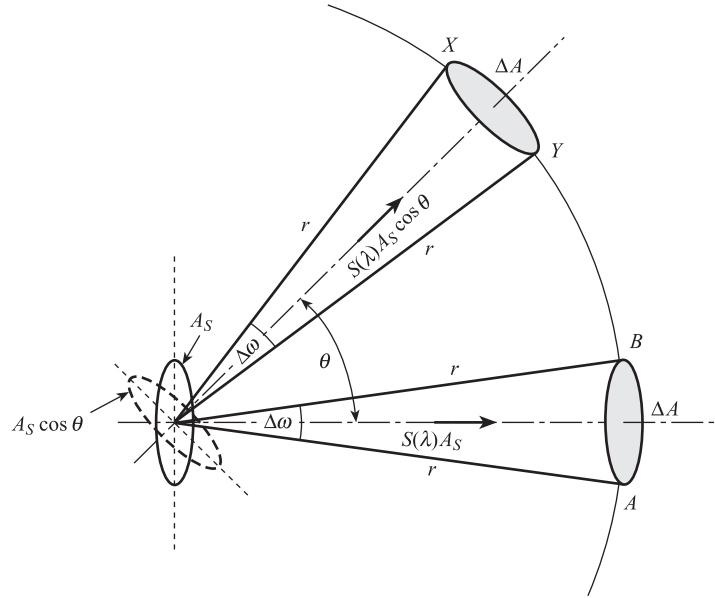
The following points should be noted.

- (a) $S(\lambda)$ is the power emitted per unit wavelength at λ . $S(\lambda)\Delta\lambda$ is the power emitted between wavelengths λ and $\lambda + \Delta\lambda$. $\int_0^\infty S(\lambda) d\lambda$ is the total power emitted over all wavelengths. This is termed the **radiance** of the source R , i.e.

$$R = \int_0^\infty S(\lambda) d\lambda \quad \text{W cm}^{-2} \text{ sr}^{-1} \quad [15.1]$$

- (b) For many of the sources used in optical measurement systems, the source $S(\lambda)$ is the same when viewed in all directions. Such a source is said to be Lambertian; a common example is a surface-emitting LED. Assuming that the source has uniform $S(\lambda)$ over its entire surface area A_s , then the radiant flux emitted by the source into unit solid angle is $A_s S(\lambda)$. This is termed the **radiant intensity** of the source, i.e.

Figure 15.3 Lambertian emitter and solid angle.



$$I_R = A_S S(\lambda) \text{ W sr}^{-1} \mu\text{m}^{-1} \quad [15.2]$$

This is the radiant intensity along the line $\theta = 0$ drawn normal to the radiating surface, in Figure 15.3. However, the projected area of the emitting surface at angle θ , relative to the normal, is $A_S \cos \theta$. The corresponding radiant intensity of the source when viewed at an angle θ is:

Lambertian angular variation in intensity

$$I_\theta = S(\lambda) A_S \cos \theta = I_R \cos \theta \quad [15.3]$$

- (c) Figure 15.3 also explains the meaning of solid angle and its importance in radiant power calculations. AB and XY are two elements of the surface of a sphere; both elements have area ΔA and are at distance r from the source. The solid angle subtended by each element at the source is:

$$\Delta\omega = \frac{\text{surface area}}{\text{distance}^2} = \frac{\Delta A}{r^2} \text{ steradians}$$

The power incident on AB is:

$$\Delta W = I_R \Delta\omega = \frac{I_R \Delta A}{r^2} \text{ W } \mu\text{m}^{-1} \quad [15.4]$$

and the power incident on XY is:

$$\Delta W_\theta = I_\theta \Delta\omega = \frac{I_R \cos \theta \Delta A}{r^2} \text{ W } \mu\text{m}^{-1} \quad [15.5]$$

15.2.2 Hot body sources

Any body at a temperature above 0 K emits radiation. The ideal emitter is termed a **black body**: from Planck's Law the spectral exitance of radiation emitted by a black body at temperature T K is:

Spectral exitance for black body radiator

$$W^{BB}(\lambda, T) = \frac{C_1}{\lambda^5 \left[\exp\left(\frac{C_2}{\lambda T}\right) - 1 \right]} \quad [15.6]$$

where

$$\begin{aligned} \lambda &= \text{wavelength in } \mu\text{m} \\ C_1 &= 37\,413 \text{ W } \mu\text{m}^4 \text{ cm}^{-2} \\ C_2 &= 14\,388 \mu\text{m K} \end{aligned}$$

Figure 15.4 is an approximate plot of $W^{BB}(\lambda, T)$ versus λ , for various values of T . The following points should be noted.

- (a) $W^{BB}(\lambda, T)$ is the power emitted per unit wavelength at λ .
 $W^{BB}(\lambda, T)\Delta\lambda$ is the power emitted between wavelengths λ and $\lambda + \Delta\lambda$.
 $\int_0^\infty W^{BB}(\lambda, T) d\lambda$ is the total power W_{TOT} emitted over all wavelengths, at temperature T .

W_{TOT} is therefore the total area under the $W^{BB}(\lambda, T)$ curve at a given temperature T . From Figure 15.4 we can see quantitatively that this area increases rapidly with T . We can confirm this quantitatively by evaluating the integral to give:

Total power emitted by a black body – Stefan's Law

$$\begin{aligned} W_{\text{TOT}} &= \int_0^\infty \frac{C_1 d\lambda}{\lambda^5 \left[\exp\left(\frac{C_2}{\lambda T}\right) - 1 \right]} \\ &= \sigma T^4 \text{ W cm}^{-2} \end{aligned} \quad [15.7]$$

where $\sigma = 5.67 \times 10^{-12} \text{ W cm}^{-2} \text{ K}^{-4}$ (Stefan–Boltzmann constant).

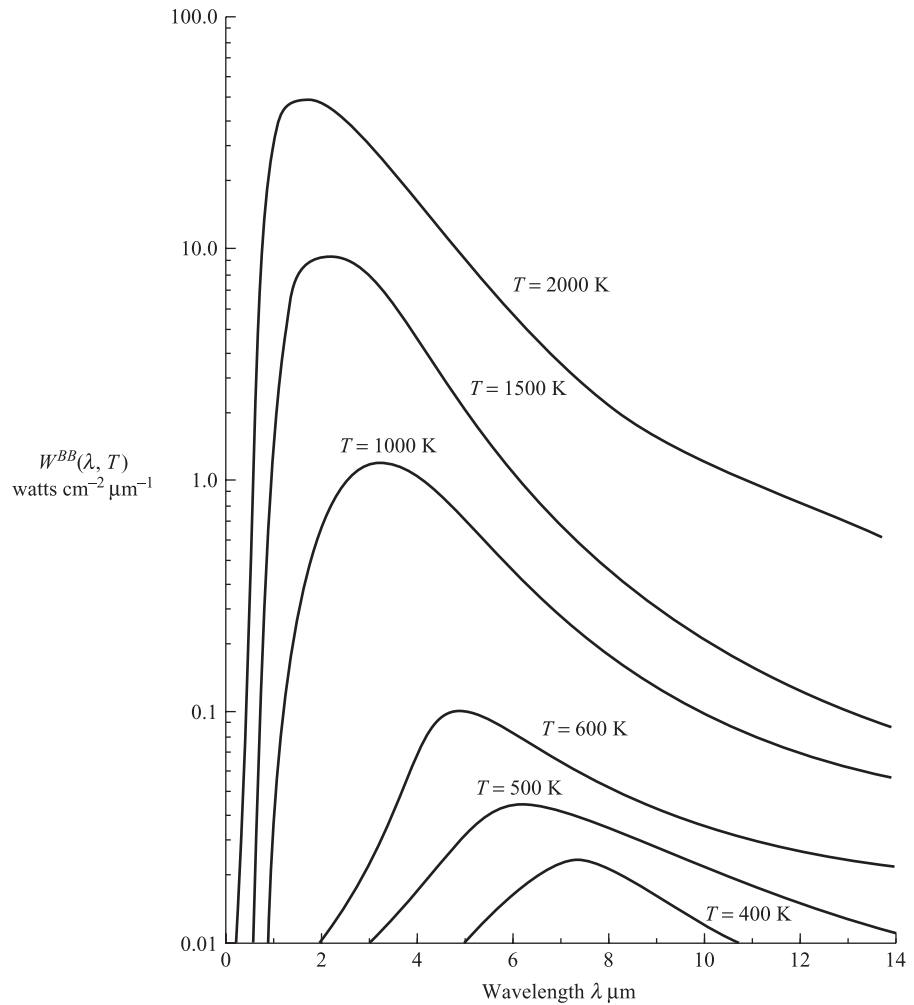
- (b) The wavelength λ_p at which $W^{BB}(\lambda, T)$ has maximum value decreases as temperature T increases according to:

$$\lambda_p = \frac{2891}{T} \mu\text{m} \quad [15.8]$$

Thus, if $T = 300 \text{ K}$, $\lambda_p \approx 10 \mu\text{m}$, i.e. most of the radiant power is infrared. However, at $T = 6000 \text{ K}$, $\lambda_p \approx 0.5 \mu\text{m}$ and most of the power is in the visible region.

- (c) Equation [15.6] is for a source in the form of a flat surface of area 1 cm^2 radiating into a hemisphere. A hemisphere is a solid angle of 2π steradians.

Figure 15.4 Spectral exitance for a black body radiator.



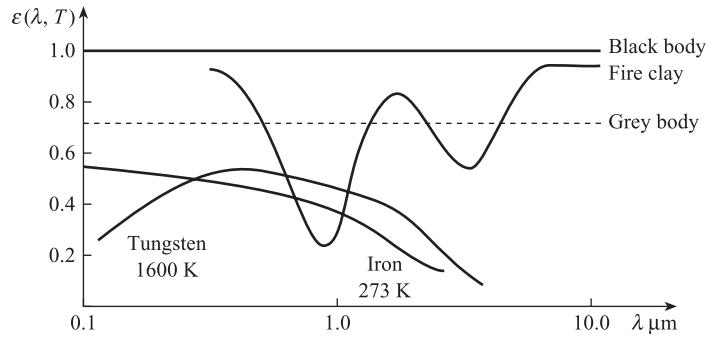
A black body is a theoretical ideal which can only be approached in practice, for example by a blackened conical cavity with a cone angle of 15° . A real body emits less radiation at temperature T and wavelength λ than a black body at the same conditions. A correction factor, termed the **emissivity** $\varepsilon(\lambda, T)$ of the body, is introduced to allow for this. Emissivity is defined by:

$$\text{Emissivity} = \frac{\text{actual radiation at } \lambda, T}{\text{black body radiation at } \lambda, T}$$

Emissivity of real body

$$\varepsilon(\lambda, T) = \frac{W^A(\lambda, T)}{W^{BB}(\lambda, T)} \quad [15.9]$$

Figure 15.5 Emissivity of various materials.



Emissivity in general depends on wavelength and temperature, although the temperature dependence is often weak. Figure 15.5 shows the emissivities of various materials. Note that a black body has $\varepsilon = 1$ by definition; a grey body has an emissivity independent of wavelength, i.e. $\varepsilon(\lambda) = \varepsilon (<1)$ for all λ . The emissivity of a real body must be measured experimentally by comparing the radiant power emitted by the body with that from a standard ‘black body’ source (typical emissivity 0.99).^[1]

Summarising, a hot body source is characterised by a broadband, continuous spectral exitance $S(\lambda, T)$ given by:

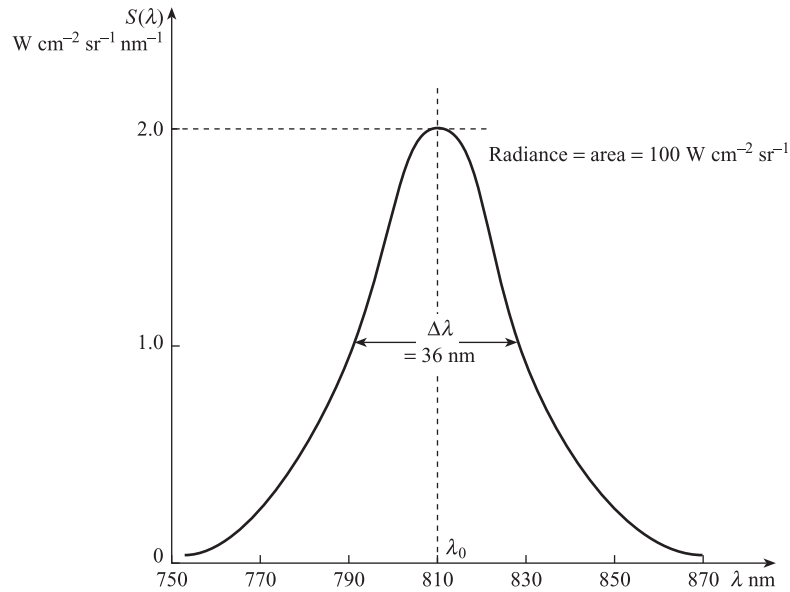
$$S(\lambda, T) = \frac{1}{\pi} \varepsilon(\lambda, T) W^{BB}(\lambda, T) \quad \text{W } \mu\text{m}^{-1} \text{ cm}^{-2} \text{ sr}^{-1} \quad [15.10]$$

In a fixed source, variable transmission medium system (Figure 15.1), source temperature T is held constant so that S depends on λ only and radiance R is approximately constant. A typical source is a tungsten halogen lamp operating at 3200 K and 50 W; most of the radiation emitted is between 0.4 μm and 3.0 μm with a maximum at 0.9 μm . In a variable source, fixed transmission medium (Figure 15.2) the source is the hot body whose temperature T is varying and is to be measured. Here S depends on both λ and T , and R depends on T . Uncertainty in the value of the emissivity of the hot body is the main source of error in this type of temperature measurement system.

15.2.3 Light-emitting diode (LED) sources^[2,3]

Light-emitting diodes have already been discussed in Section 11.4. These are pn junctions formed from p -type and n -type semiconductors, which when forward biased emit optical radiation. LEDs emitting visible radiation are widely used in displays. Examples are gallium arsenide phosphide (GaAsP) which emits red light ($\lambda \approx 0.655 \mu\text{m}$) and gallium phosphide (GaP) which emits green light ($\lambda \approx 0.560 \mu\text{m}$). Infrared LED sources are often preferred for use with optical fibre transmission links because their wavelength characteristics $S(\lambda)$ are compatible with the fibre transmission characteristics $T(\lambda)$. LEDs based on gallium aluminium arsenide (GaAlAs) alloys emit radiation in the 0.8 to 0.9 μm wavelength region, and those using indium gallium arsenide phosphide (InGaAsP) emit in the 1.3 to 1.6 μm region. Light-emitting diodes emit radiation over a narrow band of wavelengths. Figure 15.6 shows a typical spectral exitance function $S(\lambda)$ for a GaAlAs LED where $S(\lambda)$ has a peak value at $\lambda_0 = 810 \text{ nm}$.

Figure 15.6 $S(\lambda)$ for GaAlAs LED.



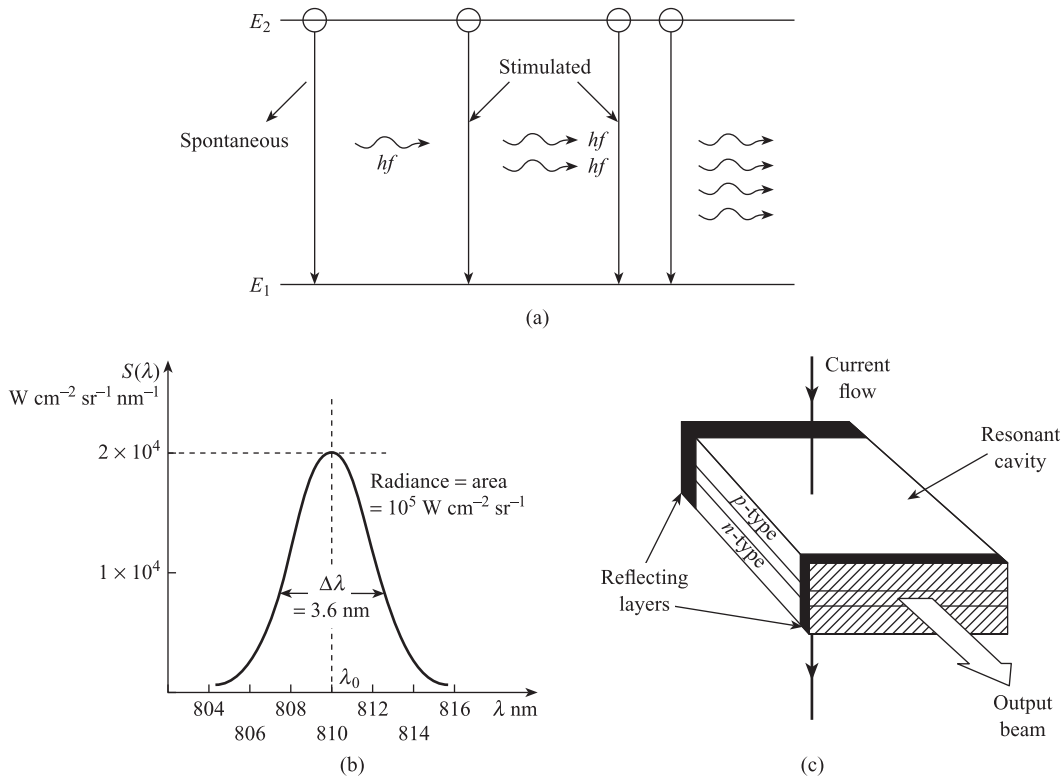
(0.81 μm) and a bandwidth $\Delta\lambda$ of 36 nm; the area under the distribution, i.e. the radiance R , is approximately $100 \text{ W cm}^{-2} \text{ sr}^{-1}$. The total radiant output power is typically between 1 and 10 mW.

15.2.4 Laser sources^[2,3]

There are several types of laser: the lasing medium may be gas, liquid, solid crystal or solid semiconductor. All types of laser have the same principle of operation, which can be explained using the energy level diagram shown in Figure 15.7(a). The ground state of the medium has energy E_1 and the excited state E_2 . A transition between these two states involves the absorption or emission of a photon of energy:

$$hf = E_2 - E_1 \quad [15.11]$$

where h is Planck's constant and f is the frequency of the radiation. If the medium is in thermal equilibrium, most of the electrons occupy the ground state E_1 and only a few have sufficient thermal energy to occupy the excited state E_2 . If, however, the laser is 'pumped', i.e. energised by an external source, then a **population inversion** occurs where there are more electrons in the excited state than in the ground state. Electrons then randomly return from the excited state to the ground state with emission of a photon of energy hf ; this is **spontaneous emission**. If this single photon causes another electron to return to the ground state, thereby generating a second photon in phase with the first, the process is called **stimulated emission**, and is the key to laser action. The two photons then create four and so on. The process is enhanced by creating a resonant cavity. This has a mirror at either end so that the photons travel forwards and backwards through the cavity, multiplication taking place all the time. The distance between the mirrors is made equal to an integral number of wavelengths λ ($\lambda = c/f$) to produce resonance. The photons leave the cavity, via a small hole in a mirror, to give a narrow, intense, **monochromatic**

**Figure 15.7**

Laser sources:

- (a) Spontaneous and stimulated emission
 (b) $S(\lambda)$ for GaAlAs injection laser diode
 (c) Construction of semiconductor laser diode.

(almost a single wavelength), **coherent beam** of light. Coherent means that different points in the beam have the same phase.

Semiconductor injection laser diodes (ILDs) are used with optical fibre links. These use the same materials, GaAlAs and InGaAsP, as LEDs, but give a narrower, coherent beam with a much smaller spectral bandwidth $\Delta\lambda$. Figure 15.7(b) shows a typical $S(\lambda)$ for a GaAlAs ILD with $\lambda_0 = 810 \text{ nm}$, $\Delta\lambda = 3.6 \text{ nm}$, and radiance $R = 10^5 \text{ W cm}^{-2} \text{sr}^{-1}$. The total radiant power is typically between 1 and 10 mW. The construction of a typical ILD is shown in Figure 15.7(c).

15.3

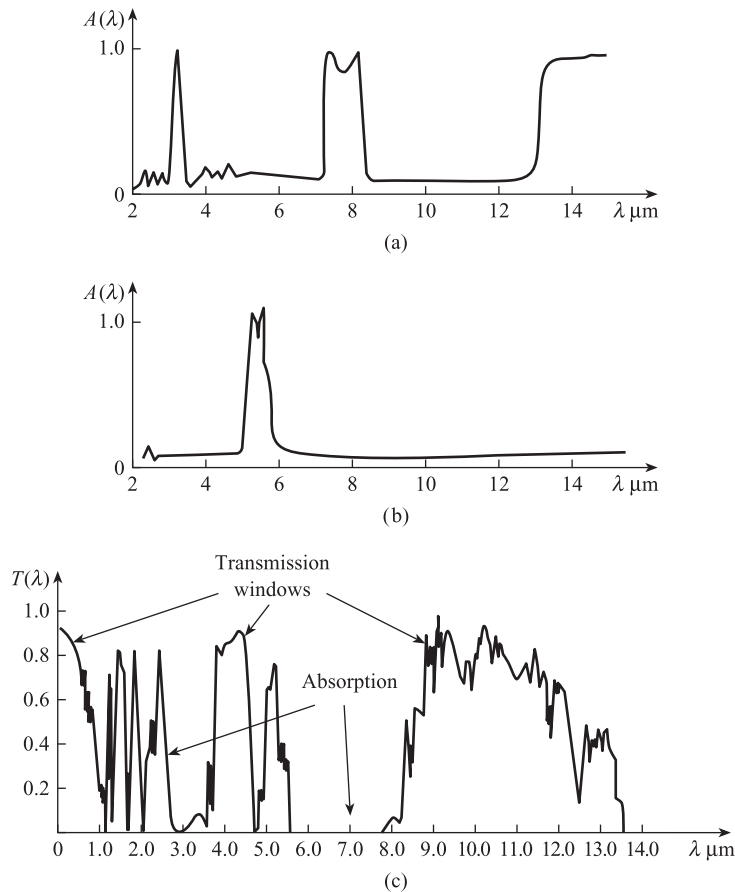
Transmission medium

15.3.1 General principles

If light is passed through any medium – gas, liquid or solid – then certain wavelengths present in the radiation cause the molecules to be excited into higher energy states. These wavelengths are thus **absorbed** by the molecules; each type of molecule is characterised by a unique **absorption spectrum** which is defined by:

$$A(\lambda) = \frac{\text{Power absorbed by medium at } \lambda}{\text{Power entering medium at } \lambda} = \frac{W_{AM}(\lambda)}{W_{IM}(\lambda)} \quad [15.12]$$

Figure 15.8 Absorption and transmission spectra:
 (a) Absorption spectrum for acetylene
 (b) Absorption spectrum for carbon monoxide
 (c) Transmission for the atmosphere over a distance of 1 mile.



Similarly the transmission spectrum $T(\lambda)$ is defined by:

$$T(\lambda) = \frac{\text{Power leaving medium at } \lambda}{\text{Power entering medium at } \lambda} = \frac{W_{OM}(\lambda)}{W_{IM}(\lambda)} \quad [15.13]$$

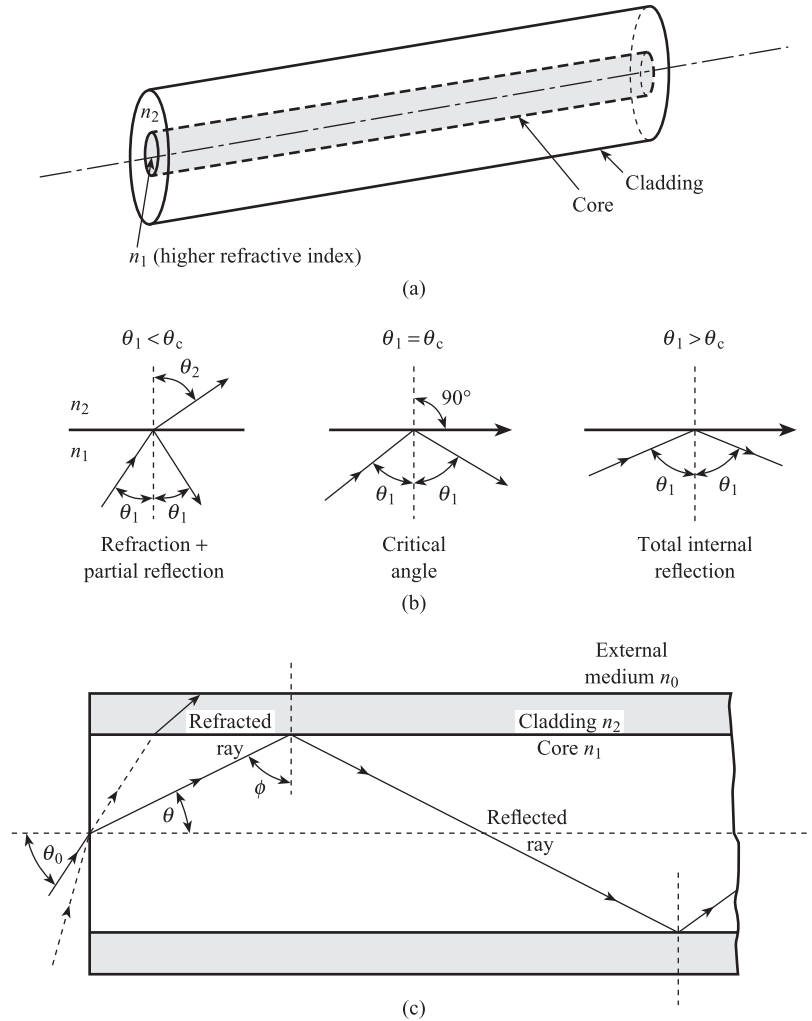
i.e. $W_{OM}(\lambda) = T(\lambda)W_{IM}(\lambda)$. From conservation of energy, $A(\lambda) + T(\lambda) = 1$ so that a transmission minimum corresponds to an absorption maximum.

Figures 15.8(a) and (b) show absorption spectra for acetylene and carbon monoxide; like many hydrocarbons and other gases these show strong absorption bands in the infrared. Figure 15.8(c) shows the transmission spectrum $T(\lambda)$ for the atmosphere; this is more complicated because there are absorption bands due to water vapour, carbon dioxide and ozone.

The above effect can be used in fixed source, variable transmission medium systems to measure the composition of gas and liquid mixtures. If the percentage of the absorbing molecule in the mixture changes, then $T(\lambda)$ changes and the amount of power leaving the medium changes. Such a system is called a **non-dispersive infrared analyser**; it could be used, for example, to measure the percentage of an absorbing component, e.g. CO, CO₂, CH₄ or C₂H₄, in a gas mixture.

The transmission characteristics of the atmosphere are also important in variable source, fixed transmission medium systems for temperature measurement. The

Figure 15.9 Optical fibre principles:
 (a) Optical fibre construction
 (b) Reflection and refraction at a boundary
 (c) Total internal reflection in a fibre.



radiation-receiving system is often designed to respond only to a narrow band of wavelengths corresponding to a **transmission window**.

15.3.2 Optical fibres

Optical fibres are widely used as transmission media in optical measurement systems.^[2,3] A typical fibre (Figure 15.9(a)) consists of two concentric dielectric cylinders. The inner cylinder, called the **core**, has a refractive index n_1 ; the outer cylinder, called the **cladding**, has a refractive index n_2 which is less than n_1 .

Figure 15.9(b) shows a ray incident on the boundary between two media of refractive indices n_1 and n_2 ($n_1 > n_2$). Part of the ray is reflected back into the first medium; the remainder is refracted as it enters the second medium. From Snell's Law we have:

$$n_1 \sin \theta_1 = n_2 \sin \theta_2 \quad [15.14]$$

and since $n_1 > n_2$ then $\theta_2 > \theta_1$. When $\theta_2 = 90^\circ$ the refracted ray travels along the boundary; the corresponding value of θ_1 is known as the **critical angle** θ_c and is given by:

$$n_1 \sin \theta_c = n_2, \text{ i.e. } \theta_c = \sin^{-1} \left(\frac{n_2}{n_1} \right) \quad [15.15]$$

Thus for a glass/air interface $n_1 = 1.5$, $n_2 = 1$ and $\theta_c = 41.8^\circ$. When θ_1 is greater than θ_c , all of the incident ray is totally internally reflected back into the first medium. Thus the above fibre will transmit, by means of many internal reflections, all rays with angles of incidence greater than the critical angle.

Figure 15.9(c) shows total internal reflections in a **step-index fibre**; this has a core with a uniform refractive index n_1 . The core is surrounded by a cladding of slightly lower refractive index n_2 and the entire fibre is surrounded by an external medium of refractive index n_0 . Total internal reflection in the core occurs if $\phi \geq \theta_c$, i.e.

$$\sin \phi \geq \frac{n_2}{n_1}, \text{ i.e. } \cos \phi \leq \sqrt{1 - \left(\frac{n_2}{n_1} \right)^2} \quad [15.16]$$

If θ_0 is the angle of incidence of a ray to the fibre, then the ray enters the core at an angle θ given by:

$$n_0 \sin \theta_0 = n_1 \sin \theta = n_1 \cos \phi \quad [15.17]$$

From eqns [15.16] and [15.17] total internal reflection occurs if:

$$\sin \theta_0 \leq \frac{n_1}{n_0} \sqrt{1 - \left(\frac{n_2}{n_1} \right)^2}$$

For air $n_0 = 1$, so that the **maximum angle of acceptance** θ_0^{MAX} of the fibre is given by:

*Numerical aperture
for step-index fibre*

$$\sin \theta_0^{\text{MAX}} = \sqrt{n_1^2 - n_2^2} = \text{NA} \quad [15.18]$$

The numerical aperture (NA) of the fibre is defined to be $\sin \theta_0^{\text{MAX}}$. Thus rays with $\theta_0 \leq \theta_0^{\text{MAX}}$ have $\phi \geq \theta_c$ and are continuously internally reflected: rays with $\theta_0 > \theta_0^{\text{MAX}}$ have $\phi < \theta_c$, refract out of the core and are lost in the cladding. θ_0^{MAX} thus defines the semi-angle of a **cone of acceptance** for the fibre.

For a step-index fibre we have:

$$n_2 = n_1(1 - \Delta) \quad [15.19]$$

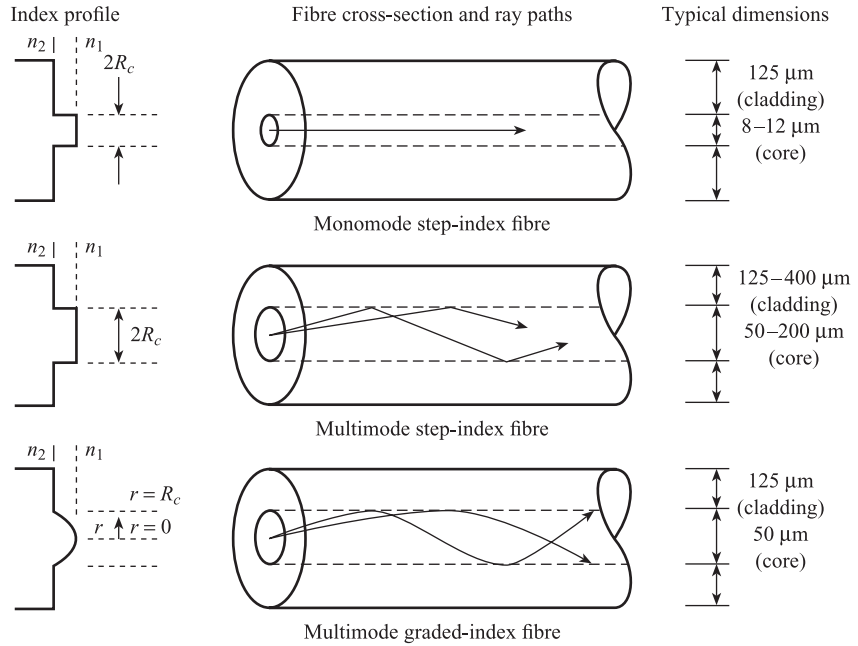
where Δ is the **core/cladding index difference**; Δ usually has a nominal value of 0.01. Since $\Delta \ll 1$, eqns [15.18] and [15.19] give the approximate equation for numerical aperture:

$$\text{NA} = \sin \theta_0^{\text{MAX}} \approx n_1 \sqrt{2\Delta} \quad [15.20]$$

Thus if $n_1 = 1.5$, then $\text{NA} = 0.21$ and $\theta_0^{\text{MAX}} = 12^\circ$.

Figure 15.10 shows the three main types of fibre in current use. The **monomode step-index fibre** is characterised by a very narrow core, typically only a few μm in

Figure 15.10 Different types of fibre (after Keiser^[2]).



diameter. This type of fibre can sustain only one mode of propagation and requires a coherent laser source. The **multimode step-index fibre** has a much larger core, typically $50\text{ }\mu\text{m}$ in diameter. Many modes can be propagated in multimode fibres; because of the larger core diameter it is also much easier to launch optical power into the fibre and also to connect fibres together. Another advantage is that light can be launched into multimode fibres using LED sources, whereas single-mode fibres must be excited with more complex laser diode sources.

Multimode graded-index fibres have a core with a non-uniform refractive index; n decreases parabolically from n_1 at the core centre to n_2 at the core/cladding boundary. These fibres are characterised by curved ray paths, which offer some advantages, but are more expensive than the step-index type.

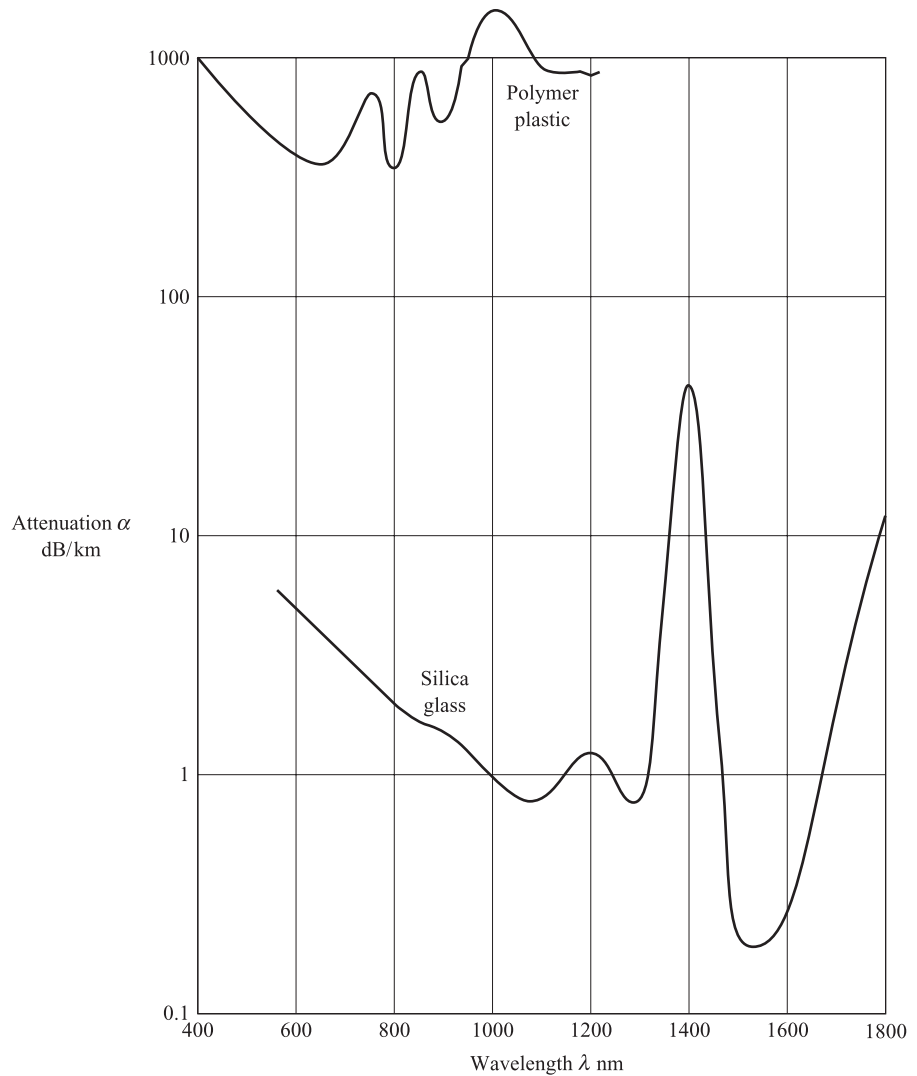
A light beam is attenuated as it propagates along a fibre; this attenuation increases with the length of the fibre. The main attenuation mechanisms are Rayleigh scattering, absorption by ions present in the fibre core, and radiation. The overall attenuation loss $\alpha\text{ dB km}^{-1}$ of a fibre of length $L\text{ km}$ is defined by:

$$\alpha = \frac{10}{L} \log_{10} \left(\frac{W_{IM}}{W_{OM}} \right) = -\frac{10}{L} \log_{10} T \quad [15.21]$$

where W_{IM} and W_{OM} are the input and output powers and T is the transmission factor. Figure 15.11 shows typical variations in α with wavelength λ for fibres made entirely of silica glass and polymer plastic. For the silica glass fibre at $\lambda = 900\text{ nm}$, $\alpha \approx 1.5\text{ dB km}^{-1}$ so that $T = 0.71$ for $L = 1\text{ km}$. For the plastic fibre at $\lambda = 900\text{ nm}$, $\alpha = 600\text{ dB km}^{-1}$ so that $T = 0.87$ for $L = 1\text{ metre}$.

Glass fibres must be used in telecommunication systems where long transmission distances are involved, but plastic fibres can be used in measurement systems where transmission links are much shorter.

Figure 15.11 Optical fibre attenuation characteristics.



15.4

Geometry of coupling of detector to source

The detector may be coupled to the source by an optical focusing system, an optical fibre or some combination of focusing systems and fibres. The aim of this section is to use the basic principles of Section 15.2.1 to study the geometry and efficiency of this coupling in some simple situations.

From eqns [15.2], [15.3] and [15.5] and Figure 15.3, the power per unit wavelength incident on an element of area ΔA of a surface, due to a Lambertian source of spectral exitance $S(\lambda)$ and area A_s is:

$$\Delta W = A_s S(\lambda) \cos \theta \Delta \omega = A_s S(\lambda) \cos \theta \frac{\Delta A}{r^2} \quad [15.22]$$

The power per unit wavelength incident on the entire surface of area A is:

$$W = A_s S(\lambda) \int_0^\omega \cos \theta \, d\omega = A_s S(\lambda) \int_0^A \frac{\cos \theta}{r^2} \, dA \quad [15.23]$$

where ω is the solid angle which the surface subtends at the source. If we make the approximations that θ is small, i.e. $\cos \theta \approx 1$, and r is a constant for all elements of the surface, then we have the approximate equations:

*Approximate equations
for power incident
on surface*

$$W(\lambda) \approx A_s \omega S(\lambda) \approx \frac{A_s A}{r^2} \cdot S(\lambda) \quad [15.24]$$

Equation [15.23] can also be used to evaluate the total power emitted by a circular source (such as an LED) in all directions, i.e. over a hemisphere which is a solid angle of 2π steradians. We have:

$$W(\lambda) = A_s S(\lambda) \pi = \pi^2 R_s^2 S(\lambda) \quad [15.23a]$$

where R_s (cm) is the radius of the source. The total source power P_s over all wavelengths is then found by integrating [15.23a]:

$$P_s = \pi^2 R_s^2 \int_0^\infty S(\lambda) \, d\lambda = \pi^2 R_s^2 R \text{ watts} \quad [15.23b]$$

where R is the radiance of the source.

15.4.1 Coupling via a focusing system

This is used in the system shown in Figure 15.2 where the transmission medium is the atmosphere. The atmosphere cannot contain a light beam and prevent it diverging, so that a converging system is necessary to focus the beam onto a detector.

We now calculate the coupling constant K_f for the situation shown in Figure 15.12(a), i.e. a circular detector receiving radiation via a circular aperture with a converging lens in the aperture. We assume that the image of the source just fills the detector area. From similar triangles we have:

$$\frac{R_D}{d} = \frac{R_2}{D}, \text{ i.e. } R_2 = \frac{D}{d} R_D \quad [15.25]$$

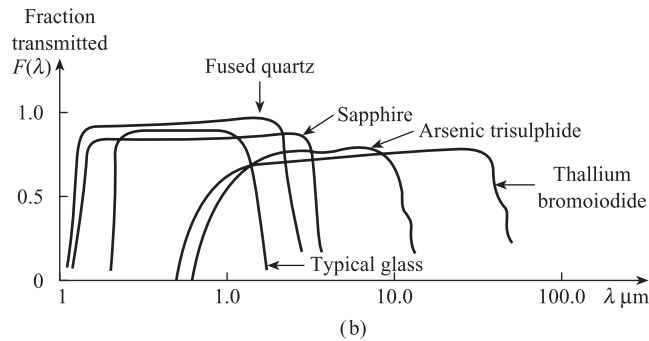
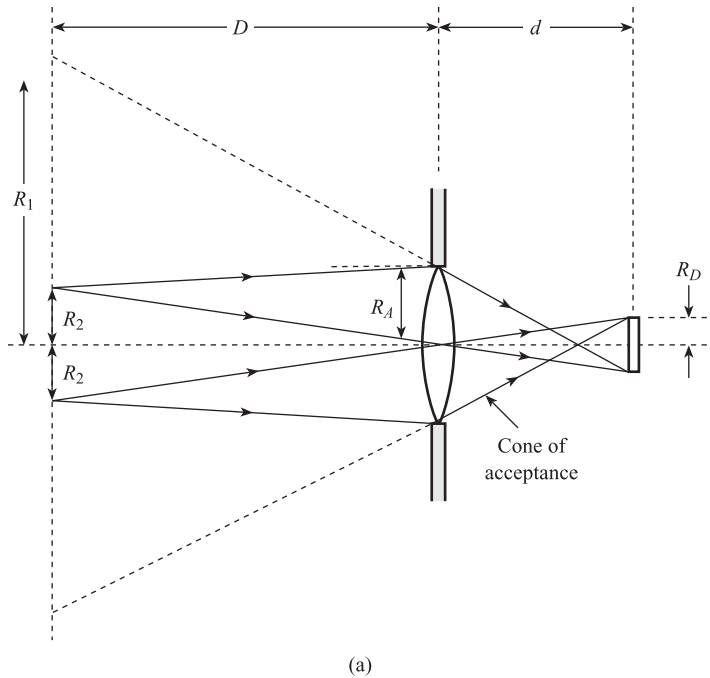
so that the area of the source scanned is:

$$A_s = \pi R_2^2 = \pi \frac{D^2}{d^2} R_D^2 \quad [15.26]$$

Assuming, for the moment, that the lens is a perfect transmitter of radiation, then all of the radiation incident onto the lens from a point on the source is focused onto the detector. This means that the appropriate solid angle is that subtended by the lens at source, i.e.

$$\omega = \frac{\pi R_A^2}{D^2} \quad [15.27]$$

Figure 15.12 Focusing systems:
(a) Geometry of lens focusing system
(b) Transmission characteristics of lens materials (after Doebelin E.O. *Measurement Systems: Application and Design*. McGraw-Hill, New York, 1976, pp. 558–61).



In eqn [15.24] the effective source power $S(\lambda)$ is the power $W_{OM}(\lambda)$ leaving the transmission medium; thus the power coupled to the detector is:

$$W_D(\lambda) = K_F W_{OM}(\lambda) \quad [15.28]$$

where

$$K_F = A_s \omega = \frac{\pi^2 R_D^2 R_A^2}{d^2} \quad [15.29]$$

We note that K_F is independent of the distance D between source and lens. This is because the amount of radiation received is limited by the ‘cone of acceptance’ which is defined by R_A , R_D and d but not D . Thus provided this cone is filled with radiation, the sensitivity of the radiation receiver will be independent of the distance

between source and receiver. This is of great practical importance since it means that an instrument will not need recalibration if its distance from the source is changed.

From Figure 15.12(a) we note that if the lens is removed, then radiation from a bigger source area A_s is required to fill the cone of acceptance. However, the appropriate solid angle ω is now that subtended by the detector at the source and is therefore smaller. Since the area of source available may be limited, or we may wish to examine a small area of the source, then solid angle is a better measure of performance and a lens is preferable. For the lens we have $1/D + 1/d = 1/f$ so that if D is large, then d may be replaced by f in eqn [15.29].

In practice the material of a lens is not a perfect transmitter and the fraction of radiation transmitted depends critically on wavelength λ . These transmission characteristics are defined by $F(\lambda)$ = fraction of power transmitted by material at λ , and eqn [15.29] must be modified to:

$$W_D(\lambda) = K_F F(\lambda) W_{OM}(\lambda) \quad [15.30]$$

Figure 15.12(b) shows $F(\lambda)$ for lens and window materials in common use. We see that glass, which will transmit visible radiation, is opaque to wavelengths greater than $2 \mu\text{m}$. For longer wavelengths either lenses of special materials, such as arsenic trisulphide, or mirrors should be used.

15.4.2 Coupling via an optical fibre

If the transmission medium is capable of containing a light beam as with an optical fibre, then it can be used to couple the detector to a source. Here there are two constants involved (Figure 15.1): K_{SM} describes the coupling of source to medium, and K_{MD} describes the coupling of the medium to the detector.

We first calculate K_{SM} for the situation shown in Figure 15.13(a), which is a step-index optical fibre with a circular core receiving radiation from a circular source. The core radius R_c is less than the source radius R_s . Only rays within the cone of acceptance defined by the maximum angle of acceptance θ_0^{MAX} can be transmitted through the core. The corresponding useful source radius R_1 is defined by the cone of acceptance, i.e.

$$\frac{R_1}{D_1} = \tan \theta_0^{\text{MAX}}$$

Assuming that $R_1 \leq R_s$ where R_s is the total source radius, then the useful source area is:

$$A_s = \pi R_1^2 = \pi D_1^2 \tan^2 \theta_0^{\text{MAX}} \quad [15.31]$$

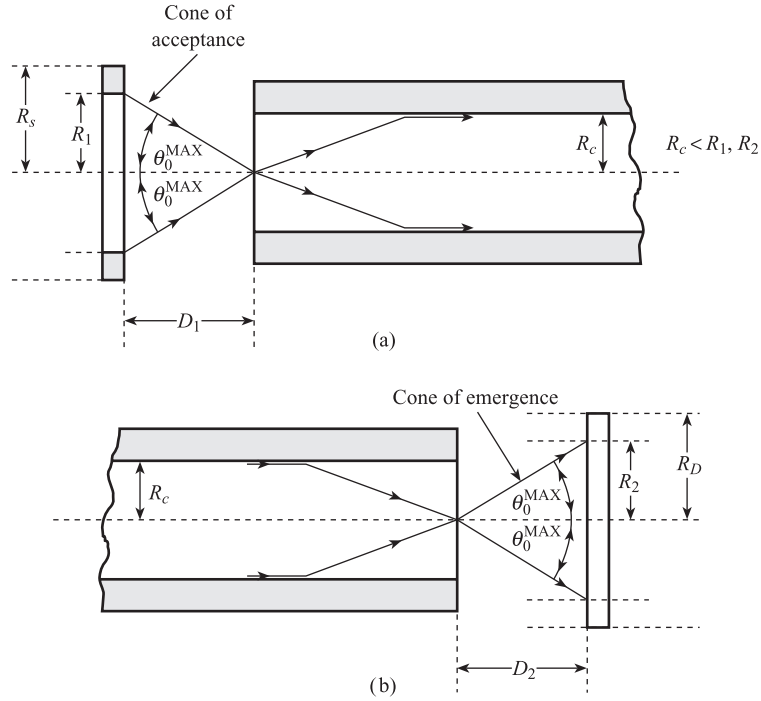
The solid angle ω which the fibre core subtends at the source is approximately:

$$\omega \approx \frac{\pi R_c^2}{D_1^2} \quad [15.32]$$

If the source spectral exitance is $S(\lambda)$ then, from eqn [15.24], the power per unit wavelength launched into the fibre is approximately:

$$W_{IM}(\lambda) \approx A_s \omega S(\lambda) \approx \pi^2 R_c^2 \tan^2 \theta_0^{\text{MAX}} S(\lambda) \quad [15.33]$$

Figure 15.13 Coupling of detector to source via an optical fibre:
(a) Coupling of source to fibre
(b) Coupling of fibre to detector.



For small θ_0^{MAX} , $\tan \theta_0^{\text{MAX}} \approx \sin \theta_0^{\text{MAX}}$; also the numerical aperture NA of a fibre surrounded by air is $\sin \theta_0^{\text{MAX}}$. Thus the coupling constant K_{SM} is given approximately by:

*Coupling constant
source to fibre $R_c < R_s$*

$$K_{SM} = \frac{W_{IM}(\lambda)}{S(\lambda)} \approx \pi^2 R_c^2 (\text{NA})^2 \quad [15.34]$$

K_{SM} is also equal to the ratio P_{IM}/R , where P_{IM} is the input power to the fibre over all wavelengths and R the source radiance. In a situation where $R_1 > R_s$, i.e. the semi-angle θ of the inlet cone is less than θ_0^{MAX} , a converging lens can be used to increase θ to θ_0^{MAX} .

If the core radius R_c is greater than the source radius R_s then the appropriate equation for K_{SM} is:

*Coupling constant
source to fibre $R_c > R_s$*

$$K_{SM} = \frac{W_{IM}(\lambda)}{S(\lambda)} = \frac{P_{IM}}{R} \quad [15.35]$$

$$= \pi^2 R_s^2 (\text{NA})^2$$

We now calculate K_{MD} for the situation shown in Figure 15.13(b), which is a circular detector receiving radiation from a step-index fibre with a circular core. The power per unit wavelength leaving the fibre is $W_{OM}(\lambda)$, which depends on the power input to the fibre $W_{IM}(\lambda)$ and the fibre transmission characteristics $T(\lambda)$. All of this power is contained within a cone of emergence whose semi-angle is equal to θ_0^{MAX} ,

the maximum angle of acceptance. The corresponding useful detector radius R_2 is defined by the cone of emergence as:

$$R_2 = D_2 \tan \theta_0^{\text{MAX}}$$

Provided $R_D \geq R_2$ where R_D is the total detector radius, then all of the power leaving the fibre is incident on the detector, i.e.

$$K_{MD} = \frac{W_D(\lambda)}{W_{OM}(\lambda)} = 1$$

If, however, $R_D < R_2$, then only radiation within a cone of semi-angle θ , less than θ_0^{MAX} , is incident on the detector. The power incident on the detector is correspondingly reduced by a factor (ω/ω_0) where ω and ω_0 are the solid angles corresponding to θ and θ_0^{MAX} respectively, i.e.

$$W_D(\lambda) = \left(\frac{\omega}{\omega_0} \right) W_{OM}(\lambda), \text{ i.e. } K_{MD} = \left(\frac{\omega}{\omega_0} \right) \quad [15.36]$$

Since $\omega \approx \frac{\pi R_D^2}{D_2^2}$, $\omega_0 = \frac{\pi R_2^2}{D_2^2}$ and $\text{NA} \approx \tan \theta_0^{\text{MAX}}$,

$$K_{MD} \approx \frac{R_D^2}{R_2^2} \approx \frac{R_D^2}{D_2^2 (\text{NA})^2} \quad [15.37]$$

15.5

Detectors and signal conditioning elements

The detector converts the incident radiant power into an electrical output, that is a resistance or small voltage. A signal conditioning element, such as a bridge and/or amplifier, is usually required to provide a usable voltage signal.

The four main performance characteristics of detectors are:

- (a) Responsivity (sensitivity), K_D
- (b) Time constant, τ
- (c) Wavelength response, $D(\lambda)$
- (d) Noise equivalent power (NEP) or factor of merit, D^* .

The sensitivity K_D is the change in detector output (ohms or volts) for a 1 W change in incident power. The wavelength response $D(\lambda)$ is the ratio between the sensitivity at wavelength λ and the maximum sensitivity; it allows for the detector not responding equally to all wavelengths, that is not *using* all wavelengths. The noise equivalent power (NEP) is the amount of incident power in watts required to produce an electrical signal of the same root-mean-square voltage as the background noise. The factor of merit D^* has been introduced in order to compare the signal-to-noise ratio of different detectors, of different sizes used with different amplifiers. It is defined by:^[4]

$$D^* = \frac{(S/N)(A\Delta f)^{1/2}}{P} \text{ cm Hz}^{1/2} \text{ W}^{-1}$$

where S/N is the signal-to-noise ratio observed when P watts of power is incident on a detector of area A cm² used with an amplifier of bandwidth Δf . There are two main types of detector in common use, thermal and photon.

15.5.1 Thermal detectors

Here the incident power heats the detector to a temperature T_D °C which is above the surrounding temperature T_S °C. The detector is usually a resistive or thermoelectric sensor which gives a resistance or voltage output; this depends on temperature difference $T_D - T_S$ and thus incident power.

Thermal detectors respond equally to all wavelengths in the incident radiation (see Figure 15.15 below), so that in effect:

$$D(\lambda) = 1, \quad 0 \leq \lambda \leq \infty$$

These detectors are used in radiation temperature measurement systems where the power emitted from a hot body source $S(\lambda, T)$ depends on temperature T .

Since $D(\lambda) = 1$ for all λ , the total power used by the detector is (see Figure 15.2):

$$P_D = K_F \int_0^\infty S(\lambda, T) T(\lambda) F(\lambda) d\lambda \quad [15.38]$$

In order to examine the factors affecting both the sensitivity and time constant of a thermal detector, we now calculate the transfer function relating detector temperature T_D to power P_D . The heat balance equation for the detector is:

$$P_D - UA(T_D - T_S) = MC \frac{dT_D}{dt} \quad [15.39]$$

where M = detector mass (kg)

C = detector specific heat ($\text{J kg}^{-1} \text{ }^\circ\text{C}^{-1}$)

A = detector surface area (m^2)

U = heat transfer coefficient ($\text{W m}^{-2} \text{ }^\circ\text{C}^{-1}$).

Rearranging, we have:

$$T_D + \tau \frac{dT_D}{dt} = \frac{1}{UA} P_D + T_S \quad [15.40]$$

where time constant $\tau = MC/UA$. The transfer function relating corresponding deviation variables ΔT_D , ΔP_D and ΔT_S is:

Transfer function for thermal detector

$$\Delta \bar{T}_D(s) = \left(\frac{1/UA}{1 + \tau s} \right) \Delta \bar{P}_D(s) + \left(\frac{\Delta \bar{T}_S(s)}{1 + \tau s} \right) \quad [15.41]$$

In the steady state, $dT_D/dt = 0$ so that [15.40] reduces to:

$$T_D = \frac{1}{UA} P_D + T_S \quad [15.42]$$

Commonly used thermal detectors are **thermopiles** (Figure 15.14(a)), which consist of a large number of thermocouples in series, and **bolometers** (Figure 15.14(b)), which are metal or semiconductor (thermistor) resistance material in the form of thin films or flakes. In both cases the surface of the detector is blackened to maximise the absorption of incoming radiation. For a thermopile consisting of n thermocouples in series,

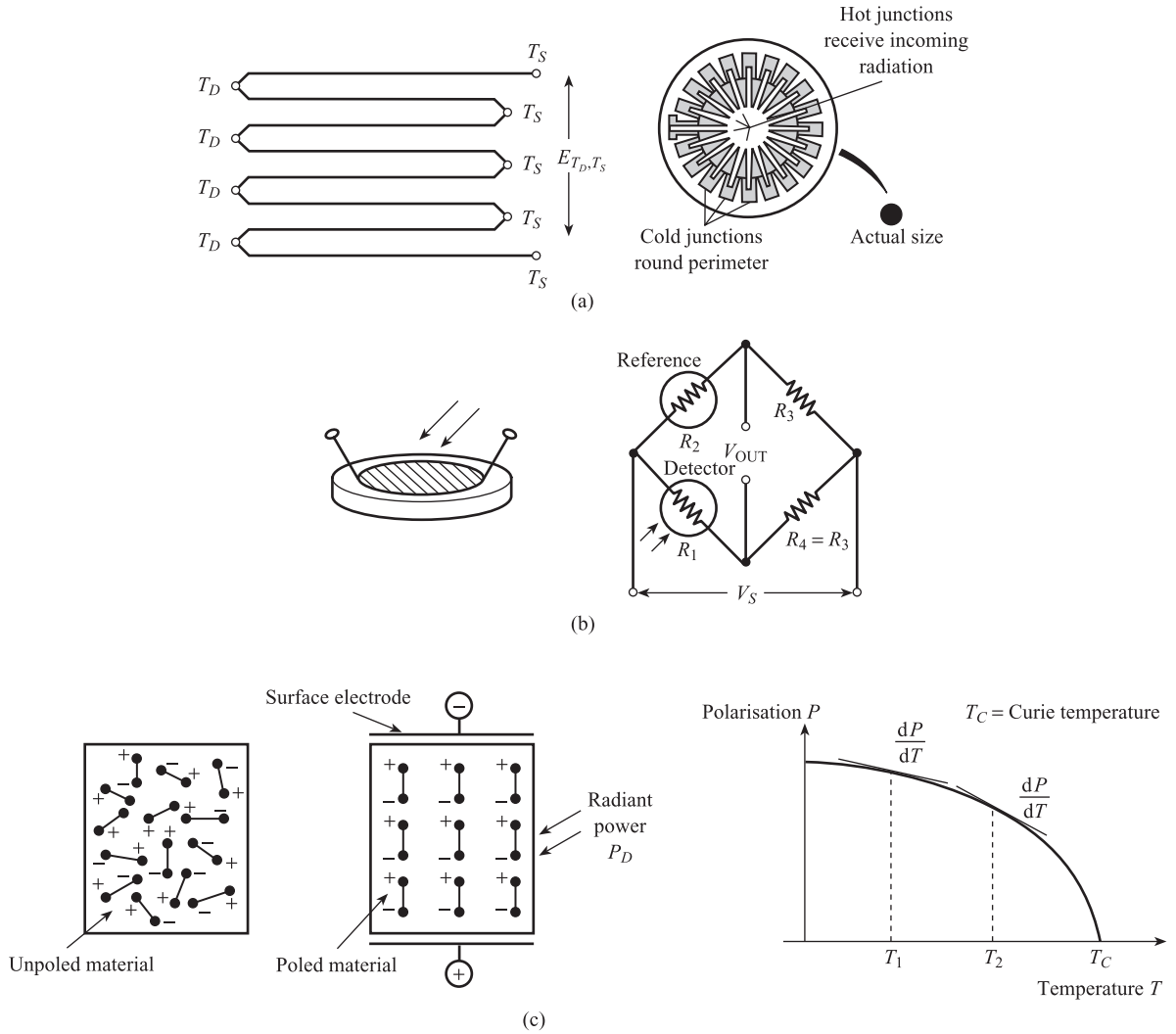


Figure 15.14
Thermal detectors:
(a) Thermopile
(b) Bolometer
(c) Pyroelectric.

with hot junction at T_D °C and reference junction at T_S °C (the temperature of the surroundings), the e.m.f. is given approximately by (Section 8.5)

$$E_{T_D, T_S} \approx na_1(T_D - T_S) \quad [15.43]$$

From [15.42] the equilibrium temperature difference is $T_D - T_S = (1/UA)P_D$, giving:

$$E_{T_D, T_S} = \left(\frac{na_1}{UA} \right) P_D \quad [15.44]$$

i.e. the detector sensitivity $K_D = \frac{na_1}{UA}$ mV/W.

The bridge circuit shown in Figure 15.14(b) gives an output voltage approximately proportional to power P_D . Here R_1 is a radiation-detecting bolometer at T_D °C, R_2 a reference bolometer at T_S °C and R_3, R_4 fixed equal resistors. This circuit has already

been discussed in Section 9.1 (Figure 9.4(a)). For metal resistive elements of temperature coefficient $\alpha \text{ K}^{-1}$ we have (from eqn [9.17]):

$$V_{\text{OUT}} \approx V_s \frac{R_0}{R_3} \alpha (T_D - T_S) \quad [15.45]$$

provided $R_3 \gg R_0$ (resistance of bolometer at 0°C). This gives:

$$V_{\text{OUT}} \approx \frac{V_s \alpha R_0}{U A R_3} \cdot P_D \quad [15.46]$$

indicating the system output voltage is approximately proportional to P_D and independent of T_S .

The time constant τ of a thermal detector is minimised by using thin flakes or films which have a large area-to-volume ratio that is a small value of M/A . However, τ cannot be reduced much below a few milliseconds because of the low heat transfer coefficient U between the detector and the surrounding air.

Certain materials exhibit the **pyroelectric** effect. These are man-made ferroelectric ceramics which also show piezoelectric properties (Section 8.7). A typical material is lithium tantalate which has a Curie temperature of 610°C . The principle of ferroelectricity is shown in Figure 15.14 (c). The ceramic is composed of a mass of minute crystallites; provided the ceramic is below the Curie temperature, each crystallite behaves as a small electric dipole. Normally the material is **unpoled**, i.e. the electric dipoles are randomly orientated with respect to each other. The material can be **poled**, i.e. the dipoles lined up, by applying an electric field when the ceramic is just below the Curie temperature. After the material has cooled and the applied field has been removed, the dipoles remain lined up, leaving the ceramic with a residual polarisation P . The pyroelectric effect arises because the incident radiant power causes the ceramic temperature T to increase; P decreases with T according to the non-linear relation shown in Figure 15.14(c). This reduction in P causes a decrease in the alignment of the dipoles and a corresponding reduction in the positive and negative charges on opposite surfaces of the crystal. The sensor is formed by depositing metal electrodes on these surfaces. The lower electrode acquires an excess positive charge which balances the negative charge on the lower surface; the upper electrode acquires an excess negative charge which balances the positive charge on the upper surface. If Δq is the excess charge caused by a temperature rise ΔT then:

$$\Delta q = \left(\frac{dP}{dT} \right) A \Delta T \quad [15.47]$$

where A is the area of the electrodes and dP/dT the slope of the P - T characteristics. The electrodes and the rectangular block of dielectric ceramic form a parallel plate capacitor C_N . The ceramic can be regarded as either a charge generator Δq in parallel with C_N or a Norton current source i_N in parallel with C_N (Section 5.1.3) where:

$$i_N = \frac{dq}{dt} = A \frac{dP}{dT} \cdot \frac{dT}{dt} \quad [15.48]$$

From eqn [15.42], we see that for constant power input P_D , the temperature rise ΔT is constant with time. If ΔT is constant with time then $dT/dt = 0$ and from eqn [15.48] $i_N = 0$; this means that the voltage across capacitance C_N is zero and the

basic sensor cannot be used for steady-state measurements of radiant power. This problem is solved by connecting the pyroelectric sensor to a **charge amplifier** (Section 8.7). This is an integrator with an output voltage proportional to $\int i_N dt$, i.e. charge Δq , temperature rise ΔT and incident radiant power P_D .

A typical pyroelectric detector of size 2.7×0.9 mm has a responsivity or sensitivity of 3200 V/W, noise equivalent power of 1×10^{-9} W and D^* of 1.4×10^8 cm Hz^{1/2} W⁻¹. When used with a standard coated silicon window, the wavelength response $D(\lambda)$ is reduced to 7 to 14 μ m.

15.5.2 Photon detectors

Photon detectors are mostly semiconductor devices in which incident photons of radiation cause electrons to be excited from the valence band to the conduction band, thereby causing a measurable electrical effect. These detectors only respond to photons whose energy hc/λ is approximately equal to the energy gap E_G between valence and conduction bands. This means that photon detectors have a narrow wavelength response $D(\lambda)$ with peak wavelength $\lambda_0 \approx hc/E_G$. Photon detectors normally have higher responsivities than thermal detectors. Because they rely on atomic processes which are inherently faster than bulk heat transfer processes, photon detectors usually have shorter time constants than thermal detectors. There are two main types of photon detector: **photoconductive** and **photovoltaic**.

Photoconductive detectors

Here the presence of excited electrons in the conduction band causes an increase in electrical conductivity and a decrease in electrical resistance. The resistance R of a photoconductive detector therefore decreases as the total power P_D increases; the relationship is extremely non-linear and is best expressed in the logarithmic form (Figure 15.15(a)):

$$\log_{10} R = a - b \log_{10} P_D \quad [15.49]$$

Figure 15.15(b) shows the wavelength response $D(\lambda)$ for three photoconductive detectors in common use. Cadmium sulphide has $\lambda_0 \approx 0.6$ μ m and is thus suitable for visible radiation. Lead sulphide with $\lambda_0 \approx 3.0$ μ m and indium antimonide with $\lambda_0 \approx 5.3$ μ m are suitable for infrared radiation.

It is important that the detector wavelength characteristics $D(\lambda)$, the source characteristics $S(\lambda)$ and the transmission medium characteristics $T(\lambda)$ all match each other as closely as possible. Thus a cadmium sulphide detector is ideal for measuring the temperature of a target at 4800 K ($\lambda_p \approx 0.6$ μ m) while indium antimonide is ideal for a target at 550 K ($\lambda_p \approx 5.3$ μ m). A typical indium antimonide detector of dimensions 6.0 mm \times 0.5 mm has $K = 7 \times 10^3$ V W⁻¹, $\tau = 5$ μ s and NEP = 1.6×10^{-11} W. Photoconductive detectors must be incorporated into deflection bridge circuits to convert their output into a voltage signal.

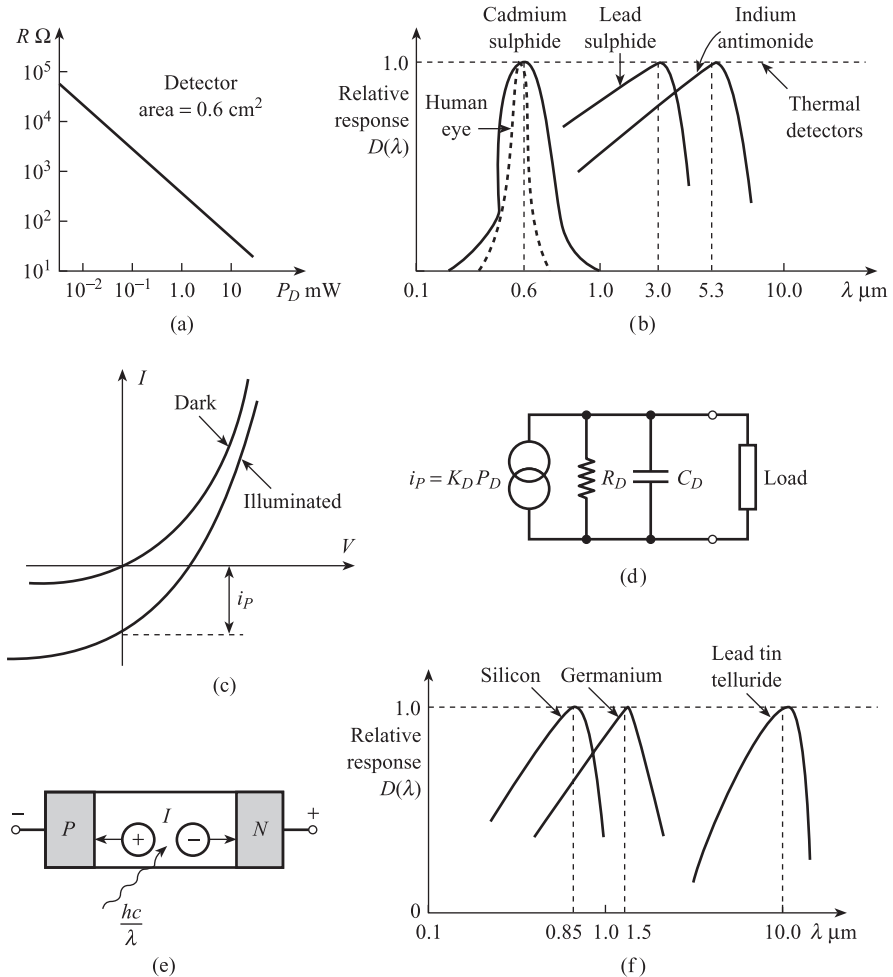
Photovoltaic detectors^[2,3,5]

These are photodiodes made by forming a junction of *p*-type and *n*-type extrinsic semiconductors. Figure 15.15(c) shows typical current/voltage characteristics for a photodiode under dark and illuminated conditions. The effect of the incident radiation

Figure 15.15

Photon detectors:

- (a) Resistance–power relation for cadmium sulphide
 (b) Wavelength response of photoconductive detectors
 (c) Current–voltage characteristics for photodiode
 (d) Norton equivalent circuit for photodiode
 (e) Construction of *pin* photodiode
 (f) Wavelength response of photovoltaic detectors.



is to increase the reverse saturation current by an amount i_p , which is termed the **photo-current**. The photocurrent is proportional to total power P_D used by the detector:

$$i_p = K_D P_D \quad [15.50]$$

where $K_D \text{ A W}^{-1}$ is the sensitivity or responsivity. This type of detector can therefore be represented as a Norton current source in parallel with the diode resistance R_D and capacitance C_D (Figure 15.15(d)). Lead–tin telluride is an example of an infrared photodiode. This operates at 77 K with a typical K_D of 5 A W^{-1} and wavelength response $D(\lambda)$ between 7 and $14 \mu\text{m}$ with peak wavelength $\lambda_0 \approx 10 \mu\text{m}$ (Figure 15.15(f)).

Figure 15.15(e) shows the construction of a *pin* diode; this has an extra layer of intrinsic (undoped) *i* material between *p* and *n* layers. The incident photons create additional electron-hole pairs in this region with a corresponding increase in photocurrent and responsivity over a comparable *pn* diode. A typical silicon *pin* photodiode has an active area of 1 mm^2 , a responsivity $K_D \approx 0.55 \text{ A W}^{-1}$, a peak wavelength $\lambda_0 \approx 0.85 \mu\text{m}$, and $D(\lambda)$ as shown in Figure 15.15(f). The wavelength response of this photodiode is therefore well matched to $S(\lambda)$ for GaAlAs LED and ILD sources; also their small size makes them ideal for coupling to optical fibres. Germanium *pin*

diodes with $K_D \approx 0.5 \text{ A W}^{-1}$ and $\lambda_0 \approx 1.5 \mu\text{m}$ have a $D(\lambda)$ more suited to longer wavelength applications.

The principle of operation of avalanche photodiode (APD) devices differs from that of *pin* diodes in one major respect. A *pin* diode converts one photon to one electron, whereas in an APD multiplication takes place, which results in many electrons at the output for each incident photon.

15.6

Measurement systems

Comprehensive reviews of optical measurement systems, especially involving optical fibre sensors, are given in references [6] and [7].

15.6.1 Modulation of intensity by source

Since the power emitted by a hot body source depends critically on source temperature (eqns [15.6] and [15.10]), systems of the type shown in Figure 15.2 are commonly used for remote temperature measurement. There are two basic types of system: **broadband** and **narrowband**.

Broadband

These systems use all wavelengths present in the incoming radiation and are often referred to as total radiation pyrometers. A thermal detector is therefore used, and from eqns [15.38], [15.10] and [15.6] the total power used by the detector is:

$$P_D = \frac{C_1 K_F}{\pi} \int_0^\infty \frac{\varepsilon(\lambda, T) T(\lambda) F(\lambda) d\lambda}{\lambda^5 \left[\exp\left(\frac{C_2}{\lambda T}\right) - 1 \right]} \quad [15.51]$$

The integral can be evaluated numerically if $\varepsilon(\lambda, T)$, $T(\lambda)$ and $F(\lambda)$ are known. However, if we assume that $\varepsilon(\lambda, T)$, $T(\lambda)$ and $F(\lambda)$ have constant values ε , T_M and F respectively for all λ , T , then using eqn [15.7]

$$P_D = \frac{1}{\pi} \varepsilon T_M K_F F \int_0^\infty \frac{C_1 d\lambda}{\lambda^5 \left[\exp\left(\frac{C_2}{\lambda T}\right) - 1 \right]} = \frac{1}{\pi} \sigma \varepsilon T_M K_F F T^4$$

The corresponding detector output signal is:

*Detector output signal
for broadband
temperature system*

$$V_T = K_D P_D = \frac{K_D}{\pi} \sigma \varepsilon T_M K_F F T^4 \quad [15.52]$$

The above assumptions represent a considerable oversimplification, and even if they are justified there is still the problem of uncertainties in the values of ε , T_M , etc. For these reasons the system should be calibrated experimentally using a standard source

of known emissivity. If the system is then used with a process source of different emissivity then a correction must be made.

Narrowband

These systems use photon detectors so that only a narrow band of wavelengths is used. In some systems a narrow pass-band radiation filter $G(\lambda)$ is used to further restrict the range of wavelengths incident on the detector. For these systems, the wavelength response $G(\lambda)D(\lambda)$ of the combined filter and detector can be approximated by the ideal band-pass filter characteristics of Figure 15.16(a). Thus the expression for total power used is:

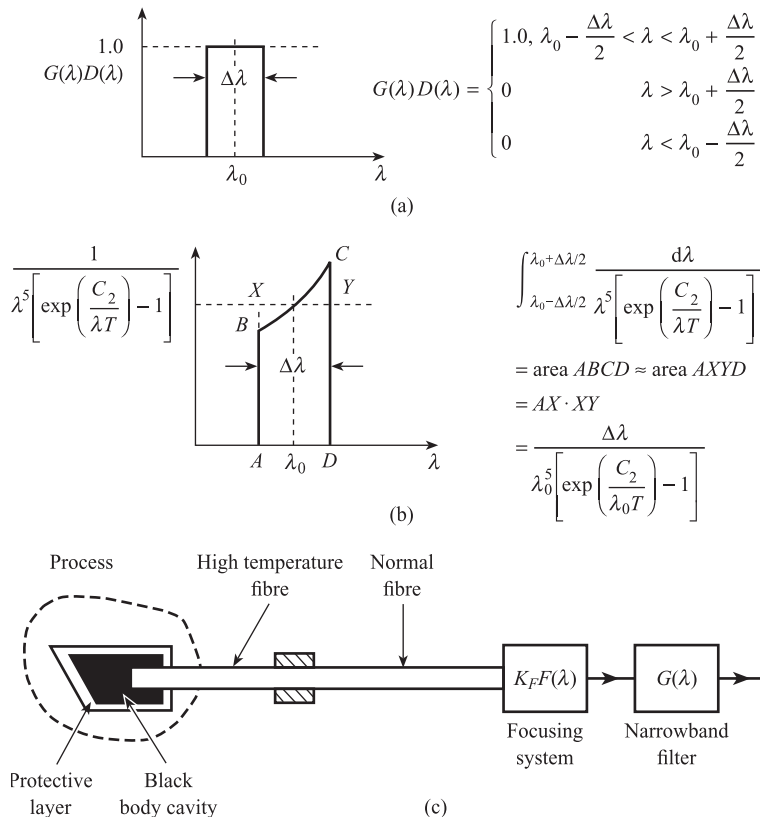
$$P_D = \frac{1}{\pi} C_1 K_F \int_0^{\infty} \frac{\epsilon(\lambda, T) T(\lambda) F(\lambda) G(\lambda) D(\lambda) d\lambda}{\lambda^5 \left[\exp\left(\frac{C_2}{\lambda T}\right) - 1 \right]} \quad [15.53]$$

which reduces to:

$$P_D = \frac{1}{\pi} C_1 K_F \int_{\lambda_0 - \Delta\lambda/2}^{\lambda_0 + \Delta\lambda/2} \frac{\epsilon(\lambda, T) T(\lambda) F(\lambda) d\lambda}{\lambda^5 \left[\exp\left(\frac{C_2}{\lambda T}\right) - 1 \right]} \quad [15.54]$$

Figure 15.16

Narrowband radiation temperature system
(a) Wavelength characteristics
(b) Evaluation of integral
(c) Black body – optical fibre system.



The assumptions $\varepsilon(\lambda, T) = \varepsilon$, $T(\lambda) = T_M$ and $F(\lambda) = F$ are far more justified for a narrow band of wavelengths and give:

$$P_D = \frac{1}{\pi} C_1 \varepsilon T_M K_F F \int_{\lambda_0 - \Delta\lambda/2}^{\lambda_0 + \Delta\lambda/2} \frac{d\lambda}{\lambda^5 \left[\exp\left(\frac{C_2}{\lambda T}\right) - 1 \right]} \quad [15.55]$$

The integral is evaluated approximately in Figure 15.16(b) to give:

$$\begin{aligned} P_D &= \frac{1}{\pi} C_1 \varepsilon T_M K_F F \frac{\Delta\lambda}{\lambda_0^5 \left[\exp\left(\frac{C_2}{\lambda_0 T}\right) - 1 \right]} \\ &\approx \frac{1}{\pi} C_1 \varepsilon T_M K_F F \cdot \frac{\Delta\lambda}{\lambda_0^5} \exp\left(-\frac{C_2}{\lambda_0 T}\right) \end{aligned} \quad [15.56]$$

The approximation is valid since $\exp(C_2/\lambda_0 T) \gg 1$; for example if $\lambda_0 = 1 \mu\text{m}$, $T = 10^3 \text{ K}$, $(C_2/\lambda_0 T) = 14.4$, $\exp(C_2/\lambda_0 T) = 1.8 \times 10^6$. The detector output signal is thus:

*Output signal for
narrowband radiation
pyrometer*

$$\begin{aligned} V(T) &= K_D P_D \\ &= \frac{1}{\pi} C_1 \varepsilon T_M K_F F K_D \frac{\Delta\lambda}{\lambda_0^5} \exp\left(-\frac{C_2}{\lambda_0 T}\right) \end{aligned} \quad [15.57]$$

The narrow band of wavelengths must be chosen to coincide with a ‘window’ in the transmission characteristics so that T_M is reasonably large. Again the system should be calibrated experimentally using a standard source of known emissivity and a correction applied if it is subsequently used with a process source of different emissivity. The above problems of variations of source emissivity and atmospheric transmission characteristics may be solved using the system shown in Figure 15.16(c). Here a black body cavity is inserted in the process and radiation is transmitted to the radiation receiver using an optical fibre system rather than the atmosphere. The fibre system consists of a short run of special fibre, which can withstand the high process temperatures, connected to a much longer length of normal fibre.

15.6.2 Modulation of intensity by transmission medium

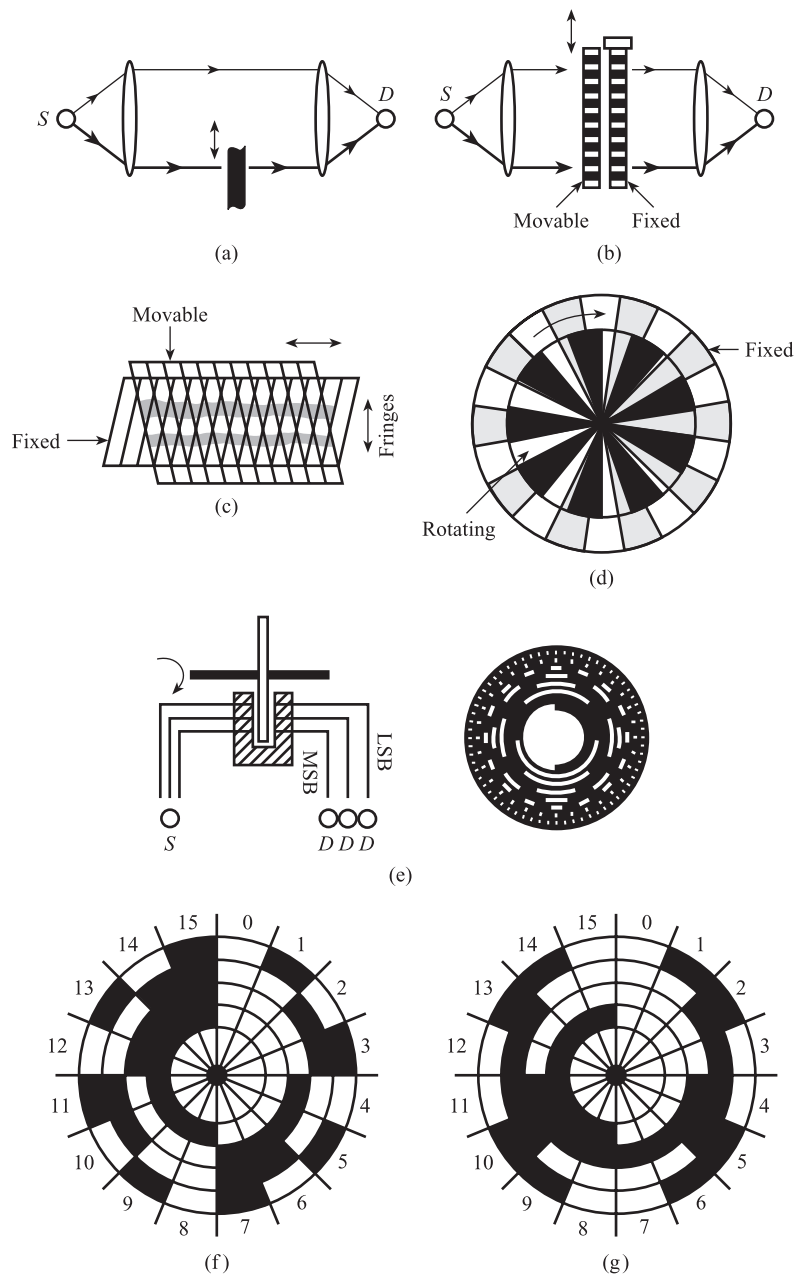
These are systems of the type shown in Figure 15.1, where the measured variable alters the characteristics of the transmission medium and so modulates the intensity of the radiation reaching the detector. There are several ways in which this modulation can be achieved.

Intensity modulation using shutters and gratings

The simplest type of shutter displacement sensor is shown in Figure 15.17(a). Figures 15.17(b), (c) and (d) show moiré fringe gratings for the digital measurement of linear and angular position. In the linear type there are two finely ruled gratings

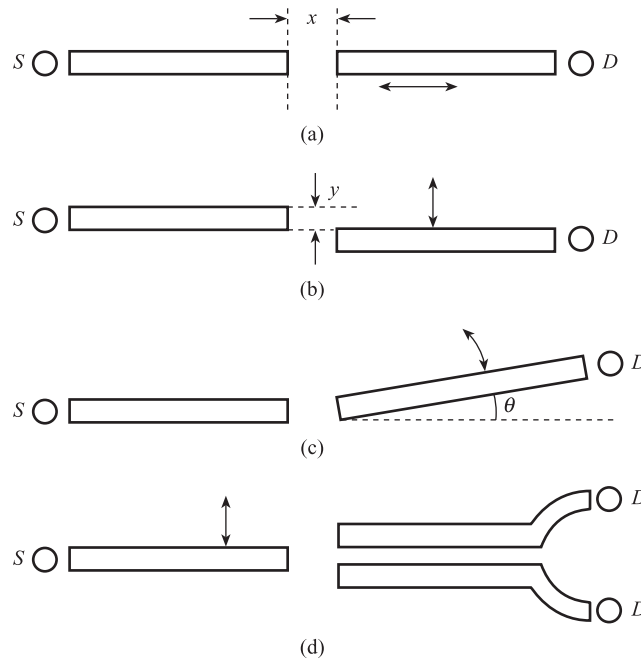
Figure 15.17 Intensity modulation using shutters and gratings:

- (a) Shutter modulator
- (b) Grating modulator
- (c) Linear displacement moiré fringe gratings
- (d) Angular displacement moiré fringe gratings
- (e) Digital encoder disc
- (f) Binary coded disc
- (g) Gray coded disc.



of the same pitch P , slightly angled to each other. Relative movement of the gratings in a horizontal direction causes a series of dark fringes to move vertically across the sensor, giving an approximately sinusoidal variation in light intensity and detector output signal. In the angular case, one grating has N lines, the other $N + 1$ lines (N is typically between 50 and 1200); for every complete revolution of the gratings there are N complete revolutions of the fringe pattern and N cycles of the detector output signal. Thus in both cases the exact displacement can only be established by counting the number of detector output cycles; moiré gratings are therefore often referred to as **incremental encoders**.

Figure 15.18 Intensity modulation using relative displacement of fibres:
 (a) Longitudinal
 (b) Transverse
 (c) Angular
 (d) Differential.



Figures 15.17(e), (f) and (g) show coded disc systems for the digital measurement of angular position. Here the disc is marked out in transparent and opaque segments according to the required digital code. **Gray code** (Figure 15.17(g)) is a cyclic code in which only one digit can change between two consecutive sectors; this is in contrast to binary code (Figure 15.17(f)), where several digits may change between consecutive sectors. If the detectors are misaligned slightly, then with a binary coded disc false codes can occur during the transition from one sector to the next. This cannot occur with Gray code; Figure 15.17(e) shows a typical eight-digit Gray coded disc. The output digital code uniquely specifies the angular position of the disc, and coded discs are often referred to as **absolute encoders**.

Intensity modulation using relative displacement of fibres

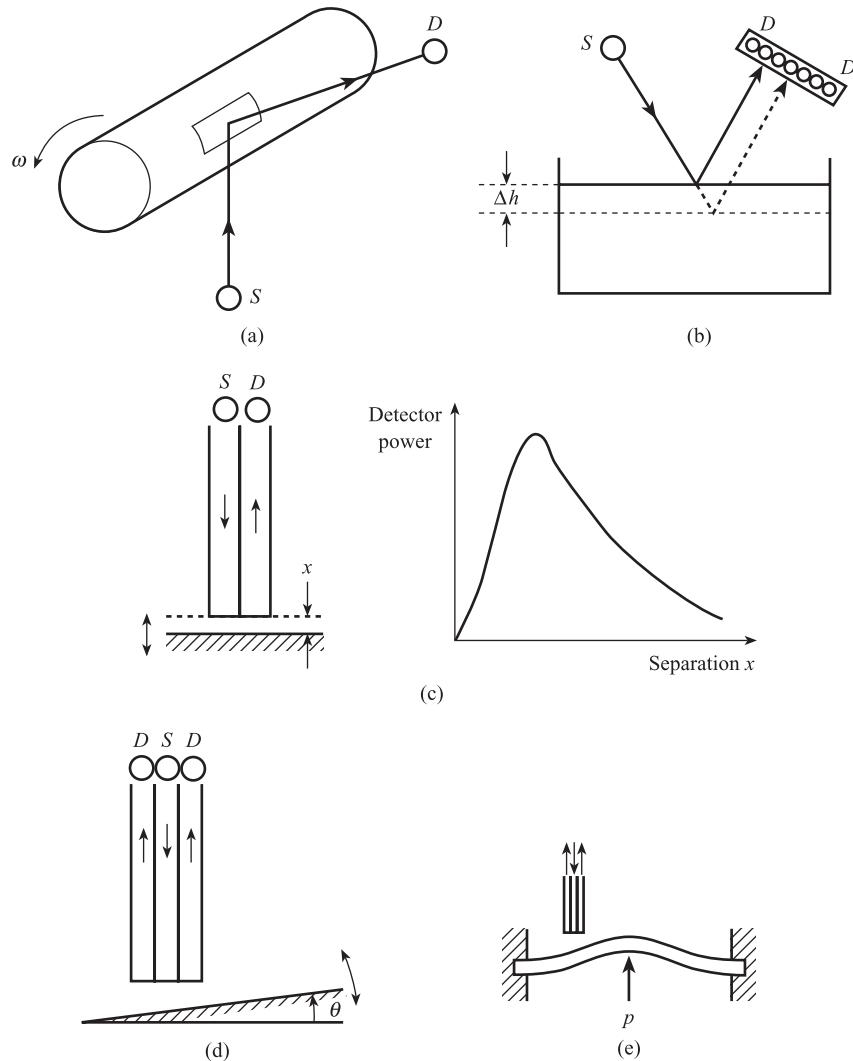
Figure 15.18 shows four possible arrangements for the measurement of small linear or angular displacements. Here the intensity of the radiation incident on the detector is modulated according to the relative displacement of two optical fibres. The underlying principles have already been discussed in Section 15.4.2. For example in Figure 15.18(a), as x is decreased the solid angle ω of the cone of rays into the second fibre increases, causing the power incident on the detector to increase. This effect continues until the cone of rays into the second fibre corresponds to the cone of emergence of the first fibre. The arrangements shown in Figures 15.18(a), (b) and (c) are affected by fibre misalignment, vibration and source variations; the differential system shown in Figure 15.18(d) should be unaffected by source variations.

Intensity modulation using reflection

Figure 15.19(a) shows a simple system for the remote measurement of angular velocity. The rotating mechanism has a reflective strip on its surface so that once in every

Figure 15.19 Intensity modulation using reflection:

- (a) Angular velocity sensor
 (b) Level sensor
 (c) Two-fibre linear displacement sensor and characteristics
 (d) Three-fibre angular displacement sensor
 (e) Three-fibre pressure sensor.



revolution light is reflected back directly to the detector. This means that the number of detector pulses per second is equal to the revolutions of the mechanism per second.

In the liquid level measurement system shown in Figure 15.19(b) a change in level Δh causes the reflected beam to be displaced laterally by an amount proportional to Δh . This change in lateral displacement is sensed by a two-dimensional array of detectors.

Figure 15.19(c) shows a two-fibre linear displacement sensor and its characteristics. These characteristics show the non-linear relationship between the power incident on the detector and the separation x of fibres and reflecting surface. For small x , the detector power increases with x because the area of overlap between the cones of emergence and acceptance increases. For larger x , detector power reaches a maximum value and then decreases according to an inverse square law. This system is affected by vibration, changes in source intensity and reflection coefficient; there are also two values of separation for a given value of detector power.

A potentially more accurate sensor is the three-fibre angular displacement sensor shown in Figure 15.19(d).^[8] Here there is a single source fibre and two detector fibres; changing the angle θ alters the ratio of the powers collected by the two return fibres and the ratio of detector output signals. This ratio depends only on θ and the refractive indices of the fibre core and cladding; it is independent of source intensity, reflection coefficient and fibre-reflector separation. One application of this is the three-fibre pressure sensor shown in Figure 15.19(e). Here the elastic element is a thin flat circular diaphragm clamped around the circumference (Figure 8.21). The fibre system is positioned close to a point on the diaphragm where the angular deformation is maximum.

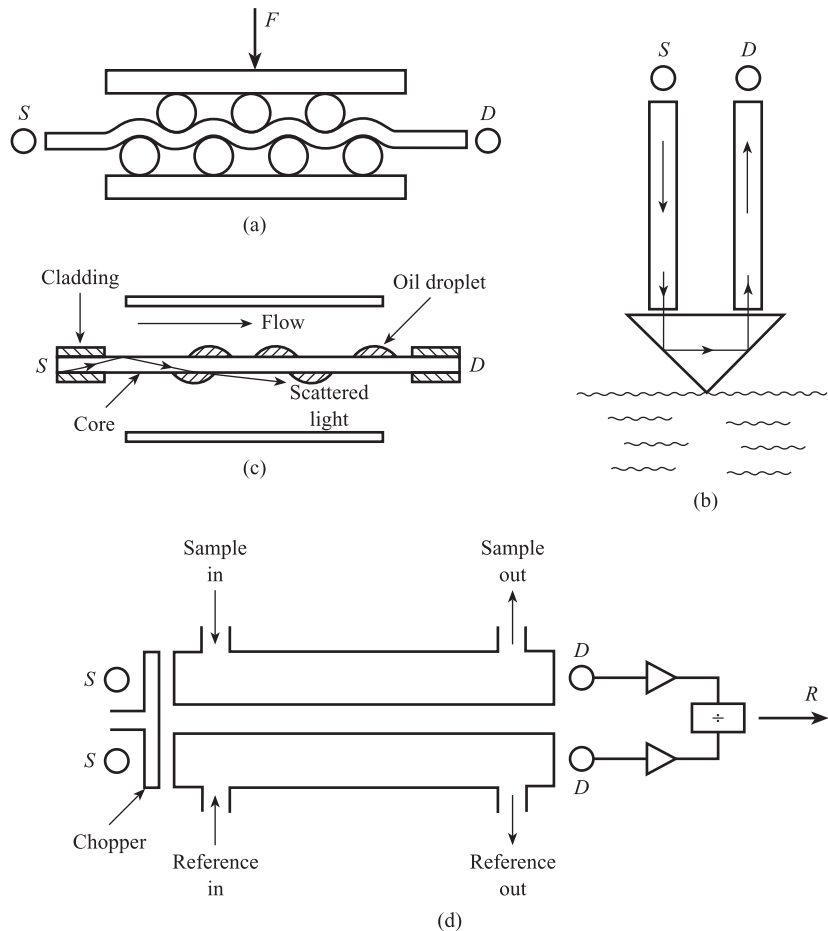
Intensity modulation using attenuation and absorption

In this type of sensor the intensity of radiation arriving at the detector is modulated either by variable attenuation in an optical fibre system or by variable absorption in gases and liquids.

Figure 15.20(a) shows an optical fibre force sensor; an increase in force F causes increased microbending of the fibre. This causes rays with ϕ just greater than the

Figure 15.20 Intensity modulation using attenuation and absorption:

- (a) Microbend force sensor
- (b) Two-fibre level detector
- (c) Oil-in-water detector
- (d) Infrared gas analyser (two-beam).



critical angle θ_c (Figure 15.9), which would normally be totally internally reflected back into the core, to be increasingly refracted into the cladding and lost from the core. The result is that the power incident on the detector decreases as F is increased.

An optical level detector is shown in Figure 15.20(b). This consists of two fibres (one inlet, one exit) cemented onto a 90° glass prism. For a low level, the prism is surrounded by air so that total internal reflection occurs at both prism faces, resulting in a high detector output signal. For a high level, the prism is surrounded by liquid so that only partial internal reflection occurs, resulting in a much lower detector output signal.

The system shown in Figure 15.20(c) can be used to detect the presence of oil droplets in water. The water flows over an optical fibre core from which the cladding has been removed. The refractive index of the core is similar to that of oil, but higher than water. This means that if an oil droplet settles on the core some rays of light are refracted out of the core, causing a reduction in detector output signal.

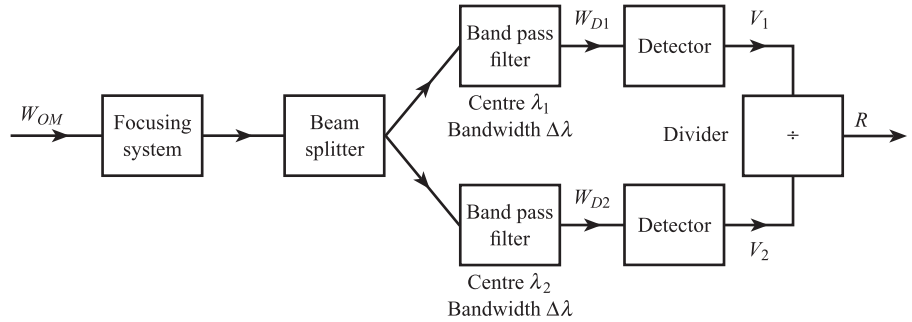
In Section 15.3 we saw that many hydrocarbon and other gases show strong absorption bands in the infrared; this means that if the percentage of the absorbing molecule in a gas mixture changes then there is a corresponding change in the transmission characteristics $T(\lambda)$. Figure 15.20(d) shows the infrared gas analyser, which uses this principle. Earlier systems were broadband with IR lamps as sources and thermopile or pyroelectric thermal detectors. Later systems are narrowband with IR LED sources and photovoltaic detectors with wavelength response matched to that of the source. In both cases the source radiation is often chopped with a rotating mechanical chopper. This means that the detector output signals are a.c. so that electronic band-pass filters and phase-sensitive detectors can be used to reject electrical interference and noise. The system shown is a two-beam type, with the sample cell containing the gas to be analysed and the reference cell containing the pure gas of interest. For example, if we wish to measure the percentage of CO in flue gas then the reference cell will contain pure CO. The detector output signals are amplified and their ratio R computed; R depends on the percentage of the absorbing molecule in the sample gas, but should be independent of modifying effects such as source variations.

15.6.3 Two-wavelength systems

The simple intensity-modulated systems discussed so far can be affected by environmental modifying and interfering inputs. For example, the source-modulated broadband and narrowband temperature systems are affected by changes in emissivity and transmission medium characteristics; the transmission medium-modulated systems are affected by changes in source intensity. Some of these problems can be solved using the two-wavelength system shown in Figure 15.21. Here the incoming radiation from the transmission medium is focused and split equally into two beams. One beam is passed through a narrow pass-band optical filter with centre wavelength λ_1 , the other through a similar filter with centre wavelength λ_2 . The detectors chosen should have the same value of wavelength response $D(\lambda)$ at λ_1 and λ_2 ; either thermal detectors or photon detectors with a suitable wavelength response could be used. An electronic divider computes the ratio R between detector output signals V_1 and V_2 .

Using eqn [15.57] for a narrowband radiation pyrometer, we can derive the equation for a two-wavelength (or two-colour) pyrometer:

Figure 15.21 Two-wavelength system.



$$R(T) = \frac{V_1(T)}{V_2(T)} = \frac{\frac{1}{\pi} (C_1 \epsilon T_M K_F F K_D)_{\lambda_1} \frac{\Delta \lambda}{\lambda_1^5} \exp\left(-\frac{C_2}{\lambda_1 T}\right)}{\frac{1}{\pi} (C_1 \epsilon T_M K_F F K_D)_{\lambda_2} \frac{\Delta \lambda}{\lambda_2^5} \exp\left(-\frac{C_2}{\lambda_2 T}\right)} \quad [15.58]$$

If λ_1 and λ_2 are close together, so that the emissivities and transmission factors are equal, then the ratio becomes:

Equation for two-colour pyrometer system

$$R(T) = \left(\frac{\lambda_2}{\lambda_1}\right)^5 \exp \frac{C_2}{T} \left(\frac{1}{\lambda_2} - \frac{1}{\lambda_1}\right) \quad [15.59]$$

This system does not require calibration and correction for emissivity variations.

The two-wavelength principle can also be used in the infrared gas analyser shown in Figure 15.20(d). Instead of using a two-beam system, with reference and sample cells, a single beam-sample cell system is used. Here λ_1 coincides with the centre of the absorption band for the component of interest and λ_2 with the centre of the band for another component.

15.6.4 Modulation of wavelength by transmission medium

All of the systems discussed so far rely on the measured variable modulating the **intensity or amplitude** of light waves. These systems are inherently susceptible to unwanted variations in source intensity and transmission characteristics. Two-channel/wavelength systems overcome some of these problems, but wavelength modulation systems, where the **wavelength** λ of the light is determined by the measured variable, are completely independent of these unwanted effects. Two such systems have been developed at the National Physical Laboratory^[9] and will now be described.

Figure 15.22(a) shows a 'Littrow' diffraction grating used as a sensor to convert angular displacement θ into changes in wavelength. Broadband radiation emerging from the input fibre is first collimated into a parallel beam; this is incident at an angle θ onto a reflection grating. The grating consists of a regular array of grooves whose spacing d is comparable to the wavelength of the incident beam. The resulting diffraction pattern is complex, but only light with wavelengths λ satisfying the equation

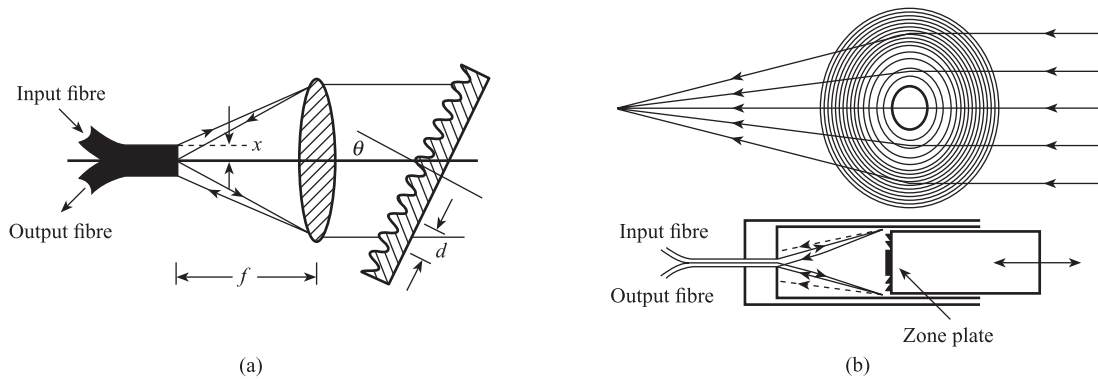
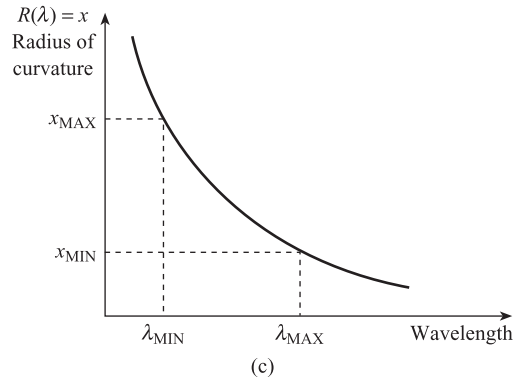


Figure 15.22
Wavelength modulation systems:
(a) Littrow grating angular displacement sensor (after Hutley^[9])
(b) Fresnel zone plate used as a lens and linear displacement sensor (after Hutley^[9])
(c) Wavelength/displacement characteristics of zone plate.



$$2d \sin \theta = m\lambda \quad [15.60]$$

where $m = 1, 2, 3, \dots$ etc., is reflected back along its own path to the output fibre. By limiting the range of incident wavelengths, only first-order effects with $m = 1$ need to be considered, giving the following unique relation between reflected wavelength λ and grating angle θ :

$$\lambda = 2d \sin \theta \quad [15.61]$$

Wavelength-encoded angular displacement sensor

The angular range of this device is limited to between 20° and 60° .

Figure 15.22(b) shows a **Fresnel zone plate**; it is a circular grating consisting of a number of concentric lines, the spacing between the lines decreasing with distance from the centre. The top diagram shows a parallel beam of monochromatic light incident on the zone plate. All rays are brought to a focus at a single point so that the plate acts as a lens of focal length f . However, the deviation of each ray depends on wavelength, so that different wavelengths are brought to a focus at different points; the focal length f is inversely proportional to wavelength λ .

The bottom diagram shows a reflecting zone plate, used as a linear displacement sensor. The plate acts as a spherical concave mirror with a radius of curvature R inversely proportional to wavelength (Figure 15.22(c)). Broadband radiation from the input fibre is incident on the zone plate a distance x away; the radiation reflected back to the output fibre is narrowband, with centre wavelength λ such that:

*Wavelength-encoded
linear displacement
sensor*

$$R(\lambda) = x \quad [15.62]$$

Thus if the range of displacement to be measured is x_{MIN} to x_{MAX} , the required range of wavelengths in the incoming radiation is λ_{MIN} to λ_{MAX} where

$$R(\lambda_{\text{MAX}}) = x_{\text{MIN}}$$

$$R(\lambda_{\text{MIN}}) = x_{\text{MAX}}$$

Because of the need to exclude overlapping higher orders, λ_{MAX} cannot usually exceed $2\lambda_{\text{MIN}}$, with corresponding limits on the displacement range.

A wavelength decoder is necessary with both of these devices to convert wavelength variations into a usable voltage signal. One possibility is to split the beam from the output fibre equally between two detectors, with very different wavelength responses $D(\lambda)$ over the wavelength range of interest. The ratio of detector output voltages should vary monotonically with wavelength.

15.6.5 Interferometers

We first need to discuss the phenomenon of **interference**, which is exhibited by any type of wave motion. Consider a monochromatic light source which is emitting light at a single angular frequency ω rad/s and corresponding wavelength λ . The light beam is then split into two beams of equal amplitude a . These beams then travel along different optical paths of lengths x_1 and x_2 before both arriving at a detector. The beams can be described by the wave equations (Section 16.3.1):

$$\phi_1 = a \sin\left(\omega t - \frac{2\pi}{\lambda} x_1\right), \phi_2 = a \sin\left(\omega t - \frac{2\pi}{\lambda} x_2\right) \quad [15.63]$$

so that the resultant light beam incident on the detector is given by:

$$\begin{aligned} \phi &= \phi_1 + \phi_2 = a \left\{ \sin\left(\omega t - \frac{2\pi}{\lambda} x_1\right) + \sin\left(\omega t - \frac{2\pi}{\lambda} x_2\right) \right\} \\ &= 2a \cos\left[\frac{2\pi}{\lambda} \left(\frac{x_2 - x_1}{2}\right)\right] \sin\left[\omega t - \frac{2\pi}{\lambda} \left(\frac{x_1 + x_2}{2}\right)\right] \end{aligned} \quad [15.64]$$

This has amplitude:

$$a_R = 2a \cos\left(\frac{\pi}{\lambda} x\right) \quad [15.65]$$

where x = optical path difference $x_2 - x_1$, and intensity:

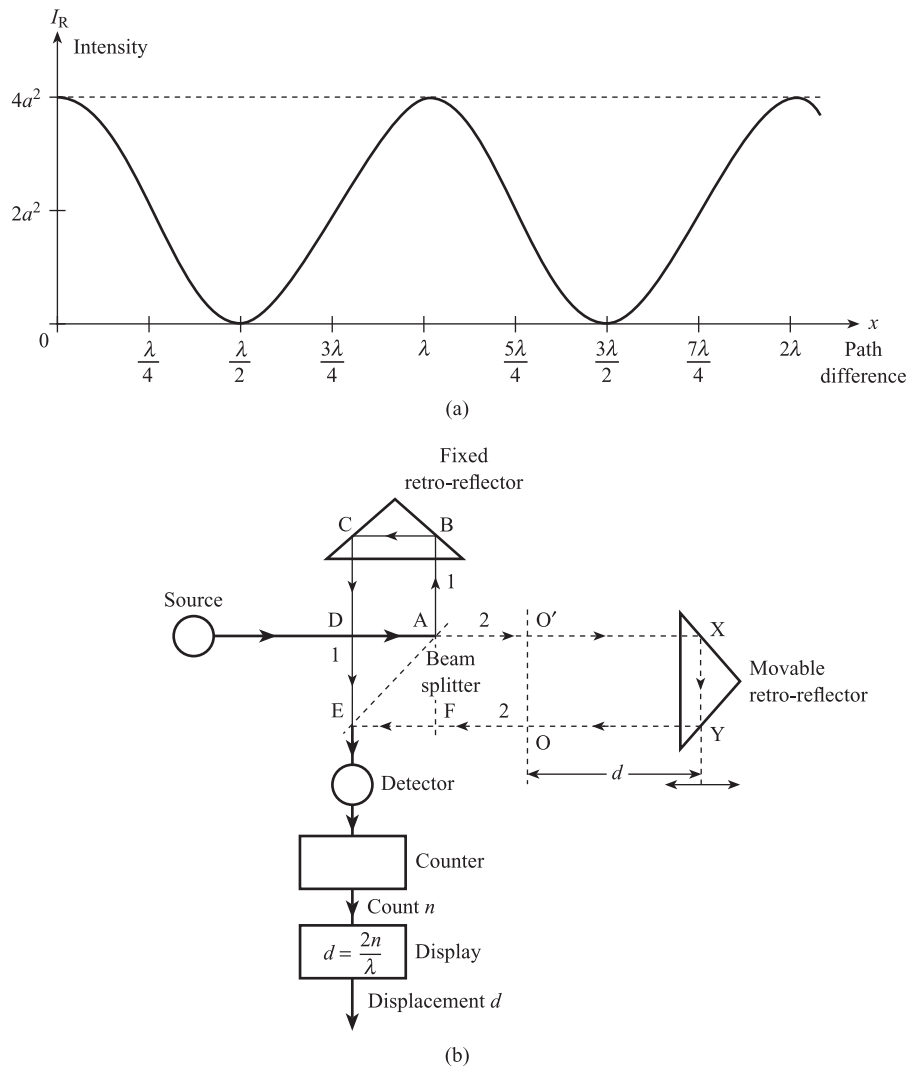
*Variation in resultant
intensity with path
difference*

$$I_R = a_R^2 = 4a^2 \cos^2\left(\frac{\pi}{\lambda} x\right) \quad [15.66]$$

Figure 15.23(a) shows the form of eqn [15.66]. We see that when $x = 0, \lambda, 2\lambda, 3\lambda$, etc., $I_R = 4a^2$, i.e. the intensity of the resultant beam corresponds to the sum $(2a)$

Figure 15.23

Interferometers:
 (a) Variation in resultant intensity with path difference
 (b) Michelson interferometer.



of the amplitudes of the individual beams, then this is **constructive interference**. When $x = \lambda/2, 3\lambda/2, 5\lambda/2$, etc., i.e. the intensity of the resultant beam corresponds to $I_R = 0$, the **difference** (i.e. 0) of the amplitudes of the individual beams, then this is **destructive interference**. Thus if path difference x is initially zero, I_R is maximum and a bright fringe is observed. If x is increased to $\lambda/2$, I_R is zero and a dark fringe is observed. If x is further increased to λ , I_R returns to maximum and a bright fringe is again observed. Thus the variation in the intensity of the light incident on the detector, and therefore the detector output signal, with path difference x , has a period equal to λ .

Figure 15.23(b) shows a **Michelson interferometer** which is used in the accurate measurement of displacement. Here a monochromatic beam of light from a laser source (Section 15.2.4) is split into two equal beams 1 and 2 at A using a beam splitter (in its simplest form this is a half-silvered mirror). Beam 1 travels to a fixed retro-reflector and is reflected back to the point E, so that the total optical path length $x_1 = ABCDE$.

Beam 2 travels to a movable retro-reflector and is again reflected back to the point E, so that here the total optical path length $x_2 = \text{AXYFE}$. The optical path difference x is therefore:

$$\begin{aligned} x &= x_2 - x_1 = \text{AXYFE} - \text{ABCDE} \\ &= (\text{AX} + \text{XY} + \text{YF} + \text{FE}) - (\text{AB} + \text{BC} + \text{CD} + \text{DE}) \end{aligned} \quad [15.67]$$

Since $\text{XY} = \text{DE}$ and $\text{FE} = \text{BC}$, then

$$x = (\text{AX} + \text{YF}) - (\text{AB} + \text{CD}) = 2\text{AX} - 2\text{AB} \quad [15.68]$$

If displacement d is measured from the line OO' , where $\text{AO}' = \text{AB}$, then $\text{AX} = \text{AB} + d$ and

$$x = 2(\text{AB} + d) - 2\text{AB} = 2d \quad [15.69]$$

This means that a change δd in d results in a change δx in x of $2\delta d$, so that if $\delta d = \lambda/2$, i.e. half a wavelength, then $\delta x = \lambda$, i.e. a full wavelength.

Thus with a Michelson interferometer the detector output signal varies periodically with displacement d , the period being equal to $\lambda/2$, one half-wavelength of the laser radiation. A Michelson interferometer used as a standard for length (Section 2.4.1) would typically use a helium-neon laser source with wavelength $\lambda = 633 \text{ nm}$. Thus a displacement $d = 1 \text{ mm}$ would produce:

$$n = \frac{d}{\lambda/2} = \frac{2 \times 10^{-3}}{633 \times 10^{-9}} = \frac{2 \times 10^6}{633} = 3159.56$$

cycles of detector output signal. This displacement can therefore be measured to within a resolution of $\pm \lambda/4$ by counting the number of whole cycles, 3160 (rounded up) in this case.

We see therefore that a basic interferometer has a very high sensitivity when used for displacement measurement. For all displacements greater than λ or $\lambda/2$ it is necessary to count the total number of cycles of intensity variation. The sensitivity can be reduced by using a source of much longer effective wavelength λ' obtained by mixing two laser beams with much shorter wavelengths λ_1 and λ_2 . This is called **synthetic wave** or **multisource heterodyne interferometry**. Thus, if we add two waves with the same amplitude a but with different frequencies ω_1 and ω_2 and wavelengths λ_1 and λ_2 , the resultant wave is:

$$\begin{aligned} \phi &= a \sin \left(\omega_1 t - \frac{2\pi}{\lambda_1} x \right) + a \sin \left(\omega_2 t - \frac{2\pi}{\lambda_2} x \right) \\ &= 2a \cos \left[\left(\frac{\omega_1 - \omega_2}{2} \right) t - 2\pi x \cdot \frac{1}{2} \left(\frac{1}{\lambda_1} - \frac{1}{\lambda_2} \right) \right] \\ &\quad \times \sin \left[\left(\frac{\omega_1 + \omega_2}{2} \right) t - 2\pi x \cdot \frac{1}{2} \left(\frac{1}{\lambda_1} + \frac{1}{\lambda_2} \right) \right] \end{aligned} \quad [15.70]$$

This is an **amplitude modulated wave**, with a carrier frequency of $(\omega_1 + \omega_2)/2$ and a much lower amplitude modulating frequency of $(\omega_1 - \omega_2)/2$. The amplitude or envelope function:

$$2a \cos \left[\left(\frac{\omega_1 - \omega_2}{2} \right) t - 2\pi x \cdot \frac{1}{2} \left(\frac{1}{\lambda_1} - \frac{1}{\lambda_2} \right) \right]$$

is a progressive wave of the form:

$$2a \cos \left(\omega' t - \frac{2\pi}{\lambda'} x \right)$$

with frequency $\omega' = (\omega_1 - \omega_2)/2$ and wavelength:

$$\frac{1}{\lambda'} = \frac{1}{2} \left(\frac{1}{\lambda_1} - \frac{1}{\lambda_2} \right), \text{ i.e. } \lambda' = \frac{2\lambda_1\lambda_2}{\lambda_2 - \lambda_1} \quad [15.71]$$

Thus if $\lambda_2 = 1001 \text{ nm}$ and $\lambda_1 = 1000 \text{ nm}$, $\lambda' = 2 \text{ mm}$. This means that if the envelope wave with wavelength λ' is used as a source in an interferometer, displacements of up to 1 mm can be detected within one cycle of the intensity variation. The carrier wave with wavelength $(\lambda_1 + \lambda_2)/2$ can still be used as an alternative source if high precision measurements are required.

Conclusion

This chapter has discussed the following:

1. The two general types of optical measurement system: fixed source, variable transmission medium; and variable source, fixed transmission medium.
2. The principles and types of sources: hot body, light-emitting diodes and lasers.
3. The principles and characteristics of optical transmission media.
4. The geometry of coupling of detector to source and the use of focusing systems and optical fibres.
5. The principles and characteristics of thermal and photon detectors.
6. Measurement systems using the modulation of intensity by source and transmission medium, two-wavelength systems, wavelength modulation and interferometry.

References

- [1] Polarizers Technical Products 1988 *Technical Information on Temperature Standards and Black Body Sources*.
- [2] KEISER G 1983 *Optical Fibre Communications*, McGraw-Hill, Tokyo, pp. 12–44, 98–115, 145–67.
- [3] CHERIN A H 1983 *An Introduction to Optical Fibres*, McGraw-Hill, Tokyo, pp. 270–4.
- [4] HOUGHTON J and SMITH S D 1966 *Infrared Physics*, Oxford University Press, London, pp. 220–3.

- [5] Plessey Optoelectronics and Microwave Ltd, *Application Notes on Pyroelectric and Lead Tin Telluride Infra-red Detectors*.
- [6] JONES B E 1985 'Optical fibre sensors and systems for industry', *J. Phys. E.: Scientific Instruments*, vol. 18, pp. 770–82.
- [7] MEDLOCK R S 1986 'Review of modulating techniques for fibre optic sensors', *Measurement and Control*, vol. 19, no. 1, pp. 4–17.
- [8] HILL S *Optical Fibre Reflectance Transducer*, Teesside Polytechnic project report, unpublished.
- [9] HUTLEY M C 1985 'Wavelength encoded optical fibre sensors', *N.P.L. News*, no. 363.

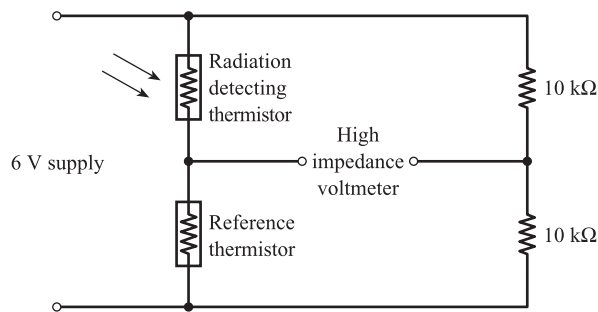
Problems

- 15.1 A broadband radiation pyrometer has a thermistor bolometer detector. The radiant power incident on the thermistor in the steady state is given by:

$$P_D = 10T^4 \text{ pW}$$

where T is the temperature of the distant target in kelvin. The beam of radiation is chopped by a semicircular disc rotating at 60 r.p.m. The thermistor is incorporated into the deflection bridge circuit shown in Figure Prob. 15.1 together with an identical thermistor at 290 K, the temperature of the detector surroundings. Using the detector data given below, sketch the form of the bridge output signal when the target temperature is 1000 K. Hint: assume a square wave variation in detector power which can be regarded as a series of steps.

Figure Prob. 1.



Thermistor data

Mass = 1 g

Surface area = 10^{-4} m^2

Specific heat = $10^2 \text{ J kg}^{-1} \text{ K}^{-1}$

Heat transfer coefficient = $10^4 \text{ W m}^{-2} \text{ K}^{-1}$

Resistance = $1.0 \exp\left(\frac{3000}{\theta}\right) \Omega$ where θ = thermistor temperature in kelvin

- 15.2 A thermocouple has an e.m.f. of 5 mV when the hot junction is at 100 °C and the cold junction is at 0 °C. A thermopile consisting of 25 such thermocouples in series is used as a detector in a chopped, broadband pyrometer. When unchopped the power in the beam of radiation incident on the hot junction of the thermopile is given by $7.5T^4 \text{ pW}$, where T is the temperature of the distant target. The beam is chopped by a semicircular disc rotating at 6000 r.p.m. The reference junction of the thermopile is at the temperature of the pyrometer

enclosure. Assuming the thermocouples are linear and the detector data given below, sketch the form of the output signal when $T = 2000$ K.

Detector data

Heat transfer coefficient = $2 \times 10^4 \text{ W m}^{-2} \text{ }^\circ\text{C}^{-1}$

Surface area = $1.6 \times 10^{-4} \text{ m}^2$

Time constant = 1 ms

- 15.3 A narrowband optical pyrometer is to be used to measure the temperature of the radiant section of a furnace in the range 1500 to 2000 K. The emissivity of the furnace wall is 0.5 at a wavelength of $0.5 \text{ } \mu\text{m}$. The transmission factor of the atmosphere between the furnace and the pyrometer is 0.90 at $0.5 \text{ } \mu\text{m}$.

Calculate the range of the pyrometer output signal given the following data:

Lens

Diameter of aperture = 3.0 cm

Focal length at $0.5 \text{ } \mu\text{m}$ = 10.0 cm

Transmission factor at $0.5 \text{ } \mu\text{m}$ = 0.95

Photoconductive detector

Diameter of detector disc = 0.5 cm

Detector sensitivity = $10 \text{ } \Omega \text{ W}^{-1}$

Centre wavelength = $0.5 \text{ } \mu\text{m}$

Bandwidth = $0.05 \text{ } \mu\text{m}$

Deflection bridge and amplifier

Overall sensitivity = $10 \text{ V } \Omega^{-1}$

Temperature for bridge balance = 1500 K

The Planck–Wien law for the hemispherical spectral intensity of radiation from a black body is:

$$W(\lambda, T) = \frac{C_1}{\lambda^5 \left[\exp\left(\frac{C_2}{\lambda T}\right) - 1 \right]}$$

where

T = absolute temperature of body (K)

λ = wavelength of radiation (μm)

$C_1 = 37\,400 \text{ W } \mu\text{m}^4 \text{ cm}^{-2}$

$C_2 = 14\,400 \text{ } \mu\text{m K}$

- 15.4 A two-colour radiation thermometer is used to measure the temperature of a body at $800 \text{ }^\circ\text{C}$. The system incorporates two detectors, one measuring radiation at $0.5 \text{ } \mu\text{m}$ and the other at $1.0 \text{ } \mu\text{m}$. What is the ratio of the detector output signals? State clearly all the assumptions made in the calculation. Explain the advantage of this system over broadband and narrowband systems.

- 15.5 An optical fibre transmission system consists of a circular LED source, a 2-metre length of optical fibre and a circular PIN diode detector. Both the source and detector are positioned $100 \text{ } \mu\text{m}$ from the ends of the fibre. Detailed data for the source, a glass fibre, a polymer fibre and the detector are given below. Use this data to perform the following calculations.

- The total power P_s emitted by the source in all directions (use eqn [15.23b]).
- The numerical aperture and maximum angle of acceptance of the glass fibre.
- The numerical aperture and maximum angle of acceptance of the polymer fibre.
- The source and detector are linked by the glass fibre; calculate the power input to the fibre, the fibre transmission factor, and power output from the fibre. (Hint: use $P_{IM}/R = K_{SM}$ and $P_{OM}/P_{IM} = T$.)

- (e) The source and detector are now linked by the polymer fibre; calculate the power input to the fibre, the fibre transmission factor, and power output from the fibre.
- (f) For both the glass system of (d) and the polymer system of (e), calculate the power incident on the detector and the detector output current. (Hint: use $P_D/P_{OM} = K_{MD}$.)

LED source

Radiance = $10 \text{ W cm}^{-2} \text{ sr}^{-1}$

Diameter = $200 \text{ }\mu\text{m}$

Centre wavelength = 810 nm

Glass fibre

Multimode step index

Core diameter = $100 \text{ }\mu\text{m}$

Core refractive index = 1.5

Core-cladding index difference = 0.015

Attenuation at 810 nm = 5 dB km^{-1}

Fibre length = 2 m

Polymer fibre

Multimode step index

Core diameter = 1.0 mm

Core refractive index = 1.65

Core cladding index difference = 0.04

Attenuation at 810 nm = 500 dB km^{-1}

Fibre length = 2 m

PIN diode detector

Diameter = 2.0 mm

Centre wavelength = 810 nm

Responsivity at 810 nm = 0.55 A W^{-1}

15.6

A system for the measurement of linear displacement consists of a reflecting Fresnel zone plate (Figure 15.22(b)), acting as a wavelength encoder, and a *pin* diode photon detector, acting as a wavelength decoder. The distance between input/output fibres and the zone plate (input displacement range) can be varied between 12.5 and 25 mm. The radius of curvature $R(\lambda)$ of the zone plate is given by $R(\lambda) = 1.25 \times 10^4 / \lambda$ where R is in mm and λ in nm. The detector has $D(\lambda) = 9 \times 10^{-4} \lambda - 0.35$. Calculate the wavelength output range for the encoder and the corresponding ratio of decoder output signals.

16 Ultrasonic Measurement Systems

Ultrasound refers to sound waves at frequencies higher than the range of the human ear, i.e. at frequencies greater than about 18 kHz. Ultrasonic waves obey the same basic laws of wave motion as lower frequency sound waves; they have, however, the following advantages:

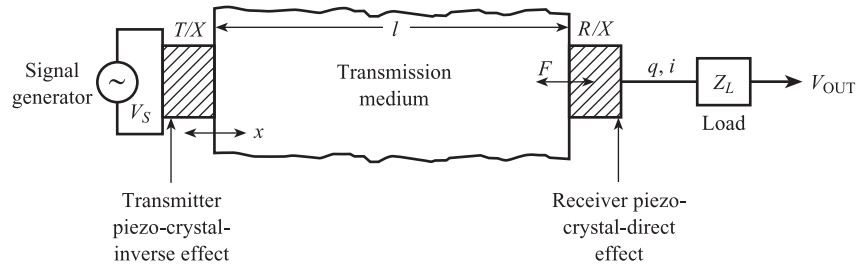
- (a) Higher frequency waves have shorter wavelengths; this means that diffraction or bending around an obstacle of given dimensions is correspondingly reduced. It is therefore easier to direct and focus a beam of ultrasound.
- (b) Ultrasonic waves can pass easily through the metal walls of pipes and vessels. This means that the entire measurement system can be mounted completely external to the fluid, i.e. is **non-invasive**. This is extremely important with hostile fluids, such as those with corrosive, radioactive, explosive or flammable properties. There is also no possibility of blockage occurring with dirty fluids or slurries.
- (c) Ultrasound can be launched into and propagated through biological tissue, making it useful for medical applications.
- (d) The silence of ultrasound means that it has important military applications.

This chapter studies ultrasonic transmitters and receivers, and the principles of transmission, and examines a range of ultrasonic measurement systems.

16.1 Basic ultrasonic transmission link

This forms the basis of any ultrasonic measurement system and is shown in Figure 16.1. It consists of an ultrasonic transmitter, the transmission medium and an ultrasonic receiver. The most commonly used devices for ultrasonic transmitters and receivers are piezoelectric sensing elements (Section 8.7). The piezoelectric effect is reversible, i.e. mechanical energy can be converted into electrical energy and electrical energy into mechanical. The ultrasonic transmitter uses the inverse piezoelectric effect; if a sinusoidal voltage $\hat{V}_s \sin \omega t$ is applied to the transmitting crystal, then the crystal undergoes a corresponding sinusoidal deformation x (eqn [8.72]). This vibration of the crystal is transmitted to the particles at the beginning of the medium, and these are set in sinusoidal motion, causing other particles to vibrate, until eventually the disturbance is transmitted to the other end of the medium. These sinusoidal particle displacements set up an accompanying sinusoidal pressure or stress in the medium.

Figure 16.1 Basic ultrasonic transmission link.



This is detected by the ultrasonic receiver, which is simply a force sensor using the direct piezoelectric effect. The fluctuating pressure causes a sinusoidal force F over the area of the crystal, thus producing a corresponding time-varying charge q and current i . This current produces a corresponding output voltage V_{OUT} across a load Z_L .

16.2

Piezoelectric ultrasonic transmitters and receivers

16.2.1 Basic principles

In Chapter 5 we introduced the concept of **effort** and **flow** variables: voltage and force are examples of effort variables; current and velocity are examples of flow variables. The interconnection of any two elements in a system is then represented by two terminals and the appropriate effort/flow pair, e.g. voltage/current at an electrical connection and force/velocity at a mechanical connection. This leads to the concept of an element being represented by a four-terminal or **two-port network**. Thus in Figure 5.17 a force sensor is represented as two-port network with a mechanical input port and an electrical output port. Two-port networks provide a good representation of piezoelectric transmitters and receivers; because the piezoelectric effect is reversible the same crystal can act as a transmitter (electrical input port/mechanical output port) or as a receiver (mechanical input port/electrical output port) and is said to be **bilateral**. Figure 16.2(a) shows transmitter and receiver two-port networks in block diagram form.

In order to derive the detailed form of these circuits we need to revise the properties of piezoelectric elements (Section 8.7). Starting with the basic equations for the direct and inverse effects we have:

$$\text{Direct effect } q = dF \quad [8.71]$$

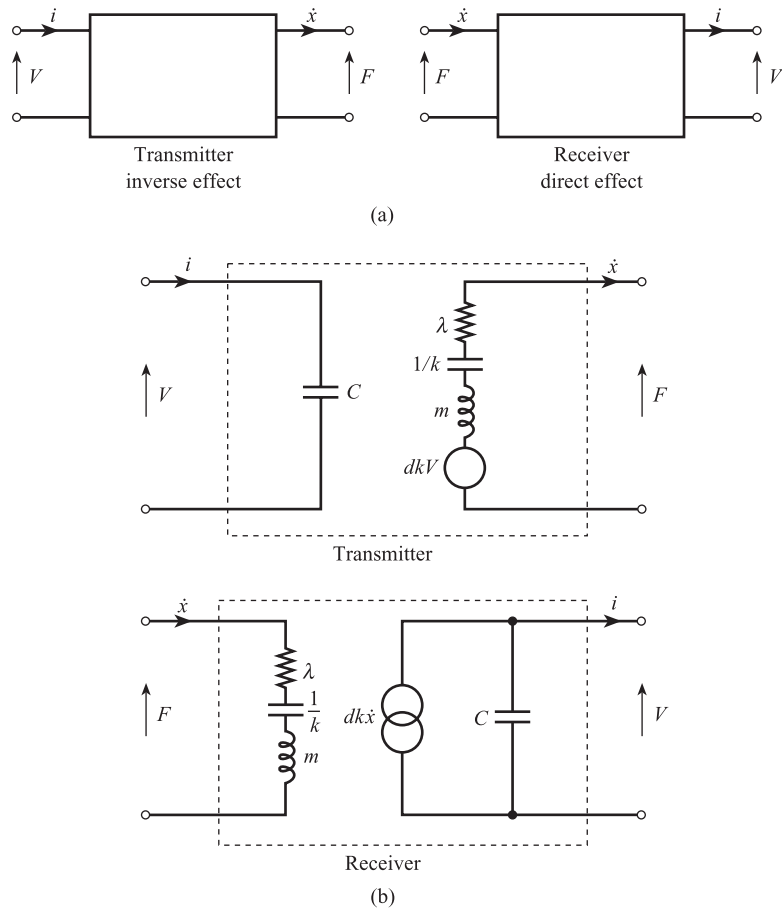
$$\text{Inverse effect } x = dV \quad [8.72]$$

We also have the equation $F = kx$ relating applied force F and deformation x of a crystal of stiffness k . Thus $q = dkx$ and:

$$i = \frac{dq}{dt} = dk\dot{x} \quad [16.1]$$

Relationship between flow variables for piezo-crystal

Figure 16.2 Two-port networks for piezoelectric transmitters and receivers:
(a) Block diagrams
(b) Detailed form.



Similarly $F/k = dV$, giving:

Relationship between effort variables for piezo-crystal

$$F = dkV$$

[16.2]

The crystal has electrical capacitance C and the corresponding electrical impedance is purely capacitive:

$$Z_E(s) = \frac{\Delta \tilde{V}(s)}{\Delta \tilde{i}(s)} = \frac{1}{Cs} \quad [16.3]$$

The mechanics of the crystal can be represented most simply using single mass (inertance m), spring (stiffness k) and damping (resistance λ) elements. The corresponding mechanical circuit consists of m , $1/k$ and λ in series and has mechanical impedance (Section 5.2):

$$Z_M(s) = \frac{\Delta \tilde{F}(s)}{\Delta \tilde{x}(s)} = ms + \lambda + \frac{k}{s} \quad [16.4]$$

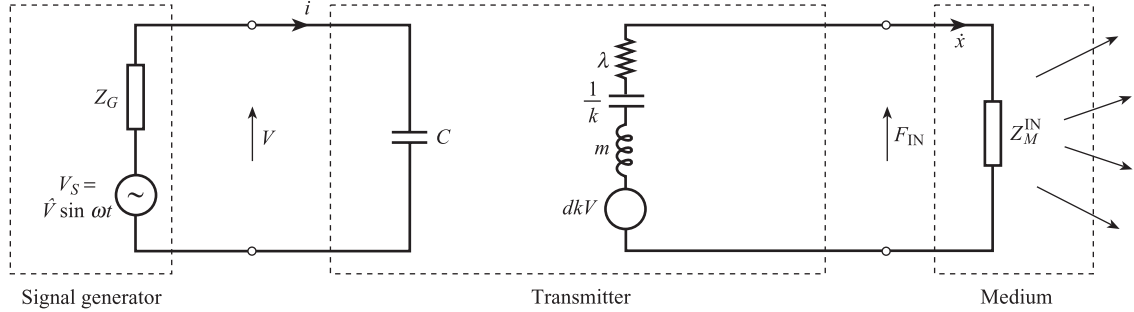
Figure 16.3 Transfer functions for transmitter and receiver systems:

(a) Signal generator/transmitter/medium

(b) Medium/receiver/external load.

Figure 16.2(b) shows the detailed form of the transmitter and receiver two-port networks. In the transmitter network, a voltage V at the input electrical port produces a force dkV which drives a velocity \dot{x} through the output mechanical impedance. In the receiver network, a force F at the input mechanical port drives a velocity \dot{x} through the input mechanical impedance; this produces a current $dk\dot{x}$ at the output electrical port.

Figure 16.3(a) shows the input electrical port of the transmitter connected to an external signal generator and the output mechanical port to the beginning of

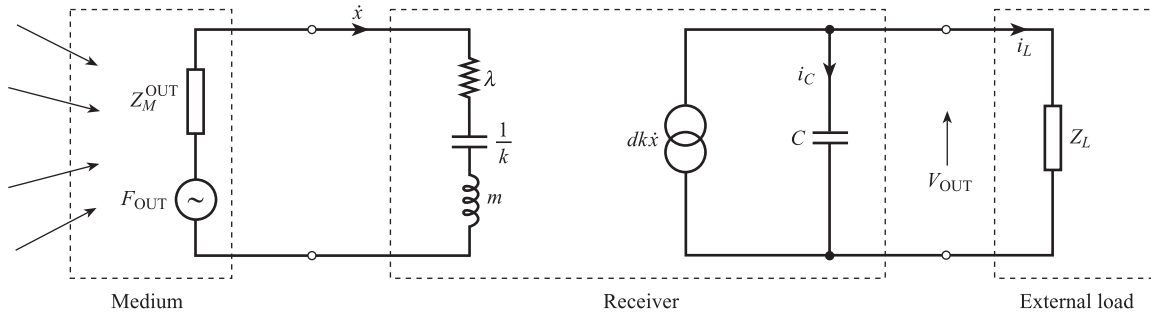


$$\frac{\Delta \bar{i}}{\Delta \bar{V}}(s) = \frac{1}{Z_G + \frac{1}{Cs}}, \quad \frac{\Delta \bar{v}}{\Delta \bar{i}}(s) = \frac{1}{Cs}$$

$$\frac{\Delta \bar{x}}{\Delta \bar{V}}(s) = \frac{dk}{(ms + \lambda + k/s) + Z_M^{\text{IN}}}, \quad \frac{\Delta \bar{x}}{\Delta \bar{x}}(s) = \frac{1}{s}$$

$$\frac{\Delta \bar{x}}{\Delta \bar{V}}(s) = \frac{dk}{s[(ms + \lambda + k/s) + Z_M^{\text{IN}}]} \left(\frac{1/Cs}{Z_G + \frac{1}{Cs}} \right)$$

(a)



$$\frac{\Delta \bar{x}}{\Delta \bar{F}_{\text{OUT}}}(s) = \frac{1}{(ms + \lambda + k/s) + Z_M^{\text{OUT}}}$$

$$\Delta \bar{V}_{\text{OUT}}(s) = \frac{\frac{1}{Cs} \cdot Z_L}{\frac{1}{Cs} + Z_L} \cdot dk \Delta \bar{x}(s), \quad \frac{\Delta \bar{V}_{\text{OUT}}}{\Delta \bar{x}}(s) = dk \frac{Z_L}{(1 + Z_L Cs)}$$

$$\frac{\Delta \bar{V}_{\text{OUT}}}{\Delta \bar{F}_{\text{OUT}}}(s) = \frac{dk}{[(ms + \lambda + k/s) + Z_M^{\text{OUT}}]} \cdot \frac{Z_L}{(1 + Z_L Cs)}$$

(b)

the transmission medium. The figure derives the overall transfer function relating crystal displacement and generator voltage. In the special case that the output impedance of the generator and the input impedance of the medium are negligible, i.e. $Z_G \approx 0$ and $Z_M^{\text{IN}} \approx 0$, the overall transfer function simplifies to the standard second-order form:

*Transmitter system
transfer function*

$$\frac{\Delta \bar{x}}{\Delta \bar{V}_s}(s) = \frac{d}{\frac{1}{\omega_n^2} s^2 + \frac{2\xi}{\omega_n} s + 1} \quad [16.5]$$

where ω_n and ξ are the mechanical natural frequency and damping ratio for the crystal (see Section 8.7).

Figure 16.3(b) shows the input mechanical port of the receiver connected to the end of the transmission medium and the output electrical port connected to an external load such as an oscilloscope or amplifier. The figure derives the overall transfer function relating voltage across the load V_{OUT} to force F_{OUT} (due to medium output pressure acting over the area of the receiver crystal). In the special case that the output impedance of the medium is negligible and the load is purely resistive, i.e. $Z_M^{\text{OUT}} \approx 0$ and $Z_L = R_L$, the overall transfer function simplifies to:

*Receiver system
transfer function*

$$\frac{\Delta \bar{V}_{\text{OUT}}}{\Delta \bar{F}_{\text{OUT}}}(s) = \frac{d}{C} \left(\frac{\tau s}{1 + \tau s} \right) \left(\frac{1}{\frac{1}{\omega_n^2} s^2 + \frac{2\xi}{\omega_n} s + 1} \right) \quad [16.6]$$

This is identical to the transfer function for the basic piezoelectric force measurement system discussed in Section 8.7: an ultrasonic receiver is simply a piezoelectric force sensor applied to the specific problem of measuring high frequency sinusoidal pressure variations.

16.2.2 Crystal oscillators and resonators

Rather than energise the crystal with an external signal generator, the crystal is usually incorporated into a closed-loop system which oscillates at the mechanical natural frequency ω_n .

In order to discuss the principles of crystal oscillators we need to find the overall electrical impedance of the crystal. Figure 16.4 shows an approximate electrical equivalent circuit for the crystal. We see that the total current i drawn by the crystal is the sum of the capacitance current i_C together with the current i_m required to drive the mechanical mass/spring/damper system. C is therefore shunted by a series electrical circuit L_1, C_1, R_1 representing these mechanical losses.

The impedance Z_E of the series circuit is given by:

$$Z_E(s) = \frac{\Delta \bar{V}}{\Delta \bar{i}_m}(s) = \frac{\Delta \bar{V}}{\Delta \bar{F}} \frac{\Delta \bar{x}}{\Delta \bar{i}_m} \frac{\Delta \bar{F}}{\Delta \bar{x}} \quad [16.7]$$

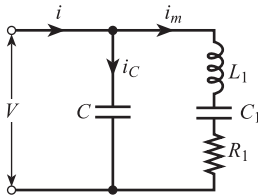


Figure 16.4 Equivalent electrical circuit for crystal.

where the ratios $\Delta\bar{V}/\Delta\bar{F}$ and $\Delta\bar{x}/\Delta\bar{i}_m$ are both equal to $1/dk$ (eqns [16.1] and [16.2]), and $\Delta\bar{F}/\Delta\bar{x}$ is the crystal mechanical impedance $Z_m(s)$ (eqn [16.4]). Thus:

$$Z_E(s) = \frac{1}{(dk)^2} \left(ms + \lambda + \frac{k}{s} \right)$$

i.e.

*Equivalent electrical
impedance of
mechanical system*

$$Z_E(s) = L_1 s + R_1 + \frac{1}{C_1 s}$$

where $L_1 = \frac{m}{(dk)^2}$, $R_1 = \frac{\lambda}{(dk)^2}$, $C_1 = d^2 k$ [16.8]

The overall electrical impedance transfer function is thus given by:

$$\frac{1}{H(s)} = \frac{1}{1/Cs} + \frac{1}{Z_E(s)} = Cs + \frac{1}{R_1 + L_1 s + 1/C_1 s} \quad [16.9]$$

For sinusoidal signals we replace s by $j\omega$ to give:

$$\frac{1}{H(j\omega)} = j\omega C + \frac{1}{R_1 + j(\omega L_1 - 1/\omega C_1)} \quad [16.10]$$

and

*Overall electrical
impedance of
piezoelectric crystal*

$$H(j\omega) = \frac{\omega R_1 C_1 - j(1 - \omega^2 L_1 C_1)}{\omega(C + C_1 - \omega^2 L_1 C C_1) + j\omega^2 C C_1 R_1} \quad [16.11]$$

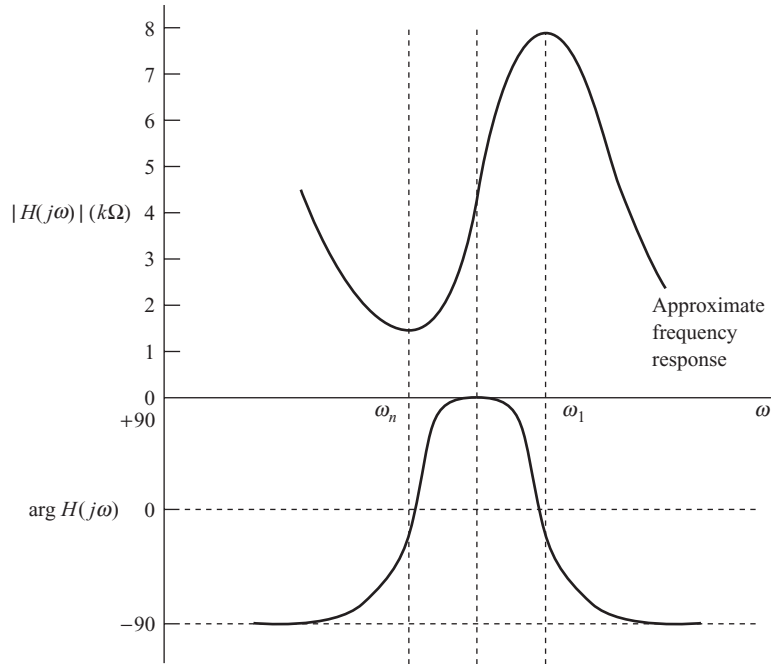
Figure 16.5 gives values of all the above parameters for a typical crystal, and shows the corresponding frequency variations of impedance magnitude $|H(j\omega)|$ and phase $\arg H(j\omega)$.

From the figure we see that there are two important frequencies. The first is the natural frequency $\omega_n = \sqrt{k/m} = 1/\sqrt{L_1 C_1}$ of the mechanical system. Here we have $1 - \omega_n^2 L_1 C_1 = 0$, so that the corresponding impedance magnitude $|H(j\omega_n)|$ is almost minimum; ω_n is termed the **series resonant frequency**. At the second frequency:

$$\omega_1 = \sqrt{\frac{C + C_1}{L_1 C_1 C}}$$

i.e. $C + C_1 - \omega_1^2 L_1 C C_1 = 0$, so that the corresponding impedance $|H(j\omega_1)|$ is almost maximum. ω_1 is termed the **parallel resonant frequency**. Below ω_n and above ω_1 , $\arg H(j\omega) = -90^\circ$, i.e. the crystal behaves as a capacitance. Between ω_n and ω_1 , $\arg H(j\omega) = +90^\circ$, i.e. the crystal is inductive.

Figure 16.5 Electrical impedance of typical piezoelectric crystal.



Crystal data

$$\begin{aligned} f_n &= 31.8 \text{ kHz} & k &= 2 \times 10^9 \text{ N/m} & m &= 5 \times 10^{-2} \text{ kg} \\ \xi &= 0.01 & \lambda &= 200 \text{ Ns/m} & d &= 2 \times 10^{-10} \text{ C/N} \\ C &= 1600 \text{ pF} & dk &= 0.4 \end{aligned}$$

$$L_1 = \frac{m}{(dk)^2} = 312.5 \text{ mH}, R_1 = \frac{\lambda}{(dk)^2} = 1250 \Omega, C_1 = d^2 k = 80 \text{ pF}$$

$$\omega_n = \sqrt{\frac{k}{m}} = \sqrt{\frac{1}{L_1 C_1}} = 2.00 \times 10^5 \text{ rad s}^{-1} \quad Q = \frac{\sqrt{mk}}{\lambda} = \frac{1}{2\xi} = 50$$

$$\omega_1 = \sqrt{\frac{C + C_1}{L_1 C_1 C}} = 2.05 \times 10^5 \text{ rad s}^{-1}$$

$$H(j\omega_n) = \frac{1250}{1 + 0.4j} \begin{cases} |H(j\omega_n)| = 1161 \Omega \\ \arg H(j\omega_n) = -22^\circ \end{cases}$$

$$H(j\omega_1) = \frac{3049 + 7512j}{j} \begin{cases} |H(j\omega_1)| = 8105 \Omega \\ \arg H(j\omega_1) = -22^\circ \end{cases}$$

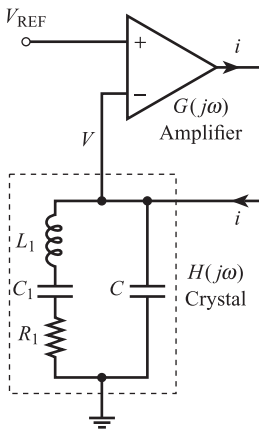


Figure 16.6 Schematic diagram of crystal oscillator.

A schematic diagram of a crystal oscillator is shown in Figure 16.6. It is a closed-loop system, with a ‘maintaining amplifier’ of impedance $1/G(j\omega)$ in the forward path, and a piezoelectric element of impedance $H(j\omega)$ in the feedback path. From Figure 16.6 we have:

$$\frac{i}{V_{\text{REF}} - V} = G(j\omega) \quad \text{and} \quad \frac{V}{i} = H(j\omega)$$

giving

$$\frac{i}{V_{\text{REF}}} = \frac{G(j\omega)}{1 + H(j\omega)G(j\omega)} \quad [16.12]$$

Using the arguments of Section 9.5, we can show that continuous oscillations at frequency ω can be maintained with $V_{\text{REF}} = 0$ if:

$$|G(j\omega)||H(j\omega)| = 1 \quad [9.52]$$

and

$$\arg G(j\omega) + \arg H(j\omega) = -180^\circ$$

Thus to maintain oscillations at ω_n we require:

$$|G(j\omega_n)| = \frac{1}{|H(j\omega_n)|} \quad [16.13]$$

and

$$\arg G(j\omega_n) = -180^\circ - \arg H(j\omega_n)$$

For the crystal specified by Figure 16.4 we require the maintaining amplifier to have:

$$|G(j\omega_n)| = \frac{1}{1161} = 8.61 \times 10^{-4}, \quad \arg G(j\omega_n) = -158^\circ \quad [16.14]$$

It is possible to adjust the frequency of oscillation slightly, by adjusting $G(j\omega)$ for the maintaining amplifier.

16.2.3 Characteristics and applications

Table 16.1 gives physical data for commonly used piezoelectric materials.^[1] **Characteristic acoustic impedance** will be discussed in Section 16.3. **Mechanical quality factor** Q is related to damping coefficient ξ by the equation $Q = 1/2\xi$. Ultrasonic transmitters and receivers are normally in the form of a thin disc of piezoelectric material with metal electrodes deposited on each face. A disc of diameter 10 mm and

Table 16.1 Physical properties of piezoelectric materials.

Material	Density ρ $\times 10^3 \text{ kg m}^{-3}$	Sensitivity d pC N^{-1}	Dielectric constant ϵ	Longitudinal velocity of sound c_L $\times 10^3 \text{ m s}^{-1}$	Characteristic acoustic impedance R_A $\times 10^7 \text{ kg m}^{-2} \text{ s}^{-1}$	Mechanical quality factor $Q = \frac{\sqrt{mk}}{\lambda}$
Quartz	2.65	2.3	4.5	5.65	1.5	> 25 000
BaTiO ₃	5.7	149	1700	4.39	2.5	< 400
PZT-5H	7.5	593	3400	4.0	3.0	< 65
PbNb ₂ O ₆	5.9	75	240	2.7	1.6	< 5
PVDF	1.8	≈10	13	2.2	0.4	14

Source: adapted in part from O'Donnell *et al.*^[1].

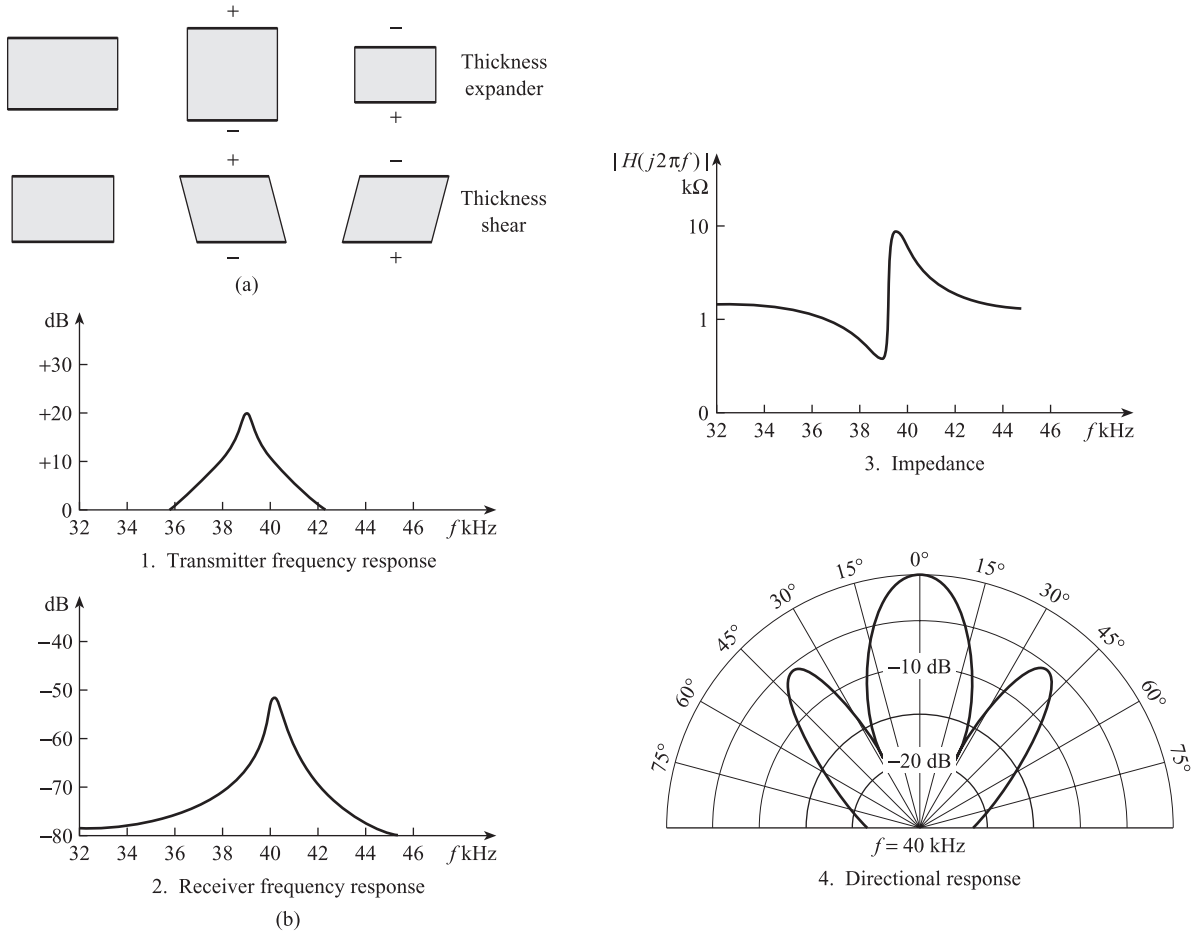


Figure 16.7 Piezoelectric transmitters and receivers: (a) Vibration displacement modes (b) Performance characteristics.

thickness 1 mm would typically have a natural frequency f_n of 5 MHz; the amplitude of the crystal deformation is around a few μm . The two usual modes of vibration are shown in Figure 16.7(a); the **thickness expander** mode is used in the generation and reception of longitudinal waves and the **thickness shear** mode in the generation of transverse waves.

The performance characteristics of piezoelectric transmitters and receivers can be summarised by four graphs: Figure 16.7(b) shows the form of the graphs in a typical case.^[2]

Graph 1 shows a decibel plot of the transmitter frequency response. This is based on the pressure/voltage transfer function $(\Delta \bar{P}_{\text{IN}} / \Delta \bar{V}_s)(s)$, which can be derived from Figure 16.3(a) using:

$$\frac{\Delta \bar{P}_{\text{IN}}}{\Delta \bar{V}_s}(s) = \frac{Z_{\text{IN}}^M}{A} s \frac{\Delta \bar{x}}{\Delta \bar{V}_s}(s) \quad [16.15]$$

where A is the area of the circular face of the disc. The decibel plot is relative to 1 μbar , i.e. $\text{dB} = 20 \log_{10}(\bar{P}_{\text{IN}} / 1 \mu\text{bar})$, and for a supply voltage V_s of 1 V rms. The graph shows a sharp resonance peak at f_n , which is characteristic of a second-order mechanical system with low ξ or high Q .

Graph 2 shows a decibel plot of the receiver frequency response. This is based on the voltage/pressure transfer function $\Delta\tilde{V}_{\text{OUT}}/\Delta\tilde{P}_{\text{OUT}}$ which can be derived from Figure 16.3(b) using

$$\frac{\Delta\tilde{V}_{\text{OUT}}}{\Delta\tilde{P}_{\text{OUT}}}(s) = A \frac{\Delta\tilde{V}_{\text{OUT}}}{\Delta\tilde{F}_{\text{OUT}}}(s) \quad [16.16]$$

The decibel plot is relative to 1 volt, i.e. $\text{dB} = 20 \log_{10}(\tilde{V}_{\text{OUT}}/1 \text{ V})$, and for a pressure of 1 μbar . The graph again shows a sharp resonance peak at f_n .

Graph 3 shows how the magnitude $|H(j2\pi f)|$ of the transducer electrical impedance varies with frequency (eqn [16.11] and Figure 16.5).

Graph 4 shows the directional response of the transmitter, i.e. how the pressure of the sound wave (at frequency f_n), launched from the transmitter, varies with angle.

Ultrasonic transmission links are usually either **narrowband** or **broadband**. In narrowband systems a narrow band of sound frequencies, close to the transducer natural frequency, is transmitted over the link. Here both transmitter and receiver should have a high Q to give a sharp resonant peak. Quartz is therefore an ideal material; a composite resonator is usually set up consisting of transmitter, transmission medium and receiver. In broadband systems either a broad band of frequencies or a pulse of sound is transmitted over the link. Here both transmitter and receiver should have a low Q to give a fairly flat frequency response. In pulse systems, Q should be ideally around 0.7, i.e. $\xi = 0.7$, give an optimum step response and minimum pulse distortion. Here low Q materials such as PbNb_2O_6 or PVDF should be used with a backing layer of absorbing material to further reduce Q (Section 16.3.5).

16.3 Principles of ultrasonic transmission

As mentioned earlier, ultrasonic waves obey the same transmission principles as lower frequency acoustic waves.

16.3.1 Propagation of plane waves

Figure 16.8 shows the transmission medium represented as a series of layers of particles. If an acoustic plane wave is passing through the medium, then each particle in a given layer, at a given time, is displaced by the same amount. For a longitudinal plane wave, the displacement d_y of a layer at position y is parallel to the direction of propagation of the wave, i.e. parallel to the Oy axis. Longitudinal plane waves are described by the partial differential equation:

$$\frac{\partial^2 d_y}{\partial y^2} = \frac{1}{c_L^2} \frac{\partial^2 d_y}{\partial t^2} \quad [16.17]$$

where d_y is the displacement of layer y at time t and c_L is the velocity of propagation of the longitudinal wave. For a progressive wave moving along the positive y direction, the solution to [16.17] is:

$$d_y = \hat{d}_y \sin \omega_L \left(t - \frac{y}{c_L} \right) \quad [16.18]$$

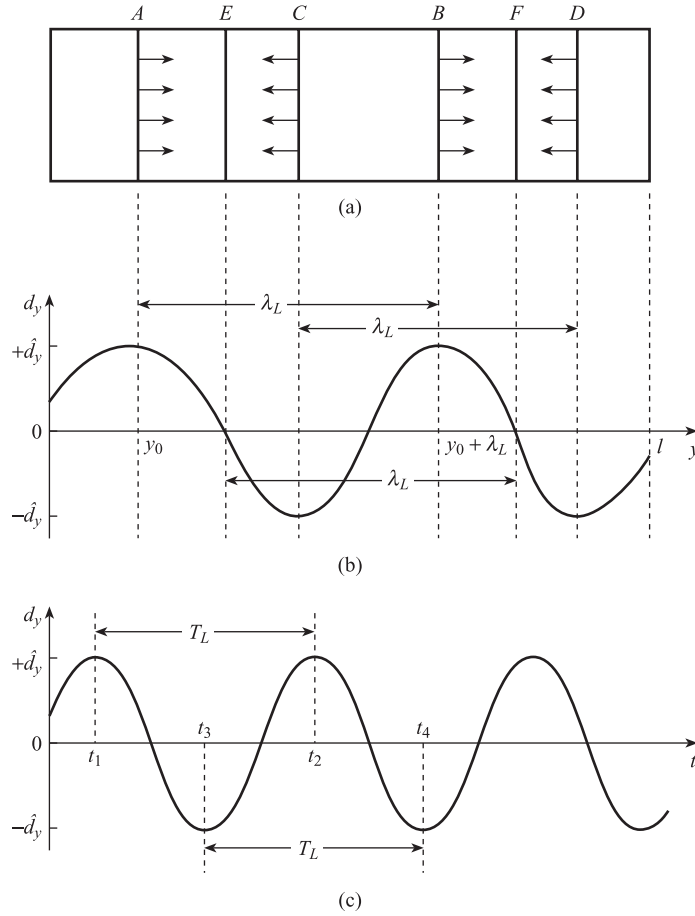
Longitudinal plane wave along positive Oy direction

Figure 16.8 Longitudinal plane waves:

(a) Wave fronts

(b) Variation of d_y with y at $t = t_0$, $d_y = \hat{d}_y \sin \omega_L(t_0 + y/c_L)$

(c) Variation of d_y with t for layer A with $y = y_0$, $d_y = \hat{d}_y \sin \omega_L(t + y_0/c_L)$.



where \hat{d}_y is the amplitude of the layer displacement and $\omega_L = 2\pi f_L$ is the angular frequency. For a progressive wave moving along the negative y direction the solution to [16.17] is:

Longitudinal plane wave along negative Oy direction

$$d_y = \hat{d}_y \sin \omega_L \left(t + \frac{y}{c_L} \right) \quad [16.19]$$

In each case, d_y is a sinusoidal function of both time t and layer position y . Figures 16.8(a) and (b) represent 'still' pictures of the displacements of each layer, taken at time $t = t_0$. Since time is now constant, d_y becomes a sinusoidal function of position y only, i.e.

$$d_y = \hat{d}_y \sin \left(\omega_L t_0 + \frac{\omega_L y}{c_L} \right) \quad [16.20]$$

The distance between layers such as A and B , C and D , E and F , which have equal displacements, is defined to be the wavelength λ_L . At A and B , $d_y = \hat{d}_y$, so that:

$$\text{at } A, \quad \omega_L t_0 + \frac{\omega_L y_0}{c_L} = \frac{\pi}{2} \quad [16.21]$$

$$\text{at } B, \quad \omega_L t_0 + \frac{\omega_L}{c_L} (y_0 + \lambda_L) = \frac{5\pi}{2}$$

Subtracting gives $\omega_L \lambda_L / c_L = 2\pi$, and since $\omega_L = 2\pi f_L$, we have

$$c_L = f_L \lambda_L \quad [16.22]$$

Relationship between velocity, wavelength and frequency for a longitudinal plane wave

Thus for a 1 MHz wave travelling with longitudinal velocity $6 \times 10^3 \text{ m s}^{-1}$ in steel, the corresponding wavelength is 6 mm. Figure 16.8(c) shows how the displacement of a given layer A , at $y = y_0$, varies sinusoidally with time t according to:

$$d_y = \hat{d}_y \sin \omega_L \left(t + \frac{y_0}{c_L} \right) \quad [16.23]$$

The period T_L of the wave is the interval between time instants t_1 and t_2 , t_3 and t_4 , where the layer displacement is the same: as usual $T_L = 1/f_L = 2\pi/\omega_L$.

For a transverse plane wave, the displacement d_z of a layer at position y is perpendicular to the direction Oy of propagation of the wave, i.e. parallel to the Oz axis. The medium is therefore subject to time-varying shear strains. The corresponding partial differential equation is:

$$\frac{\partial^2 d_z}{\partial y^2} = \frac{1}{c_T^2} \frac{\partial^2 d_z}{\partial t^2} \quad [16.24]$$

where d_z is the transverse displacement of layer y at time t , and c_T is the transverse wave velocity. For a progressive wave travelling in the positive y direction, the solution to [16.24] is similar to [16.18], i.e.

Transverse plane wave along positive Oy direction

$$d_z = \hat{d}_z \sin \omega_T \left(t - \frac{y}{c_T} \right) \quad [16.25]$$

where \hat{d}_z is displacement amplitude and $\omega_T = 2\pi f_T$ is the angular frequency. Using arguments similar to those above, we can show that the relationship between velocity, wavelength and frequency of a transverse wave is similar to [16.22], i.e.

$$c_T = f_T \lambda_T \quad [16.26]$$

The velocity of sound in a medium depends on the appropriate elastic modulus and density ρ , according to the general equation:

$$c = \sqrt{\frac{\text{elastic modulus}}{\rho}} \quad [16.27]$$

Gases will support compressive and tensile stresses but not shear stresses, so that only longitudinal acoustic waves can be passed through gases. The corresponding velocity is given by:

Velocity of longitudinal sound waves in a gas

$$c_L = \sqrt{\frac{\gamma P}{\rho}} \quad [16.28]$$

where P is the pressure of the gas and γ the specific heat ratio. In general, liquids collapse under the action of shear stresses, so that usually transverse waves cannot be transmitted through liquids. The velocity of longitudinal waves in liquids is given by:

Velocity of longitudinal waves in a liquid

$$c_L = \sqrt{\frac{B}{\rho}} \quad [16.29]$$

where B is the bulk modulus of elasticity of the liquid. Since solids will support compressive/tensile and shear stresses, both longitudinal and transverse waves can be transmitted through solids. The corresponding velocities are given by^[3]

Velocity of longitudinal and transverse waves in a solid

$$c_L = \sqrt{\frac{E(1-\nu)}{(1+\nu)(1-2\nu)\rho}}$$

$$c_T = \sqrt{\frac{s}{\rho}} \quad [16.30]$$

where E is Young's modulus, s is the shear modulus and ν is Poisson's ratio for the solid.

16.3.2 Acoustic impedance and power

In Chapter 5 we saw that mechanical force F and velocity \dot{x} were an effort/flow pair, so that the product $F\dot{x}$ represents mechanical power and the ratio F/\dot{x} represents mechanical impedance. In acoustic work the particle velocity $u = \partial d/\partial t$ is the flow variable, and the accompanying pressure or stress P is the effort variable. Specific acoustic impedance is thus defined by:

Specific acoustic impedance

$$Z_A = \frac{P}{u} \quad [16.31]$$

As with electrical impedance, Z_A is, in general, a complex quantity of the form $Z_A = R_A + jX_A$. However, for plane progressive waves, the imaginary component X_A is zero,

Table 16.2 Characteristic impedance of some common materials.

Material	Longitudinal velocity of sound c_L m s ⁻¹	Density ρ kg m ⁻³	Characteristic impedance $R_A = \rho c_L$ kg m ⁻² s ⁻¹
Steel	6.0×10^3	7.80×10^3	4.7×10^7
Iron	5.90×10^3	7.90×10^3	4.7×10^7
Brass	3.50×10^3	8.60×10^3	3.0×10^7
Aluminium	6.40×10^3	2.70×10^3	1.7×10^7
Bone	$\approx 5.3 \times 10^3$	$\approx 1.5 \times 10^3$	$\approx 0.8 \times 10^7$
Glass	5.50×10^3	2.50×10^3	1.3×10^7
Biol. tissue	$\approx 1.5 \times 10^3$	$\approx 1.0 \times 10^3$	$\approx 0.15 \times 10^7$
Polystyrene	2.35×10^3	1.10×10^3	0.25×10^7
Oil	1.40×10^3	0.90×10^3	0.13×10^7
Water	1.50×10^3	1.0×10^3	0.15×10^7
Air	0.34×10^3	1.3	430

Source: adapted from Blitz^[3].

leaving $Z_A = R_A$. It can be shown that R_A is the product of density ρ and velocity of sound c for the material, i.e.

Characteristic impedance of a medium

$$R_A = \rho c$$

[16.32]

Table 16.2 (adapted from Blitz^[3]) gives values of longitudinal velocity, density and characteristic impedance for commonly used materials.

The power or intensity at any point in an acoustic field is the product Pu of through and across variables. For a plane progressive wave, we can use eqn [16.31] to give three equations for acoustic intensity:

Acoustic intensity or power

$$W = Pu = \frac{P^2}{R_A} = u^2 R_A$$

[16.33]

W is the rate of flow of acoustic energy, through unit area, at right angles to the direction of propagation of the wave, and has the units of $W\ m^{-2}$.

16.3.3 Attenuation of a plane wave in a medium

So far we have assumed that as a plane acoustic wave travels through a material, the amplitudes \hat{d} and \hat{P} of particle displacement and pressure variation respectively remain constant. In practice the wave becomes attenuated as it passes through the medium, so that the amplitudes decrease exponentially with distance y travelled.

Thus for displacement amplitudes we have:

Displacement attenuation for a plane wave

$$\hat{d}(y) = \hat{d}(0) \exp(-\alpha_d y)$$

[16.34]

where $\hat{d}(0)$ is the amplitude at the beginning of the medium, $\hat{d}(y)$ is the amplitude at position y , and $\alpha_d \text{ m}^{-1}$ is the displacement attenuation coefficient. A similar equation relates the acoustic intensity $W(y)$ at position y to the intensity $W(0)$ at $y = 0$, i.e.

Power attenuation for a plane wave

$$W(y) = W(0) \exp(-\alpha_w y) \quad [16.35]$$

where $\alpha_w \text{ m}^{-1}$ is the power attenuation coefficient. Various mechanisms are responsible for this power loss. In liquids viscous friction effects are important; in solids scattering at grain boundaries and absorption at crystal lattice defects are the main loss mechanisms.

16.3.4 Reflection and refraction at a boundary between two materials

Figure 16.9 shows a plane wave incident on a plane boundary separating two materials of different characteristic impedances. From the figure, we see that part of the incident wave I is reflected (R), and part is transmitted (T). The laws relating the angles θ_i , θ_R and θ_T of incidence, reflection and transmission are those for any wave motion. Figure 16.9 takes no account of possible conversion of longitudinal waves into transverse waves, and vice versa, at the boundary. The ratio between intensity W_R and incident intensity W_I is termed the reflection coefficient α_R ; the ratio between transmitted intensity W_T and incident intensity W_I is the transmission coefficient α_T , i.e.

$$\alpha_R = \frac{W_R}{W_I}, \quad \alpha_T = \frac{W_T}{W_I} \quad [16.36]$$

Figure 16.9 Reflection and refraction of sound at a boundary between two materials.

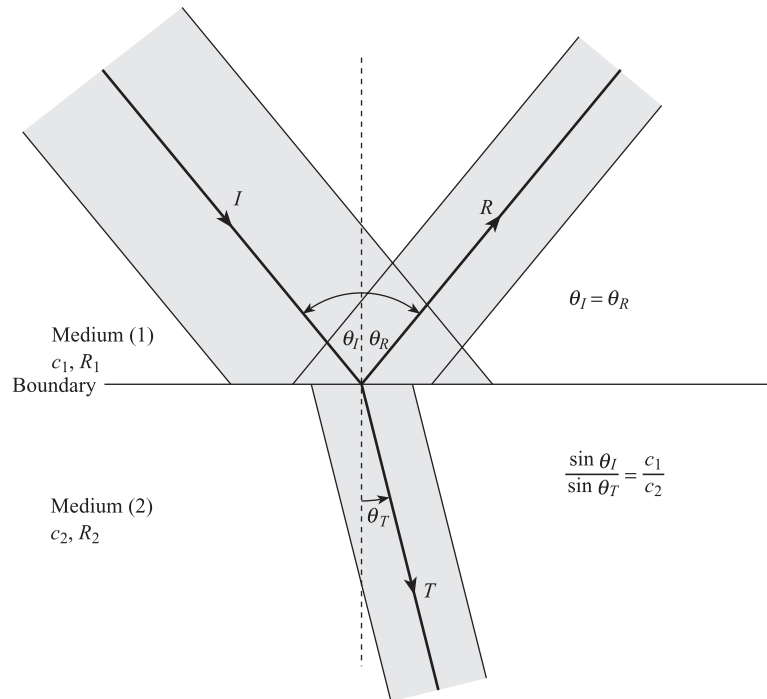


Table 16.3 Values of α_R and α_T at the boundaries of five common materials.

	Steel	Quartz	Polystyrene	Water	Air
Steel	0.0, 1.0	0.27, 0.73	0.81, 0.19	0.88, 0.12	$\approx 1.0, 3.7 \times 10^{-5}$
Quartz		0.0, 1.0	0.51, 0.49	0.67, 0.33	$\approx 1.0, 1.1 \times 10^{-4}$
Polystyrene			0.0, 1.0	0.06, 0.94	$\approx 1.0, 6.9 \times 10^{-4}$
Water				0.0, 1.0	$\approx 1.0, 1.1 \times 10^{-3}$
Air					0.0, 1.0

For normal or near-normal angles of incidence, i.e. $\theta_i \approx \theta_R \approx \theta_T \approx 0$, it can be shown that^[4]

Reflection and transmission coefficients for near-normal incidence

$$\alpha_R = \frac{(R_2 - R_1)^2}{(R_2 + R_1)^2}, \quad \alpha_T = \frac{4R_1R_2}{(R_2 + R_1)^2} \quad [16.37]$$

We note that $\alpha_R + \alpha_T = 1$; this is a consequence of energy conservation, i.e. $W_R + W_T = W_I$. Table 16.3 uses R values from Table 16.2 to give α_R and α_T values for boundaries of five important materials. We see that the α_T values for quartz/steel and steel/water are reasonably large. This is of great practical value, because it means that sound waves can be launched from quartz crystal transmitters into solid metal bars, and also into liquids contained in metal pipes and vessels. The α_R values for steel/air and water/air are very close to unity (α_T very small); this means there is almost perfect reflection of sound waves at these boundaries. Detection of cracks and flaws in metal samples and at the liquid/gas interface in level measurement is therefore possible.

We can now examine the efficiency of the simple transmission link of Section 16.1 and Figure 16.1. As an example, consider a quartz transmitter and receiver attached to opposite sides of a steel billet 10 cm thick. The ratio $W_{R/X}/W_{T/X}$ of received power to transmitted power depends on attenuation losses in the steel, together with interface losses at the quartz/steel and steel/quartz boundaries. Using eqns [16.35] and [16.36] we have:

$$\frac{W_{R/X}}{W_{T/X}} = (\alpha_T)_{Q/S} e^{-\alpha_W l} (\alpha_T)_{S/Q} \quad [16.38]$$

Since $(\alpha_T)_{Q/S} = (\alpha_T)_{S/Q} = 0.73$, $l = 0.1$ m, and assuming $\alpha_W = 2.0$ for steel,

$$\frac{W_{R/X}}{W_{T/X}} = (0.73)^2 e^{-0.2} = 0.53 \times 0.82 = 0.44$$

i.e. the efficiency of energy transmission is 44%.

From Table 16.3 we see that the α_T values for quartz/air and steel/air are very small. This means that it is very difficult to launch a sound wave from a piezoelectric transmitter into a gas, either directly or via a steel pipe. One way of overcoming this problem is to place a **matching layer** between the transmitter and the gas. If R_1 , R and R_2 are the characteristic impedances of the transmitter, matching layer and gas respectively then:

$$\alpha_{T,M} = \frac{4R_1R}{(R_1 + R)^2}, \quad \alpha_{M,G} = \frac{4RR_2}{(R + R_2)^2} \quad [16.39]$$

and the overall transmission coefficient between transmitter and gas is:

$$\alpha_{T,G} = \alpha_{T,M} \times \alpha_{M,G} = \frac{16R_1R_2R^2}{(R_1 + R)^2(R + R_2)^2} \quad [16.40]$$

It can be shown (Problem 16.9) that this overall transmission coefficient is a maximum when:

*Optimum impedance
of matching layer*

$$R = \sqrt{R_1R_2} \quad [16.41]$$

Thus in order to maximise power transfer between quartz ($R_1 = 1.5 \times 10^7$) and air ($R_2 = 430$) a matching layer with $R \approx 8 \times 10^4$ is required. From Table 16.1, we see that $R_A \approx 0.4 \times 10^7$ for PVDF, and from Table 16.2, $R_A \approx 0.15 \times 10^7$ for biological tissue. Acoustic power can therefore be efficiently launched from PVDF transducers directly into the human body without the need for matching layers.

16.3.5 Stationary waves and resonance

Consider a progressive plane wave travelling along the positive y direction through a medium with zero attenuation coefficient. If it meets the boundary with a medium of very different characteristic impedance then almost perfect reflection occurs. This means that there is now a reflected wave travelling along the negative y direction with equal amplitude to the incident wave. For longitudinal waves the incident wave is:

$$d_y = \hat{d}_y \sin \left[\omega_L \left(t - \frac{y}{c_L} \right) \right]$$

and the reflected wave is:

$$d_y = \hat{d}_y \sin \left[\omega_L \left(t + \frac{y}{c_L} \right) \right]$$

The resultant particle displacement is therefore:

$$d_y^R = \hat{d}_y \left\{ \sin \omega_L \left(t - \frac{y}{c_L} \right) + \sin \omega_L \left(t + \frac{y}{c_L} \right) \right\}$$

*Equation for
stationary wave*

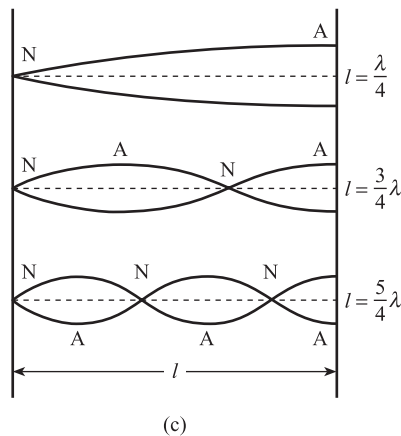
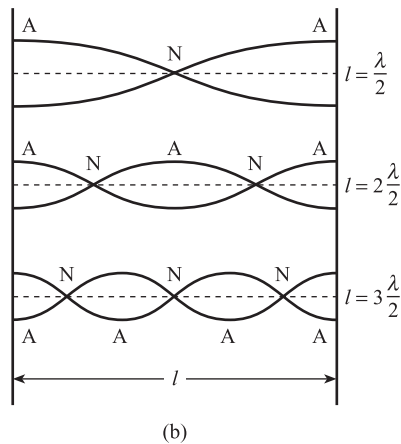
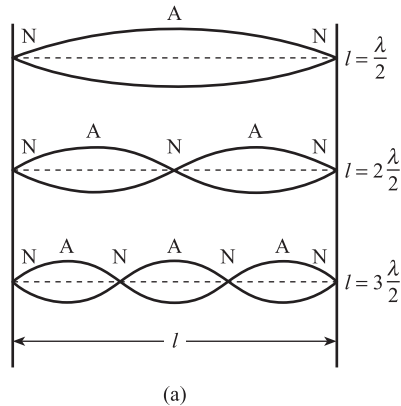
$$d_y^R = 2\hat{d}_y \cos \left(\frac{\omega_L y}{c_L} \right) \sin(\omega_L t) \quad [16.42]$$

The function $2\hat{d}_y \cos(\omega_L y/c_L)$ defines the wave amplitude or envelope. Since this is independent of t , i.e. does not move forward with time, the wave is **stationary**. At values of y where $\cos(\omega_L y/c_L) = 0$, the envelope has a minimum value of zero; these

are **nodes**. At values of y where $\cos(\omega_L y/c_L) = 1$, the envelope has a maximum value of $2\hat{d}_y$; these are **antinodes**.

In practice the medium will have finite length l , and the type of stationary or **standing wave** set up will depend on the boundary conditions at each end of the medium, i.e. whether there are nodes or antinodes. In the special cases that the frequency of the sound wave is such that l is a whole number of either half or quarter wavelengths, then **resonance** is produced where \hat{d}_y has a large resonant value.

Figure 16.10 Resonant stationary wave patterns:
(a) Half wave resonance – node at each end
(b) Half wave resonance – antinode at each end
(c) Quarter wave resonance – node at one end, antinode at other end.



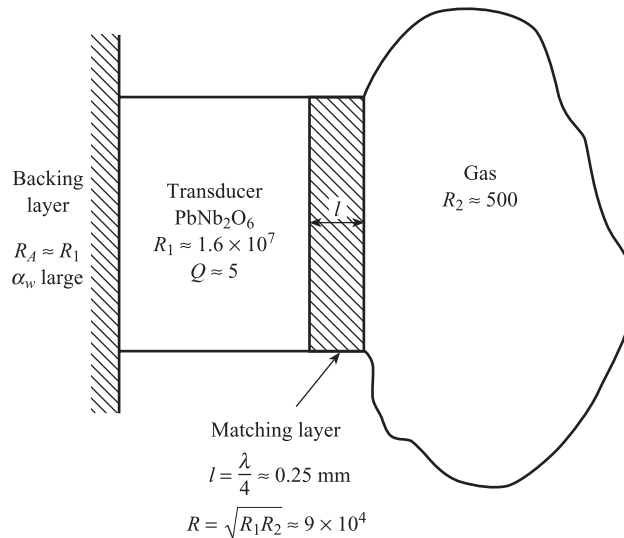
Two types of resonance are possible. In **half wave resonance** (Figures 16.10(a) and (b)) there are identical boundary conditions at each end of the medium. Figure 16.10(a) shows possible resonant modes for a node at each end; these modes could occur if a medium of low characteristic impedance is bounded on both sides by a medium of high impedance, for example a gas inside a metal pipe. Figure 16.10(b) shows possible resonant modes for an antinode at each end; these modes could occur if a medium of high impedance is bounded on both sides by a medium of low impedance, for example a metal bar surrounded by gas. The other type of resonance is **quarter wave resonance**; here there are different boundary conditions, i.e. a node and antinode, at each end of the medium. Figure 16.10(c) shows the possible resonant modes; these modes could occur if a medium of intermediate impedance is bounded on one side by a material of high impedance and on the other by a material of low impedance.

The principles discussed in this and previous sections are important in the design of efficient transmitters. As an example, consider the problem of launching a pulse of ultrasound from a piezoelectric transducer into a gas. There are three essential requirements:

1. The sound wave launched from the rear face of the transducer should not enter the gas, otherwise pulse transit time measurements will be confused.
2. The overall Q should be ideally around 0.7 to minimise pulse distortion.
3. Maximum power should be transmitted from the front face of the transducer into the gas.

The transmitter shown in Figure 16.11 fulfils these requirements. The backing layer, with characteristic impedance similar to that of the transducer and high attenuation coefficient, accepts and absorbs the wave from the rear face. This layer also reduces the Q of the overall transmitter to a value well below that of the transducer itself. The matching layer has length $l = \lambda/4$, so that a quarter wave resonant mode is present, and impedance $R = \sqrt{R_1 R_2}$. This ensures maximum power transfer from transducer front face to the gas.

Figure 16.11 Transmitter for launching sound pulses into a gas.



16.3.6 Doppler effect

When a source (or transmitter) and observer (or receiver) of sound waves are in relative motion, then the frequency of the received signal differs from the frequency of the transmitted signal by an amount that depends on the relative velocities of source and observer. This shift in apparent frequency is called the Doppler effect and occurs in all types of wave motion. There are two cases to consider.^[5] One is where the source is stationary and the observer is moving; the other is where the source is moving and the observer stationary.

Figure 16.12(a) shows a stationary source of sound S with frequency f and a stationary observer O . If the disturbance takes time Δt to travel from S to O , then O receives $f\Delta t$ cycles in this time and the distance $OS = f\lambda\Delta t$. If O moves towards S with velocity v , then in time Δt it travels a distance $v\Delta t$ to O' (Figure 16.12(b)), and receives an additional $v\Delta t/\lambda$ cycles of sound. The total number of cycles received in Δt is thus $(f + v/\lambda)\Delta t$ and the apparent frequency is:

$$f' = f + \frac{v}{\lambda} = f + \frac{f}{c} v = f \left(\frac{c + v}{c} \right) \quad [16.43]$$

since $1/\lambda = f/c$. If O moves away from S with velocity v , then $(f - v/\lambda)\Delta t$ cycles are received in time Δt , so that the apparent frequency is:

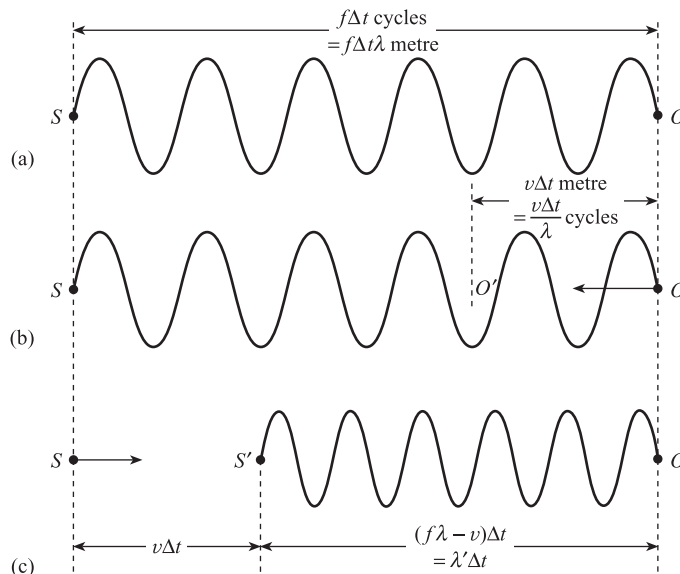
$$f' = f \left(\frac{c - v}{c} \right) \quad [16.44]$$

We can generalise these two results by the single equation:

*Doppler shift: fixed
source, moving
observer*

$\frac{f'}{f} = \frac{\text{velocity of waves relative to observer}}{\text{normal wave velocity}}$	[16.45]
--	---------

Figure 16.12 Doppler effect.



If S now moves towards O (stationary) with velocity v , then in time Δt it travels a distance $v\Delta t$ to S' (Figure 16.12(c)). In this case $f\Delta t$ cycles of sound occupy the distance $S'O = (f\lambda - v)\Delta t$. The apparent wavelength is thus:

$$\lambda' = \frac{\text{total distance}}{\text{total number of cycles}} = \frac{(f\lambda - v)\Delta t}{f\Delta t} = \lambda - \frac{v}{f} \quad [16.46]$$

Since

$$\frac{1}{f} = \frac{\lambda}{c}, \quad \lambda' = \lambda - \lambda \frac{v}{c} = \lambda \left(\frac{c - v}{c} \right) \quad [16.47]$$

If S moves away from O we have:

$$\lambda' = \lambda \left(\frac{c + v}{c} \right) \quad [16.48]$$

and we can generalise these two results by the single equation:

Doppler shift: moving source, fixed observer

$$\frac{\lambda'}{\lambda} = \frac{\text{velocity of waves relative to source}}{\text{normal wave velocity}} \quad [16.49]$$

16.4 Examples of ultrasonic measurement systems

16.4.1 Pulse reflection or pulse echo systems

Figure 16.13(a) shows a typical system. A piezoelectric crystal acting as a transmitter/receiver is attached to medium 1; the characteristic impedances of media 1 and 2 are substantially different. When the crystal acts as a transmitter, an oscillator giving a sinusoidal voltage at radio frequency f is connected to the crystal for a time T_w using switch A. Thus a pulse of ultrasound of width T_w enters medium 1 and most of the pulse energy is reflected at the boundary of medium 1 with medium 2. The reflected pulse returns to the crystal at a time T_T after the outgoing pulse. Since T_T is the time for the 'round trip' of distance $2l$ then:

Transit time for pulse echo system

$$T_T = \frac{2l}{c} \quad [16.50]$$

where l is the distance of the interface from the crystal and c is the velocity of sound in medium 1.

The crystal now acts as a receiver and converts the reflected pulse into a voltage pulse. Switch B is now closed so that the pulse passes to the echo signal conditioning circuit where it is amplified, rectified and 'squared up' using a Schmitt trigger. Figure 16.13(b) shows the idealised outgoing and reflected pulse waveforms. These pulse waveforms pass to a logic circuit which detects the leading edge of the outgoing pulse and that of the first reflected pulse; the resulting output is a pulse signal

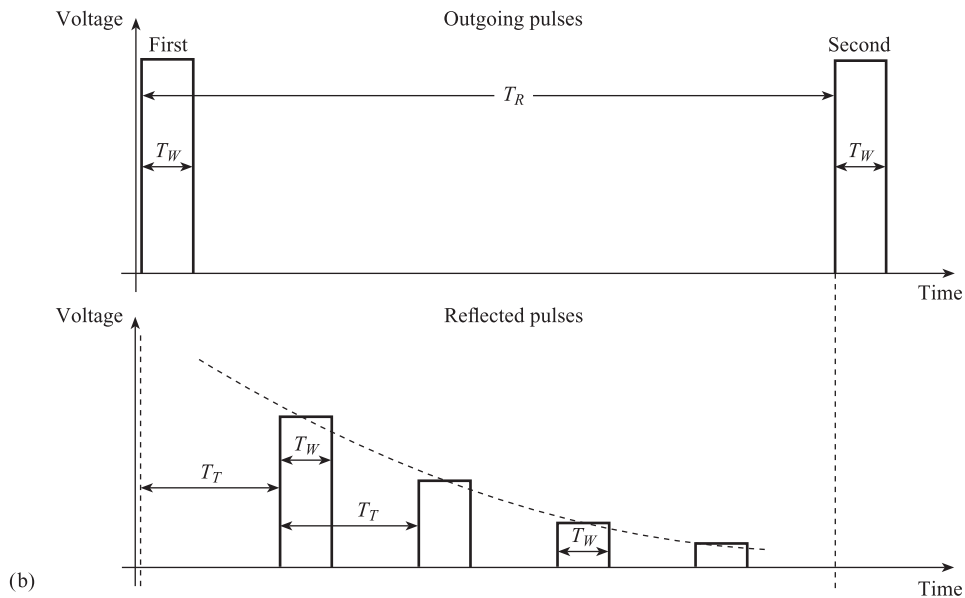
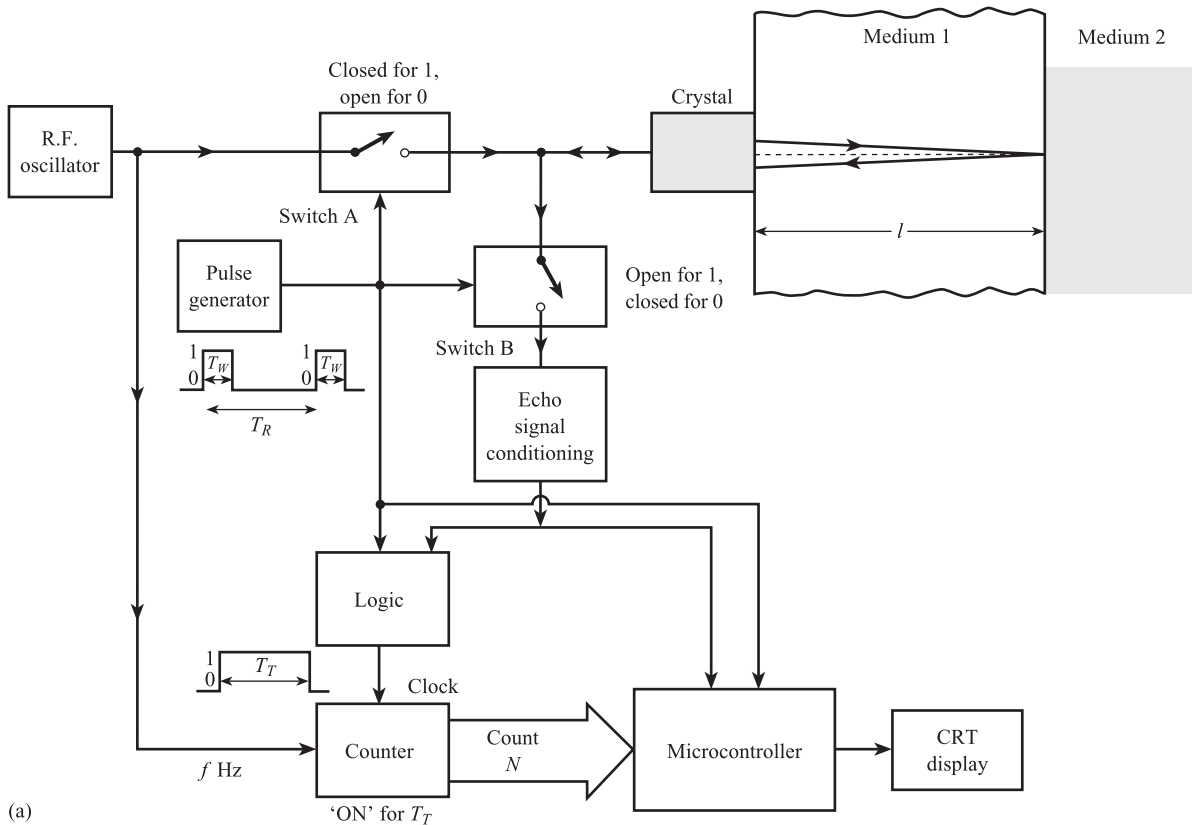


Figure 16.13 Pulse reflection techniques

(a) Typical system

(b) Idealised outgoing and reflected pulse waveforms.

which is in the '1' state during the transit time T_T . This is used to control a counter which also receives clock pulses at frequency f from the signal generator. The total count N during the 'on' time is therefore $N = fT_T$. This is transferred to a micro-controller using a parallel digital signal. The computer calculates T_T from N and uses equation [16.50] with a known value of c to find l .

The measurement is complicated by the creation of multiple reflections or 'echoes'. Part of the first reflected pulse is reflected at the boundary of medium 1 and the crystal, and reflected again at the boundary of media 1 and 2 to give a second reflected pulse. The process is repeated many times, the amplitude of the reflected pulses dying away due to attenuation losses in medium 1 and reflection losses at the boundaries. Figure 16.13(b) shows these multiple reflected pulses. The following conditions should be obeyed by the pulse signal:

- (a) The pulse width T_W should be large compared with the period $1/f$ of the sound wave; this ensures that there are many cycles, i.e. sufficient energy, in each pulse:

$$T_W \gg \frac{1}{f} \quad [16.51]$$

- (b) The transit time T_T should be large compared with the pulse width T_W to avoid interference between outgoing and reflected pulses:

$$T_T \gg T_W \quad [16.52]$$

- (c) The repetition time T_R between successive outgoing pulses should be large compared with transit time T_T ; this ensures that all reflections, following one outgoing pulse, are attenuated before the next enters the material:

$$T_R \gg T_T \quad [16.53]$$

Thus for a metal specimen with $l = 0.2$ m and $c = 5 \times 10^3$ m s⁻¹, $T_T = 80$ μs. If $f = 1$ MHz, then the above conditions are satisfied with $T_W = 15$ μs, $T_R = 1$ ms.

Because of the large difference in characteristic impedance between most solids and air, this method can be used for thickness measurement. Pulse reflection techniques are also commonly used for the detection of flaws in metals.^[6] Here frequency f is chosen so that the sound wavelength is small compared with the size of defects it is desired to detect.

The large difference in characteristic impedance between gases and liquids means that almost perfect reflection occurs at a liquid/gas interface and that these techniques are applicable to level measurement. Analysis of the interface losses (Problem 16.2) would suggest that it is better to mount the crystal at the base of the vessel, directing the waves upwards through the liquid, rather than mount the crystal at the top of the vessel, directing the waves downwards through the gas. However, most commercial ultrasonic level measurement systems^[7-10] use the latter method, because it offers greater ease of installation and maintenance.

Another important application of pulse reflection techniques is in the 'imaging' of areas of the human body.^[11] Figure 16.14(a) shows, in simplified form, the various layers of tissue.^[12] The characteristic impedance of these layers will be different: for example, the impedance of bone is around 0.8×10^7 whereas that of soft biological tissue is around 0.15×10^7 (Table 16.2). A piezoelectric transducer is placed on the epidermis layer, which has either a characteristic impedance close to that of soft tissue (e.g. PVDF) or a matching layer. This minimises internal reflections at the transducer/epidermis boundary and the problem of multiple echoes.

Figure 16.14 Ultrasonic imaging of human body (adapted from Payne^[12]):
 (a) Layers and coordinate system
 (b) A-scan display
 (c) B-scan display.

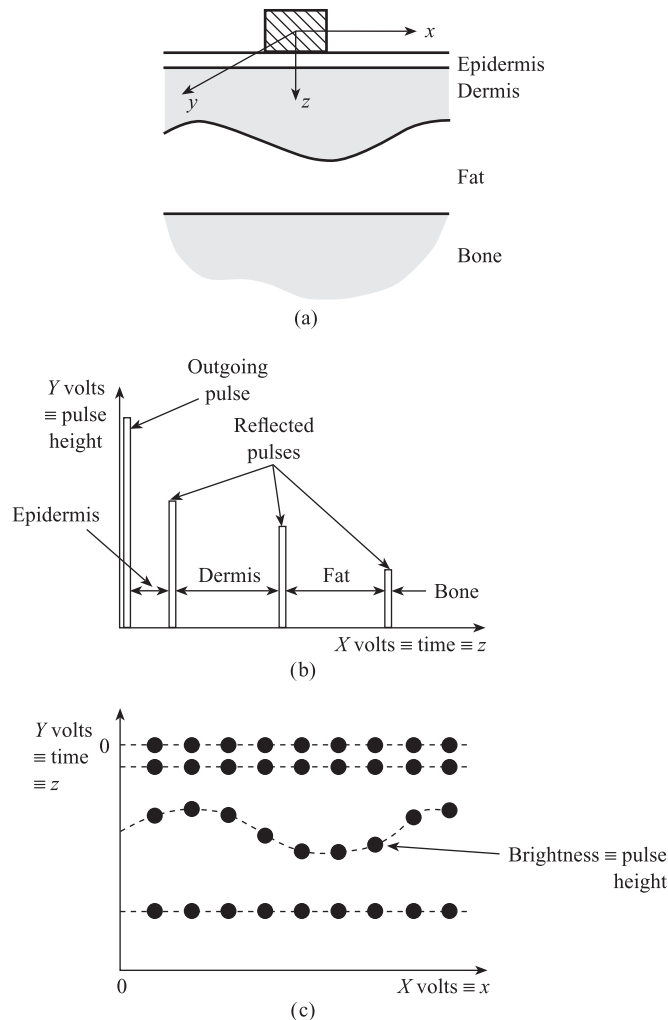


Figure 16.14(b) shows the CRT trace obtained when the system of Figure 16.13 is used with the layer system of Figure 16.14(a). The three reflected pulses correspond to reflections at the epidermis/dermis, dermis/fat and fat/bone boundaries respectively; the time intervals between successive reflected pulses are proportional to the thickness of each layer. This trace, referred to as an **A-scan display**, is rather difficult to interpret; a more realistic image is obtained using a **B-scan display**. Here the transducer is connected to two displacement sensors which measure transducer x and y position coordinates on the body surface. The output voltage of the x sensor is applied to the X plates of the CRT and a voltage proportional to time, i.e. distance z travelled through the body, is applied to the Y plates. The brightness of the image on the screen is proportional to the transducer output voltage (Z modulation) so that a bright spot corresponds to a reflected pulse. By keeping the transducer y -coordinate fixed and adjusting the x -coordinate, an image of the body in the x - z plane is built up and stored (Figure 16.14(c)). Thus the B-scan images a 'slice' through the body, normal to the surface. Another alternative is the **C-scan display**; this is an image of the body in the x - y plane, i.e. a slice parallel to the surface of the body. This is obtained

Figure 16.15 C-scan display of human foetus (by permission of Nottingham City Hospital NHS Trust and Sarah Morton).



by applying x sensor output voltage to the CRO X plates and y sensor output voltage to the Y plates and using Z modulation. Figure 16.15 shows a C-scan display of a human foetus.

16.4.2 Ultrasonic Doppler flowmeter

This flowmeter uses the Doppler effect discussed in Section 16.3.6 and is shown in Figure 16.16. We see that the flowmeter is completely external to the pipe; it is thus suitable for the 'difficult' flowmetering problems discussed in Section 12.5 (i.e. corrosive fluids, slurries) and as a 'clip-on' flowmeter.^[13] The transmitting crystal sends an ultrasonic wave of frequency f and velocity c into the fluid, at an angle θ relative to the direction of flow. Bubbles, solid particles or eddies in the flow stream can be regarded as 'observers', moving with velocity v relative to the fixed transmitter.

The velocity of sound waves relative to the observer is $c + v \cos \theta$, so that from eqn [16.45] the apparent frequency f' seen by the observer is given by:

$$\frac{f'}{f} = \frac{c + v \cos \theta}{c} \quad [16.54]$$

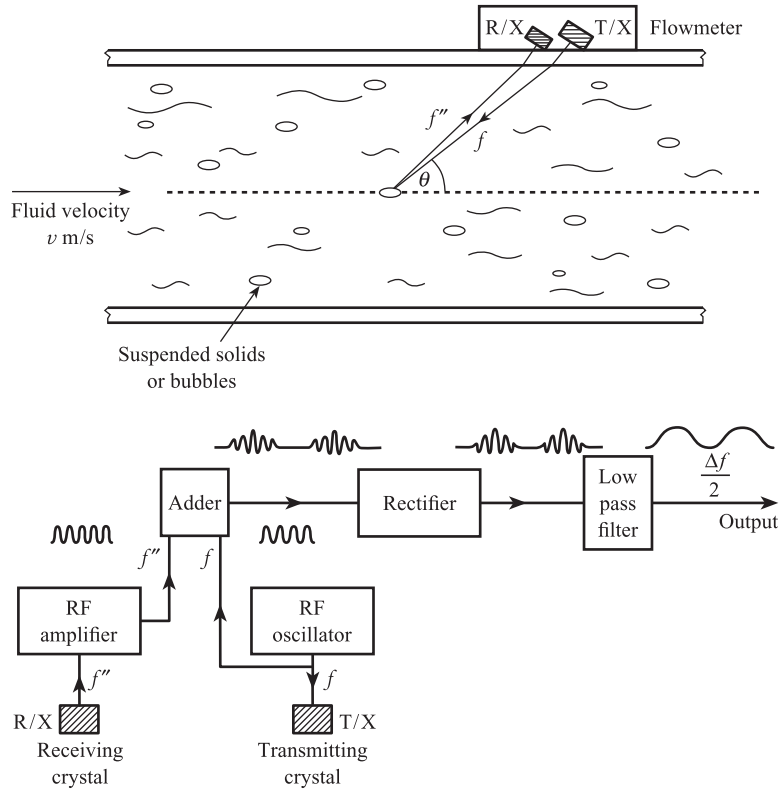
The particle scatters the incident sound wave in all directions, but a small proportion is back-scattered in the direction of the receiving crystal. The particle now acts as a 'source' moving with velocity v relative to the receiving crystal, acting as a fixed observer. The velocity of the sound waves relative to the source is $c - v \cos \theta$, so that from eqn [16.49] the apparent wavelength seen by the receiving crystal is given by:

$$\frac{\lambda''}{\lambda'} = \frac{c - v \cos \theta}{c} \quad [16.55]$$

Since $\lambda'' f'' = \lambda' f' = c$, the corresponding received frequency f'' is:

$$\frac{f''}{f'} = \frac{c}{c - v \cos \theta} \quad [16.56]$$

Figure 16.16 Doppler flowmeter – layout and signal processing.



Eliminating f' between [16.54] and [16.56] gives:

$$f'' = f \left(\frac{c + v \cos \theta}{c - v \cos \theta} \right) = f \left(\frac{1 + \frac{v}{c} \cos \theta}{1 - \frac{v}{c} \cos \theta} \right) \quad [16.57]$$

Typically we have $c \approx 10^3 \text{ m s}^{-1}$ and $v \approx 10 \text{ m s}^{-1}$, i.e. $v/c \approx 10^{-2}$. Thus we can ignore terms involving second and higher powers of v/c . With this approximation [16.57] reduces to:

*Frequency shift in
Doppler flowmeter*

$$\Delta f = f'' - f = \frac{2f}{c} (\cos \theta) v \quad [16.58]$$

Thus the frequency difference Δf is proportional to fluid velocity v , and thus volume flowrate. If $f = 1 \text{ MHz}$ and $\theta = 30^\circ$, then $\Delta f = 17.3 \text{ kHz}$ for the above values of c and v .

Figure 16.16 shows a possible system for processing the electrical signal from the receiver crystal. Due to attenuation, interface and scattering losses, the receiver signal is at a low level, and is first amplified to the amplitude \hat{V} of the transmitter drive signal. Both signals are input to an adder. The adder output signal is:

$$\begin{aligned}
 V_{\text{ADD}} &= \hat{V} \sin 2\pi f''t + \hat{V} \sin 2\pi ft \\
 &= 2\hat{V} \cos \frac{2\pi(f'' - f)t}{2} \sin \frac{2\pi(f + f'')t}{2}
 \end{aligned}
 \quad [16.59]$$

This is a sine wave of frequency $(f + f'')/2$ and amplitude $2\hat{V} \cos(2\pi\Delta f t/2)$, which is an amplitude modulated signal with a carrier frequency of $(f + f'')/2$ and a modulating frequency of $\Delta f/2$. The signal is demodulated to give a final output sinusoidal signal whose frequency $\Delta f/2$ is proportional to fluid velocity v .

16.4.3 Ultrasonic cross-correlation flowmeter

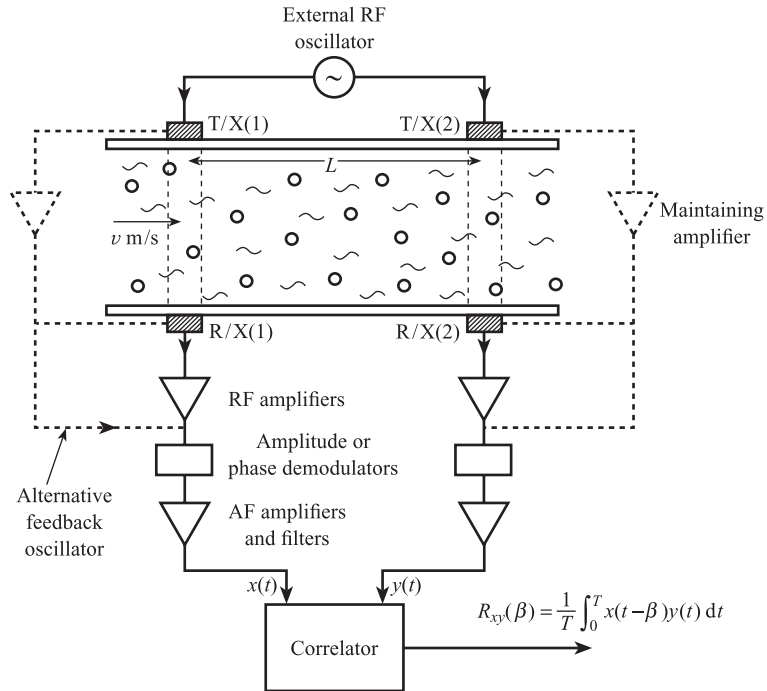
The principle of the cross-correlation flowmeter has already been explained in Section 12.5. In general it consists of two sensors, at distance L apart, which detect random fluctuations in some property of the fluid. The sensor output signals $x(t)$ (upstream) and $y(t)$ (downstream) are input to a correlator which evaluates the cross-correlation function:

$$R_{xy}(\beta) = \lim_{T \rightarrow \infty} \frac{1}{T} \int_0^T x(t - \beta)y(t) dt$$

This has a maximum at $\beta = L/v$, when there is maximum similarity between the delayed upstream signal $x(t - \beta)$ and the downstream signal $y(t)$.

Figure 16.17 shows an ultrasonic cross-correlation flowmeter^[14,15] consisting of two transmission links T/X(1)–R/X(1) and T/X(2)–R/X(2). The meter is completely external to the pipe and is especially suitable for two-phase flow measurements, that

Figure 16.17 Ultrasonic cross-correlation flowmeter.



is liquids with suspended gas bubbles or solid particles. A bubble or particle has a different acoustic impedance from that of the liquid. This means that if one is present in either of the transmission links, there are two extra interfaces and corresponding reflection losses. The ultrasonic wave reaching the receiver is reduced in amplitude and changed in phase relative to the received wave with no particles present. The number of particles in either link varies randomly with time, causing the received ultrasonic waves to be randomly modulated, in both amplitude and phase. The receiver signals are first amplified and then demodulated to remove the high-frequency carrier signal. The demodulated signals, representing the random fluctuations in flow, are then amplified and input to the correlator. Each transmission link can be either energised by an external r.f. oscillator (solid line), or incorporated into a feedback oscillator system of the type described in Section 16.2 (dotted line).

16.4.4 Ultrasonic transit time flowmeter

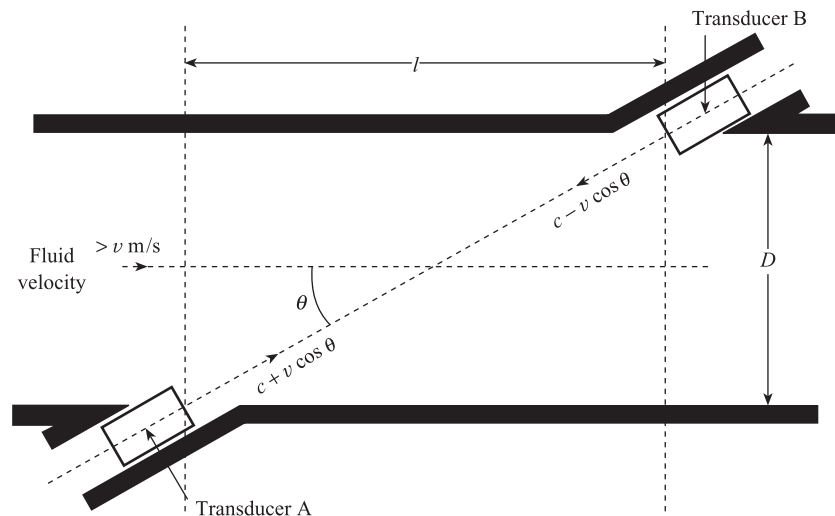
Figure 16.18 shows an ultrasonic transit time flowmeter of the ‘wetted sensor’ type where the piezoelectric transducers are in contact with the fluid. This is suitable for clean, single-phase liquids and gases. For dirty, hostile or multiphase flows, a ‘clamp on’ type, with the transducers mounted on the outside of the pipe, is preferred. Firstly, transducer B acts as a transmitter and sends a pulse of ultrasound to transducer A, acting as a receiver. The corresponding transit time from B to A is:

$$T_{BA} = \frac{L}{c - v \cos \theta} \quad [16.60]$$

where path length $L = D/\sin \theta$ and c is the velocity of sound in the fluid. If then A acts as a transmitter and sends a pulse to B acting as a receiver, the corresponding transit time from A to B is:

$$T_{AB} = \frac{L}{c + v \cos \theta} \quad [16.61]$$

Figure 16.18 Ultrasonic transit time flowmeter.



The **differential transit time** ΔT is therefore given by:

$$\begin{aligned}\Delta T = T_{BA} - T_{AB} &= \frac{D}{\sin \theta} \left(\frac{L}{c - v \cos \theta} - \frac{1}{c + v \cos \theta} \right) \\ &= \frac{2D \cot \theta v}{c^2 \left(1 - \frac{v^2}{c^2} \cos^2 \theta \right)}\end{aligned}\quad [16.62]$$

As with the Doppler flowmeter the ratio v/c is typically 10^{-2} so that $(v^2/c^2) \cos^2 \theta \ll 1$ and eqn [16.62] reduces to:

Differential transit time

$$\Delta T = \frac{2D \cot \theta}{c^2} v \quad [16.63]$$

Thus differential transit time ΔT is proportional to fluid velocity v but is normally very small. For water in a 0.1 m diameter pipe, the transit time at $\theta = 45^\circ$, in the stationary fluid, is 95 μs . If the water velocity is 1 m s^{-1} the corresponding differential transit time is 89 ns. Thus to obtain a measurement error within 1% of reading, the maximum error in ΔT should be 0.9 ns. This high degree of precision can be obtained using a **sing-around system** where transducers A and B are continuously switched between transmitter and receiver modes.^[16] Here the differential transit time is converted into a frequency difference $\Delta f = (\sin 2\theta/D)v$ which is independent of sound velocity c .

16.4.5 Ultrasonic vortex flowmeter

This is described in Section 12.3.3.

Conclusion

This chapter began by explaining the basic ultrasonic transmission link, which consists of a **transmitter**, a **transmission medium** and a **receiver**. The next section examined the detailed characteristics of ultrasonic transmitters and receivers based on **piezoelectric** crystals. The following section studied the principles of ultrasonic transmission including **plane wave propagation**, **acoustic impedance and power**, **attenuation**, **reflection**, **refraction** and **stationary** waves. The final section looked at examples of ultrasonic measurement systems including **pulse reflection**, **Doppler**, **cross-correlation** and **transit time** systems.

References

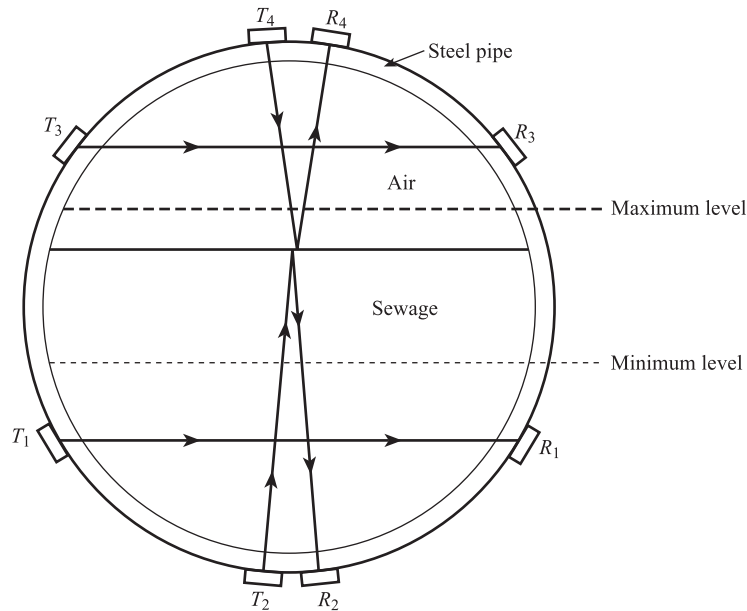
- [1] O'DONNELL M, BUSSE L J and MILLER J G 1981 'Piezoelectric transducers', *Methods of Experimental Physics*, vol. 19, Academic Press.

- [2] Massa Products Corporation 1983 *Technical Information on Model Tr-89/B Series Transducers*.
- [3] BLITZ J 1971 *Ultrasonics: Methods and Applications*, Butterworths, London.
- [4] BLITZ J 1967 *Fundamentals of Ultrasonics*, 2nd edn, Butterworths, London.
- [5] LONGHURST R S 1963 *Geometrical and Physical Optics*, Longman, London, pp. 112–14.
- [6] WHITTLE M J 1979 'Advances in ultrasonic flaw detection', *CEGB Research*, no. 10, November.
- [7] BENSON F W 1967 'Ultrasonics for liquid level control', *Measurement and Control*, vol. 9, no. 11, November.
- [8] Robertshaw Controls Co., Industrial Instrumentation Division 1979 *Publicity Material for Model 165 Ultrasonic Level System*.
- [9] Bestobell Mobrey Ltd 1979 *Instruction Manual for 'Sensall' Continuous Level Monitoring System*.
- [10] Endress and Hauser (UK) Ltd, *Technical Information, DU 210, DU 211 Ultrasonic Level Sensors*.
- [11] CRECRAFT D I 1983 'Ultrasonic instrumentation: principles, methods and applications', *J. Phys. E. Scientific Instruments*, vol. 16, pp. 181–9.
- [12] PAYNE P A 1985 'Medical and industrial applications of high resolution ultrasound', *J. Phys. E. Scientific Instruments*, vol. 18, pp. 465–73.
- [13] Bestobell Mobrey Ltd, *Publicity Material for Doppler Flowmeter*.
- [14] MEDLOCK R S 1985 'Cross correlation flow measurement', *Measurement and Control*, vol. 18, no. 8, pp. 293–7.
- [15] KEECH R P 1982 'The KPC multichannel correlation signal processor for velocity measurement', *Transactions of the Institute of Measurement and Control*, vol. 4, no. 1, Jan.–Mar.
- [16] SANDERSON M L 1982 'Electromagnetic and ultrasonic flowmeters: their present states and future possibilities', *Electronics and Power*, vol. 28, no. 2, pp. 161–4.

Problems

- 16.1 A piezoelectric crystal has an effective mass of 10^{-2} kg, stiffness of 10^{10} N m $^{-1}$ and damping constant 200 Ns m $^{-1}$. The electrical capacitance of the crystal is 1000 pF and the charge sensitivity is 2×10^{-10} C N $^{-1}$.
- (a) Calculate the series and parallel resonant frequencies of the crystal.
 - (b) Calculate the magnitude and phase of the overall electrical impedance of the crystal at the above frequencies.
 - (c) The crystal is incorporated into a closed-loop oscillator system which is to oscillate at the crystal series resonant frequency. Calculate the required gain and phase of the maintaining amplifier at this frequency.
- 16.2 Figure Prob. 2 shows a cross-section through a steel pipe through which sewage is flowing. The level of sewage in the pipe can also vary between the limits shown. Quartz crystals are attached to the outside of the pipe to form the four transmission links: T_1-R_1 , T_2-R_2 , T_3-R_3 and T_4-R_4 .
- (a) Assuming that only interface losses take place, calculate the fraction of received power to transmitted power for each link. Use the data given in Tables 16.1 and 16.2, and assume that sewage has the same transmission characteristics as water.

Figure Prob. 2.



- (b) Explain how these links can form the basis of systems to measure:
- the level of sewage;
 - the velocity of sewage.

16.3 An open steel vessel contains liquid metal to a depth of about 0.75 m. It is proposed to measure the depth of liquid using ultrasonic pulse reflection techniques. A quartz crystal attached to the base of the vessel is to act alternatively as a transmitter and receiver. Using the data given below and in Tables 16.1 and 16.2:

- Calculate the 'round trip' time T_r and the fraction of received power to transmitted power.
- Choose suitable values for pulse width and repetition times.

Data

Velocity of sound in liquid metal	$= 1.5 \times 10^3 \text{ m s}^{-1}$
Density of liquid metal	$= 5 \times 10^3 \text{ kg m}^{-3}$
Power attenuation coefficient	$= 0.1 \text{ m}^{-1}$
Natural frequency of quartz crystal	$= 1 \text{ MHz}$

16.4 An ultrasonic Doppler flowmeter is to be used to measure the volume flow rate of a slurry in a steel pipe of diameter 0.2 m. Two piezoelectric crystals, each having a natural frequency of 1 MHz, are positioned, a few millimetres apart, on the outside of the pipe to form an ultrasonic transmission link. The transmitting crystal directs an ultrasonic beam into the pipe so that the beam is moving in an opposite direction to the flowstream. The angle between the ultrasonic beam and the direction of flow is 60° . On average 10% of the ultrasonic power reaching each solid particle is scattered back in the direction of the receiving crystal. Assume that the slurry has the same density and sound velocity as water (Table 16.2) and a power attenuation coefficient of 1.0 m^{-1} .

- Find the difference between the frequencies of the transmitted and received beams when the flow rate is $1.13 \times 10^3 \text{ m}^3 \text{ h}^{-1}$.
- Estimate the ultrasonic power incident on the receiving crystal for each watt of ultrasonic power leaving the transmitting crystal. State any assumptions made in your calculation.

- 16.5
- An ultrasonic transmitter is in the form of a piezoelectric disc of diameter 2.5 cm and thickness 1.0 cm. The front face of the disc is placed directly onto biological tissue; the rear face is in contact with air. A pulse launched from the centre of the disc divides into two equal pulses, each of power 1 W and width 0.5 μs , one travelling towards the front face and one towards the rear face.
- (a)

Use the data given below to derive the form of the signal entering the tissue.
- (b)

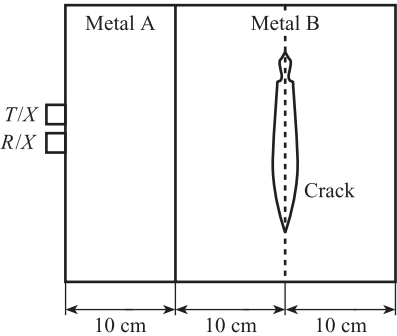
Explain in detail what modifications should be made to the transducer so that the signal entering the tissue is a close approximation to a single pulse.

Data

Material	Velocity of sound (m s^{-1})	Density (kg m^{-3})
Piezoelectric	5×10^3	2.6×10^3
Tissue	1.3×10^3	1.0×10^3
Air	0.3×10^3	1.33

- 16.6
- Figure Prob. 6 shows transmitting and receiving quartz crystals attached to a composite metal slab. The composite slab consists of a slab of metal *A* bonded to a slab of metal *B*; metal *B* contains an air-filled crack of negligible thickness in the position shown. An ultrasonic pulse of mean power 1 W and duration 5 μs is launched from the transmitting crystal into the slab. Use the data given below to discuss the main features of the signal at the receiving crystal. Estimates of times and power levels should be made.

Figure Prob. 6.



Data

Material	Velocity of sound (m s^{-1})	Density (kg m^{-3})	Power attenuation coefficient (m^{-1})
Metal A	6.0×10^3	3.0×10^3	2.0
Metal B	6.0×10^3	8.0×10^3	4.0
Quartz	6.0×10^3	2.5×10^3	—
Air	0.30×10^3	1.33	—

- 16.7
- A differential transit time ultrasonic flowmeter is to measure gas velocities between 0.3 and 24 m s^{-1} to an accuracy within $\pm 1\%$. Use the data given below to critically assess the feasibility of the flowmeter according to the following criteria.

- Ratio of received pulse power to transmitted pulse power. Explain how this ratio may be improved.
- Accuracy of pulse transit time measurement necessary to meet the above specification.

Data

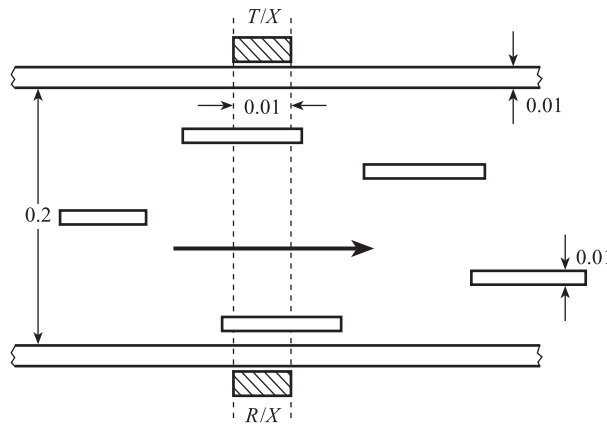
Material	Velocity of sound (m s^{-1})	Density (kg m^{-3})
Quartz	5700	2600
Natural gas	500	50

Pipe diameter $D = 300$ mm, flowmeter length $l = 600$ mm.

16.8

An organic liquid containing suspended plastic pellets is flowing in a steel pipe of internal diameter 0.2 m and thickness 0.01 m. An ultrasonic transmission link is set up across the pipe; this consists of identical transmitting and receiving quartz discs as shown in Figure Prob. 8. The plastic pellets can be regarded as discs of thickness 0.01 m and diameter 0.02 m, moving parallel to the direction of flow.

Figure Prob. 8.



Using the data given in the table below, calculate the power incident on the receiver for each watt of transmitter power in the following cases:

- no pellets present in the transmission link;
- a single pellet completely intersecting the transmission link;
- n pellets completely intersecting the transmission link, all pellets being separated by the liquid phase.

Material	Velocity of sound (m s^{-1})	Density (kg m^{-3})	Power attenuation coefficient (m^{-1})
Steel	6.0×10^3	7.8×10^3	4.0
Quartz	5.7×10^3	2.6×10^3	—
Plastic	2.4×10^3	1.1×10^3	2.0
Liquid	1.5×10^3	1.0×10^3	1.0

16.9

The overall transmission coefficient $\alpha_{T,G}$ between a transmitter of characteristic impedance R_1 and a gas of impedance R_2 separated by a matching layer of impedance R is given by eqn [16.40]. By differentiating [16.40] and setting the derivative equal to zero (or any other method), show that $\alpha_{T,G}$ is a maximum when $R = \sqrt{R_1 R_2}$.

- 16.10 (a) Explain briefly the meaning of the following terms used in ultrasonics:
- (i) Attenuation
 - (ii) Matching layer
 - (iii) Resonant stationary wave.
- (b) An ultrasonic transmitter is in the form of a piezoelectric disc of diameter 1.0 cm and thickness 2.0 mm. The transmitter is to be used to launch 1 MHz pulses into biological tissue. Use the concepts of part (a) and the data below to detail what modifications are made to the transmitter so it meets the following specification:
- (i) Maximum power for pulse transmission from the front face into the tissue
 - (ii) Minimum power for pulse transmission from the rear face into the tissue.

Data

Material	Velocity of sound (m s^{-1})	Density, (kg m^{-3})	Power attenuation coefficient (m^{-1})
Piezoelectric	5×10^3	2.6×10^3	5×10^2
Tissue	1.3×10^3	1.0×10^3	—
Air	0.3×10^3	1.33	—

17 Gas Chromatography

In many industrial processes, the materials passing between different stages of the process are mixtures of compounds or elements. These mixtures are often a single phase, i.e. gas, liquid or solid, but may be multiphase, e.g. gas and liquid. In order to operate many processes at maximum throughput or efficiency, it is essential to have some information on the **composition** of important process streams. In some cases a detailed analysis giving the fraction of each component in the mixture may be required; in others it is sufficient to know the percentage of a single key component.

Important industrial examples are:

- Complete analysis of the hydrocarbon gas stream leaving a naphtha cracking furnace
- Percentage of carbon monoxide in boiler flue gas
- Acidity/alkalinity of boiler feed water
- Concentration of dissolved metal ions in industrial effluent discharged into rivers.

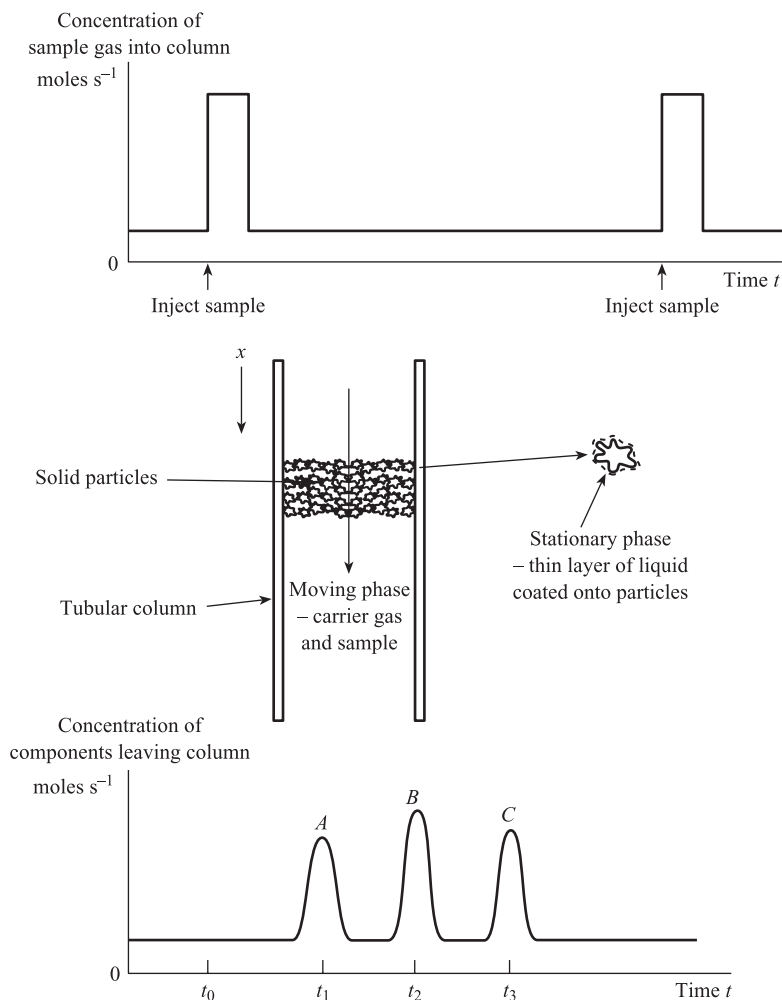
The measurement of composition is usually referred to as **analysis** and the corresponding systems as **analytical measurement systems**. The study of analytical techniques and systems is a wide subject which warrants a complete book in itself; the interested reader is referred to References 1–3. This chapter discusses the widely used technique of **gas chromatography** and the systems based on this technique. The use of katharometer and non-dispersive infrared systems for analysing gases has already been discussed in Chapters 14 and 15. The use of electrochemical sensors for measuring the concentration of ions in solution has been discussed in Section 8.9.

17.1 Principles and basic theory

Gas chromatography is a technique for measuring the composition of a gas or volatile liquid sample by separating the sample into its constituent components. The separation is performed using two phases: a moving gas phase, and a stationary phase which is either liquid or solid. In **gas–liquid chromatography** the stationary phase is a thin layer of non-volatile liquid, coated onto solid particles acting only as a support. In **gas–solid chromatography** the solid particles themselves provide the stationary phase.

A typical column for **gas–liquid chromatography** (GLC) is shown in Figure 17.1. The moving gas phase is called the carrier gas; this is an inert gas such as helium,

Figure 17.1 Typical GLC column and gas flow rates in gas–liquid chromatography.



argon or nitrogen which does not react with the sample and is not dissolved by the liquid phase. A known volume of sample gas is injected into the carrier at time t_0 . This causes a pulse increase in the flow rate of gas into the column. The column is a long coiled tube, typically 2–3 m long and of 3 mm internal diameter, packed with small particles of solid ceramic material such as ground firebrick. The particles are coated with the liquid phase to give a large surface area for dissolving the gas. The liquid should not react with any of the components, and should have negligible vapour pressure at the column temperature. Commonly used liquids are silicones and polyglycols.

The carrier gas ‘sweeps’ the sample through the packing and brings it into intimate contact with the liquid phase. A dynamic equilibrium is set up, with molecules passing from gas to liquid and from liquid to gas at equal rates. However, molecules of different components spend, on average, different amounts of time in the liquid phase. When molecules are dissolved in the liquid phase they have zero velocity down the column. The overall result is that the different components of the sample emerge or ‘elute’ from the end of the column at different times.

Figure 17.1 shows the variation in the flow rate of gas leaving the column with time; this is called a **chromatogram**. Component A spends very little time in the liquid phase and elutes from the column first (at time t_1) whereas component C spends a lot longer in the liquid phase and is last to emerge from the column (time t_3).

The average time for the i th component of the sample mixture to travel through the column is termed the **retention time** T_i . This is the sum of the time T_{Mi} spent in the moving gas phase and the time T_{Si} spent in the stationary phase, i.e.

$$T_i = T_{Mi} + T_{Si} \quad [17.1]$$

The time T_{Mi} depends only on the length L of the column and the average carrier gas velocity \bar{u} ; this is the same for all components, i.e.

$$T_{Mi} = \frac{L}{\bar{u}} \quad \text{for all } i \quad [17.2]$$

Time T_{Si} is usually different for each component and depends on the distribution ratio K_i of the component between the two phases, i.e.

$$K_i = \frac{T_{Si}}{T_{Mi}} \quad [17.3]$$

From [17.1]–[17.3] we have

*Retention time for
ith component*

$$T_i = \frac{L}{\bar{u}} (K_i + 1) \quad [17.4]$$

Figure 17.2 is an idealised distance/time graph for four components, with $K_i = 0, 1, 2$ and 3 , travelling down the column. The component with $K_i = 0$ spends no time in the liquid phase and the graph is a straight line of slope \bar{u} . The components with $K_i = 1, 2$ and 3 spend increasing time in the liquid phase and the corresponding graphs are straight lines of slope $\frac{1}{2}\bar{u}$, $\frac{1}{3}\bar{u}$ and $\frac{1}{4}\bar{u}$ respectively. The average carrier gas velocity \bar{u} can be found using^[4]

$$\bar{u} = \frac{3(P^2 - 1)}{2(P^3 - 1)} \bar{u}_0 \quad [17.5]$$

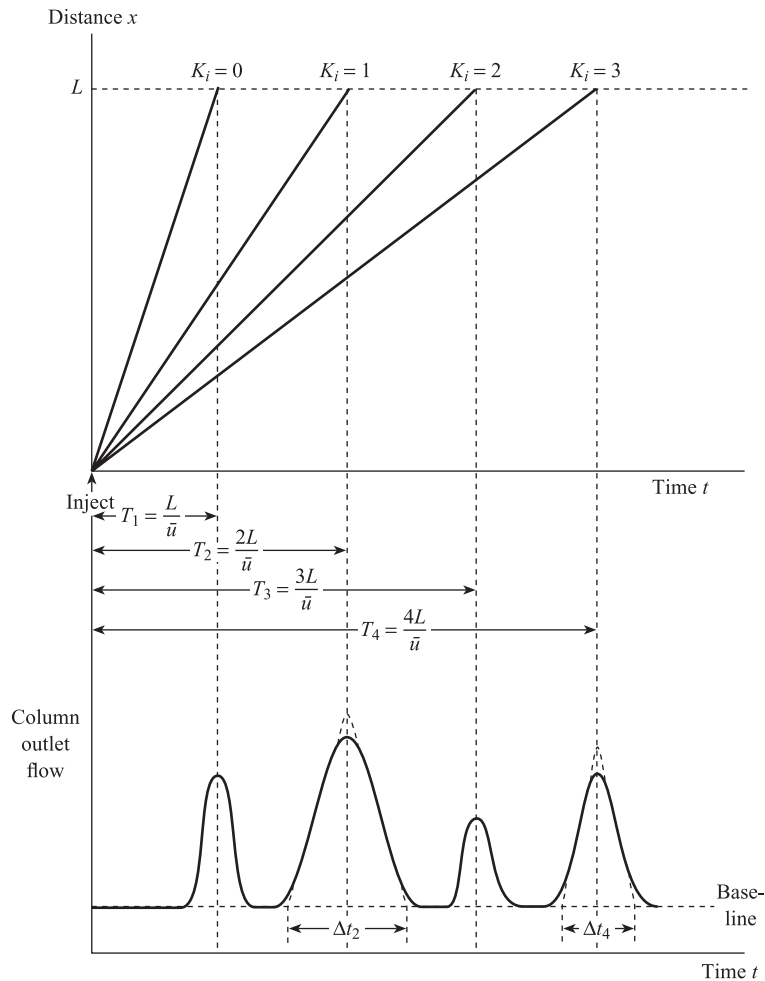
where \bar{u}_0 is the velocity at the column outlet, and $P = P_i/P_0$ is the ratio of column inlet and outlet pressures.

The molecules of the i th component do not all elute at the same time; there is a statistical distribution of times (usually normal) about the mean value T_i . The width of the distribution depends on the width of the original injection pulse, as well as molecular diffusion effects inside the column, and can be described by a standard deviation σ_i . An alternative measure is the base width Δt_i defined by the points of intersection of the base line and tangents drawn to the distribution at the half-peak height values (Figure 17.2). For a normal distribution $\Delta t_i = 4\sigma_i$.

The resolution R_{ij} of two adjoining components i, j is defined by:

*Resolution of adjacent
components*

$$R_{ij} = \frac{2(T_j - T_i)}{\Delta t_i + \Delta t_j} \quad [17.6]$$

Figure 17.2 Retention times and peak widths.

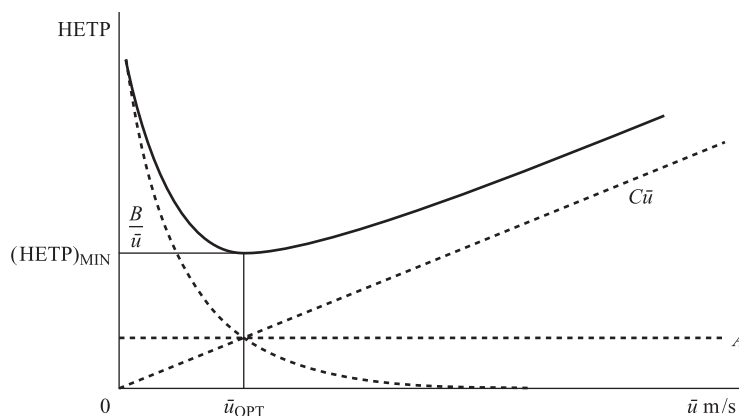
A resolution of 1.5 for two identical normal peaks means that $T_j - T_i$ is equal to six standard deviations and that the peaks are almost completely separated. A commonly used measure of the separating efficiency of a column is **height equivalent to a theoretical plate (HETP)**. This quantity arises because of the similarity between packed chromatograph columns and packed distillation columns, and the need to find the height of a packed column equivalent to one theoretical stage in a plate column. To calculate HETP for a given column of length L , we first calculate the number of theoretical plates N in the column, which is defined by

$$N = 16 \left(\frac{T_i}{\Delta t_i} \right)^2 \quad [17.7]$$

and then

$$\text{HETP} = \frac{L}{N} \quad [17.8]$$

Figure 17.3 Relation between HETP and carrier gas velocity \bar{u} .



For a typical column we may have $L = 1$ m, $T_i = 120$ s and $\Delta t_i = 10$ s, giving $N = 2304$ and $\text{HETP} \approx 0.44$ mm. HETP is not a constant for a given column, but depends on the mean carrier gas velocity \bar{u} and column temperature T °C. The relationship between HETP and \bar{u} is given by the Van Deemter equation:

$$\text{HETP} = A + \frac{B}{\bar{u}} + C\bar{u} \quad [17.9]$$

where A , B and C are constants for a given system at a given temperature. The individual terms represent diffusion and mass transfer effects and are plotted in Figure 17.3. We see that there is an optimum carrier gas velocity \bar{u}_{OPT} at which HETP is a minimum, i.e. the best separation of components is obtained.

17.2 Typical gas chromatograph

Figure 17.4 shows a typical gas chromatograph system for composition measurement. Because column HETP depends on carrier gas velocity and column temperature, it is essential to control the flow rate of carrier gas and to place the sample injection valve, column and detector in a temperature-controlled enclosure. The sample injection valve is used to inject the sample into the carrier gas stream.

Figure 17.5 shows the principle of operation of a sliding plate valve used with a gas sample. The valve consists of a plastic plate with grooved channels, sandwiched between two metal blocks. Prior to injection the valve is in position A such that the carrier gas passes directly to the column and the sample gas passes through the sample loop before being vented. This ensures that the sample loop is filled with sample gas; typically the sample loop has a volume of a few millilitres. On receiving an 'injection' signal from the computer the plate moves across to position B . The carrier gas now passes through the sample loop and flushes the sample volume into the column. The sample gas stream passes directly to vent. The valve is then returned to position A ready for the next injection. The operation is similar for a liquid sample, except that the volume of the sample is much smaller; this vaporises on entering the carrier gas stream.

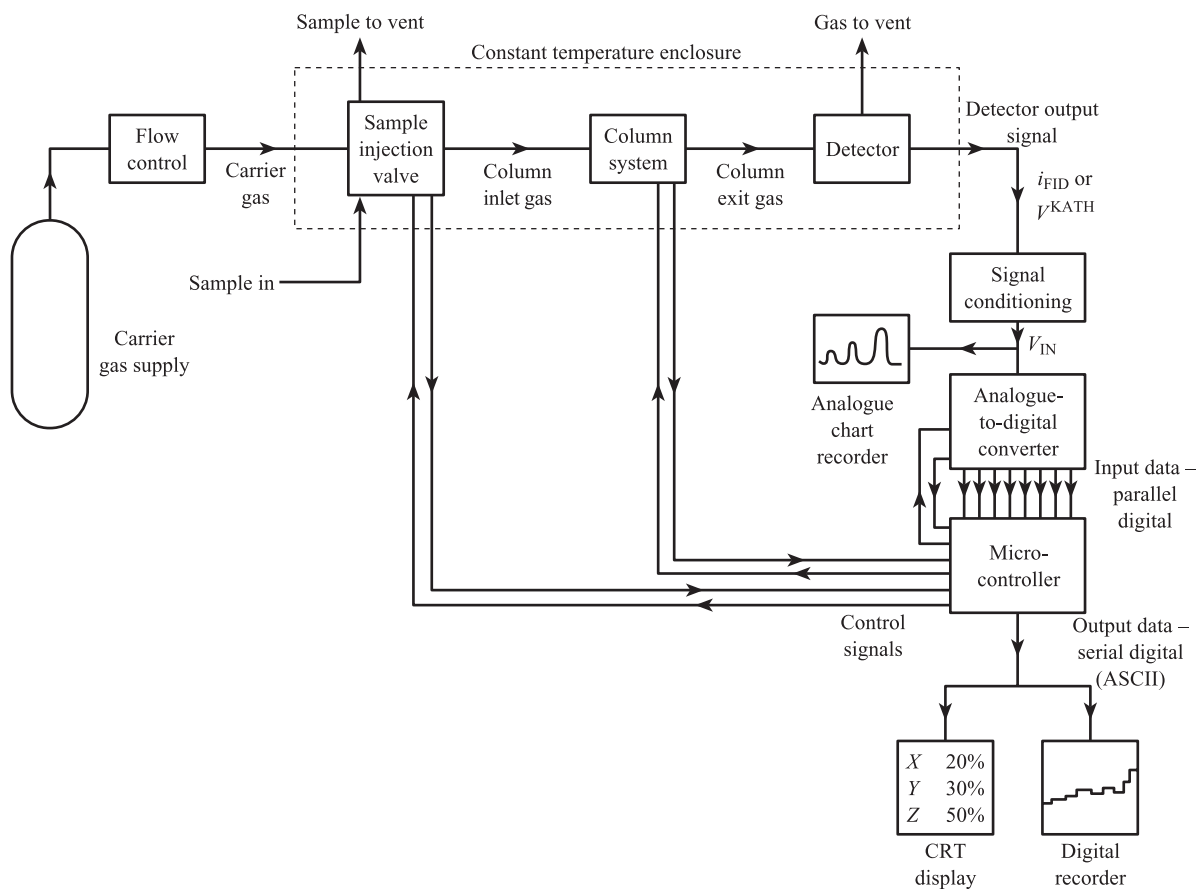


Figure 17.4 Typical gas chromatograph system for composition measurement.

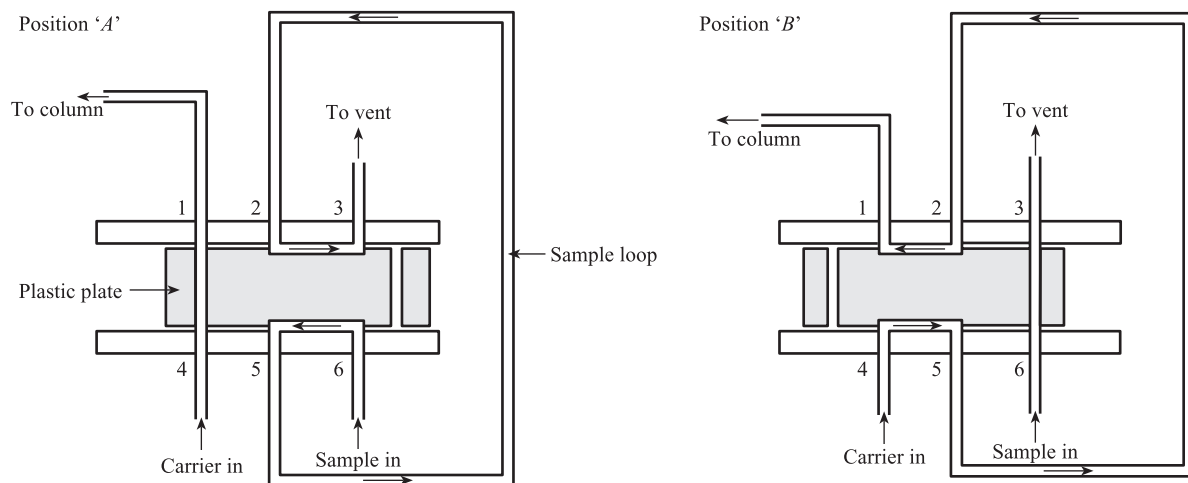


Figure 17.5 Injection of a gas sample with a sliding plate valve (after Pine^[5]).

The construction of a typical GLC column has already been described. A column for **gas-solid chromatography** (GSC) is similar, except that the solid particles themselves provide the active stationary phase rather than just acting as a support. Materials such as charcoal, silica gel, activated alumina and molecular sieve can adsorb gas molecules onto their surface. Many chromatograph systems incorporate more than one column, enabling sample and gas streams to be switched between columns.

The purpose of the detector is to give a voltage or current output, depending on either concentration or flow rate, for each of the component gases eluting from the column. An ideal detector will give an output proportional to either component concentration or component flow rate.^[1] The detector sensitivity (e.g. current/flow rate) should be high and the same for all components. The detector should also have good repeatability and fast speed of response.

The **katharometer** (Section 14.4) has medium sensitivity, and is widely used as a detector in gas chromatograph systems for measuring compositions from several per cent down to around 1000 p.p.m. It consists of four heated, matched metal filaments arranged in a deflection bridge energised by a constant current $2i_0$. Pure carrier gas is passed over two of the filaments (Figure 14.7), and the gas eluting from the column over the other two. The bridge is balanced when pure carrier gas leaves the column, but for each eluting component there is an output voltage given approximately by:

$$V_i^{\text{KATH}} = D \frac{(k_c - k_i)x_i}{k_c[x_i k_i + (1 - x_i)k_c]} \quad [14.52]$$

$$D = \frac{i_0^3 R_{TF}^2 \alpha d}{0.24A} \quad [14.50]$$

where k_c = thermal conductivity of carrier, k_i = thermal conductivity of the eluting component, and x_i = molar concentration of component i in the carrier + component mixture. From [14.52] we see that the carrier thermal conductivity must be substantially different from all the component conductivities. For small x_i ,

$$V_i^{\text{KATH}} \approx D \left(\frac{k_c - k_i}{k_c^2} \right) x_i$$

i.e. there is an approximately linear relation between V_i^{KATH} and x_i . However, sensitivity depends on k_i , i.e. sensitivity is different for different components. The **flame ionisation detector** has a high sensitivity for organic molecules and is used in the measurement of low compositions down to a few p.p.m. Here the gas eluting from the column is passed to a controlled oxy-hydrogen flame. The flame causes the organic molecules to be split up into charged ions, which flow to the collector electrode under the action of an applied d.c. voltage. This ionisation current is proportional to component flow rate, i.e. the number of molecules per second of component eluting from the column.

The detector output signal is at a low level (see Problem 14.5, for example) and requires amplification before being input to the A/D converter. This typically (Chapter 10) accepts an input signal of 0 to +5.0 V and converts it into an 8-, 12- or 16-bit binary parallel digital signal, which is passed to the microcontroller for further processing. The microcontroller performs two main functions, which are explained more fully in the following section. These are as follows:

- *Control of sequence of operations.* Several operations must be performed on the system of Figure 17.4, including sample injection, column switching, control of A/D converter, signal processing and control of data presentation elements. These must be performed in the correct order and at the correct times.
- *Signal processing.* The time variation of converter input voltage is closely related to the flow rate of gas leaving the column as a series of peaks. The computer calculates the area under each peak, which is approximately proportional to the total mass of the corresponding component. The composition of the sample mixture can then be found. These data can then be presented to the observer, possibly as a complete analysis of the sample on the CRT display or as a record showing the trend of a key component.

17.3

Signal processing and operations sequencing

The input voltage V_{IN} to the A/D converter will be proportional to the detector output signal. For a flame ionisation detector, the detector output current is proportional to the number of molecules \dot{n}_i of the i th component, eluting from the column per second. In this case the converter input voltage is:

$$V_i^{\text{IN}} = G\dot{n}_i \quad [17.10]$$

where G is a constant, ideally the same for all components.

Integrating [17.10], we have:

$$n_i = \frac{1}{G} \int V_i^{\text{IN}} dt = \frac{1}{G} A_i \quad [17.11]$$

which shows that the total number of molecules n_i of the i th component in the sample is proportional to the integral of converter input voltage, i.e. to the **area** A_i under the i th peak. Thus the total number M of molecules present in a sample of m components is given by:

$$M = \sum_{i=1}^m n_i = \frac{1}{G} \sum_{i=1}^m A_i \quad [17.12]$$

i.e. M is proportional to the sum of the areas under all peaks. The percentage molar concentration c_i of the i th component in the sample is therefore given by:

*Calculation of
concentrations in
ideal case*

$$c_i = \frac{n_i}{M} \times 100\% = \frac{A_i}{\sum_{i=1}^m A_i} \times 100\% \quad [17.13]$$

Thus in the ideal case, the composition of the sample can be found by evaluating the area under each component peak. The output voltage of the katharometer, however, is different for different components, and is approximately proportional to the concentration x_i of the component in the component/carrier mixture. If \dot{n}_c is the number of molecules of carrier leaving the column per second, then:

$$x_i = \frac{\dot{n}_i}{\dot{n}_c + \dot{n}_i} \approx \frac{\dot{n}_i}{\dot{n}_c} \quad \text{for small } x_i \quad [17.14]$$

Thus for dilute mixtures, x_i is proportional to \dot{n}_i provided that \dot{n}_c is a constant, so that there is tight control of carrier gas flow rate. The A/D converter input voltage for a katharometer detector is therefore given approximately by:

$$V_i^{\text{IN}} \approx G_i \dot{n}_i \quad [17.15]$$

where G_i is the sensitivity for the i th component, which depends on thermal conductivity k_i . In this case the corresponding expression for the concentration of the i th component in the original sample is:

Calculation of concentrations in practical case

$$c_i = \frac{(1/G_i)A_i}{\sum_{i=1}^m \frac{1}{G_i} A_i} \times 100\% = \frac{A_i^*}{\sum_{i=1}^m A_i^*} \times 100\% \quad [17.16]$$

where the A_i^* are the corrected peak areas $A_i^* = (1/G_i)A_i$.

The input to the computer is a sampled, coded version of the A/D converter input signal V_{IN} . The converter has, typically, a conversion time of a few milliseconds, so that samples can be read by the computer at intervals of a few milliseconds. These sampled values may be affected by high-frequency interference or noise, and should be filtered. One simple filtering method is to calculate the average value of a group of several samples. Thus if the A/D conversion time is 5 ms an average of 40 samples is available every 0.2 s. The computer uses these filtered values to estimate the area of the peak by dividing it into a series of rectangular elements, as shown in Figure 17.6.

If y_j is the j th filtered value and ΔT the interval between values, then the area of the j th rectangle is $y_j \Delta T$, giving:

Approximate expression for peak area

$$A \approx \sum_{j=1}^P y_j \Delta T = \Delta T \sum_{j=1}^P y_j \quad [17.17]$$

Figure 17.6 Calculation of peak area.

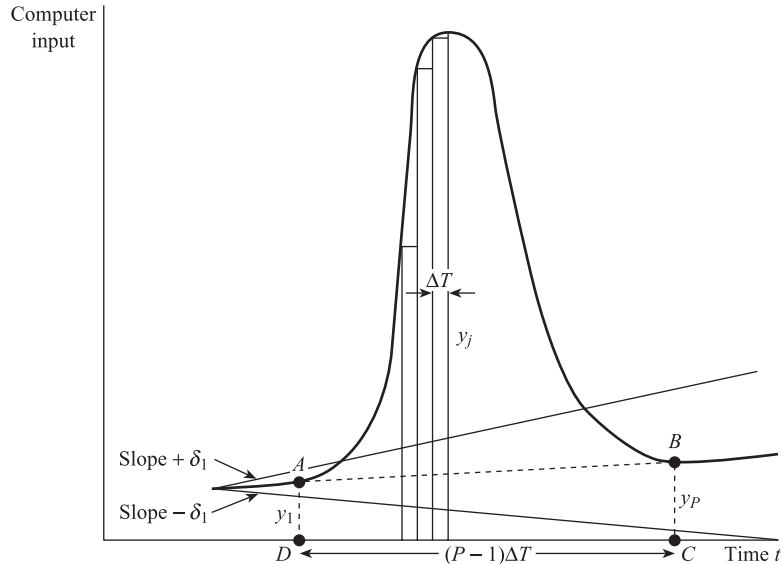
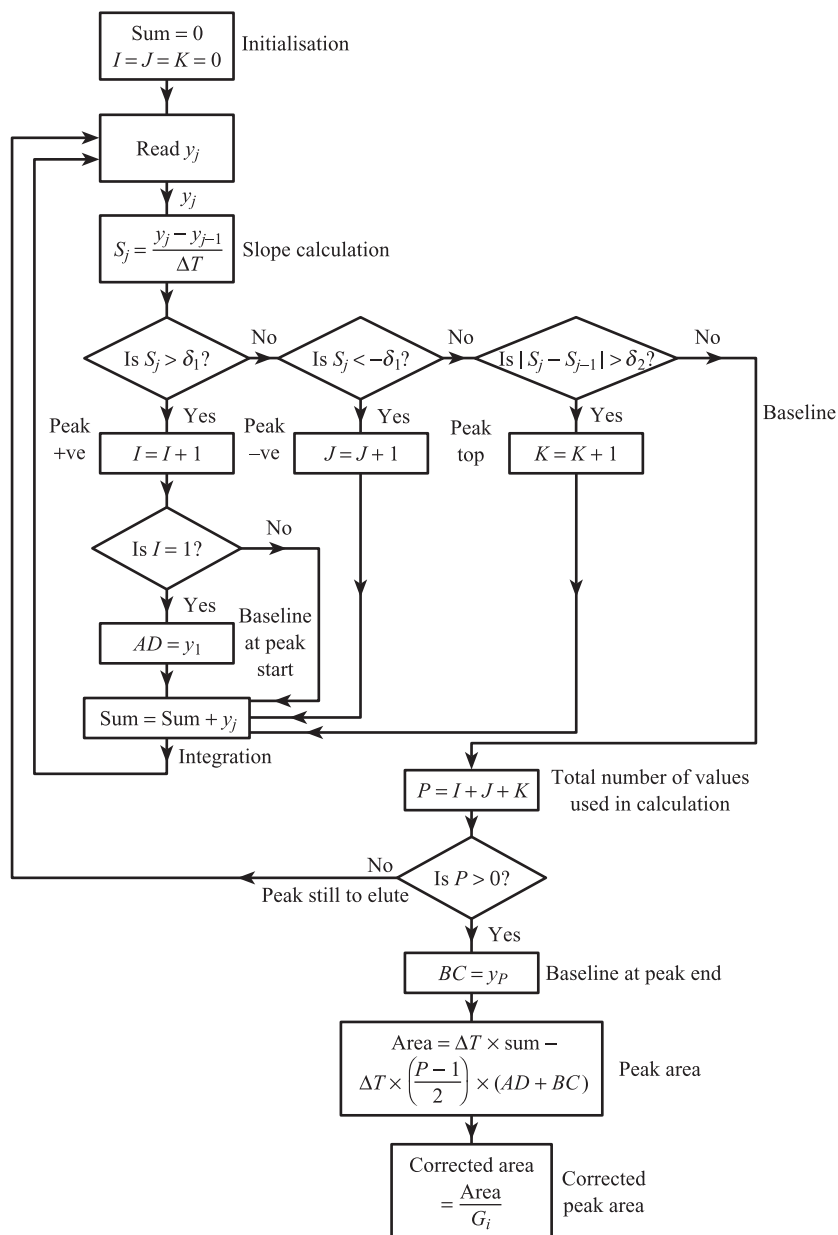


Figure 17.7 Flowsheet of program for evaluating corrected peak area.



where P is the number of filtered values used in the calculation. The above expression is accurate if ΔT is small compared with the peak standard deviation σ . Thus if $\sigma = 2.5$ s, a ΔT of 0.2 s is suitable, giving $P = 75$ for the complete peak of width 6σ .

Figure 17.7 shows a flowsheet of a simple program for evaluating the area of a given peak. After initialisation, the computer reads the current filtered value y_j and then evaluates the corresponding slope or gradient s_j . This is given by:

$$s_j = \frac{y_j - y_{j-1}}{\Delta T} \quad [17.18]$$

where y_{j-1} is the previous filtered value and ΔT the interval between values. This slope value is used to decide whether or not a peak is eluting from the column. The baseline will not always be constant with time but may drift either upwards or downwards. If the maximum slope of the baseline is $+\delta_1$ or $-\delta_1$, then the condition for a peak is:

$$\text{Peak: } s_j > +\delta_1 \quad \text{or} \quad s_j < -\delta_1 \quad [17.19]$$

and the condition for baseline is:

$$\text{Baseline: } s_j \leq +\delta_1 \quad \text{or} \quad s_j \geq -\delta_1 \quad [17.20]$$

The integration, i.e. summation of y_j values, proceeds only while the peak condition is satisfied. However, integration must also be carried out around the top of the peak where the slope is small, which means that the baseline condition rather than the peak condition is obeyed. At the baseline there is only a small difference between current and previous slopes s_j and s_{j-1} , whereas at the top of a peak the difference between these slopes is large. Thus we can differentiate between baseline and peak top using the conditions:

$$\text{Baseline: } s_j \leq +\delta_1 \quad \text{or} \quad s_j \geq -\delta_1 \quad \text{and} \quad |s_j - s_{j-1}| \leq \delta_2 \quad [17.21]$$

$$\text{Peak top: } s_j \leq +\delta_1 \quad \text{or} \quad s_j \geq -\delta_1 \quad \text{and} \quad |s_j - s_{j-1}| > \delta_2 \quad [17.22]$$

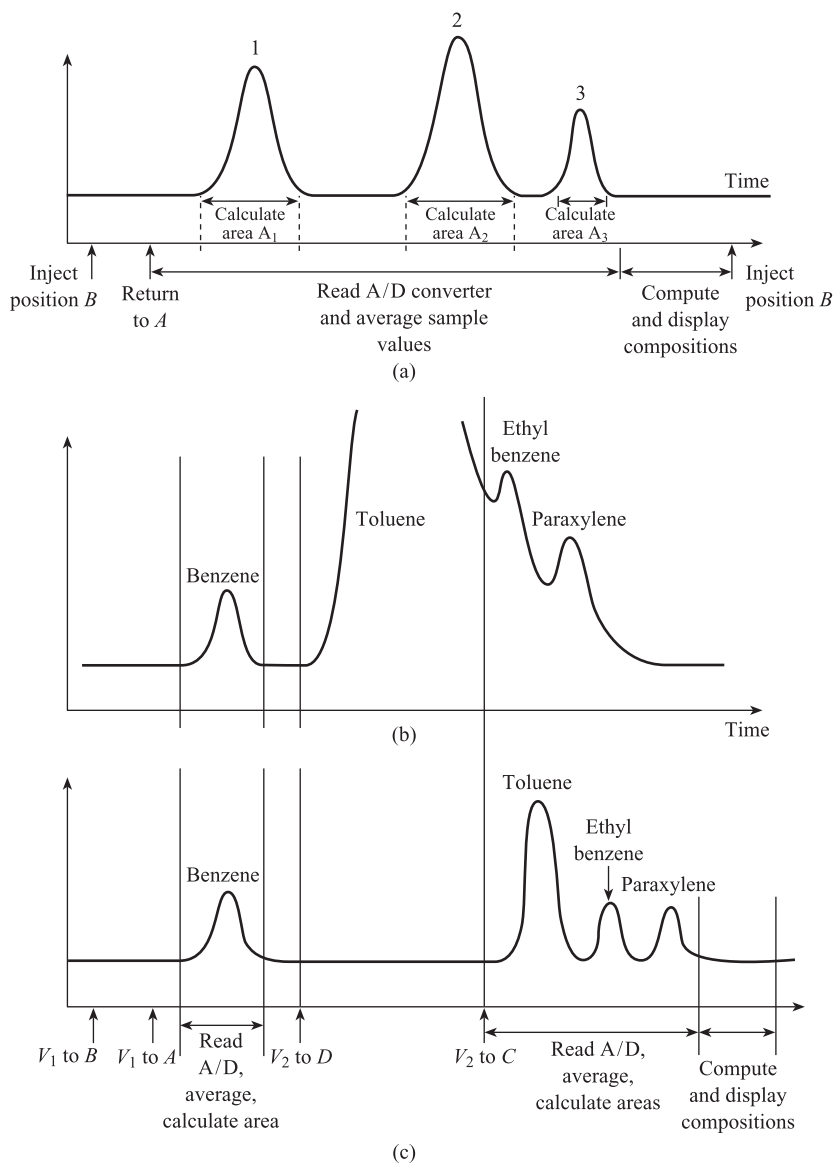
The computer counts the total number of times $I + J + K$ that conditions [17.19] and [17.22] are satisfied; this gives the total number of values P used in the calculation. The computer finds the first value to satisfy the condition $s_j > \delta_1$, which is the first value used in the integration and is designated y_1 . This gives the position A of the baseline at the start of the peak. The position B of the baseline at the end of the peak is the last value to satisfy the condition $s_j < -\delta_1$, that is the last value y_p used in the integration. The baseline is assumed to follow the straight line AB , and the peak area A_i is calculated by subtracting the area of trapezium $ABCD$ from eqn [17.17], i.e.

$$A_i = \Delta T \sum_{j=1}^P y_i - \Delta T \left(\frac{P-1}{2} \right) (y_1 + y_p) \quad [17.23]$$

As mentioned earlier, the detector sensitivity may be different for different components i . The corrected area A_i^* is evaluated using $A_i^* = A_i/G_i$, where G_i is the sensitivity for the i th component. The G_i values can be found experimentally by injecting a standard mixture of known composition and comparing the areas of the corresponding voltage peaks. The computer uses eqn [17.16] to calculate component concentrations c_i from the A_i^* .

Figure 17.8(a) shows the sequence of operations for a simple system involving one column and one carrier stream. There are, however, many analyses which require multiple column and carrier operation.^[5] One example is the measurement of small concentrations of benzene, ethyl benzene and paraxylene in a mixture which is mainly toluene. The resulting chromatogram, for a single column, is shown in Figure 17.8(b). We see that the peaks are not clearly resolved; the small ethyl benzene and paraxylene peaks sit high on the 'tail' of the large toluene peak. The problem is solved using the technique of **heartcutting**, which involves switching gas streams between

Figure 17.8 Sequences of operations in gas chromatography:
 (a) Normal sequence
 (b) Chromatogram without 'heartcutting'
 (c) Chromatogram and sequence of operations with 'heartcutting'.



two columns, as shown in Figure 17.9. Two sliding plate valves are used, one for sample injection (V_1) and one for column switching (V_2). The sample is injected into column 1 using V_1 , in the normal way. Valve V_2 is initially in position C , which enables the benzene peak to pass from column 1 to column 2. As the toluene peak is about to elute from column 1, V_2 is switched to position D , so that the gas leaving column 1 is vented and carrier gas 2 is passed through column 2. When most of the toluene has been vented, V_2 is returned to position C . Thus the remainder of the toluene peak, together with the associated ethyl benzene and paraxylene peaks, enters column 2. These peaks can then be effectively separated in column 2 without having to use very long retention times. The resulting chromatogram is shown in Figure 17.8(c), together with the operations sequence.

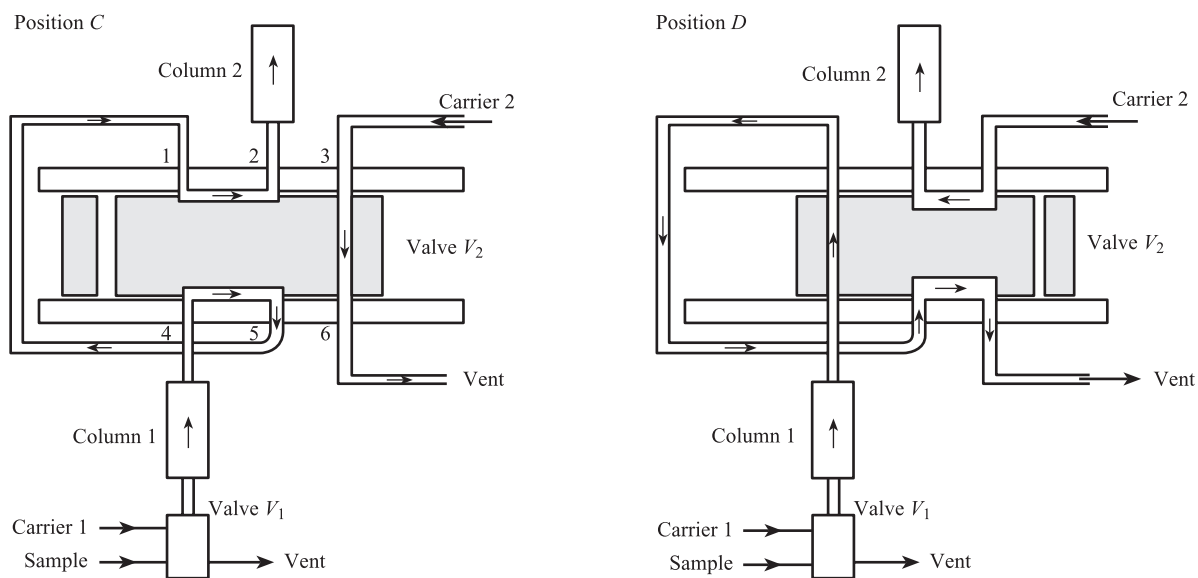


Figure 17.9 Heartcutting using two sliding plate valves.

Another switching technique involving two columns and two carrier supplies is called **backflushing**. This technique allows components of interest to pass through columns 1 and 2 to the detector. Components not required for the analysis, or which may harm the detector, are prevented from entering column 2 and 'flushed' to vent by carrier 2 flowing through column 1 in a reverse direction.

Conclusions

The chapter first discussed the principles of **gas chromatography** and a typical **chromatograph** for measuring the compositions of gas mixtures. Associated **signal processing** and **sequencing operations** were then studied.

References

- [1] EWING G W 1975 *Instrumental Methods of Chemical Analysis*, 4th edn, McGraw-Hill, New York.
- [2] STROBEL H A 1973 *Chemical Instrumentation: A Systematic Approach*, 2nd edn, Addison Wesley, New York.
- [3] WILLARD H H, MERRITT L L and DEAN J A 1974 *Instrumental Methods of Analysis*, 5th edn, Van Nostrand, New York.
- [4] AYERS B O, LLOYD R J and DEFORD D D 1961 'Principles of high speed gas chromatography with packed columns', *Analytical Chemistry*, vol. 33, no. 8, July, pp. 986–91.
- [5] PINE C S F 1967 'Process gas chromatography', *Talanta*, vol. 14, pp. 269–97.

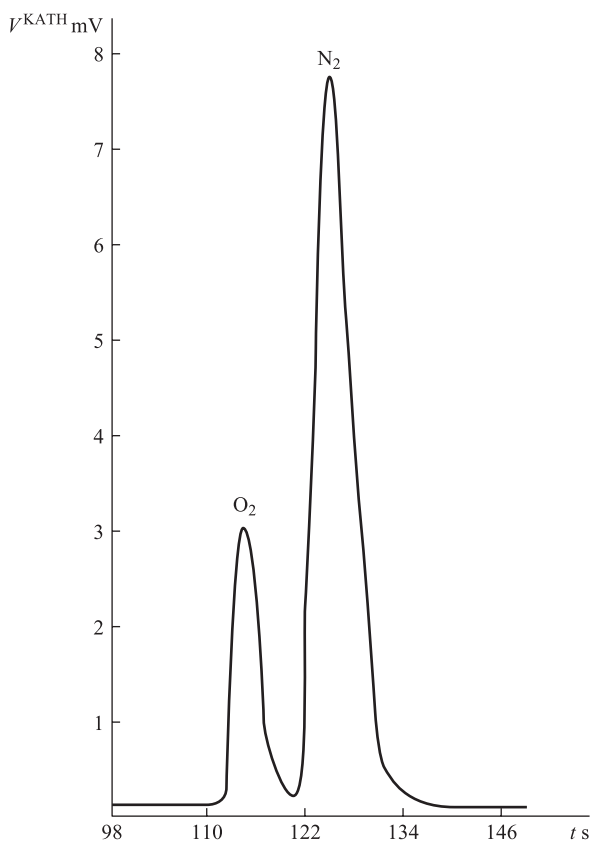
Problems

17.1

A sample containing oxygen and nitrogen is injected into a helium carrier at time $t = 0$. The sample is swept through a column 1.0 m long packed with molecular sieve. The eluting components are detected by a katharometer detector which has an equal sensitivity for oxygen and nitrogen. The time variation in katharometer output voltage is shown in Figure Prob. 1.

- (a) Assuming that the distribution ratio K for oxygen is 2.0, estimate the mean carrier velocity \bar{u} and K for nitrogen.
- (b) Estimate base width Δt for both peaks and hence find the resolution R .
- (c) Estimate the number of theoretical plates N and HETP.
- (d) Estimate the percentage composition of the sample (assume peaks are approximately triangular).

Figure Prob. 1.



18 Data Acquisition and Communication Systems

All of the measurement systems discussed so far have presented the measured value of a single variable to an observer; i.e. the systems were single input/single output. However, there are many applications where it is necessary to know, simultaneously, the measured values of several variables associated with a particular process, machine or situation. Examples are measurements of flow rates, levels, pressures and compositions in a distillation column, temperature measurements at different points in a nuclear reactor core, and components of velocity and acceleration for an aircraft. It would be extremely uneconomic to have several completely independent systems, and a single multi-input/multi-output **data acquisition system** is used. Here several elements are 'time shared' amongst the different measured variable inputs. This technique of **time division multiplexing** is discussed in the first section of this chapter, and a typical data acquisition system is described in the following section.

The oil, water and gas industries are characterised by complex distribution systems involving the transfer of fluids by long pipelines from producing to consuming areas. Similarly, an electricity distribution system involves the transfer of electrical power from power stations to consumers, via a network of high voltage cables. These systems also include several items of equipment or plant, e.g. pumping stations, compressors, storage tanks and transformers, each with associated measured variables. These plant items are often located several miles from each other, in remote areas. It is essential for the effective supervision of these distribution systems that all relevant network measurement data are transmitted to a central control point.

To do this a complex **communications system** is required. This usually consists of a **master station** (at the central control point) and several **outstations** (at the plant items). The system must be capable of transmitting large amounts of information in two directions (M/S to O/S and O/S to M/S), over long distances, in the presence of interference and noise. This chapter discusses the principles of **parallel digital signalling**, **serial digital signalling**, **error detection/correction** and **frequency shift keying**, which are used in communications systems, and concludes by describing the implementation of communications systems for measurement data with special regard to the **Fieldbus standard**.

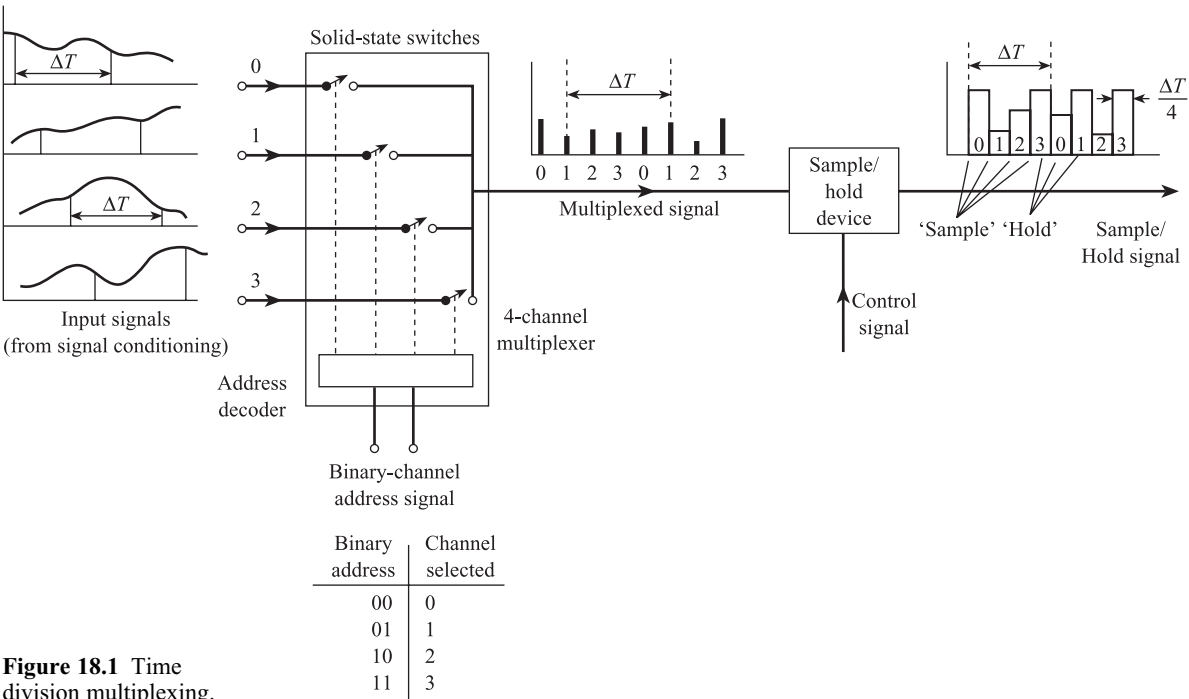


Figure 18.1 Time division multiplexing.

18.1

Time division multiplexing

Figure 18.1 shows a simple schematic diagram of a time division multiplexer, with four channels labelled 0, 1, 2 and 3. The input signal at each channel is a continuous voltage corresponding to a measured variable. The multiplexer also requires a two-bit parallel channel address signal to specify which input signal is connected to the output line. Thus if the binary address signal is 10, the switch in channel 2 is closed and input 2 is connected momentarily to the output line. The multiplexer output signal is thus a series of samples (Chapter 10) taken from different measurement signals at different times. In **sequential** addressing the channels are addressed in order, i.e. first 0, followed by 1, then 2 and 3, returning to channel 0 and repeating, so that the pattern of samples for the multiplexed signal is as shown in the diagram. **Random** addressing, whereby an observer selects a channel of interest at random, is also possible.

If ΔT is the sampling interval, i.e. the time interval between samples of a given input, e.g. 0 or 1, then the corresponding sampling frequency $f_s = 1/\Delta T$ must satisfy the conditions for the Nyquist sampling theorem (eqn [10.1]). These require that f_s be greater than or equal to $2f_{MAX}$, where f_{MAX} is the highest significant frequency present in the power spectral density of the measurement signal.

In Figure 18.1 four samples occur during ΔT , so that the number of samples per second for the *multiplexed* signal is $4f_s$. In general, for m signals, each sampled f_s times per second, the number of samples per second for the multiplexed signal is:

Sample rate for m multiplexed signals

$$f_s^M = mf_s$$

[18.1]

Different measured variables may have frequency spectra with different maximum frequencies: thus the power spectrum of a flow measurement may extend up to 1 Hz, but that of a temperature measurement only up to 0.01 Hz. The sampling frequency of the flow measurement must therefore be 100 times that of the temperature measurement. In the multiplexed signal there will be 100 samples of the flow measurement between each temperature sample. The multiplexed signal is normally fed to a sample-and-hold device (Section 10.1). Figure 18.1 shows the sample-and-hold waveform.

18.2 Typical data acquisition system

Figure 18.2 shows a typical microcontroller-based data acquisition system.^[1,2] The signal conditioning elements are necessary to convert sensor outputs to a common signal range, typically 0 to 5 V; Table 18.1 gives sensing and signal conditioning elements for different measured variables. The voltage signals are input to a 16-channel time division multiplexer, and the multiplexed signal is passed to a single sample/hold device and analogue-to-digital converter (Section 10.1). In cases where all the sensors are of an identical type, for example 16 thermocouples, it is more economical to multiplex the sensor output signals. Here the multiplexed sensor signal is input to a single signal conditioning element, such as the reference junction circuit and instrumentation amplifier, before passing to the sample/hold and ADC.

The ADC gives a parallel digital output signal which passes to one of the parallel input interfaces of the microcontroller. Another parallel input/output (I/O) interface provides the address and control signals necessary for the control of multiplexer, sample/hold and ADC. These are a four-bit multiplexer address signal, a **sample/hold** control signal, an **initiate conversion** signal to the ADC, and a **data valid** signal from the ADC. The microcontroller performs whatever calculations (on the input data)

Figure 18.2 Typical microcontroller based data acquisition system.

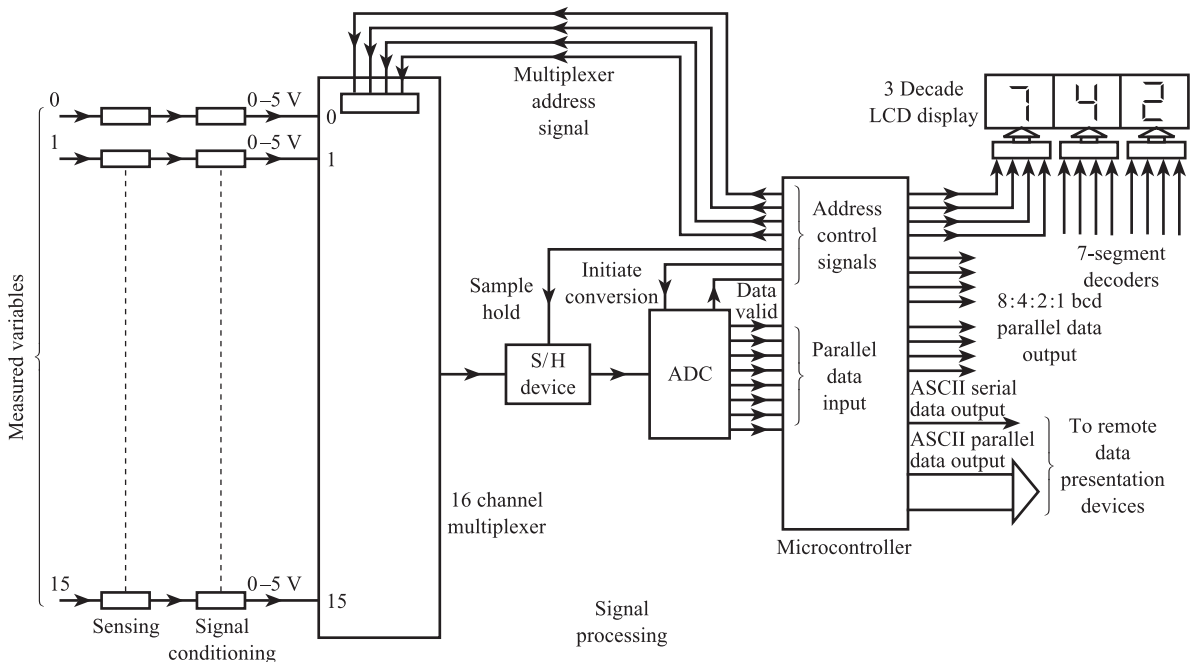


Table 18.1 Typical measured variables, sensing and signal conditioning elements.

Measured variable	Sensing element(s)	Signal conditioning elements
Temperature	Thermocouple	Reference junction circuit + instrumentation amplifier
Temperature	Platinum resistance detector	Deflection bridge + instrumentation amplifier
Flow rate	Orifice plate	Electronic D/P transmitter (4–20 mA) + current-to-voltage converter
Weight	Strain gauge load cell	Deflection bridge + instrumentation amplifier
Level	Electronic D/P transmitter (4–20 mA)	Current (e.g. 4 to 20 mA) to voltage (e.g. 0 to 5 V) converter
Angular velocity	Variable reluctance tachogenerator	Frequency-to-voltage converter
Linear displacement	Linear variable differential transformer (LVDT)	A.C. amplifier + phase-sensitive demodulator + low pass filter
Pressure	Diaphragm + capacitance displacement sensor	A.C. bridge + a.c. amplifier + phase sensitive demodulator + LPF
Acceleration	Piezoelectric crystal	Charge amplifier

are necessary to establish the measured value of the variable. A common example is the solution of the non-linear equation relating thermocouple e.m.f. and temperature (Section 10.4). The computer converts the measured value from hexadecimal into binary-coded decimal form (Section 10.3). This b.c.d. data is written into a computer parallel output interface. Each decade is then separately converted into seven-segment code and presented to the observer using a seven-segment LCD display (Section 11.4). The computer also converts each decade of the b.c.d. to ASCII form (Section 10.4). The resulting ASCII code is then written into a serial and/or parallel output interface. These can transmit ASCII data in serial and/or parallel form to remote data representation devices such as a monitor, printer or host computer.

18.3 Parallel digital signals^[3]

Parallel digital signals were introduced in Section 10.1; one path is required for each data bit and all the bits are transmitted at the same time. Therefore, if eight data bits (one byte) are to be transmitted there are eight paths in parallel, the voltage on each path being typically 5 V for a 1 and 0 V for a 0. The total collection of parallel paths is called a **data bus** or **data highway** and is similar to the internal data bus in a computer. Since, however, an internal computer bus can only handle low power levels, it must be connected to an external data highway via a buffered interface. One commonly used parallel data highway conforms to the IEE 488/IEC 625 standard. This is a bit-parallel, byte-serial transmission system capable of a maximum transmission rate of 1 Mbyte s⁻¹ up to a maximum transmission distance of 15 m. The standard is intended for high-speed, short-distance communication in a laboratory-type environment, where there is relatively low electrical interference. The bus comprises 16 lines: eight lines are used for data (usually 7-bit ASCII + parity check bit), three for ‘handshaking’ (see following section) and five for bus activity control. Up to 15 devices can be connected onto the bus. Each device must be able to perform at least one of the following three functions:

- *Listener* – a device capable of receiving data from other devices, e.g. a printer or monitor.
- *Talker* – a device capable of transmitting data to other devices, e.g. a counter or the data acquisition system of Figure 18.2.
- *Controller* – a device capable of managing communications on the bus by sending addresses and commands, e.g. a computer.

If the transmission distance for parallel signals is increased beyond a few metres, imperfections in the transmission line result in some of the bits in a given byte arriving out of synchronisation with the rest. Similarly the presence of external interference again results in loss of synchronisation or corruption of data. In conclusion, parallel digital signals are suitable for high-speed, short-distance communication in laboratory, environments. They are not suitable for long-distance communication in industrial environments where significant external interference may be present.

18.4 Serial digital signals

18.4.1 Introduction

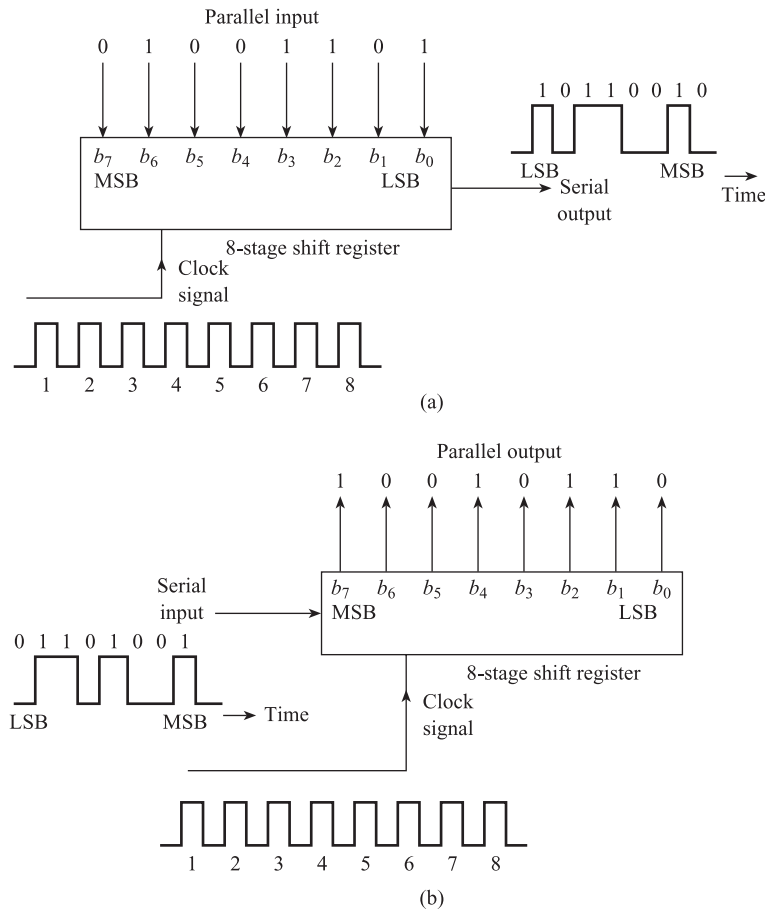
Serial digital signals can be used to transmit data over much longer distances (typically up to around 1 km) and are therefore commonly used in telemetry systems.^[3] Here all the data bits are transmitted one bit at a time in a chain along a single path. A serial digital signal is therefore a time sequence of two voltage levels, for example 0 V for a 0, 5 V for a 1 (**unipolar**), or -2.5 V for a 0, $+2.5$ V for a 1 (**bipolar**). The transmission path can vary from a standard twisted-pair cable to a low-loss coaxial cable or an optical fibre cable. Serial digital signalling is often referred to as **pulse code modulation**.

Figure 18.3(a) shows the use of an eight-stage shift register to convert an 8-bit parallel digital signal into serial form. The parallel signal $b_7 \dots b_0$ is first loaded into the register and a clock signal applied. On receipt of the first clock pulse the contents of the register are shifted one place to the right, causing the least significant bit b_0 to appear at the register output, i.e. the least significant bit is transmitted first. The second clock pulse causes the register contents again to be shifted one place to the right, causing the next bit b_1 to be transmitted. The process is repeated until the register is empty: the most significant bit b_7 is the last to be transmitted. Figure 18.3(b) shows the register used to convert a serial signal into parallel form. On receipt of the first clock pulse the least significant bit is loaded into the storage element on the extreme left of the register. The second clock pulse causes the register contents to move one place to the right, allowing the next significant bit to enter the register. After eight clock pulses the entire signal is loaded into the register, with the LSB b_0 on the extreme right and the MSB b_7 on the extreme left.

Digital transmission links may be divided into three categories, depending on whether the communication is one-way or two-way. These categories are:

- **Simplex.** One way communication from A to B where B is not capable of transmitting back to A. This may be sufficient where a remote outstation is merely sending data to a master station. However, the master station cannot acknowledge receipt of data or request retransmission of corrupted data.

Figure 18.3 Parallel and serial digital signals:
 (a) Parallel to serial conversion
 (b) Serial to parallel conversion.

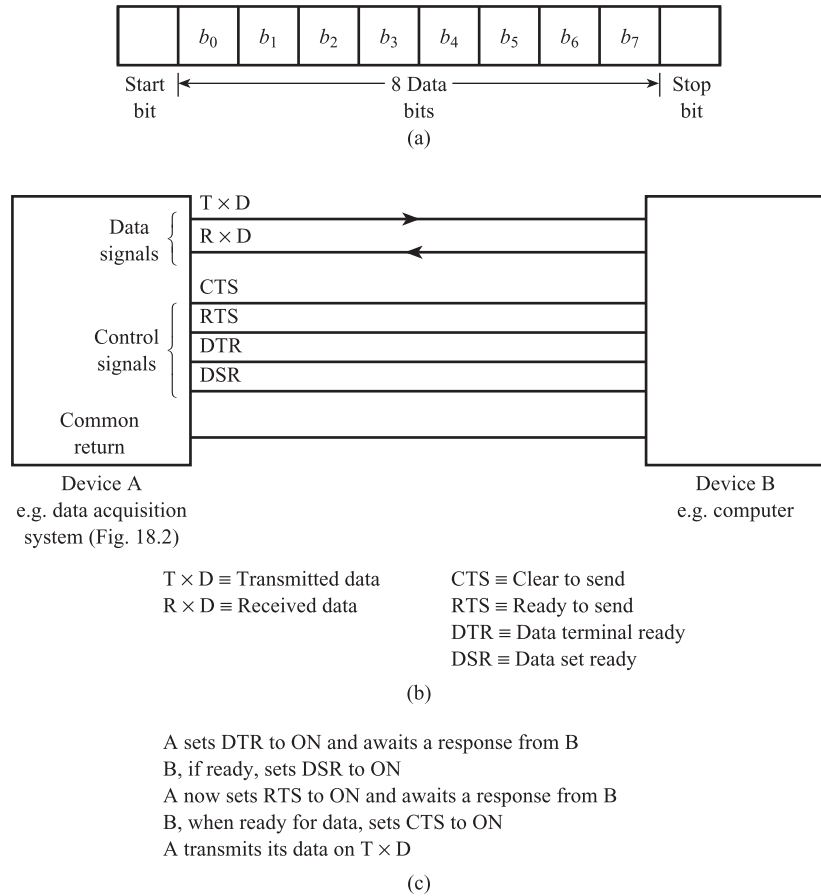


- **Half duplex.** Transmission from A to B and from B to A but not simultaneously. With this system, after an outstation has transmitted data to a master station, the master station can then send an acknowledgement and if necessary request retransmission.
- **Full duplex.** Simultaneous transmission from A to B and from B to A. This can be done using two paths; however, using modulation techniques, it is possible to transmit in two directions along a single path.

In each of the above systems it is important that the receiver is ready to receive and identify each set of data from the transmitter. There are two ways in which this can be achieved: **asynchronous transmission** and **synchronous transmission**. In asynchronous transmission each byte or **frame** of data is preceded by a start bit and concluded by a stop bit (Figure 18.4(a)), so that the receiver knows exactly where the data starts and finishes. The transmission rate of serial digital signals is specified using **bit rate** R ; this is the number of bits transferred in unit time, usually expressed in bits per second. Because of the need to check start and stop bits, the maximum transmission rate possible with asynchronous transmission is around 1200 bits s^{-1} . This method is therefore more suited to slower transmission systems.

Figure 18.4

Asynchronous transmission and 'handshaking':
 (a) Asynchronous data framing
 (b) Connection for asynchronous transmission using RS 232
 (c) 'Handshaking' sequence – A transmitting to B.



For rates greater than 1200 bits s^{-1} synchronous transmission is used. Here a regular clocking signal is used to keep the receiver exactly in step with the transmitter. The transmitted data is preceded by a synchronising character which acts as a clocking pulse at the receiver. The receiver will then 'clock in' each bit of data.

There are several standard methods of **serial digital communication** available. The choice of method depends on several criteria, including the following:

- Transmission distance
- Bit rate R
- Resistance to external interference and noise
- Number of multiplexed signals over a single link.

These criteria are often conflicting; for example, a high bit rate is incompatible with a long transmission distance and high noise immunity. From Section 18.4.2, we see that the bandwidth required for transmission of PCM is proportional to the bit rate R , i.e. the greater R the higher the required bandwidth. However, the available bandwidth of a given electrical cable decreases with length as the effects of resistance and capacitance increase. From Section 18.4.3, we see that for PCM affected by 'white' noise, the standard deviation of noise present at the PCM receiver is proportional to \sqrt{R} , i.e. the greater R the greater the noise present. However, since the receiver has

simply to decide whether a 1 or a 0 has been transmitted, this decision can be made correctly even if the pulses are severely distorted by noise. Any errors that do occur, as a result of noise and interference, can be detected by adding check bits to the serial data signal (Section 18.5).

From Section 18.4.2, the bit rate R for m multiplexed signals is m times greater than for a single signal, so that high m is again incompatible with long transmission distance and high noise immunity. Finally, the amount of external noise and interference will generally increase with transmission distance.

One commonly used standard for serial digital signals is the **RS 232 C/V 24 interface**. This specifies a 25-line connector and can be used for asynchronous and synchronous communication. In asynchronous communication only seven lines are used: two for data (transmitted and received), four for control signals and one for a common return (Figure 18.4(b)). Figure 18.4(c) shows how the control signals are used in a ‘**handshaking**’ sequence; this is necessary to ensure that the receiver is ready to receive data from the transmitter. RS 232 is capable of a bit rate of up to 20 kbits s^{-1} over short distances, i.e. up to 15 m; longer transmission distances can be used at lower bit rates. However, RS 232 is vulnerable to external interference and cable resistance/capacitance effects and is best used over short transmission distances.

For higher bit rates over longer distances, RS 232 is gradually being replaced by a new standard **RS 449**, which is capable of a bit rate of 10 kbits s^{-1} over a distance of 1 km. The reason for this longer transmission distance is that, in RS 449, the transmitting and receiving data lines each have their own separate return lines (rather than sharing a common return). Each data line and return line can then form a twisted pair to give shielding from inductively coupled interference (Section 6.5.2). However, in industrial environments, where there is high external interference, RS 449 cannot be used successfully even at low bit rates. The solution here is to use **current loop transmission**: as explained in Section 6.3, a current transmission system has far greater immunity to series-mode interference than an equivalent voltage transmission system. Here the current in the loop is serially switched between 0 and 20 mA; 0 mA corresponds to a 0 and 20 mA to a 1. With current loop transmission the bit rate is normally limited to 4800 bits s^{-1} ; also in order to transmit data to and from a computer a converter is necessary to convert the current serial signal into computer-compatible RS 232.

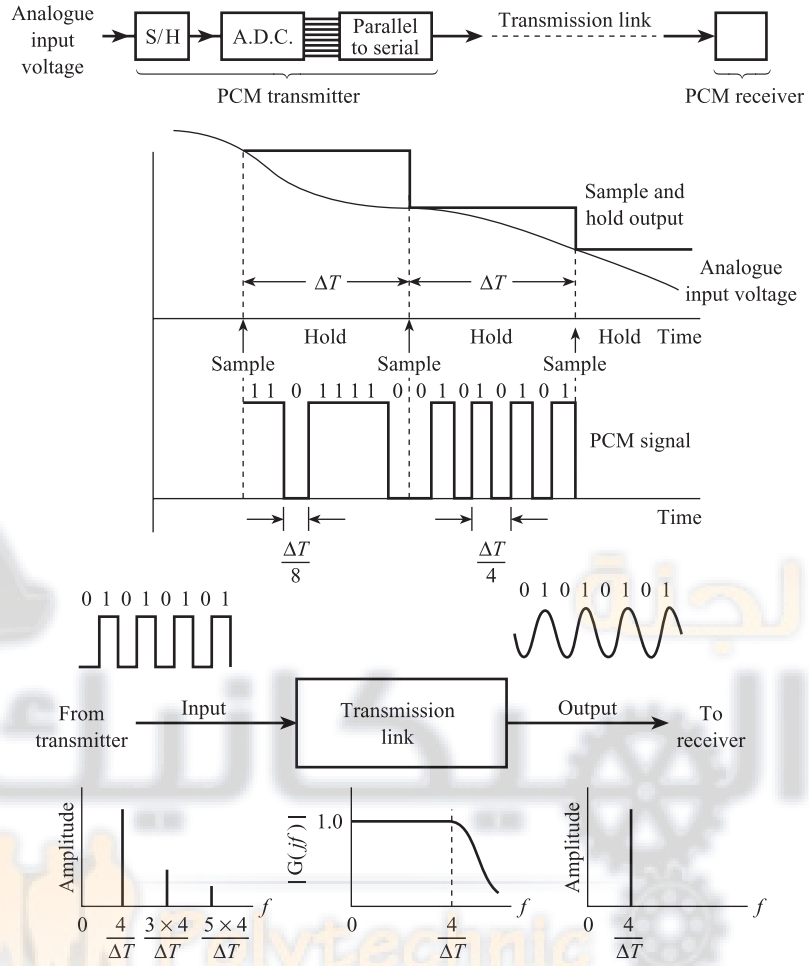
The serial digital techniques discussed above are suitable for transmission distances up to around 1 km. Successful transmission over longer distances in the presence of high interference can be obtained by frequency modulating the serial digital signal onto a carrier (Section 18.6).

18.4.2 Transmission bandwidth

Figure 18.5 shows a simple PCM transmission system. A transmitter, consisting of a sample/hold device, ADC and parallel-to-serial converter, converts an input analogue voltage into a serial digital signal, which is sent over a transmission link to a receiver. The transmission link may be cable, radio link or optical fibre.

In order to estimate the bandwidth required for the transmission link it is necessary to find the extent of the frequency spectrum of the PCM signal. We first need to find the **bit rate** of the PCM signal; this is the number of bits per second or **baud** (1 baud = 1 bit s^{-1}).

Figure 18.5 Calculation of PCM transmission bandwidth.



Consider a single signal, sampled f_s times per second, each sample being encoded into an n -bit code. There are f_s samples per second and n bits per sample, so that the bit rate is:

Bit rate for a single signal

$$R = nf_s \quad [18.2]$$

For m multiplexed signals, each sampled f_s times per second, there are mf_s samples per second, so that in this case the bit rate is:

Bit rate for m multiplexed signals

$$R = nmf_s \quad [18.3]$$

Figure 18.5 shows corresponding time variations in input analogue voltage, sample-and-hold output signal and PCM signal. The graphs assume that the sample/hold device is in the SAMPLE state for an infinitely short time. This means that, for a single signal, the time in the HOLD state is equal to the sampling interval ΔT . If the ADC

has an 8-bit encoder, i.e. $n = 8$, then eight bits (either 0 or 1) of information must be transmitted during this time interval ΔT . Thus the width of each bit of information in the PCM signal is $\Delta T/8$. There are 256 possible pulse patterns during each sampling interval, but the pulse pattern corresponding to 01010101 has the shortest period and the highest frequency components.

From Figure 18.5 we see that this pulse pattern is a square wave of period $\Delta T/4$. The frequency spectrum of this square wave (Section 4.3) consists of a fundamental of frequency $4/\Delta T$ Hz, together with harmonics at frequencies $3 \times 4/\Delta T$, $5 \times 4/\Delta T$, $7 \times 4/\Delta T$, etc. If this square wave signal is transmitted over a link with bandwidth between 0 and a little over $4/\Delta T$ (Figure 18.5), then the received signal contains only the fundamental frequency $4/\Delta T$, i.e. it is a sine wave of frequency $4/\Delta T$ Hz. The receiver can still decide correctly that the transmitted message was 01010101, so that the minimum bandwidth required for transmission of the square wave is 0 to $4/\Delta T$, i.e. 0 to $4f_s$ Hz (since $f_s = 1/\Delta T$). Since this square wave has the highest frequency components of all possible pulse patterns, then the minimum bandwidth required for transmission of the PCM signal is 0 to $4f_s$. Thus in the general case of a single signal, sampled at f_s and encoded into an n -bit code, we have:

*Minimum PCM
bandwidth for
a single signal*

$$\text{PCM bandwidth} = 0 \text{ to } \frac{1}{2}nf_s \quad [18.4]$$

For m multiplexed signals, each sampled at $f_s = 1/\Delta T$, the time in the HOLD state is $\Delta T/m$. This means that n bits of information must be transmitted during time $\Delta T/m$; i.e. the width of each bit of information is now $\Delta T/mn$. The corresponding PCM bandwidth in this case is:

*Minimum PCM
bandwidth for m
multiplexed signals*

$$\text{PCM bandwidth} = 0 \text{ to } \frac{1}{2}mnf_s \quad [18.5]$$

From [18.2]–[18.5] we see that a single general expression for minimum PCM bandwidth is:

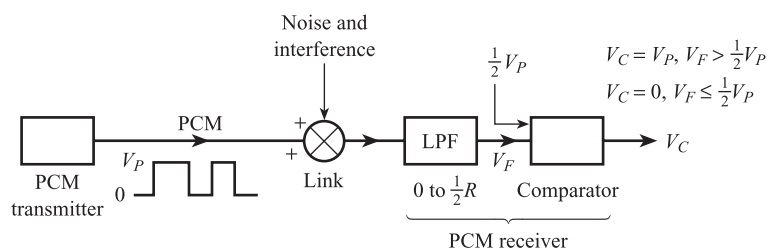
$$\text{PCM bandwidth} = 0 \text{ to } \frac{1}{2}R \quad [18.6]$$

Thus a PCM signal, derived from 16 multiplexed signals, each sampled once per second and encoded into 12 bits, has a bit rate of $16 \times 12 = 192$ bauds and requires a transmission link with a minimum bandwidth of 0 to 96 Hz.

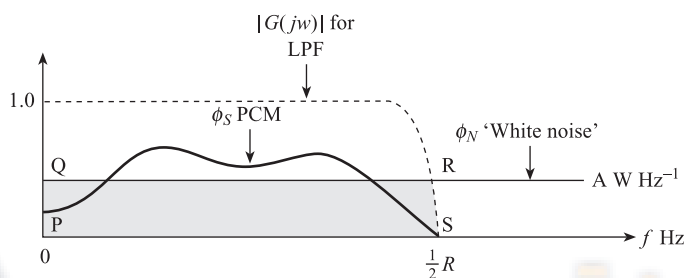
18.4.3 Effect of noise on PCM signal

The transmission link connecting PCM transmitter and receiver may be affected by external interference and noise as shown in Figure 18.6(a). Figure 18.6(b) shows the power spectral density ϕ_s of the PCM signal, extending effectively from 0 to $\frac{1}{2}R$ Hz. The figure also shows the power spectral density ϕ_N of ‘white’ noise; here ϕ_N has a constant value of $A \text{ W Hz}^{-1}$ over an infinite range of frequencies. The first stage of the receiver is a low-pass filter of bandwidth between 0 and $\frac{1}{2}R$ Hz. This rejects noise frequencies greater than $\frac{1}{2}R$, but noise frequencies inside the signal bandwidth, i.e. between 0 and $\frac{1}{2}R$, are allowed to pass to the comparator. The total power W_N of the noise in the comparator input signal is given by the area $PQRS$ under the noise power spectral density curve (eqn [6.23]), i.e.

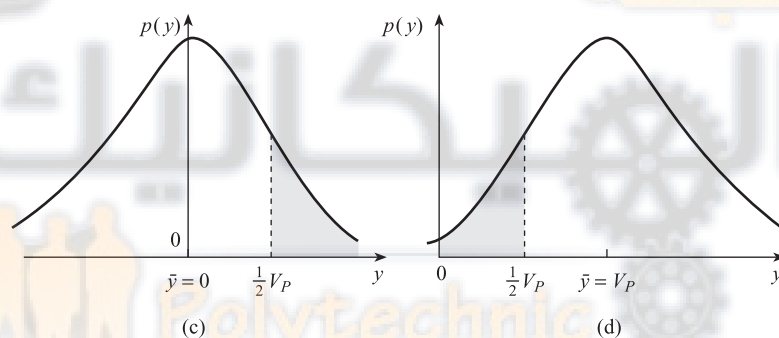
Figure 18.6 Effect of noise of PCM signal.



(a)

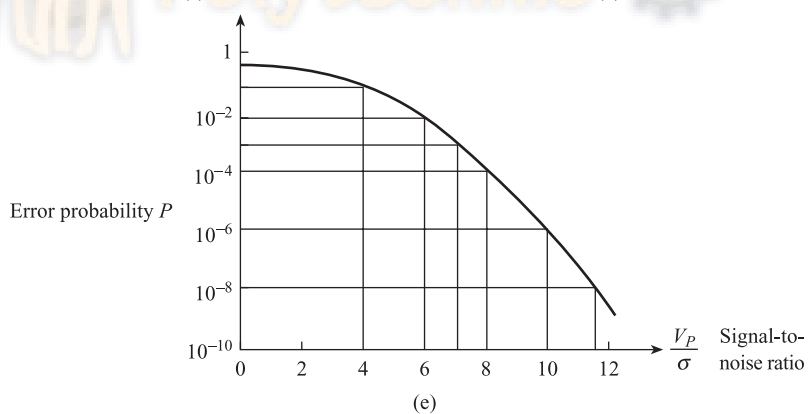


(b)



(c)

(d)



(e)

$$W_N \approx \frac{1}{2}AR \text{ watts}$$

[18.7]

Assuming the noise signal has zero mean \bar{y} , then the standard deviation σ is equal to the root mean square value y_{RMS} . From eqn [6.33] $y_{\text{RMS}}^2 = W_N$, so that the standard deviation of the noise present in the comparator input signal is given by:

$$\sigma = \sqrt{W_N} = \sqrt{\frac{AR}{2}} \text{ volts} \quad [18.8]$$

The PCM signal leaving the transmitter has a value V_p volts for a 1 and 0 V for a 0. The second stage of the receiver is a comparator which compares the filter outputs V_F with $\frac{1}{2}V_p$, i.e. one half of the original pulse amplitude. The comparator output voltage is given by:

$$\begin{aligned} V_C &= V_p, & \text{if } V_F > \frac{1}{2}V_p \\ V_C &= 0, & \text{if } V_F \leq \frac{1}{2}V_p \end{aligned} \quad [18.9]$$

so the receiver decides that a 1 has been transmitted if $V_F > \frac{1}{2}V_p$, and a 0 has been transmitted if $V_F \leq \frac{1}{2}V_p$. This decision is often made correctly, even if the received pulses are distorted by noise. The presence of noise, however, does mean that some decisions are made incorrectly, i.e. the receiver decides that a transmitted 1 is a 0 or a transmitted 0 is a 1. The probability of these errors occurring can be evaluated using the probability density function $p(y)$ for the noise.

Suppose that a 0 is transmitted: we can assume, then, that the comparator input signal is noise alone with standard deviation σ and zero mean value ($\bar{y} = 0$). The probability of a wrong decision here is the probability of the noise being greater than $\frac{1}{2}V_p$, i.e. $P_{y > \frac{1}{2}V_p}$. This probability is equal to the shaded area under the $p(y)$ curve in Figure 18.6(c), i.e.

*Probability of a 0
being received as a 1*

$$P_{y > (1/2)V_p} = \int_{(1/2)V_p}^{\infty} p(y) dy \quad [18.10]$$

If a 1 is transmitted, then the comparator input signal is noise superimposed on a d.c. voltage of V_p , i.e. noise with a mean value of V_p . The probability of a wrong decision in this case is the probability that the noise will be less than $\frac{1}{2}V_p$. This probability is equal to the shaded area in Figure 18.6(d), i.e.

*Probability of a 1
being received as a 0*

$$P_{y < (1/2)V_p} = \int_{-\infty}^{(1/2)V_p} p(y - V_p) dy \quad [18.11]$$

In the special case of noise with a normal probability density function:

$$p(y) = \frac{1}{\sigma\sqrt{2\pi}} \exp\left[-\frac{(y - \bar{y})^2}{2\sigma^2}\right] \quad [6.14]$$

it can be shown^[3] that both the above probabilities are equal and given by

*PCM error probability
(error rate) for
normal noise*

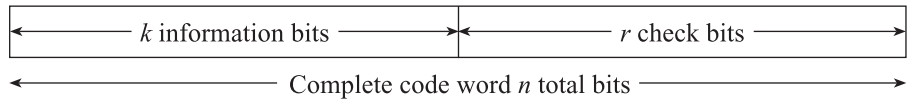
$$P\left(\frac{V_p}{\sigma}\right) = \frac{1}{2} - \frac{1}{\sqrt{\pi}} \int_0^{V_p/2\sqrt{2}\sigma} \exp(-x^2) dx \quad [18.12]$$

Assuming that a given digit is equally likely to be 0 or 1, then [18.12] gives the probability of an error in the decoding of any digit. Figure 18.6(e) shows how error probability varies with V_p/σ (signal-to-noise ratio). We see that for V_p/σ greater than around 8, a small increase in V_p/σ causes a very large reduction in error probability. Thus increasing V_p/σ from 8 to 12 reduces the error probability from approximately 10^{-4} to 10^{-8} . At $V_p/\sigma = 7$, the probability of error in a single bit is approximately 10^{-3} . This means that the probability of error in a 16-bit signal is 0.016. There is an equal probability that the error will occur in any of the digits in the PCM signal. If the error occurs in the least significant bit (LSB) then the resulting measurement error will be small; if the error occurs in the most significant bit (MSB) then the measurement error will be 50% of full scale.

18.5

Error detection and correction

For the reasons given above, it is important that any errors occurring during the decoding of a noise-affected PCM signal are detected, and in some cases corrected. This is achieved by the use of **redundancy**. Redundancy here means the addition of extra **check** digits to the **information** digits containing the measurement data. Thus each complete code word consists of n digits made up of k information (measurement) digits and $r = n - k$ check digits as shown below. Such a code word is referred to as an (n, k) code and has a redundancy of $(r/n) \times 100\%$.



18.5.1 Single parity check bit system

The simplest error detection system uses a single check bit, i.e. $r = 1$. The check bit is chosen using the concept of **parity**.^[4] A complete code word has **even parity** if the total number of 1s is even, and **odd parity** if the total number of 1s is odd. Thus in an even parity check system the check digit is set so that the total number of 1s in the complete code word is even; in an odd parity check system the check digit is set so that the total number of 1s is odd. Examples are given below:

Information bits	Even parity code word	Odd parity code word
1011	10111	10110
1000	10001	10000
0101	01010	01011
1111	11110	11111

The parity check bit is added to the information bits at the PCM transmitter using **modulo 2** addition. This process is characterised by the rules:

$$0 \oplus 0 = 0, \quad 0 \oplus 1 = 1, \quad 1 \oplus 0 = 1, \quad 1 \oplus 1 = 0$$

and can be implemented by either an **exclusive-or** logic gate or a read only memory. The transmitter performs modulo 2 addition on the information bits. Thus in the above example:

$$1 \oplus 0 \oplus 1 \oplus 1 = 1$$

$$1 \oplus 0 \oplus 0 \oplus 0 = 1$$

$$0 \oplus 1 \oplus 0 \oplus 1 = 0$$

$$1 \oplus 1 \oplus 1 \oplus 1 = 0$$

In an even parity system the check bit is the result of modulo 2 addition of the information bits; in an odd parity system the check bit is the inverse of this result.

The PCM receiver checks the parity of the complete received code word for correctness. Thus in an even parity system, a received code word with even parity is deemed to be correct, one with odd parity incorrect. This checking is performed by modulo 2 addition of *all* the digits in the code word. For an even parity system the result of addition is zero if there is no error.

This simple system has several limitations. It only detects the presence of an odd number of errors, e.g. 1 or 3 in the above example. An even number of errors, e.g. 2 or 4, gives the correct code word parity and goes undetected. Even if an error is detected, this system cannot decide which bit or bits are in error and therefore cannot correct the code word.

18.5.2 Practical error detecting systems

In industrial telemetry systems the amount of random noise present is often small; i.e. there is usually a high signal-to-noise ratio V_p/σ and consequently a low probability of errors. Occasionally, however, large interference voltages lasting a short time occur; these voltage transients are often caused by switching electrical equipment on or off. In this situation it is obviously important to detect as many error combinations as possible, but it is not worth attempting to correct errors. If the receiver detects an error it simply requests a retransmission of the code word. Since substantial interference and corresponding 'single burst' errors occur infrequently, interruptions to normal operation due to requests for retransmission also occur infrequently.

By using several check bits, each checking the parity of a different combination of information bits, it is possible to detect practically all error combinations. A typical arrangement used in an industrial telemetry system^[5] is shown below:

Information bits												Check bits			
b_{11}	b_{10}	b_9	b_8	b_7	b_6	b_5	b_4	b_3	b_2	b_1	b_0	c_3	c_2	c_1	c_0
X		X		X		X		X		X		X			
X	X			X	X			X	X				X		
X	X	X	X					X	X	X	X			X	
X	X	X	X	X	X	X	X	X	X	X	X				X

18.6 Frequency shift keying

In the previous section we saw that the frequency spectrum of the PCM signal extends, effectively, from 0 to $\frac{1}{2}R$ Hz. This means that part of the PCM spectrum may coincide with the spectrum of interference voltages, usually at 50 Hz, due to nearby power circuits (Figure 6.13(b)). Also the bandwidths of practical transmission links do not normally extend down to 0 Hz: for example, a British Telecom landline may have a bandwidth between 300 and 3300 Hz, and a VHF radio link bandwidth between 107.9 and 108.1 MHz. These two problems can be solved by modulating the PCM signal onto a carrier signal, whose frequency lies within the bandwidth of the transmission link. The spectrum of the signal is now shifted up to the carrier frequency, away from the interference spectrum, so that the latter can be rejected by a band pass filter (Figure 6.13(d)).

Two types of modulation were discussed in Chapter 9. In amplitude modulation (AM) the modulating signal alters the amplitude of a sinusoidal carrier; in frequency modulation (FM) the modulating signal alters the frequency of the carrier. It will be shown later in this section that FM requires a greater bandwidth than AM. However, provided the change in carrier frequency is sufficiently large, an FM receiver is better at improving a given signal-to-noise ratio than an AM receiver.

For this reason, in most telemetry systems, the PCM signal is frequency modulated onto a carrier; this is called *frequency shift keying* (FSK).

18.6.1 FSK transmitters and receivers

The **voltage controlled oscillator** (VCO) is the basis of both FSK transmitters and receivers. The principle of feedback oscillators was discussed in Section 9.5; we saw that the frequency of an electrical oscillator depends on the inductance and capacitance of an L - C - R circuit. The frequency of oscillation of a VCO is determined by the magnitude of the input voltage. Thus if V and f are corresponding values of input voltage and oscillation frequency, we have:

Frequency of voltage controlled oscillator

$$f = f_c + kV \quad [18.15]$$

where f_c is the frequency at zero voltage (unmodulated carrier frequency), and k Hz V^{-1} is the VCO sensitivity. The corresponding VCO output signal is:

$$V_{VCO} = \hat{V} \sin 2\pi(f_c + kV)t \quad [18.16]$$

If a PCM signal is input to a VCO (Figure 18.7(a)), the VCO output is an FSK signal; this has two frequencies, f_1 for a 1 and f_0 for a 0. For bipolar PCM with $V = +V_p$ for a 1 and $V = -V_p$ for a 0, the FSK frequencies are:

$$\begin{aligned} f_1 &= f_c + kV_p = f_c + D, \text{ for a 1} \\ f_0 &= f_c - kV_p = f_c - D, \text{ for a 0} \end{aligned} \quad [18.17]$$

where $D = kV_p$ is the maximum frequency deviation of the carrier. A typical FSK transmitter, suitable for a British Telecom landline, has $f_c = 1080$, $f_0 = 960$, $f_1 = 1200$, i.e. $D = 120$ Hz.^[7]

Figure 18.7 FSK transmitter and receiver:
(a) Transmitter
(b) Receiver.

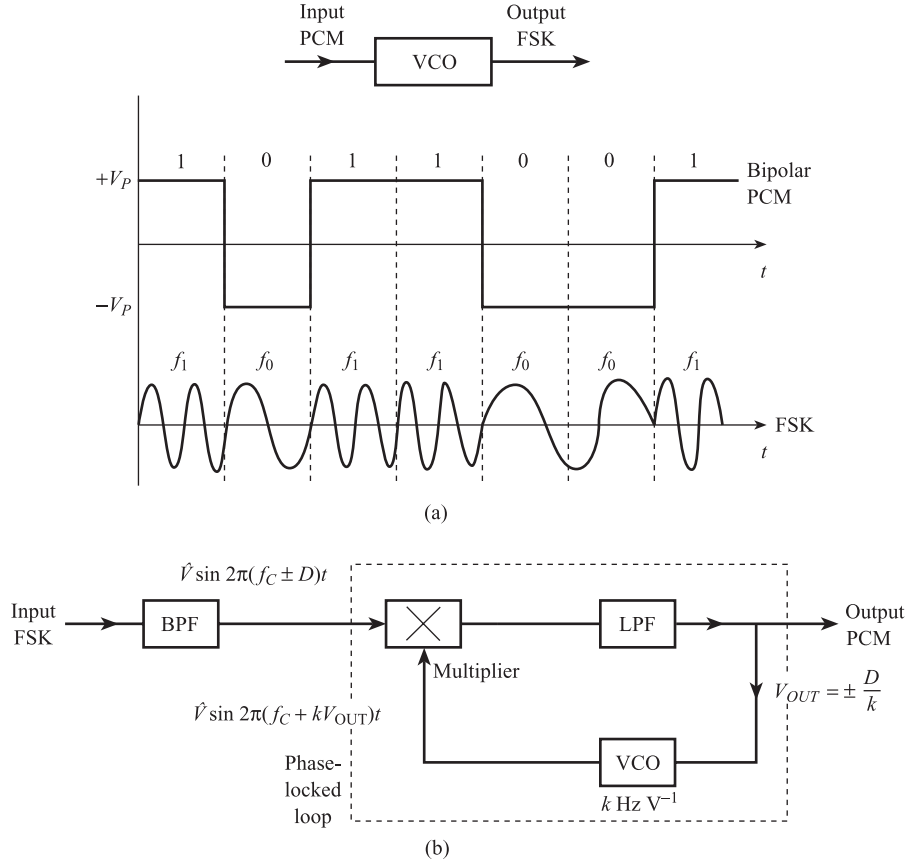


Figure 18.7(b) shows an FSK receiver which converts an incoming FSK signal back to PCM. The first stage of the receiver is a band pass filter which rejects all noise and interference outside the FSK bandwidth. The second stage is a phase locked loop (PLL), which consists of a VCO, a multiplier and a low pass filter in a closed loop system. The multiplier detects any difference in phase between the input signal and the VCO signal.

Suppose that the input signal is $\hat{V} \sin 2\pi(f_C + D)t$ (corresponding to a 1) and initially $V_{OUT} = 0$, so that the VCO output signal is $\hat{V} \sin 2\pi f_C t$. The multiplier output signal contains sum and difference frequencies, i.e. $2f_C + D$ and D ; the LPF removes the $2f_C + D$ component so that now V_{OUT} is a low amplitude signal of frequency D . This causes the frequency of the VCO output signal to increase until it is equal to that of the input signal, i.e. until $f_C + kV_{OUT} = f_C + D$. At the same time the frequency of V_{OUT} falls from D to zero as the amplitude of V_{OUT} increases. When the system settles out, V_{OUT} is equal to a d.c. voltage of magnitude $+D/k$ (for a 1). Similarly, when the input frequency is $f_C - D$, the system settles out with $f_C - D = f_C + kV_{OUT}$ and V_{OUT} a d.c. voltage of magnitude $-D/k$ (for a 0). In both cases the VCO frequency is said to 'lock' onto the input frequency.

18.6.2 Bandwidth of FSK signal

In Section 9.3 we saw that if a single sine wave of frequency f_i is amplitude modulated onto a sinusoidal carrier of frequency f_s , then the spectrum of the AM signal

consists of two lines at frequencies $f_s - f_i$ and $f_s + f_i$. This means that if a random signal, with spectrum between 0 and f_M , is amplitude modulated onto f_s , the spectrum of the AM signal lies between $f_s - f_M$ and $f_s + f_M$. If a single sine wave $\hat{V}_i \sin 2\pi f_i t$ is frequency modulated onto a sinusoidal carrier using a VCO, then from eqn [18.15] the instantaneous frequency of the FM signal is:

$$\begin{aligned} f &= f_c + k\hat{V}_i \sin 2\pi f_i t \\ &= f_c + D \sin 2\pi f_i t \end{aligned} \quad [18.18]$$

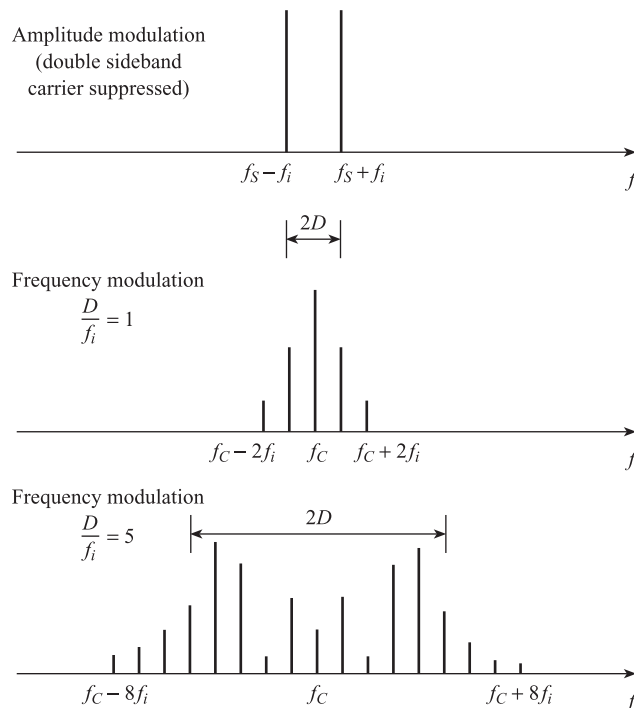
Here f_c is the unmodulated carrier frequency and $D = k\hat{V}_i$ is the maximum deviation of f from f_c . The resulting FM signal is given by:

$$V_{FM} = \hat{V} \sin 2\pi(f_c + D \sin 2\pi f_i t)t \quad [18.19]$$

From Figure 18.8 we see that the spectrum of this FM signal is wider and more complex than the corresponding AM spectrum. In FM there are several lines, symmetrically arranged about f_c , the number and relative amplitudes of the lines depending on the **modulation index** D/f_i .^[8]

For a random modulating signal containing frequencies between 0 and f_M , the FM spectrum consists of a large number of lines. In this case, the number of lines and the width of the spectrum depend on the appropriate modulation index D/f_M . For very small and very large values of D/f_M , i.e. $D/f_M \ll 1$ and $D/f_M \gg 1$, the frequency spectrum of the FM signal extends approximately from $f_c - (D + f_M)$ to $f_c + (D + f_M)$.^[8] For $D/f_M \approx 1$, the FM spectrum extends approximately from $f_c - (D + 2f_M)$ to $f_c + (D + 2f_M)$.

Figure 18.8 Comparison of AM and FM spectra.



Summarising these results we have:

*Approximate FM
bandwidth*

$$\begin{aligned} &\text{Approximate FM bandwidth} \\ &= f_c - (D + f_M) \quad \text{to} \quad f_c + (D + f_M), \quad \frac{D}{f_M} \ll 1, \frac{D}{f_M} \gg 1 \\ &= f_c - (D + 2f_M) \quad \text{to} \quad f_c + (D + 2f_M), \quad \frac{D}{f_M} \approx 1 \end{aligned} \quad [18.20]$$

In FSK the modulating signal is PCM. The PCM signal has a frequency spectrum effectively between 0 and $\frac{1}{2}R$ (Section 18.4.2); here $f_M = \frac{1}{2}R$, where R is the PCM bit rate. Equations [18.20] can therefore be used to give corresponding expressions for the bandwidth necessary to transmit an FSK signal, i.e.

*Approximate FSK
bandwidth*

$$\begin{aligned} &\text{Approximate FSK bandwidth} \\ &= f_c - (D + \tfrac{1}{2}R) \quad \text{to} \quad f_c + (D + \tfrac{1}{2}R), \quad \frac{2D}{R} \ll 1, \frac{2D}{R} \gg 1 \\ &= f_c - (D + R) \quad \text{to} \quad f_c + (D + R), \quad \frac{2D}{R} \approx 1 \end{aligned} \quad [18.21]$$

Thus an FSK signal with $f_c = 1080$ Hz, $D = 120$ Hz and $R = 200$ baud has $2D/R = 1.2$, and requires a bandwidth approximately between 760 and 1400 Hz.

18.7

Communication systems for measurement

18.7.1 Introduction

In the introduction to this chapter, we saw that in many industrial situations it will be necessary to transmit measurement data from transducers/transmitters (outstations, O/S), located at different items of plant equipment, to signal processing and data presentation elements (master stations, M/S), located in a central control room. The distances between individual plant items and between the items and the control room may be up to a few kilometres. A communications system is therefore required which is capable of transmitting large amounts of information in two directions (M/S to O/S and O/S to M/S), over long distances in the presence of external interference and noise. Such systems are often referred to as **telemetry systems**.

In Section 9.4.3 we discussed **intelligent** or **smart transmitters**. These transmitters incorporate a microcontroller which is used not only to calculate the measured value of the variable but also to control a **digital communications module**. Since this module can both transmit and receive digital information, an intelligent transmitter can therefore act as an outstation in a telemetry system. The main problem here is that there are a large number of digital communication standards in current use. This means that transmitting/receiving equipment made by one manufacturer may not be

compatible with that made by another manufacturer. There is a need therefore for an agreed signal standard for the digital communication of measurement data, just as a 4–20 mA current loop has been used as an analogue transmission standard.

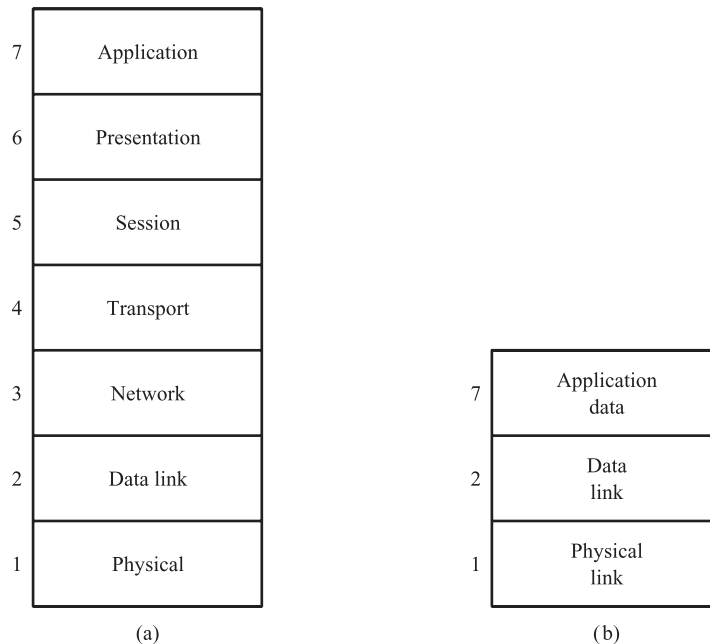
18.7.2 Reference Model for Open Systems Interconnection (OSI)

In 1983 the International Standards Organisation (ISO) approved the Reference Model for Open Systems Interconnection (OSI) as an international communication standard. The aim of the standard is to allow open communication between equipment from different vendors. It will be many years before this aim is achieved but the OSI model will provide the basis of the aim. In the meantime the model can act as a bridge between two different proprietary systems which previously could not communicate.

The OSI model is an abstract concept consisting of seven layers (Figure 18.9(a)). Each layer represents a group of related functions or tasks. **OSI protocols** are used to define these functions but do not define how these functions are implemented. The main purpose of the model is to provide a structure whereby vendor independent systems can be implemented. The functions of the seven layers can be summarised as follows:

- **Application Layer (7)** This is the highest-order layer in the model and its purpose is to ensure that a user application program can both receive and transmit data.
- **Presentation Layer (6)** This layer ensures that an application correctly interprets the data being communicated by translating any differences in representation of data.
- **Session Layer (5)** This layer is responsible for controlling communication sessions between applications programs.

Figure 18.9 Layered protocol models:
(a) ISO OSI model
(b) Fieldbus model.



- **Transport Layer (4)** This layer provides those layers above it with a reliable data-transfer mechanism which will be independent of any particular network implementation.
- **Network Layer (3)** This layer provides the actual communication service to the transport layer; it controls communications functions such as routing, relaying and data link connection.
- **Data Link Layer (2)** This layer controls the transfer of data between two physical layers and provides for (ideally) error-free sequential transmission of data over a link in a network.
- **Physical Layer (1)** This layer defines the actual signalling method employed, together with the type of transmission medium, e.g. copper wire, fibre optic, radio waves, etc.

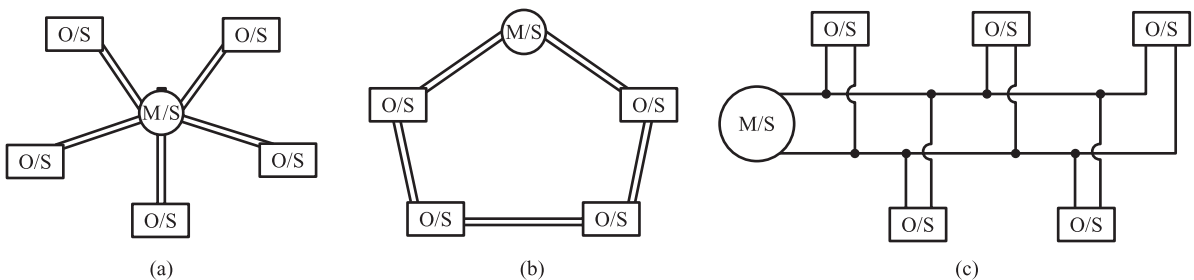
18.7.3 Fieldbus

Work is currently in progress to produce a single standard for two-way digital communication of measurement and control data between intelligent sensors/transmitters located in the field and a computer-based master station located in a control room. This standard is referred to as 'Fieldbus' and is particularly, but not exclusively, applicable to the process industries. The standard is based on a simplified three-layer version of the seven-layer OSI model (Figure 18.9(b)): the **physical layer (1)**, the **data link layer (2)** and the **application layer (7)**. Detailed discussion has taken place over many years with the aim of producing an agreed standard for each of the three layers. These standards are now in the process of being finalised. We now discuss how each of the layers can be implemented.

Physical layer^[9]

The first decision to be made is the **network topology**, i.e. the geometry of the interconnection between the outstations and the master station. Figure 18.10(a) shows three classic network topologies: **star**, **ring** and **multi-drop**. In any given link in the star arrangement there is only communication between the master station and a single outstation. This means that less multiplexing but more wiring is required; also if the master station fails the whole network fails. The ring arrangement also has limited reliability. The network will only function if all the stations are working; if any station fails then all stations beyond the failed station are also inaccessible. In the multi-drop arrangement several outstations and master stations share a common transmission path. Some method of multiplexing is therefore required to separate the signals from each outstation. In **time division multiplexing** (TDM, Section 18.1) the

Figure 18.10 Network topologies:
(a) Star
(b) Ring
(c) Multi-drop.



signals are separated in time so that, for example, O/S 1 transmits to M/S during a given time slot, O/S 2 transmits to M/S during the next time slot and so on. The alternative is **frequency division multiplexing** (FDM) where the signals are separated in frequency by modulating them onto different carrier frequencies (Sections 9.3 and 18.6). However, FDM requires more complex hardware so that TDM is usually preferred. A protocol will be necessary to arbitrate between the different outstations and avoid data collisions. The multi-drop arrangement has high reliability: the network will still function if any outstation fails, and if a suitable protocol is used it will still function, to a limited extent, if the master station fails. The multi-drop arrangement is therefore the preferred topology for Fieldbus.

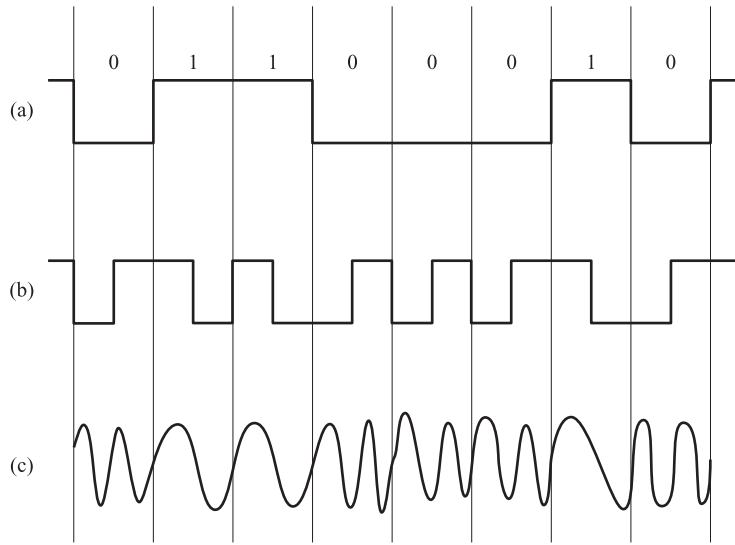
The next decision to be made concerns the **interconnection medium** to be used to implement the bus arrangement. This could be copper wire, optical fibre or a radio link. It is generally extremely difficult to implement the bus arrangement using optical fibres and there are problems in making reliable fibre/fibre connections in hostile environments. If the distances between the outstations and master station are many kilometres then radio links may be required. However, in many industrial situations these distances are only a few kilometres at most; this means that copper wire is feasible. Since it is also the cheapest practical way of implementing the bus arrangement, it is preferred for Fieldbus. In order to minimise the effects of inductive and capacitive coupling to interference sources (Section 6.5), screened twisted-pair wires should be used.

The final decision in the physical layer is the **signalling method** to be used. There are two methods of transmitting digital data: either in **parallel** form (Section 18.3) or in **serial** form (Section 18.4). We saw in Section 18.3 that parallel digital signals are suitable for high-speed, short-distance (up to 15 m) communication in laboratory environments where there is low-level electrical interference. Serial digital signals (pulse code modulation) are more suited to longer transmission links where significant electrical interference is present. If the serial signal is not modulated onto a carrier so that the signal bandwidth is determined entirely by the bit rate R (eqn [18.6]), this is referred to as **base-band** transmission.

Figures 18.11(a) and (b) show two base-band transmission methods: **non-return to zero** (NRZ) and **bi-phase Manchester**. NRZ is characterised by one voltage level (e.g. 0 V) corresponding to binary 0 and another (e.g. 5 V) corresponding to binary 1. The major disadvantage of this method is that a long sequence of 1s or 0s results in the voltage on the line remaining constant. This problem is overcome in the bi-phase method where one phase, e.g. \sqcap , corresponds to a 0 and another phase, e.g. \sqcup , corresponds to a 1; this guarantees a change in voltage at least once per bit period. The noise immunity of the serial signal can be increased by modulating it onto a carrier signal; this is **carrier band** transmission. Figure 18.11(c) shows **frequency shift keying** (FSK, Section 18.6). Here there are two distinct frequencies: the lower frequency corresponds to binary one and the higher frequency to binary zero.

One possible implementation of the physical layer is provided by the HART protocol which is marketed by Fisher-Rosemount.^[10] This is compatible with the smart transmitters discussed in Section 9.4.3. A multi-drop bus topology is used which can accommodate up to 15 smart devices with one power source. The interconnection medium is a single shielded twisted pair (maximum length 3 km) or multiple twisted pairs with an overall shield (maximum length 1.5 km). The signalling method is FSK based on the Bell 202 communications standard which uses 1200 Hz to represent binary 1 and 2200 Hz to represent 0; the bit rate is 1200 bits/s. This FSK signal is

Figure 18.11 Serial digital signalling:
 (a) Non-return to zero (NRZ)
 (b) Bi-phase Manchester
 (c) Frequency shift keying (FSK).



superimposed on the normal 4–20 mA analogue signal in a current loop (Figure 9.23). The amplitude of the FSK signal is 0.5 mA, so that if the normal analogue current is 12 mA, the minimum and maximum instantaneous currents are 11.5 and 12.5 mA. The average value of loop current is therefore unchanged at 12 mA. The Bell 202 communications system also allows smart devices to be directly connected to leased telephone lines. This allows the device to communicate with a central control point many kilometres away. Since the transmitter power is also isolated from the communications in leased line applications, any number of devices can be networked.

Data Link layer^[9]

As a result of the above discussions, the physical layer will be a single multidrop bus which is shared between several intelligent devices using time division multiplexing. The data link layer is concerned with the transfer of data between these devices. The first requirement is for a method of controlling the bus which specifies the time interval during which a given device will transmit and receive information. The simplest method is to have a single fixed central master station which controls the times at which each of the outstations transmits and receives. This method has limited reliability, however, since if the master station fails then the whole network fails even though all of the outstations may be working correctly. The reliability is increased if two or more stations are designated to be masters. Another method is decentralised mastership; here each of the stations connected to the bus takes it in turn to be the master for a given period of time. This can be achieved using **token passing**. The station holding the token is responsible for initiating all communications on the network for a given period of time. At the end of the period it must pass on the token to the next station.

In order that data is correctly routed between stations, addressing information must be added to the data. Thus if a given station is transmitting data to another station, then the data should be preceded by an **address code** which uniquely defines the source and destination addresses. An 8-bit address code could specify up to 16 source

Figure 18.12 Typical frame format.

Start flag	Address field	Command field	Information field	Parity check field	Stop flag
------------	---------------	---------------	-------------------	--------------------	-----------

addresses and up to 16 destination addresses. There is also a requirement for **control** or **command instruction codes** where, for example, a given device is required either to receive (read) incoming data or to transmit (write) data to another device. Finally, there is a need for any errors present in the transmitted information to be detected and ideally corrected. This is done by adding additional **parity check bits** (Section 18.5).

The total information transmitted from one outstation to another now consists of different types, one type following another in time. It is essential therefore that the data is arranged in **packets** or **frames**. Each frame should have a **format** which clearly separates and distinguishes between different types of data, for example addressing codes and check codes. Figure 18.12 shows a typical frame format; it commences with a beginning of message or **START flag code**, followed by an address field, a command field, an information field and a parity check field, and concludes with an end-of-message or **STOP flag code**.

Application layer

The role of the application layer can be summarised as follows:

1. It enables the master station to obtain measurement data from the data link layer in a form suitable for further processing in a user applications program. An example is a master station obtaining volume flow rate data Q and density data ρ from smart field transmitters in a form suitable for an applications program to calculate mass flow rate $\dot{M} = \rho Q$.
2. It enables the master station to output data from an applications program to the data link layer in a form suitable for transmission to outstations. An example is an applications program in the master station changing the input range of a smart field differential pressure transmitter from 0 to 2.5 m of water to 0 to 3.0 m of water.

The application layer therefore specifies a set of control or command instructions which occur as a corresponding code in the data frame (Figure 18.12). Three necessary basic instructions are:^[10]

- READ, e.g. Master station reads measured value; Transmitter reads input range data
- WRITE, e.g. Master station specifies identification number and input range of transmitter; Transmitter outputs measured value
- CHANGE, e.g. Master station changes transmitter input range.

18.7.4 Fieldbus development

Figure 18.13 shows a possible future development of Fieldbus.^[11] It consists of a low-speed bus and a high-speed bus linked by a bridge.

The low-speed bus can be implemented using the HART protocol described earlier. This uses multi-drop bus topology, with up to 15 smart transmitters (Section 9.4.3)

Figure 18.13
Development of Fieldbus.

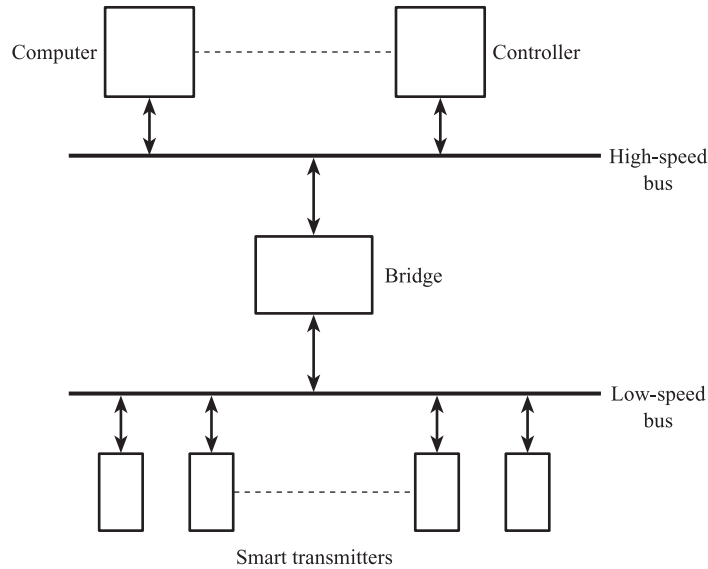


Figure 18.14
Frame format for
HART protocol.^[10]

Start character	Address field	Command field	Byte count	Status field	Data field	Parity check
-----------------	---------------	---------------	------------	--------------	------------	--------------

or other field devices connected to the bus. The interconnection medium is twisted pairs and the signalling method is FSK, based on the Bell 202 modem standard; the bit rate is 1200 bits/s.

Figure 18.14 shows the general format of a message frame in the HART protocol. Each field of information can consist of several bytes; each byte of information consists of a start bit, eight data bits, an odd parity bit and a stop bit.^[10]

There are three classes of commands in the HART command set. Universal commands are recognised and implemented by all field devices. Common-practice commands provide functions implemented by most, if not all, field devices. Device-specific commands represent functions that are unique to each field device. Typical commands are 'read measured variables', 'identify device' and 'read device information'.

The high-speed bus can be implemented using an **Ethernet** network. Ethernet is the most widely installed **local area network** (LAN) and is specified in the IEEE 802.3 standard. The most commonly installed Ethernet systems are called 10BASE-T and use ordinary telephone twisted-pair wire. Bit transmission rates of up to 10 Mbits/s are obtained with this standard; the signalling method is bi-phase Manchester. Other allowed transmission media at 10 Mbits/s are thin wire coaxial cable (up to 185 m), thick wire coaxial cable (up to 500 m), broadband coaxial cable (up to 3500 m) and optical fibre. For Fieldbus development it is proposed to use fast Ethernet, based on the 100BASE-T standard. This uses twisted-pair wires and operates at 100 Mbits/s. A variety of intelligent devices, including computers and controllers, can be connected on to the high-speed bus using multi-drop topology.

Conclusion

This chapter commenced by discussing the principles of **time division multiplexing** and its use in **data acquisition systems**. This was followed by a discussion of the principles of a range of techniques which form the basis of **communications systems**. These are **parallel digital signalling**, **serial digital signalling**, **error detection/correction** and **frequency shift keying**. The chapter concluded by studying how communication systems for measurement data can be implemented, making special reference to the emerging **Fieldbus** standard.

References

- [1] Mowlem Microsystems 1985 *Technical Information on ADU Autonomous Data Acquisition Unit*.
- [2] RDP Electronics 1986 *Technical Information on Translog 500 Data Acquisition System*.
- [3] MATTHEWS P R 1982–83 ‘Communications in process control’, *Measurement and Control*, Nov. and Dec. 1982, Jan. 1983.
- [4] CARLSON A B 1975 *Communication Systems*, 2nd edn, McGraw-Hill–Kogakusha International Student Edition, pp. 410–17.
- [5] Kent Process Control 1985 *Technical Information on Kent P4000 Telemetry Systems*.
- [6] Serck Controls 1977 *Product Data Sheet on a Telemetry Drive Module PDS 10/9*.
- [7] A.T.S. (Telemetry) Ltd 1987 *Technical Information on Type 1100 F.S.K. Data Modules*.
- [8] CARLSON A B 1975 *ibid.*, pp. 225–37.
- [9] ATKINSON J K 1987 ‘Communications protocols in instrumentation’, *J. Phys. E: Scientific Instrumentation*, vol. 20, pp. 484–91.
- [10] BOWDEN R 1996 *HART Field Communications Protocol*, Fisher-Rosemount Technical Publication.
- [11] Fisher-Rosemount 2002 *The Basics of Fieldbus – Technical Data Sheet*.

Problems

18.1

Sixteen analogue input voltages, each with a frequency spectrum between 0 and 5 Hz, are input to a time division multiplexer. The multiplexed signal passes to a serial digital (PCM) transmitter consisting of a sample/hold device, 12-bit binary ADC and a parallel-to-serial converter. The PCM signal is transmitted to a distant receiver over a link affected by ‘white’ noise with a power spectral density of 0.2 mW Hz^{-1} .

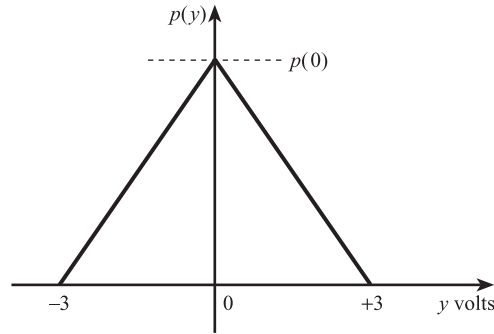
- (a) Suggest a suitable sampling frequency for each input signal.
- (b) What is the corresponding number of samples per second for the multiplexed signal?
- (c) What is the maximum length of time the sample/hold device can spend in the hold state?
- (d) What is the maximum percentage quantisation error for the ADC?
- (e) Find the bit rate and minimum transmission bandwidth for the PCM signal.

- (f) The first stage of the PCM receiver is a low-pass filter with a bandwidth 'matched' to the frequency spectrum of the PCM signal. Estimate the standard deviation of the noise present at the filter output.

18.2 A PCM transmitter sends out a 12-bit serial digital signal with 5 V corresponding to a 1 and 0 V corresponding to a 0. The signal passes over a transmission link, affected by random noise, to a PCM receiver consisting of a low-pass filter and a comparator. The comparator input signal is the PCM signal with noise superimposed on it; the probability density $p(y)$ of this noise is the triangular function shown in Figure Prob. 2. The comparator decides that a 1 has been transmitted if the comparator input signal is greater than 2.5 V, and that a 0 has been transmitted if the comparator input signal is less than or equal to 2.5 V.

- Calculate $p(0)$ such that $p(y)$ is normalised.
- Find the probability that y is greater than +1.0 V.
- Find the probability that a 0 is received as a 1.
- Find the probability that a 1 is received as a 0.
- What is the probability that a single error occurs in a complete code word?

Figure Prob. 2.



18.3 Ten measurement signals are input to a multiplexer so that each one is sampled twice per second. The multiplexed signal is input to a serial digital transmitter incorporating a 10-bit ADC. The resulting PCM signal is converted into FSK such that 720 Hz corresponds to a 1 and 480 Hz corresponds to a 0. Estimate the bandwidth required by the FSK signal.

- 18.4**
- Random noise is characterised by a Gaussian probability density function of standard deviation $\sigma = 1.0$ V and mean value $\bar{y} = 0$ V. Using the probability values given below, calculate the probability that the noise voltage:
 - exceeds +0.5 V
 - lies between -1.0 and +1.0 V
 - is less than -1.5 V.
 - Information in binary form is sent with a 0 represented by 0 V and a 1 represented by 5 V. During transmission the above random noise is added to it. The receiver decides that a 0 has been transmitted if the total input voltage is less than 2.5 V and that a 1 has been transmitted if the total input voltage is greater than 2.5 V. Use the probability values below to estimate the probable number of errors if 1600 bits of information are transmitted.

$$P_{y > \bar{y} + 0.5\sigma} = 0.3085, \quad P_{y > \bar{y} + \sigma} = 0.1587$$

$$P_{y > \bar{y} + 1.5\sigma} = 0.0668, \quad P_{y > \bar{y} + 2.5\sigma} = 0.0062$$

19 The Intelligent Multivariable Measurement System

In Section 9.4 we introduced the concept of the **intelligent transmitter** which has the capability of calculating an estimate of the measured value of a variable. The concept of computer estimation of measured value was also explained in Section 3.3. This chapter discusses the principles and implementation of **intelligent multivariable** measurement systems, which have the ability to estimate the measured values of a number of process variables. This type of system will require several sensors, usually one for each measured variable. The output of a given sensor may also be affected by some of the other process variables, so that **inverse sensor models** (Section 3.3) are required which take account of this. The system should also have the ability to calculate estimates of the values of process variables which are not measured from estimates of variables which are measured, using **process models**. This is the concept of the **virtual instrument** discussed in Section 10.3.

This chapter first discusses the structure of a typical intelligent multivariable system and the elements which are present. It then considers the types of modelling methods which are used in these systems.

19.1

The structure of an intelligent multivariable system

Figure 19.1 shows the general structure of an intelligent multivariable measurement system. The purpose of the system is to present the observer with a set of measured values of the process variables. We now discuss the elements which are present in the system.

19.1.1 The process

The process could be a chemical plant, power station, steel mill, oil refinery, car, ship or aircraft, for example. In all cases there may be a number of information variables which describe the process. Examples of these are given in Table 1.1. In this chapter we define $\{P\}$ to be the set of n process information variables or simply **process variables**. Thus the set of process variables for a gas pipeline could be:

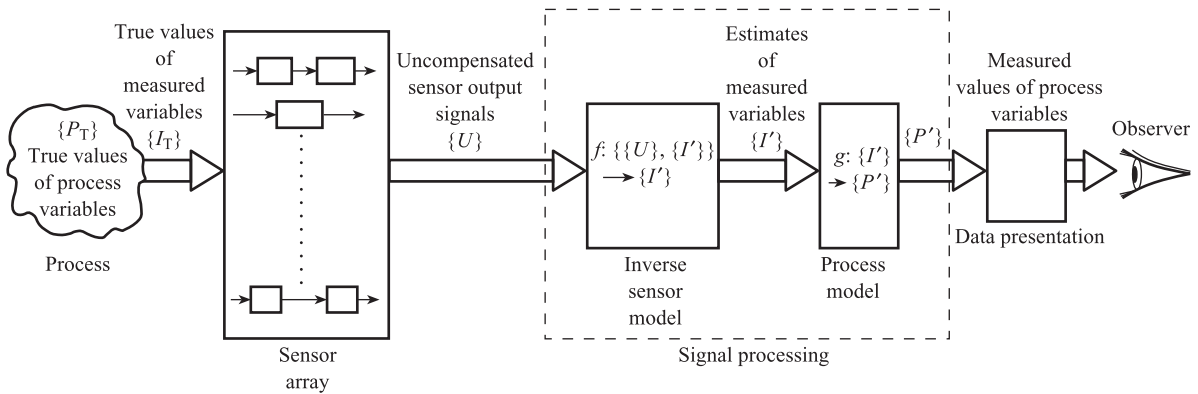


Figure 19.1 The intelligent multivariable measurement system.

$$\{P\} = \{\text{volume flow rate, temperature, pressure, density, mass flow rate, enthalpy flow rate}\}$$

We can then define $\{P_T\}$ as the set of n numbers which are the **true values** of these process variables.

However, it may be impossible, impractical or uneconomic to **measure** all n process variables. We define $\{I\}$ as the set of m **measured variables** ($m \leq n$). $\{I\}$ is therefore a subset of $\{P\}$; in the gas pipeline example above we could have:

$$\{I\} = \{\text{volume flow rate, temperature, pressure}\}$$

The system should therefore have the ability to calculate the $n - m$ unmeasured variables from the m measured variables. In the example given, mass flow rate, density and enthalpy flow rate are calculated from volume flow rate, temperature and pressure. We can define $\{I_T\}$ as the set of m numbers which are the true values of the measured variables.

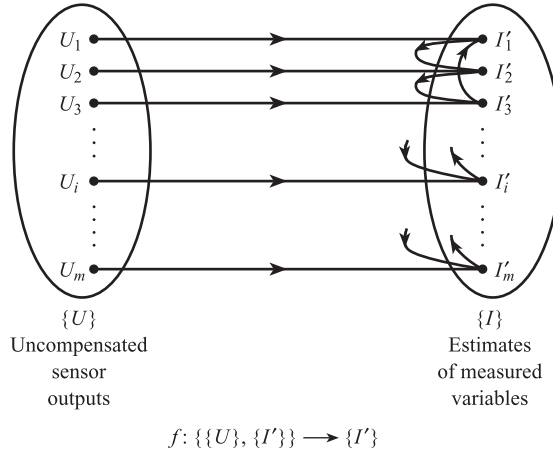
19.1.2 The sensor array

Assuming that one sensor is required for each measured variable, an array of m sensors is required. The principles and characteristics of a range of sensing elements in widespread current use are discussed in Chapter 8. Each sensor will require associated signal conditioning elements, such as bridges, amplifiers and resonators; these are discussed in Chapter 9. Furthermore, analogue-to-digital and frequency-to-digital converters (Section 10.1) are required to give parallel or serial digital output signals. $\{U\}$ is the set of m uncompensated digital sensor output signals. $\{U\}$ is passed to a signal processing element; this is a computer with software to implement two types of model.

19.1.3 Inverse sensor models

This model is shown in Figure 19.2. Here, for a given sensor i , with an uncompensated output U_i , the model calculates an estimate I'_i of the i th measured variable I_i . $\{I'\}$ is the set of m numbers which are estimates of the measured values. We can say that the model maps the set $\{U\}$ into the set $\{I'\}$. However, an individual estimate I'_i may also depend on estimates of other measured variables $\{I\}$. In general, the

Figure 19.2 The inverse sensor model.



model therefore provides a function f which maps the sets $\{U\}$ and $\{I'\}$ into the set $\{I'\}$, i.e.

$$f: \{\{U\}, \{I'\}\} \rightarrow \{I'\} \quad [19.1]$$

In the example of Figure 19.2, I'_1 depends on U_1 and I'_3 , I'_2 depends on U_2 and I'_1 , and I'_3 depends on U_3 and I'_2 .

In many cases this mapping can be represented by m inverse sensor equations of the form (eqn [3.20]):

$$I' = K'U + N'(U) + a' + K'_M I'_M U + K'_I I'_I \quad [19.2]$$

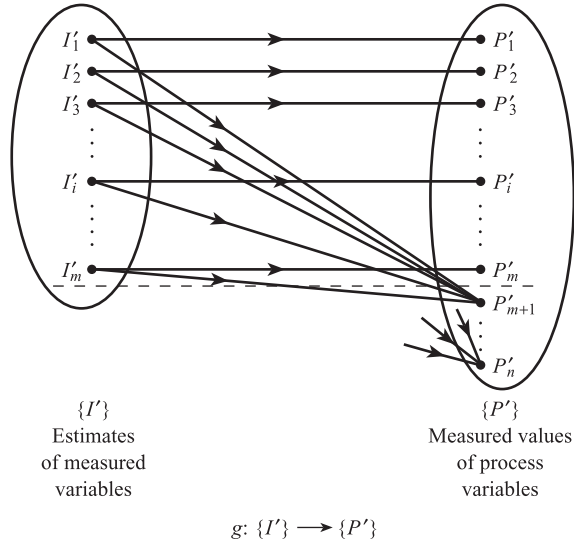
which describe non-linear characteristics, a single modifying input I'_M and a single interfering input I'_I . If eqn [19.2] can be applied to the three variables I'_1, I'_2 and I'_3 in Figure 19.2 then we have:

$$\begin{aligned} I'_1 &= K'_1 U_1 + N'_1(U_1) + a'_1 + K'_{M13} U_1 I'_3 \\ I'_2 &= K'_2 U_2 + N'_2(U_2) + a'_2 + K'_{I21} I'_1 \\ I'_3 &= K'_3 U_3 + N'_3(U_3) + a'_3 + K'_{M32} U_3 I'_2 + K'_{I32} I'_2 \end{aligned} \quad [19.3]$$

Here I'_3 acts as a modifying input on I'_1 , I'_1 as an interfering input on I'_2 , and I'_2 as both a modifying and an interfering input on I'_3 . In general, a given sensor may be affected by several modifying and interfering variables. The three eqns [19.3] can be solved to give I'_1, I'_2 and I'_3 .

19.1.4 Process models

This model is shown in Figure 19.3. Here the model uses the set $\{I'\}$ of estimates of the m measured variables to calculate the set $\{P'\}$ of measured values of the n process variables. We can say that the model provides a function g which maps the set $\{I'\}$ into the set $\{P'\}$, i.e.

Figure 19.3 The process model.

$$g: \{I'\} \rightarrow \{P'\}$$

[19.4]

If we consider the relationship between individual members I'_i and P'_i of the sets, then we have:

$$\begin{aligned} P'_i &= I'_i & \text{for } i = 1, \dots, m \\ P'_i &= g_i\{I'\} & \text{for } i = m + 1, \dots, n \end{aligned} \quad [19.5]$$

where g_i is the i th function of the set $\{I'\}$.

In some cases this mapping may be implemented by a number of simple equations. If we return to the gas pipeline example of Section 10.1.1 we have the set of six process variables:

$$\{P\} = \{\text{volume flow rate } Q, \text{ absolute temperature } \theta, \text{ absolute pressure } P, \text{ density } \rho, \text{ mass flow rate } \dot{M}, \text{ enthalpy flow rate } \dot{H}\}$$

and the set of three measured variables:

$$\{I\} = \{Q, \theta, P\}$$

The three non-measured process variables ρ , \dot{M} and \dot{H} can be calculated from Q , θ and P using:

$$\begin{aligned} \rho &= \frac{P}{R\theta} \\ \dot{M} &= \rho Q \\ \dot{H} &= C_p \dot{M} \theta \end{aligned} \quad [19.6]$$

where R is the gas constant and C_p the specific heat at constant pressure.

The set of measured values $\{P'\}$ are then transferred to the data presentation element for display to the observer.

19.2 Modelling methods for multivariable systems

19.2.1 The general multivariable modelling problem

In the previous section we saw the need for both inverse sensor and process models. This section examines different modelling methods that can be used.

Figure 19.4 shows the general multivariable modelling problem. Given a set $\{x\}$ of p input variables and a set $\{y\}$ of r output variables, we need to find a function f which maps the set $\{x\}$ into the set $\{y\}$, i.e. a function f such that:

$$f: \{x\} \rightarrow \{y\}$$

[19.7]

In many cases this mapping may be represented by a number of equations. In Section 19.2.2 we show how the basic equations of **physics** and **chemistry** can be used in modelling. Section 19.2.3 explains the derivation and applications of **regression** equations using experimental data. Finally Section 19.2.4 shows how **artificial neural networks** can be used to implement the mapping in situations where suitable equations cannot be found.

19.2.2 Physical and chemical model equations

Table 19.1 lists some physical and chemical equations which can be used to model sensors. It should be noted that in some cases the fundamental equation has to be corrected for practical use by introducing correction factors whose values are found from experimental data.

The equation for an ion-selective electrode can be used in a measurement system to measure the concentration or activity a of dissolved sodium (Na^+), potassium (K^+) and calcium (Ca^{2+}) ions in a sample of water. An array of three ion-selective electrodes is required, one for each ion. However, the e.m.f. of each electrode depends not only

Figure 19.4 The general multivariable model.

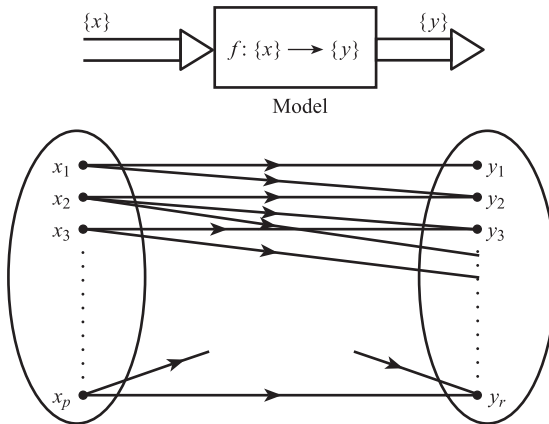


Table 19.1 Physical and chemical equations used in sensor models.

Resistive – strain gauge	$R = R_0(1 + Ge)$	Elastic	$x = \frac{1}{k}F$
Resistive – thermistor	$R = K \exp\left(\frac{\beta}{\theta}\right)$	Accelerometer	$x = \frac{ma}{k}$
Capacitive	$C = \frac{\epsilon\epsilon_0 A}{d}$	Differential pressure flowmeter	$\dot{M} = C_D E \epsilon \frac{\pi}{4} d^2 \sqrt{2\rho_1 \Delta P}$
Inductive	$L = \frac{n^2}{\mathcal{R}}$	Vortex flowmeter	$f = \frac{Sv}{d}$
Hall effect	$V = -\left(\frac{R_H}{t}\right)IB$	Coriolis flowmeter	$T = 4lr\omega\dot{M}$
Electromagnetic – tachogenerator	$E = b\omega, \sin(m\omega, t)$	Thermal sensor	$T_D = \frac{1}{UA}P_D + T_s$
Electromagnetic – flowmeter	$E = Blv$	Density transmitter	$\rho = \frac{A}{f_n^2} + \frac{B}{f_n} + C$
Thermoelectric	$E_{T_1,0} = E_{T_1,T_3} + E_{T_3,0}$	pH electrode	$E = E_0 - 0.0592 \text{ pH}$
Piezoelectric	$q = dF$	Ion-selective electrode	$E = E_0 + \frac{R\theta}{F} \log_e(a_X + K_{X/Y}a_Y)$

on the activity a_X of the selected ion X but also on the activities a_Y, a_Z of the other ions Y and Z. The sensor array can be described by the three equations:

$$\begin{aligned}
 E_{\text{Na}^+} &= E_{0\text{Na}^+} + \frac{R\theta}{F} \log_e(a_{\text{Na}^+} + K_{\text{Na}^+/\text{K}^+}a_{\text{K}^+} + K_{\text{Na}^+/\text{Ca}^{2+}}a_{\text{Ca}^{2+}}) \\
 E_{\text{K}^+} &= E_{0\text{K}^+} + \frac{R\theta}{F} \log_e(a_{\text{K}^+} + K_{\text{K}^+/\text{Na}^+}a_{\text{Na}^+} + K_{\text{K}^+/\text{Ca}^{2+}}a_{\text{Ca}^{2+}}) \\
 E_{\text{Ca}^{2+}} &= E_{0\text{Ca}^{2+}} + \frac{R\theta}{F} \log_e(a_{\text{Ca}^{2+}} + K_{\text{Ca}^{2+}/\text{Na}^+}a_{\text{Na}^+} + K_{\text{Ca}^{2+}/\text{K}^+}a_{\text{K}^+})
 \end{aligned} \tag{19.8}$$

If the e.m.f. values are measured and the values of the cross-sensitivity constants $K_{X/Y}$ are known, then eqn [19.6] can be solved to give a_{Na^+} , a_{K^+} and $a_{\text{Ca}^{2+}}$.

Table 19.2 lists some physical and chemical equations which are used to model processes. These equations can be used to calculate process variables which are not measured from variables which are measured. Simple examples are the calculation of velocity from acceleration and the calculation of current from voltage.

From Table 19.2 we see that we can calculate the volume flow rate Q of fluid flowing through a pipe by measuring the velocity v at an area element dA and integrating over the total cross-sectional area A_T of the pipe to give:

$$Q = \int_0^{A_T} v \, dA \tag{19.9}$$

Table 19.2 Physical and chemical equations used in process models.

Acceleration	$\ddot{x} = \frac{F}{m}$	Mass	$M = \rho V$
Velocity	$\dot{x} = \int \ddot{x} dt$	Volume	$V = \int Q dt$
Displacement	$x = \int \dot{x} dt$	Volume flow rate	$Q = \int v dA$
Mechanical power	$W = F\dot{x}$	Gas density	$\rho = \frac{P}{R\theta}$
Energy	$E = \int W dt$	Liquid density	$\rho = \frac{\rho_0}{1 + \alpha(T - T_0)}$
Electric current	$i = \frac{V}{R}$	Liquid viscosity	$\eta = \eta_{15} \exp \left[\frac{E}{R_0} \left(\frac{1}{T} - \frac{1}{288} \right) \right]$
Charge	$q = \int i dt$		
Electrical power	$W = iV$	Gas enthalpy flow rate	$\dot{H} = C_p \dot{M} \theta$

If we then divide A_T into 12 area elements A_i , $i = 1, \dots, 12$, and measure the velocity v_i at each area element, then eqn [19.9] becomes:

$$Q = \sum_{i=1}^{12} v_i A_i \quad [19.10]$$

The v_i can then be measured by an array of 12 vortex shedding sensors.^[1]

Each sensor i is located at area element A_i and detects vortices shed downstream from a bluff body. If f_i is the frequency of vortex shedding measured by the i th sensor, then from Table 19.1 we have:

$$f_i = \frac{S}{d} v_i \quad \text{or} \quad v_i = \frac{d}{S} f_i \quad [19.11]$$

where S is the Strouhal number and d the width of the bluff body. From eqns [19.10] and [19.11] we have:

$$Q = \frac{d}{S} \sum_{i=1}^{12} f_i A_i \quad [19.12]$$

so that Q can be found from the measured f_i if the constants A_i , S and d are known.

19.2.3 Multivariable regression equations

There are many situations where an equation with a well-defined form does not exist to describe a given physical or chemical effect. One example is the e.m.f. of a thermocouple $E_{T,0}$ (Section 8.5) with the measured junction at $T^\circ\text{C}$ and the reference junction at 0°C ; here the non-linear relation between $E_{T,0}$ and T has to be described by a polynomial or power series of the form:

$$E_{T,0} = a_1 T + a_2 T^2 + a_3 T^3 + a_4 T^4 + \dots \quad [19.13]$$

The coefficients a_1, a_2, a_3 , etc., are found from experimental data values of $E_{T,0}$ and T using **regression** analysis. In the multivariable modelling problem of Section 19.2.1 it is even more likely that some of the equations will have to be found using regression techniques.

We consider a model which has a single output variable y which depends on p input variables $\{x_1, \dots, x_p\}$ and we wish to establish a regression equation of the form:

$$y = f(x_1, x_2, \dots, x_p) \quad [19.14]$$

To do this we need q sets of experimental data; in general q will be much greater than p . The input data is defined by the matrix:

$$\mathbf{X} = \begin{bmatrix} x_{11} & x_{12} & \dots & x_{1p} \\ x_{21} & x_{22} & \dots & x_{2p} \\ \vdots & \vdots & & \vdots \\ x_{k1} & x_{k2} & \dots & x_{kp} \\ \vdots & \vdots & & \vdots \\ x_{q1} & x_{q2} & \dots & x_{qp} \end{bmatrix} \quad [19.15]$$

The output data is defined by the column vector:

$$\mathbf{Y} = \begin{bmatrix} y_1 \\ y_2 \\ \vdots \\ y_k \\ \vdots \\ y_q \end{bmatrix} \quad [19.16]$$

and

$$\mathbf{Y} = f(\mathbf{X}) \quad [19.17]$$

As an example we consider

$$y = f(x_1, x_2) \quad [19.18]$$

where y is a function of two independent variables x_1 and x_2 , and we need to find an equation of the form:

$$y = b_0 + b_1x_1 + b_2x_2 + b_{11}x_1^2 + b_{22}x_2^2 + b_{12}x_1x_2 \quad [19.19]$$

where there are six coefficients to be found. We use q sets of data ($q \gg 6$); the k th set is $\{y_k, x_{1k}, x_{2k}\}$ where $k = 1, \dots, q$.

From eqn [19.19] the k th estimate of y is:

$$y_{k,\text{est}} = b_0 + b_1x_{1k} + b_2x_{2k} + b_{11}x_{1k}^2 + b_{22}x_{2k}^2 + b_{12}x_{1k}x_{2k} \quad [19.20]$$

Since the k th observed value of y is y_k , the k th value of error is:

$$e_k = y_k - y_{k,\text{est}} \quad [19.21]$$

and the k th value of square error is:

$$e_k^2 = (y_k - y_{k,\text{est}})^2 \quad [19.22]$$

The sum of square errors SSE is therefore:

$$\begin{aligned} \text{SSE} &= \sum_{k=1}^q e_k^2 = \sum_{k=1}^q (y_k - y_{k,\text{est}})^2 \\ &= \sum_{k=1}^q (y_k - b_0 - b_1 x_{1k} - b_2 x_{2k} - b_{11} x_{1k}^2 - b_{22} x_{2k}^2 - b_{12} x_{1k} x_{2k})^2 \end{aligned} \quad [19.23]$$

The coefficients $b_0, b_1, b_2, b_{11}, b_{22}$ and b_{12} are chosen so that SSE has a minimum value; this occurs when:

$$\frac{\partial \text{SSE}}{\partial b_0} = \frac{\partial \text{SSE}}{\partial b_1} = \frac{\partial \text{SSE}}{\partial b_2} = \frac{\partial \text{SSE}}{\partial b_{11}} = \frac{\partial \text{SSE}}{\partial b_{22}} = \frac{\partial \text{SSE}}{\partial b_{12}} = 0 \quad [19.24]$$

These conditions give rise to a set of six simultaneous equations which can be expressed in matrix form:

$$\mathbf{A}\mathbf{b} = \mathbf{g} \quad [19.25]$$

Figure 19.5 Regression matrix equations.

$$\mathbf{A} = \begin{bmatrix} q & \sum_{k=1}^q x_{1k} & \sum_{k=1}^q x_{2k} & \sum_{k=1}^q x_{1k}^2 & \sum_{k=1}^q x_{2k}^2 & \sum_{k=1}^q x_{1k} x_{2k} \\ \sum_{k=1}^q x_{1k} & \sum_{k=1}^q x_{1k}^2 & \sum_{k=1}^q x_{1k} x_{2k} & \sum_{k=1}^q x_{1k}^3 & \sum_{k=1}^q x_{1k} x_{2k}^2 & \sum_{k=1}^q x_{1k}^2 x_{2k} \\ \sum_{k=1}^q x_{2k} & \sum_{k=1}^q x_{1k} x_{2k} & \sum_{k=1}^q x_{2k}^2 & \sum_{k=1}^q x_{1k}^2 x_{2k} & \sum_{k=1}^q x_{2k}^3 & \sum_{k=1}^q x_{1k} x_{2k}^2 \\ \sum_{k=1}^q x_{1k}^2 & \sum_{k=1}^q x_{1k}^3 & \sum_{k=1}^q x_{1k}^2 x_{2k} & \sum_{k=1}^q x_{1k}^4 & \sum_{k=1}^q x_{1k}^2 x_{2k}^2 & \sum_{k=1}^q x_{1k}^3 x_{2k} \\ \sum_{k=1}^q x_{2k}^2 & \sum_{k=1}^q x_{1k} x_{2k}^2 & \sum_{k=1}^q x_{2k}^3 & \sum_{k=1}^q x_{1k}^2 x_{2k}^2 & \sum_{k=1}^q x_{2k}^4 & \sum_{k=1}^q x_{1k} x_{2k}^3 \\ \sum_{k=1}^q x_{1k} x_{2k} & \sum_{k=1}^q x_{1k}^2 x_{2k} & \sum_{k=1}^q x_{1k} x_{2k}^2 & \sum_{k=1}^q x_{1k}^3 x_{2k} & \sum_{k=1}^q x_{1k} x_{2k}^3 & \sum_{k=1}^q x_{1k}^2 x_{2k}^2 \end{bmatrix}$$

$$\mathbf{b} = \begin{bmatrix} b_0 \\ b_1 \\ b_2 \\ b_{11} \\ b_{22} \\ b_{12} \end{bmatrix} \quad \mathbf{g} = \begin{bmatrix} \sum_{k=1}^q y_k \\ \sum_{k=1}^q x_{1k} y_k \\ \sum_{k=1}^q x_{2k} y_k \\ \sum_{k=1}^q x_{1k}^2 y_k \\ \sum_{k=1}^q x_{2k}^2 y_k \\ \sum_{k=1}^q x_{1k} x_{2k} y_k \end{bmatrix}$$

where the matrix \mathbf{A} and the column vectors \mathbf{b} and \mathbf{g} are defined in Figure 19.5.^[2] The vector of coefficients \mathbf{b} is then given by:

$$\mathbf{b} = \mathbf{A}^{-1}\mathbf{g}$$

where \mathbf{A}^{-1} is the inverse of \mathbf{A} .

The regression equation [19.19] has a similar form to the inverse sensor equation [19.2]. Comparing the equations, if we set:

$$\begin{aligned} y &= I', \quad x_1 = U, \quad x_2 = I'_M = I'_1 \\ b_0 + b_1 x_1 + b_{11} x_1^2 &= a + K'U + N'(U) \\ b_2 &= K'_1, \quad b_{12} = K'_M, \quad b_{22} = 0 \end{aligned} \quad [19.26]$$

then this regression equation can be used as an inverse sensor equation.

A more extensive version of eqn [19.19] has been used to model a resonant silicon pressure sensor (Section 9.5.2) and an associated temperature sensor.^[3] Here the inverse model equation for the pressure sensor is of the form:

$$y = \sum_{i=0}^3 \sum_{j=0}^3 k_{ij} x_1^i x_2^j \quad [19.27]$$

where: y = pressure in millibar
 x_1 = output frequency in Hz
 x_2 = temperature sensor output in millivolts
 k_{ij} = calibration constant for a given sensor.

Sixteen calibration constants are therefore required. Here temperature is both a modifying and an interfering input, and the temperature sensor is a forward-biased diode. The voltage drop across the diode depends non-linearly on temperature.

19.2.4 Artificial neural networks

In complex multivariable processes and sensor arrays, well-defined physical and chemical equations may not exist to provide a sufficiently accurate model of the system. Furthermore, it may be impossible to predict the form of a suitable multivariable regression equation; this will be especially so if a large number of variables are required to represent the system accurately. In these situations **artificial neural networks** can be used as a modelling technique. These are empirical models which approximate the behaviour of **neurons** in the human brain.

Figure 19.6 shows a typical artificial neural network. It consists of three layers: the **input** layer, the **hidden** layer and the **output** layer. In this example there are four input variables, x_1, x_2, x_3 and x_4 , i.e. $p = 4$, and a single output variable y , i.e. $r = 1$. Beginning with the input layer, each of the inputs x_s is multiplied by the input weighting w_{1s} to give four weighted inputs $w_{1s}x_s, s = 1, \dots, 4$. There are four summing elements in the input layer. Each summer s has five inputs, the four weighted inputs $w_{1s}x_s$ and an input bias b_{1s} . The output of each summer is therefore:

$$g_s = b_{1s} + \sum_{s=1}^4 w_{1s}x_s, \quad s = 1, \dots, 4 \quad [19.28]$$

The four g_s signals are passed to the hidden layer. Each g_s is input to a function block S. The form of this function is:

Figure 19.6 Example of artificial neural network.

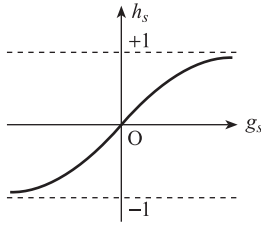
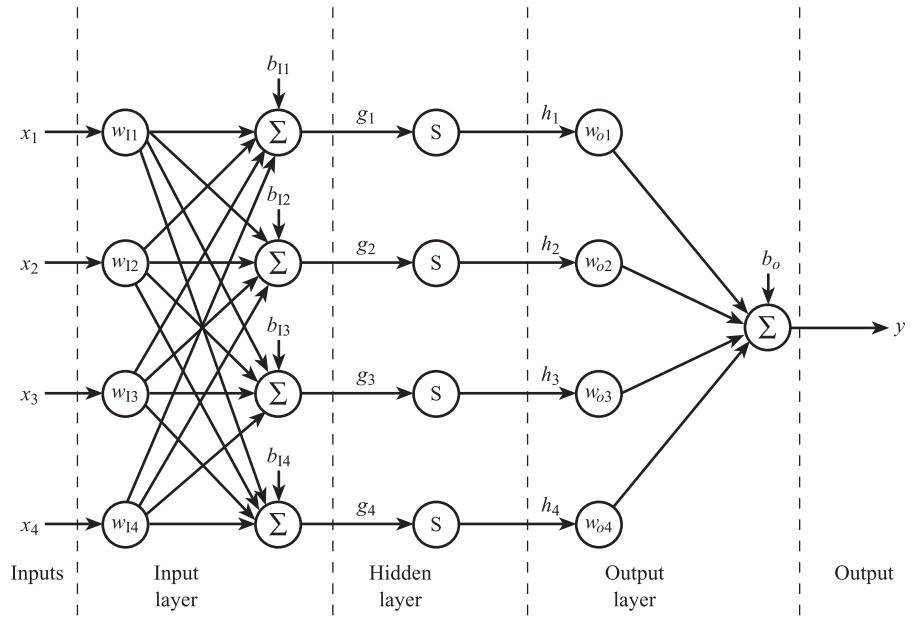


Figure 19.7
The balanced
sigmoid function.

$$h_s(g_s) = \frac{1 - \exp(-g_s)}{1 + \exp(-g_s)} \quad [19.29]$$

and it is referred to as a **balanced sigmoid** or hyperbolic tangent. It has the S-shaped form shown in Figure 19.7. This function has the advantages of being within the range -1 to $+1$, being able to approximate almost any other function and having derivatives that can be conveniently calculated. It would, for example, be easier to calculate derivatives of the function $h(g) = 1 + g + g^2 + g^3 + g^4$ but this would be less flexible as an approximation to other functions.

The four signals h_s are then passed to the output layer. Here each is multiplied by an output weighting w_{os} to give four signals $w_{os}h_s$. These are input to a summing element, together with an output bias b_o . The output y of the summer is therefore:

$$y = b_o + \sum_{s=1}^4 w_{os}h_s \quad [19.30]$$

and this is the final output of the network.

We see that the network of Figure 19.6 involves eight weights w and five biases b . The values of w and b are chosen so that for q sets of experimental input data

$$\{x_{1k}, x_{2k}, x_{3k}, x_{4k}\}, \quad k = 1, \dots, q$$

the corresponding network output values $y_{k,\text{est}}$ are as close as possible to the observed values y_k . This process is called **training** the network, and one method of achieving this is **back propagation**. Here the errors $e_k = y_k - y_{k,\text{est}}$ are calculated and the sum of square errors, SSE, is found. The partial derivatives of SSE with respect to w and b are then calculated and the values of w and b adjusted according to the magnitude and sign of these derivatives. This process is continued iteratively until values of w and b are found which minimise SSE.

One application of neural networks is to model an array of semiconductor sensors used to measure small concentrations of pollutant gases in air.^[4] Here there is an array of six sensors; each sensor is formed by depositing a thin film of a given metal phthalocyanine onto a planar configuration of thick film platinum electrodes (Section 8.1.4). Metals such as Zn, Pb, Ag, Co and Cu are used to measure the concentrations of gases such as NO₂, Cl₂, H₂S, HCl, NH₃ and water vapour. The resistance of a given metal sensor can depend on the concentration of all the gases present in the mixture; these relationships can also be non-linear. These cross-sensitivity and non-linear effects can be modelled by a neural network which has six inputs, corresponding to the six sensor resistances, and six outputs, corresponding to the six gas concentrations.

A process modelling application of neural networks is the prediction of the concentration of NO_x components present in the exhaust gas from an industrial boiler.^[5] Here 10 input variables were identified as being necessary for an accurate model of the process; these included fuel flow rate, air flow rate, stack gas recirculation flow rate, humidity, temperatures and pressures. A 10-input, single-output neural network gave predicted NO_x concentrations within approximately 1% of values obtained with an NO_x analyser.

Conclusion

This chapter has first discussed the structure of **intelligent multivariable measurement** systems and then shown the need for **inverse sensor** and **process** models. It went on to discuss multivariable modelling methods based on **physical/chemical equations**, **multivariable regression** and **artificial neural networks**.

References

- [1] MUDD J and BENTLEY J P 2002 'The development of a multi-channel vortex flowmeter using a twelve sensor array', *Measurement and Control*, vol. 35, no. 10, pp. 296–8.
- [2] WALPOLE R E and MYERS R H 1978, *Probability and Statistics for Engineers and Scientists*, 2nd edn, Collier MacMillan, pp. 314–25.
- [3] FROST D (Druck Ltd) 1999 'Resonant silicon pressure transducers', *Sensor and Transducer Conf.*, NEC Birmingham.
- [4] JEFFEREY P D *et al.* 1998 'Thick film chemical sensor array allows flexibility in specificity', *Sensor and Transducer Conf.*, NEC Birmingham.
- [5] HAYES R L *et al.* 'Using neural networks to monitor NO_x on an industrial boiler', *Advances in Instrumentation and Control*, vol. 51, part 1, pp. 259–71.

Answers to Numerical Problems

Chapter 2

- 1 $6.06 \mu\text{V } ^\circ\text{C}^{-1}$, $3.61 \times 10^{-3} \mu\text{V } ^\circ\text{C}^{-2}$, $2.59 \times 10^{-6} \mu\text{V } ^\circ\text{C}^{-3}$
- 2 $\beta = 2946 \text{ K}$, $\alpha = 1.86 \times 10^{-4} \text{ k}\Omega$, $3.64 \text{ k}\Omega$
- 3 (a) $+25.9\%$ (b) 0 , $53.3 \text{ mV cm}^{-1} \text{ V}^{-1}$ (c) 19.3 mV cm^{-1}
- 4 13.2%
- 5 (b) 208.6 Hz , 0.6 Hz
- 6 $R_T = 100(1 + 3.908 \times 10^{-3}T - 5.82 \times 10^{-7}T^2)$
- 7 (a) $a = 4.0 \text{ mA}$, $K = 1.6 \text{ mA bar}^{-1}$, $K_I = +0.4 \text{ mA } ^\circ\text{C}^{-1}$, $K_M = 0.4 \text{ mA bar}^{-1} \text{ V}^{-1}$
(b) 18.0 mA
- 8 $O = 2.0 \times 10^{-3}I + 1.0$
- 9 $O = 8.0 \times 10^{-4}I + 4.0$
- 10 $+0.2 \text{ V}$, $+4\%$
- 11 -0.5 mV , -2.5%
- 12 (a) $E = 54.78T$ (b) $-210 \mu\text{V}$, -0.77% ; $-109 \mu\text{V}$, -0.40%
- 13 $K_I = 0$, $K_M = 0.005 \text{ V kN}^{-1} ^\circ\text{C}^{-1}$
- 14 $K_M = 0$, $K_I = 0.02 \text{ V } ^\circ\text{C}^{-1}$
- 15 $K_M = +6 \times 10^{-6} \text{ mA Pa}^{-1} \text{ K}^{-1}$, $K_I = +0.02 \text{ mA } ^\circ\text{C}^{-1}$
- 16 (a) 19.6 mV , 0.392% (b) $76.3 \mu\text{V}$, 0.00153%
- 17 1.0%

Chapter 3

- 1 $\bar{E} = -0.425 ^\circ\text{C}$, $\sigma_E = 1.93 ^\circ\text{C}$
- 2 (a) 120.7 Pa (b) -500 Pa
- 3 (a) (i) 4.95 V (ii) 4.97 V
- 4 (b) Increase of $10^{-6} \text{ rad V}^{-1}$
- 5 (a) $\bar{E} = +5.0 ^\circ\text{C}$, $\sigma_E = 2.6 ^\circ\text{C}$
- 6 (a) $\bar{E} = +0.08 \text{ m/s}$, $\sigma_E = 0.35 \text{ m/s}$
- 7 $\bar{E} = -0.67 \text{ K}$, $\sigma_E = 4.87 \text{ K}$
- 8 -0.5 kN
- 9 $+0.32 \text{ m}$

Chapter 4

- 1 $-29.4, -10.8, -0.5, +24.1, +0.7$ °C
- 2 (a) 5×10^{-3} m N⁻¹, 20 rad s⁻¹, 0.3 (b) 1 cm
(c) $1.0 + 0.5 [1 - e^{-6t}(\cos 19t + 0.32 \sin 19t)]$ cm
- 3 $50[1.07 \sin(10t - 3^\circ) - 1.00 \sin 10t]$
 $+ \frac{50}{3}[2.16 \sin(30t - 19^\circ) - 1.00 \sin 30t]$
 $+ \frac{50}{5}[1.62 \sin(50t - 156^\circ) - 1.00 \sin 50t]$ N
- 4 (a) 0 to 0.1 rad s⁻¹ (b) 0 to 0.033 rad s⁻¹ (c) 0 to 0.33 rad s⁻¹
- 5 (a) 10 rad/s, 7.0, $\frac{0.1}{10^{-2}s^2 + 1.4s + 1}$ (b) Approx. $\frac{1}{10^{-4}s^2 + 1.4 \times 10^{-2}s + 1}$
- 6 (a) $\omega_n = 10$ rad/s, $\xi = 0.1$, $V(t) = 0.49[1 - e^{-t}(\cos 10t + 0.1 \sin 10t)]$
- 7 (a) $50[0.734 \sin(10t + 40^\circ) - 1.00 \sin 10t]$
 $+ \frac{50}{3}[1.39 \sin(30t - 2^\circ) - 1.00 \sin 30t]$
 $+ \frac{50}{5}[2.44 \sin(50t - 79^\circ) - 1.00 \sin 50t]$
- 9 (a) (i) $T_M(t) = 10[0.894 \sin(0.1t - 26.5^\circ) + \frac{0.707}{2} \sin(0.2t - 45^\circ) + \frac{0.555}{3} \sin(0.3t - 56.3^\circ)]$
(ii) $E(t) = 10[0.894 \sin(0.1t - 26.5^\circ) - \sin 0.1t] + \frac{10}{2}[0.707 \sin(0.2t - 45^\circ) - \sin 0.2t]$
 $+ \frac{10}{3}[0.555 \sin(0.3t - 56.3^\circ) - \sin 0.3t] - \frac{10}{4} \sin 0.4t$

Chapter 5

- 1 (a) 2.92×10^8 Ω, 0.15 pH mV⁻¹ (b) -20.5%
- 2 (a) 2.0 V cm⁻¹ (b) 500 Ω, 50 V
- 3 -56 Pa
- 4 $\frac{0.1s^2 + 10s + 1000}{5.1s^2 + 30s + 1100}$
- 5 9.09 mV
- 6 4.5 V, 10.5 kΩ
- 7 (a) 2.0 V, 1.6 kΩ, 1.72 V
(b) 5.0 V, 2.5 kΩ, 4.0 V
(c) 8.0 V, 1.6 kΩ, 6.9 V
- 8 (a) 10 V (b) $E_{Th} = 7$ V, $R_{Th} = 21$ Ω (c) 399 Ω
- 9 (a) 0.5 cm (b) $E_{Th} = 5.0$ V, $R_{Th} = 2.5$ kΩ (c) 4.0 V

Chapter 6

- 1 (a) 0.15 V, 1.0 V
- 2 +1.0, +0.6, +0.2, -0.2, -0.6, -1.0, -0.6, -0.2, +0.2, +0.6, +1.0
- 3 (a) 10^{-4} W, 10^{-2} V, 10^{-2} V (b) -20 dB
(d) Increased to +10 dB (e) Increased to +30 dB
- 4 (a) 3.14 mV, 100 V (b) 4.15 mV, 15.85 mV
- 5 (a) 1.5 mW (b) 8.5 mW (c) -7.5 dB
(d) 55 mV (e) 300 Hz (f) 92 mV

Chapter 7

- 1 (a) MDT = 6.2 h (b) MTBF = 10 074 h (c) $\lambda = 0.87 \text{ yr}^{-1}$ (d) $A = 0.99940$
- 2 (a) 0.62 (b) 0.24 (c) 0.31
- 3 TLOC = £19 000 for system (1), TLOC = £15 350 for system (2)

Chapter 8

- 1 (a) $3.91 \times 10^{-3} \text{ }^{\circ}\text{C}^{-1}$, $-5.85 \times 10^{-7} \text{ }^{\circ}\text{C}^{-2}$ (b) +0.76%
- 2 $R_1 = R_3 = 120.0025 \text{ } \Omega$, $R_2 = R_4 = 119.9975 \text{ } \Omega$
- 3 88.5, 55.3, 22.1 pF
- 4 7.6, 3.4 mH
- 5 521 mH, 5.6 mH
- 6 3.46 V, 367 Hz; 34.6 V, 3670 Hz
- 7 (a) -1.07%, -0.65% (b) $51.8 \text{ } \mu\text{V }^{\circ}\text{C}^{-1}$, $8.68 \times 10^{-3} \text{ } \mu\text{V }^{\circ}\text{C}^{-2}$ (c) $248 \text{ }^{\circ}\text{C}$
- 8 (a) 20 N m^{-1} , 0.51 N s m^{-1} (b) 0 to 1.24 cm (c) $1333 \text{ } \Omega$
- 9 -0.25 to +0.25 rad
- 10 (a) 1.2 mm (b) 0 to 0.17 mm
- 11 (a) $G(s) = 0.02 \left(\frac{10^{-3}s}{1 + 10^{-3}s} \right) \left(\frac{5.4 \times 10^{10}}{s^2 + 4.65 \times 10^3 s + 5.4 \times 10^{10}} \right)$
 (c) $G(s) = 0.002 \left(\frac{0.1s}{1 + 0.1s} \right) \left(\frac{5.4 \times 10^{10}}{s^2 + 4.65 \times 10^3 s + 5.4 \times 10^{10}} \right)$
- 12 (a) 100 g (b) (ii) 1 V
- 13 (a) 625 N m^{-1} (b) 1 mm (c) 3.40 to 7.58 mH
- 14 $62.5 \text{ }^{\circ}\text{C}$
- 15 $60 \text{ } \Omega$
- 16 $12\,320 \text{ } \Omega$
- 17 -5×10^{-4} , $+2 \times 10^{-4}$
- 18 $119.88 \text{ } \Omega$, $120.048 \text{ } \Omega$
- 19 169.9 pF
- 20 2.78 pF
- 21 $120.126 \text{ } \Omega$
- 22 (a) -4.87% (b) $255 \text{ }^{\circ}\text{C}$
- 23 $201 \text{ }^{\circ}\text{C}$
- 24 2 kHz
- 25 0 to 5 mm
- 26 60 mV

Chapter 9

- 1 (a) $R_2 = 100 \text{ } \Omega$, $R_3 = 5770 \text{ } \Omega$, $R_4 = 5770 \text{ } \Omega$
 (b) $R_2 = 100 \text{ } \Omega$, $R_3 = 6000 \text{ } \Omega$, $R_4 = 6000 \text{ } \Omega$
 (c) $R_2 = 100 \text{ } \Omega$, $R_3 = 5000 \text{ } \Omega$, $R_4 = 6000 \text{ } \Omega$
- 2 $R_2 = 10 \text{ } \Omega$, $R_3 = 1650 \text{ } \Omega$, $R_4 = 1650 \text{ } \Omega$

- 3 (a) (i) 0 to 1.0 V (approx.) (ii) -1.5% (b) 0 to 0.6 V (approx.)
4 $R_2 = 1000\ \Omega$, $R_3 = 264\ \Omega$, $R_4 = 2370\ \Omega$, $V_s = 2.40\ \text{V}$
5 (b) 9.1 mV
6 2584
7 0 to 44.2 mV
8 (a) 64.2 nF (b) 0.178 V (c) 0.3%
9 (a) Since $f_n = 32\ \text{Hz}$, $\xi = 0.7$, $|G(j\omega)| = 1$ up to 10 Hz (c) $+0.2 \sin 2000\pi t$ and $-0.2 \sin 2000\pi t$
10 1.9 k Ω
11 $R_{\text{IN}} = 10\ \text{k}\Omega$, $R_F = 1\ \text{M}\Omega$, $C_{\text{IN}} = 0.159\ \mu\text{F}$, $C_F = 0.159\ \text{nF}$
12 (a) $4.8 \times 10^3\ \text{N/A}$, 19.3 N (b) 1.0, 0.2
13 81.6 kHz at 1 mm to 122.4 kHz at 3 mm
14 $|G(j\omega_n)| = 20$ and $\arg G(j\omega_n) = -90^\circ$, between 2.60 and 4.56 kHz
15 (b) $L = 4.7\ \text{mH}$ (c) At $f_n = 100\ \text{kHz}$, $|G(j\omega_n)| = 0.0295$, $\arg G(j\omega_n) = -90^\circ$
At $f_n = 120\ \text{kHz}$, $|G(j\omega_n)| = 0.0354$, $\arg G(j\omega_n) = -90^\circ$
17 (a) 10^5 to $10^6\ \text{Pa}$ (b) $|G(j\omega_n)| = 200$, $\arg G(j\omega_n) = -90^\circ$ between 1.0 and 3.0 kHz
18 (a) 0.1 V (b) 0.01 V
19 (a) 10 k Ω (b) 25.6 V
20 (a) 5×10^{-4} (b) 15 mV

Chapter 10

- 1 (a) (i) $\pm 0.0122\%$ (a) (ii) 000111000010, 100001101010 (b) 1C2, 86A
(c) (i) $\pm 0.05005\%$ (c) (ii) 0001 0001 0000, 0101 0010 0101
2 (a) 85.3 Ω (b) 1.97 V
3 (a) 0 to $1/\tau\ \text{rad s}^{-1}$ (d) 0 to $\pi/4\tau\ \text{rad s}^{-1}$
4 32

Chapter 11

- 1 (a) 7.5 rad V^{-1} , 1.0 Hz, 35.6 (b) approx. 10 k Ω in series, 0.15 rad V^{-1}
2 (a) 0 to 15 cm

Chapter 12

- 1 (a) 10 m s^{-1} (b) 0.883 kg s^{-1} (c) 1.5×10^5 (d) 5.84 cm
2 (a) $Re = 1.2 \times 10^5$ at max. flow (b) 7.68 cm
3 (a) 0.14 m (b) $2.86 \times 10^5\ \text{Pa}$
4 (a) $Re = 2.7 \times 10^6$ at max. flow (b) 0.146 m (c) 0.135 m
5 23.8 mV and 4.3 Hz at min. flow, 499 mV and 90.2 Hz at max. flow
6 (a) 69.9 to 699 Hz (b) 10^4 (c) 14.3 m^3
7 432 pulses m^{-3}
8 $\tau = 150\ \text{ms}$, $\frac{1}{f_c} = 10\ \text{ms}$
9 (a) 7200 kg h^{-1} (b) 9.4×10^5 (d) 7610 kg h^{-1}
10 45 to 450 μs

Chapter 13

- 1 (b) (i) 0.200 to 1.00 bar (b) (ii) 0.202 to 1.007 bar
- 2 $E_{\text{MAX}} = 1.9 \mu\text{J}$ safe to use with hydrogen-air

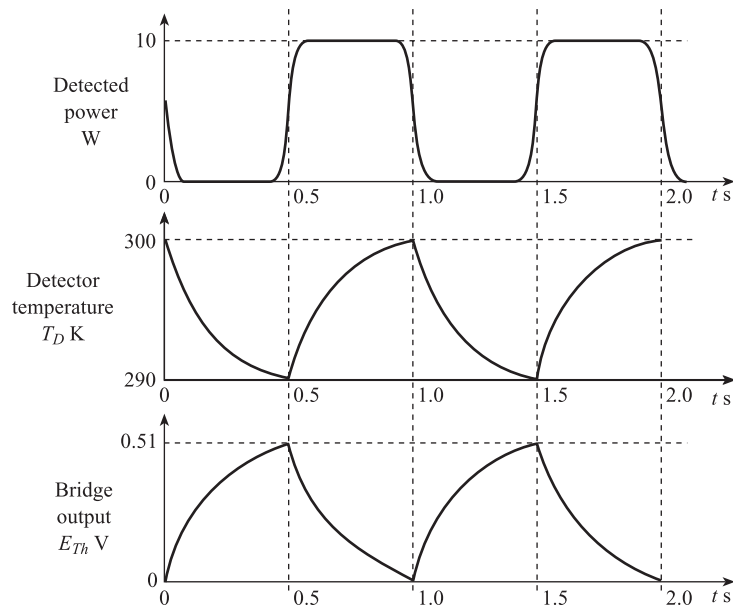
Chapter 14

- 1 $E_{\text{OUT}} = (3.93 + 6.55\sqrt{\nu})^{1/2}$
- 2 (a) $4.27 + 0.33\sqrt{\nu}$ (b) $\tau_v = 4 \text{ ms}$, therefore unsuitable
- 3 $\tau_v = 2.7 \text{ s}$, i.e. bandwidth 0 to 0.06 Hz, therefore unsuitable
- 4 (a) $G(s) = \frac{1}{6.4 \times 10^4 s^2 + 1068s + 1}$
 $|G(j\omega)| = 0.144$ at $\omega = 2\pi \times 10^{-3}$, therefore cannot follow variations
 (b) $G(s) = \frac{1}{1600s^2 + 93s + 1}$
 $|G(j\omega)| = 0.91$ at $\omega = 2\pi \times 10^{-3}$, can follow variations more closely
- 5 (a) 0 to 10.6 mV

Chapter 15

- 1 See Figure Soln Prob. 15.1
- 2 Period $T_p = 10 \text{ ms}$, maximum $T_D - T_s = 37.5^\circ\text{C}$,
 thermocouple constant $a_1 = 5 \times 10^{-2} \text{ mV } ^\circ\text{C}^{-1}$, output voltage range = 0 to 46.9 mV
- 3 0 to 5.97 mV
- 4 2.10×10^4
- 5 (a) 10 mW (b) 0.26, 15.1° (c) 0.47, 27.8° (d) $170 \mu\text{W}$, 0.998, $169.7 \mu\text{W}$
 (e) 2.2 mW, 0.794, 1.75 mW (f) Glass $169.7 \mu\text{W}$, $93.3 \mu\text{A}$; Polymer 1.75 mW, $961 \mu\text{A}$
- 6 500 to 1000 nm, 5.5

Figure Soln Prob. 15.1.



Chapter 16

- 1 (a) $\omega_n = 1.00 \times 10^6 \text{ rad s}^{-1}$, $\omega_1 = 1.18 \times 10^6 \text{ rad s}^{-1}$
(b) 50Ω , $-2^\circ 52'$ at ω_n , $14.1 \text{ k}\Omega$, $-3^\circ 27'$ at ω_1 (c) 0.02 A V^{-1} , -177°
- 2 (a) 7.7×10^{-3} , 7.7×10^{-3} , 7.3×10^{-10} , 7.3×10^{-10}
- 3 (a) 1 ms, 0.103 (b) $T_w = 30 \mu\text{s}$, $T_R = 10 \text{ ms}$ for example
- 4 (a) 6.7 kHz (b) $6 \times 10^{-4} \text{ W}$
- 5 (a) See Figure Soln Prob. 16.5(a)
- 6 See Figure Soln Prob. 16.6
- 7 (a) 4.67×10^{-7} (b) $115 \mu\text{s}$ at 24 m s^{-1} , $1.5 \mu\text{s}$ at 0.3 m s^{-1}
- 8 (a) 5.8 mW (b) 4.96 mW (c) $5.8 e^{-0.01n}(0.93)^{2n} \text{ mW}$

Figure Soln
Prob. 16.5(a).

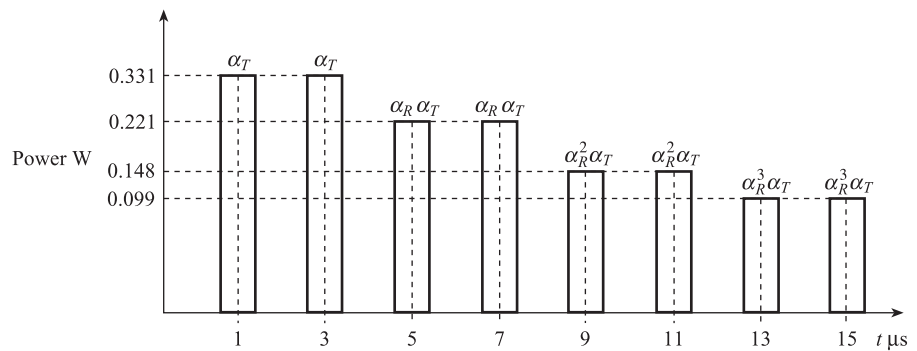
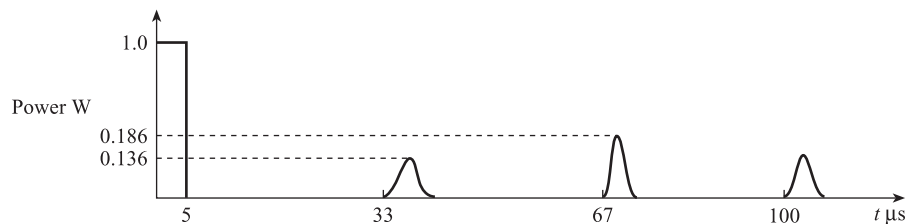


Figure Soln Prob. 16.6.



Chapter 17

- 1 (a) $2.63 \times 10^{-2} \text{ m s}^{-1}$, 2.26 (b) 6 s, 7 s, 1.54
(c) average $N \approx 5400$, $1.85 \times 10^{-4} \text{ m}$ (d) 18% O_2 , 82% N_2

Chapter 18

- 1 (a) 15 samples s^{-1} for example (b) 240 samples s^{-1} (c) 4.17 ms
(d) $\pm 0.0122\%$ (e) 2880 baud, 0 to 1440 Hz (f) 0.54 V
- 2 (a) 0.333 (b) 0.222 (c) 1.39×10^{-2} (d) 1.39×10^{-2} (e) 0.167
- 3 280 to 920 Hz
- 4 (a) 0.309, 0.683, 0.067 (b) 10

Index

- absolute encoders, 412
- a.c. amplifier, 219–20, 224–7
- a.c. carrier system, 224–7
- a.c. loading, 80
- accelerometers
 - negative feedback type, 72–3
 - piezoelectric type, 187–8
 - principle, 177–8
 - strain gauge type, 180–1
- accuracy, 35–47
- acoustic impedance, 434–5, 439–40
- acoustic matching, 443–5
- acoustic power, 439–40
- across (effort) variables, 84–93
- active sensing elements, 149–50
- address bus, 261–3
- address code, 261–5
- address map, 261–5
- address register, 261–5
- address signal, 261–5
- addressing, 261–5
- aliasing, 249
- alphanumeric displays, 289–92
- ampere, 23–7
- amplifiers
 - a.c., 219–20
 - buffer, 216–17
 - charge, 185–6
 - chopper stabilised, 224–7
 - differential, 216–19
 - ideal operational, 214–15
 - instrumentation, 223–4
 - inverting, 215–16
 - non-inverting, 216
 - operational, 214–27
 - practical limitations, 221–3
 - relay, 356–7
 - strain gauge, 218–19
 - voltage adder, 220–1
 - voltage follower, 216–17
- amplitude modulation (AM), 224–7
- amplitude ratio, 61–5
- analogue chart recorders, 304–6
- analogue filter, 117–18, 219–20
- analogue to digital conversion, 256–60
- analogue to digital converters (ADC), 256–60
 - dual slope, 256–8
 - flash, 259–60
 - successive approximation, 257–9
- anemometer (constant temperature), 374–8
- angular accelerometer, 178
- angular velocity measurement system, 270–2
- angular velocity sensor, 170–2, 414
- application layer, 494–8
- argument of complex number, 62–5
- arithmetic/logic unit, 262–3
- artificial neural networks, 512–14
- ASCII code, 272–3, 307–9
- assembly language, 264–5
- attenuation of ultrasonic wave, 440–1
- autocorrelation, 104–7, 121
- availability, 129
- averaging, 119–21
- backlash, 13
- balanced amplitude modulation, 224–7
- balanced bridge, 207–14
- band limited white noise, 104
- band pass filter, 117–18
- band stop filter, 117–18
- bandwidth, 71
- base units, 23
- BASIC language, 266
- bathtub curve, 131
- baud, 479–84
- bellows, 178–82
- bilateral transducers, 92–3
- binary coded decimal (bcd), 251–2
- binary codes, 251–4
- binary counter, 254–6
- biphase Manchester, 496–7
- bit, 251–4
- bit rate, 479–84
- black body, 389–90
- block diagram symbols, 7
- bolometer, 404–6
- Bourdon tube, 181–2
- bridges, *see* deflection bridges, 205–14

- buffer amplifier, 216–17
- byte, 251–4, 262–3
- C language, 267–8
- calibration: static, 28–31
- cantilever, 179–80
- capacitance: electrical, fluidic thermal, 84–7
- capacitive coupling, 114–16
- capacitive sensing elements, 160–5
- capsule, 181–2
- carrier gas, 462–7
- carrier signal, 224–7, 490–3
- cathode ray tube (CRT), 295–9
 - displays, 295–9
- character displays, 289–92
- characteristic acoustic impedance, 439–40
- charge amplifier, 185–6
- chart recorders, 304–6
- CHEMFET, 194–6
- chemical equations, 507–9
- check bits (digits), 487–9
- chopped radiation systems, 416
- chromatography, gas, 461–79
- clock pulses (signals), 254–6, 479–80
- closed-loop recorders, 304–306
- closed-loop systems, 42–3, 72–3, 228–30, 235–6, 304–6, 374–8
- code word, 251–4
- codes, 251–4
- common mode interference, 108–13, 116–17
- common mode rejection ratio, 116–17, 221–2
- communication systems, 475–501
- comparator, 258, 485
- compensation, 41–7
 - dynamic, 70–3
- compensation leads (thermocouple), 174–6
- compliance, 85
- composition measurement, 159–60, 190–6, 461–73
- compressible fluids, 314–20
- compressive stress, strain, 156–8
- computer
 - software, 264–9
 - system, 260–3
- conduction of heat, 367
- cone of acceptance, 399–401
- convection, 367–8
- convolution integral, 346
- Coriolis mass flowmeter, 340–2
- correlation, 104–7, 121, 344–7
- corrugated diaphragm, 181–2
- cost penalty function, 141–4
- counter, 254–9
- critical damping, 59–65
- cross-correlation flowmeter, 344–7
- crystal oscillator, 431–4
- crystal: piezoelectric, 182–8, 428–36
- cumulative power function, 102–4
- cumulative probability distribution function, 100–1
- Curie temperature, 405–7
- current source, 82–4
- current transmission, 82–4, 108–9
- current transmitters, 228–35
- Dall tube, 324–8
- damped angular frequency, 60–1
- damping force, 56–7, 177–82
- damping ratio, 56–65
- data acquisition systems, 477–8
- data bus, 260–3
- data link layer, 494–8
- data presentation elements
 - cathode ray tube (CRT), 295–9
 - chart recorders, 304–6
 - electroluminescence display (EL), 302–4
 - laser printers, 307–9
 - light emitting diode (LED), 292–5
 - liquid crystal displays (LCD), 299–302
 - paperless recorder, 306–7
 - pointer-scale indicator, 287–9
- decibel, 71, 108–9, 435–6
- decoder: 7 segment, 291–2
- deflection bridges
 - capacitive differential displacement sensor, 212–13
 - capacitive level sensor, 212–13
 - inductive differential displacement sensor, 212–14
 - resistive
 - katharometer, 378–81
 - platinum resistance detector, 209
 - strain gauge, 208–12
 - temperature difference, 210–11
 - thermistor, 209–10
 - Thevenin equivalent circuit, 205–6
- demodulation – frequency, 491
- demodulation – phase sensitive amplitude, 226–7
- denary numbers, 251–4
- density transducer, 239–40
- derived units, 24–5
- deterministic signal, 97–8
- diaphragm, 181–2
- dielectric, 160–5
- differential amplifier, 216–19
- differential capacitance displacement sensor, 161–2
- differential equations, 51–7
- differential pressure flowmeters, 321–9
- differential pressure (D/P) transmitters
 - applications, 231–2
 - closed loop-electronic, 228–30
 - open loop-electronic, 230–3
 - pneumatic-torque balance, 357–61
 - smart, 233–5
 - vibrating plate resonator, 239–40
- differential reluctance displacement sensor, 166–8
- differential transformer, 168–70
- digital codes, 251–4
- digital communications, 475–99
- digital displays, 289–304

- digital filter, 275–82
- digital filtering, 275–82
- digital printers, 307–9
- digital signals
 - parallel, 478–9
 - serial, 479–90
- digital to analogue converter (DAC), 256–7
- diodes, 292–5, 407–9
- direct model, 15–17, 44–5
- discharge coefficient, 323–9
- displacement sensors, 149–70, 411–13, 417–22
- displays, 287–304
- Doppler effect, 446–7
- Doppler flowmeter, 451–3
- drift (amplifier), 221–2
- dual slope ADC, 256–8
- dummy leads, 209, 245
- dynamic characteristics
 - of first order elements, 51–5, 58–9, 61–3
 - of second order elements, 56–7, 59–61, 63–5
- dynamic compensation, 70–3
- dynamic errors, 65–70

- earth loops, *see* multiple earths
- effort variable, 84–93
- elastic modulus, 156
- elastic sensing elements, 177–82
- electrical oscillators, 236–8
- electrochemical sensing elements, 190–6
- electroluminescence displays, 302–6
- electromagnetic coupling, 111, 114
- electromagnetic flowmeter, 343–4
- electromagnetic radiation, 385
- electromagnetic sensing elements, 170–2, 343–4
- electromagnetic shielding, 114
- electromechanical oscillators, *see* resonators
- electronic transmitters, 228–35
- electrostatic coupling, 112
- electrostatic deflection (in CRT), 295–6
- electrostatic screening and shielding, 114–16
- emissivity, 390–1
- encoders, 412–13
- encoding, 251–4
- environmental effects, 11–13
- error bands, 14–15
- error detection and correction (PCM), 487–9
- error probability function
 - measurement, 36–41
 - PCM, 484–7
- error reduction techniques
 - dynamic, 70–3
 - steady state, 41–7
- errors in measurement
 - dynamic, 65–70
 - steady state, 35–41
- errors in PCM transmission, 484–90
- Ethernet, 499
- estimation of measured value, 44–7

- even parity, 487–9
- exclusive OR, 488
- expansibility factor, 323–6
- extension leads, 174–6

- failure rate
 - data, 135–8
 - definition, 126–31
 - function, 131–2
 - models, 135–8
- farad, 23–6
- Faraday's law, 170
- feedback
 - accelerometer, 72–3
 - constant temperature anemometer, 374–8
 - differential pressure transmitter, 228–30
 - in dynamic compensation, 72–3
 - in static error reduction, 42–4
 - oscillators and resonators, 235–40
 - pneumatic transmitters, 357–61
- field effect transistors (FET), 194–6
- Fieldbus, 495–9
- filtering, 117–18
- filters, frequency response, 117–18
- first-order differential equation, 275–82
- first-order elements, 51–5
 - sinusoidal response, 61–3
 - step response, 58–9
- flapper/nozzle, 353–6
- flash ADC, 259–60
- flat screen displays, 299–304
- floating point, 253–4
- flow measurement systems, 313–47
- flow variable, 84–93
- flowmeters
 - Coriolis, 340–2
 - cross-correlation, 344–7, 453–4
 - differential pressure, 321–9
 - electromagnetic, 343–4
 - inferential mass, 339–40
 - turbine, 330–2
 - ultrasonic Doppler, 451–3
 - ultrasonic transit time, 454–5
 - vortex, 332–7
- fluid mechanics, 313–19
- fluid velocity sensor
 - hot wire and film sensors, 374–8
 - pitot tube, 319–21
- flux (magnetic), 165–8
- foil strain gauge, 157–8
- force balance systems, 228–30, 357–61
- force sensing elements, 177–81, 182–7
- Fourier analysis, 67–70
- Fourier transform, 106–7, 277
- frame, 498–9
- frame format, 498–9
- frequency demodulation, 491
- frequency modulation (FM), 490–3

- frequency response
 - of amplifiers, 219–23
 - of first and second order systems, 61–5
- frequency shift keying (FSK), 490–3
- frequency signals, 235–40
- frequency to digital conversion, 254–6
- Fresnel zone plate, 417–19
- fundamental frequency, 67–70
- fundamental interval, 153
- full-scale deflection (FSD), 10–11
- gain (amplifiers)
 - closed loop, 215–19
 - d.c. open loop, 214
- gain: bandwidth product, 222–3
- gain and phase conditions, 70, 236
- gallium aluminium arsenide (GaAlAs), 391–3
- gallium arsenide phosphide (GaAsP), 295, 391–3
- gallium phosphide (GaP), 295, 391–3
- gas sensors, 159–60, 193–4
- gauge factor, 157–8
- gauge pressure, 189–232
- Gaussian probability density function, 17–20
- gears, 13
- graphic displays, 292, 297–304
- Hall effect sensors, 196–7
- HART protocol, 496–500
- harmonics, 67–70
- heat balance equation, 51–2, 369–71, 404
- heat flow rate, 51–2, 369–71, 400
- heat transfer coefficient, 367–8
- heat transfer effects, 367–81
- henry, 24
- hexadecimal
 - code, 253
 - operand, 264–5
 - to decimal conversion, 272
- high-level language, 265–9
- high pass filter, 117–18
- histogram, 30–1, 100–1
- hum, 110
- humidity sensors, 154–5, 161–3
- hysteresis, 13
- ideal straight line, 9–10
- identification of characteristics
 - dynamic, 58–65
 - static, 28–31
- impact pressure, 319–20
- impedance
 - acoustic, 439–40
 - general definition, 84–7
- impulse response, 345–6
- incremental encoders, 412
- index register, 262–3
- indicators, pointer scale, 287–9
- inductive sensing elements, 165–70
- inertance, 85
- information bits (digits), 487
- infrared detectors, 403–9
- infrared radiation, 385–93
- initiate conversion, 258–9
- injection laser diode (ILD), 392–3
- input impedance, 77–80, 214
- input offset voltage, 214, 221
- input/output interface, 261
- instruction, 264–8
- instruction decoder, 262–3
- instruction register, 262–3
- instrumentation amplifier, 223–4
- integrator, 185–6, 269, 279–80
- intelligent systems, 503–14
- intelligent transmitters, 233–5
- interference – effect on measurement circuit, 107–17
- interference signals
 - common mode, 110–13
 - series mode, 110–13
- interfering input, 11–12
- interferometers, 419–22
- International Practical Temperature Scale (IPTS), 27–8
- intrinsic safety, 362–3
- inverse element models, 44–6, 504–5
- inverting amplifier, 215
- ion selective electrodes, 190–3
- j* operator, 62
- Johnson noise, 110
- junction, thermoelectric, 172–6
- junction diode, 292–5, 407–9
- katharometer, 378–81
- kelvin, degree, 23
- kilogram, 23
- kinetic energy (fluids), 317–18
- lag, first order, 52–5
- laminar flow, 315–16
- Laplace transform
 - definition 52–3
 - tables, 52–3
- lasers, 392–3
- laser printers, 307–9
- least significant bit (LSB), 251–4
- least squares fit, 28–9, 509–12
- level measurement, *see* liquid level
- light-emitting diode (LED), 292–5, 391–2
- linear differential equations, 52, 55, 56–7
- linear systems
 - frequency response, 63
 - principle of superposition, 68
- linear variable differential transformer (LVDT), 168–70
- linearity, 9–11
- liquid crystal displays (LCD), 299–302
- liquid level measurement, 161–3, 231–2, 456–7
- live zero, 228

- load cells, 179–80
- loading
 - electrical, 77–84
 - generalised, 84–93
- logarithmic amplitude ratio (decibel), 71, 108–9
- longitudinal wave (sound), 435–6
- look-up table, 272–4
- low pass filter, 117–18
- magnetic circuit, 165–8
- magnetic flux, 165
- magnetic reluctance, 165
- magnetomotive force (mmf), 165
- magnitude of complex number, 62–3
- mass, seismic, 177–8, 180–1, 187–8
- mass flow rate, 317, 326, 339–42
- mean down time (MDT), 127–9
- mean time between failures (MTBF), 129
- mean time to fail (MTTF), 126–7
- mean value
 - of element output, 19–20
 - of probability density function, 17–20, 101
 - of random signal, 99
 - of system error, 36–41
- measured value, 3–4
- measured variables, 3
- memory
 - random access (RAM), 261–3
 - read only (ROM), 261–3
- metre, 23–6
- Michelson interferometer, 420–2
- microcontroller
 - in chromatography, 466–73
 - in error reduction, 44–7
 - in flow measurement, 339–40
 - in speed measurement, 270–2
 - software, 264–5
 - system, 263
- microprocessor, 261–3
- mineral insulated thermocouple, 176
- modifying input, 11–13
- models
 - process, 505–6
 - element, 504–5
- modelling methods, 507–14
- modulation
 - amplitude (AM), 224–7
 - frequency (FM), 235, 490–3
- modulo 2 addition, 487–9
- modulus of elasticity, 156
- moment of inertia, 177–8
- monitors, 295–304
- most significant bit (MSB), 251–3
- motors, 304–6
- moving coil indicator, 287–9
- multiple earths, 111–16
- multiplexer, 477–8
- multiplexing, time division, 477–8, 483, 495–6
- multiplier, 7, 264–72, 281–2
- multivariable
 - modelling, 507–14
 - systems, 503–7
- narrow band
 - radiation thermometer, 410–11
 - ultrasonic link, 436
- National Measurement System, 23–8
- National Physical Laboratory (NPL), 23–8
- natural frequency, 56–7
- negative feedback, 42–3, 72–3, 228–30, 235–6, 304–6, 374–8
- noise
 - effect on measurement circuit, 107–9
 - methods of reduction, 113–21
 - sources, 110
 - statistical quantities, 98–107
- non-linearity
 - definition, 10–11
 - methods of compensation, 41–7
 - of deflection bridges, 206–12
 - of loaded potentiometer, 80–2
- non-return to zero (NRZ), 496–7
- normal distribution, *see* Gaussian probability density function
- Norton equivalent circuits, 82–4
- nozzle (flow), 324–7
- nozzle/flapper, 353–6
- number systems, 251–4
- Nusselt number, 367–8
- Nyquist sampling theorem, 247–9
- observation period, 97–8
- odd parity, 487–9
- offset voltage, 214, 221
- opcode, 264–5
- open-loop dynamic compensation, 72
- open-loop transmitter, 230–3
- opposing environmental inputs, 41–2
- optical fibres, 395–8, 413–15
- optical measurement systems, 385–422
- optical radiation, 385
- optical sources, 387–93
- optimum damping ratio, 60, 72
- orifice plate, 322–9
- oscillators
 - crystal, 433–4
 - electrical, 236–8
 - electromechanical, 238–40
 - voltage controlled (VCO), 490–1
- oscilloscope, cathode ray, 295–9
- OSI model, 494–5
- overshoot, 60–1
- paperless recorders, 306–7
- parallel digital signals, 254–60, 478–9
- parallel impedances, 82–4

- parallel reliability, 133–5
- parallel to serial conversion, 479–80
- parity check digits, 487–9
- partial fractions, 59–62
- passive axis, 157
- periodic signals, 67–70
- permeability, 165–8
- permittivity, 160
- persistence, 296
- pH electrode, 191–2
- phase difference, 61–5
- phase locked loop (PLL), 491
- phase-sensitive demodulator (PSD), 226–7
- phosphor, 295–9, 302–4
- phosphorescence decay, 295–6
- photon detectors, 407–9
 - photoconductive, 407–9
 - photovoltaic, 407–9
- physical equations, 507–9
- piezoelectric
 - effect, 182–3
 - sensing elements, 182–8, 428–36
- pitot-static tube, 319–21
- pixel matrix, 292–3
- Planck's Law, 389–90
- platinum resistance sensor, 152–5
- pneumatic
 - displacement sensor, 353–6
 - measurement systems, 353–62
 - relay amplifier, 356–7
 - torque-balance transmitters, 357–61
- pointer-scale indicator, 287–9
- Poisson's ratio, 156–7
- polarisation, 299–302
- polynomial, 11, 28–9, 509–12
- potential energy (fluid), 317–18
- potentiometer displacement sensor, 149–52
- power
 - acoustic, 439–40
 - cumulative function, 102–4
- power spectral density function, 102–4
- power spectrum, 102–4
- Prandtl number, 367–8
- pressure
 - absolute, 189, 232
 - differential, 189, 232
 - gauge, 189, 232
- pressure energy, 318
- pressure sensing elements, 160–4, 177–82
- pressure tappings, 322–7
- primary sensing elements, 149–50
- printers, 307–9
- probability
 - for random signal, 100–1
 - of failure, 125–6
- probability density function
 - definition, 14–15, 100–1
 - for measurement system error, 36–7
 - for random signal, 100–1
 - for repeatability, 17–19
 - for tolerance, 19–20
- process, 3, 503–4
- process models, 505–6
- program, 264–9
- pulse code modulation (PCM), 479–87
- pulse echo system, 447–51
- pyroelectric detectors, 405–7
- pyrometer thermal radiation, 409–11, 416–17
- quantisation, 249–51
- quantum level, 249–51
- quartz, 434–6
- R-2R ladder network, 256–7
- radiance, 387
- radiation sources, 387–93
- radiation (thermal) measurement systems, 409–11, 416–17
- random signals
 - introduction, 97–8
 - statistical characteristics, 98–107
- RAM, 261–3
- range, 9
- raster display, 296–8
- recorders
 - chart, 304–6
 - paperless, 306–7
- redundancy
 - in PCM error detection, 487–9
 - to improve reliability, 133–5
- reference junction, 172–6
- reference junction compensation circuit, 174–5
- refresh displays, 295–9, 302–4
- register
 - address, 262–3
 - data, 262–3
 - instruction, 262–3
 - shift, 479–80
- regression analysis, 28–9, 509–12
- regression matrix equations, 509–12
- relative permeability, 165–8
- relay, pneumatic, 356–7
- reliability
 - data, 135–8
 - design and maintenance, 139–40
 - fundamental principles, 125–35
- reluctance displacement sensors, 166–8
- reluctance (magnetic), 165
- repair time, 127–30, 139–40
- repeatability
 - definition, 17–19
 - measurement of, 30–1
- resistive deflection bridges, 206–12
- resistive sensing elements, 149–60
- resolution, 13–14, 249–51
- resonance, 64, 235–9, 435–6, 443–5

- resonant frequency, 64, 235–9, 435–6, 443–5
- resonators
 - vibrating plate, 239
 - vibrating tube, 239
- response
 - sinusoidal input, 61–5
 - step input, 58–61
- Reynolds number, 315–16
- rise time, 301
- ROM, 261–3
- root mean square (r.m.s.) value, 99
- rotational mechanical systems, 177–8
- sample and hold device, 249–50
- sampling, 247–9
- scaled variables, 273–5
- scales design of, 287–9
- Schmitt trigger, 254–6, 270–1
- screening, 114–16
- second-order
 - elements, 56–7
 - sinusoidal response, 63–5
 - step response, 59–61
- seismic mass, 177–8, 180–1, 187–8
- semiconductor
 - diodes, 292–5, 407–9
 - photon detectors, 407–9
 - strain gauges, 158
 - temperature detectors, 153–6
 - sensor array, 159–60, 514
- sensing elements (sensors), 149–97
- sensitivity (steady state), 11–12
- serial digital signalling, 479–87
- shear modulus of elasticity, 156, 181
- shear stress–strain, 156, 313–14
- shielding, 114–16
- shift register, 479–80
- shot noise, 110
- SI units, 23–8
- sidebands, 225–6, 492
- signal
 - autocorrelation function, 104–7, 121
 - averaging, 119–21
 - conditioning, 205–40
 - deterministic, 97–8
 - filtering, 117–18
 - modulation, 118–19, 224–7, 235, 490–3
 - processing, 247–82
 - random, 98–107
- signal conditioning, 205–40
- signal processing, 247–82
- signal-to-noise ratio, 107–9
- sinusoidal response, 61–5
- span, 9
- spectral density, 102–4
- spectrum of a signal, 102–4
- speed measurement system, 270–2
- speed sensing elements, 170–2, 413–14
- spring, 177
- standard deviation
 - from calibration experiment, 30–1
 - of error distribution, 36–40
 - of random signal, 99
 - of repeatability distribution, 17–19
 - of tolerance distribution, 19–20
- standards, 21–8
- static characteristics
 - statistical, 17–20
 - systematic, 9–17
- static (steady-state) calibration, 21–31
- statistical characteristics of element, 17–20
- statistical representation of random signal, 98–107
- steady-state characteristics, *see* static characteristics
- steady-state compensation, 41–7
- Stefan–Boltzmann constant, 389
- step response, 58–61
- stiffness, 177–82
- Stolz equation, 325
- storage elements, 261–3
- strain
 - definition, 156–7
 - in elastic elements, 156–8, 177–82
 - types, 156
- strain gauge, 156–8, 179–81
- stress, 156
- subtraction, 7, 216–18, 264–8
- successive approximation ADC, 257–9
- summing amplifier, 220–1
- superposition principle, 68
- tachogenerator, variable reluctance, 170–2
- telemetry, 493–9
- temperature coefficient of resistance, 152–5
- temperature measurement, thermal radiation, 409–11, 417
- temperature sensing elements
 - resistive, 152–5
 - thermoelectric, 172–6
- temperature standards, 27–8
- tensile strain, 156
- thermal capacitance, 84–7
- thermal detectors, 368–81, 404–7
- thermal noise, 110
- thermal resistance, 84–7
- thermal sensing elements
 - dynamics of, 369–71
 - fluid velocity detectors, 371–8
 - thermal conductivity detectors, 378–81
 - thermal power detectors, 404–7
- thermistor, 153–4
- thermocouple, 172–6
- thermoelectric sensing elements, 172–6
- thermopile, 404–5
- Thévenin equivalent circuits, 77–82, 205–6
- Thévenin impedance, 77–82, 205–6
- Thévenin theorem, 77

- thickness measurement (ultrasonic), 447–9
- through variables, 84–94
- time constant
 - electrical, mechanical, fluidic elements, 55
 - thermal elements, 52
- time delay measurement, 344–7
- time division multiplexing (TDM), 477–8, 483, 495–6
- time standards, 23–6
- torque-balance transmitters, 228–30, 357–60
- torque sensing element, 180–1
- total lifetime operating cost (TLOC), 141–4
- traceability, 22–3
- transducer, *see* density transducer *and* sensing elements
- transfer function
 - definition, 54
 - first-order, 54–5
 - second-order, 56–7
- transformer
 - linear variable differential, 168–70
- transient response, *see* step response
- transit time flowmeters, 454–5
- translational mechanical system, 84–7
- transmission bandwidth
 - FSK, 493
 - PCM, 484
- transmission characteristics
 - optical lens materials, 400
 - optical transmission media, 393–8
 - ultrasonic transmission medium, 436–45
- transmission of data, 475–500
- transmitters
 - current, 228–35
 - pneumatic, 357–61
 - smart, 233–5
 - ultrasonic, 428–36
- transverse wave (ultrasonics), 438–9
- triple point of water, 23
- true value (of measurement variable), 22
- turbine flowmeter, 330–2
- turbulent flow, 315–16
- two-phase flow measurement, 342, 344–7
- two port networks, 87–93, 428–31
- ultrasonic
 - imaging, 447–51
 - measurement systems, 427–55
 - transmission link, 427–8
 - transmission principles, 436–55
 - transmitters and receivers, 428–31
- unavailability, 130
- United Kingdom Accreditation Service (UKAS), 22
- units
 - SI base, 23
 - SI derived, 24–8
- unreliability, 126
- value measured and true, 3–4
- variables, measured, 3
- velocity measurement system, 270–2
- velocity of approach factor, 323–6
- velocity of fluid
 - pitot tube sensor, 319–21
 - thermal sensor, 371–8
- velocity sensing elements, 170–1, 413–14
- vena contracta, 322–3
- Venturi tube, 322–7
- virtual instrument
 - concept, 503–7
 - software, 268–9
- viscosity, 313–14
- viscous damping, 56–7, 177–82
- visual (video) display unit (VDU), 295–9
- volt, standard of, 27
- voltage balance recorder, 304–6
- voltage controlled oscillator (VCO), 490–1
- voltage follower, 216–17
- voltage summer, 220–1
- volume flow rate, 316–17
- vortex flowmeters, 332–8
- vortex shedding, 332–3
- wave, acoustic plane, 436–43
- waveform
 - deterministic, 97–8
 - periodic, 67–70
 - random, 97–8
- wavelength, 436–8
- weighting resistors, 256–7
- Wheatstone bridge, 206–7
- white noise, 104
- Wiener–Khinchin relationship, 106–7
- X deflection (in CRT), 295–9, 450–1
- Y deflection (in CRT), 295–9, 450–1
- Young’s modulus, 156
- Z modulation (in CRT), 295–9, 450–1
- Z transform, 275–81
- zener barrier, 362–3
- zero intercept, 9–10
- zirconia, 193–4

